

AD-754 903

ADVANCED AUXILIARY POWER SYSTEM

Andrew D. Meshow, et al

AiResearch Manufacturing Company

Prepared for:

Air Force Aeropropulsion Laboratory

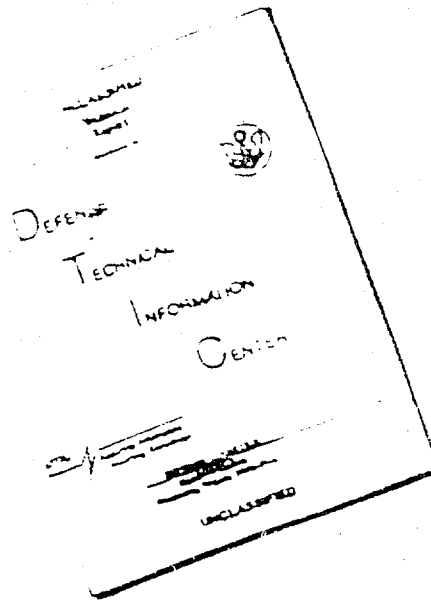
30 November 1972

DISTRIBUTED BY:

NTIS

National Technical Information Service
U. S. DEPARTMENT OF COMMERCE
5285 Port Royal Road, Springfield Va. 22151

DISCLAIMER NOTICE



THIS DOCUMENT IS BEST
QUALITY AVAILABLE. THE COPY
FURNISHED TO DTIC CONTAINED
A SIGNIFICANT NUMBER OF
PAGES WHICH DO NOT
REPRODUCE LEGIBLY.

REPRODUCED FROM
BEST AVAILABLE COPY

UNCLASSIFIED

AFAPL-TR-72-58

AD754903

ADVANCED AUXILIARY
POWER SYSTEM

MesheW, A.D., Swenski, D.F., et al
AirResearch Manufacturing Company of Arizona

TECHNICAL REPORT AFAPL-TR-72-58
November 1972

Approved for Public Release, Distribution Unlimited

Reproduced by
NATIONAL TECHNICAL
INFORMATION SERVICE
U S Department of Commerce
Springfield VA 22151

Air Force Aero Propulsion Laboratory
Air Force Systems Command
Wright-Patterson Air Force Base, Ohio

NOTICE

When Government drawings, specifications, or other data are used for any purpose other than in connection with a definitely related Government procurement operation, the United States Government thereby incurs no responsibility nor any obligation whatsoever; and the fact that the Government may have formulated, furnished, or in any way supplied the said drawings, specifications, or other data, is not to be regarded by implication or otherwise as in any manner licensing the holder or any other person or corporation, or conveying any rights or permission to manufacture, use, or sell any patented invention that may be related thereto.

Copies of this report should not be returned unless return is required by security considerations, contractual obligations, or notice on a specific document.

DOCUMENT CONTROL DATA - R & D

(Security classification of title, body of abstract and indexing annotation must be entered when the overall report is classified)

1. ORIGINATING ACTIVITY (Corporate author) GARRETT CORP., AIRESEARCH DIV., 402 SOUTH 36TH STREET PHOENIX, ARIZONA 85034		2a. REPORT SECURITY CLASSIFICATION	
		2b. GROUP	
3. REPORT TITLE ADVANCED AUXILIARY POWER SYSTEM PROGRAM			
4. DESCRIPTIVE NOTES (Type of report and inclusive dates) FINAL TECHNICAL REPORT November 1968 through May 1972			
5. AUTHOR(S) (First name, middle initial, last name) Andrew D. Meshew, Donald F. Swenski, et al.			
6. REPORT DATE November 30, 1972		7a. TOTAL NO. OF PAGES 556 486	7b. NO. OF REFS 0
8a. CONTRACT OR GRANT NO. F33615-69-C-1100		9a. ORIGINATOR'S REPORT NUMBER(S) SC-6308 SY-6055-R8, Rev. 1	
b. PROJECT NO. 3145		9b. OTHER REPORT NO(S) (Any other numbers that may be assigned this report) AFAPL-TR-72-58	
c.			
d.			
10. DISTRIBUTION STATEMENT Approved for Public Release; Distribution Unlimited			
11. SUPPLEMENTARY NOTES Details of discussions in this document may be better studied on microfiche.		12. SPONSORING MILITARY ACTIVITY AIR FORCE AEROPROPULSION LABORATORY WRIGHT-PATTERSON AFB, OHIO	
13. ABSTRACT This is a report of the Advanced Technology Auxiliary Power System (APS) Research and Development Program. The purpose of the program was to advance the technology of small APUs, using the secondary power system requirements of a hypothetical fighter aircraft of mid-1970 as a goal and an auxiliary power system as a test bed for exploratory development. The APU was 10 in. in diameter by 24 in. long, and the design-point performance goal was 300 equivalent shaft horsepower at 2200°F turbine inlet temperature and sea level, 130°F ambient conditions. Other design-point goals included an 11:1 cycle pressure ratio, 55-lb/min bleed-air at 6:1 pressure ratio, and a total system weight under 200 lb, including the starting system. Due to the technical difficulties in attempting to reduce to practice an advanced turbine wheel alloy, AF2-1DA, the average turbine inlet temperature was limited to 2000°F. Technical difficulties in perfecting the notched centrifugal compressor were also encountered, with the result that the maximum equivalent shaft horsepower produced was 162 instead of the 300 goal. The program resulted in technological advancements in the axial-centrifugal compressor, including variable inlet guide vanes, uncooled 2200°F combustion, an advanced radial in-flow cooled-turbine, uncooled columbium nozzles, and an advanced high-speed torque converter with lockup feature.			

DD FORM 1 NOV 68 1473

I-a

UNCLASSIFIED

Security Classification

14	KEY WORDS	LINK A		LINK B		LINK C	
		ROLE	WT	ROLE	WT	ROLE	WT
	AUXILIARY POWER UNIT TORQUE CONVERTER SMALL GAS TURBINE ENGINE ACCESSORY DRIVE GEARBOX						

I-6

UNCLASSIFIED

Security Classification

UNCLASSIFIED

AFAPL-TR-72-58

ADVANCED AUXILIARY
POWER SYSTEM

Mesheh, A.D., Swenski, D.F., et al

Approved for Public Release, Distribution Unlimited

I-C

FOREWORD

This report was prepared by The AiResearch Manufacturing Company of Arizona. The work under this contract was performed under Air Force Contract F33615-69-C-1100 from November 1968 to April 1972. This contract was administered by the U.S. Air Force Aeronautical Systems Group (AFSC), Wright-Patterson Air Force Base, Ohio. Mr. R. E. Quigley was the Air Force Project Engineer, and Mr. D. F. Swenski was the Project Engineer for AiResearch, during the final demonstration phase of the program.

The authors and contributors to the program and the final report include: D. G. Furst, L. W. Norman, and D. F. Swenski, Advanced Technology Supervision; R. W. Vershure, M. D. Toomey, N. M. Hughes, G. Amarel, G. L. Reese, D. F. Heuer, and K. E. Leach, Advanced Technology Project; B. H. Nicholls, Systems Engineering; L. J. Fitzjarrald, C. W. Warner, H. P. Gorman, B. Tice, and N. G. Walker, Design; E. Nelson, W. L. Womack, J. R. Hadley, and C. S. Chang, Applied Mechanics; R. O. Bullock and W. L. Hull, Aerodynamics; D. R. Seyler, G. L. Perrone, and C. Paine, Compressor Aerodynamics; W. Caan and K. W. Hansen, Combustion; J. J. Rebeske and F. F. Holman, Turbine Aerodynamics; M. F. Lasker, A. Pakvis, and D. A. Tummond, Gears, Bearings and Seals; R. P. Craig and D. M. Kreiner, Controls; and A. D. Meshew, Performance.

This report is assigned supplementary report number SY-6055-R8 by AiResearch and was submitted for approval in May 1972.

Publication of this report does not constitute Air Force approval of AiResearch findings or conclusions. It is published only for the exchange and stimulation of ideas.



Major Karl H. Muller, Chief
Laser & Aircraft Power Branch
Aerospace Power Division

TABLE OF CONTENTS

	<u>Page</u>
ABSTRACT	iii
FOREWORD	v
LIST OF ILLUSTRATIONS	xii
LIST OF TABLES	xxiii
LIST OF SYMBOLS	xxv
 SECTION I. INTRODUCTION AND SUMMARY	 1
 SECTION II. PROGRAM GOALS	 7
1. SYSTEM REQUIREMENTS	7
2. SYSTEM OPTIMIZATION	15
3. SYSTEM DEMONSTRATION UNIT	29
4. SYSTEM AND COMPONENT PERFORMANCE	31
 SECTION III. COMPRESSOR DESIGN AND DEVELOPMENT	 49
1. AXIAL COMPRESSOR STAGE	51
1.1 Aerodynamic Design and Development	51
1.2 Mechanical Wheel Design Analysis	69
2. RADIAL COMPRESSOR STAGE	73
2.1 Aerodynamic Design and Development	73
2.2 Mechanical Wheel Design Analysis	84
2.3 Structural Design Analysis	89
 SECTION IV. COMBUSTION SYSTEM DESIGN AND DEVELOPMENT	 99
1. DESIGN OBJECTIVES	100
2. COMPONENT SELECTIONS	101
2.1 Combustor	101
2.2 Fuel Injection System	101
2.3 Ignition System	102

TABLE OF CONTENTS (Contd)

	<u>Page</u>
3. PNEUMATIC INJECTOR DESIGNS	102
3.1 Combustor	102
3.2 Fuel Injector	104
3.3 Test Rig	107
4. PNEUMATIC INJECTOR COMBUSTION SYSTEM DEVELOPMENT	109
4.1 Fuel Injector	109
4.2 Combustor	112
4.3 System Performance	121
5. PRESSURE INJECTOR COMBUSTION SYSTEM DESIGN	123
5.1 Combustor	123
5.2 Fuel Injector	124
5.3 Combustion Rig	127
6. PRESSURE ATOMIZING COMBUSTION SYSTEM DEVELOPMENT	127
6.1 System Development	127
6.2 System Performance	129
 SECTION V. TURBINE DESIGN AND DEVELOPMENT	 141
1. RADIAL STAGE	142
2. AXIAL STAGE	148
2.1 Preliminary Design	148
2.2 Exhaust Diffuser	149
2.3 Stage Efficiency and Off-Design Performance	149
3. AERODYNAMIC DEVELOPMENT	150
3.1 Two-Stage Testing	150
3.2 Radial-Stage Testing	159
3.3 Axial-Stage Performance	175
3.4 Predicted Radial Stage Off-Design Performance	175
4. MECHANICAL DESIGN AND DEVELOPMENT	183
4.1 Uncooled Turbine Nozzle	183
4.2 Structural Heat-Transfer Analysis	189
4.3 Radial Turbine Wheel	202
4.4 AF2-1DA Radial Turbine Wheel Material	226
4.5 Axial Turbine Wheel	239

TABLE OF CONTENTS (Contd)

	<u>Page</u>
SECTION VI. TORQUE CONVERTER	251
1. DESIGN GOALS	251
1.1 Program Goals	251
1.2 Lockup Device	252
2. DESIGN ANALYSES	253
2.1 Torque Converter Design	253
2.2 Lockup Elements	265
3. DEVELOPMENT	276
3.1 Tests 1, 2, 3	278
3.2 Tests 4, 5, 6	279
3.3 Test 7	280
3.4 Test 8	282
3.5 Test 9 (Steady State)	282
3.6 Test 10 (Acceleration)	284
3.7 Test 11 (Acceleration)	284
3.8 Test 12 (Steady State)	284
3.9 Test 13 (Acceleration)	285
3.10 Test 14 (Acceleration)	285
3.11 Test 15 (Acceleration)	285
3.12 Test 16	288
3.13 Tests 17, 18, 19	288
SECTION VII. CONTROL SYSTEM	293
1. AUTOMATIC CONTROL SYSTEMS DESIGNS	293
1.1 Speed Control Systems	293
1.2 Speed Switching Control and DC Power Supply	300
1.3 APU Overtemperature Control System	300
1.4 Surge Control System	305
1.5 Load Compressor Systems	306
1.6 Gas-Diverting Valve System	311
1.7 Variable Geometry Control System	312
1.8 Oil Hydraulic System	317
2. APS DEMONSTRATOR CONTROL SYSTEM	317
2.1 Control Components	318
2.2 Control System Operation	325

TABLE OF CONTENTS (Contd)

	<u>Page</u>
SECTION VIII. APU DESIGN ANALYSIS	329
1. THERMAL ANALYSIS OF ROTATING GROUP	329
2. RELATIVE DISPLACEMENT ANALYSES	331
3. ROTATING GROUP DYNAMIC ANALYSIS	331
4. ROTATING GROUP TIE-BOLT	333
4.1 Hollow Radial Turbine Tie-Bolt Configuration	336
4.2 Solid Radial Turbine Tie-Bolt Configuration	343
5. BEARING SYSTEM	345
5.1 APU Main Shaft	345
5.2 Accessory Drive Gearbox	347
6. SEALS	350
6.1 Compressor Bearing Cavity	350
6.2 Rotating Knife Labyrinth Seals	350
6.3 Turbine Bearing Cavity	352
SECTION IX. GEARBOX DEVELOPMENT	355
1. GENERAL DESIGN	355
2. LUBRICATION SYSTEM	360
3. ACCESSORIES	363
3.1 Standby Generator	363
3.2 Main Engine Generator	364
3.3 Hydraulic Pumps	364
3.4 Starter Motor	364
SECTION X. APU TEST HISTORY	367
1. BUILD 1	367
2. BUILD 2	367
2.1 Configuration	367
2.2 Testing	375
2.3 Teardown Inspection	375
2.4 Teardown Failure Analysis	378

TABLE OF CONTENTS (Contd)

	<u>Page</u>
SECTION XI. CONCLUSIONS	399
REFERENCES	401
APPENDIX. Illustrations and Their Tabular Coordinates for the Technologically Advanced Auxiliary Power System Program	403

LIST OF ILLUSTRATIONS

	<u>Page</u>
1. Selected Auxiliary Power System	3
2. Estimated Performance GTCP305 Advanced Technology APU Maximum Bleed Condition	4
3. Estimated Performance GTCP305 Advanced Technology APU Maximum Shaft Power Condition	5
4. Main Engine Starting Characteristics	12
5. System I - Single-Shaft Integral Bleed APS	16
6. System II - Single Shaft Load Compressor APS	17
7. System III - Free Turbine Integral Bleed APS	18
8. System IV - Free Turbine Load Compressor APS	19
9. Radial Impeller Bleed Extraction System	21
10. Estimated Performance With Theoretical Compressors	33
11. Estimated Performance With Theoretical Compressors	34
12. Cooling Flow and Leakage Parametric Data	35
13. Cooling Flow and Leakage Parametric Data	36
14. Pressure Drop Parametric Data	37
15. Pressure Drop Parametric Data	38
16. Compressor Efficiency Parametric Data	39
17. Compressor Efficiency Parametric Data	40
18. Burner Efficiency Parametric Data	41
19. Burner Efficiency Parametric Data	42
20. Turbine Efficiency Parametric Data	43
21. Efficiency Parametric Data	44
22. Axial -1 Compressor Rotor Performance Map	52

LIST OF ILLUSTRATIONS (Contd)

	<u>Page</u>
23. Axial -1 Compressor Stage Performance Map	54
24. Axial -2 Compressor Rotor Performance Map	55
25. Axial -2 Compressor Rotor Performance Map With Increased Tip Clearance	56
26. Axial -1 Compressor Rotor Performance Map With Increased Tip Clearance	58
27. Axial -2 Compressor Rotor Performance Map at Various IGV Settings	59
28. Axial Compressor Stage VIGV Effects	60
29. Axial (-3) Compressor Stage	62
30. Axial (-3) Compressor Stage	63
31. Axial Compressor Stage Flowpath	64
32. Axial -3 Compressor Stage Performance Map	66
33. Centrifugal Compressor Inlet Flow Distribution Comparison	67
34. Tangential Stress Distribution of GTCP305 Axial Compressor	71
35. Axial Compressor Stage Interference Diagram	72
36. Reference Centrifugal Compressor	74
37. Reference Notched Impeller Test Results	75
38. Centrifugal Compressor Vector Triangles of Inducer Leading Edge	76
39. Centrifugal Compressor Vector Triangles of Diffuser Leading Edge	78
40. Centrifugal Compressor Performance Map	81
41. Centrifugal Compressor Tangential Stress Distribution . . .	86
42. Centrifugal Compressor Temperature Distribution	87

LIST OF ILLUSTRATIONS (Contd)

	<u>Page</u>
43. 6AL-25Ni-4Zr-2M Titanium Tensile Properties	88
44. Axial Deflection	90
45. Radial Deflection	91
46. Centrifugal Compressor Interference Diagram	92
47. Bleed Plenum, Flow Splitter, and Shroud Assembly	93
48. Bleed Plenum, Flow Splitter, and Shroud Assembly Steady-State Temperature Estimates	95
49. Bleed Plenum, Flow Splitter, and Shroud Assembly Steady-State Pressure Estimates	96
50. Bleed Plenum, Flow Splitter, and Shroud Assembly Steady-State Stresses	97
51. Bleed Plenum, Flow Splitter, and Shroud Assembly Steady-State Deflections	98
52. Combustor Loading During Start Cycle	103
53. Combustor Air Distribution	105
54. Pneumatic Injector Assembly	106
55. Fuel Injector Test Fixture	108
56. Pneumatic Injector Fuel Atomizer, Total Pressure Survey . .	110
57. Pneumatic Injector Fuel Atomizer, Static Pressure Survey	111
58. Pneumatic Injector Flow Calibration	113
59. Ignition Test Results	114
60. Combustor	117
61. Combustor Temperature Distribution	118
62. Combustor	120
63. Acceleration Temperature Spread	122

LIST OF ILLUSTRATIONS (Contd)

	<u>Page</u>
64. Combustor Airflow Distribution, Configuration 1	125
65. Combustor Airflow Distribution, Configuration 2	126
66. Fuel Nozzle Cross Section	128
67. Fuel System Flow Calibration	130
68. Temperature Spread Factor	132
69. Temperature Spread Factor	133
70. Temperature Spread Factor	134
71. Temperature Spread Factor	135
72. Temperature Spread Factor	136
73. Temperature Spread Factor	137
74. Sea-Level Ignition Characteristics	138
75. 25,000-Ft Altitude Ignition Characteristics	139
76. Combustor	140
77. Radial Turbine Vector Diagram	144
78. Radial Turbine Vector Diagrams, Rotor Exits	145
79. Axial Turbine Vector Diagrams	146
80. Scalloped Radial Wheel and Axial Turbine Assembly	151
81. Turbine Section Efficiency, 80% $N/\sqrt{\theta}$	153
82. Turbine Section Efficiency, 90% $N/\sqrt{\theta}$	154
83. Turbine Section Efficiency, 100% $N/\sqrt{\theta}$	155
84. Turbine Section Efficiency, 110% $N/\sqrt{\theta}$	156
85. Turbine Section Efficiency, 115% $N/\sqrt{\theta}$	157
86. Turbine Section Flow	158
87. Radial Rotor Efficiency Survey Design Pressure Ratio . . .	160

LIST OF ILLUSTRATIONS (Contd)

	<u>Page</u>
88. Radial Turbine Efficiency Survey Design Speed (From Turbine Section Test)	161
89. Radial Turbine Stage Efficiency, 80% $N/\sqrt{\theta}$	162
90. Radial Turbine Stage Efficiency, 90% $N/\sqrt{\theta}$ (Unscalped Wheel)	163
91. Radial Turbine Stage Efficiency, 100% $N/\sqrt{\theta}$ (Unscalped Wheel)	164
92. Radial Turbine Stage Efficiency, 110% (Unscalped Wheel)	165
93. Radial Turbine Stage Efficiency, 120% $N/\sqrt{\theta}$ (Unscalped Wheel)	166
94. Radial Turbine Flow (Unscalped Wheel)	167
95. Radial Turbine Mean Exit Swirl Angle	168
96. Radial Turbine Shroud Pressure Loading	170
97. Radial Turbine Efficiency Survey	171
98. Radial Turbine Delta T/T Survey	172
99. Radial Turbine Pressure Ratio Survey	173
100. Radial Turbine Swirl Angle Survey	174
101. Axial Turbine Efficiency, 80% $N/\sqrt{\theta}$	176
102. Axial Turbine Efficiency, 91% $N/\sqrt{\theta}$	177
103. Axial Turbine Efficiency, 101% $N/\sqrt{\theta}$	178
104. Axial Turbine Efficiency, 112% $N/\sqrt{\theta}$	179
105. Axial Turbine Efficiency, 117% $N/\sqrt{\theta}$	180
106. Axial Turbine Efficiency	181
107. Radial Turbine Test 3 (Unscalped Open Wheel) and Predicted Turbine Performance Comparison	182

LIST OF ILLUSTRATIONS (Contd)

	<u>Page</u>
108. Radial Turbine Test Data Match	184
109. Uncooled Turbine Nozzle Vane Cascade	187
110. Design Boundary Conditions, Cooled Turbine Nozzles	190
111. Cooled Turbine Nozzle Configuration	191
112. Cooled Turbine Nozzle Steady-State Temperatures	193
113. Cooled Turbine Nozzle Transient Temperatures	194
114. Cooled Turbine Nozzle Cooling-Flow Distribution	195
115. Cooled Turbine Nozzle Temperature Distribution	197
116. Turbine Shroud Maximum Calculated Stress Locations	199
117. Film and Internal Cooling Schemes for Radial Turbine Wheel	203
118. Progression of Radial Turbine Aerodynamic Configuration	204
119. Radial Turbine Film-Cooling Test Results	206
120. Radial Turbine Wheel Temperature Distribution	208
121. Radial Turbine Wheel Radial Stress	209
122. Radial Turbine Wheel Tangential Stress	210
123. Equivalent Stress	211
124. Radial Turbine Wheel Combined Centrifugal and Thermal Stresses and Deflections	212
125. Engine Start Transients, Radial Turbine Inlet Temperature and Wheel Speed	215
126. Radial Turbine Wheel Maximum Temperature and Stress Transients, Engine Start	216
127. Radial Turbine Wheel, Life Fraction Distribution	220
128. Manufacturer's Stress-Rupture Properties of Unitemp AF2-1DA	222

LIST OF ILLUSTRATIONS (Contd)

	<u>Page</u>
129. Radial Turbine Wheel 2500-Hr Creep Distribution	223
130. Low-Cycle Fatigue Test for Inertia Welded AF2-1DA Wheel and Inconel 718	225
131. Typical AF2-1DA Forging Cracks	231
132. Yield Strength of AF2-1DA, 0.2%	233
133. Ultimate Tensile Strength of AF2-1DA	234
134. AF2-1DA Stress-Rupture Curve From AFML-TR-69-25, With AiResearch Data	235
135. Axial Turbine Wheel Centrifugal Stress Distributions . . .	240
136. Axial Turbine Blade Characteristics	241
137. Axial Turbine Combined Thermal and Centrifugal Stress Distributions	242
138. Axial Turbine Inlet Temperature and Wheel Speed Transients, Engine Start	245
139. Axial Turbine Wheel Maximum Temperature and Stress Transients, Engine Start	246
140. Axial Turbine, Modified Goodman Diagram	248
141. Axial Turbine, Interference Diagram	249
142. Estimated Torque Converter Performance at 20,000-rpm Impeller Speed	254
143. Torque Converter Design Vector Diagram	256
144. Advanced APU Torque Converter Final Meridional Shape . . .	257
145. Torque Converter Impeller Vector Diagram	259
146. Torque Converter Turbine Vector Diagram	260
147. Torque Converter Reactor Vector Diagram	261
148. Effect of Varying Reactor Exit Angle	264
149. Torque Converter Configuration	266

LIST OF ILLUSTRATIONS (Contd)

	<u>Page</u>
150. Torque Converter Impeller (Top) and Turbine (Bottom) . . .	267
151. Torque Converter Fixed Reactor	268
152. Torque Converter Variable Reactor	269
153. Lockup Clutch and Torque Converter Layout	271
154. Lockup Clutch and Torque Converter Schematic	273
155. Estimated Performance Lockup Torque Converter	275
156. Estimated Lockup Torque Converter Efficiency	277
157. Torque Converter Reactor Interference Diagram	281
158. Steady-State Torque Converter Performance	283
159. Comparison of Torque Converter Tests 10 and 14 at 100 psig Charge Pressure	286
160. Performance Comparison of Torque Converter Flow Control Orifice Sizes at 0.5 Speed Ratio	287
161. Final Torque Converter Test Results	289
162. Capacity Factor Final Torque Converter Test Results	290
163. Overall Control System Diagram	295
164. Subsystem Diagram, Speed Control	297
165. Power Supply and Switching Schematic (APU/ADS System) Single-Shaft Version	301
166. Subsystem Diagram, APU Overtemperature System	303
167. Subsystem Diagram, Surge Control	307
168. Subsystem Diagram, Load Compressor Systems	309
169. Subsystem Diagram, Gas Diverting Valve System	313
170. Subsystem Diagram, Variable Geometry	315
171. Subsystem Diagram, Oil Hydraulic System	319

LIST OF ILLUSTRATIONS (Contd)

	<u>Page</u>
172. APU Demonstrator Control System	321
173. APU Demonstrator Fuel Control System	326
174. APU Demonstrator, Fuel Control System Characteristics . . .	327
175. Rotating Group Temperature Distribution, °F	330
176. Seal Displacement During Transient Operation	332
177. Bearing Loads vs Engine Speed	334
178. Hollow Radial Turbine Configuration, APU Temperature Distribution	337
179. Solid Radial Turbine Configuration, APU Temperature Distribution	339
180. Low-Cycle Fatigue for Inconel 718 at 1200°F	341
181. Tie-Bolt Load Relaxation, Hollow Radial Turbine Configuration	342
182. Turbine Transient Temperature Response	344
183. Tie-Bolt Relaxation Solid Radial Turbine	346
184. Bearing Test Rig	348
185. Comparison of Bearing Rig Tests and APU Tests	349
186. Compressor Face Seal Assembly	351
187. Typical Hydrodynamic Seal	353
188. Installation Drawing - Advanced Technology Gearbox	357
189. APS Gear Schematic	359
190. Flow Diagram, Oil, Gas Turbine Engine Accessory Drive . .	361
191. APS Gearbox and Accessories	368
192. APU and Gearbox	369
193. APS Test Setup	370

LIST OF ILLUSTRATIONS (Contd)

	<u>Page</u>
194. Builds, 1, 2, 3	371
195. Build 4	383
196. Build 5	389
197. Build 5 APU Instrumentation	392
198. First-Stage Turbine Nozzles	405
199. Axial Compressor	406
200. Axial Compressor Blade Stacking	407
201. Axial Compressor Blade Stacking	408
202. Axial Compressor Blade Stacking	409
203. Axial Compressor Blade Stacking	410
204. Axial Compressor Blade Stacking	411
205. Axial Compressor Blade Stacking	412
206. Axial Compressor Blade Stacking	413
207. Axial Compressor Blade Stacking	414
208. Axial Compressor Blade Stacking	415
209. Axial Compressor Blade Stacking	416
210. Axial Compressor Blade Stacking	417
211. Axial Compressor Blade Stacking	418
212. Swept Inlet Stator	419
213. Duct Assembly, Diffuser, Interstage	420
214. Rectilinear Stator	421
215. Coordinates for Figure 202	422
216. Coordinates for Figure 202	423
217. Coordinates for Figure 200	424

LIST OF ILLUSTRATIONS (Contd)

	<u>Page</u>
218. Centrifugal Compressor Ref. Figure 207	425
219. Centrifugal Compressor	427
220. Radial Turbine	429
221. Radial Turbine	431
222. Radial Turbine, Coordinates for Figure 208	433
223. Radial Turbine, Coordinates for Figure 209	435
224. Axial Turbine	436
225. Axial Turbine	437
226. Torque Converter, Impeller	438
227. Axial Turbine Coordinates for Figures 212 and 213	439
228. Torque Converter, Impeller	441
229. Torque Converter, Turbine	442
230. Torque Converter, Turbine	443
231. Torque Converter, Reactor	444
232. Torque Converter, Reactor	445
233. Torque Converter, Reactor	446
234. Torque Converter, Reactor	447
235. Torque Converter, Reactor Airfoil Data	448

LIST OF TABLES

	<u>Page</u>
I APS Performance Requirements	8
II Reference Duty Cycle for Advanced Auxiliary Power System	10
III APS Component Performance Comparison	13
IV APU Variable Geometry Requirements	20
V Cycle Assumptions for Design-Point Performance Calculations	24
VI System Evaluation Comparison	25
VII Fuel Flows for Bleed-Air Modes, lb/hr	27
VIII APU Shaft Horsepower Requirements and Performance . .	28
IX APS Design-Point Parameters	32
X APU Design-Point Influence Coefficients	45
XI Turbine Aerodynamic Design Goals	143
XII Uncooled Turbine Nozzle Tests	186
XIII Effective Turbine Shroud Stresses due to Steady- State Pressures	200
XIV Effective Turbine Shroud Stresses due to Steady- State Pressure and Temperature	201
XV Transient Turbine Shroud Thermal, Effective Stresses .	213
XVI Radial Turbine Wheel Centrifugal Deflections	214
XVII Radial Turbine Wheel Centrifugal and Thermal Deflections	219
XVIII Maximum Radial Turbine Wheel Life Fraction Summation .	224
XIX Influence of Duty Cycle on Radial Turbine Disc Bore Creep	227
XX Room Temperature Tensile Properties of AF2-1DA From Various Forgings	228

LIST OF TABLES (Contd)

	<u>Page</u>
XXI 1400°F Tensile Properties of AF2-1DA From Various Forgings	229
XXII AF2-1DA Experimental Heat Treat Cycles	236
XXIII Stress-Rupture Properties of AF2-1DA Wheel Forging, Using the Cookie-Cutter Technique	237
XXIV Comparison of AF2-1DA Published, Cookie-Cutter, and Astroloy Stress-Rupture Data	238
XXV Radial Turbine Duty Cycle	244
XXVI Component Design Data	356
XXVII Exceptions to GTCP305 Assembly P/N 380977-1, Rev. A, Build 1	373
XXVIII GTCP305 Light-Off Tests, Build 2A, Test 2, Run 46, Scans 56-63, 4/14/71	376
XXIX Self-Sustaining Runs, GTCP305, Build 3, Test 2, 5/24/71	380
XXX Hot Runs, GTCP305, Build 4, 7/26/71	386
XXXI Self-Sustaining Runs, GTCP305, Build 5, 1-21, 1-28, and 2-17-72	398

LIST OF SYMBOLS

A'_{cr}	$\frac{2r}{r+1} gRT'$ Critical Velocity
APU	Auxiliary power unit (gas turbine)
APS	Auxiliary power system (APU, plus gearbox, accessories, etc.)
B'	Time for one bearing out of 100 to fail
BPR	Bypass ratio = $W_B / (W_A - W_B)$
C_A	Axial clearance, in.
C_R	Radial clearance, in.
DN	Bearing diameter (mm) X rpm
EGT or T_5	Exhaust gas temperature, °F or °R
eshp	Equivalent shaft horsepower
esfc	Equivalent specific fuel consumption (lb/hr of fuel per eshp)
g_c	Gravitational constant, 32.17 ft/sec ²
gg	Gas generator
H	Enthalpy, Btu/lb
hp	horsepower
N	Speed, rpm
N_s	Specific speed, rpm-ft ^{3/4} /sec ^{1/2}
P	Total pressure, psia
P/P or PR	Pressure ratio
R	Gas constant, 1544/mol. wt
sfc	Specific fuel consumption (lb/hr of fuel per shp)

LIST OF SYMBOLS (Contd)

shp	Shaft horsepower
T	Total temperature, °F or °R
T'	Total temperature, °R
TIT	Turbine inlet temperature, °F or °R
T-T	Total-to-total (pressure)
T-S	Total-to-static (pressure)
TSF	Temperature spread factor, calculated from combustor exit and inlet temperatures =

$$\frac{T_{\max} - T_{\text{avg}}}{T_{\text{avg}} - T_{\text{in}}}$$

V_u	Peripheral (wheel) velocity
V_x	Tangential velocity
V	Axial velocity, ft/sec
VIGV ₁ or IGV ₁	Variable inlet guide vane to Compressor 1
VIGV ₂₃ or IGV ₂₃	Variable inlet guide vane to Compressors 2 and 3
VSCF	Variable-speed, constant speed (generator)
W_A	Actual air inlet flow rate, lb/sec
W_B	Bleed-air flow rate, lb/sec
$W\sqrt{\theta}/\phi$	Corrected flow
ϕ	P/14.696
γ	Adiabatic efficiency
ϕ	V_x/V
ρ	Mass density, slug/ft ³
θ	T/518.7, T _{in} °R

SECTION I
INTRODUCTION AND SUMMARY

The Exploratory Development Program reported herein was performed by the AiResearch Manufacturing Company of Arizona, A Division of The Garrett Corporation. The objective of the program was to provide the advancements in technology required to improve the performance, weight, and volume of a small auxiliary power unit accessory drive system to the extent that this type of system would become practical for use on advanced fighter, attack, and light cargo aircraft. Since the objective was technological advancement, the resulting power system was not directed toward any one specific aircraft but was designed to be adaptable to a variety of future envelopes and requirements and, therefore, included a high degree of flexibility.

The major program goals were:

(a) APU

APU size	= 10-in. diam x 24-in. length
Cycle pressure ratio	= 11:1
Bleed pressure ratio	= 6:1
Equivalent shaft horsepower	= 300 at 130°F sea level
Output shaft horsepower	= 160
Turbine inlet temperature	= 2200°F
Specific fuel consumption	= 0.51

(b) System

Weight = 200 lb (including APU, gearbox, start system)
TBO = 2500 hr

(c) Maximum Technological Flexibility

The program consisted of three phases:

- (a) System preliminary design
- (b) Component development
- (c) System demonstration

The results of an Auxiliary Power System study, completed by the AiResearch Manufacturing Company and reported under AFAPL-TR-67-135, formed a basis for the initial work accomplished in the Preliminary Design Phase. Approximately 184 APU cycle and configuration analyses were completed, including variable geometry, multispool, and recuperated versions. Potential candidates were narrowed to four nonrecuperated systems of which 12 variations were considered:

- (a) Single shaft - Integral bleed/gearbox
- (b) Single shaft - Load compressor/gearbox
- (c) Free turbine - Integral bleed/gearbox
- (d) Free turbine - Load compressor/gearbox

The system selected for the Exploratory Development Program was the single-shaft integral bleed APU, which offered the maximum potential for technological advancement while fulfilling the requirements set forth in the Statement of Work including maximum flexibility (Figure 1). The APU design characteristics at the maximum bleed conditions are shown in Figure 2 and the performance parameters at the maximum shaft power condition in Figure 3.

The component technology goals and demonstrated test results are demonstrated in Section II, with technology advancements that are compared to the 1968 state of the art. The results of the final Build 5 demonstrator unit performance testing are discussed in Section IV.

- **APU - SINGLE SHAFT, INTEGRAL BLEED**

COMPRESSOR - AXIAL PLUS RADIAL

- SPLIT FLOW IMPELLER

- VAR INLET GUIDE VANES

COMBUSTOR - ANNULAR

TURBINE - RADIAL PLUS AXIAL

- COOLED FIRST STAGE

START SYSTEM - HYDRAULIC ACCUMULATOR

• GEARBOX - MODULAR CONSTRUCTION

TORQUE CONV - LOCKUP FEATURE

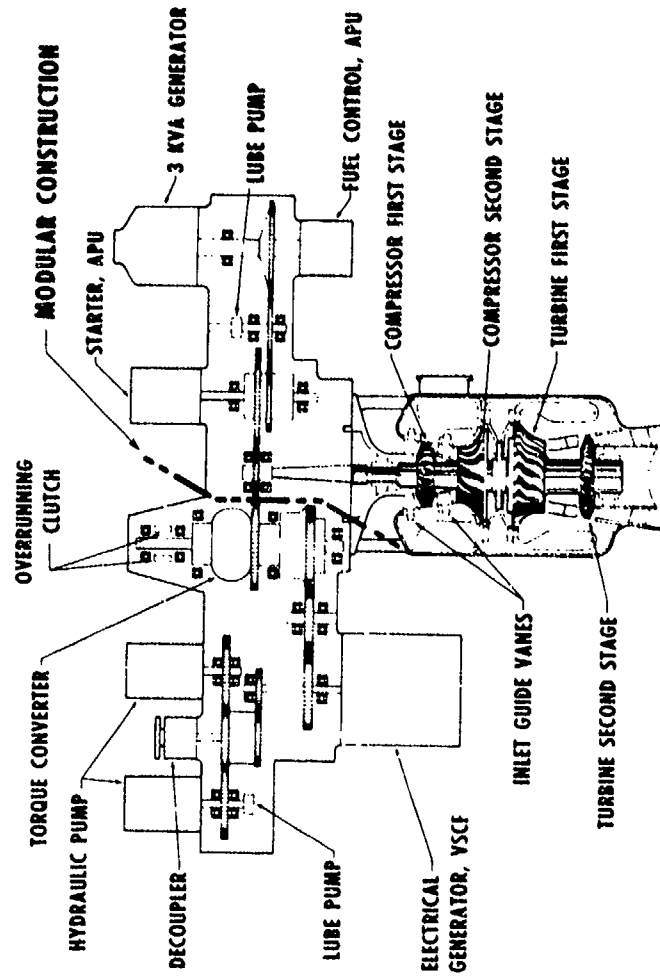


Figure 1. Selected Auxiliary Power System.



NOTES:

1. AMBIENT CONDITIONS: 130°F, 14.7 PSIA
2. MISCELLANEOUS DATA:
 - ACCESSORY HORSEPOWER - 13.6
 - SHAFT HORSEPOWER - 74.8
 - BLEED HORSEPOWER - 212.8
 - COOLING FLOW - 6%
 - IGV SETTING, C_1 - 100%
 - IGV SETTING, C_{2-3} - 100%

3. NOMENCLATURE:

- P - TOTAL PRESSURE, PSIA
- P/P - PRESSURE RATIO
- W_C - CORRECTED FLOW, LB/SEC
- W_B - BLEED AIRFLOW RATE, LB/MIN
- W_A - ACTUAL THROUGHFLOW, LB/SEC
- T - TOTAL TEMPERATURE, °F
- η - EFFICIENCY
- δ - RATIO OF STATION TO AMBIENT PRESSURE

$W_A = 3.40$ $W_C = 2.244$ $W_B = 69.29$ $W_C = 0.292$ $P/P = 4.167$
 $W_C = 3.663$ $\delta = 1.792$ $\delta = 11.448$ $W_C = 0.447$ $\eta = 0.88$ $W_C = 1.736$
 $\delta = 0.99$ $\delta = 6.163$ $\delta = 10.873$ $\delta = 2.47$

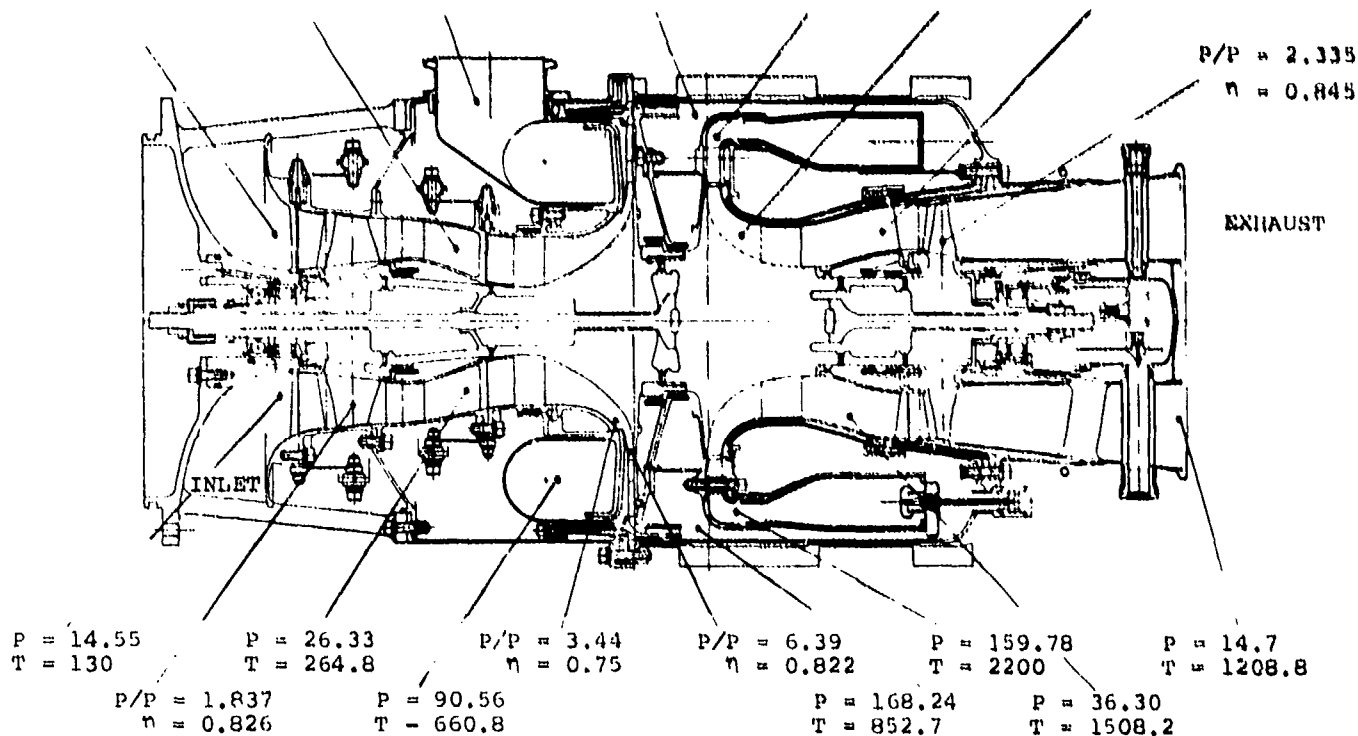


Figure 2. Estimated Performance GTCP305 Advanced Technology
APU Maximum Bleed Condition.



NOTES:

1. AMBIENT CONDITIONS: 130°F, 14.7 PSIA
2. MISCELLANEOUS DATA:
 ACCESSORY HORSEPOWER = 13.6
 SHAFT HORSEPOWER = 163.0
 BLEED HORSEPOWER = 124.0
 COOLING FLOW = 6%
 IQV SETTING, C_1 = 95%
 IQV SETTING, C_{2-1} = 107.5%

3. NOMENCLATURE:

- P = TOTAL PRESSURE, PSIA
 P/P = PRESSURE RATIO
 W_C = CORRECTED FLOW, LB/SEC
 W_B = BLEED AIRFLOW RATE, LB/MIN
 W_A = ACTUAL THROUGHFLOW, LB/SEC
 η = EFFICIENCY
 δ = RATIO OF STATION TO AMBIENT PRESSURE

$W_A = 2.908$ $W_C = 2.03$ $W_C = 0.292$ $P/P = 4.180$
 $W_C = 3.1227$ $\delta = 1.667$ $W_B = 39$ $\delta = 11.51$ $W_C = 0.447$ $\eta = 879$ $W_C = 1.71$
 $\delta = 0.993$ $\delta = 6.25$ $\delta = 10.927$ $\delta = 2.47$

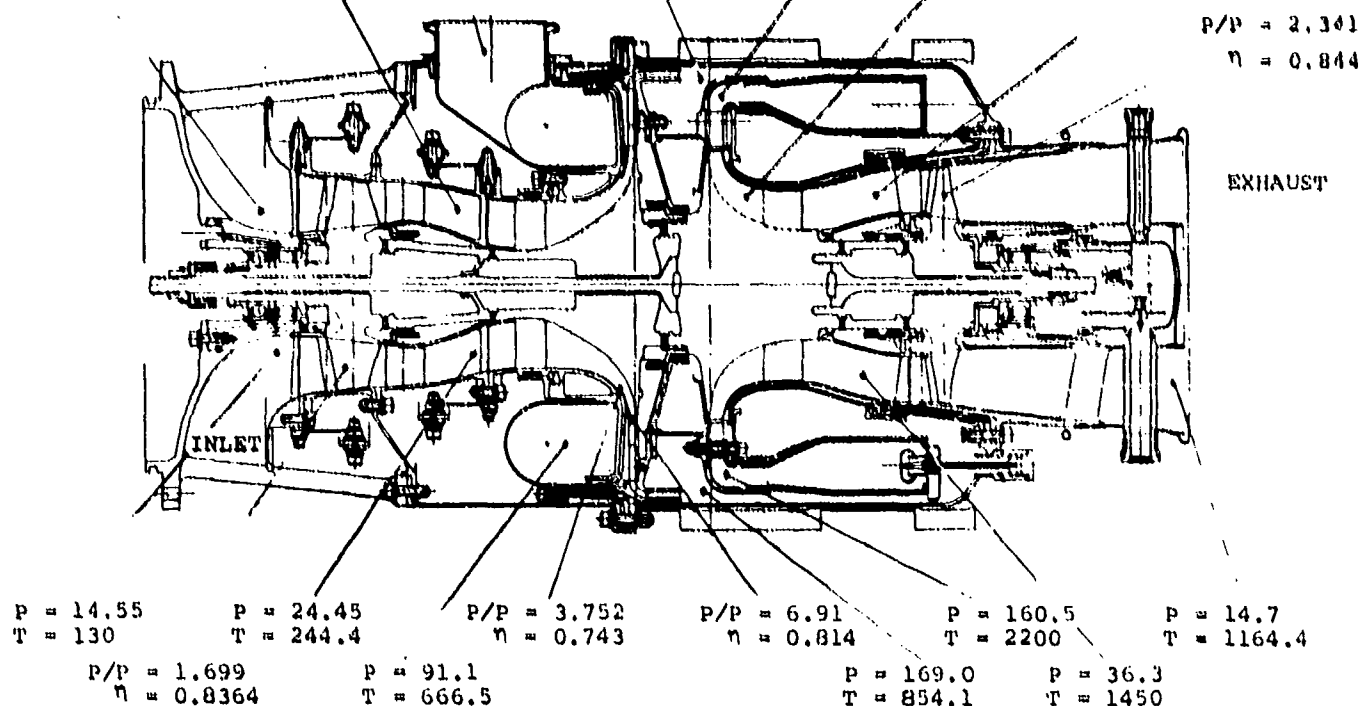


Figure 3. Estimated Performance GTCP305 Advanced Technology APU Maximum Shaft Power Condition.

The developed technology is directly relevant to a wide variety of applications. Major technology advancements have been made in the following components:

- (a) Axial compressor
- (b) Centrifugal compressor
- (c) 2200°F uncooled combustor
- (d) Radial turbine
- (e) 20,000 rpm torque converter

The existing APU has the capability, with additional development, of being configured to provide all shaft power as well as conversion to a free-turbine version. The centrifugal compressor and radial turbine can be used either separately or together and are readily scaled to provide a basis for various possible high-performance applications.

SECTION II

PROGRAM GOALS

The overall goal of this program was to advance the state of the art of small auxiliary power systems (APS). The program was centered about the design and technological development of a typical auxiliary power system for an advanced fighter aircraft, based on the recommendations of AFAPL-TR-67-135. The final system was to be a technological development vehicle capable of demonstrating the component and APU performance requirements with technology adaptable to a wide variety of future aircraft applications.

1. SYSTEM REQUIREMENTS

The reference auxiliary power system upon which this advanced technology program was based consisted of a gas turbine power unit and integral accessory gearbox. The aircraft electrical generators and hydraulic pumps, which are normally mounted on one of the main aircraft engines, were mounted on this gearbox. The auxiliary power system was designed to be mounted separately from the main engine in the aircraft but was to be capable of being engine-driven by a power take-off shaft. On the ground, the auxiliary power unit would supply shaft power to the gearbox for checkout of aircraft systems, for aircraft standby power requirements, and for starting the main engine. Bleed-air would be supplied by the APU during ground operation for an air-cycle aircraft air conditioning system. The APU was also required to provide emergency in-flight start power.

The power requirements for the preliminary design phase of this effort are shown on Table I for each of the operating modes. The system-sizing condition occurs at ground check, when there is an electrical load of 22 kva plus simultaneous bleed-flow of 55 lb/min at 130°F, sea-level ambient conditions. Sizing at this time provides

TABLE I

APS PERFORMANCE REQUIREMENTS

Operating Mode	T _{amb} , °r	WB (P/P=6), lb/min	Elect. Load, kva	Hydraulic Load, gpm/psi	eshp	Time/ Mission
Checkout, sea level*	130	55	22	0	199	15 min
Checkout, sea level**	↓	0	0	15/3000	35	15 min
Standby, sea level**	↓	55	3	0	168	0.5-4 hr
Engine Start, sea level**	59	0	↓	↓	>208	20 sec
Engine Start, 20,000 ft at Mach 0.5, inlet recovery = 0.75	-12.3	0			61.5	Negligible
Normal inflight [†]						
Maximum power	N/A	-	76	54/3000	246	5 sec
Normal power	N/A	-	38	27/3000	123	Continuous
Emergency inflight, 40,000 ft	-69.7	-	-	-	56	10 min

*Design-point. Ground operation required from -65° to 130°F.

**Ground operation required from -65° to 130°F.

[†]One gearbox

compatibility with the engine start requirements (20 sec at 59°F, sea-level temperature and at altitude), as well as with emergency auxiliary power requirements. The equivalent shaft horsepower shown on Table I are for the cycle assumptions and are shown for the listed requirements only. The additional power required for the surge bleed during shaft-power-only modes or excess bleed pressure is not included.

The design ambient conditions were 130°F at sea level. The original design objectives for the APU and gearbox components are:

- (a) APU cycle pressure ratio, 11:1
- (b) APU bleed-air pressure ratio, 6:1
- (c) APU bleed-flow, 55 lb/min
- (d) Turbine inlet temperature, 2200°F
- (e) Fuel flow, 100 lb/hr
- (f) Torque converter weight, 5 lb
- (g) APU basic size, 10-in. diam x 24-in. length
- (h) Total system weight including APU, gearbox, and APU start-system, 180 lb

Prior to the final hardware design, the goals of the program were revised from those given on Table I to include a maximum system weight of 200 lb and a minimum power rating of 300 eshp at 130°F ambient temperature. This represents the growth potential of the unit within the original APU envelope limitations of a 10-in. diam by 24-in. length.

Establishment of the system duty cycle is critical to component design, since it determines the operating time at maximum load and temperature. The duty cycle (Table II) was based on the mission, the

TABLE II
REFERENCE DUTY CYCLE FOR ADVANCED AUXILIARY POWER SYSTEM

Operating Mode	T _{amp} , °F	W _B (P/P=6), lb/min	Electrical Load, kva	Hydraulic Load, gpm/psi	eshp	Required TIT, °F	Time/Mission	APU Operating Time, hr
Checkout, S.L.	130 120 110	55	22	0	188	1950 1925 1900	15 min	36 72 119
S.L.	130	0	0	15/3000	35	1835		226
Standby, S.L. S.L.	130 120 110	55	3	0	155	1855 1790 1725	0.5-4 hr	210 422 1407
Engine Start S.L.	59	0			208	2140	20 sec	2
Engine Start 20,000, M ₀ = 0.5 5.75q recovery	-12.3	0			61.5	--	Negligible	>0.5
Emergency in-flight	-69.7	-	-	-	66	2050	10 min	3
							TOTAL	2500

*Based on average time duration. TBO assumed 2500 hr.

operating time in each of the operating modes, and the assumed 2500-hr TBO, with assumptions regarding the number of APU and main-engine starts per mission. Table I indicates the duration of each of the various operating sequences with which the auxiliary power system is associated. On this basis, a total of 910 aircraft missions was assumed, based on an average standby time of 2.25 hr/mission, and the total number of APU starts was assumed to be 1500. From these data, the turbine inlet temperature as a function of time was established (Table II) and the maximum life fraction computed (Section III).

The assumed engine-starting drag torques of 59° and -65°F are given in Figure 4. Included is an approximate starter torque curve required to obtain an engine start within 20 sec at 59°F.

The program objective was to provide technological advancement applicable to an on-board auxiliary power system for equipment check-out, environmental control, and engine starting for fighter, attack, and light cargo aircraft. The demonstrator power system was not directed toward any specific aircraft but rather was designed to provide technology applicable to an advanced high-performance power unit with maximum attention to technological flexibility in related and similar systems. Component performance parameters, existing at the start of the program (1968), are compared with the goals of the program and the results of the testing (Table III). The corrected flows are included for comparison between APU-size and test-rig size components. The APU design goal of a 10-in. diam was maintained, but the addition of the case flanges increased the envelope to 11.5 in.

NOTES:

1. Polar moment of inertia at starter drive including accessories, but excluding starter = 11.02 slug-ft²
2. Light-off will occur 8 sec after reaching 488 rpm starter drive-speed
3. Starter torque must be maintained for 15 sec minimum

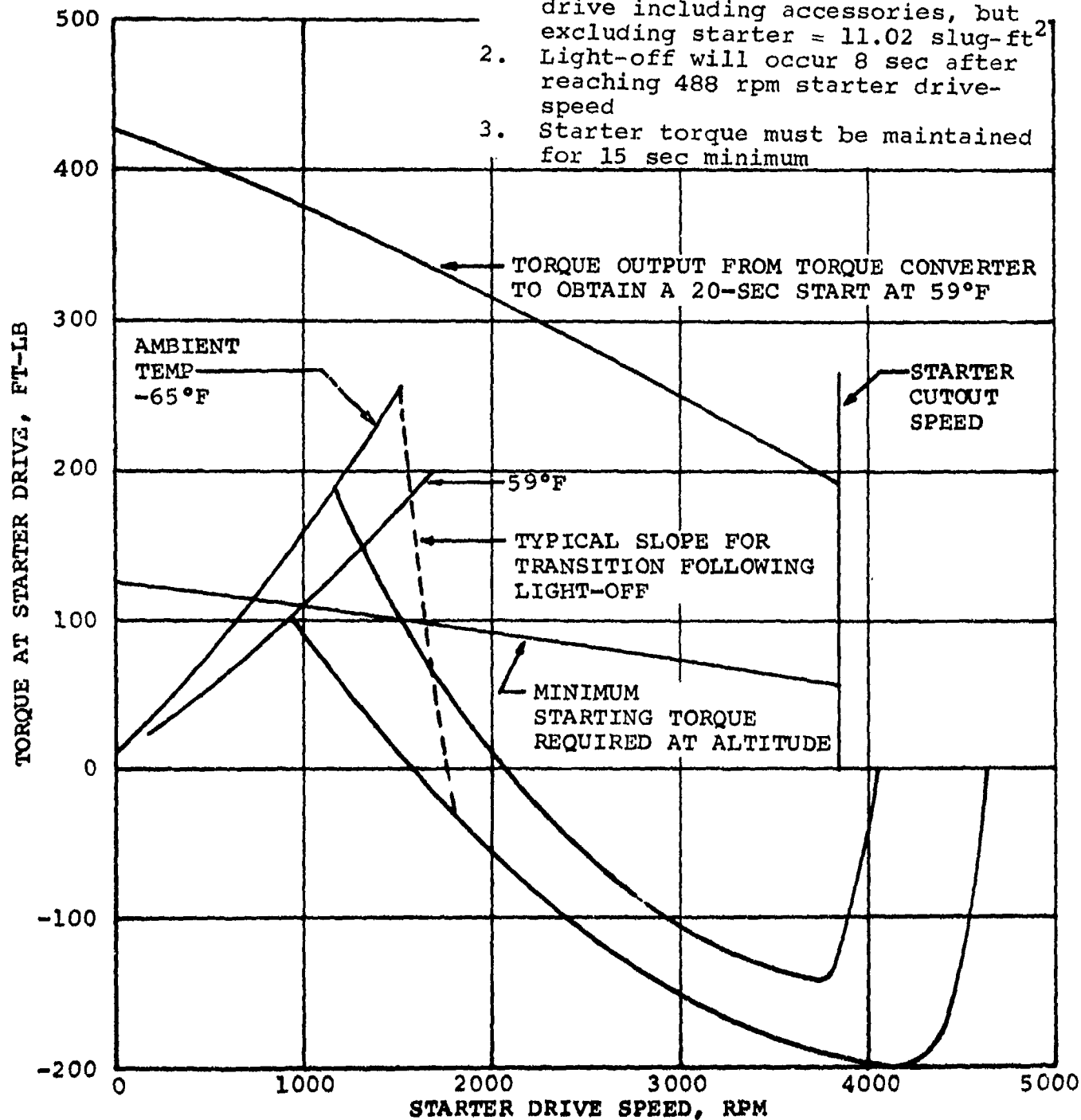


Figure 4. Main Engine Starting Characteristics.

TABLE III

APS COMPONENT PERFORMANCE COMPARISON

Item	Parameter	1968 Technology (a)	Program Goal	Maximum Test Results (b)	Test Data Source
Axial Compressor Dash 1	Corr Flow (c)	-	3.66	22.5	Extrapolated from reference rotor test rig
	P/P	1.4	1.837	1.8	
	Eff	0.826	0.826	0.72	
Dash 3		-	3.66	22.5	Reference stage test rig
		1.4	1.837	1.85	
		0.826	0.826	0.84	
Centrifugal Compressor Bleed Low-Pressure Side		-	0.762	4.7	Reference stage test split flow rig
		-	4.33	2.85	
		-	0.75	0.58	
Centrifugal Compressor Power High-Pressure Side		7.0	1.482	3.45	Reference stage test rig
		5.3	6.39	6.39	
		0.79	0.822	0.78	
Radial Turbine (Total-to-Total)		1.35	0.447	0.539	APU-size cold air test rig
		3.1	4.167	4.167	
		0.893	0.897	0.887	
		1650	2200	N/A	
		1800	2180	N/A	
		30.8	37.6	37.6	
Combined Turbines (Total-to-Static)		N/A	0.447	0.53	APU-size cold air test rig
		↓	10.9	10.9	
			0.86	0.867	

(a) Where applicable, technological levels at the beginning of the program for similar components are listed.

(b) Further rig and APU test data may be found in the succeeding sections.

(c) $\dot{m} = \text{lb/sec}$, $\phi = T_{in}/518.7$, $T_{in} = ^\circ R$, $\delta = P_{in}/14.696$, and $P_{in} = \text{psia}$.

TABLE III (Contd)

Item	Parameter	1968 Technology	Program Goal	Maximum Test Results	Test Data Source
Cycle Pressure Ratio	N/A	N/A	11.0	8.79	Scan 144, 77,067 rpm
Bleed Pressure Ratio		↓	6.0	4.349	Scan 144, 77,067 rpm
Bleed Flow Rate, lb/min			69.0	64.0	Scan 109, 73,700 rpm
APU Speed (Physical), rpm			81,822	81,100	Scan 138
Torque Converter Power Input, hp		280	280	324	APU-size test rig
Torque Converter Stall Torque Ratio		N/A	2.24	2.0	
Torque Converter Efficiency		-	0.80	0.77	
Speed, rpm		8000	20,000	20,000	
Torus Diameter, in.		11.5	3.74	3.74	
Combustor Temperature Spread Factor (d)		0.18	0.12	0.112	
(e)		0.18	0.12	0.16	
Combustor Heat Release Rate (f)		3.5×10^6	5.0×10^6	5.2×10^6	
(d) Test rig data at 1200°F ΔT, final (atomizer) configuration					
(e) Test rig data at 1330°F ΔT (design ΔT), pneumatic impact injector configuration					
(f) Units are Btu/hr-ft ³ atm. Comparison is for similar reverse-flow annular combustors.					

2. SYSTEM OPTIMIZATION

Thirty-seven candidate systems were considered for this application, but most of these were eliminated early in the evaluation because of complexity, size, and weight. The potential candidates were reduced to four that appeared to have merit (Figures 5 through 8). A preliminary design analysis was then conducted to select the APS configuration most capable of satisfying the requirements set forth in the Statement of Work.

Variable inlet guide vanes (VIGVs) for all the candidate systems were required to not only obtain a better match of the compressors under various operating conditions (to keep the size of the APU to a minimum) but also to minimize the fuel consumption at the standby operating condition. In all APU configurations, VIGVs for both the first-stage (axial) and the second-stage (radial) compressors were included (Table IV) to aid in the evaluation of the prototype unit.

For the integral bleed systems (I and III), VIGVs for the first-stage compressor are required for efficient engine operation over the bleed-flow range. For the bleed-air to be extracted at a 6:1 pressure ratio from a higher cycle pressure ratio APU, the second-stage (radial) impeller was notched to enable the bleed-flow to be split off at a lower pressure ratio (Figure 9). The flow range requirement varies from no-flow to 55 lb/min, but due to the interstage bleed-flow extraction configuration, some bleed-air must always be extracted to prevent surge in the radial impeller. The justification for including VIGVs at the APU compressor stages for Systems II and IV would be to increase the operating efficiency under certain conditions. VIGVs would be required for the load compressors to modulate the flow and to minimize the load when no bleed-air was required.

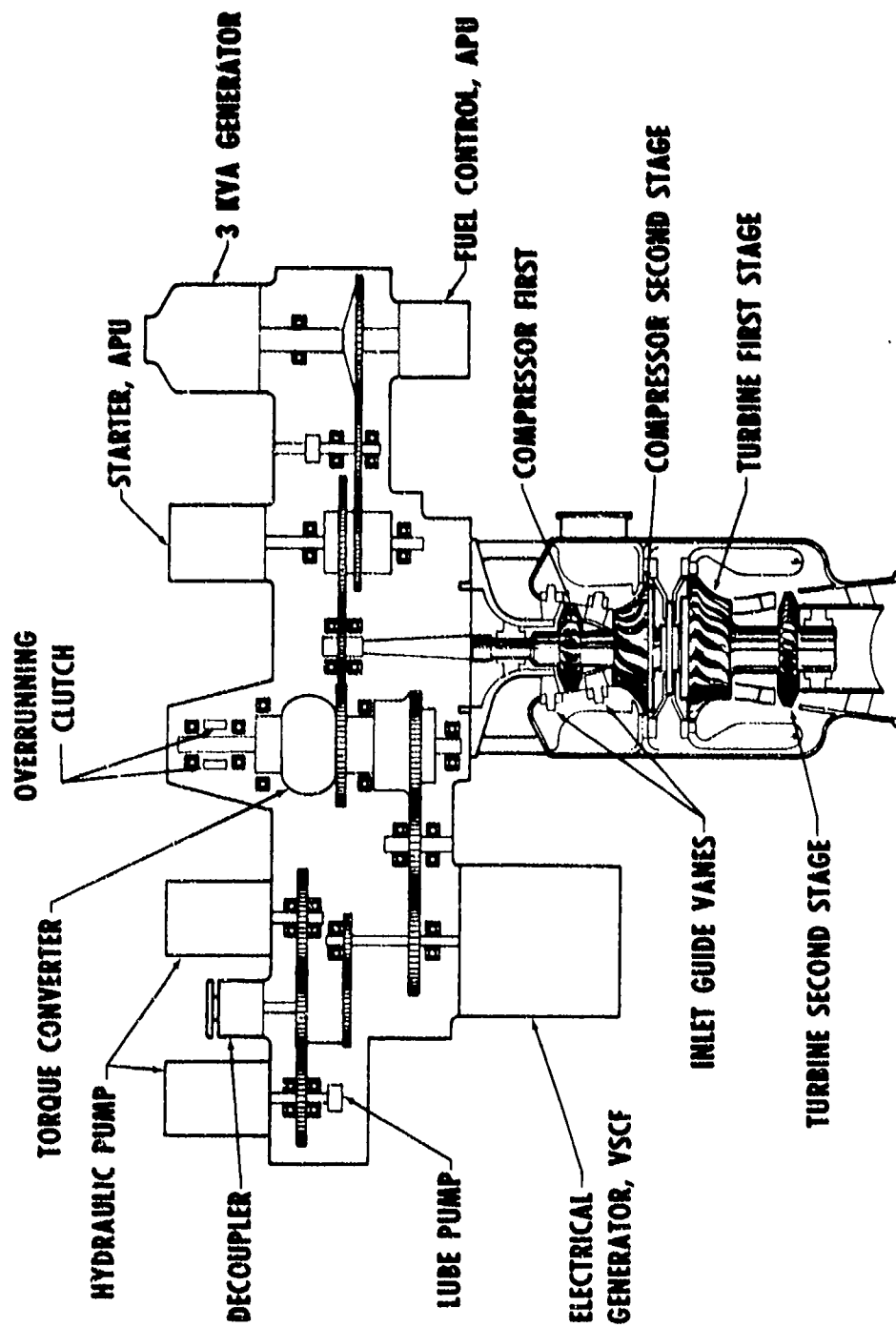


Figure 5. System I - Single-Shaft Integral Bleed APS.

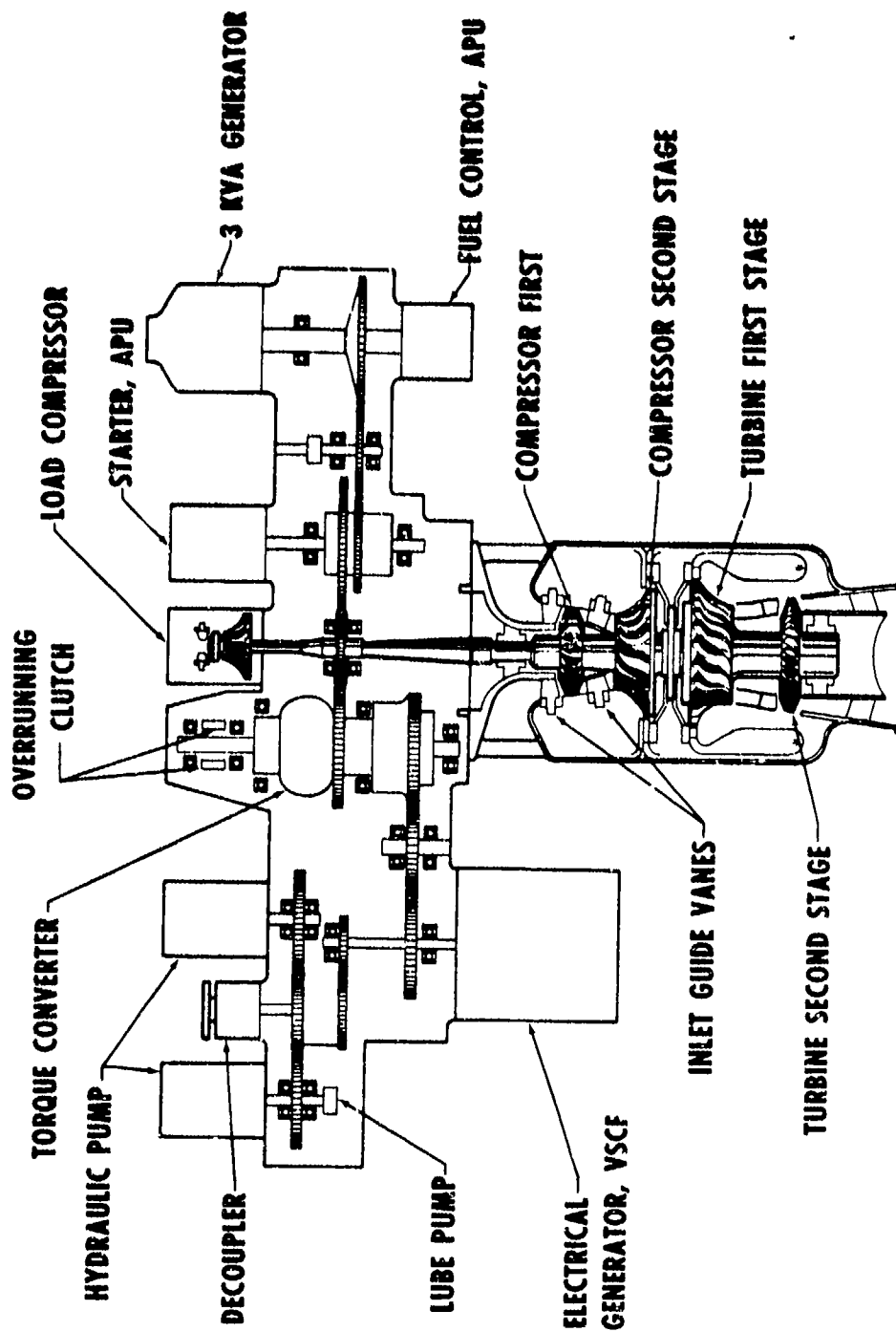


Figure 6. System II - Single-Shaft Load Compressor APS.

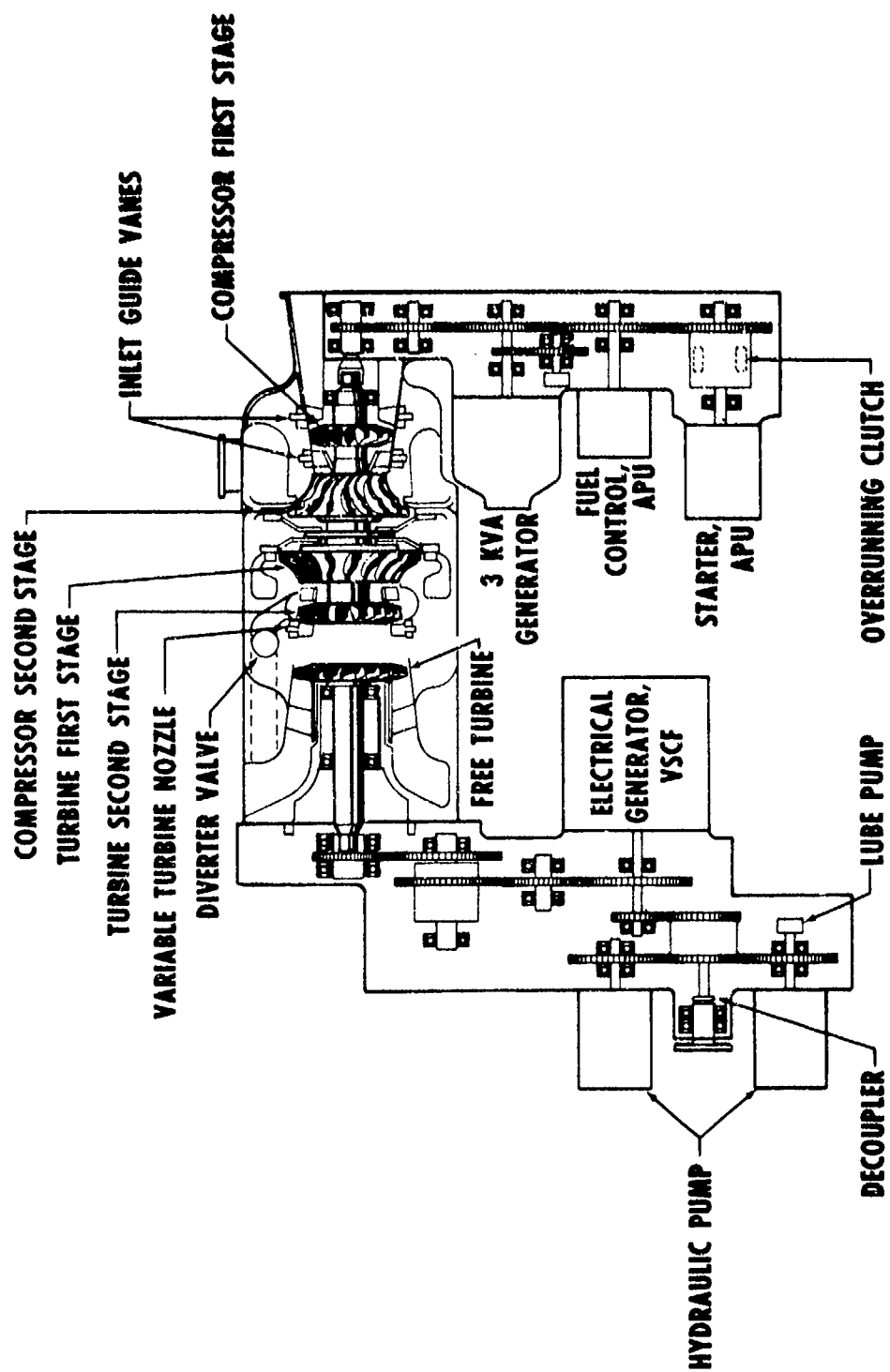


Figure 7. System III - Free Turbine Integral Bleed APS.

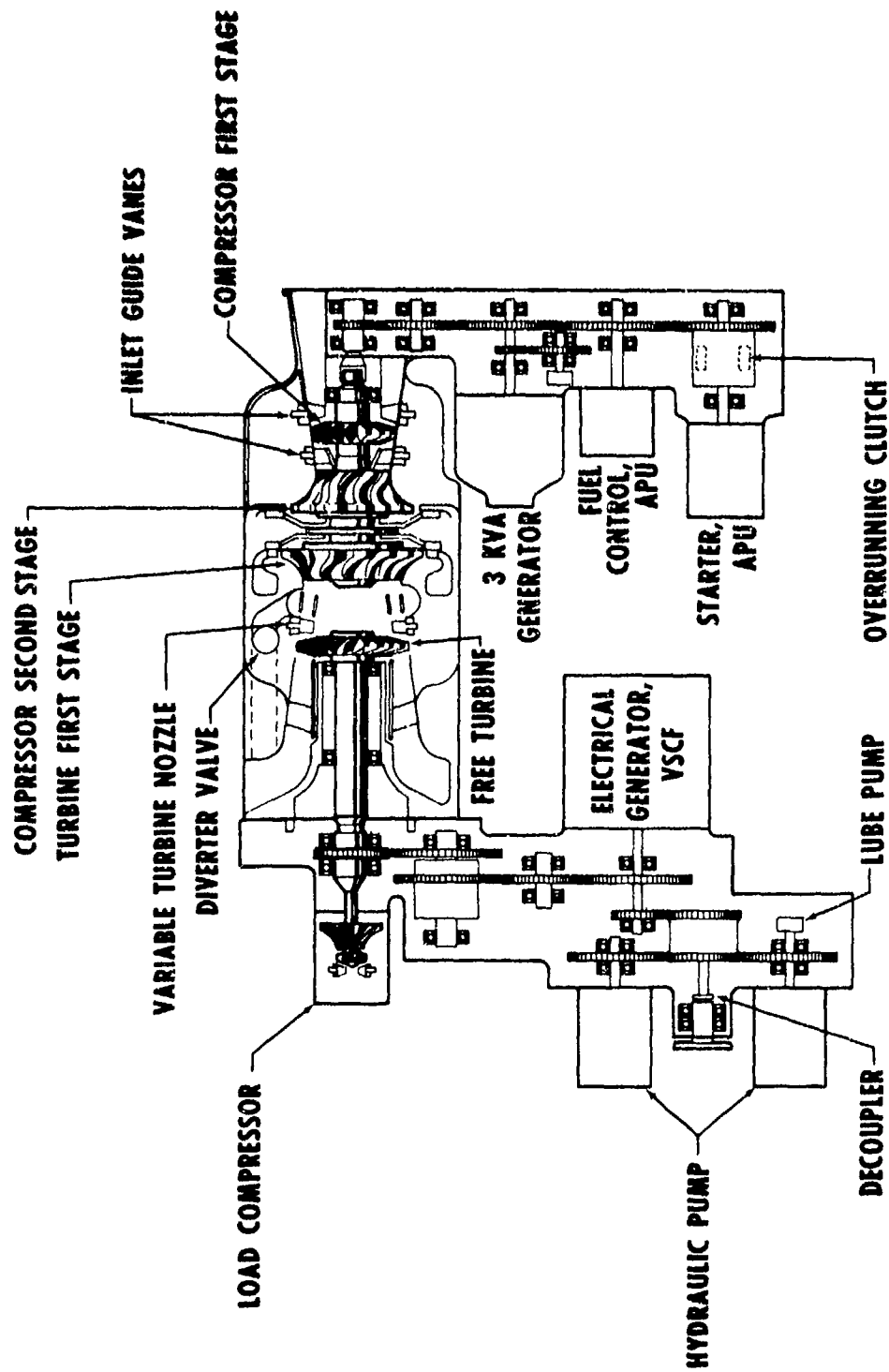


Figure 8. System IV - Free Turbine Load Compressor APS.

TABLE IV
APU VARIABLE GEOMETRY REQUIREMENTS

System	Compressors		Turbine		Diverter Valve	Load Compressor
	1	2	1	2		
I Single-shaft, integral-bleed	IGV	IGV	None	None	N/A	N/A
II Single-shaft, load-compressor	→	→	→	None	N/A	IGV
III Free-turbine integral-bleed	→	→	→	Nozzles	Yes	N/A
IV Free-turbine, load-compressor	→	→	→	None	Yes	IGV

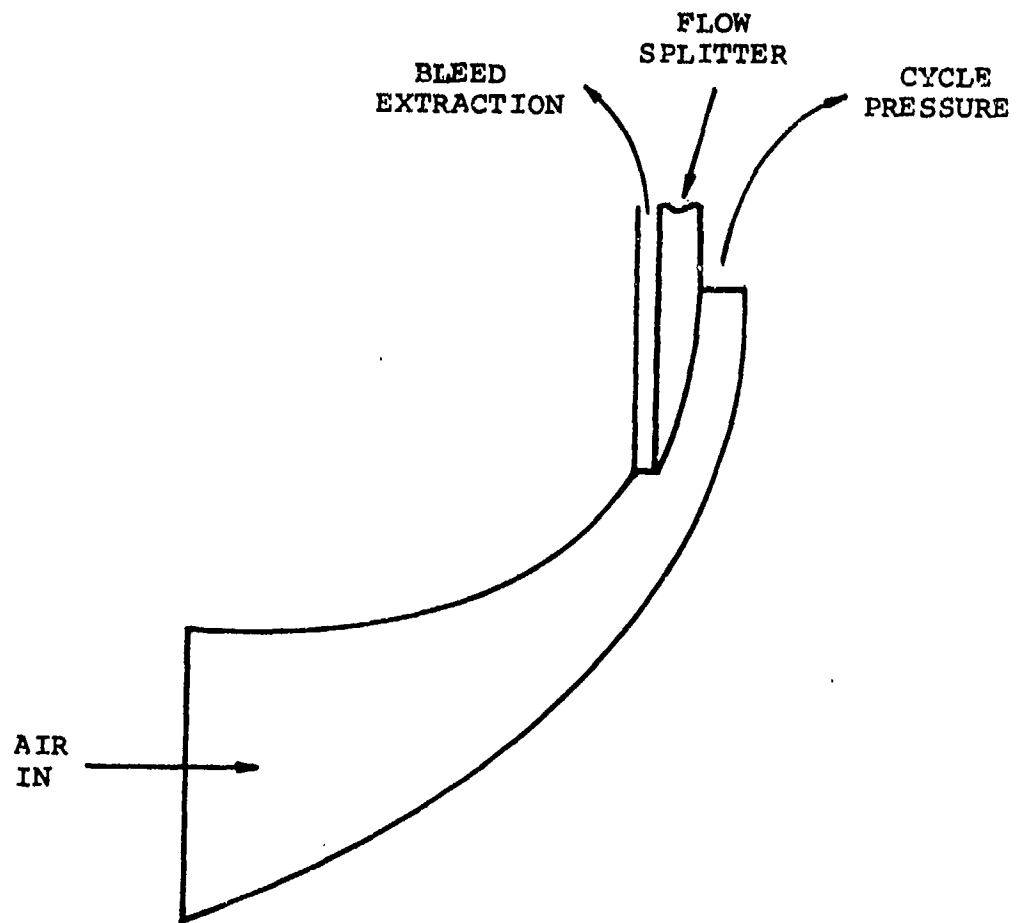


Figure 9. Radial Impeller Bleed Extraction System

For a free-turbine engine that is required to produce shaft power only from the free-turbine (System IV), modulating the fuel flow (resulting in the modulation of the gas generator speed and burner temperature) results in an efficient method of supplying varying amounts of power to the free-turbine. For a main engine start, 3 kva of power at constant frequency must be furnished by the gas generator. A constant-speed drive or a variable-speed, constant-frequency system is required if the gas generator speed is allowed to vary according to the required shaft power load from the free-turbine. The alternate solution to this problem would be to maintain a constant gas generator speed and modulate compressor VIGVs and a diverter valve. (This valve would divert the gas generator exhaust from the free-turbine to the atmosphere at low shaft power loads.) A detailed analysis would be required to choose between the variable and constant gas generator speed configurations, but for purposes of comparing the four candidate systems, the constant-speed gas generator configuration was chosen.

For conventional engines that furnish bleed-air at the engine cycle pressure, the excess bleed-air could be diverted into the turbine to convert it into shaft power. However, for the APU of this program, the bleed-air is at a pressure considerably lower than the engine-cycle pressure and, therefore, cannot be profitably used in the turbine to generate power. Hence, no variable turbine nozzles are recommended in the first stage of any of these engines. Variable turbine nozzles are required for the free-turbine of the integral-bleed free-turbine engine (System III) because of the power shift from the gas generator turbine (during bleed-power modes) to the free-turbine (during shaft power modes). To enable the APU to operate as efficiently as possible and maintain a constant gas generator speed (maintain a constant 3-kva generator speed and bleed pressure), a modulating gas diverter valve would be required in addition to the compressor and turbine VIGVs.

The APS performance requirements used in the performance analyses have been given on Table I. All four APU configurations were analyzed to determine size, fuel flow, and operating characteristics at design-point, which was the electrical checkout mode on a 130°F day, provided the required shaft power would also be available for an engine start. The load-compressor APUs (Systems II and IV) would not have any difficulty in meeting this requirement, since the maximum power needed at checkout is greater than at engine starting. However, for the integral-bleed units, the available shaft power for engine starting was marginal, and the APUs were analyzed for both checkout and starting modes.

To form a basis for the performance studies, the design-point cycle parameters were estimated (Table V). The compressor and turbine efficiencies, combustor efficiency, pressure losses, leakage, cooling, and accessory and drag horsepowers were estimated from previous experience and the literature.

Based upon these design-point cycle parameters, the four systems were evaluated. The APU size, system weight, and fuel flow at the design-point were determined. Each system was diagramed, and the relative control simplicity, cost, and maintainability were estimated. A comparison of the final evaluation is shown on Table VI. For these comparisons, each system was designed to function in all required operating modes. An analysis of all parasitic and drag-power losses was conducted for each of the candidate systems, in order to perform realistic system comparisons. The data (Table VI) show that System I is the optimum selection.

Although System I was selected as the reference design for the program, the component technology development is directly applicable to any of the other three systems. The notched radial impeller of the selected system can easily be recontoured to become a conventional radial impeller for a pure shaft power APU or an APU with bleed-air

TABLE V
CYCLE ASSUMPTIONS FOR DESIGN-POINT PERFORMANCE CALCULATIONS

Parameter	I	II	III	IV
	Single-Shaft		Free-Turbine	
	Integral-Bleed	Load-Compressor	Integral-Bleed	Load-Compressor
I. Pressure Drop, $\Delta P/P$				
Inlet	0.01	0.01	0.01	0.01
Between C_1 and C_2	0.015	0.015	0.015	0.015
Compressor	0.01	0.01	0.01	0.01
Burner	0.04	0.04	0.04	0.04
Turbine Diffuser	0.01	0.01	0.04	0.04
II. Cooling Flow, W_c/W_a	0.06	0.06	0.06	0.06
III. Burner Efficiency	0.98	0.98	0.98	0.98
IV. Leakage, W_1/W_a , C_2 Discharge	0.01	0.01	0.01	0.01
V. Burner Exit Temperature, $^{\circ}F$	2200	2200	2200	2200
VI. Cycle Pressure Ratio, Burner Inlet to Ambient	11:1	11:1	11:1	11:1
VII. Bleed-Air Valve $\Delta P/P$	0.03	0.03	0.03	0.03
VIII. Compressor P.R./ η				
First Stage	1.833/0.826	1.833/0.817	1.833/0.826	1.833/0.817
Second Stage ³	3.460/0.810	6.217/0.781	3.460/0.810	6.217/0.781
Third Stage ³	1.778/0.827	-	1.778/0.827	-
IX. Turbine η				
First Stage	-	-	0.87	0.87
Second Stage (Power Turbine)	-	-	0.84	0.84
Overall	0.87	0.87	-	-
X. Accessory and Drag Power Losses				
Gas Generator	-	-	4.9	4.9
Power Turbine	13.6	22.8	9.7	18.8
XI. Load Compressor Pressure Ratio η				
Pressure Ratio		6.32/0.7785		6.32/0.7785
Horsepower Required for 55 lb/min		163		163
XII. Ambient Conditions				
Pressure, Sea Level Static, psia	14.696	14.696	14.696	14.696
Temperature, $^{\circ}F$	130	130	130	130
NOTES:				
1. 130 $^{\circ}F$, sea level, standard day				
2. Actual flow paths and design speed to be based on 89,000 rpm				
3. Second-stage compressor is assumed to be the bleed portion of the notched impeller, and the third-stage is the power portion.				

A34722

TABLE VI
SYSTEM EVALUATION COMPARISON

Configuration	APU Size, in.			System Weight, lb	Fuel Flow (Checkout), lb/hr	Relative Control Simplicity	Relative Ccost	Relative Maintainability
	L	W	H					
Design Goals	24	10	10	180*	100	--	--	--
System I Single-Shaft Integral Bleed	18	10	10	179	120	1.0	1.0	1.0
System II Single-Shaft Load Compressor	18	10	10	193	131	0.98	1.18	0.98
System III Free-Turbine Integral Bleed	38	21	13	205	141	0.93	1.24	0.90
System IV Free-Turbine Load Compressor	42	21	13	220	136	0.90	1.32	0.88
*System weight goal was changed from 180 to 200 lb at the conclusion of the preliminary design phase.								

extraction at the cycle pressure. The axial turbine may become the power turbine in a free-turbine version of the APU. The torque converter is acceptable to a variety of applications.

An off-design performance analysis of the four auxiliary power systems was conducted to further verify the selection of System I. Optimum variable geometry settings were obtained from parametric studies. The fuel consumption for the design-point is included on Table VII and is compared to standby fuel flows on 130° and 59°F days. For the 59°F day, standby fuel flows are included for 80-percent of the 55 lb/min requirement (44 lb/min) for comparison, since this is more nearly the actual requirement. Fuel flows at the standby condition are more significant because of the length of time in that operating mode. The fuel flows at all other conditions are then relatively insignificant, especially the engine-starting conditions.

Performance estimates for engine-starting (sea level and 20,000 ft) and emergency power (40,000 ft) were made for each of the four candidate systems (Table VIII). System III is the only configuration that did not meet the required power in all modes, indicating that if System III were chosen as the optimum, the engine starting requirement would size the engine. All shaft powers are the result of parametric studies that determined the optimum variable geometry settings. The integral bleed systems (I and III) require a minimum of expended bleed-air to avoid surge in both the axial and radial compressor stages.

The required power for System III (Table VIII) is based on the actual peak shaft power required to start the engine within the 20-sec time limit. For System I, the required power includes the torque transmission and efficiency characteristics of the torque converter. System II required-power includes those losses and characteristics associated with the torque converter, as well as the power drag of the load compressor. For System IV, the load compressor drag is added to the required shaft power of System III.

TABLE VII
FUEL FLOWS FOR BLEED-AIR MODES, LB/HR

System	130° Day		59° Day	
	Checkout, 55 lb/min 6:1 P.R. 36 shp	Standby, 55 lb/min 6:1 P.R. 5 shp	Standby, 55 lb/min 7.2:1 P.R. 5 shp	Standby, 44 lb/min 6:1 P.R. 5 shp
I Single-shaft integral-bleed	120	107	112	106
II Single-shaft load-compressor	131	114	113	107
III Free-turbine integral-bleed	141	120	130	124
IV Free-turbine load-compressor				
Constant gg speed	131	114	113	107
Variable gg speed	128	114	108	106

TABLE VIII
APU SHAFT HORSEPOWER REQUIREMENTS AND PERFORMANCE

System	59°F Day Engine Start (20-sec minimum)		20,000 ft Engine Start		40,000 ft Emergency Power	
	Required	Available	Required	Available	Required	Available
I Single-Shaft Integral-Bleed	208	208	61.5	90.6	82.5	86.3
II Single-Shaft Load-Compressor	224	250	69.5	111.8	82.5	103.4
III Free-Turbine Integral-Bleed	146	140	43.0	61.2	66.0	73.0
IV Free-Turbine Load-Compressor	162	200	51.0	97.0	66.0	103.1

3. SYSTEM DEMONSTRATION UNIT

The selected system comprised an integral bleed APU with an accessory gearbox (System I, Figure 5). The APU was mounted on, and drives directly into, the gearbox, which provides the mounting and power transmission to a 40-kva aircraft system generator, a 3-kva standby generator, and two hydraulic pumps. The pumps and large generator could be driven by the APU or the main engine. The APU represented a unit designed for 2500 hr between overhauls. During this overhaul life, the APU would be started 1500 times, and the APU would activate the main engine 910 times.

A program goal was to demonstrate the production of power in all the modes listed on Table I. The electrical checkout and standby modes are combinations of bleed-air and shaft power and were to be demonstrated by absorption of electrical energy into a load bank and then dumping the bleed air. In the hydraulic checkout mode, shaft power absorption would be demonstrated by dissipating the pressurized hydraulic fluid into a sump. The engine starting mode was to be demonstrated by accelerating a flywheel sized to approximate the combination of engine inertia and drag torque through the starter cutout speed. However, due to a reduction in the power goal during the course of the program, the engine starting demonstration was deleted.

The torque converter operation was to be developed and proven on test rig prior to installation in the demonstration system. As an additional contract item, a clutch and lockup device was to be developed for the torque converter. This device was to increase the ratio of output shaft speed to input shaft speed from 0.9 to 1.0 and then positively lock the shafts together. The entire sequence was to take place while maximum shaft power was being transmitted.

The technology development vehicle was configured as a compact, lightweight, single-shaft integral-bleed auxiliary power system. It comprises VIGVs for both compressor stages, a reverse-flow annular combustor, and a two-stage turbine section. Bleed-air is extracted from a notch on the radial impeller wheel. The fuel pump, starter, 3-kva generator, PMG (permanent magnet generator) for ignition and control power generation, and a lube pump are mounted on the APU section of the gearbox.

The gearbox design consists essentially of two separate gear trains coupled by a torque converter. The first is coupled to the APU shaft and contains the APU starter motor shaft, accessories, and torque converter drive. The other gear train is coupled to the main engine input and drives the hydraulic pumps, a lube pump, and the VSCF generator. The main engine drive is coupled to the torque converter output through an overrunning clutch mechanism, thus starting the main engine with APU shaft power but not allowing the main engine to drive the APU. When the engine speed exceeds the torque converter output speed, the clutch will overrun. At this point, the APU may continue to operate or may be shut down, since it no longer furnishes power to the engine or accessories. With the main engine decoupled, the APU will be capable of driving the main engine accessories at a speed corresponding to engine-idle.

4. SYSTEM AND COMPONENT PERFORMANCE

The justification for selecting System I (Figure 5), the integral-bleed single-shaft APU system, was presented in the previous section. The selected system was designed as a demonstrator unit, with emphasis on component development, performance, technological flexibility, and the interchangeability of the gearbox sections rather than on a flight-weight system.

The fuel component and system design-point parameters are given on Table IX. The estimated performance of the APU is depicted in Figures 10 and 11 as a function of bleed-flow rate. Parametric studies showed that very little, if any, advantage could be realized from the the VIGVs for the centrifugal compressor; hence, all data are shown for the centrifugal compressor VIGVs set at 0 deg. Some efficiency gain is theoretically possible at low bleed-flow rates, but this would be mostly negated by the efficiency loss associated with leakage around the ends of the variable guide vanes.

Design-point parametric studies were completed early in the study phase to enable the designers to conduct simple trade-off analyses. Several cycle variables were investigated to determine their influence on specific fuel consumption and specific power: cooling and leakage rates; inlet, combustor, and turbine exit pressure drop; and compressor, combustor, and turbine efficiencies. The results are presented in the form of carpet plots in Figures 12 through 21 and are summarized on Table X. Note that if the design cooling-flow schedule is used (Note b, Table X), the sfc does not change, but the specific power increases 11.25 percent per 100°F burner temperature.

TABLE IX

APS DESIGN POINT PARAMETERS

Physical speed, rpm	81,800
Ambient temperature, °F	130
Inlet pressure loss, $\Delta P/P$	0.01
Axial Compressor corrected flow, lb/sec	3.667
Pressure ratio	1.837
Efficiency, T-T	0.826
Interstage duct pressure loss, $\Delta P/P$	0.015
Centrifugal bleed compressor corrected flow, lb/sec	0.48
Pressure ratio	3.5
Efficiency, T-T	0.75
Bleed valve pressure loss, $\Delta P/P$	0.03
Centrifugal power compressor corrected flow, lb/sec	1.78
Pressure ratio	6.38
Efficiency, T-T	0.82
Leakage, $\Delta W/W$	0.005
Turbine cooling flow, $\Delta W/W$	0.06
Burner pressure loss, $\Delta P/P$	0.05
Efficiency	0.98
Discharge temperature, °F	2200
Turbine inlet corrected flow, lb/sec	0.447
Efficiency, T-S at diffuser exit	0.87
Accessory and drag loss, hp	13.6
Cycle pressure ratio	11.4:1
Bleed-air pressure ratio	6:1
Bleed-flow rate, lb/min	55
Torque converter weight, lb	5
APU diameter, in.	10
APU length, in.	24
APS weight, including start system, lb	180
APU eshp	300
Fuel consumption, lb/hr	120

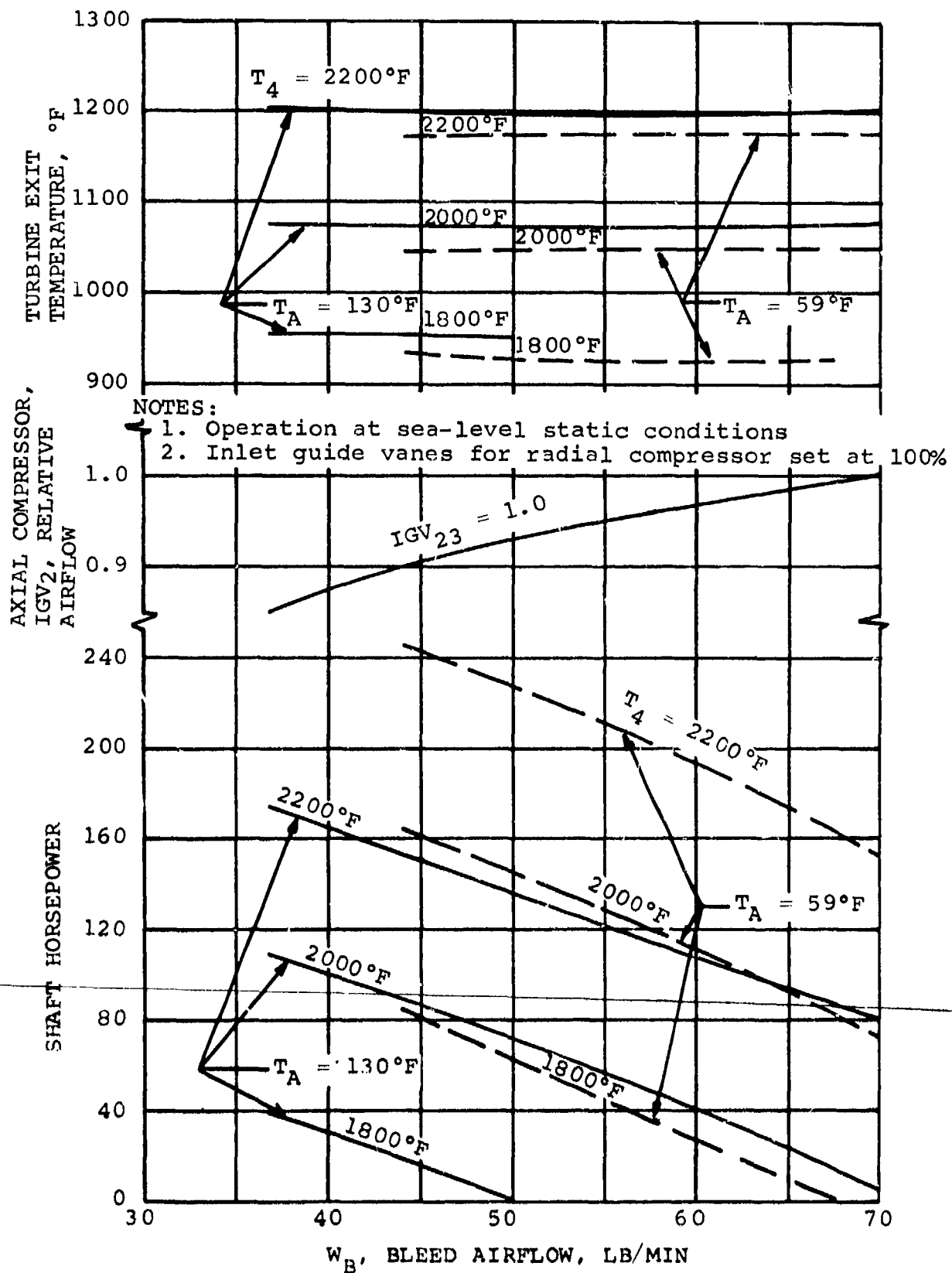


Figure 10. Estimated Performance With Theoretical Compressors.

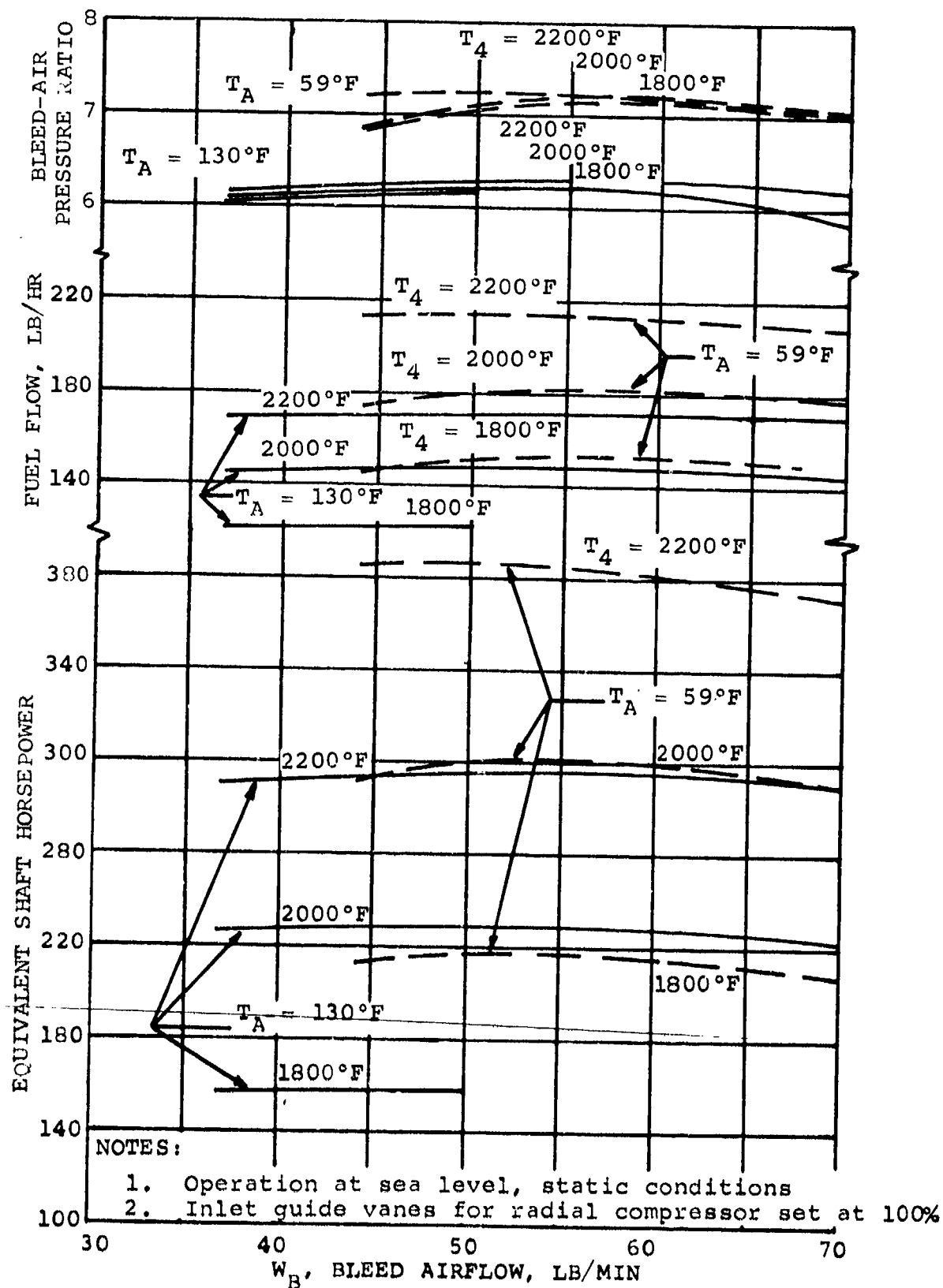


Figure 11. Estimated Performance With Theoretical Compressors.

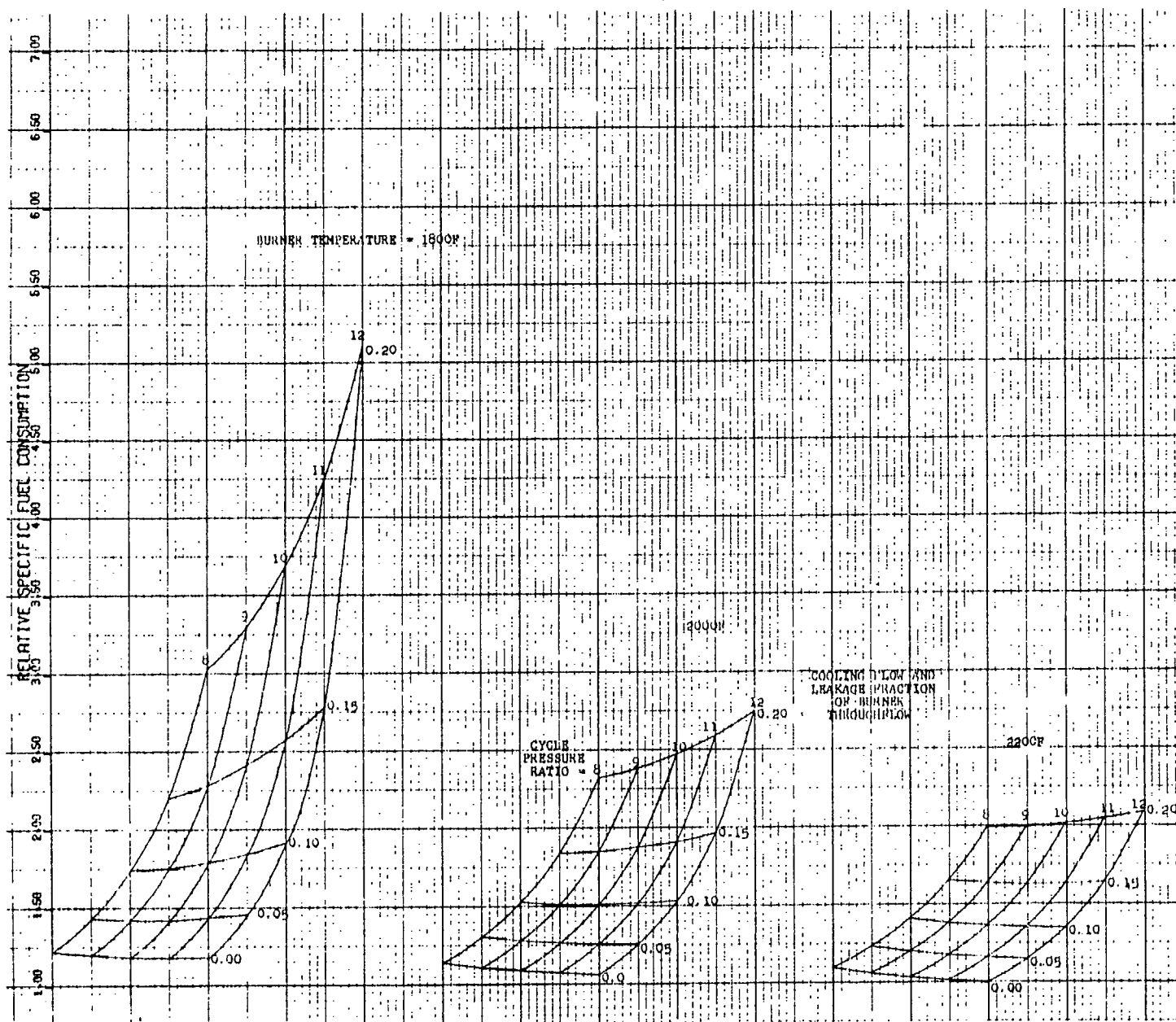


Figure 12. Cooling Flow and Leakage Parametric Data.



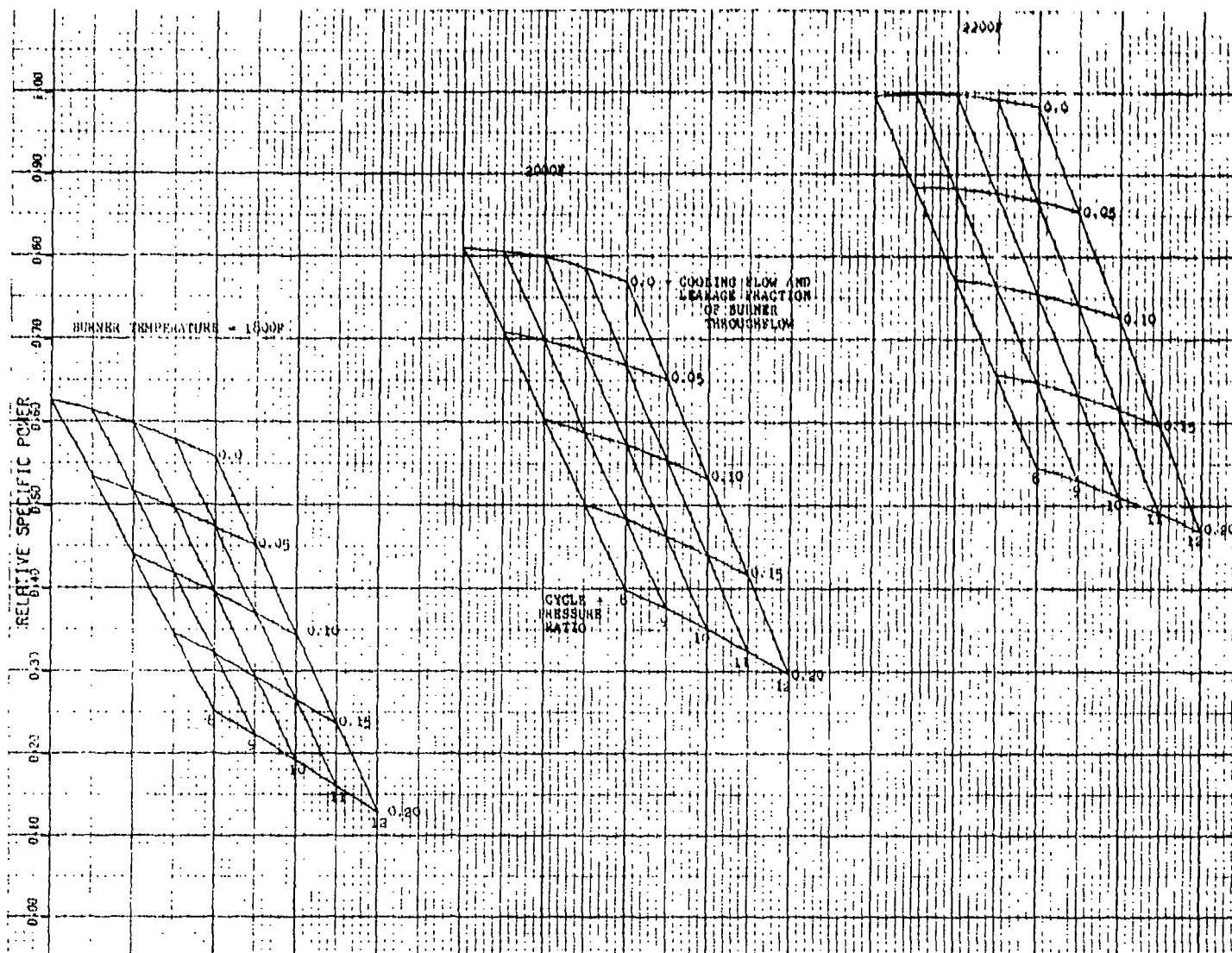


Figure 13. Cooling Flow and Leakage Parametric Data.

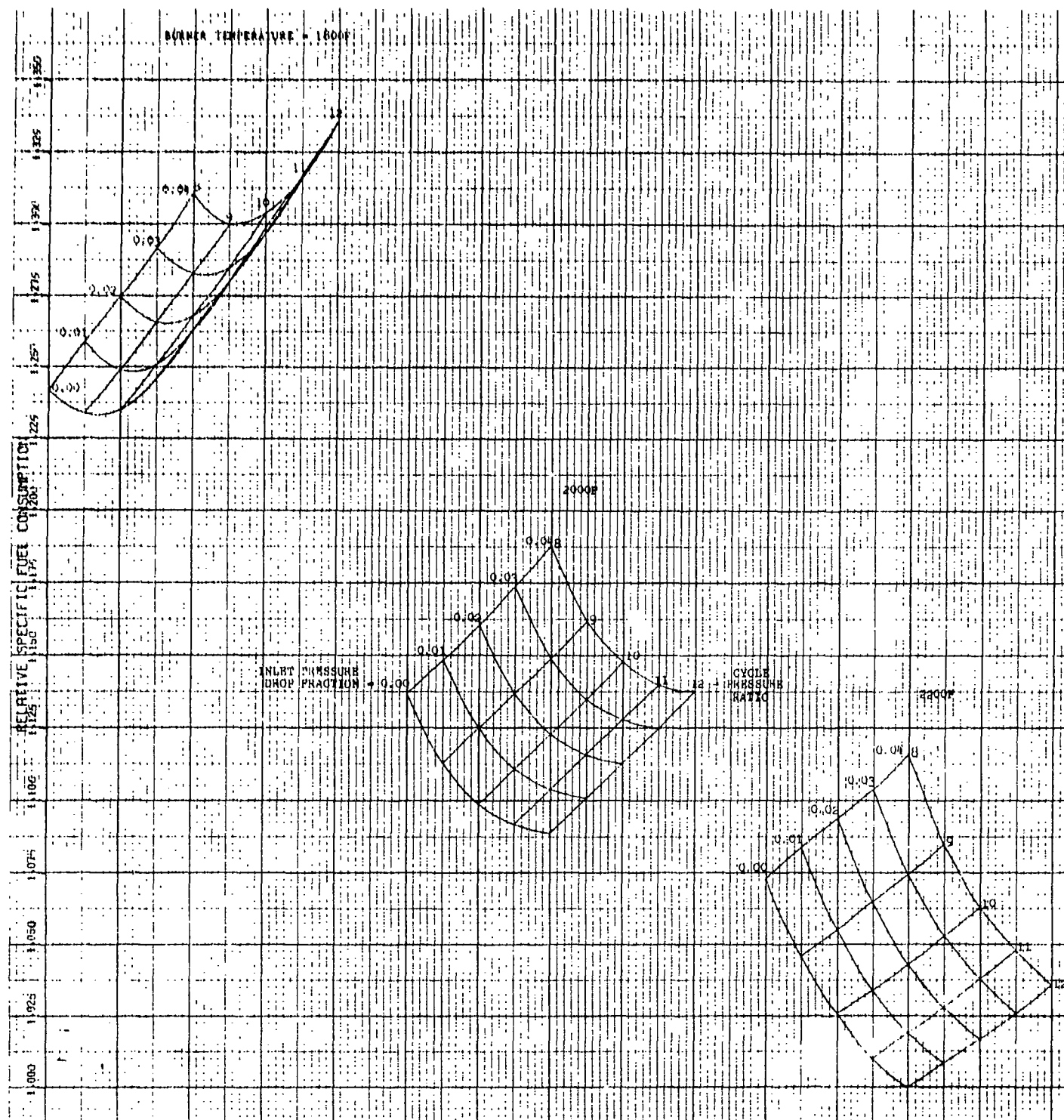


Figure 14. Pressure Drop Parametric Data.

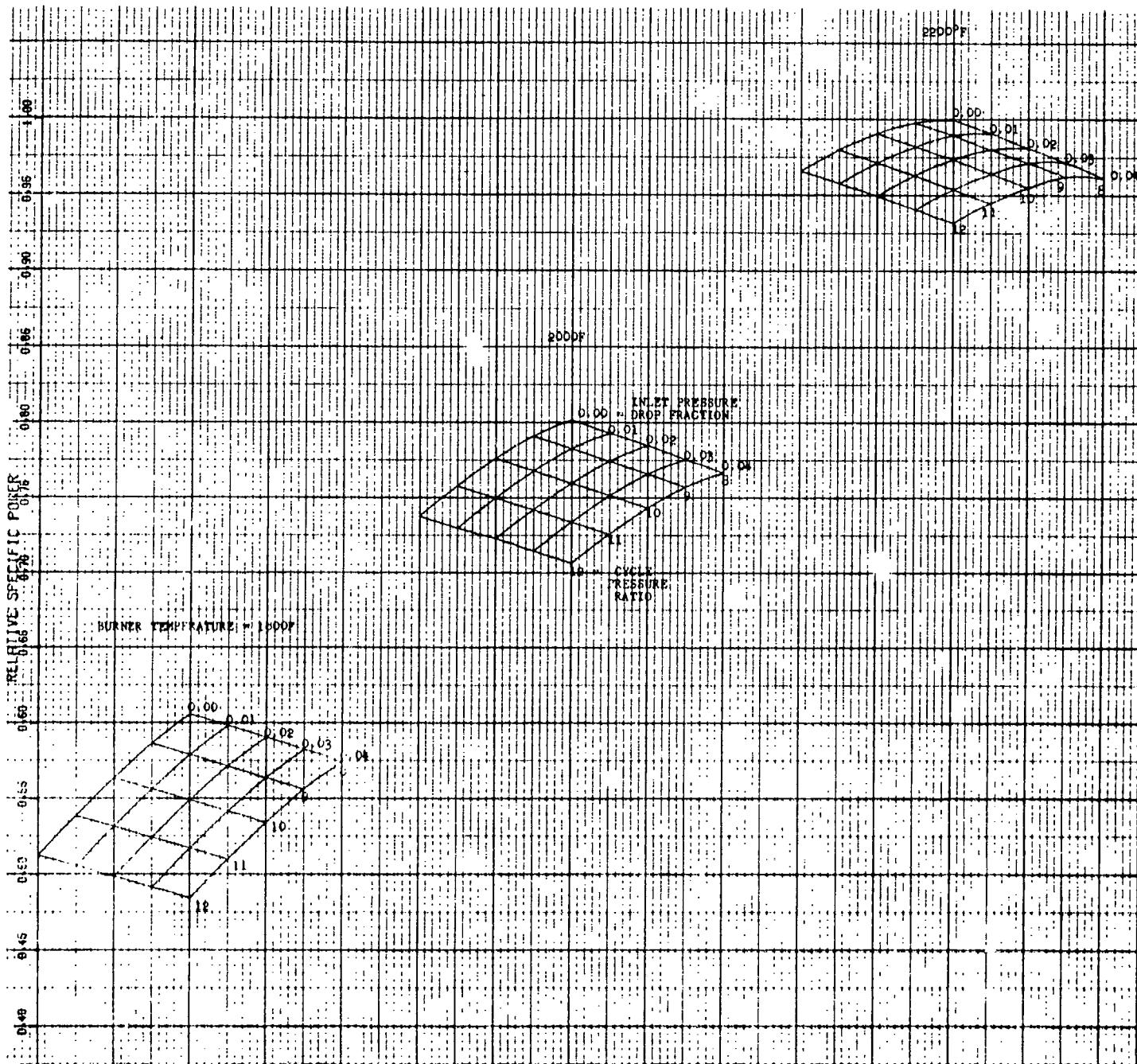


Figure 15. Pressure Drop Parametric Data.

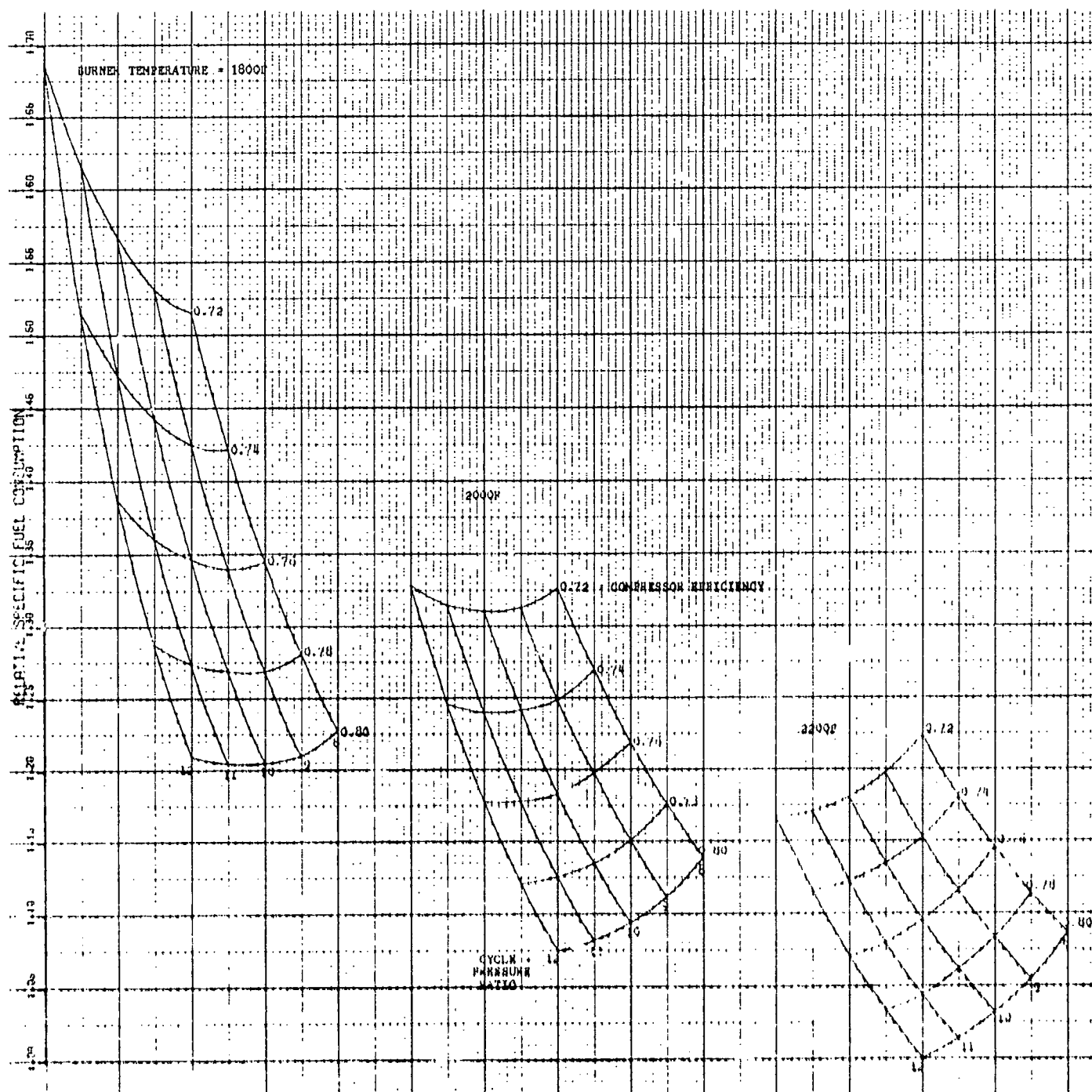


Figure 16. Compressor Efficiency Parametric Data.

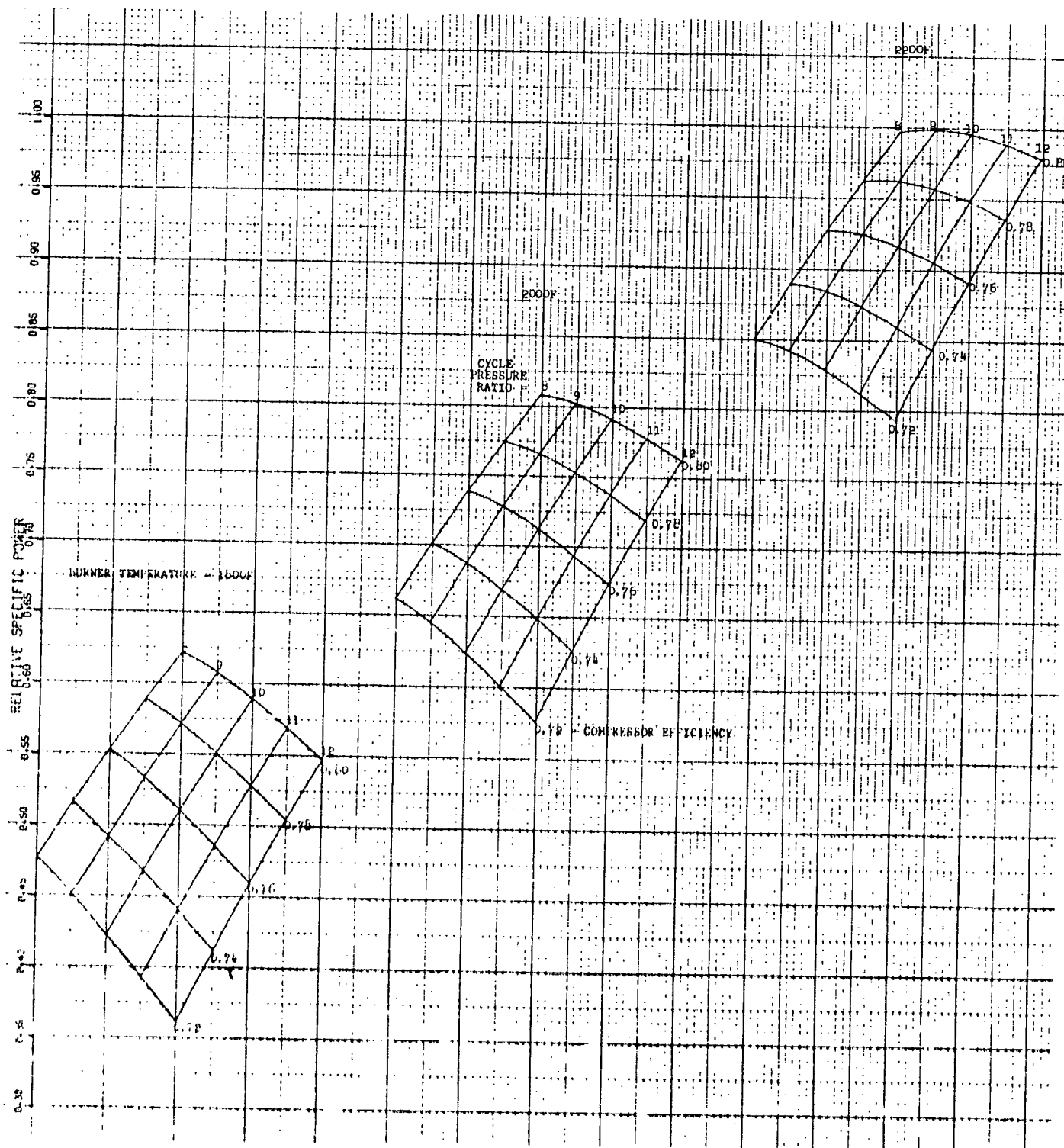


Figure 17. Compressor Efficiency Parametric Data.

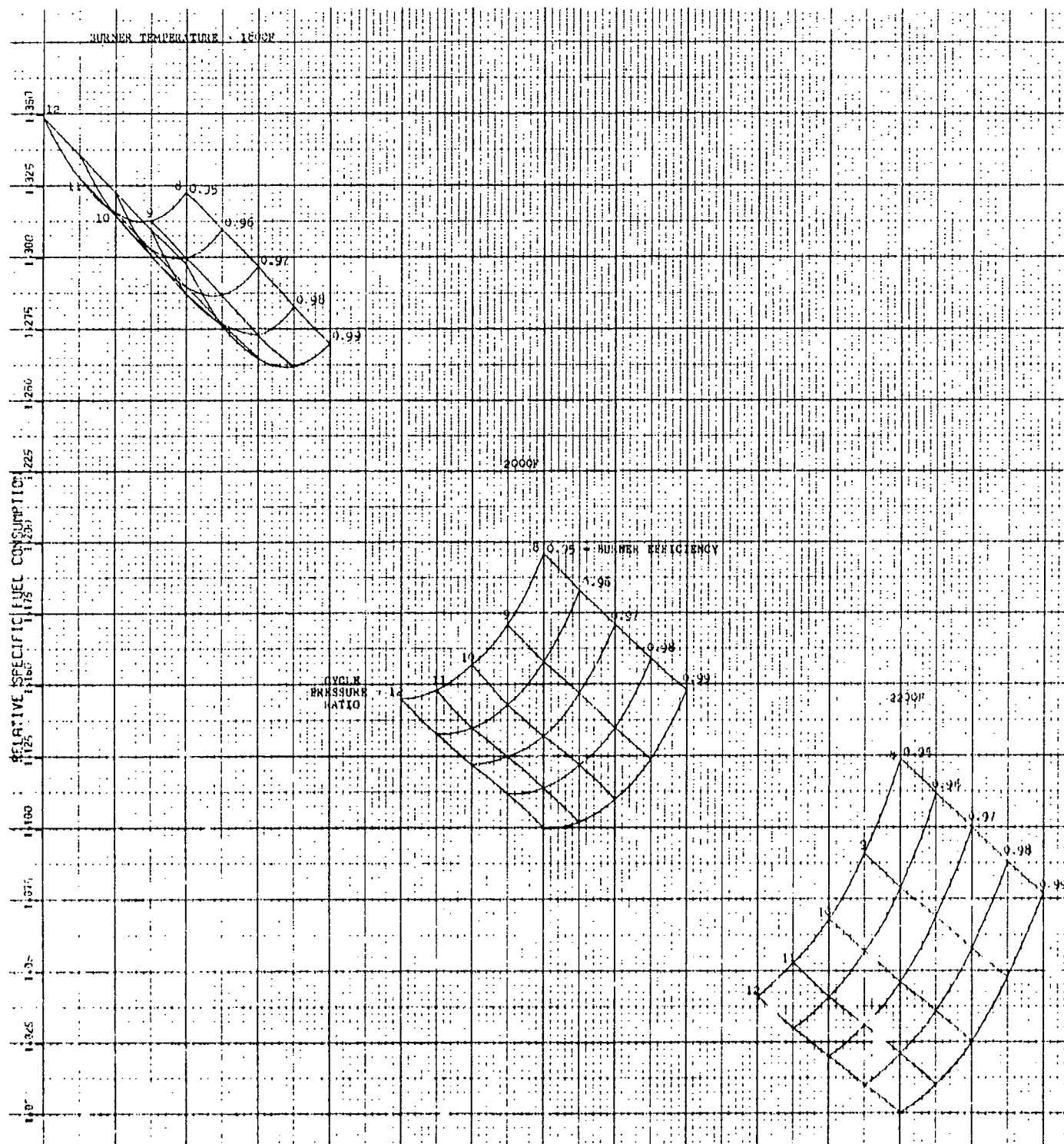


Figure 18. Burner Efficiency Parametric Data.

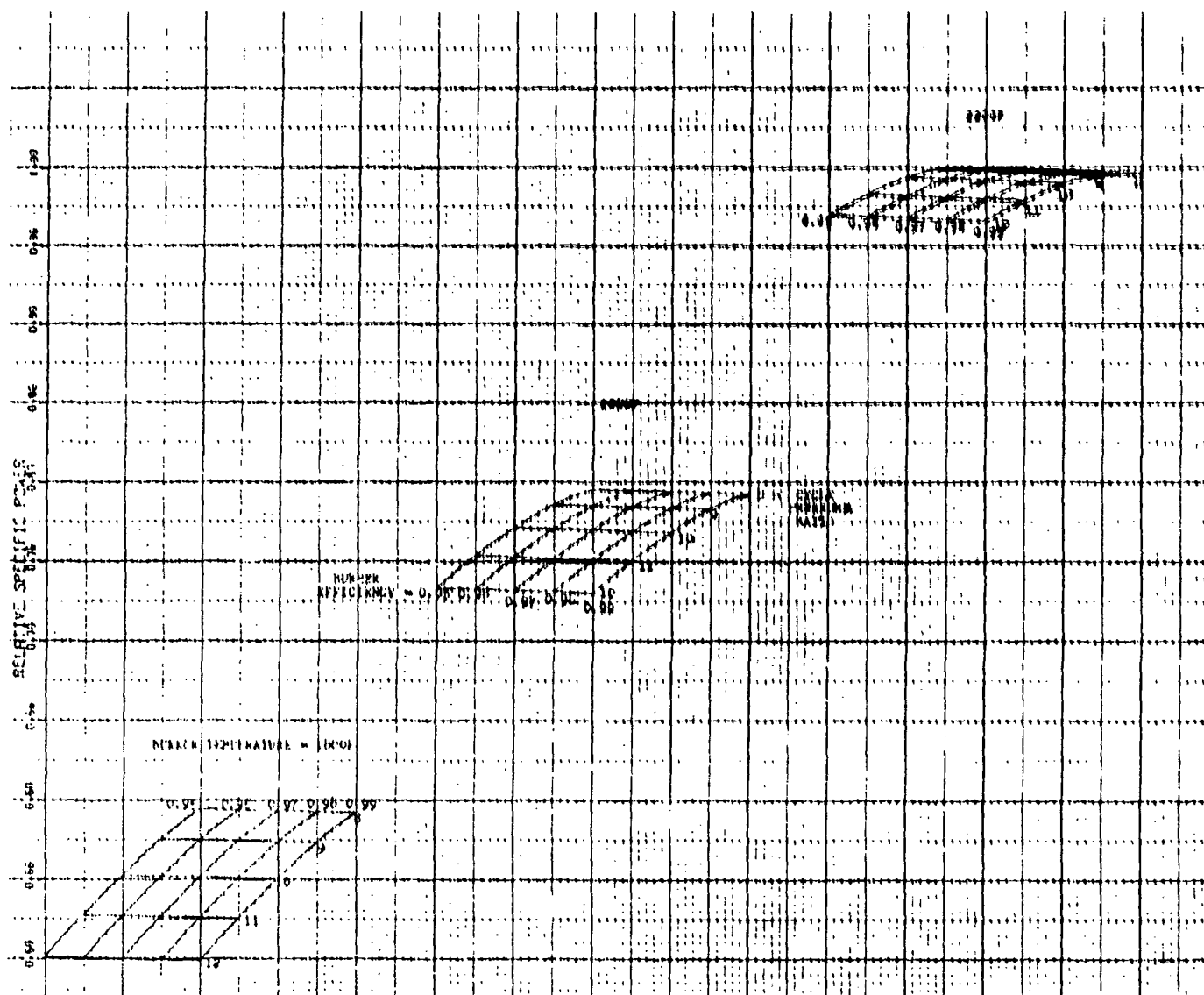


Figure 19. Burner Efficiency Parametric Data.

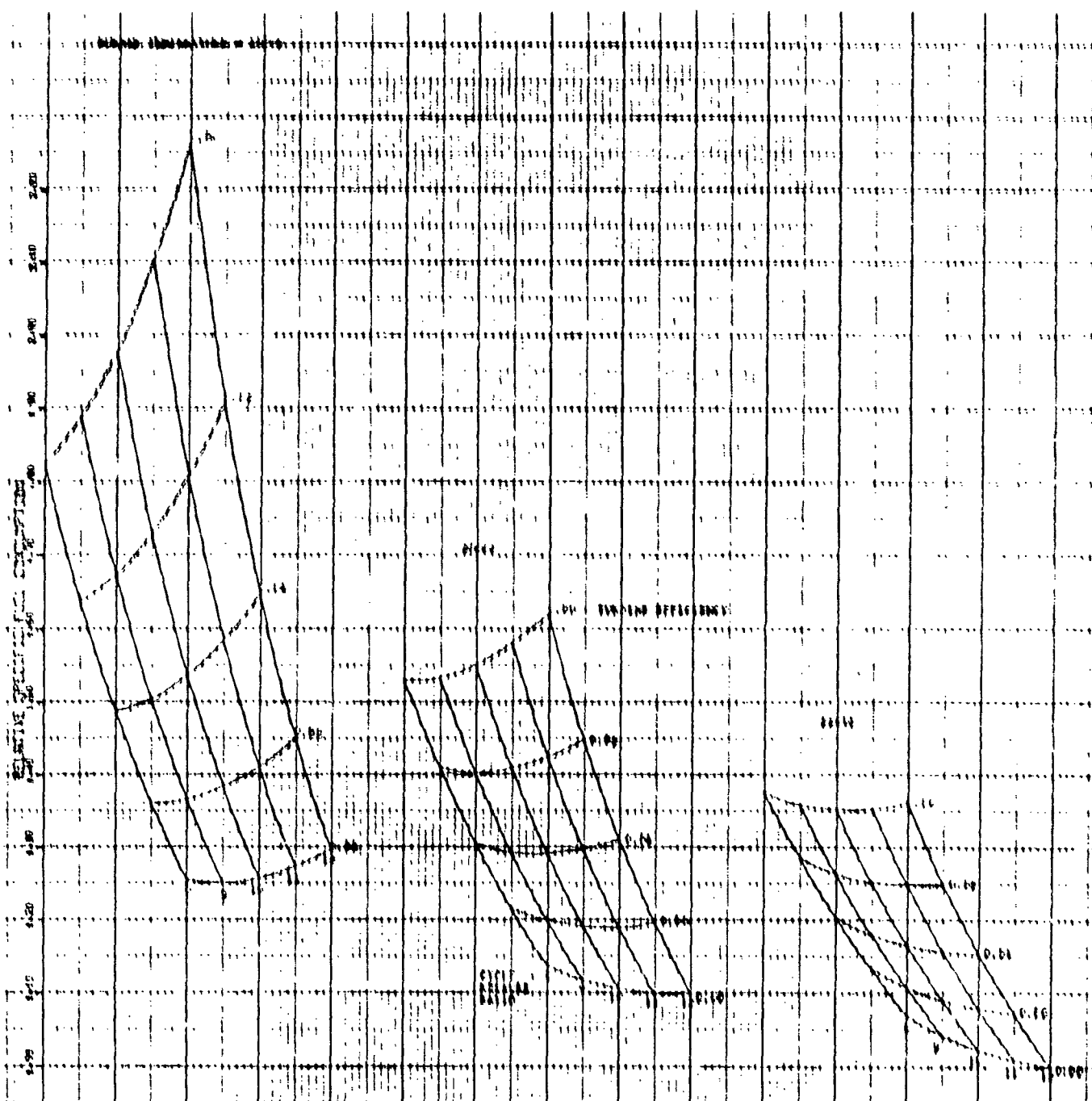


Figure 20. Turbine Efficiency Parametric Data.

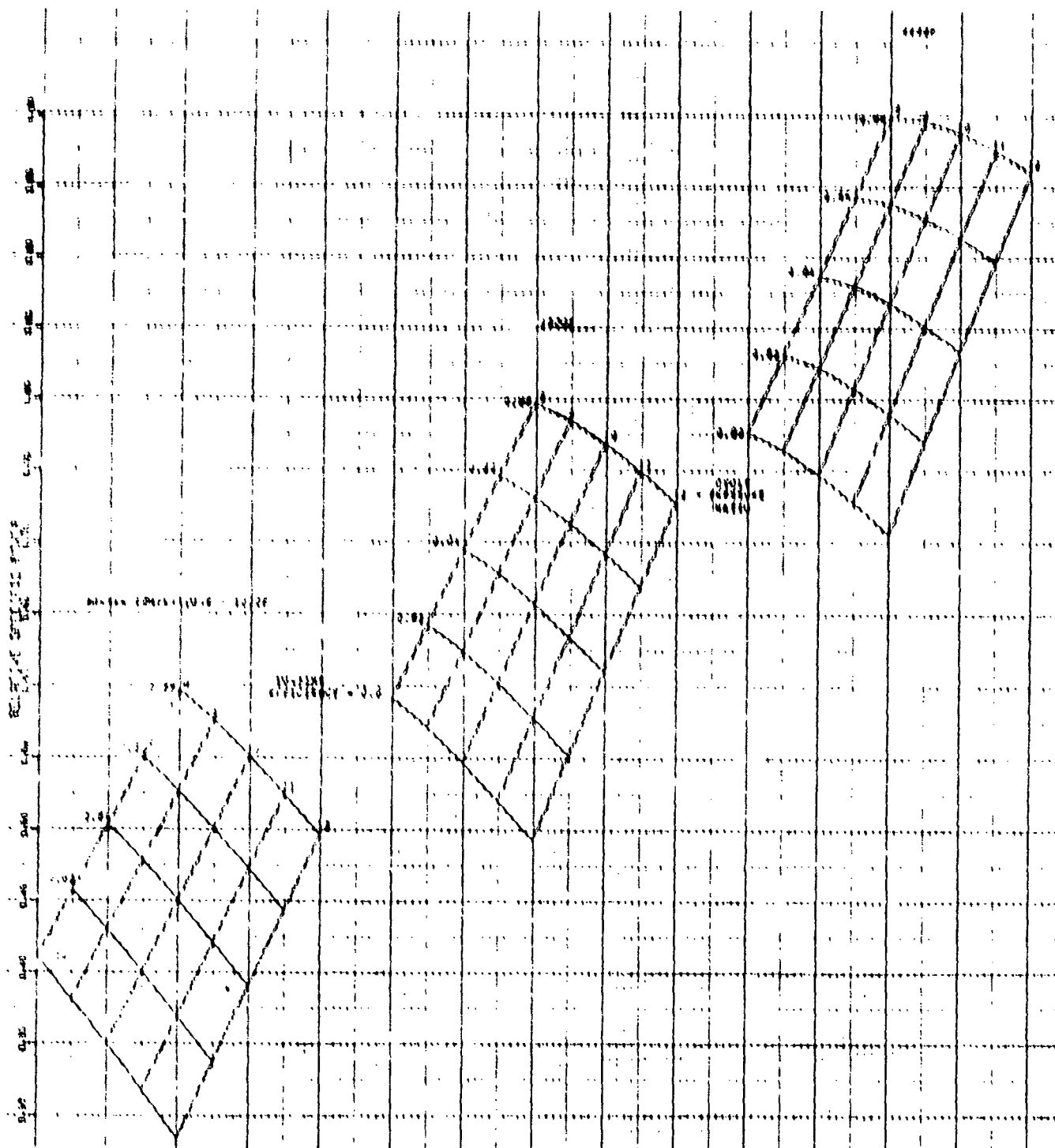


Figure 21. Efficiency Parametric Data.

TABLE X
AFU DESIGN-POINT INFLUENCE COEFFICIENTS (a)

Performance	Parameter	Percent sfc	A Parameters		
			Fuel Flow (d)	Percent Spec Pwr	eshp
100°F	Δ Burner Temperature (b)	0	0	-11.25	-33.70
100°F	Δ Burner Temperature (c)	-5.00	-6.00	-17.70	-53.00
%W/W	Leakage or Cooling	+3.5	+4.20	-2.50	-7.50
%P/P	Pressure Loss	-0.875	+1.05	-0.875	-2.62
%N _C	Compressor Efficiency	-1.50	-1.80	-2.63	-7.80
%N _B	Burner Efficiency	-1.0	-1.2	0	0
%N _T	Turbine Efficiency	-3.16	-3.79	-4.19	-12.52
Δ Cycle	Pressure Ratio	-1.58	-1.89	-1.05	-3.15
(a) Based on the design-point parameters from Table IX, unless otherwise specified.					
(b) Based on the following cooling flow schedule:					
	Burner Temperature:	1800°F	2000°F	2200°F	
	Percent Cooling Flow:	0	3	6	
(c) Based on 6 percent cooling flow					
(d) Fuel flow is based on 120 lb/hr					

Carpet plots are constructed so that the vertical grid lines are used to interpolate between the main lines of each of the two parameters on the grids. This method of data presentation allows the user to interpolate either of the independent variables with a higher degree of accuracy. There is a carpet plot grid for each of three burner temperatures, and the grids are spaced so that data may be interpolated between the grids.

Any sfc carpet plot may be used to determine the effect on sfc of a change of pressure ratio, burner temperature, the particular influence parameter in question, or a combination of all three. For example (Figure 12), for the sfc of a cooled 2200°F turbine to equal that of an uncooled turbine at 1800°F with a total leakage fraction of 0.01, the total leakage and cooling fraction will be 0.07 at 11:1 pressure ratio. These leakage and cooling fractions are approximately those expected, which indicates that no sfc advantage is to be gained by the higher turbine inlet temperatures. However, according to Figure 12, the relative specific power at 1800°F burner temperature and 0.01 leakage is 0.558, and at 2200°F burner temperature and 0.07 leakage, it is 0.900. From these relative specific power ratios, a 72-percent increase in specific power is indicated for the higher temperature burner.

In most cases, the influence of an increase or decrease of a given cycle parameter will allow engineering judgment to refine the design. For example (Figure 12), by assuming the design-point pressure ratio of 11:1 and burner temperature of 2200°F, a cooling-flow fraction of 6 percent gives a relative sfc of 1.2. An increase of this parameter to 10 percent increases the sfc to 1.35. The fuel consumption of a machine designed for 10-percent cooling-flow would, therefore, be 112.5 percent of that designed for 6-percent cooling-flow.

In many cases, one variable is dependent upon the value of another, and the net effect must be obtained by combining the two influence coefficients. That is, a design-point burner temperature increase (tending to decrease sfc) must be accompanied by an increase in cooling flow (tending to increase sfc). The calculated decrease and increase must be multiplied together to determine the net effect. Other examples of trade-off include decreasing compressor efficiency and increasing turbine efficiency as a result of increasing the cycle pressure ratio.

SECTION III

COMPRESSOR DESIGN AND DEVELOPMENT

The compressor section comprises an axial first stage and a radial second stage. Bleed-air is extracted from a notch in the second-stage impeller. This arrangement is referred to as a split-flow radial compressor or a notch bleed system.

Cycle analysis (from estimated maps for each compressor, based on test data for similar compressors) showed that VIGVs may have been required for each stage to achieve the off-design goal of maximum shaft power and for compressor matching at part-speed. Later testing showed that the second-stage VIGVs were not necessary.

All compressor development work was conducted with scaled-up components, as the small size of the APU components prevented the inclusion of an adequate quantity of instrumentation. Also, the probe sizes become large, relative to the height of the annular passage, invalidating the assumption of a "point" measurement.

Scaling test results to any other geometrically similar size is based upon similarity of tip speed and the premise that inlet flow velocity remains the same. For the -3 axial compressor, the design inlet flow rate of the reference rig was 6.147 times that of the APU-size compressor. Since the flow rate is proportional to the flow area at the same average velocity, the reference rig compressor scale was made proportional to the square root of the flow ratio, or 2.479 times as large. The tip velocity (and all other wheel velocities in the flow path) is maintained by decreasing the rpm to $1/2.479$ (40.33 percent) of the APU-size component. The compressor performance maps, thus derived, are scaled by the corrected flow ratio, with the pressure ratio and efficiency remaining the same.

When scaling from an optimum large compressor to a smaller size, three main factors can contribute to pressure and efficiency losses:

- (a) Clearance Effects - Generally, clearance is difficult to scale. As compressors become smaller with correspondingly smaller blade heights both axially and radially, the clearance to blade-height ratio increases with an accompanying drop in performance.
- (b) Reynolds Number Effects - The Reynolds number decreases with reduced size. This can cause an increase in the friction losses of the compressor if a lower limit of Reynolds number is violated.
- (c) Manufacturing Effects - The effect of manufacturing limitations on the performance of small compressors is subtle but important. As blades become smaller, a point is reached where it becomes impractical or impossible to scale tolerances. Similarly, blade thicknesses cannot be scaled indefinitely. The requirements for resistance to erosion and vibratory stresses usually define a minimum thickness that is independent of compressor size. The size of the tooling to fabricate compressor blades has a practical limit, so that tool deflection and breakage can be controlled. For small compressors, there is a relative increase in the thickness of the blades near the fillets that adversely affects the performance. The relative surface smoothness cannot be maintained, thus contributing to increased friction losses.

The combination of these factors can cause large adverse effects on the performance of components scaled to a smaller size. Therefore, the reference compressor rigs were made large enough to enable accurate aerodynamic measurements and to keep the adverse effects of scaling to a minimum. In an effort to eliminate as many of the losses as possible, the reference rig blade thickness, fillets, surface smoothness, and clearances were all scaled from the APU-size design. Estimates of pressure and efficiency degradation were applied to the reference rig tests results, to approximate losses by scaling to the small size.

1. AXIAL COMPRESSOR STAGE

1.1 Aerodynamic Design and Development

The design requirements of the low-pressure stage were:

(a) Stage pressure ratio	1.837
(b) Corrected flow	3.66
(c) Total-to-total efficiency	0.826

From these, the following rotor characteristics evolved:

(a) Rotor tip speed (corrected, ft/sec)	1590
(b) Inlet hub-tip ratio	0.5
(c) Rotor tip solidity*	1.3
(d) Hub solidity*	2.53
(e) Number of rotor blades	15.0
(f) Rotor aspect ratio (blade height/chord)	0.87

Two rotor configurations were evaluated on the size (11.66-in. tip diam) test rig. The first, designated -1, was a research compressor designed for a 1400-ft/sec corrected tip speed. The second design (-2) was a restaggered version of the -1 rotor blade. A stagger increase was made to accommodate higher air angles coincident with the 1590-ft/sec tip-speed required for the design pressure.

Testing the inlet guide vane design was accomplished with the -2 axial rotor configuration. The guide vanes were intended to match the compressors at part-speed and at varying bleed flows. The scale rig test results for both configurations are summarized as follows:

- (a) Test 1 - The first test was performed using the -1 rotor design. Figure 22 shows a map of rotor performance. The

*Solidity = (chord) x (number of blades/ $2\pi R$)

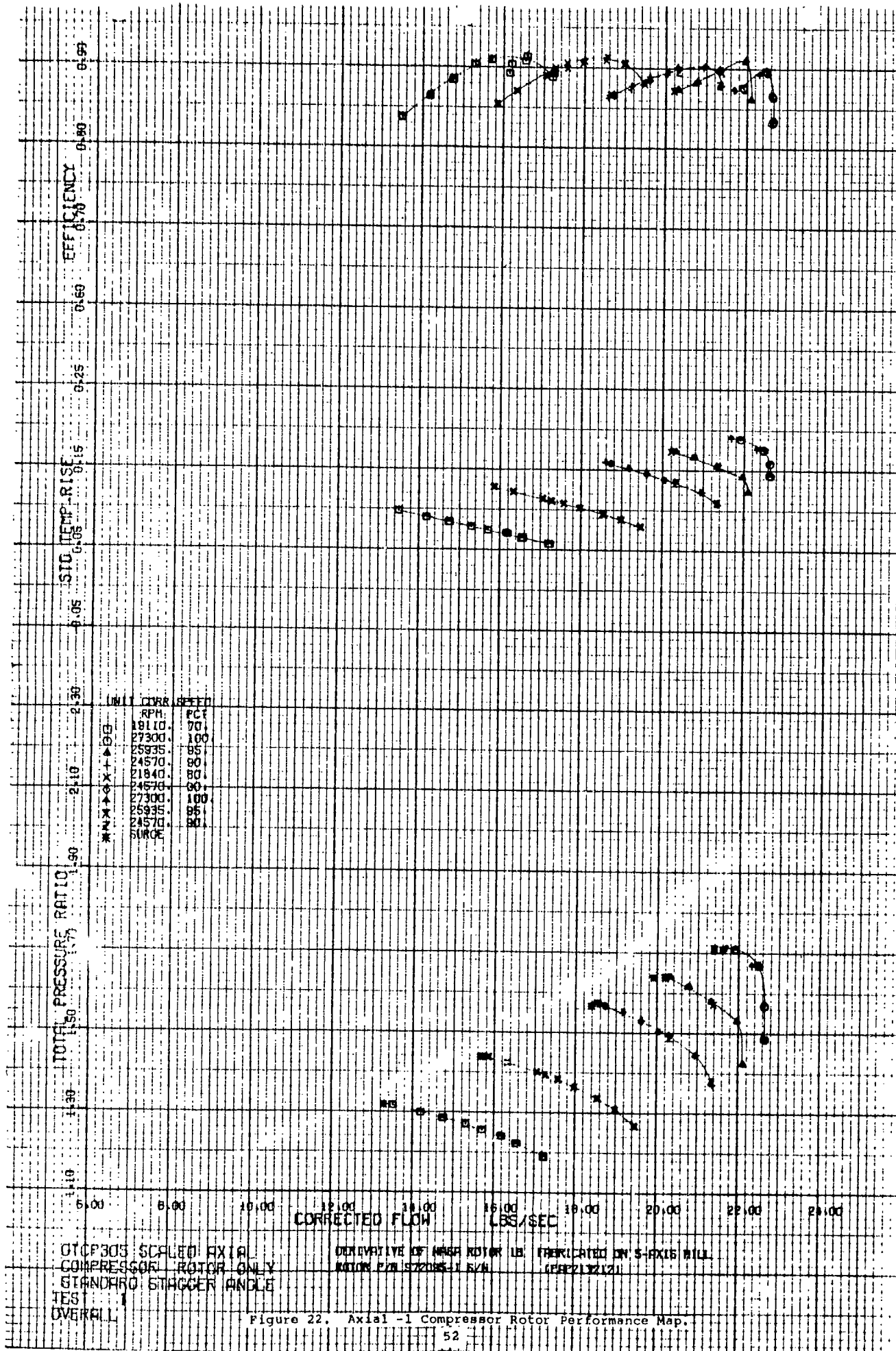
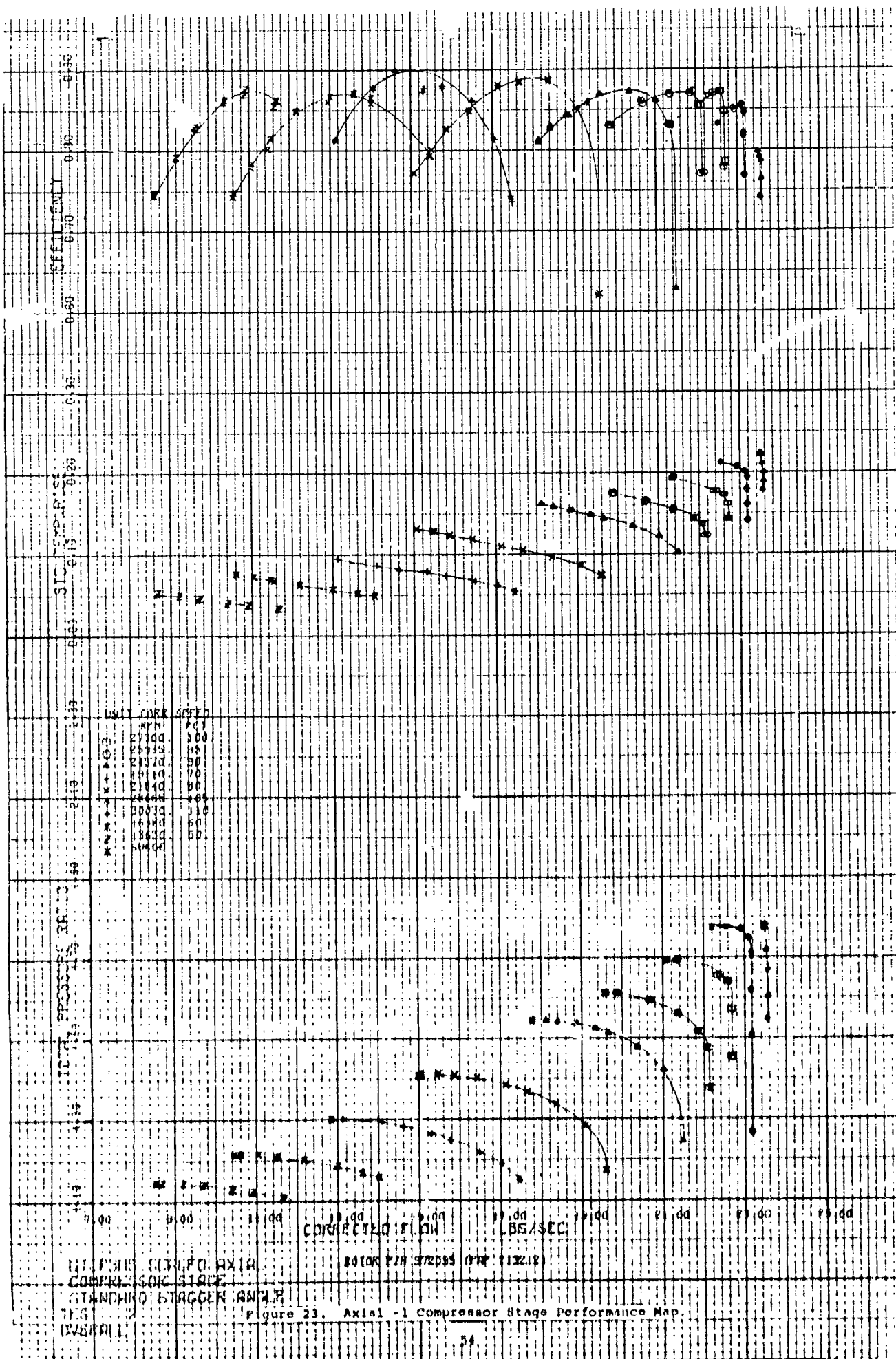
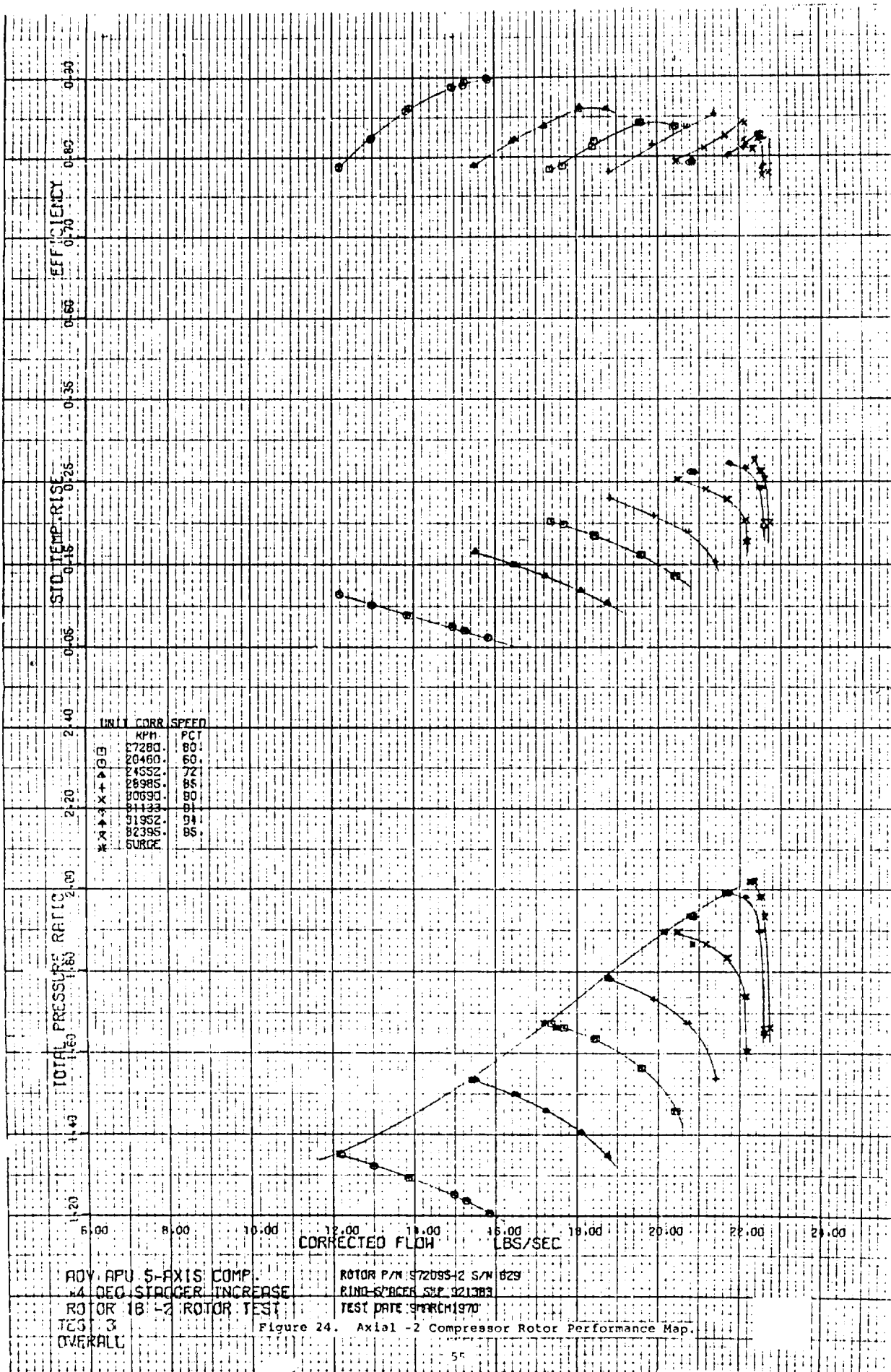


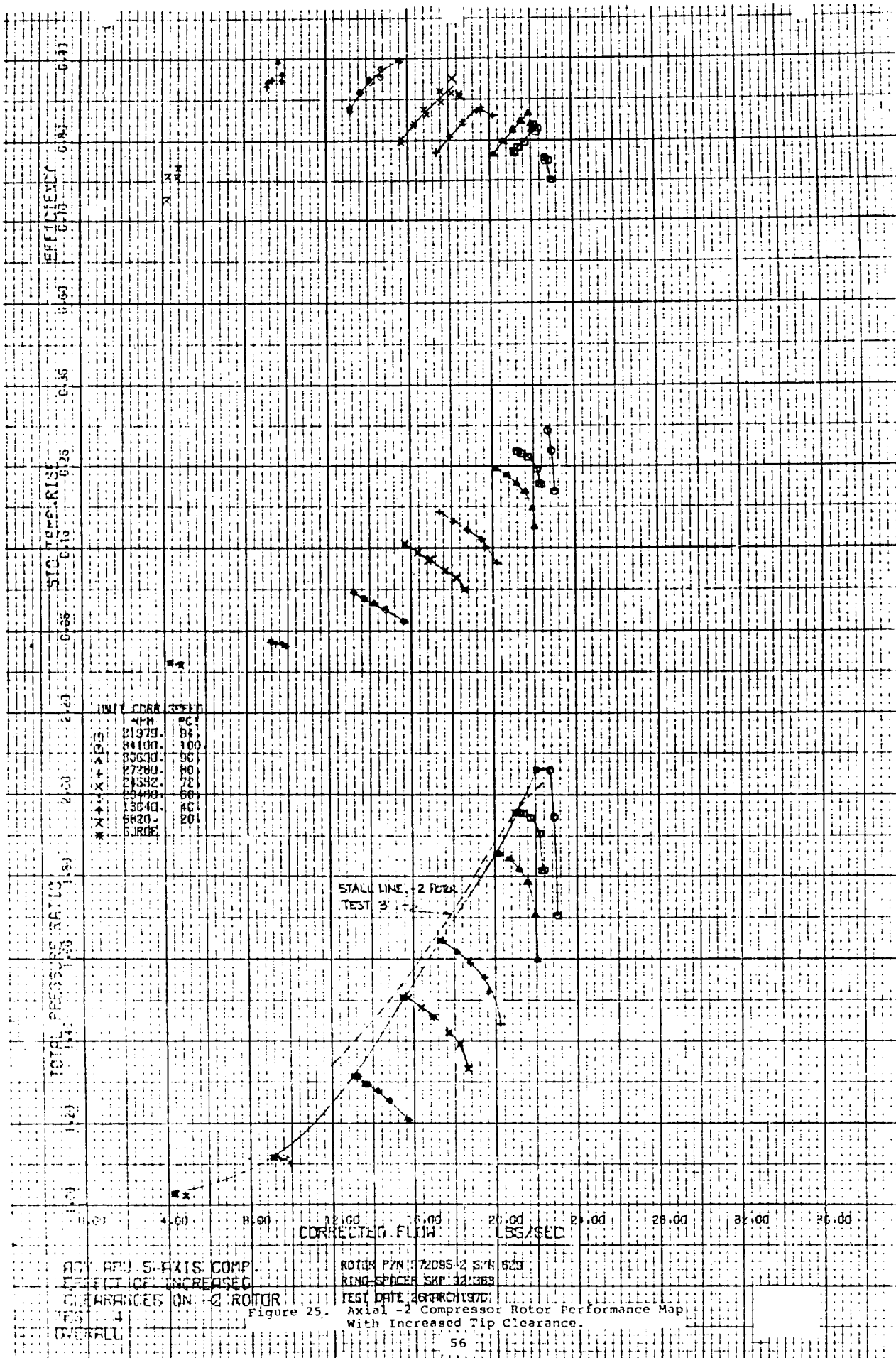
Figure 22. Axial -1 Compressor Rotor Performance Map.

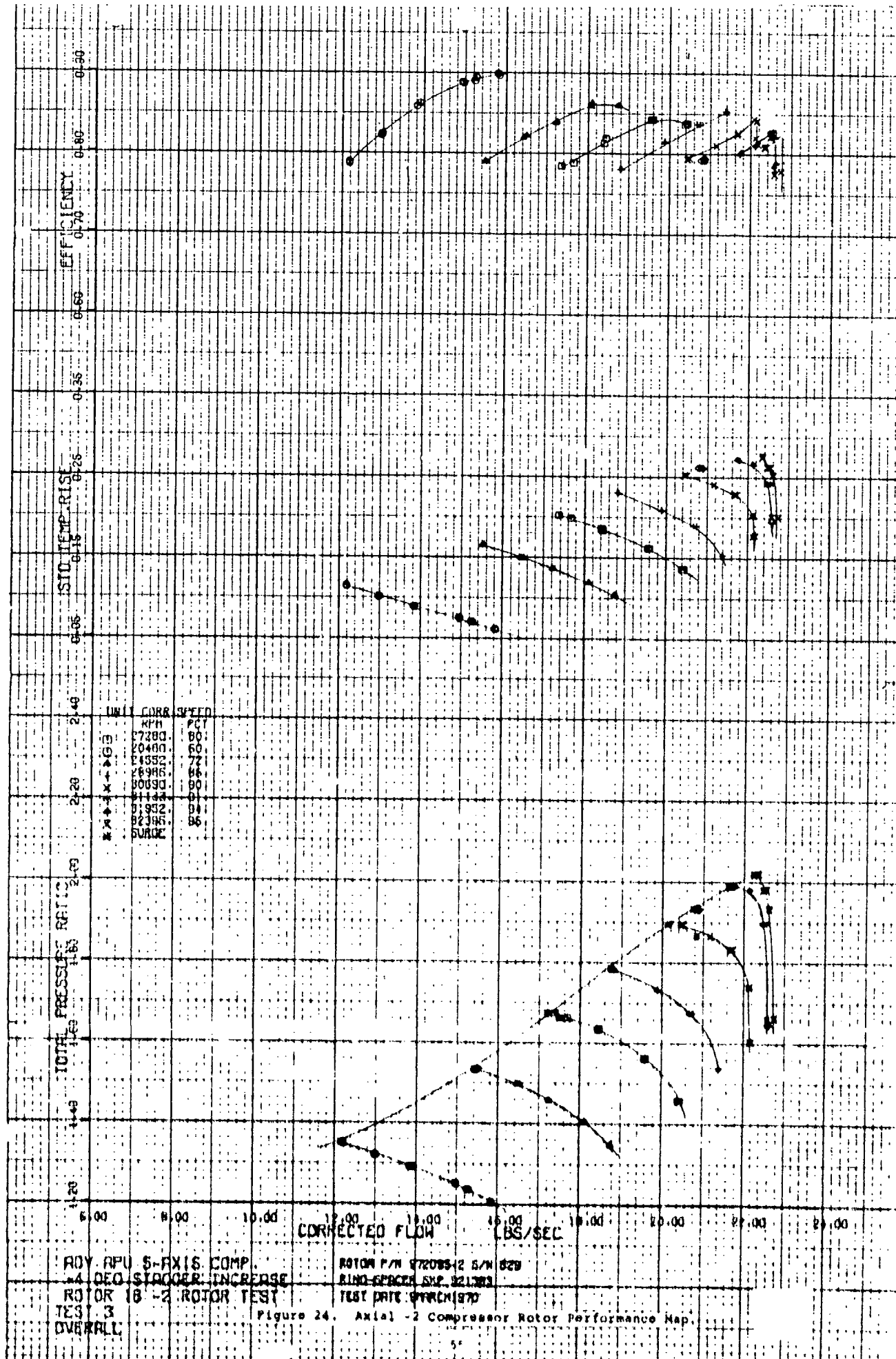
-1 rotor obtained approximately 1 percent higher efficiency than predicted, but the surge margin at higher operating speeds was lower. Tip clearances was 0.3 percent of chord.

- (b) Test 2 - This was a stage test performed with both the stator and the rotor. The rotor tip clearance was opened slightly to allow overspeed operation. The results (Figure 23) again indicate reduced surge margin. It was theorized that stall margin loss could be blade isolation caused by small clearances during the first two tests. Another possibility was blade untwist in the tip region. Both effects were investigated in subsequent tests.
- (c) Test 3 - The -2 rotor efficiency and stall margin were lower than predicted at APU design speed (Figure 24). The instrumentation included capacitance probes at the leading and trailing edges to measure blade untwist. Data indicated a blade untwist of 0.6 deg, compared to an analytical estimate of 1.1 deg. The flow change associated with this incidence change is approximately 33 percent of the measured range loss, but this is considered a secondary effect. Rotor clearance was 0.6 percent of chord.
- (d) Test 4 - A fourth test was conducted to determine the effects of increased tip clearance on the -2 rotor surge margin. Tip clearance was opened to approximately 1.3 percent of the chord at APU design speed. The efficiency and pressure ratio decreased with no beneficial change in surge margin (Figure 25).
- (e) Test 5 - Following the fourth test, the higher efficiency suggested scaling the -1 rotor design for use in the initial APU testing. As a result, Test 5 was performed on the -1 rotor to establish the streamline location at the rotor leading and trailing edges necessary to match the APU flow conditions. Tip clearances were increased to 1.6 percent



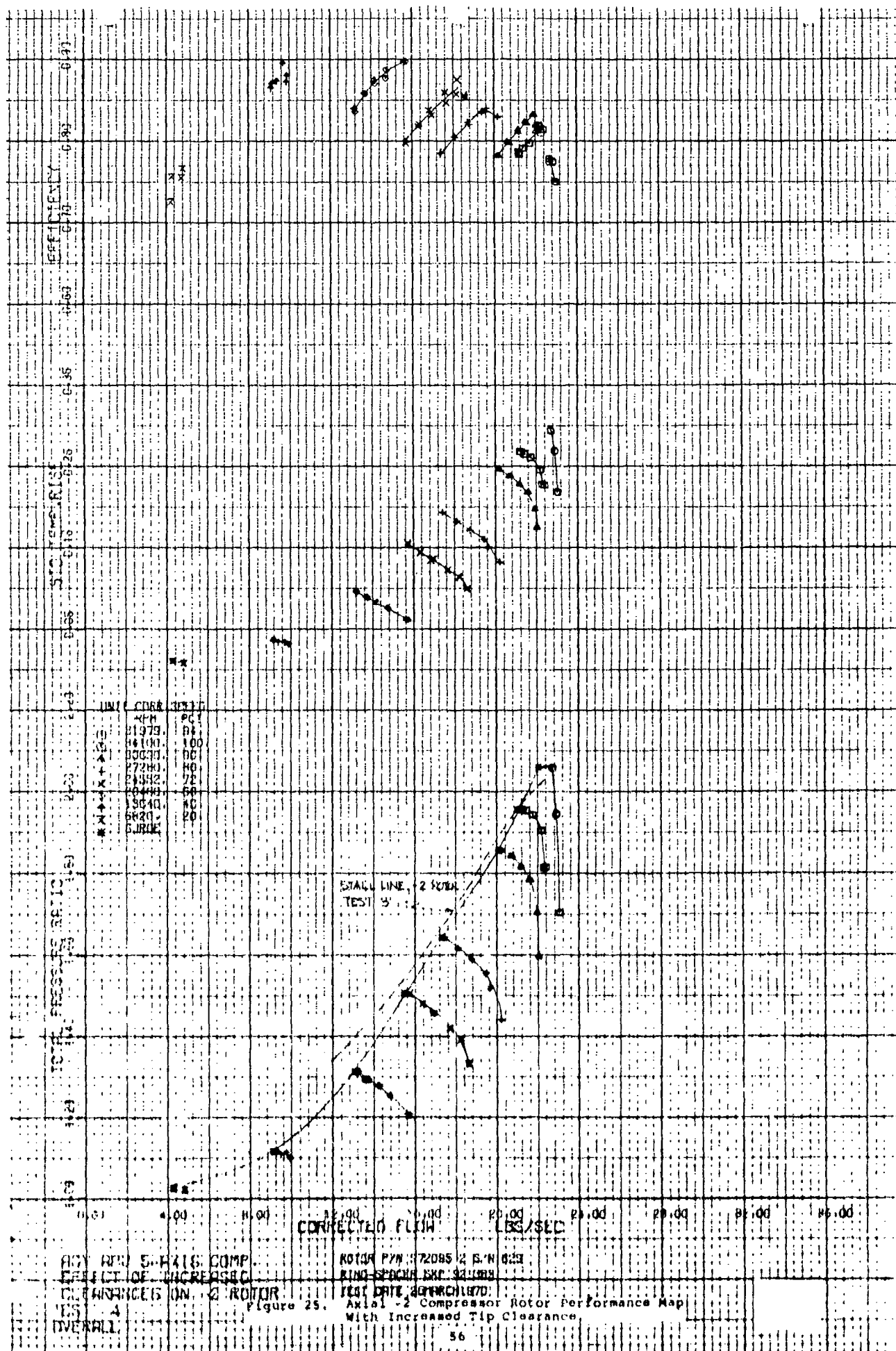






Reproduced from
best available copy.





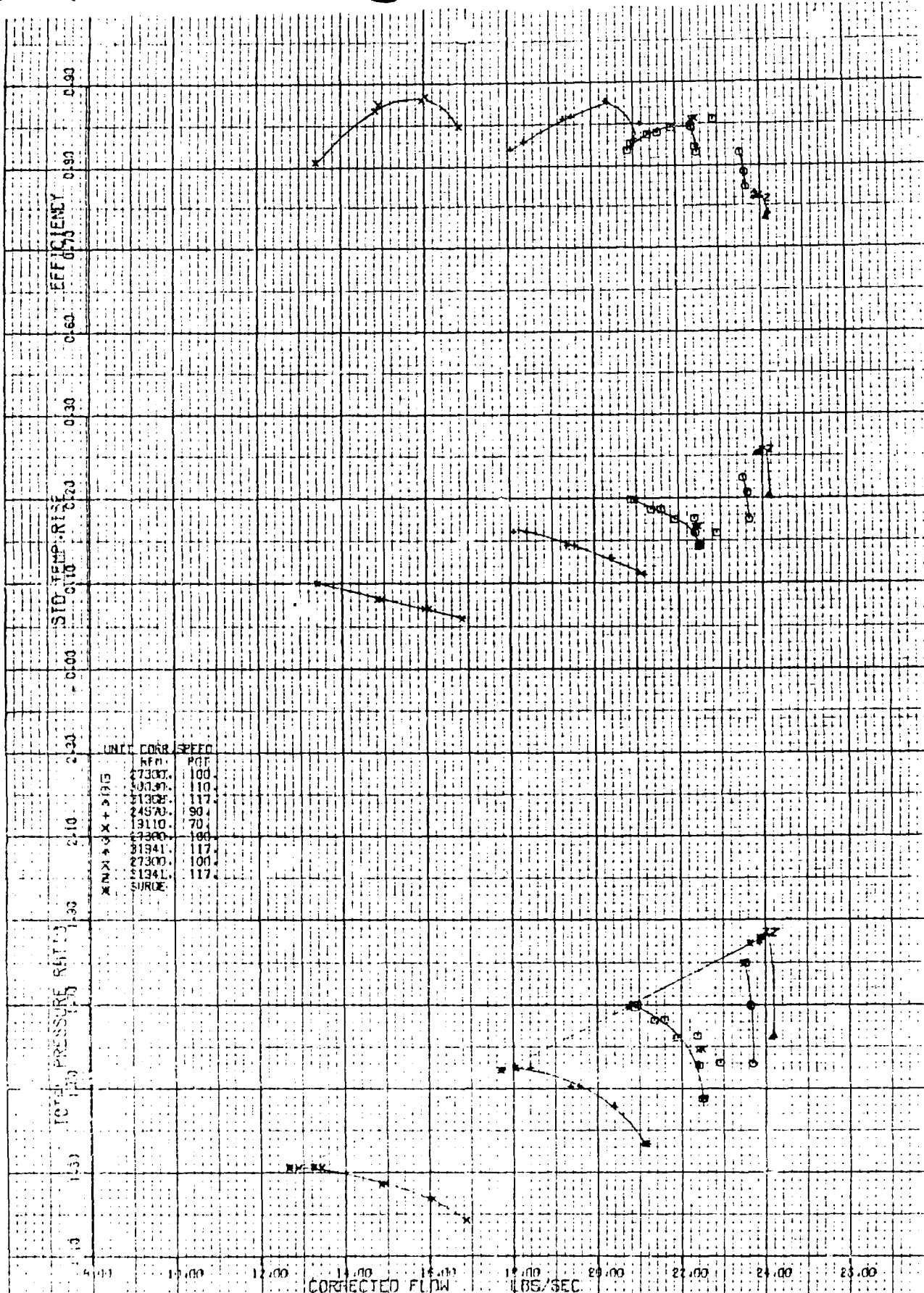
of chord as in the -2 rotor; the results (Figure 26) indicated a reduction of efficiency with no beneficial change in surge margin.

- (f) Test 6 - The sixth test was conducted to determine the effects of variable inlet guide vanes on the -2 rotor performance. Data were recorded for vane settings of 10 deg open (flow turned opposite to rotor rotation), zero deg (axial), and 10-, 20-, and 30-deg closed, for seven speed lines from 20 to 93.78 percent corrected speed. Figure 27 shows a typical constant-speed map for these inlet guide vane settings.

Normalized inlet guide vane data are compared in Figure 28 with assumed theoretical performance during initial cycle studies. The peak efficiency for each speed line without inlet guide vanes was used as the basis for normalizing the peak efficiency at various inlet guide vane settings and speed lines. With the exception of the 90- and 94-percent speeds at normalized flows greater than 1.0, the trend of the data approaches that of the assumed APU efficiency reference line. Analysis of the high-speed, high-flow data indicates that this deviation is caused by stator choking.

The selection of the initial APU axial compressor configuration was based upon data obtained from the axial compressor tests. The higher efficiency of the -1 over the -2 dictated its use. The -1 rotor shroud contour was modified from the inlet to the second-stage inlet guide vane leading edge to match the flow conditions between the axial and centrifugal compressor at the APU design-point conditions.

Analysis of the rig test data led to the conclusion that the severely reduced surge margin was caused by the low rotor aspect ratio. Based on this and the low efficiency achieved by the -2 configuration at the APU design-point, a third-stage design (-3) for the low-pressure compressor was initiated with a higher aspect ratio.

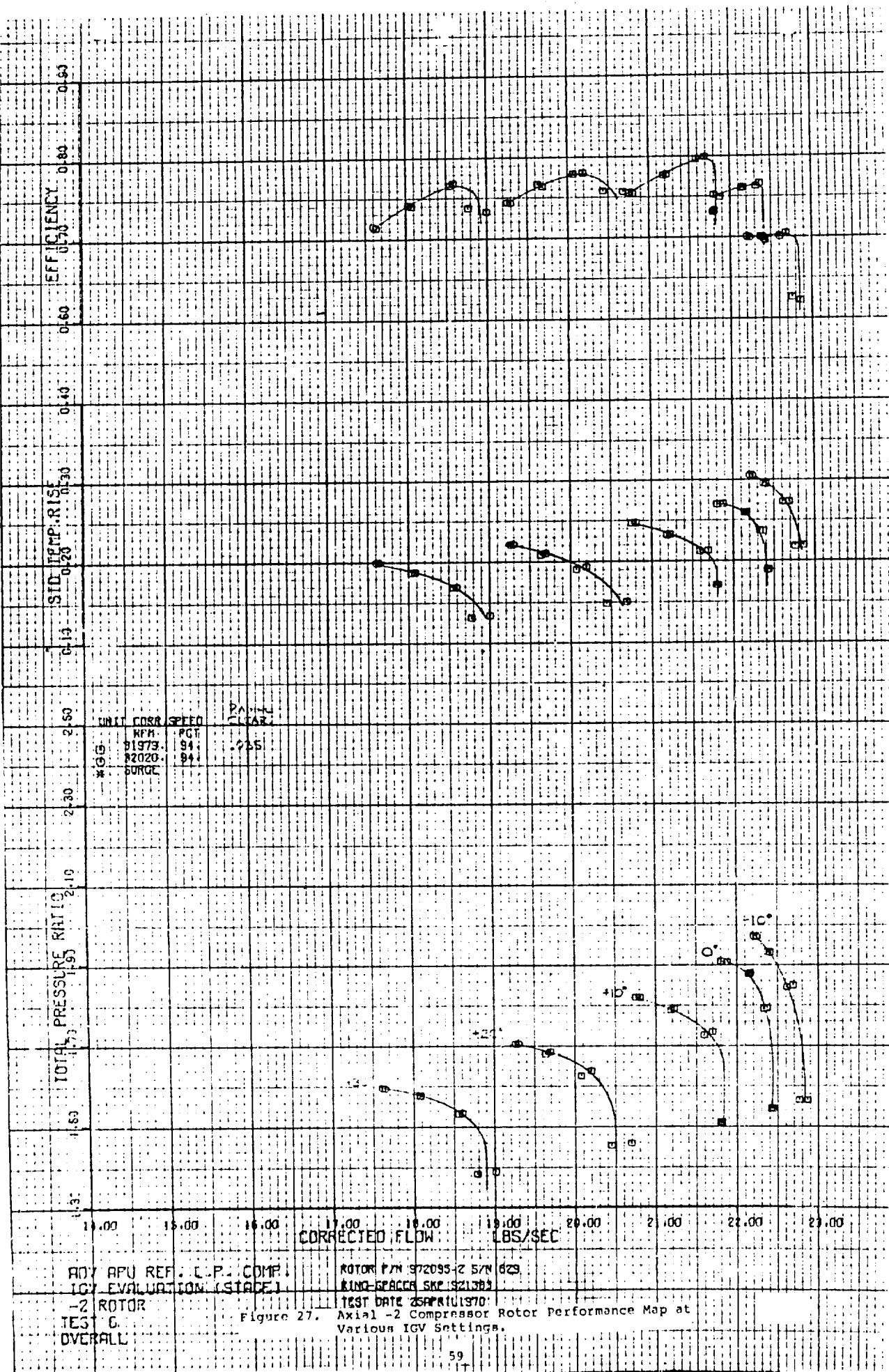


RD7 APL 5-1415 COMPL
 THE COMpressor Rotor
 Rotor Only

ROTOR P/N 372035-11 GYN 508 (P/N 218212)
 SHROUD P/N 372036-11 GYN 508
 CAPACITANCE PROBE CALIBRATION Y-150

TEST DATE APRIL 1970

Figure 26. Axial-1 Compressor Rotor Performance Map
 with Increased Tip Clearance



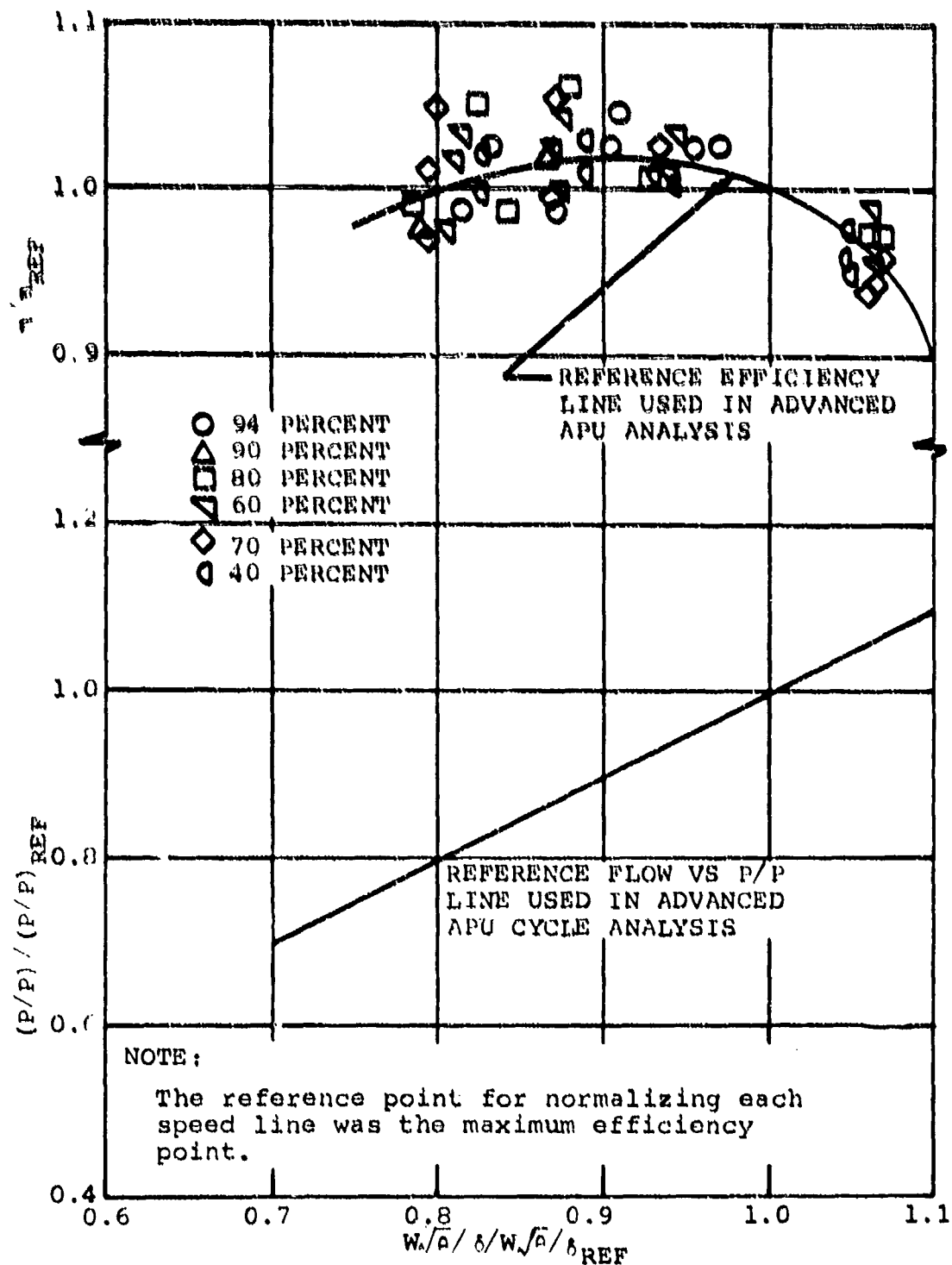


Figure 28. Axial Compressor Stage VIGV Effects.

The following -3 rotor characteristics evolved:

(a) Rotor tip speed (corrected, ft/sec)	1590
(b) Inlet hub-tip ratio	0.5
(c) Rotor tip solidity	1.297
(d) Number of rotor blades	24
(e) Rotor aspect ratio	1.26

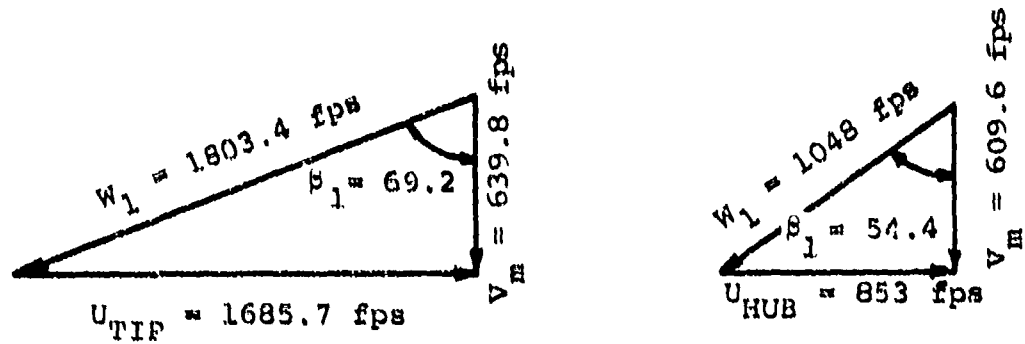
The rotor was scaled from a NASA design [1]*. A portion approximately 3 percent) of the tip was removed to achieve the correct flow at the APU design speed. The aspect ratio was altered to maintain a minimum chord length of 0.8 in. for manufacturing accuracy. The design-point vector diagrams for the rotor are shown in Figure 29 and the diagrams for the stator in Figure 30.

The stator system design for the -3 rotor (Figure 31) incorporated a swept stator followed by a rectilinear stator. The tandem stator concept evolved from two considerations:

- (a) Due to the high stator hub Mach number, a conventional stator would suffer unusually high losses. "Sweeping" the blade would reduce the loss, since the loss is proportional to the Mach number normal to vane leading edge.
- (b) The sweep effect on the hub wall boundary layer was advantageous. Sweeping the blade rearward from hub to tip with approximately constant cross-span loading caused a static pressure gradient on the vane that decreased radially outward. This pressure gradient provided a driving force on the hub wall boundary layer, causing it to migrate across the vane away from the hub. This would provide a hub wall with reduced boundary layer at the rectilinear stator inlet.

*Elevated numbers refer to List of References following Section XI.

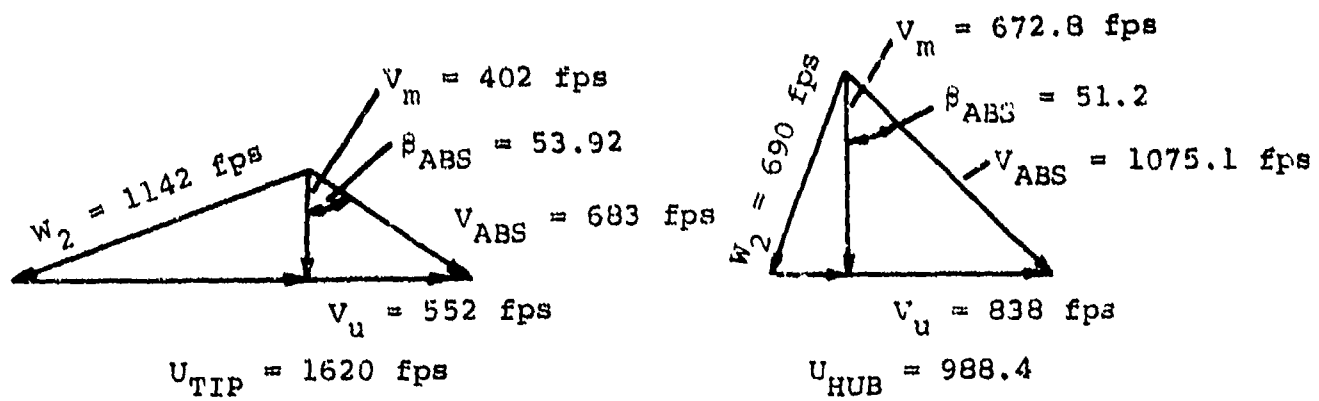
ROTOR LEADING EDGE



TIP

HUB

ROTOR TRAILING EDGE

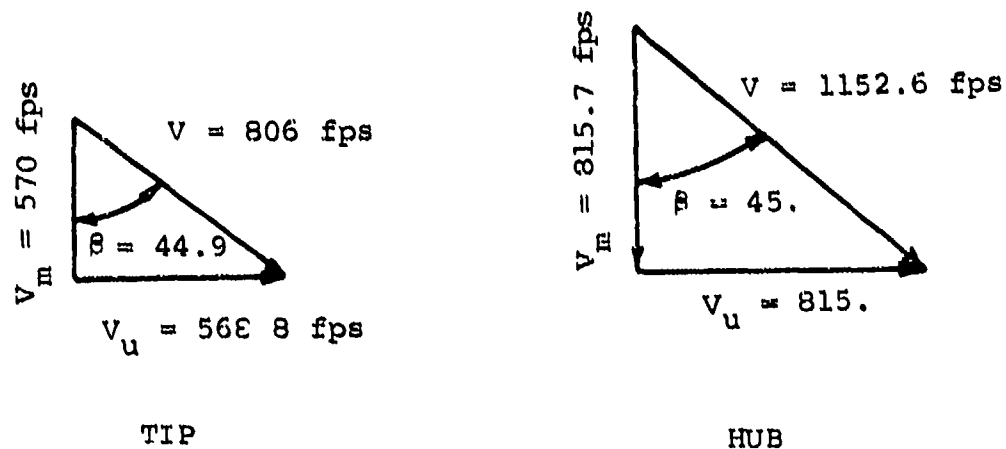


TIP

HUB

Figure 29. Axial (-3) Compressor Stage.

SWEPT STATOR INLET



SWEPT STATOR EXIT RECTILINEAR STATOR INLET

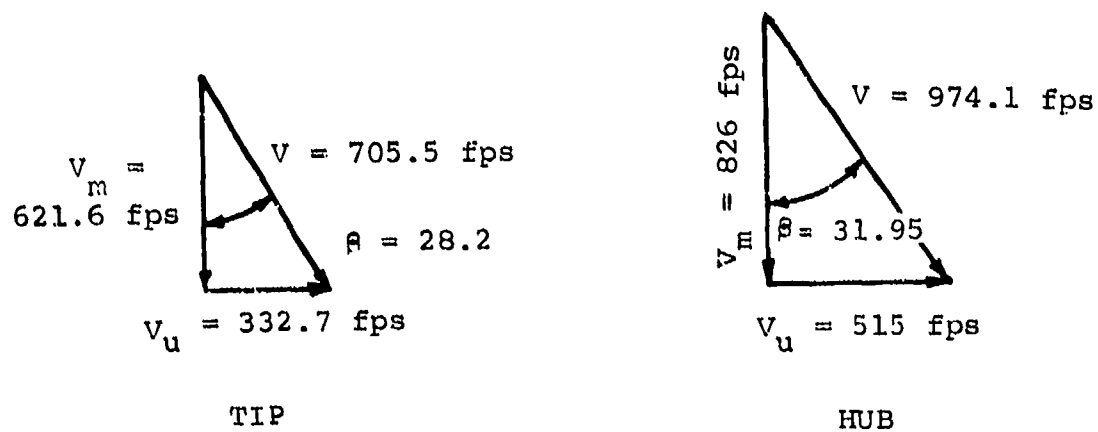


Figure 30. Axial (-3) Compressor Stage.

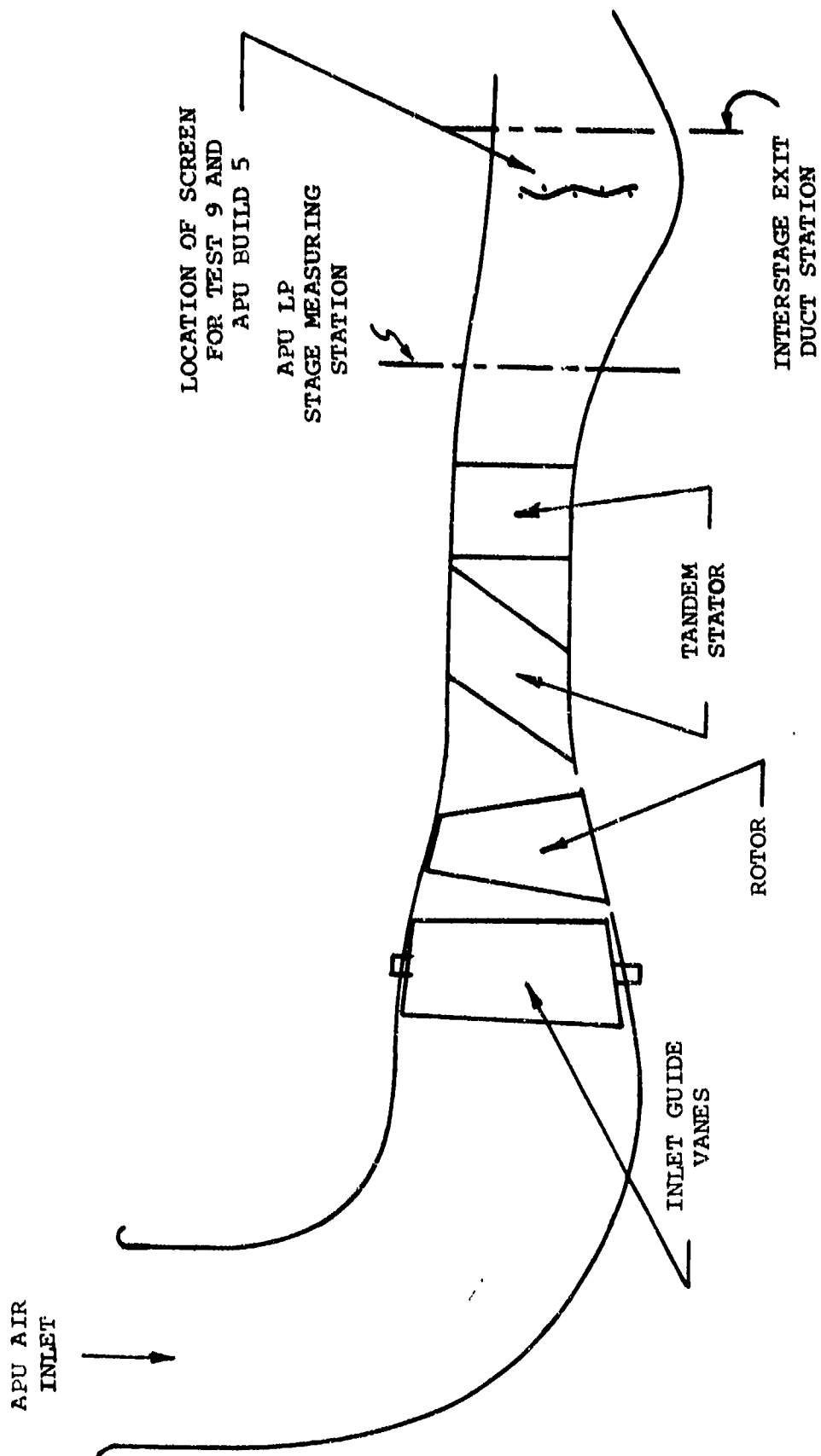
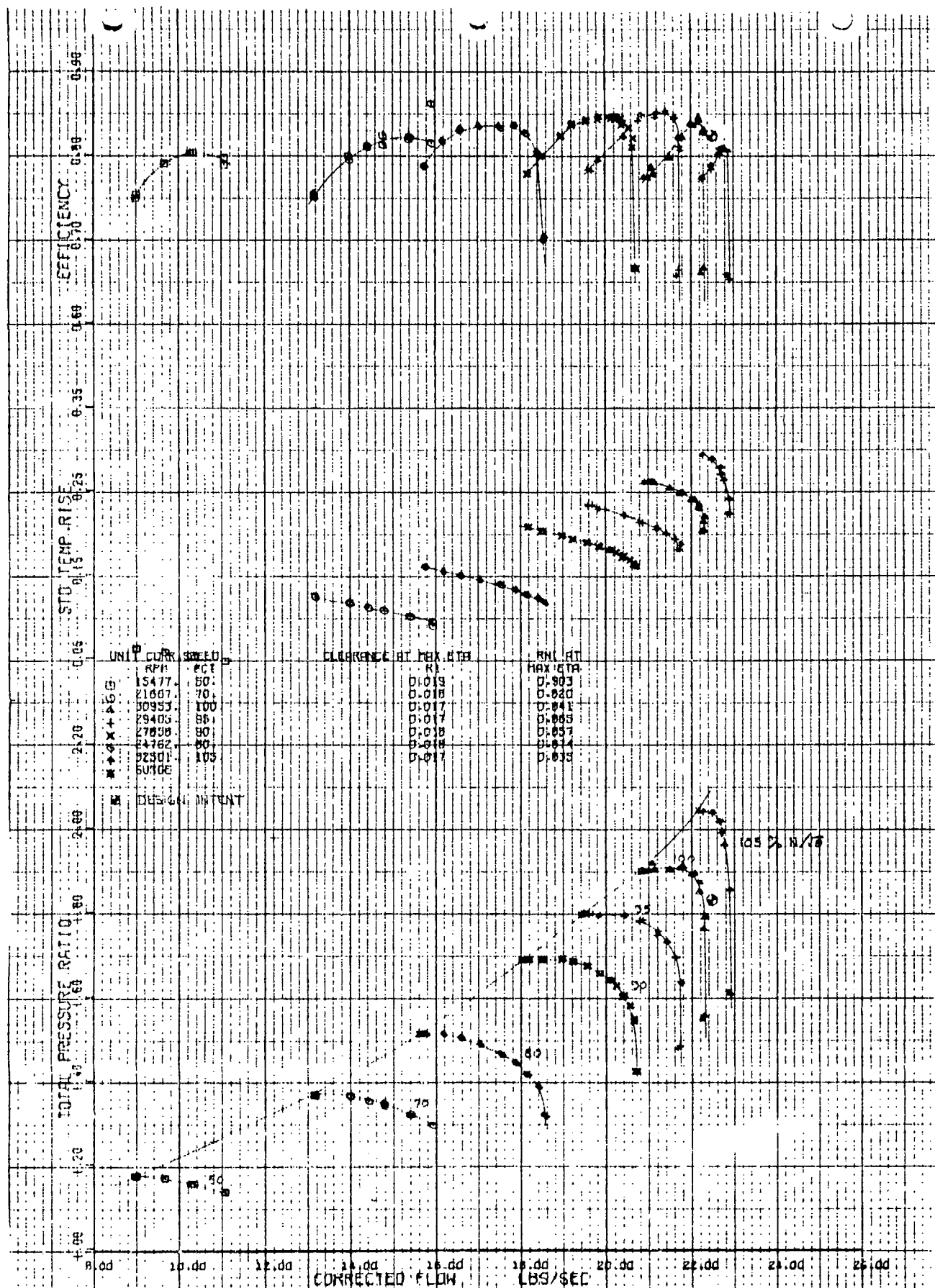


Figure 31. Axial Compressor Stage Flowpath.

Four tests were conducted with this configuration in the reference size as summarized below:

- (a) Test 7 - This test included the entire -3 stage from the inlet to the high-pressure compressor inlet station. (The inlet guide vanes were not available for this or subsequent tests.) The range from choke to surge flow (Figure 32) exceeded the design estimate by 1 percent, while the peak adiabatic efficiency at design-corrected speed and work-input conditions was 0.84, compared to the APU-size design estimate of 0.826. Corrected-flow at the design work input was 2 percent below the estimated value. Instrumentation at the high-pressure-compressor-inlet station indicated that a separated flow region existing in the lower 20 percent of the passage (Figure 33). An average residual swirl angle of 5 percent was measured.
- (b) Test 8 - This was a test of the rotor and swept stator only. The data revealed that the performance characteristics for the rotor and swept stator were very close to design intent at the design-corrected speed and work input. A large wake was measured in the upper 10 percent of the passage and was probably caused by either an excessive stator angle of attack or accumulation of the boundary layer that flows across the stator span from hub to shroud. Comparison of these data with the full-stage data showed that a large loss occurred in the lower 10 percent of the rectilinear stator. Review of the results of Tests 7 and 8 resulted in the decision not to make any major changes in the current stage design.
- (c) Test 9 - As the data points (represented by squares in Figure 33 from Test 7), the relative air angle and absolute Mach number did not coincide with the design intent, especially at the hub region. As an interim fix to improve the APU operation, a screen was sized and placed in the core



DTCP 305 REF. LP COMPRESSOR ORIGINAL DTCP 305 FOR SCALE -3 STAGE DESIGN INCLUDING TRANS DUCT
 KKK -3 STAGE * NISSAI PWA SCALED NISSAI COMPRESSOR * SPEC. RATIO=1.5 DESIGN SPEED=10500 RPM
 DTCP 305 * TANDEM STATOR *
 TEST 7
 OVERALL TAPER AVG. 7
 DTCP 305

Figure 12. Axial -3 Compressor Stage Performance Map.

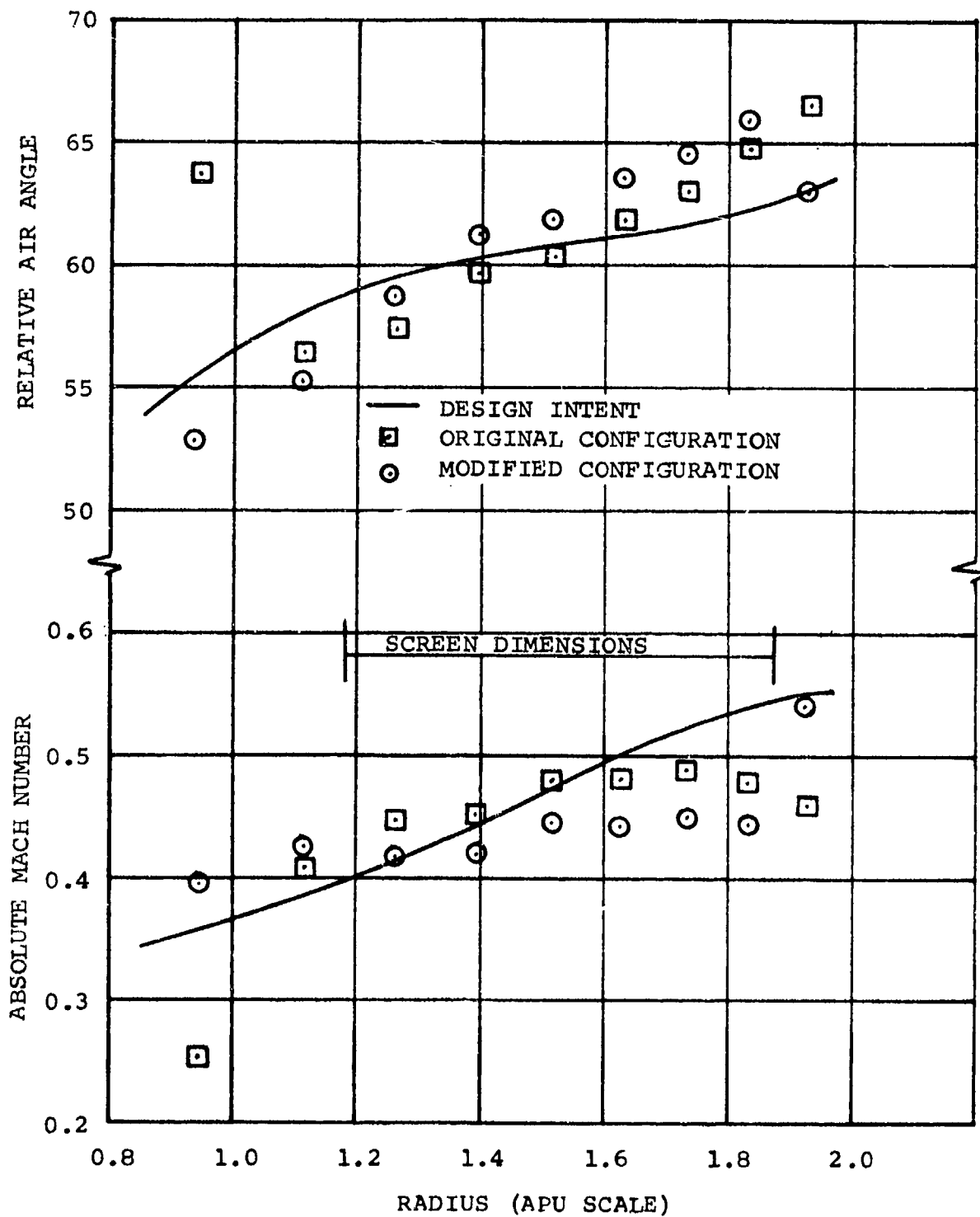


Figure 33. Centrifugal Compressor Inlet Flow Distribution Comparison.

of the annular flow passage 9.45 in. upstream from the centrifugal compressor inducer (Figure 31). The solidity and annular dimensions were based on Morgan's test data^[2]:

$$(T/S)(2.0 - T/S) = 0.30$$

where:

T = wire thickness

S = center-to-center spacing

Corresponding to this, the dynamic loss coefficient was

$$\Delta P / (1/2 \rho V^2) = 0.4$$

where:

ΔP = screen pressure loss, lb/ft²

ρ = mass density, slug/ft³

V = velocity, ft/sec

from Figure 5 of Reference 2. Test 9 on the reference rig showed that the addition of the screen added approximately 2-percent pressure loss and eliminated the flow separation at the hub region. The shroud velocity was raised to design intent. However, the cross-passage, relative air-angle distribution remained similar to that without the screen.

- (d) Test 10 - This test evaluated the effect of a boundary-layer fence on the swept stator. (The screen was installed downstream.) The objective was to force the cross-span flow of the boundary layer to be dumped at mid-stream rather than accumulating in the shroud region. However, no change in cross-passage pressure profile was observed.

Compressor performance measurements in the APU were kept to a minimum to minimize the detrimental effects of the instrumentation on APU performance. The measured performance of Builds 1, 2, and 3 indicated that the efficiency levels of the -1 compressor were considerably

less than anticipated. Operation of the APU at its design-corrected speed was not possible, due to insufficient axial compressor flow range at the design-corrected speed.

In Build 4, which utilized the -3 configuration, the low-pressure compressor exhibited considerably better performance than the previous builds with the -1 configuration. The improved flow range, which was exhibited by the reference-size stage, was evident. However, the data from the Build 5 tests did not reflect this performance improvement. Due to minimal instrumentation, the problem was not able to be adequately diagnosed.

1.2 Mechanical Wheel Design Analysis

The 1590-ft/sec tip speed of the first-stage axial compressor allows a choice of materials for added strength. The selection was a titanium alloy (6Al-4V). While this material exhibits more than adequate strength for the application, it was chosen because of its relatively light weight, which allows a maximum first-bending critical speed.

1.2.1 Stress and Life Analyses

The calculated tangential and radial stresses in the rotor are:

(a) Maximum tangential stress, ksi	63,300
(b) Maximum radial stress, ksi	43,000
(c) Average tangential stress, ksi	21,700

The burst speed and its margin of safety are determined by the following calculations:

$$N_B = N_{OP} \left(\frac{0.08 \sigma_{ult}}{\sigma_{avg}} \right) = 175,000 \text{ rpm}$$

where:

N_B = Burst speed

N_{OP} = Operating speed

σ_{ult} = Material ultimate strength

σ_{avg} = Average stress

$$\text{Margin of Safety} = \frac{(\text{Min-Burst Speed}) - (\text{Design Speed})}{(\text{Design Speed})} = 114\%$$

Figure 34 shows the calculated tangential stress distribution in the rotor.

The maximum material temperature is estimated as less than 200°F. The material strength at this temperature is more than sufficient to maintain adequate burst margin and stress-rupture life. For forged titanium (6Al-4V), the ultimate tensile strength required for 125-percent speed at 200°F is 80 ksi. The typical material ultimate strength is 145 ksi, and the stress rupture-life attains 710,000 hr.

1.2.2 Blade Vibration Analysis

Figure 35 is a Campbell Interference Diagram showing computed blade frequencies and possible sources of excitation. Possible problem areas could result from interference between the blade first-natural frequency and a 3-rev excitation source. (These 1-, 2-, and 3-rev excitation sources generally result from aerodynamic distortions in the gas flow.) Although no other regions of interference are apparent, analytical predictions of the higher blade frequencies are difficult, and it is possible that other interference regions do exist.

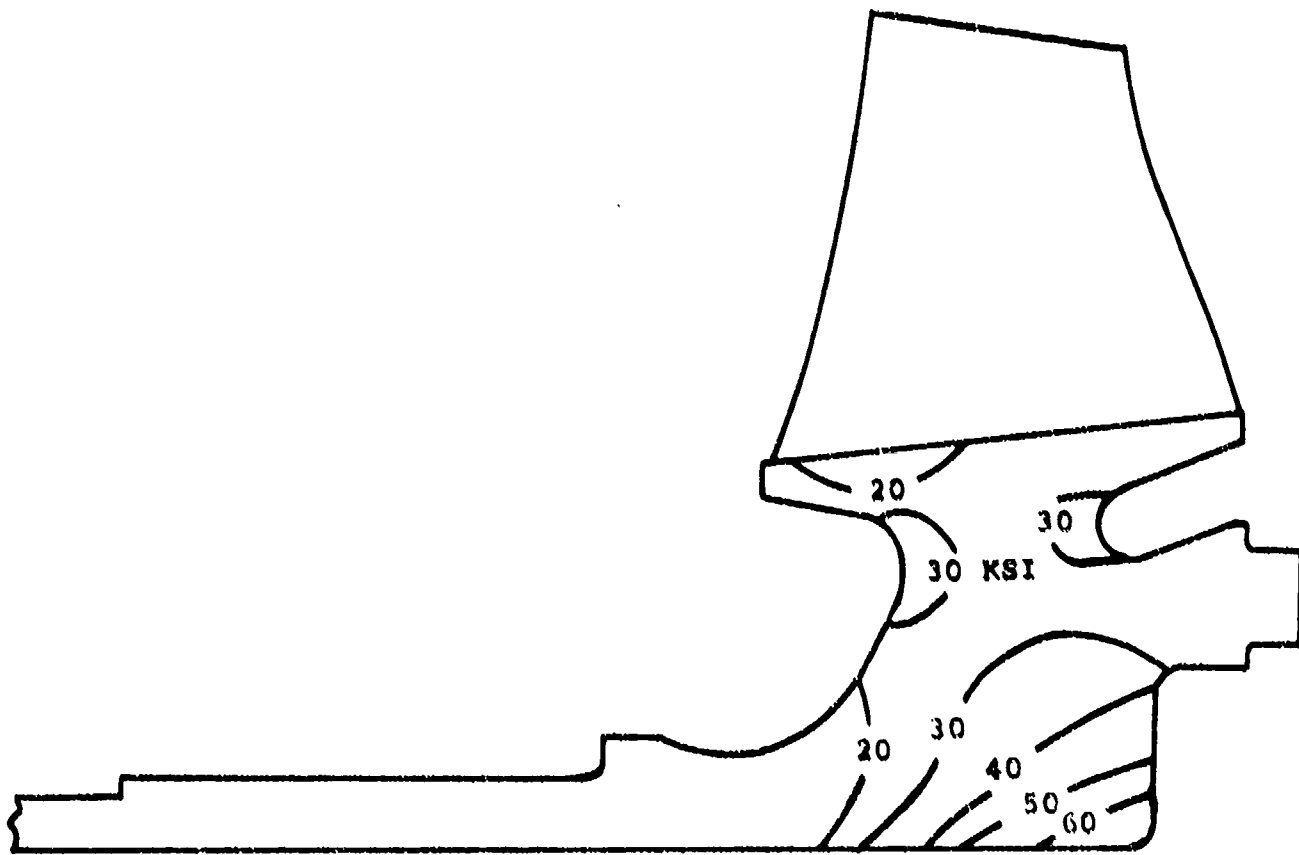


Figure 34. Tangential Stress Distribution of GTCP305 Axial Compressor.

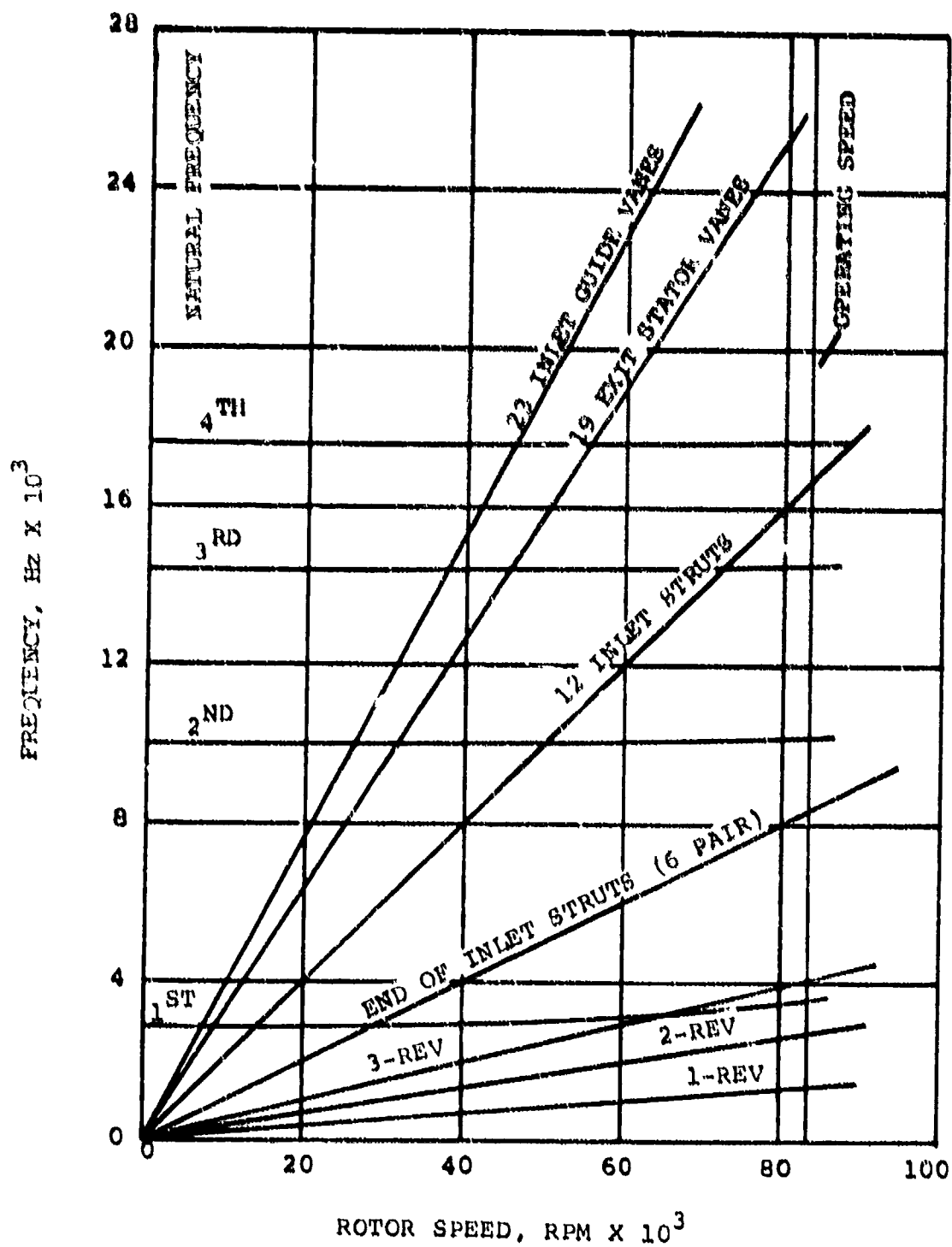


Figure 35. Axial Compressor Stage Interference Diagram.

If the vibratory fatigue problems occur in engine operation, strain-gauge tests will be required to determine the source and magnitude of interference.

2. RADIAL COMPRESSOR STAGE

2.1 Aerodynamic Design and Development

The split-flow radial compressor is a new concept. To test the feasibility and to partially map the characteristics of this compressor, 6:1 pressure ratio centrifugal compressor wheel was notched (Figure 36) and tested. Both stages used the APU diffuser designs (vaneless in the bleed diffuser and second-stage radial-axial tandem vanes the the centrifugal stage). Testing was limited due to mechanical difficulties, but some useful data were obtained (Figure 37).

When the through-flow resistance was held constant and the bleed flow downstream resistance increased (similar to APU operation), the flow rate pressure ratio and efficiency on the through-flow side decreased slightly (Figure 37) from Point B to A (a bypass ratio of 0.247) to wide-open bleed conditions at Point B (a bypass ratio of 0.487). With the bleed valve wide open, the through-flow speed line was mapped by varying the flow from surge Point C (bypass ratio of 0.552) to choke conditions at Point D (bypass ratio of 0.432). In this instance, the bleed-flow and pressure ratio decreased slightly, with an accompanying increase in efficiency. Mechanical difficulties with the rig prevented the acquisition of a full map. The sizing of the notch was based on an analysis of data taken from the split-flow impeller tests. The vector diagrams for the centrifugal wheel are shown in Figure 38.

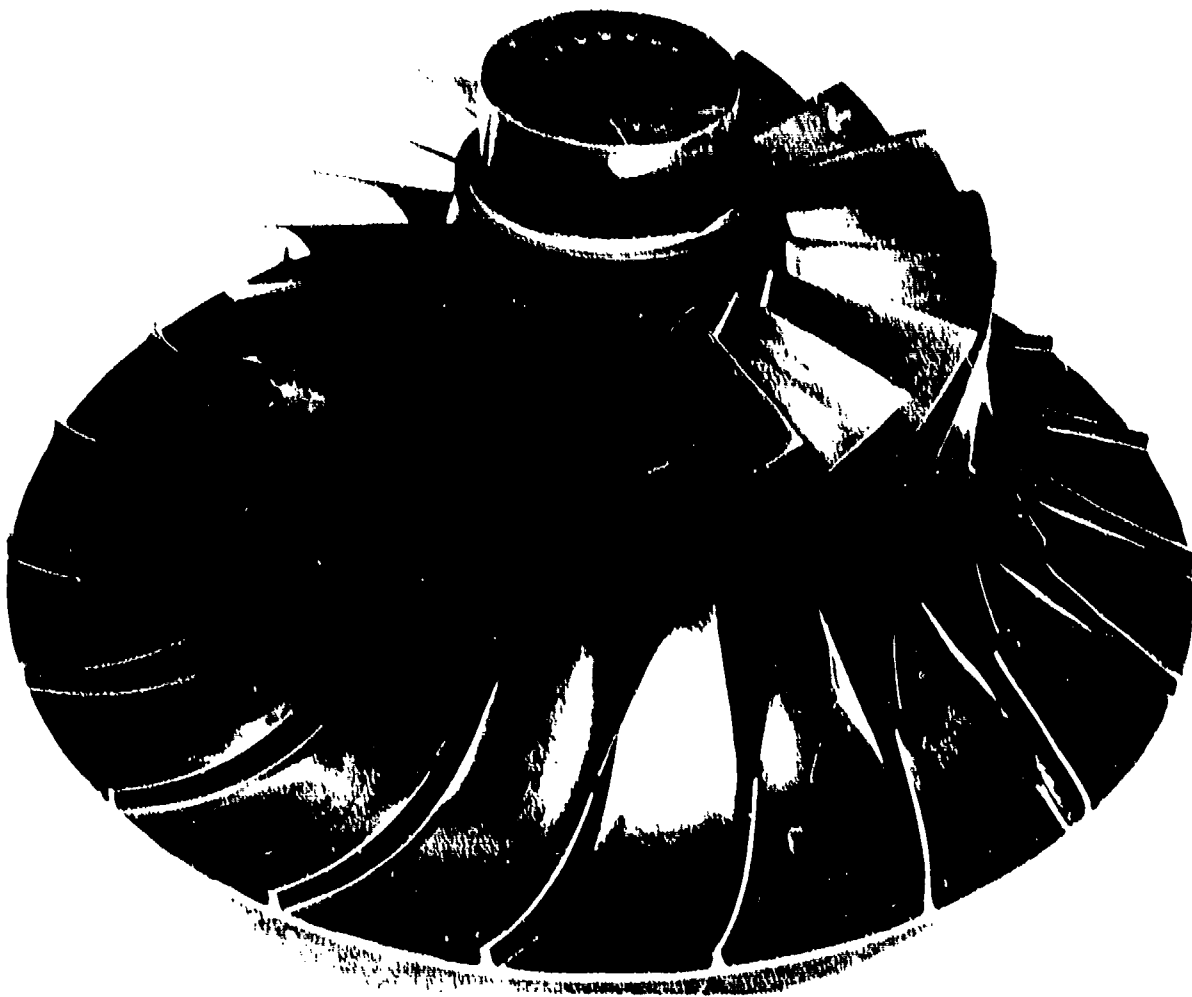


Figure 36. Reference Centrifugal Compressor.

NOTE: Corrected-speed is 102 percent of APU design

- = Design point
- = Constant bleed-flow resistance
- △ = Constant throughflow resistance

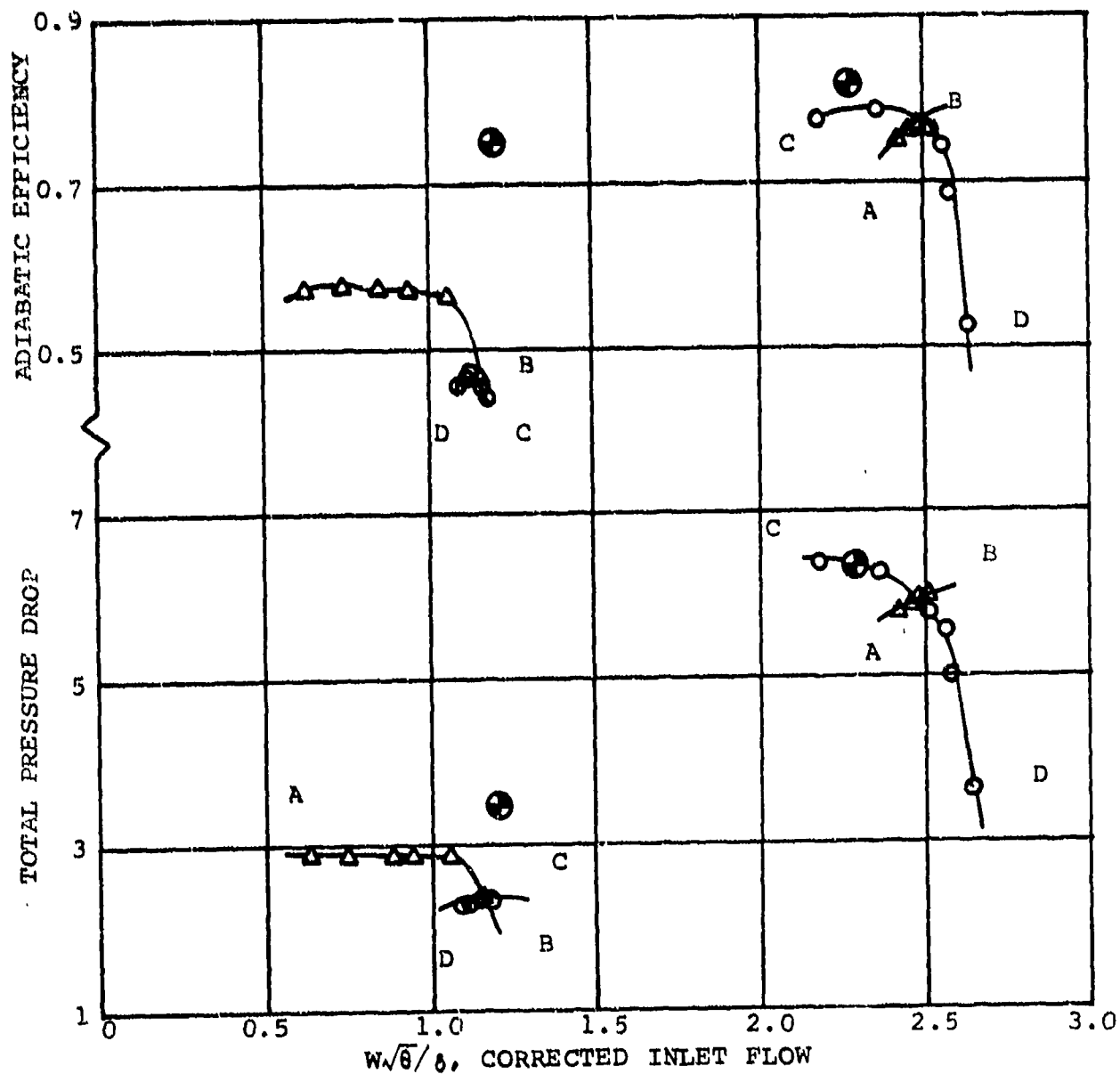


Figure 37. Reference Notched Impeller Test Results.

INDUCER LEADING EDGE

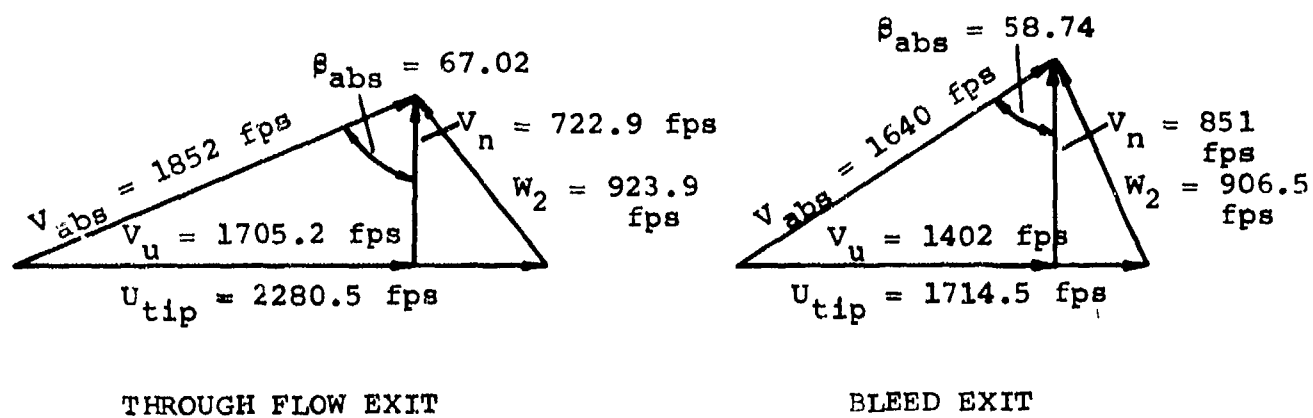
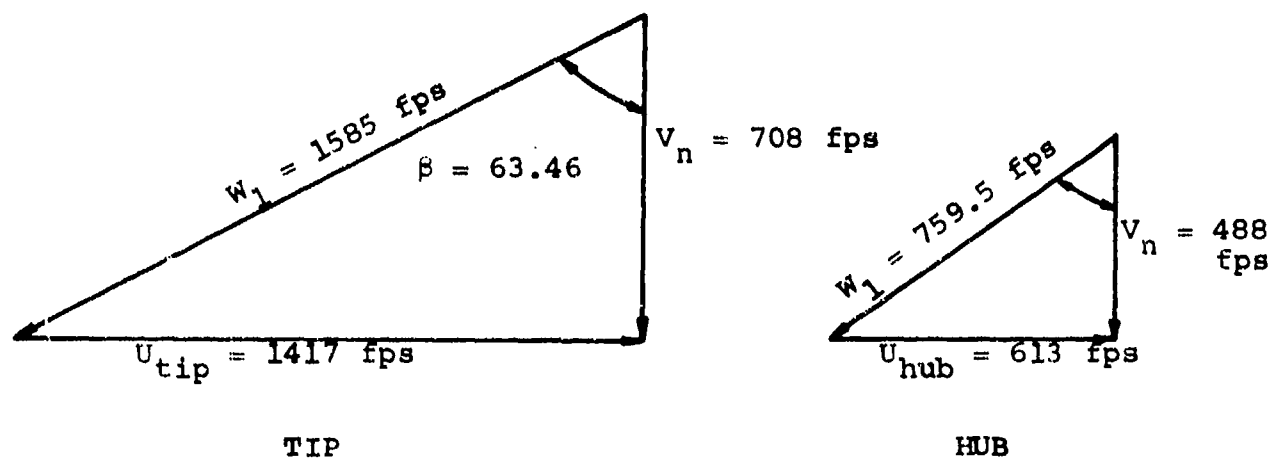


Figure 38. Centrifugal Compressor Vector Triangles of Inducer Leading Edge.

2.1.1 Rotor Aerodynamic Design

A preliminary analysis indicated that a scale of an existing AiResearch 6:1 pressure ratio stage with a cutback leading edge would allow passage of the design-point flow. However, rig tests proved otherwise, and the APU scale radial compressor incorporated a recontoured shroud that increased the flow 10 percent.

2.1.2 Through-flow Diffuser Design

Due to size limitations in the radial direction, a two-stage (radial-axial) diffuser design was required. The first-stage (radial) diffuser employed current design diffusion rates with somewhat less static pressure recovery than normal. The remaining diffusion was accomplished with an axial cascade. The vector diagrams for the diffuser are shown in Figure 39.

A 27-vane radial diffuser design was selected to achieve the maximum static pressure rise without severely limiting the surge margin.

2.1.3 Bleed Passage Diffuser Design

Due to the large variation in impeller bleed exit air angle from the design bleed condition to minimum bypass ratio and the high absolute exit Mach number, a vaneless diffuser design was chosen. This alleviated the incidence angle variation that would occur on a vaned diffuser.

2.1.4 Rig Tests

The design flow and pressure ratio were achieved on the through-flow side, but the efficiency was 3.5 percentage points low. On the

DIFFUSER LEADING EDGE

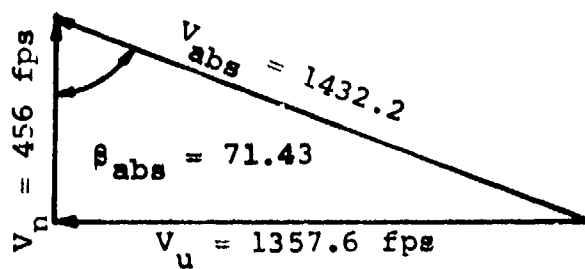


Figure 39. Centrifugal Compressor Vector Triangles of Diffuser Leading Edge.

bleed side, the maximum flow was approximately 3 percent low, the maximum pressure ratio and the maximum efficiency were 15 and 17 percent, respectively, lower than design. This was apparently due to a choking condition, with associated high losses in the vaneless space bleed-diffuser.

The overall requirements of the compressor stage at design-point operation required that each portion of the APU centrifugal compressor be designed for the following stage conditions:

	<u>Bleed-Flow Portion</u>	<u>Through-Flow Portion</u>
Total pressure ratio	3.440	6.39
Corrected flow, lb/sec	0.7618	1.4818
Total-to-total efficiency	0.75	0.8218

For these design requirements, the following impeller (19 blades) geometry evolved:

Tip diameter, in.	
Bleed flow side	4.765
Engine flow side	6.337
Inducer tip diameter, in.	3.942
Inducer hub diameter, in.	1.704
Blade width at tip, in.	
Bleed flow side	0.070
Engine flow side	0.129
Impeller exit	
Absolute flow angle (engine flow), deg	67.78
Blade angle, deg	
Blade flow side	58.75
Engine flow side	35.00

- (a) Test 7 - This test was on the unnotched wheel to measure impeller exit flow conditions at the design-corrected flow and speed. These measured quantities were used to establish loss, deviation, and blockage. The impeller notch was then designed to the analytical model.
- (b) Test 9 - This test was an evaluation of the unnotched rotor, with the 27-vane radial diffuser installed. The favorable efficiency and flow range characteristics of this configuration established the selection of this through-flow diffuser design (Figure 40).
- (c) Test 10 - This test was an evaluation of the inlet guide vanes and the impeller and diffuser from Test 9. Results were inconclusive, due to failure of the diffuser vanes.
- (d) Test 11b - A repeat of Test 7 with the impeller trailing edges cut to print. A gain of approximately 1 efficiency-point was realized at design speed and flow.
- (e) Test 13 - This was a test of the split-flow compressor similar to that designed for the APU. (The shroud was not recontoured to pass the additional 10-percent flow required by the APU.) A minimum bypass ratio (BPR) of 0.25 was achieved. A through-flow efficiency of 0.782 at the design pressure ratio of 6.39 was measured and compared to the design goal of 0.8218. The peak bleed-port efficiency at design speed was 0.58 compared to the design goal of 0.75. This poor recovery was attributed to a strong flow separation in the vaneless diffuser space. Failure of the flow splitter caused early termination of this test.

EFFICIENCY

TEMPERATURE RISE

PRESSURE RATIO

CORRECTED SPEED	AXIAL CLEARANCE
KRPM	AT PEAK EFF.
PC1	
58000	100 0.0131
54080	102 0.0117
55350	105 0.0100
50350	95 0.0123
47700	90 0.0095
42400	80 0.0134
31800	60 0.0104
21200	40 0.0193
10600	20 0.0186
21200	40 0.0184
47700	90 0.0095
58000	100 0.0108
51080	102 0.0102
58350	110 0.0097
50350	115 0.0081

INLET TEMPERATURE
12.5 ATPOPMEL

CORRECTED FLOW (BOLLHOUS) LBS/SEC

ADV. REV. REF. RADIAL
COMPRESSOR RISE 36-111
27 VANE SHORT DIFFUSER
TEST 9
FIRST STAGE

ROTOR 771372553 5/4 101
TEST DATE 24 JUNE 1971
PERFORMANCE FROM CALIBRATION 7-173
FIGURE 1-3-4

Figure 40. Centrifugal Compressor Performance Map.

2.1.5 Engine Performance

Following is a summary of the radial compressor performance from APU Builds 1 and 2:

- (a) The bypass ratio at which stall occurred was approximately 0.33 rather than 0.25, as determined from the reference rig tests.
- (b) The bleed pressure ratio was lower than design. This was attributed to a high-pressure loss in the vaneless diffuser.
- (c) The APU pressure ratio was lower than expected. This was attributed to either an oversized turbine nozzle, blockage of the radial compressor by the variable inlet guide vanes, excessive turbine nozzle bypass air (calculated as cooling airflow), or a choked diffuser for the through-flow portion.
- (d) The second-stage VIGVs were not required. (Variations of guide-vane position did not improve the performance.)
- (e) The maximum bleed-flow obtainable decreased as APU speed was increased above approximately 90 percent of the design-corrected speed. This occurred with no throttling of the bleed port.

In an effort to overcome these deficiencies, the following changes were incorporated into Build 3:

- (a) The second-stage VIGVs were eliminated.
- (b) The bleed diffuser forward wall was recontoured to increase the diffuser width.

- (c) The high-pressure compressor radial diffuser passage width was increased about 5 percent, and the compressor wheel blade height was increased 0.025 in.

These modifications resulted in marked improvement in the radial compressor performance, but the bleed-flow rate still exhibited a drop-off at about the same corrected speed.

In Build 4 (the first build utilizing the -3 low-pressure compressor stage), the bleed passage was again recontoured to increase the vaneless diffuser passage width. The radial wheel was also modified at the bleed exit to decrease running clearance.

Serious difficulties were encountered with the radial compressor in Build 4 testing. Above approximately 67,000 rpm, the through-flow compressor efficiency dropped sharply. At 77,000 rpm, the total-to-total efficiency was approximately 0.58.

Two possibilities existed: (1) A flow separation existed in the hub region of the interstage duct, and (2) There was poor distribution of flow within the impeller. The flow separation (distortion) could cause high incidence losses in the inducer region, while the oversized bleed discharge diffuser could cause the impaired flow.

Based on discussions concerning the above points, two changes were made for Build 5:

- (a) A screen was designed to remove the separated-flow condition at the hub and improve the inducer incidence angles.
- (b) The bleed diffuser passage was recontoured to the configuration used in Build 3.

The combination of changes improved the radial compressor performance sufficiently to allow self-sustaining operation at 93-percent corrected APU speed. Both sides of the high-pressure compressor were approximately three efficiency percentage points below the peak values measured on Build 3 and the reference scale rig.

2.2 Mechanical Wheel Design Analysis

The high tip speed (2260 ft/sec) and temperature (700°F) requirements of the radial compressor resulted in the selection of 6Al-25Ni-4Zr-2Mo titanium as the wheel material. Unlike the axial compressor, the high-pressure ratio of the second stage resulted in operating temperatures sufficiently high to cause creep; therefore, the higher rupture strength alloy was chosen.

2.2.1 Stress and Life Analyses

The calculated tangential and radial stresses for the impeller are:

(a) Maximum tangential stress, psi	85,340
(b) Maximum radial stress, psi	74,750
(c) Average tangential stress, psi	38,350

The burst speed and its margin of safety are determined by the following calculations:

$$N_B = N_{OP} \left(\frac{0.8 \sigma_{ult}}{\sigma_{avg}} \right) = 132,000 \text{ rpm}$$

where:

N_B = Burst speed

N_{OP} = Operating speed

σ_{ult} = Material ultimate strength

σ_{avg} = Average stress

$$\text{Margin of Safety} = \frac{(\text{Min-Burst Speed}) - (\text{Design Speed})}{(\text{Design Speed})} = 61\%$$

Figure 41 shows the tangential stress distribution in the impeller. Figure 42 presents the detailed temperature distribution for the analysis. Tensile strength properties of the alloy are shown in Figure 43.

In general, AiResearch designs criteria limit creep to 0.20 percent over the design life of an impeller. Based on an elastic stress analysis and the maximum operating temperatures for a 130°F day (Figure 42), the GTCP305 radial impeller would reach this allowable limit at a local region in the disk bore after 2500 hr. This estimate is conservative in two ways:

- (a) The 2500-hr engine duty cycle contains only about 500 hr of operation at a high ambient temperature condition.
- (b) The elastic assumption allows no creep-relaxation, as could occur. Therefore, because of the conservative nature of the estimate, creep is not expected to be a design problem over the 2500-hr duty-cycle life of the engine.

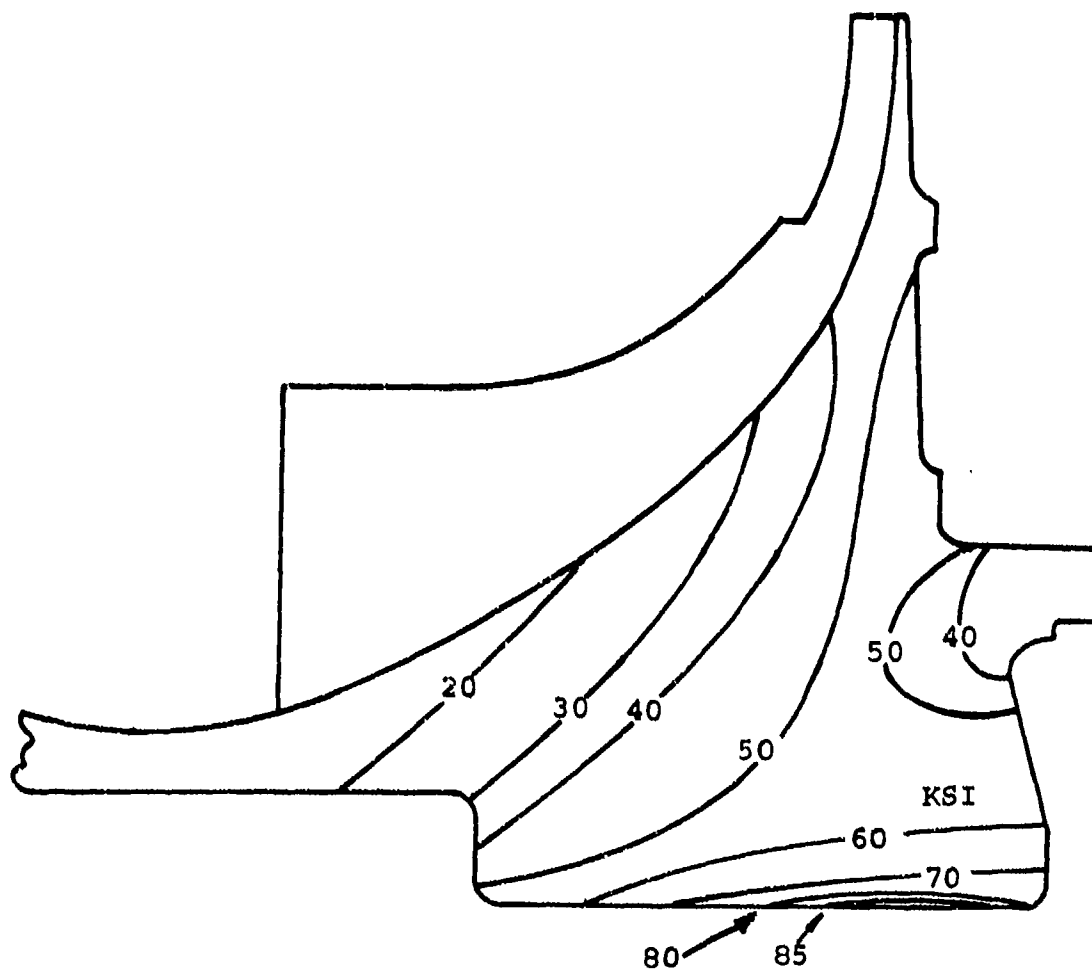


Figure 41. Centrifugal Compressor Tangential Stress Distribution.

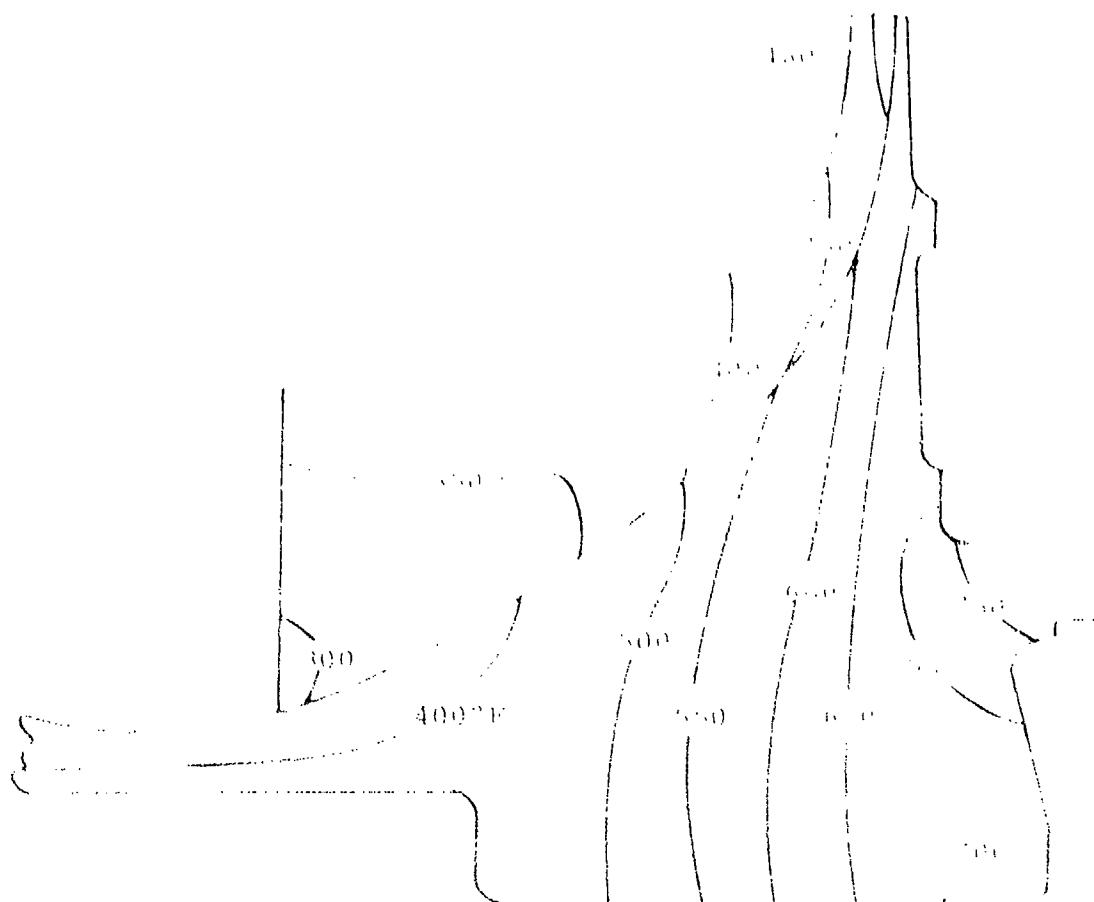


Figure 11. Centrifugal Compressor Distribution.

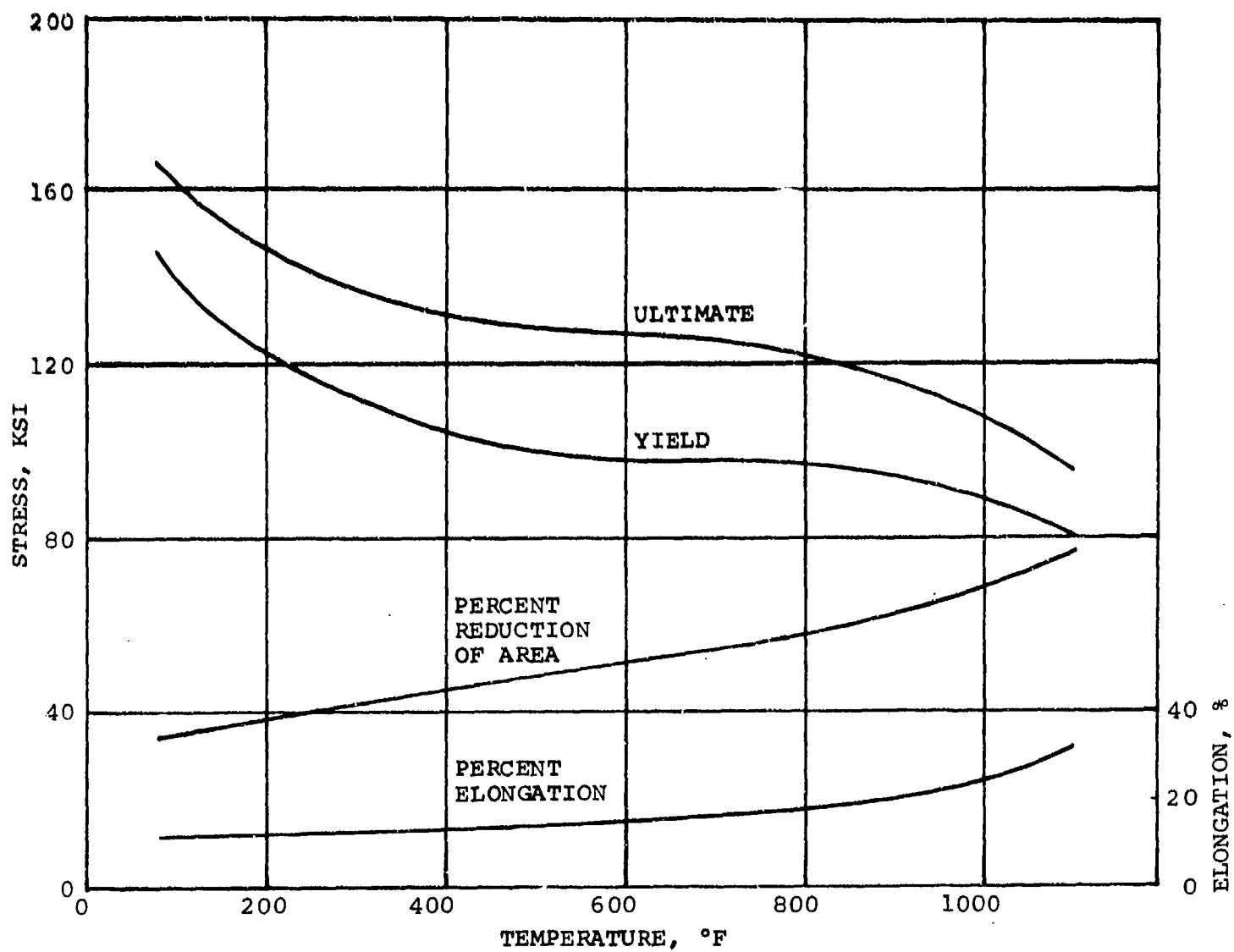


Figure 43. 6Al-25Nb₁-4Zr-2M Titanium Tensile Properties.

Axial deflections (Figure 44) and radial deflections (Figure 45) are shown at various points along the blade shroud line, during an engine start and at steady-state conditions.

2.2.2 Blade Vibration Analysis

Blade resonant frequencies for the radial compressor were experimentally determined by salt-pattern tests on a shake table. Figure 46 shows these frequencies (without centrifugal stiffening effects), possible sources of excitation (due to aerodynamic distortions in the gas flow), and the 19-rev source created by the 19 first-stage stators.

Although possible regions of interference are noted, no conclusions regarding the strength of the source can be ascertained. This information can be determined only by strain-gauge tests on an engine.

2.3 Structural Design Analysis

To ensure that the performance goals of the GTCP305 would be successfully attained, the structures influencing the aerodynamics were necessarily optimized. This required that the bleed diffuser passage width, the blade tip-flow splitter clearance, and the blade tip-shroud clearance be precisely controlled or, at least, a configuration derived that could be optimized during early runs of the engine. These criteria dictated that the design allow the flexibility of axially locating the bleed passage walls; the assembly shown in Figure 47 fulfills this requirement. The flow splitter was axially located by shims at A, to eliminate discontinuities in the diffuser passage at Point B. The shroud was then bolted to the bleed-air plenum with Bolt C, and this assembly machined to a specific contour, as specified by a deflection analysis. The assembly was then bolted to the diffuser structure at D. The operating axial position of the assembly was then determined by shims at E.

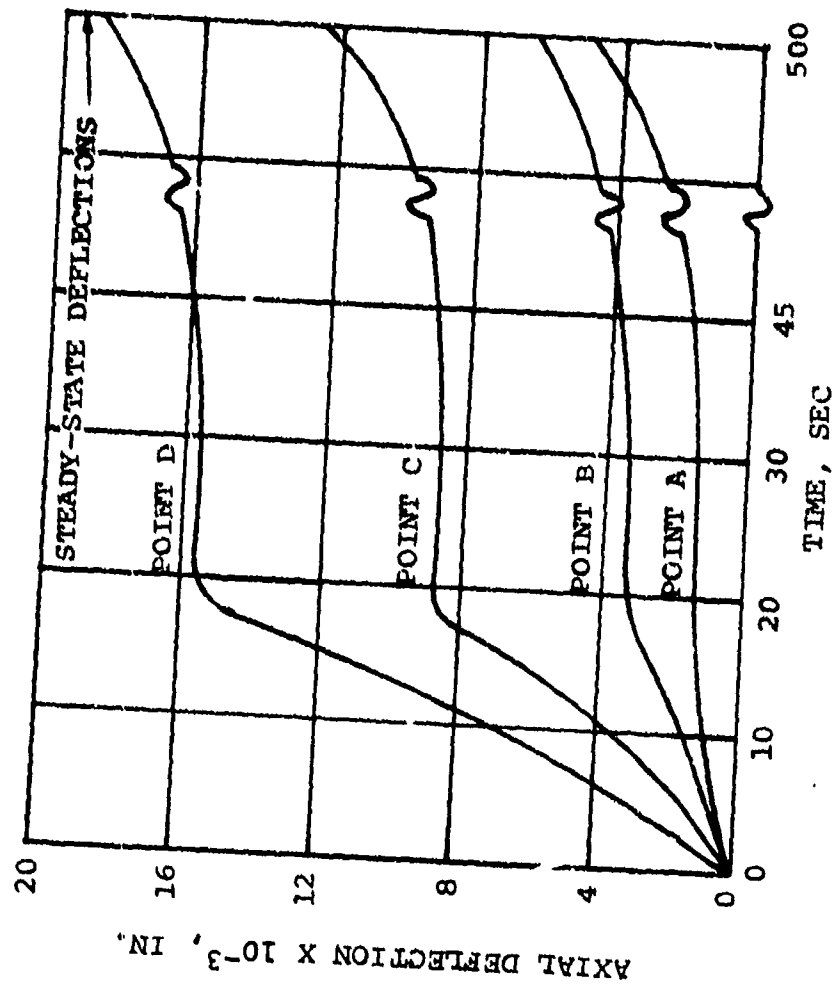
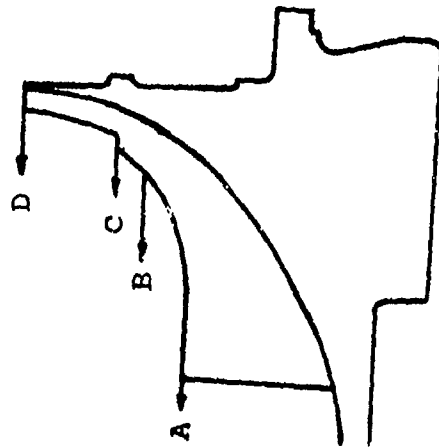


Figure 44. Axial Deflection.



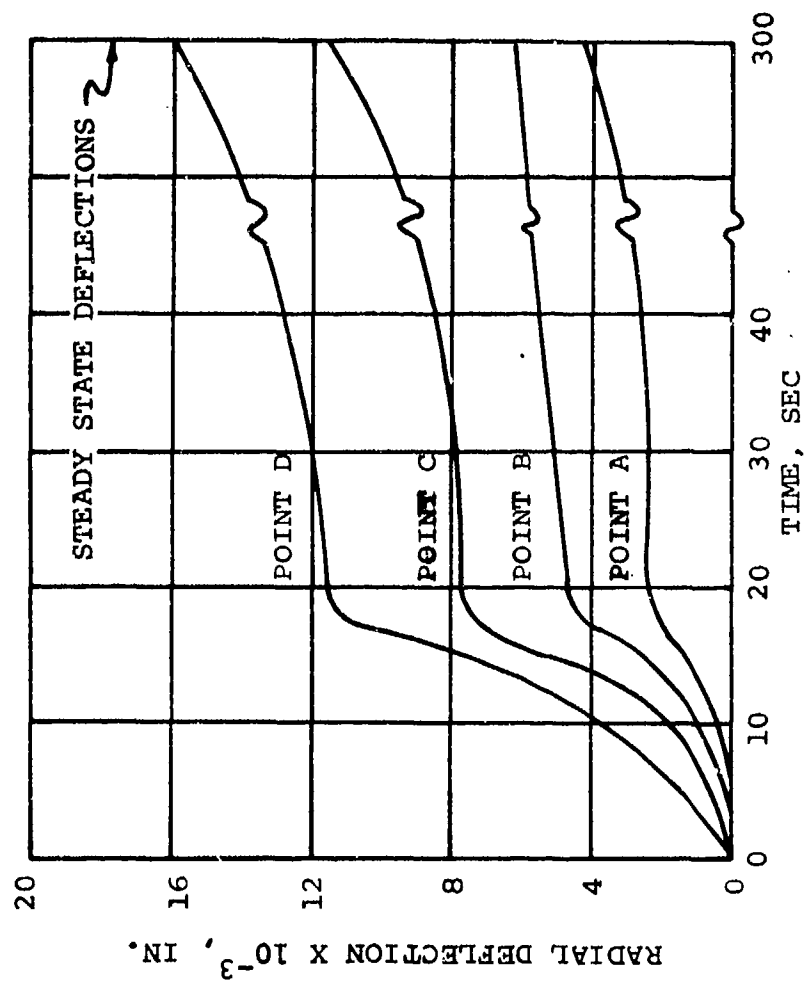
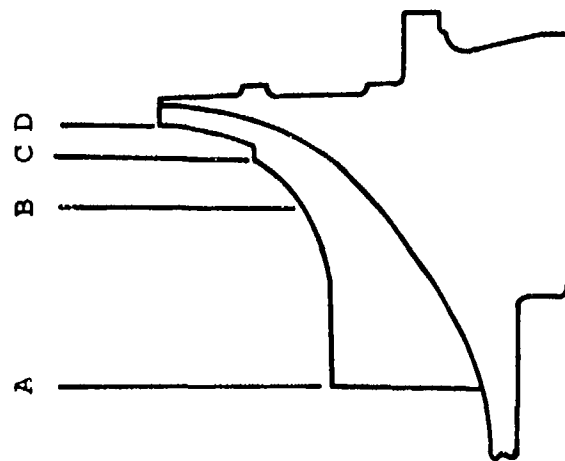


Figure 45. Radial Deflection.



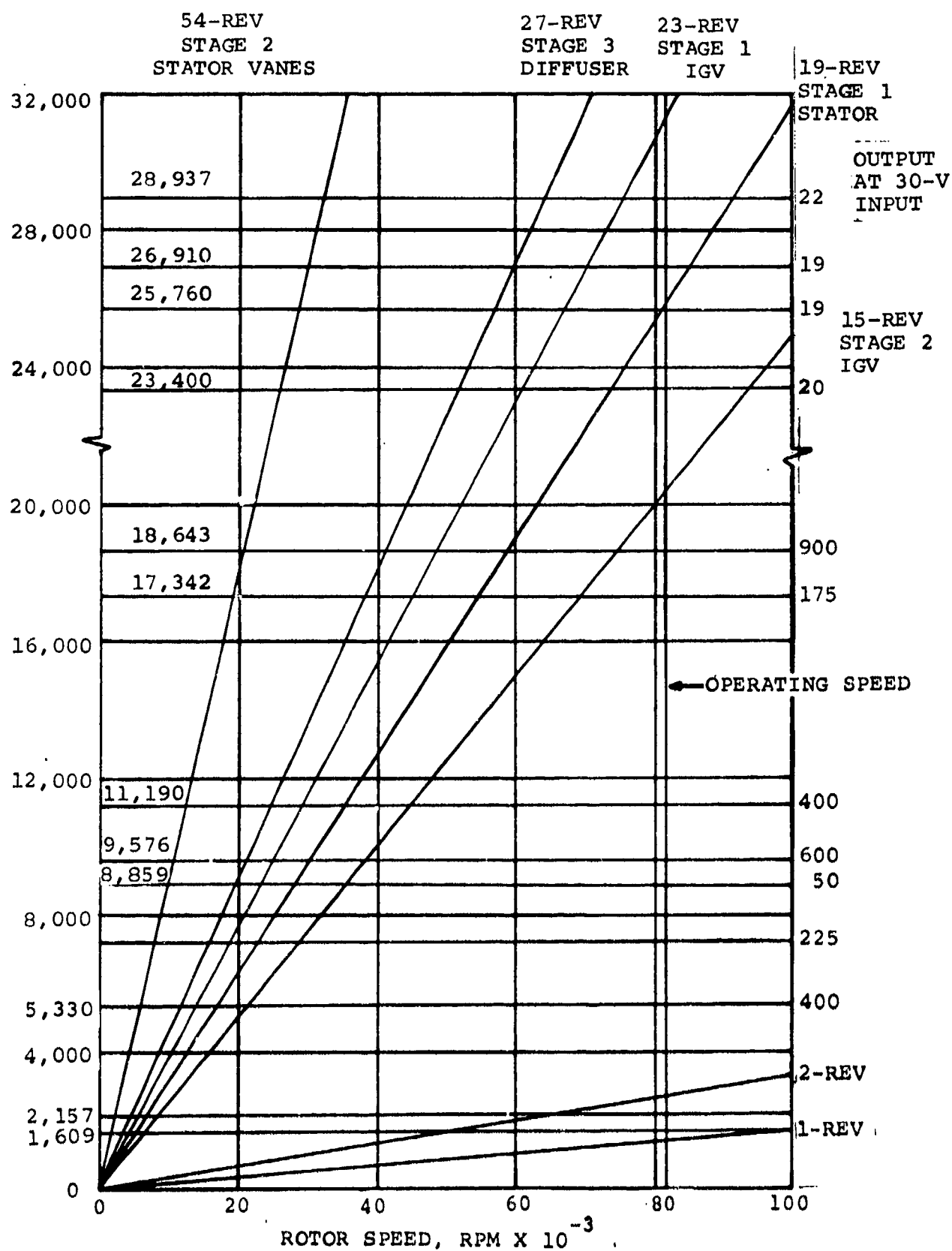


Figure 46. Centrifugal Compressor Interference Diagram.

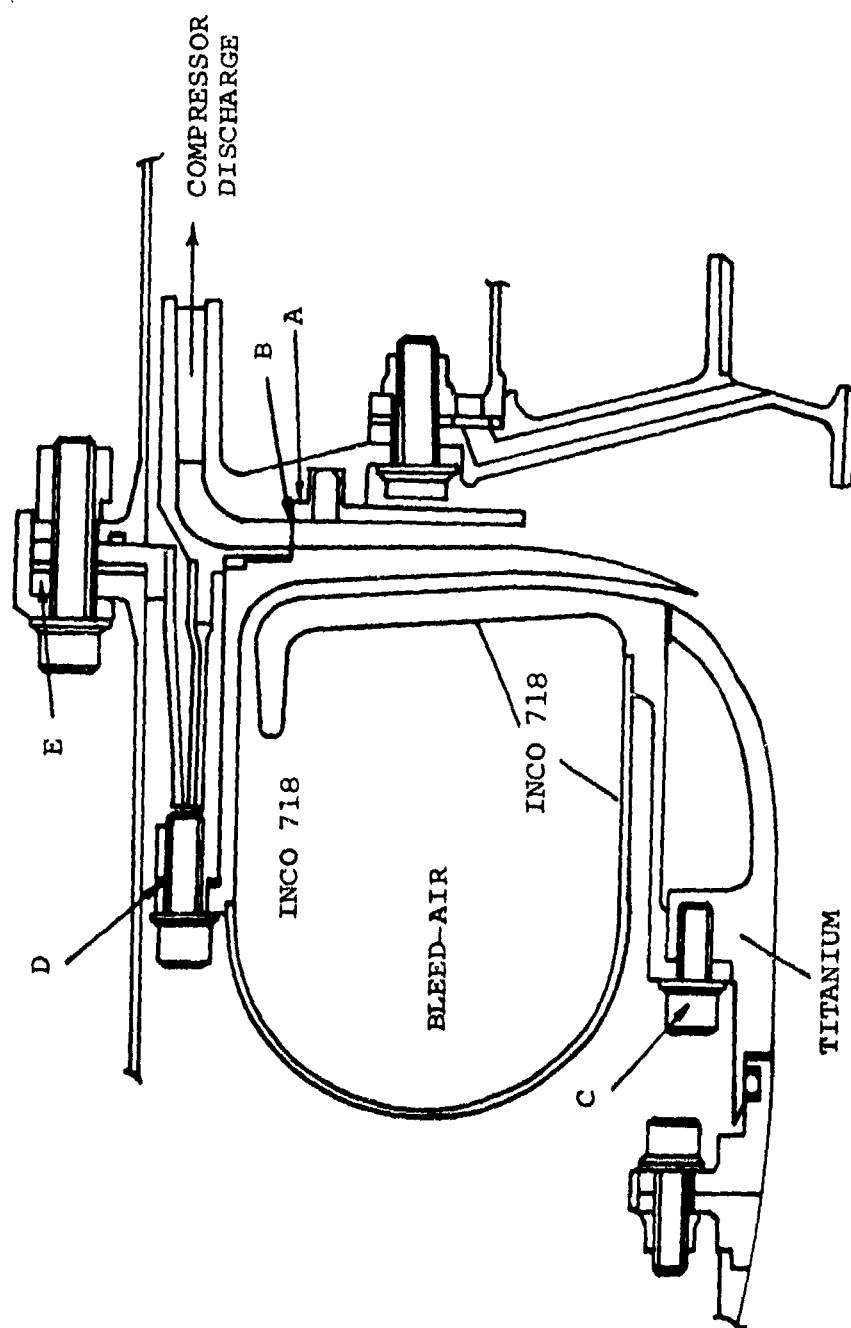


Figure 47. Bleed Plenum, Flow Splitter, and Shroud Assembly.

Throughout this design, the use of shims at strategic locations virtually eliminated tolerance stacking and created a system that is amenable to optimization.

To establish the limitations for the necessary dimensional analysis, a deflection study of the structures was completed, and the results combined with predicted rotor deflections. This analysis was accomplished with an AiResearch digital computer program for thin-walled shells. Predicted steady-state thermal and pressure loads are shown in Figures 48 and 49, respectively.

Predicted stress levels were low, making the design very conservative relative to the high strength INCO 718 used throughout the assembly (Figure 50). This material is justified, however, since it minimizes the design effect of stresses, leaving greater flexibility for the control of deflections. The shroud is the only part of the assembly cut from a dissimilar material--titanium--because the low coefficient of expansion permitted better deflection control.

Minimum blade-tip clearance occurs at the second critical speed during shutdown when the rotor and the structures are still at steady-state temperatures. The radial shroud clearance allows for an estimated 0.0075-in. excursion of the shaft, when passing this critical speed.

Predicted steady-state deflections of the shroud and flow splitter are shown in Figure 51.

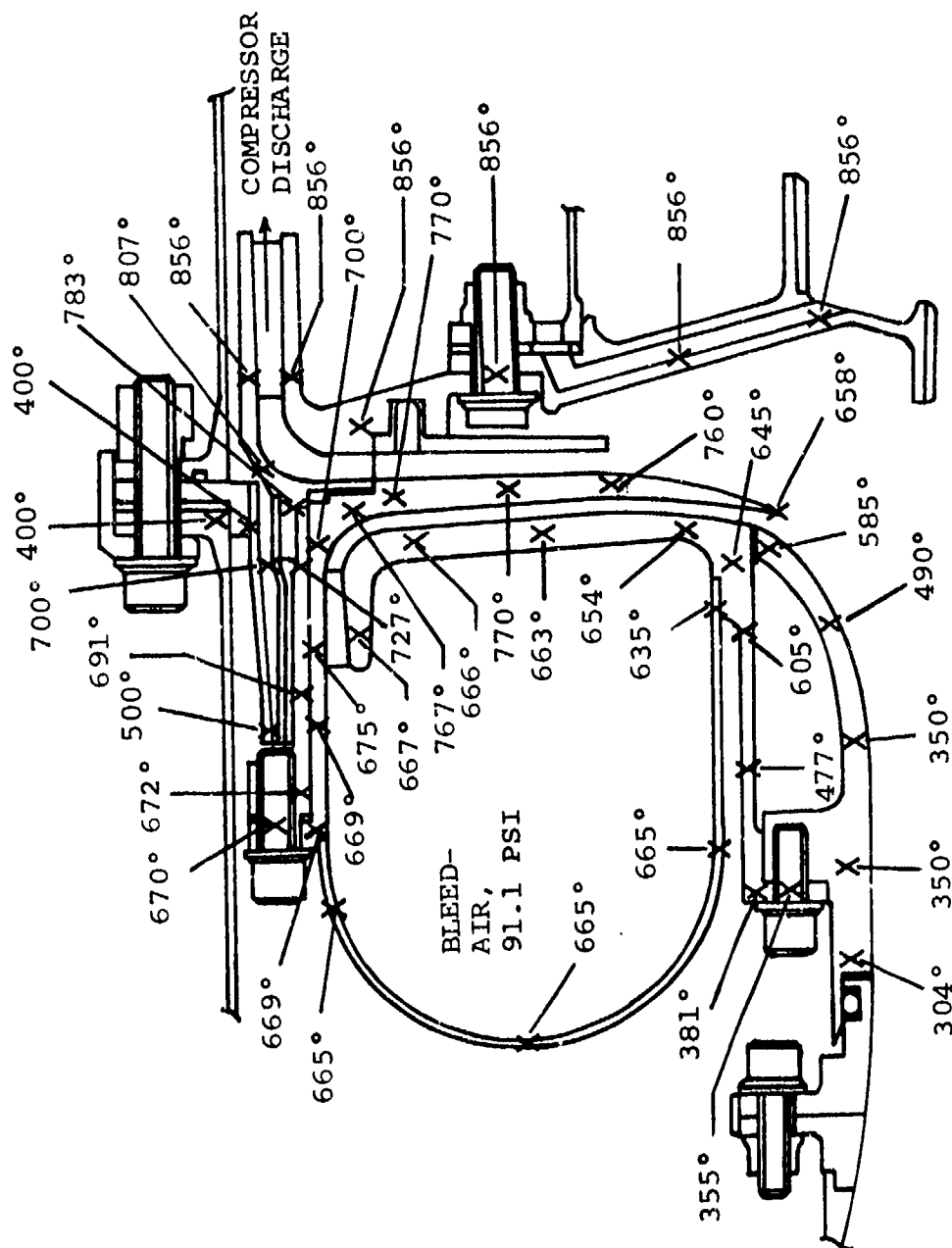


Figure 48. Bleed Plenum, Flow Splitter, and Shroud Assembly Steady-State Temperature Estimates.

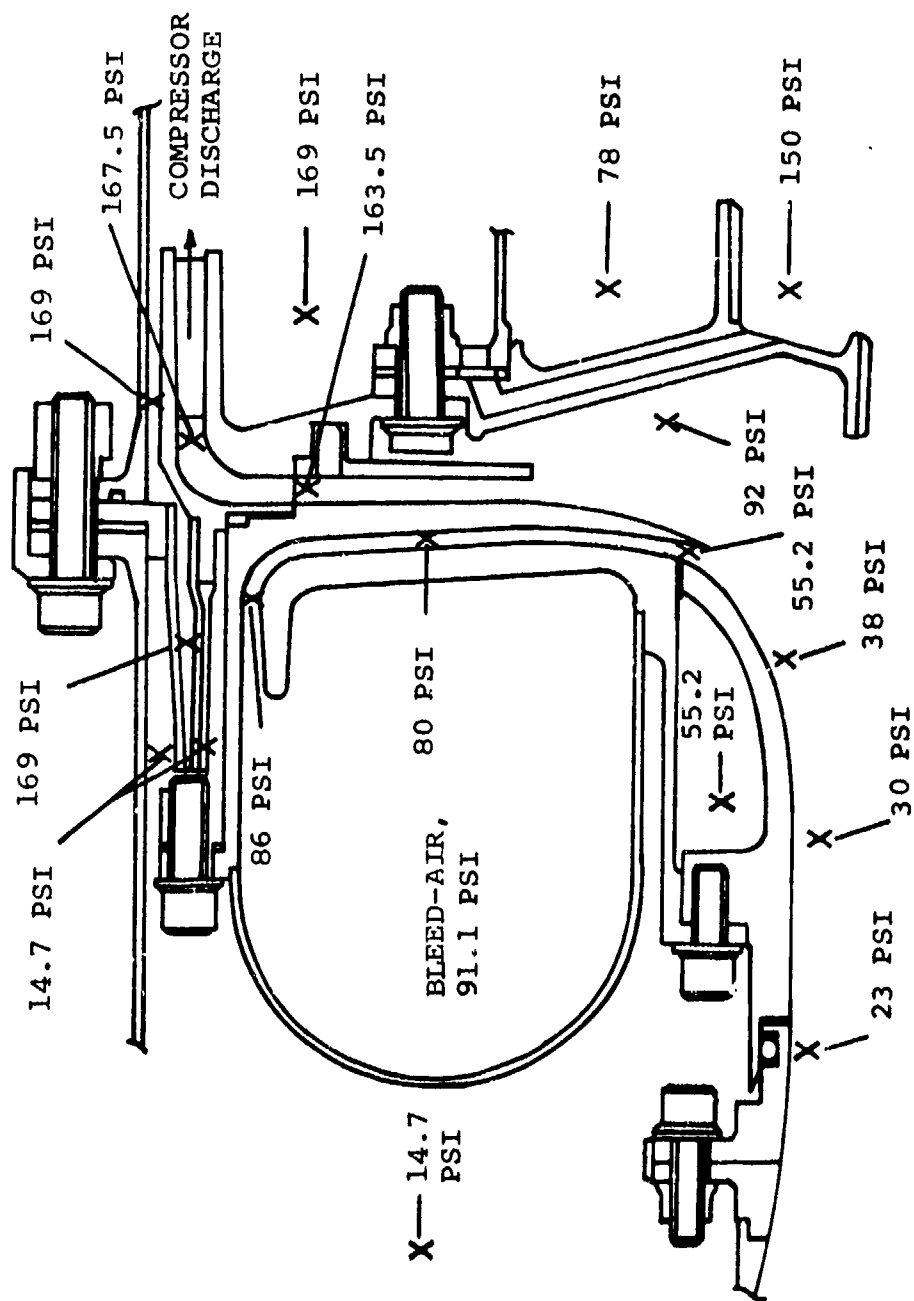


Figure 49. Bleed Plenum, Flow Splitter, and Shroud Assembly
Steady-State Pressure Estimates.

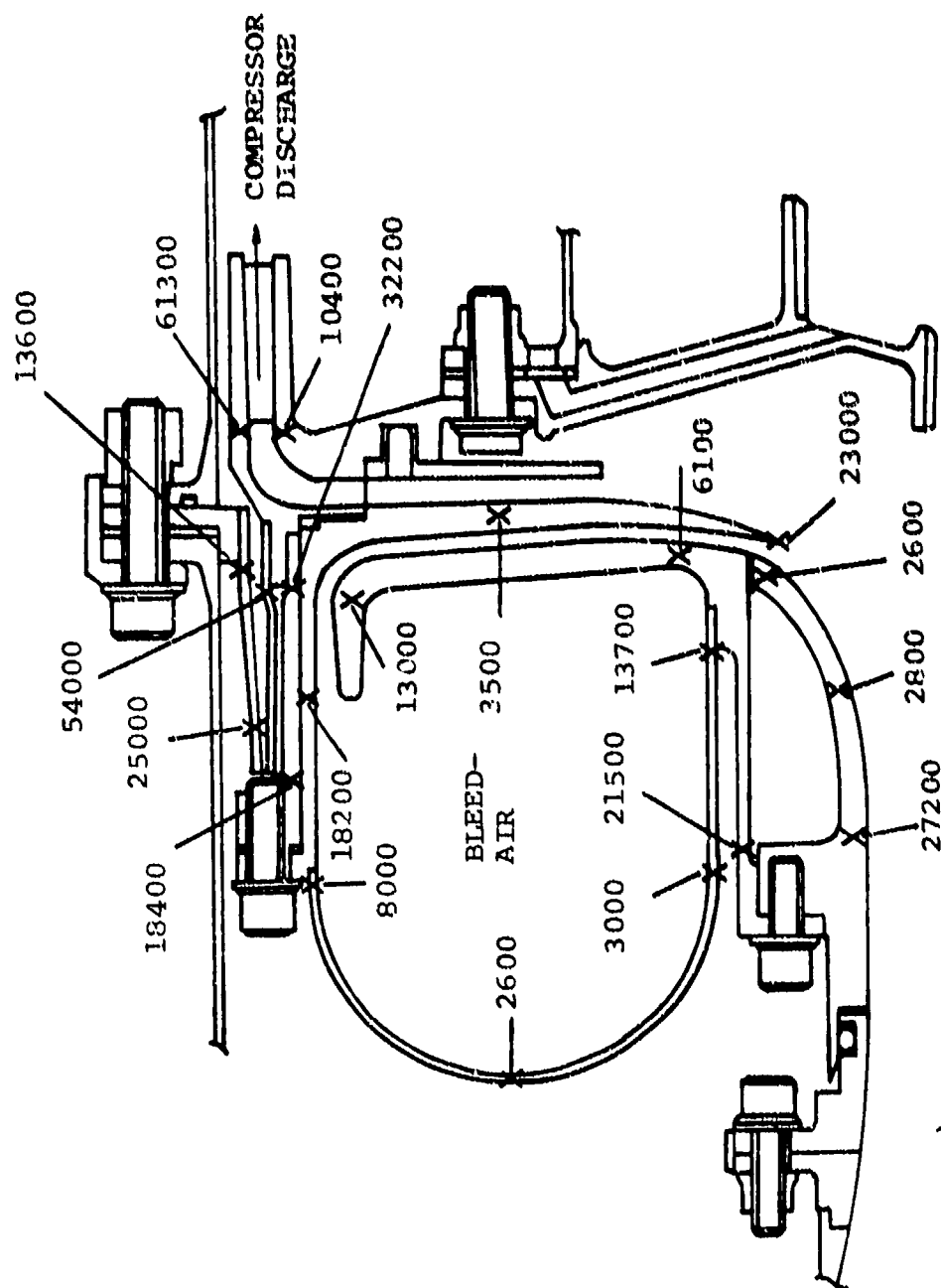


Figure 50. Bleed Plenum, Flow Splitter, and Shroud Assembly
Steady-State Stresses.

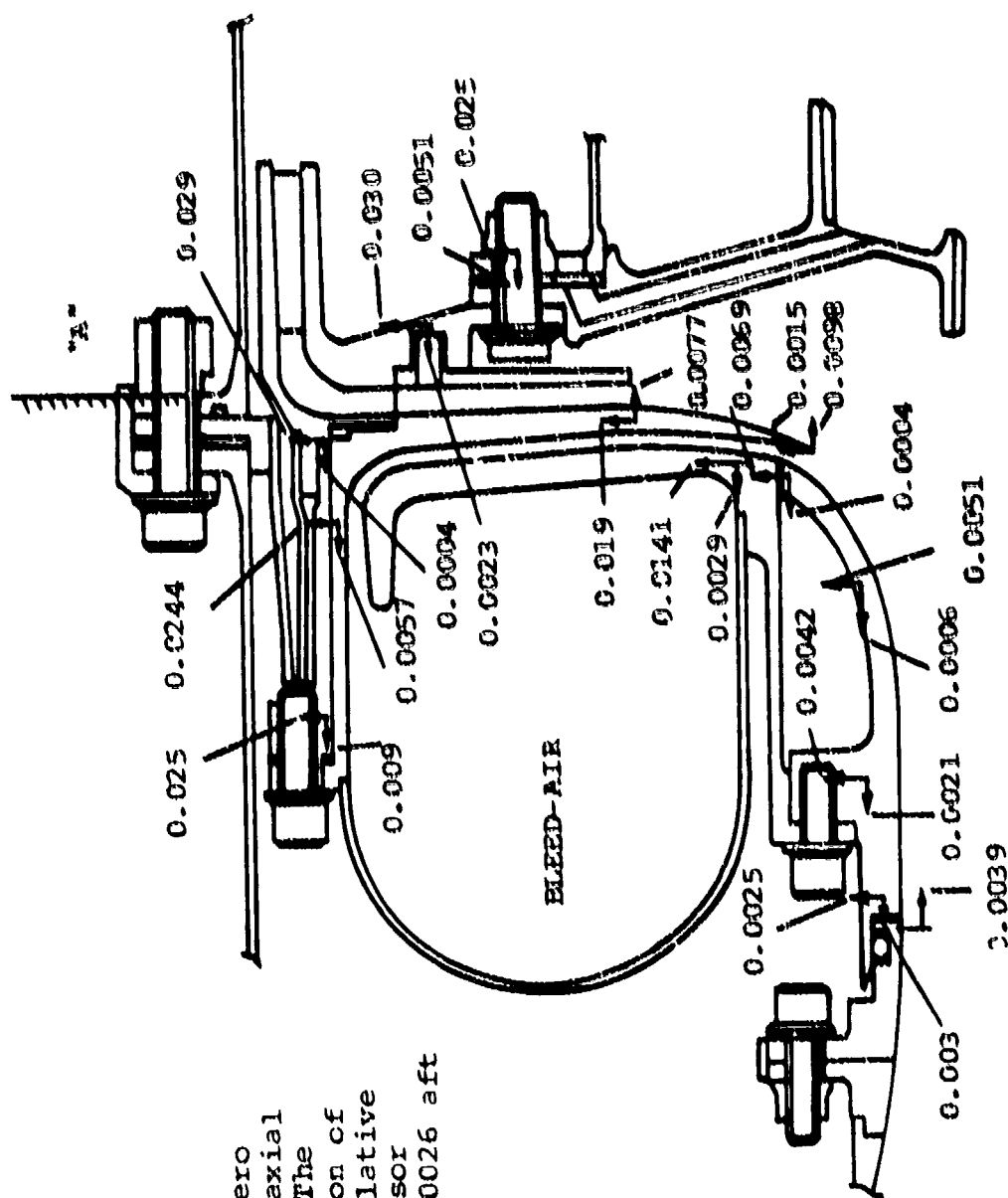


Figure 51. Bleed Plenum, Flow Splitter, and Stator Assembly Steady-State Deflections.

SECTION IV

COMBUSTION SYSTEM DESIGN AND DEVELOPMENT

The trend toward smaller, higher power gas turbines, operating at high turbine inlet temperatures with low airflow, places increasing demands on the combustion system. Usually these requirements are most easily satisfied by a single-can combustor with one atomizer, but unless the combustor can be located on the turbine shaft centerline at the rear of the engine, a plenum to accommodate the can must be added to the engine outline, causing asymmetry of the engine compressor case so that the combustor inlet airflow is distorted. As a result, the development of an alternate combustor type (an annular combustor) was undertaken.

The major technical problems associated with annular combustor development occur when the engine through-flow is low, which poses two problems:

- (a) It has the largest surface area for a given volume, thereby compounding the wall-cooling problem.
- (b) The fuel flow requirement of the multiple injectors is reduced to the point of introducing manufacturing, flow tolerance, and contamination problems associated with small flow passages.

Therefore, the objective was to develop a reverse-flow annular combustor for an advanced-technology low-flow gas turbine. An additional constraint imposed upon the system was a specified turbine inlet temperature spread factor well below state of the art values for annular combustors at a relatively low (3 percent) pressure drop and a volumetric heat release rate of 30×10^6 Btu/hr-ft³.

1. DESIGN OBJECTIVES

The preliminary design objectives established for the combustion system are listed below:

- (a) The maximum engine diameter of 10 in., the maximum airflow velocity into the combustor plenum, and the minimum turbine diameter determined the maximum combustor size.
- (b) Peak turbine inlet temperature was to be 2300° at 2200°F average inlet temperature, which translates into a temperature spread factor (TSF) of 0.074. This indicated a substantial improvement in the state of the art for annular combustor temperature distribution at high exit temperatures.
- (c) Design combustor pressure drop was to be from 3 to 5 percent of inlet total pressure. This further complicated the temperature spread requirement, since increased pressure drop is beneficial to dilution zone mixing.
- (d) The initial combustor was designed for a heat intensity of 5×10^6 Btu/hr/ft³/atm, which represented an increase over production reverse-flow annular combustors. Increased heat intensity also compounded the temperature distribution problem.
- (e) A maximum metal temperature goal of 1600°F was set for the initial design.
- (f) A minimum efficiency of 99 percent at the design-point and 80 percent for the combustor was established at altitude starting conditions.

(g) A design goal of a 1000°F controlled-temperature rise at light-off was established to minimize thermal shock in the turbine components. This corresponds to a fuel-air ratio of approximately 0.014.

(h) An altitude start capability to 40,000 ft was specified.

2. COMPONENT SELECTIONS

2.1 Combustor

Selection of the combustor-type for the GTCP305 was governed primarily by the engine envelope limitations. The short overall length of the engine precluded use of a straight-cylindrical, single-can, or straight-through annular combustor, while a radial first-stage turbine and component arrangement eliminated the possibility of a can-type combustor on the engine shaft centerline. The layout of the engine restricted the combustor to the annular volume around the turbine stages, resulting in a short overall length. Therefore, an annular reverse-flow combustor was selected primarily, because swirl in the dilution zone could be utilized to increase the effective mixing length, thereby improving the temperature distribution at the turbine inlet without contributing to increased engine length.

2.2 Fuel Injection System

A low-pressure fuel injection system was selected for maximum reliability and maintainability. The low-pressure system was least sensitive to fuel contamination and could utilize the least complicated fuel pump and control components.

Seven double-venturi pneumatic injectors, using combustor pressure drop to atomize the fuel, were designed. The double-venturi was to increase the throat velocity above that induced by combustor pressure drop. The increased throat velocity resulted in improved atomization through higher relative velocity difference, hence higher shearing stress between the fuel and air.

2.3 Ignition System

A high-energy, low-voltage, capacitor-discharge ignition unit was chosen as the best compromise between ignition capability and system size and weight. The high energy (4 joule stored) was required for satisfactory light-off at altitude with a small-volume combustion chamber. The low-voltage system was chosen from a minimum weight, maximum reliability standpoint. Such a system requires minimum shielding on the ignition unit and cable to avoid electromagnetic interference problems. A single shunted-surface gap, low-voltage igniter is required for the system.

3. PNEUMATIC INJECTOR DESIGNS

3.1 Combustor

The pneumatic atomizing combustor was sized for a corrected airflow of 0.292 lb/sec at the maximum bleed design-point. The fuel flow at this operating point was 163.5 lb/hr. The design heat-release rate was 5×10^6 Btu/hr-ft³-atm, which determined the combustor volume of 95 in.³. The design efficiency was 98 percent at a total pressure drop of 4 percent, with a minimum efficiency of 80 percent at maximum combustor loading during acceleration; estimated combustor loading during a start cycle is shown in Figure 52. The exit axial Mach number of the combustor was 0.045.

NOTES:

W = Combustor airflow, lb/sec

P = Combustor inlet air pressure, atm

T = Combustor inlet air temperature, °R

A_e = Combustor liner cross section area, ft²

D_e = Combustor liner channel height, ft

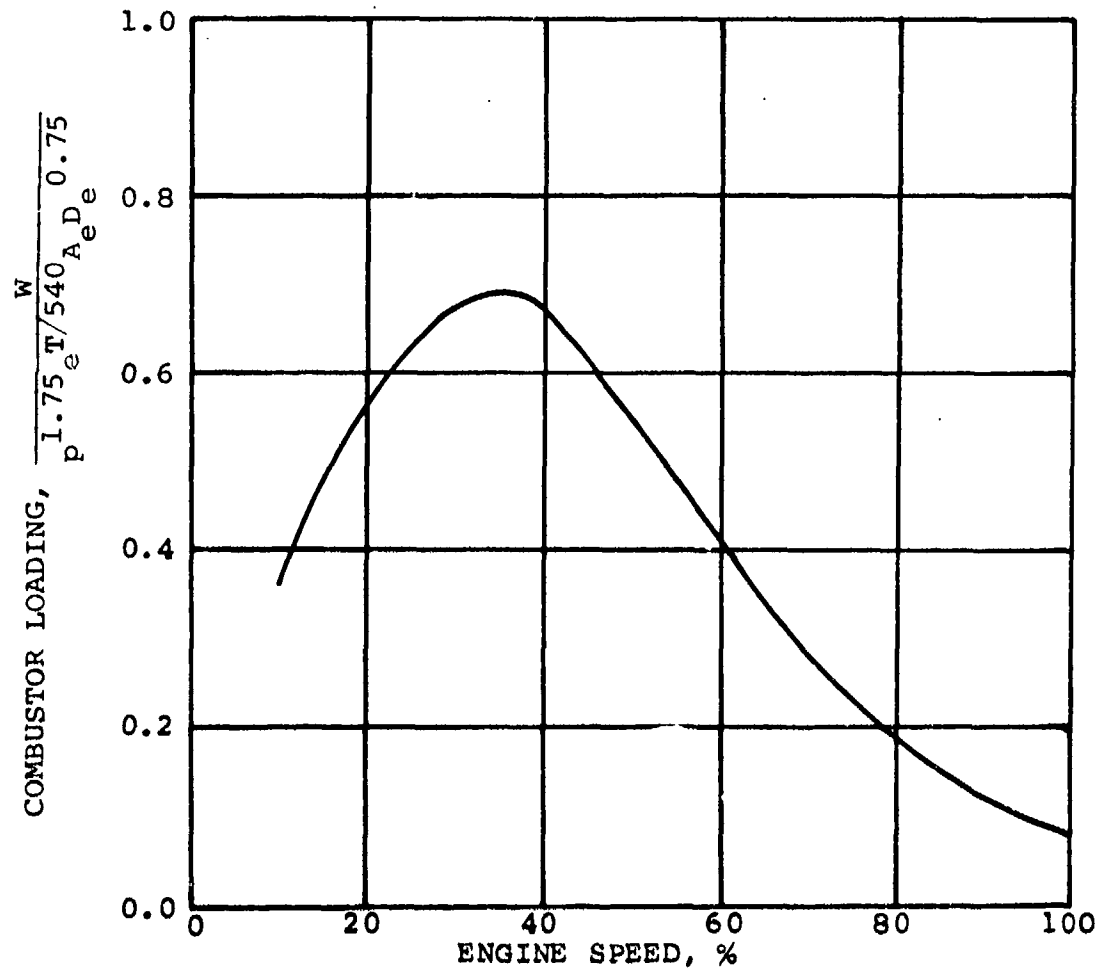


Figure 52. Combustor Loading During Start Cycle

The combustor was designed so that the airflow distribution (Figure 53) would provide a near stoichiometric mixture in the primary zone. Seventeen percent of the combustor airflow passed through the pneumatic fuel injectors for atomization and premixing. The remaining primary air (16 percent of the total airflow) was introduced through slot in the end plate of the combustor and directed along the inner surface of the combustor walls. This flow pattern, with the flow directed by the fuel injectors, was intended to establish a strong primary zone recirculation pattern. The remaining 67 percent of the airflow passed around the end of the combustor into the annulus between the combustor and the turbine shroud. This diluted air entered the combustor in 28 evenly spaced orifices near the discharge end. A single-sided dilution-zone design allowed all of the diluting air to flow over the entire outer surface of the liner to provide cooling.

Because of the low airflow and the relatively large surface area involved, a porous metal material (poroplate), with an internal ceramic zirconium oxide coating, was chosen for the combustor to eliminate the need for film cooling. The purpose of the nonporous ceramic was to insulate the parent metal from the hot gases and to protect the liner from oxidation. Nickel base alloy, L-605, was chosen as the parent material, and a flame spray process for application of the ceramic was established that gave a nominal 0.04 ceramic thickness in an allowable range of 0.02 to 0.06 in. The airflow that would normally have been used for cooling was, therefore, made available to the dilution zone for improved mixing.

3.2 Fuel Injector

Seven pneumatic fuel injectors were utilized to inject the fuel into the combustion chamber. A cross section of the fuel injector is shown in Figure 54. The convergent-divergent nozzle, where the fuel was injected, was designed to utilize high velocity at the throat for

DISTRIBUTION

17% 7 NOZZLES
 16% 14 SLOTS
 67% 28 DILUTION HOLES

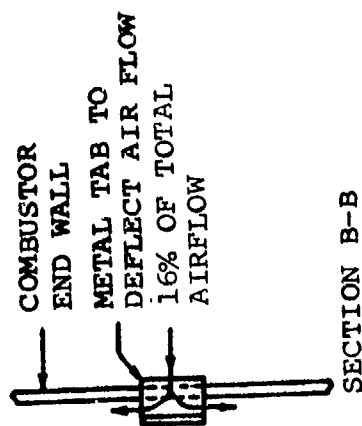
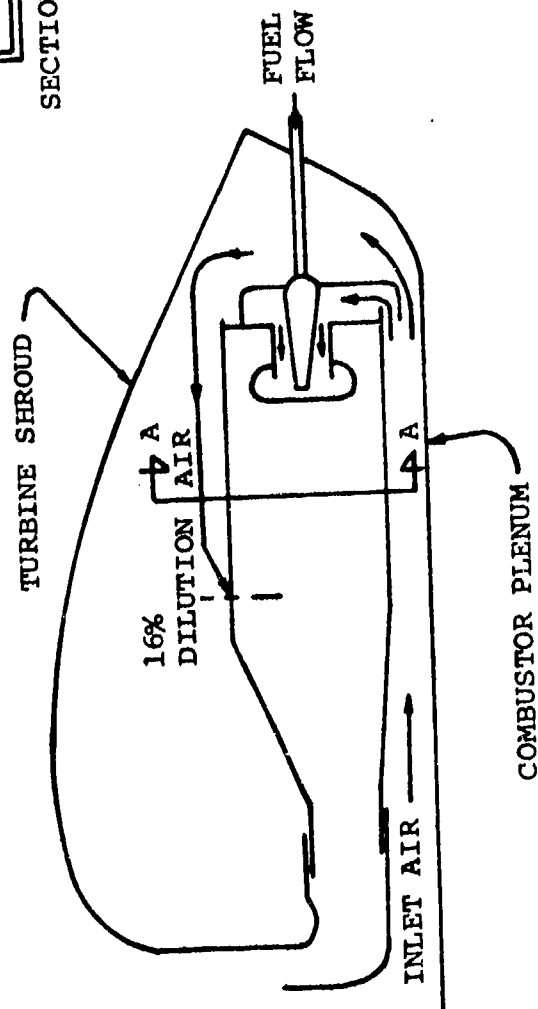
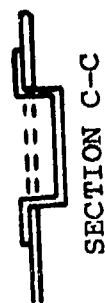
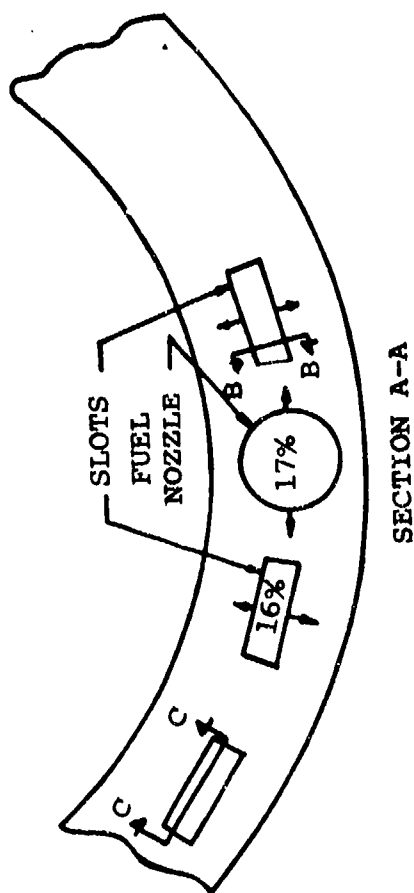


Figure 53. Combustor Air Distribution.

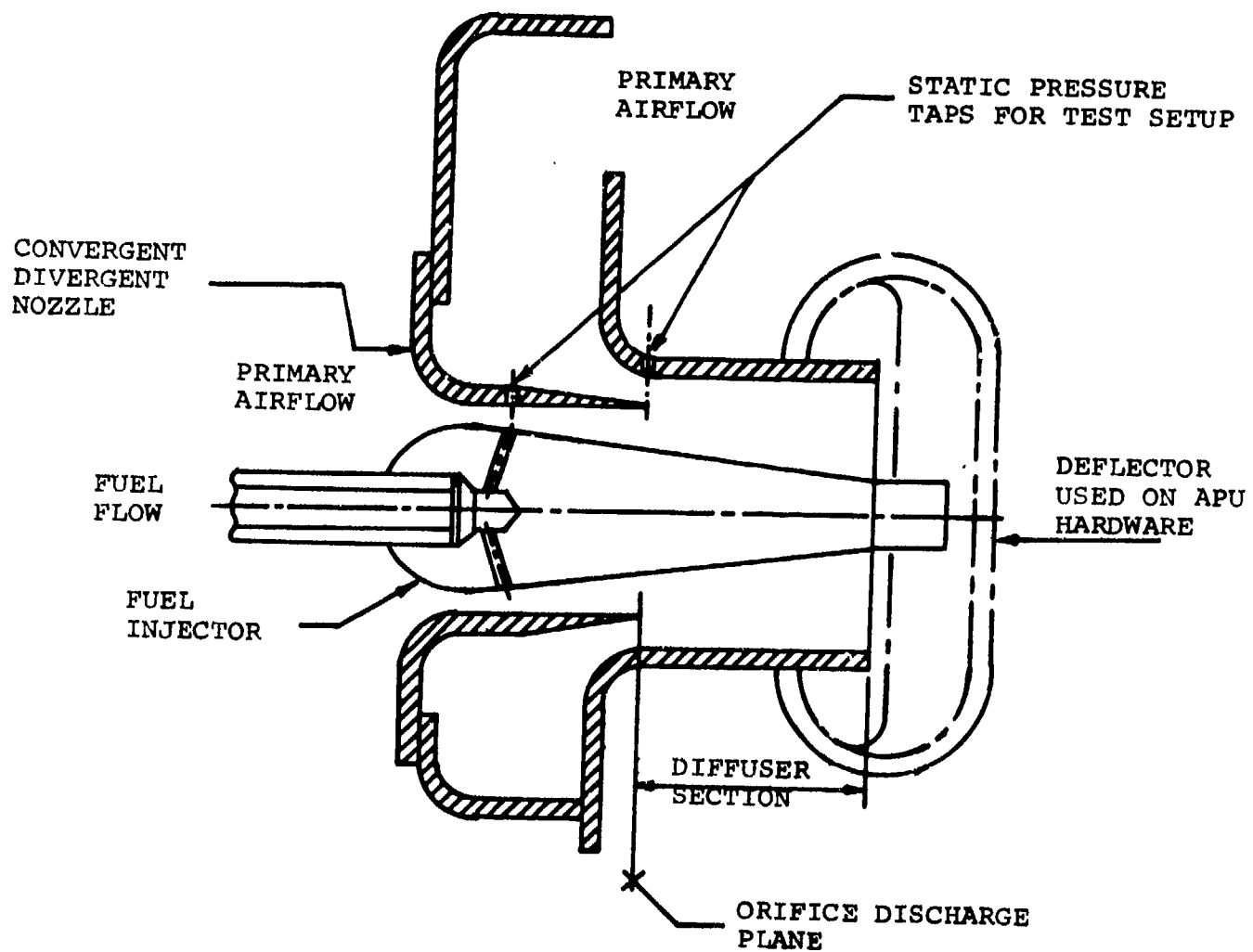


Figure 54. Pneumatic Injector Assembly.

the most efficient fuel atomization. To increase the throat velocity above that induced by the 4-percent pressure drop across the burner, additional air was introduced into the fuel nozzle system through an orifice at the discharge of the convergent-divergent nozzle, effectively lowering the discharge pressure of the nozzle and thereby increasing the throat velocity. The air and fuel mixture was then diffused before striking a diverter cup to prevent coalescing the fuel on the cup. The diverter cup was used to direct the fuel-air mixture tangentially in the combustor annulus to obtain complete circumferential distribution.

3.3 Test Rig

Two test rigs were designed for the program:

- (a) Fuel Injector - The test rig for measuring fuel-injector diffuser efficiency is shown in Figure 55. The schematic of the test section (Figure 54) shows the location of static pressure taps. Additional instrumentation consisted of a total pressure probe mounted on a traversing mechanism capable of moving radially and axially (Figure 55).
- (b) Combustor - A combustor test rig was designed to provide inlet air conditions simulating those in the engine by using actual engine hardware where possible. A rotating probe measured the combustor discharge pressure and temperature. The probe established both circumferential and lateral variations in the discharge profile. Additional instrumentation recorded inlet and exit pressures and temperatures and could also be used to determine overall pressure drop and combustion efficiency. Temperature-indicating paint defined the combustor metal temperature profile.

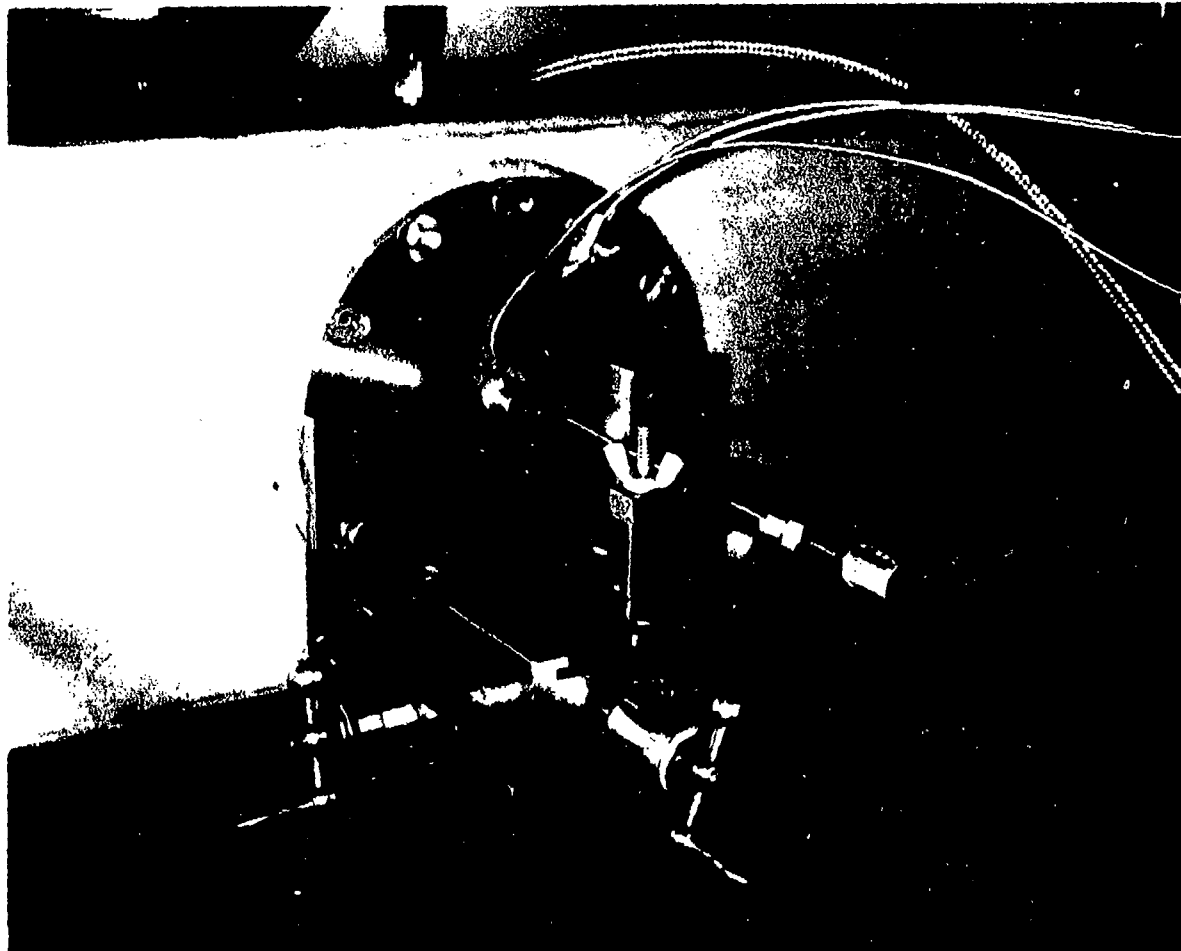


Figure 55. Fuel Injector Test Fixture.

4. PNEUMATIC INJECTOR COMBUSTION SYSTEM DEVELOPMENT

4.1 Fuel Injector

Testing in the fuel injector test rig was conducted with the end cup deflector removed to allow access to the internal passages. These tests were in addition to the normal flow calibrations run on the nozzle stand. The following development problems were identified and resolved on the injector rig:

- (a) Initial pressure traverses indicated that the injector stem was not concentric with the inner venturi, so that a significant difference in static pressure depression was observed between two probe positions 180 deg apart. This problem was corrected by redesign, incorporating three fins to maintain concentricity.
- (b) Several end-cup modifications were made and tested to determine an optimum compromise between adequate airflow for atomization and satisfactory circumferential distribution of the mixture.
- (c) A 25-percent loss in total pressure was measured at the throat of the outer venturi, resulting in lower-than-design diffuser efficiency. The loss was attributed to swirl induced in the inlet chamber of the nozzle. Figures 56 and 57 show typical pressure traverses taken on the injector rig.
- (d) The initial configuration of the injector discharge ports created a surface tension problem that resulted in fuel adhering to the centerbody, rather than being injected into the airstream. This was overcome by a redesign that allowed the injector centerbody to be fabricated with discharge ports

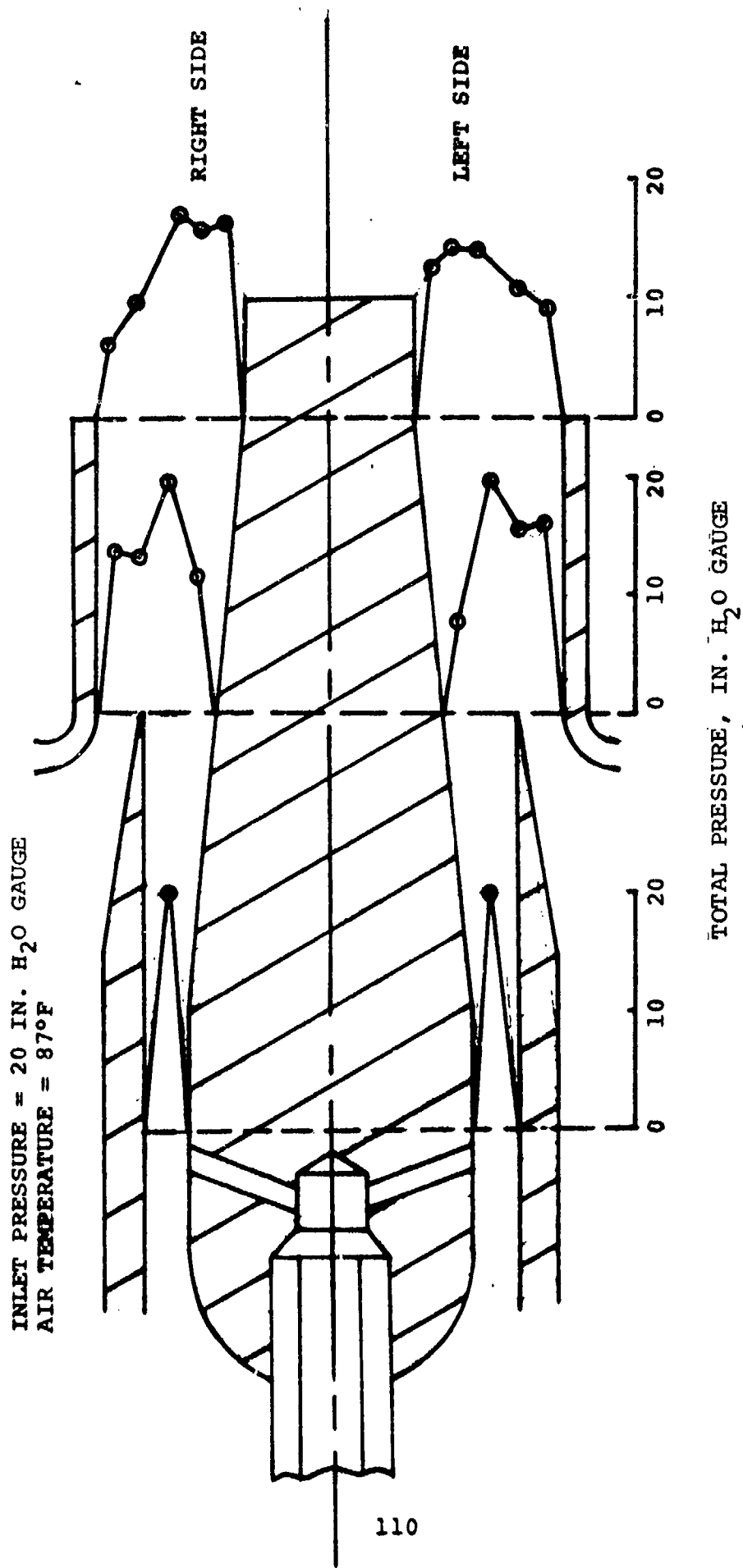


Figure 56. Pneumatic Injector Fuel Atomizer, Total Pressure Survey



AIR TEMPERATURE = 85°F

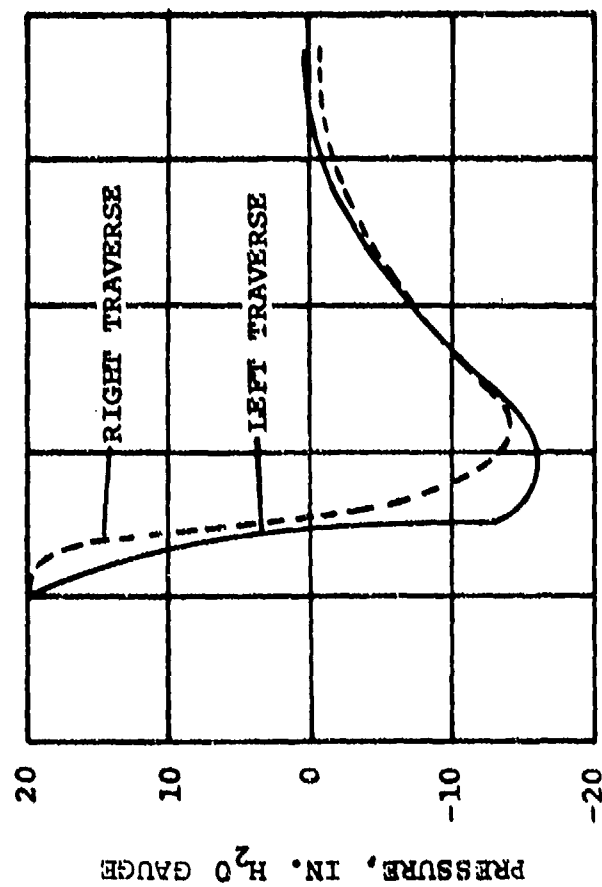


Figure 57. Pneumatic Injector Fuel Atomizer, Static Pressure Survey.

consisting of sections of capillary tubing protruding slightly above the centerbody surface and brazed to it. Use of the tubing also resulted in closer tolerance on the discharge port diameters for better flow matching. A typical flow calibration of a pneumatic injector is shown in Figure 58.

An additional injector problem, which was identified in the combustion rig rather than in the fuel injector rig, concerned flow-matching multiple injectors on a manifold. The system was initially designed to incorporate 20 psi check-valves in the fuel injector housings, both as a means of filling the manifold prior to ignition (thereby ensuring satisfactory temperature distribution during acceleration) and of providing some back pressure to the fuel control to improve fuel metering characteristics. The valves were plagued by contamination problems and reseating malfunctions as a result of the installation technique and were subsequently replaced by "visco-jet" flow restrictors to minimize head effects. The new restrictors resulted in a fuel system pressure increase over the entire engine operating range.

4.2 Combustor

4.2.1 Ignition Studies

Preliminary rig tests indicated that the combustion system was atomization-limited at light-off. A series of combustor modifications was tested in an attempt to improve the ignition capability, but only igniter penetration proved to have any significant effect on ignition. Some improvement was attained, but required-to-light, fuel-air ratio remained quite high (Figure 59).

The requirement for matching the fuel flows from individual injectors on the manifold, to ensure satisfactory temperature distribution, was compounding the ignition problem by decreasing the fuel

NOTE: Nozzle internal check valves removed for test

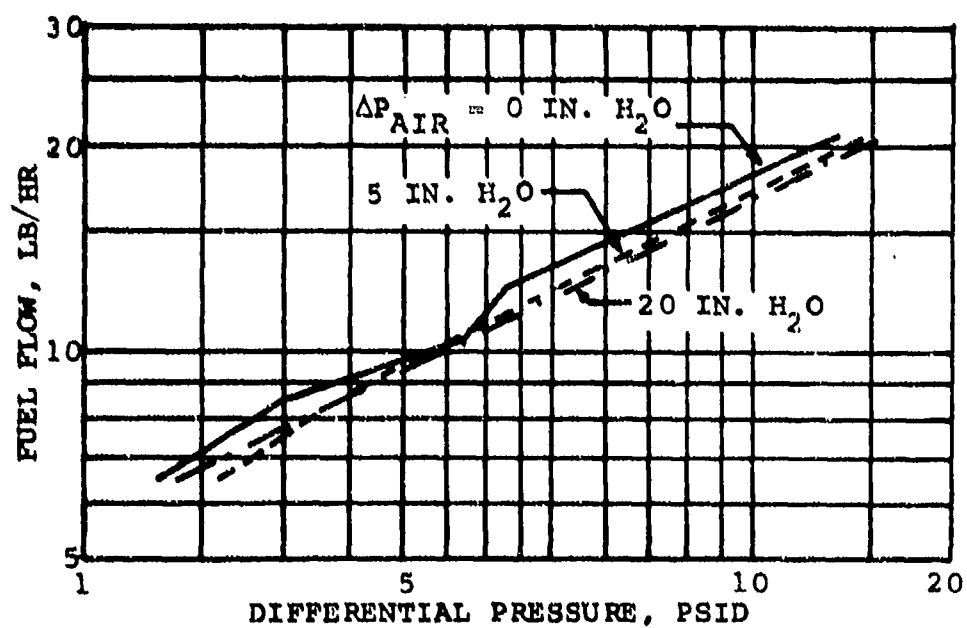


Figure 58. Pneumatic Injector Flow Calibration.

LEGEND:

1. First test - standard configuration
2. Igniter penetration test
3. Blocked dome tabs either side of igniter
4. Longer, wider dome tabs; valved fuel manifold; start air manifold
5. Removed dome tabs; valved fuel manifold; modified start air

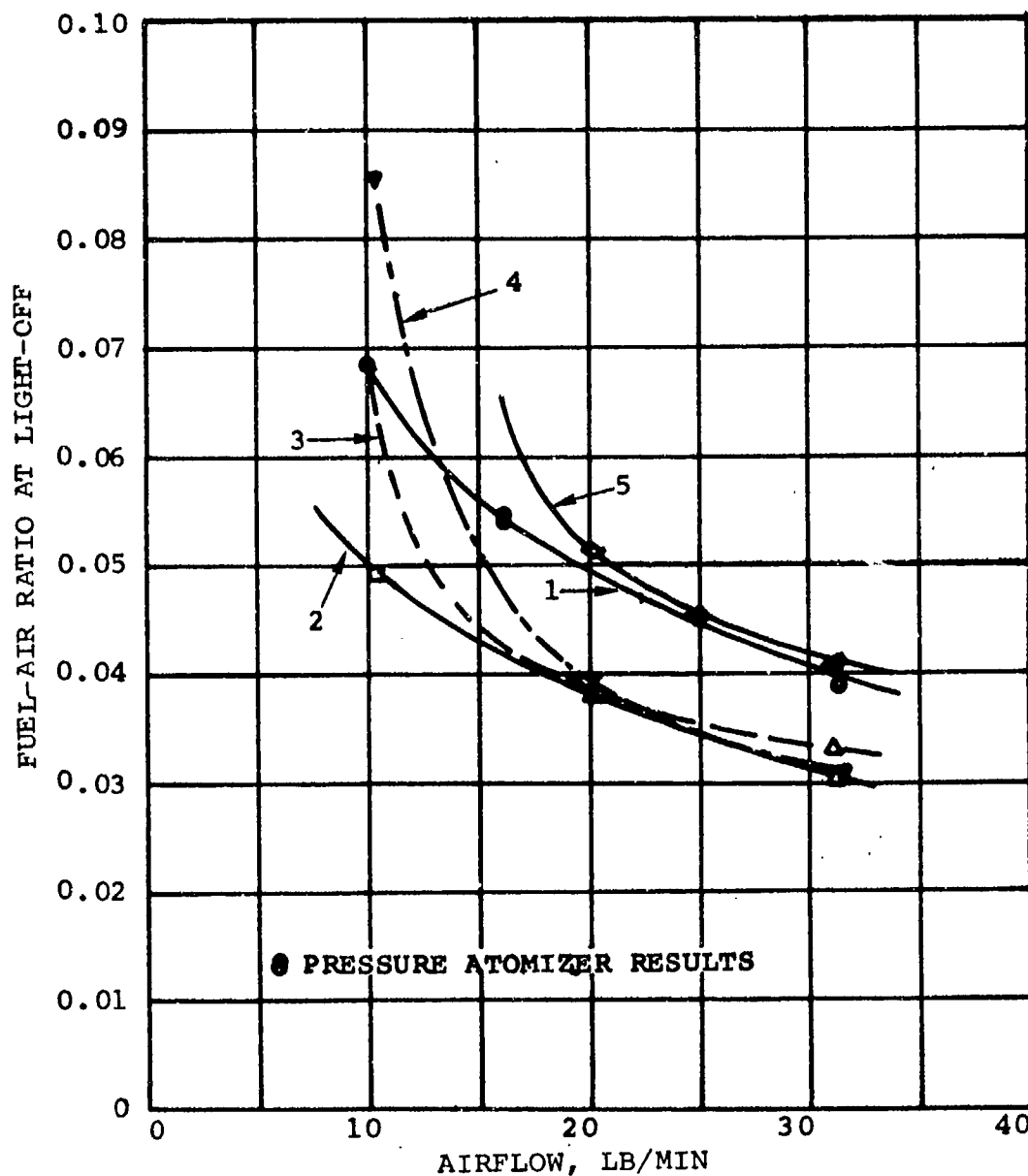


Figure 59. Ignition Test Results.

flow through the two lowest nozzles (positioned on either side of the igniter). A reduced local fuel-air ratio accompanied the reduced flow from the ignition nozzles and, therefore, a higher overall fuel flow was required to deliver an ignitable mixture to the plug. As a result, a new igniter location immediately adjacent to one fuel injector was chosen.

A single-pressure atomizer was installed in the combustor to improve ignition capability, but resultant poor temperature distribution immediately after light-off and instability encountered during the transition from the start nozzle to the seven pneumatic nozzles rendered the system impractical.

4.2.2 Temperature Spread Reduction

Initial rig tests showed the TSF in excess of 0.8. The temperature spread factor is defined as the maximum gas temperature minus the average gas temperature divided by the combustor temperature rise,

$$TSF = \frac{T_{\max} - T_{\text{avg}}}{T_{\text{avg}} - T_{\text{in}}}$$

and is generally measured at the turbine nozzle inlet. The excessive spread was traced to a combination of fuel maldistribution due to wide manufacturing tolerances on the fuel injectors and to an over-rich primary zone, requiring a portion of the dilution air to complete the combustion process. Several chamber modifications, allowing increased primary zone airflow, were made and tested until a configuration was obtained that exhibited good temperature distribution without deterioration in ignition capability or lean stability.

The configuration incorporated air admission holes in the dome, equally spaced with respect to the fuel injectors (Figure 60); the TSF was 0.16. A typical circumferential temperature distribution plot is shown in Figure 61. The low-temperature area at the 150-deg circumferential position resulted from an oversized dome-cooling tab that was required to maintain the correct open area distribution, when the igniter location was moved closer to the fuel injector nearest that point. The change resulted in asymmetry of the combustor at that circumferential position.

4.2.3 Efficiency and Lean Stability

Combustion efficiency of the initial combustor configuration was 95 percent at the design-point and dropped below 90 percent with decreasing combustor temperature rise. The low efficiency was attributed to an over-rich condition in the primary zone, resulting from too little airflow through the injector venturis. The increased primary zone airflow modifications that improved temperature distribution also increased combustion efficiency to 99+ percent at the design-point and above 93 percent, over a range of fuel-air ratios from 0.008 to 0.20.

Lean blowout fuel-air ratio at design conditions for the original design was 0.004; this value was increased to 0.005 for the increased primary airflow modification. Lean blowout occurred at combustion efficiencies of slightly less than 40 percent.

4.2.4 Pressure Loss

Combustor total pressure drop at design-corrected airflow and 1050°F combustor temperature rise for the original design was greater than 7 percent of combustor inlet total pressure compared with a design goal of 3 percent and initial design sizing of 4 percent. The high loss was attributed to too little primary zone open area, resulting

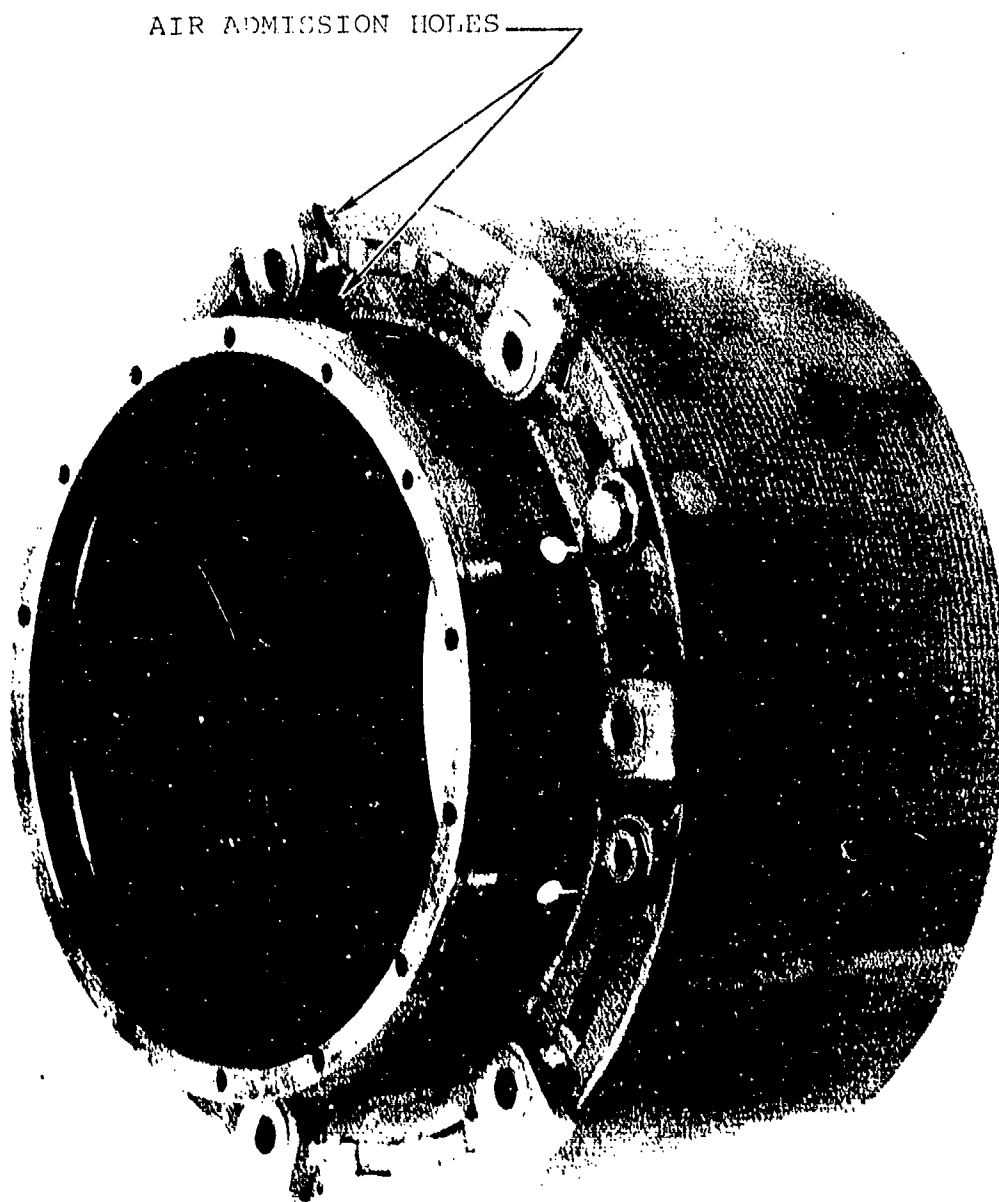
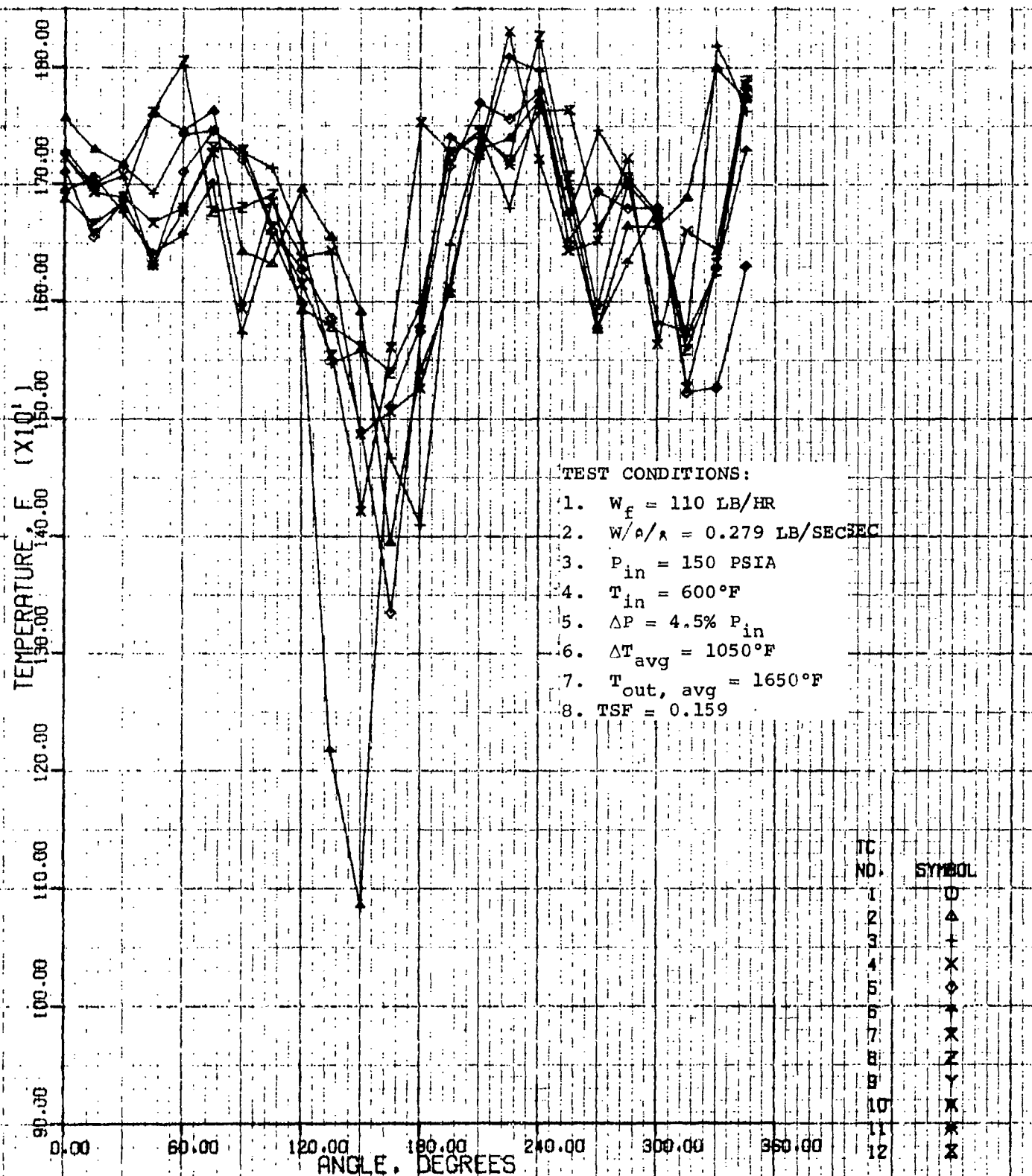


Figure 60. Combustor.



GTCP 305-1 RIG DATA SHEET 25, TEST 25-1
 UNIT 305 S/N 0 TEST 25 SCAN 1

Figure 61. Combustor Temperature Distribution.

from lower-than-anticipated flow coefficients for the injector venturis. The increased primary zone airflow modification reduced the loss to 4.5 percent of inlet total pressure. Corresponding isothermal pressure loss reduction was 2.5 percent from an initial value of 6.5 percent down to 4 percent of inlet total.

4.2.5 Combustor Durability

During the development phase, several endurance and combustor metal temperature tests were conducted at rated combustor temperature rise or higher. The first Therminex paint test results indicated that the ceramic-coating cooling concept was effective on most inner and outer liners, except at local areas near the fuel injector bosses on the outer liner, as shown in Figure 62.

Attempts to accumulate endurance time on the combustor configuration with increased primary air identified a durability problem with the fuel injector deflector cups. The tabs supporting the cups failed, due to overtemperature, and allowed the cup to separate from the injector venturi housing. The overtemperature condition was the result of a flame-front reposition that accompanied the primary zone airflow modification. The problem was solved by a cup redesign incorporating integral air cooling of the cup supports. An additional safety feature of the design was that the cup was supported so that failure of the outside support surface material would not result in separation of the cup from the venturi housing.

Evaluation of the combustor performance with the newly designed venturi housings showed a deterioration in TSF from 0.16 to 0.21 and a pressure loss increase to 5.7 percent of inlet total pressure. The new end-cup design had increased the back pressure on the venturi, resulting in throttled injector diffuser performance and a corresponding decrease in venturi through-flow.

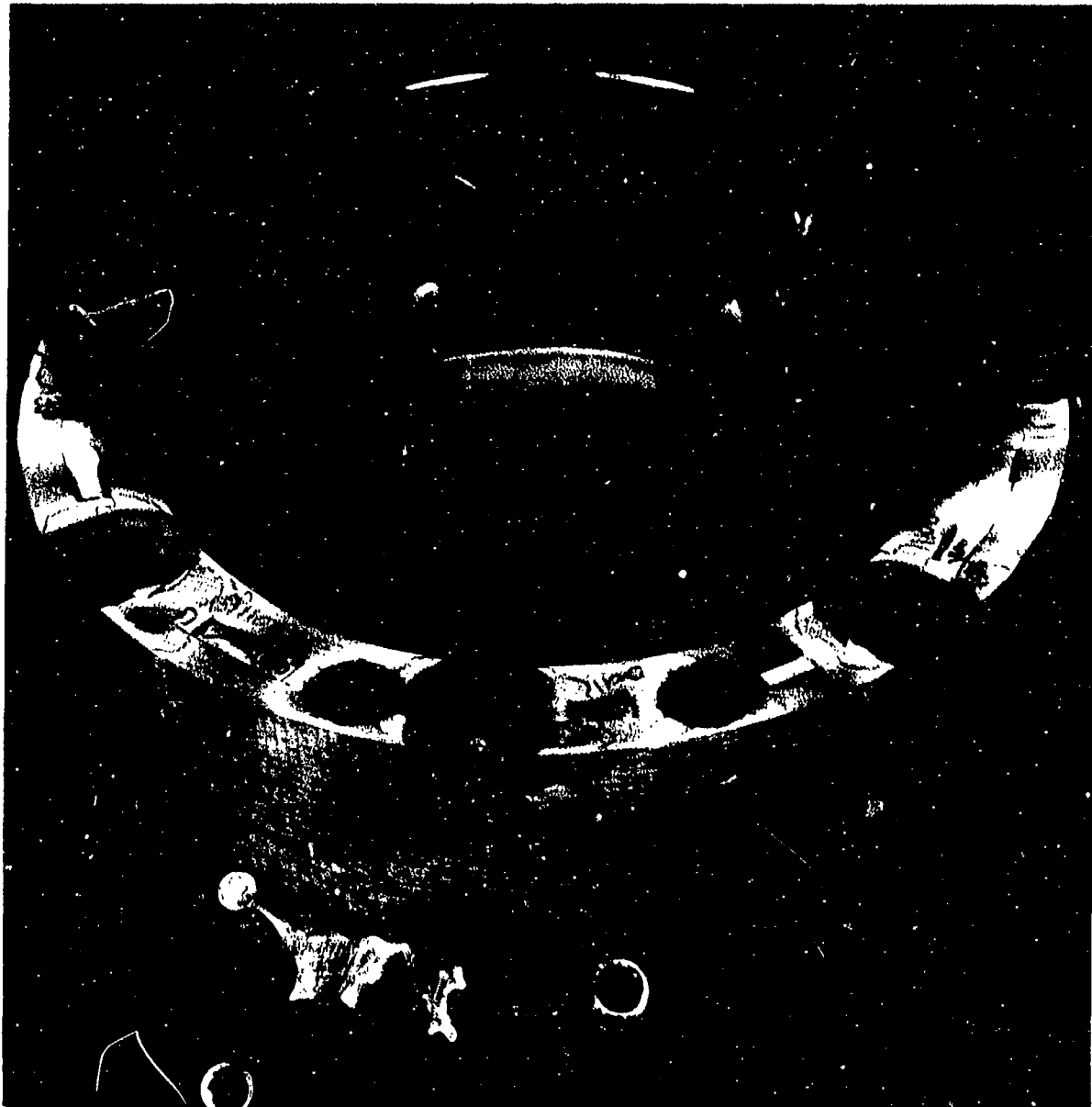


Figure 62. Combustor.

As a result of the durability problems with the pneumatic injectors and because of the limited ignition capability of the system, development emphasis was shifted to a backup system incorporating pressure atomizers. The backup system was even more attractive since the potential benefits of a low-pressure fuel system had already been compromised as a result of a back pressure device to overcome head effects.

4.3 System Performance

A total of 38 combustion rig development tests were conducted on the system. When the pneumatic injector approach was abandoned, the following performance levels had been achieved:

- (a) Isothermal pressure loss, $\Delta P/P_T$
 - 5 percent with cooled deflectors
 - 4 percent with uncooled deflectors
- (b) Design-point TSF
 - 0.21, cooled deflectors
 - 0.16, uncooled deflectors
- (c) Start cycle TSF
 - Figure 63
- (d) Ignition fuel-air ratio
 - 0.03 min at sea level, 50 percent N
- (e) Lean blowout fuel-air ratio
 - 0.005 at design inlet conditions
- (f) Efficiency
 - 97 percent, cooled deflectors
 - 99+ percent, uncooled deflectors
 - 40 percent, incipient blowout

The overall system was tested at a maximum heat release rate of 5.2×10^6 Btu/hr-ft³-atm.

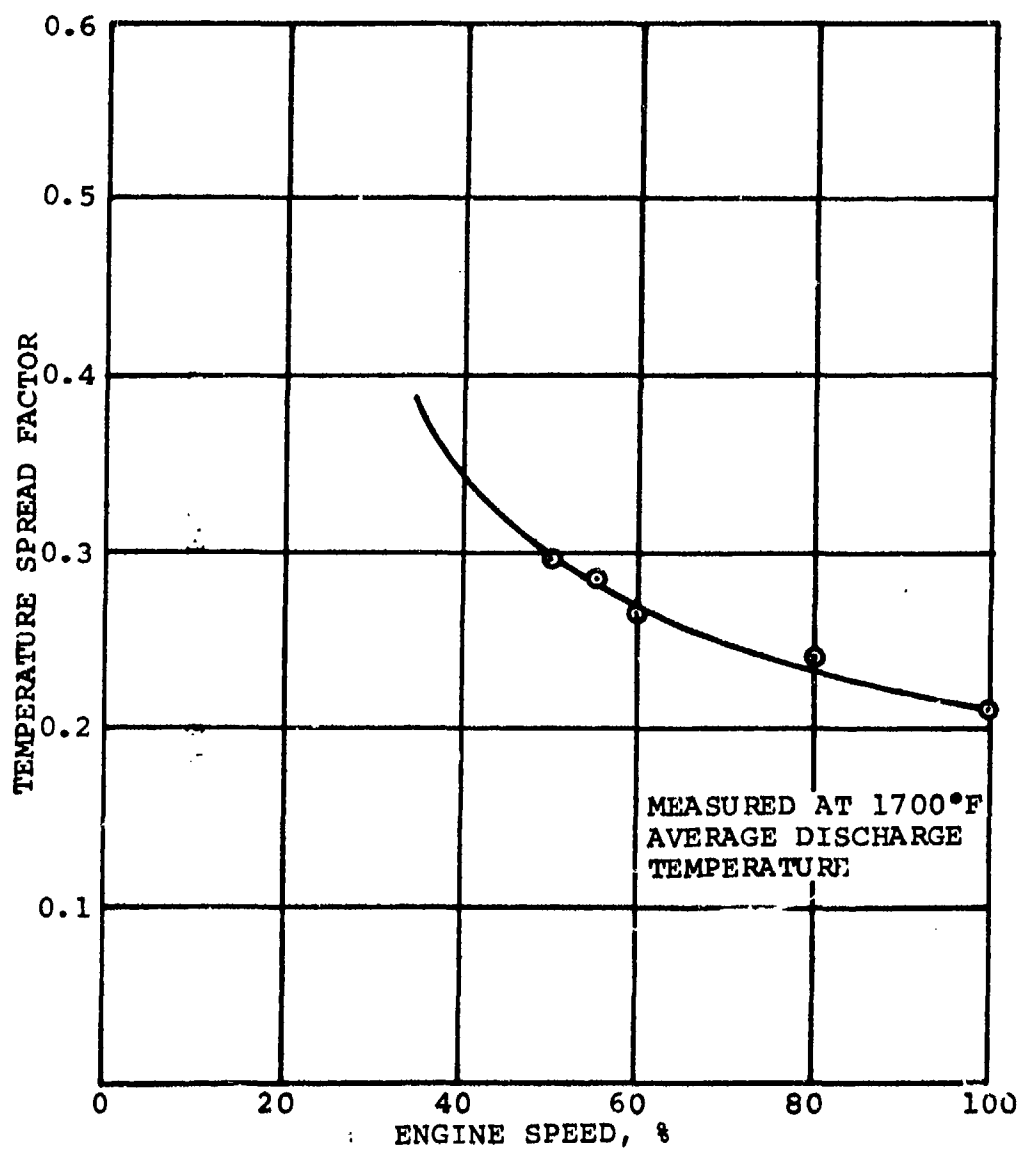


Figure 63. Acceleration Temperature Spread.

5. PRESSURE INJECTOR COMBUSTION SYSTEM DESIGN

5.1 Combustor

Two pressure injector combustor configurations were designed for the backup system. Both incorporated a lengthened, increased channel height (1.25 in.) combustor with 12 equally spaced Simplex atomizers inserted radially through the turbine plenum. The atomizers were oriented to spray in the direction of the inlet air swirl and back toward the combustor dome. In addition, the atomizers were placed so every other nozzle was sized for satisfactory spray quality at ignition. The ceramic-coating cooling concept and the combustor-turbine nozzle interface seal configuration were carried over from the pneumatic injector design.

Both configurations were sized at the maximum bleed design-point for 4-percent pressure drop. Liner OD was 9.65 in.; injector pitch diameter was 9.25 in., and nozzle spacing ratio (pitch diameter nozzle spacing divided by channel height) was 1.93. Single-sided inner liner air entry was retained, and the combustor length was increased from 3.875 to 4.89 in.

The increased length and channel height resulted in a volume increase from 95 to 144 in.³ and a corresponding design heat-release rate reduction from 5×10^6 to 3.3×10^6 Btu/hr-ft³-atm. The volume increase was made possible by the removal of the pneumatic injector venturi housings from the combustor base-plate; no increase in turbine plenum size was required.

The basic difference between the two pressure-atomizing configurations was in the primary zone flame-stabilizing mechanism. The first configuration, P/N 25549, employed a single-recirculation primary zone with a film-cooled dome. The cooling air is introduced to

strengthen the recirculation. All other airflow is introduced through the inner liner to utilize its cooling potential over the maximum combustor surface area. This configuration, with its flow area distribution, is shown in Figure 64. The lip at the mean diameter of the dome was added to allow butt-welding without jeopardizing the ceramic coating.

The second configuration, P/N 25687, incorporated a toroidal recirculation primary zone established by tangential louvers in the combustor dome. The dome air was injected tangentially to strengthen the natural recirculation established by the inlet air swirl. All remaining airflow was again admitted through the inner liner (Figure 65).

5.2 Fuel Injector

The fuel injection system was built into a six-primary, six-secondary nozzle system to ensure adequate ignition capability. The primary nozzles were sized for a minimum pressure differential of 25 psi at light-off, while the secondary nozzles were sized to pass the total required fuel flow without necessitating a fuel pump change. These constraints resulted in primary and secondary atomizer flow requirements of 6.7 and 15 lb/hr, respectively, at 100 psid. A compromise 6.8- and 16-lb/hr system was selected because of hardware availability. The system was set up so a flow divider would allow more even matching of the primary and secondary nozzle flows at the design-point.

Mechanical constraints imposed upon the fuel injectors included minimum radial protrusion above the turbine plenum, a common primary and secondary housing, a mounting configuration to allow a pitch diameter of 9.25 in., and a fabrication technique to minimize coking at high combustor inlet temperatures. The injection angle of 32 deg below horizontal was required to obtain the optimum fuel distribution at the specified pitch diameter, with a standard fuel atomizer tip having a spray angle of 75 deg.

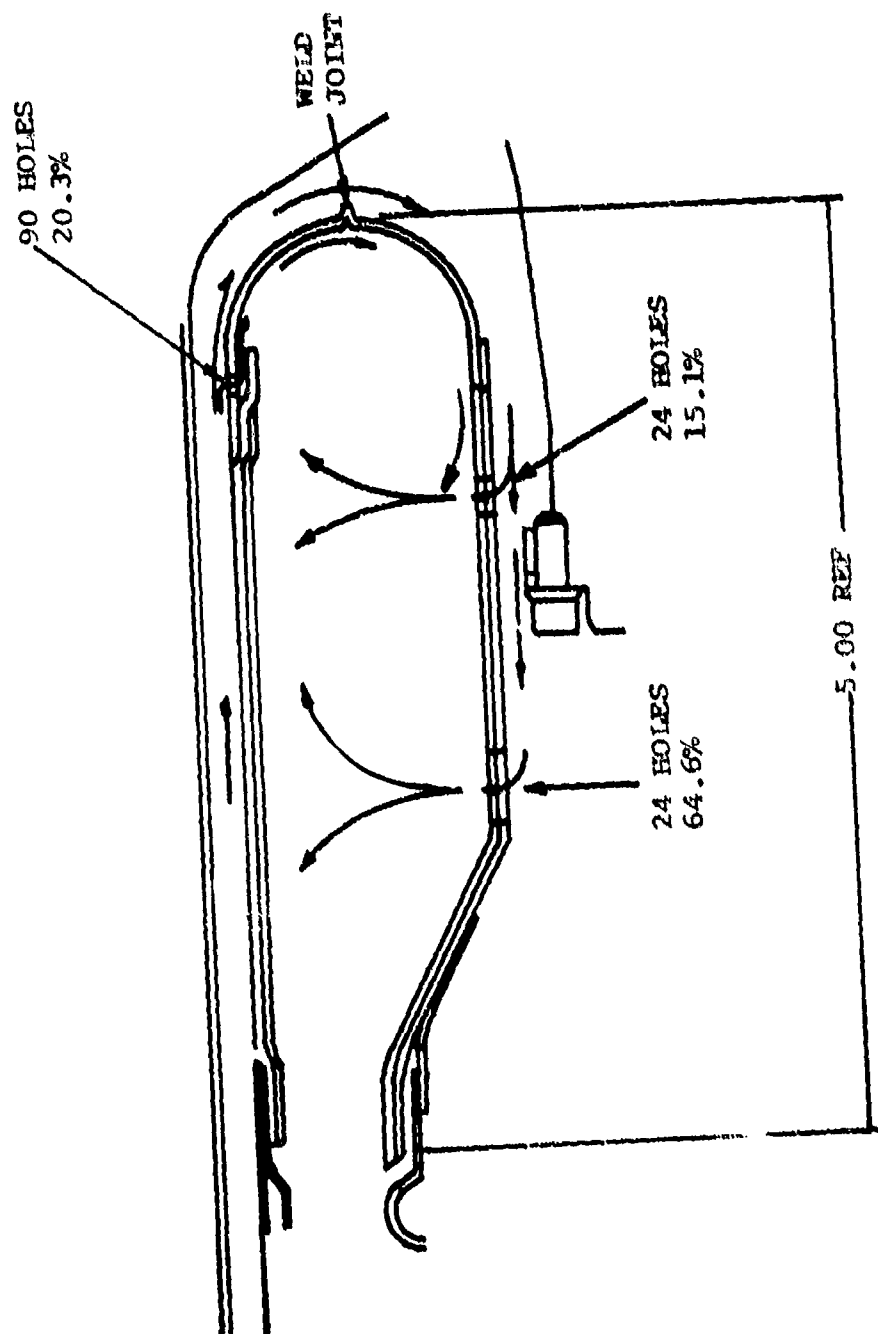


Figure 64. Combustor Airflow Distribution, Configuration i.

TANGENTIAL LOUVER
FLOWS INTO PLANE
OF PAPER

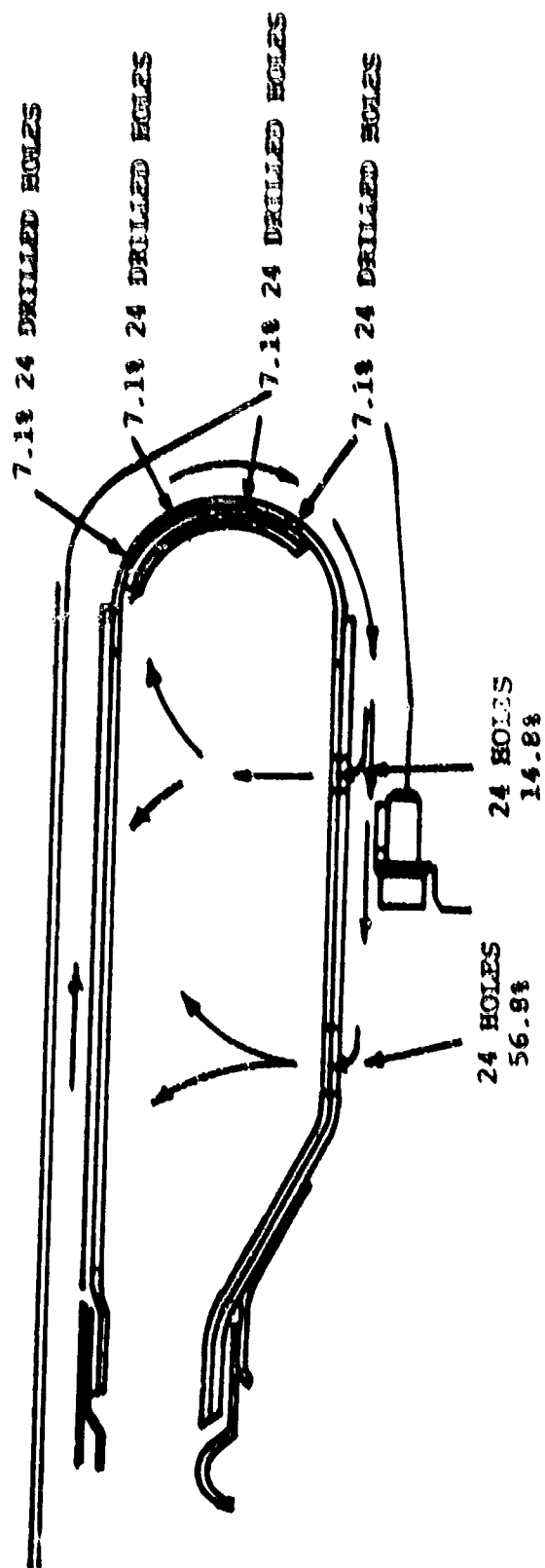


Figure 65. Combustor Airflow, Distribution, Configuration 2.

A fuel nozzle cross section is shown in Figure 66. A double-tube vacuum braze assembly procedure was adopted to minimize fuel coking.

5.3 Combustion Rig

A combustor test rig was designed to accommodate the pressure-atomizing combustion system. The rig layout and instrumentation were similar to the pneumatic injector combustor test rig.

6. PRESSURE ATOMIZING COMBUSTION SYSTEM DEVELOPMENT

6.1 System Development

Fabrication difficulties were experienced with the first pressure atomizer combustor configuration because the L-605 Poroplate could not be formed to the contour of the inner liner without tensile failure of the metal fibers. The first inner liner was, therefore, fabricated from sheet stock. Initial combustion rig tests indicated a bonding problem, between the Rockide coating and the nonporous sheet metal inner liner, that was solved by fabricating the cylindrical section of the inner liner from more ductile N-155 Poroplate and by using sheet metal for the transition section.

Ignition characteristics and temperature distribution were evaluated on P/N 25549 with a 4-primary, 8-secondary and a 6-primary, 6-secondary fuel injection system. Although ignition capability of the 4, 8 system was superior to the 6, 6 system, the temperature distribution on primary nozzles was significantly worse. Therefore, the 6, 6 system was selected for development tests. A fuel injector spray angle, with a centerline of 25 deg from tangential rotated back toward the combustor dome, was determined to give the optimum combination of ignition capability and temperature distribution. A flow divider with a cracking pressure of 75 psi was selected as the best available compromise between matching the primary and secondary fuel flows at the

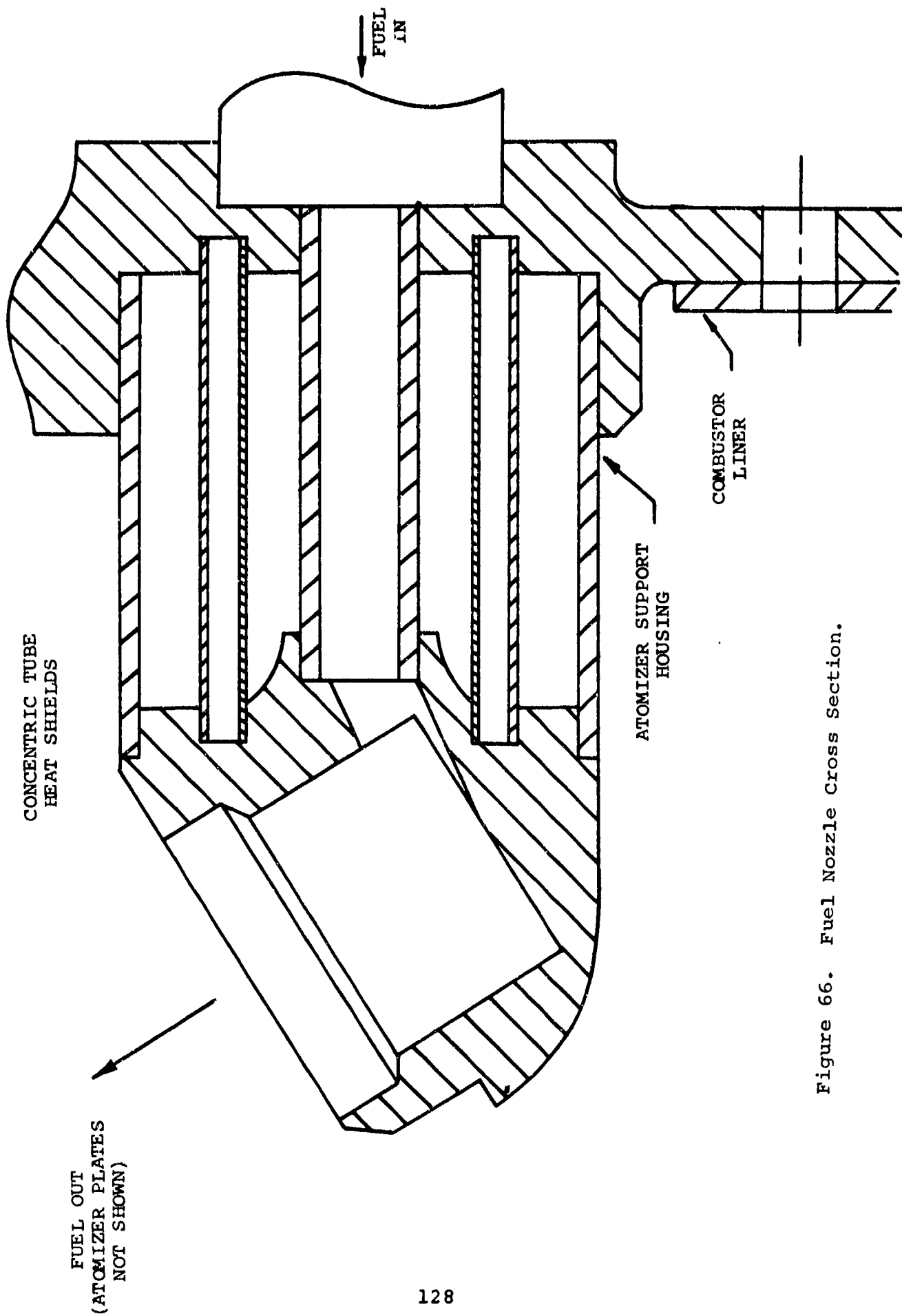


Figure 66. Fuel Nozzle Cross Section.

design-point and maintaining sufficient fuel flow for acceleration and cold-day operation, without exceeding the fuel pump capability. A flow calibration of the fuel injection system is shown in Figure 67.

Axial locations of the combustor orifices had been fixed from pneumatic system development tests and proved satisfactory for the pressure-atomizing system. The number of orifices was changed to 24 to maintain symmetry with the number of fuel injectors.

The toroidal recirculation combustor, P/N 26587, was also evaluated for ignition capability and temperature distribution. Test results indicated that ignition was slightly improved, but the temperature spread was significantly worse. Therefore, development emphasis was placed on P/N 25549, and no further effort was expended on P/N 25687.

After development test results had defined injection angle and flow divider characteristics for P/N 25549, additional testing verified that combustor durability and altitude ignition at 25,000 ft were satisfactory. With the exception of one local hot spot on the inner liner transition section at 1700°F, the combustor wall temperatures were at or below the 1600°F maximum design-goal. A total of 13 development tests were conducted on the pressure-atomizing combustion system.

6.2 System Performance

The system was developed to the following levels of performance:

- (a) Isothermal pressure - 3.6 percent
 loss, $\Delta P/P_T$

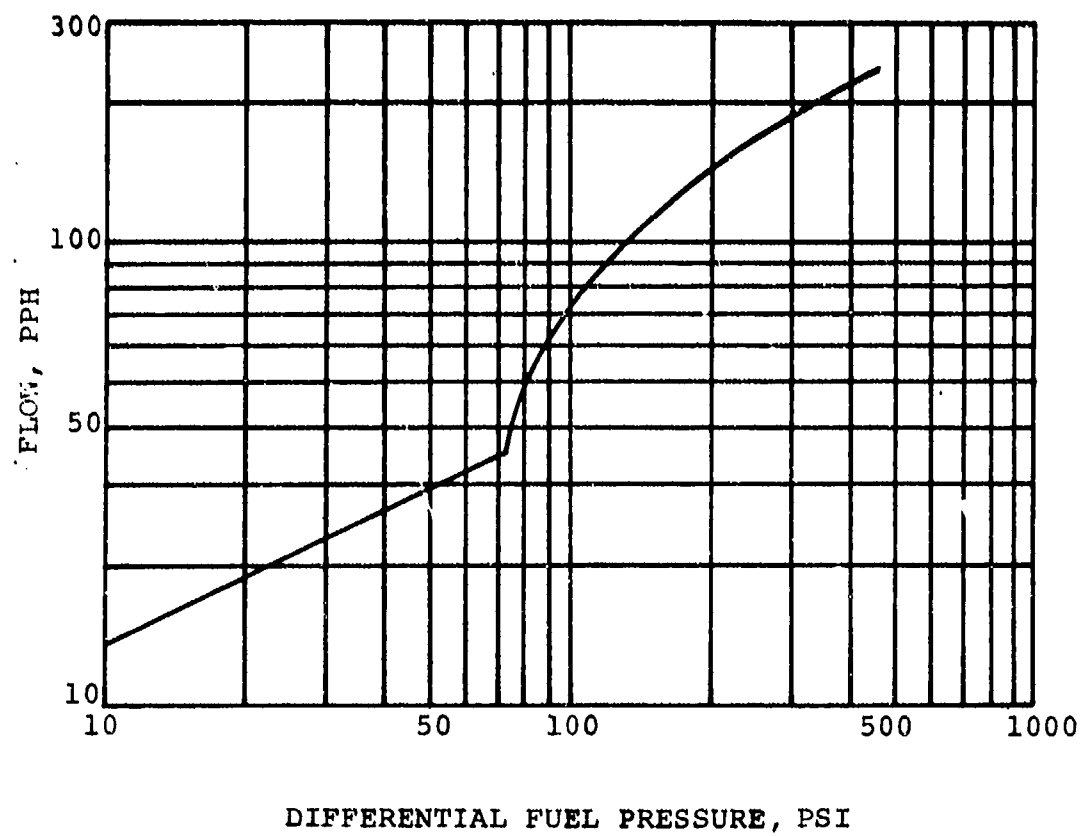


Figure 67. Fuel System Flow Calibration.

- | | |
|--|--|
| (b) Temperature spread factor | <ul style="list-style-type: none"> - 0.11 on rig at 1200°F ΔT (Figures 68 and 69) - 0.15 on engine at no-load (Figure 68) - 0.18 on rig at 118 percent of design ΔT and 2200°F discharge temperature. (Figures 70 and 71) - 0.38 on primaries only (Figures 72 and 73) |
| (c) Sea-level ignition fuel-air ratio | <ul style="list-style-type: none"> - 0.025 at sea level 25 percent N - 0.063 at sea level 13 percent N (Figure 74) |
| (d) Sea-level, lean-blowout fuel-air ratio | <ul style="list-style-type: none"> - 0.008 at design inlet conditions |
| (e) 25,000-ft altitude ignition fuel-air ratio | <ul style="list-style-type: none"> - 0.062 at 25 percent N (Figure 75) |
| (f) Efficiency | <ul style="list-style-type: none"> - 97 percent at 75 percent of design ΔT - 99 percent at design ΔT - 99+ percent at 118 percent of design ΔT |
| (g) Durability | <ul style="list-style-type: none"> - Tested at 250°F above design ΔT - Heat release rate = 4×10^6 Btu/hr-ft³-atm (Figure 76) |

The performance data show that for the pressure-atomizing combustion system, only lean stability is inferior to the pneumatic atomizing system.

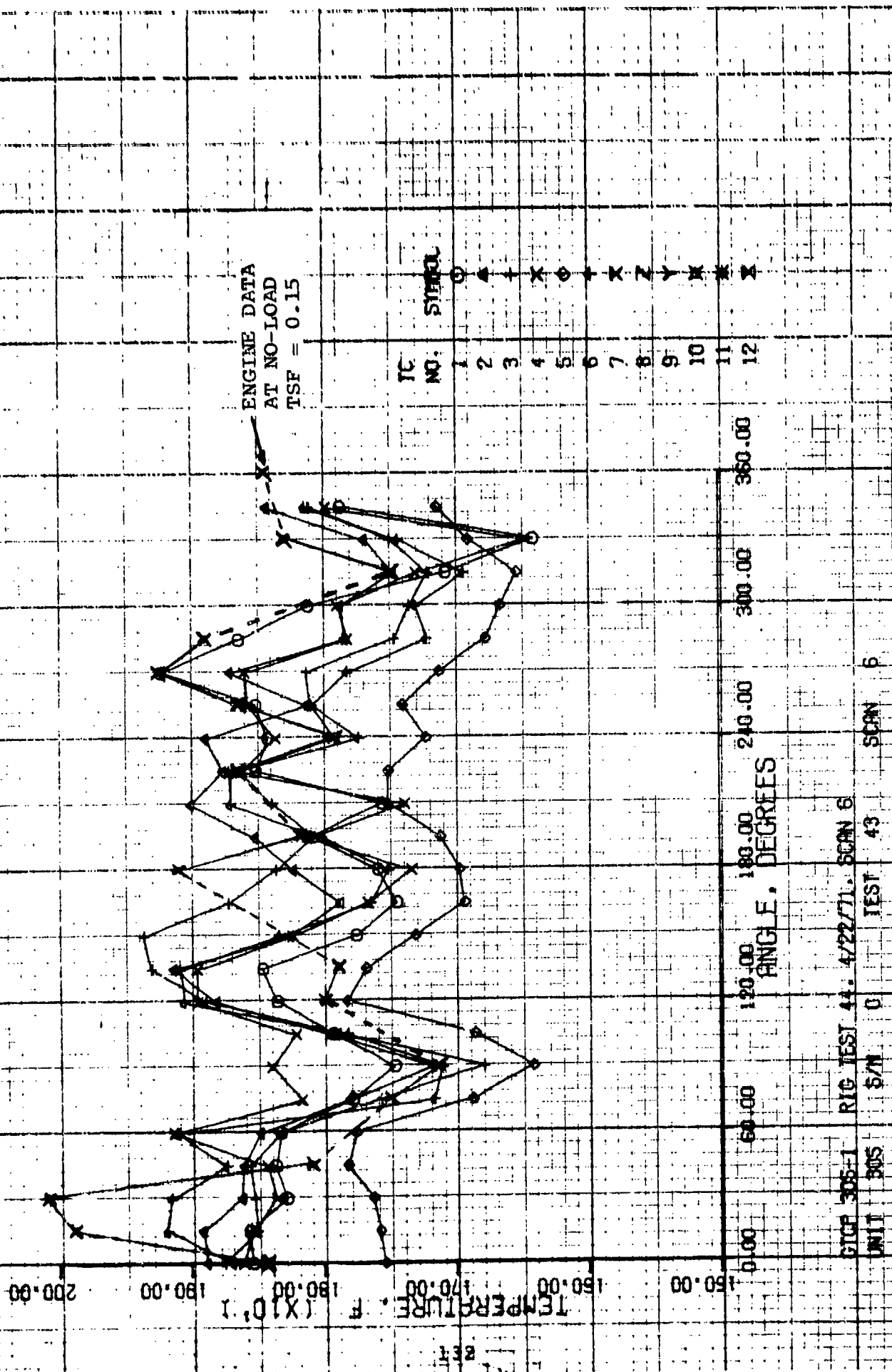


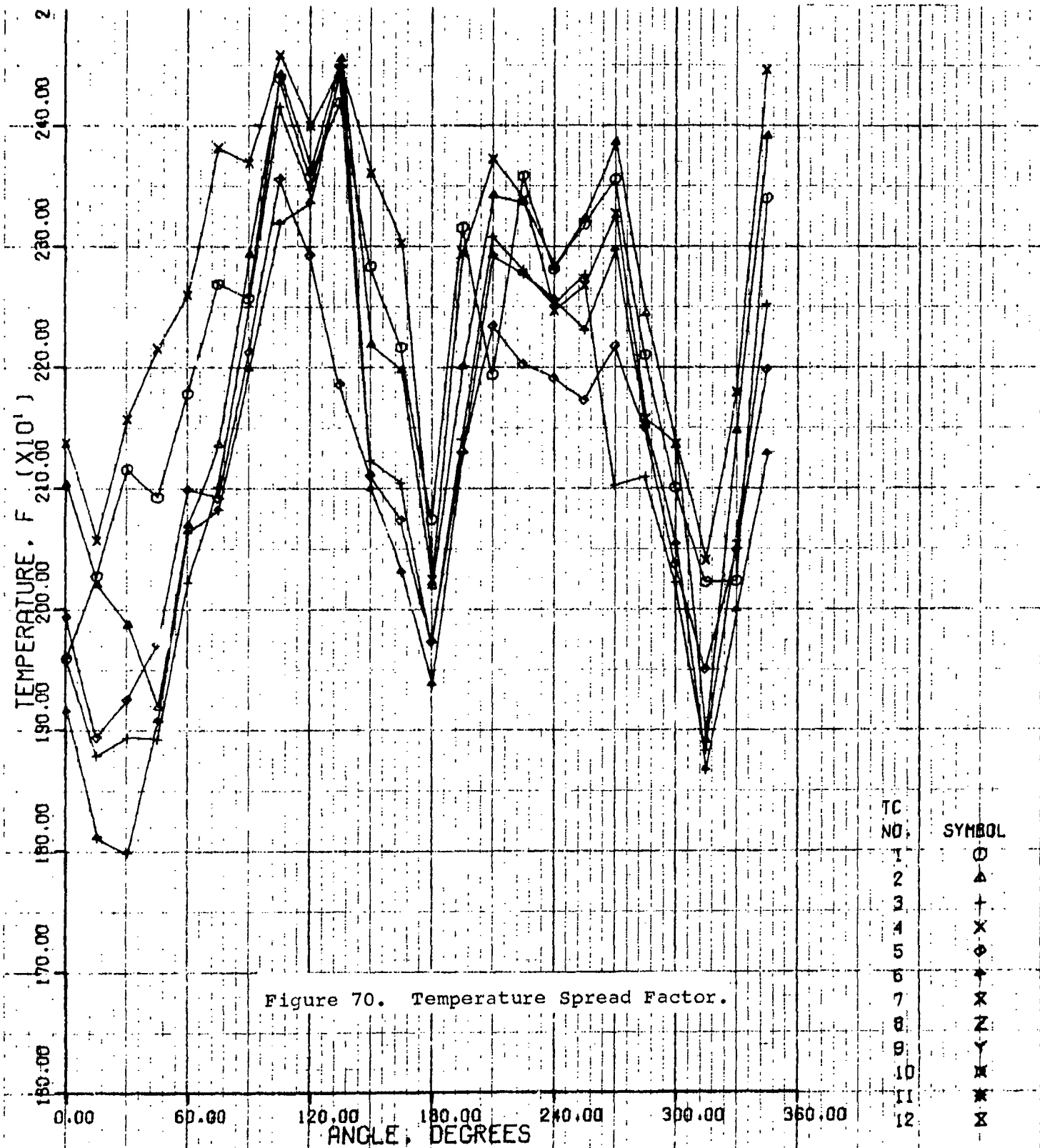
Figure 68. Temperature Spread Factor.

GTCP 305-1 RIG TEST 44, 4/22/71, SCAN 6

UNIT 305 S/N 0 TEST 43 SCAN 6

THERMOCOUPLE NO.																	RADIAL VALUES-											
RADIUS, IN.																												
ANGLE, DEG.																												
1	2	3	4	5	6	7	8	9	10	11	12	AVG	MAX	MIN	SPREAD													
1853	1888	1875	1861	1753	1898	0	0	0	0	0	0	1850	1888	1753	135													
1856	1871	1850	1853	1757	1918	0	0	0	0	0	0	1854	1918	1757	160													
1828	1841	1852	1835	1763	1914	0	0	0	0	0	0	1842	1914	1763	152													
1836	1860	1855	1842	1782	1872	0	0	0	0	0	0	1841	1872	1782	91													
1832	1867	1831	1912	1775	1910	0	0	0	0	0	0	1851	1912	1775	137													
1778	1780	1756	1816	1687	1716	0	0	0	0	0	0	1755	1816	1687	129													
1746	1717	1678	1838	1641	1710	0	0	0	0	0	0	1722	1838	1641	197													
1792	1793	1787	1820	1685	1781	0	0	0	0	0	0	1777	1820	1685	135													
1836	1820	1888	1894	1782	1904	0	0	0	0	0	0	1864	1904	1782	123													
1845	1912	1929	1894	1767	1908	0	0	0	0	0	0	1876	1929	1767	162													
1776	1826	1935	1823	1730	1833	0	0	0	0	0	0	1820	1935	1730	205													
1748	1796	1871	1766	1692	1764	0	0	0	0	0	0	1770	1871	1692	179													
1753	1822	1835	1733	1686	1750	0	0	0	0	0	0	1766	1835	1686	139													
1810	1851	1806	1803	1711	1800	0	0	0	0	0	0	1798	1851	1711	140													
1755	1899	1837	1734	1751	1863	0	0	0	0	0	0	1808	1899	1734	161													
1850	1875	1862	1861	1750	1870	0	0	0	0	0	0	1845	1875	1750	125													
1840	1888	1790	1835	1721	1772	0	0	0	0	0	0	1808	1888	1721	166													
1851	1811	1804	1856	1739	1808	0	0	0	0	0	0	1812	1856	1739	117													
1921	1849	1811	1858	1711	1781	0	0	0	0	0	0	1825	1921	1711	209													
1862	1793	1745	1781	1676	1720	0	0	0	0	0	0	1761	1862	1676	186													
1810	1786	1738	1788	1685	1729	0	0	0	0	0	0	1752	1810	1685	145													
1705	1746	1720	1729	1652	1692	0	0	0	0	0	0	1708	1746	1652	94													
1641	1748	1748	1446	1689	1742	0	0	0	0	0	0	1706	1748	1440	128													
1788	1841	1810	1797	1713	1812	0	0	0	0	0	0	1793	1841	1713	128													
CIRCUIT NO. VALUES-																	PATTERN FACTORS BASED ON INLET TEMP OF SOA.											
AVERAGE TEMP.																	ALL TEMPS ARE FAHRENHEIT											
MAXIMUM TEMP.																												
MINIMUM TEMP.																												
SPREAD, MAX-MIN																												
SPREAD, MAX-AVG																												
STANDARD DEVIATION																												
MAX TEMP GRADIENT																	OVERALL VALUES BASED ON- WEIGHTED											
MAX TEMP GRAD/YUCH																	STRAIGHT BY INPUT											
PATTERN FACTOR																	AVE AGE AREAS											
.007 .065 .096 .079 .055 .049 0.000 0.000 0.000 0.000 0.000 0.000																	*****											
THERMOCOUPLE FUNCTIONS ARE CHROMEL/ALUMEL																	1800. 1904. 1900.											
																	***** 1935. *****											
																	***** 1935. *****											
																	***** 1640. *****											
																	***** 295. *****											
																	135. 131. 135.											
																	.112 .109 .112											
																	.109											

Figure 69. Temperature Spread Factor.



GTCP 305-1 RIG TEST 50, 6/16/71, SCAN 1
 UNIT 305 S/W 0 TEST 50 SCAN 1
 134

```

*****
SS: *****
SS: *****

```

GTCP 305-1 RIG TEST 50 4/16/71, SCAM 1

UNIT 305 S/N 0 TEST 50 SCAN 1

THERMOCUPLE NO.												
RADIUS, IN.												

ANGLE, DEG.	1	2	3	4	5	6	7	8	9	10	11	12

1	1551	2104	1245	2137	1493	1415	0	0	0	0	0	0
2	2027	2000	1474	2156	1402	1410	0	0	0	0	0	0
3	2116	1327	1424	1456	1425	1404	0	0	0	0	0	0
4	2022	1419	1372	2015	1471	1407	0	0	0	0	0	0
5	2177	2009	2027	2050	2094	2082	0	0	0	0	0	0
6	2264	2129	2101	2332	2091	2081	0	0	0	0	0	0
7	2244	2273	2251	2347	2212	2196	0	0	0	0	0	0
8	2437	2443	2417	2454	2354	2318	0	0	0	0	0	0
9	2357	2340	2307	2400	2292	2255	0	0	0	0	0	0
10	2412	2455	2447	2447	2184	2448	0	0	0	0	0	0
11	2244	2214	2124	2351	2110	2094	0	0	0	0	0	0
12	2214	2127	2104	2303	2172	2094	0	0	0	0	0	0
13	2073	2114	1472	2124	1772	1934	0	0	0	0	0	0
14	2314	2200	2147	2204	2122	2124	0	0	0	0	0	0
15	2103	2312	2307	2372	2234	2291	0	0	0	0	0	0
16	2354	2314	2294	2432	2202	2277	0	0	0	0	0	0
17	2281	2272	2251	2244	2100	2255	0	0	0	0	0	0
18	2312	2323	2274	2267	2172	2230	0	0	0	0	0	0
19	2344	2306	2103	2327	2217	2294	0	0	0	0	0	0
20	2214	2264	2154	2157	2154	2151	0	0	0	0	0	0
21	2103	2135	2022	2136	2036	2053	0	0	0	0	0	0
22	2022	1401	1403	2040	1454	1466	0	0	0	0	0	0
23	2024	2147	2050	2173	2042	1997	0	0	0	0	0	0
24	2347	2391	2252	2444	2124	2128	0	0	0	0	0	0

IRADIANT, CAL/IN ²												

AVERAGE TEMP.	2217	2274	2124	2266	2114	2109	0	0	0	0	0	0
MAXIMUM TEMP.	2437	2455	2447	2451	2354	2448	0	0	0	0	0	0
MINIMUM TEMP.	1450	1401	1474	1424	1493	1404	0	0	0	0	0	0
SPREAD, DEG.	427	544	544	455	467	450	0	0	0	0	0	0
STANDARD DEVIATION	223	241	314	124	243	339	0	0	0	0	0	0
MAX TEMP GRADIENT	144	144	171	131	121	174	0	0	0	0	0	0
MAX TEMP GRADIENT	341	289	324	303	295	349	0	0	0	0	0	0
PATTERN FACTOR	118	157	276	116	112	226	0.000	0.000	0.000	0.000	0.000	0.000

THERMOCUPLE LOCATIONS ARE CIRCUMFERENCE												

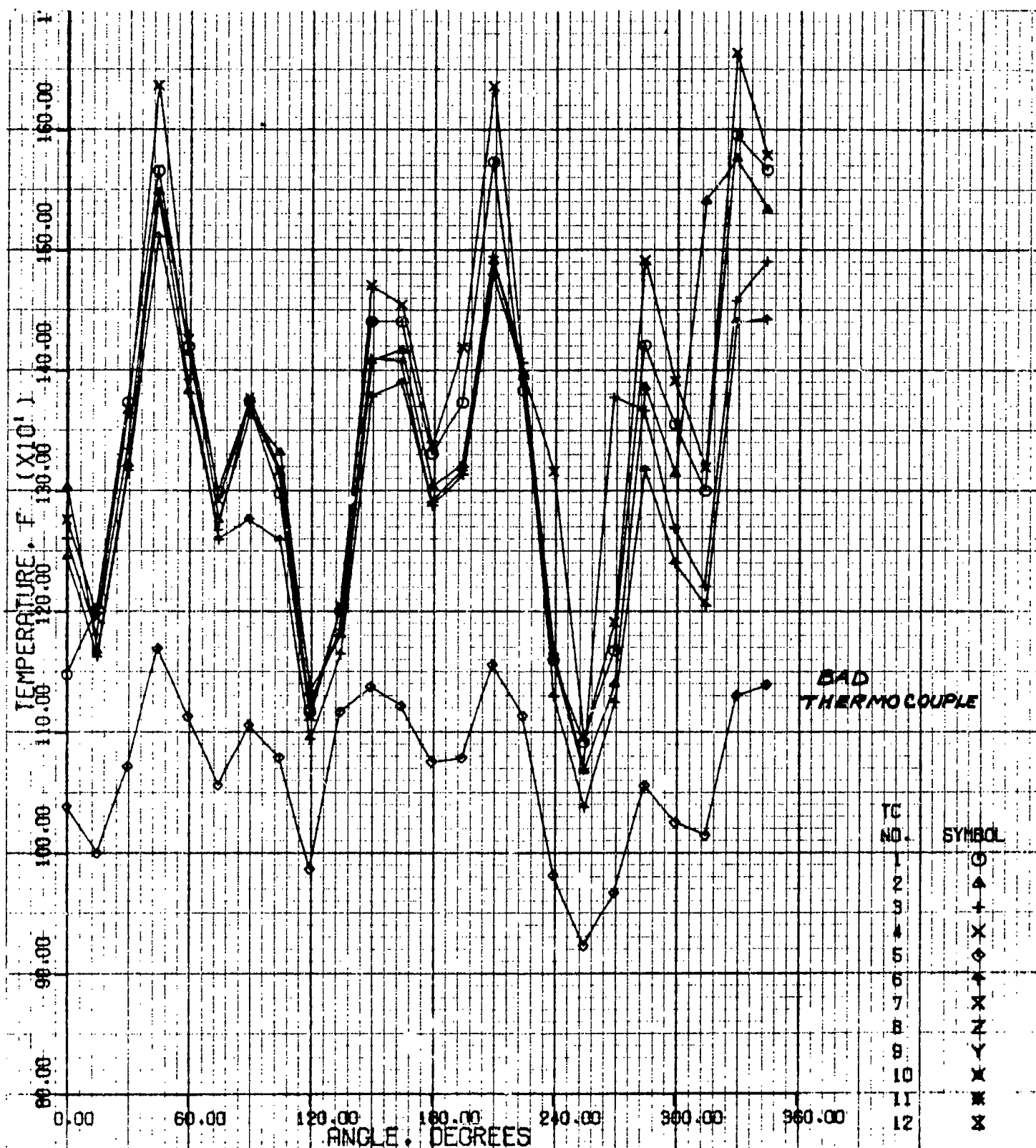
PATTERN FACTORS BASED ON INLET TEMP OF GAS												

ALL TEMPS ARE FAHRENHEIT												

OVERALL VALUES BASED ON STRAIGHT LINE INPUT AVERAGE AREAS												

AVERAGE	2173	2174	2200	2174	2174	2200	0	0	0	0	0	0
MAXIMUM	2459	2459	2459	2459	2459	2459	0	0	0	0	0	0
MINIMUM	1794	1794	1794	1794	1794	1794	0	0	0	0	0	0
MAX-MIN	665	665	665	665	665	665	0	0	0	0	0	0
AVG TO PEAK SPREAD	236	236	236	236	236	236	0	0	0	0	0	0
PATTERN FACTOR BASED ON SINGLE AVERAGE	.183	.183	.183	.183	.183	.183	0	0	0	0	0	0
PATTERN FACTOR, (T MAX - T INLET) / (INPUT AVG - T INLET)	.179	.179	.179	.179	.179	.179	0	0	0	0	0	0

Figure 71. Temperature Spread Factor.



GTCP 305-1 RIG TEST 41 4/17/71L SCAN 3
 UNIT 305 S/N 01 TEST 41 SCAN 8

Figure 72. Temperature Spread Factor.

GRCS 5-1 RIG TEST 410 4/17/71, SEC 1

UNIT 315 C/W 0 TEST 41 SCAN 3

TEMPERATURE NO.	1	2	3	4	5	6	7	8	9	10	11	12	RADIAL VALUES-
410-10	410	410	410	410	410	410	410	410	410	410	410	410	
1	1144	1274	1261	1274	1030	1244	0	0	0	0	0	0	AVG MAX MIN SPREAD
2	1003	1104	1181	1105	1000	1163	0	0	0	0	0	0	0 1212 1304 1039 205
3	1374	1354	1334	1344	1072	1317	0	0	0	0	0	0	0 1152 1203 1000 202
4	1464	1404	1544	1437	1170	1511	0	0	0	0	0	0	0 1298 1374 1072 302
5	1424	1415	1301	1426	1114	1382	0	0	0	0	0	0	0 1497 1637 1170 468
6	1300	1274	1244	1293	1057	1260	0	0	0	0	0	0	0 1358 1426 1114 312
7	1374	1365	1374	1378	1104	1277	0	0	0	0	0	0	0 1242 1300 1057 244
8	1294	1332	1317	1317	1079	1259	0	0	0	0	0	0	0 1312 1378 1166 271
9	1117	1144	1124	1114	487	1004	0	0	0	0	0	0	0 1267 1332 1079 253
10	1201	1111	1185	1205	1117	1165	0	0	0	0	0	0	0 1095 1134 947 147
11	1441	1404	1411	1471	1134	1379	0	0	0	0	0	0	0 1176 1205 1117 17
12	1441	1417	1401	1455	1129	1390	0	0	0	0	0	0	0 1375 1471 1138 333
13	1441	1417	1401	1434	1074	1284	0	0	0	0	0	0	0 1372 1455 1122 333
14	1474	1472	1414	1424	1074	1314	0	0	0	0	0	0	0 1271 1338 1076 262
15	1474	1472	1472	1472	1134	1344	0	0	0	0	0	0	0 1304 1420 1070 340
16	1444	1444	1444	1444	1114	1344	0	0	0	0	0	0	0 1472 1637 1156 481
17	1444	1444	1444	1444	1114	1344	0	0	0	0	0	0	0 1349 1407 1114 293
18	1444	1444	1444	1444	1114	1344	0	0	0	0	0	0	0 1153 1317 982 335
19	1444	1444	1444	1444	1114	1344	0	0	0	0	0	0	0 1048 1096 923 172
20	1444	1444	1444	1444	1114	1344	0	0	0	0	0	0	0 1162 1378 967 411
21	1444	1444	1444	1444	1114	1344	0	0	0	0	0	0	0 1340 1402 1056 434
22	1444	1444	1444	1444	1114	1344	0	0	0	0	0	0	0 1266 1392 1026 366
23	1444	1444	1444	1444	1114	1344	0	0	0	0	0	0	0 1267 1542 1015 527
24	1444	1444	1444	1444	1114	1344	0	0	0	0	0	0	0 1478 1665 1131 534
25	1444	1444	1444	1444	1114	1344	0	0	0	0	0	0	0 1459 1580 1140 440

TEMPERATURE NO.	1	2	3	4	5	6	7	8	9	10	11	12	RADIAL VALUES-
410-10	410	410	410	410	410	410	410	410	410	410	410	410	
1	1144	1274	1261	1274	1030	1244	0	0	0	0	0	0	AVG MAX MIN SPREAD
2	1003	1104	1181	1105	1000	1163	0	0	0	0	0	0	0 1212 1304 1039 205
3	1374	1354	1334	1344	1072	1317	0	0	0	0	0	0	0 1152 1203 1000 202
4	1464	1404	1544	1437	1170	1511	0	0	0	0	0	0	0 1298 1374 1072 302
5	1424	1415	1301	1426	1114	1382	0	0	0	0	0	0	0 1497 1637 1170 468
6	1300	1274	1244	1293	1057	1260	0	0	0	0	0	0	0 1358 1426 1114 312
7	1374	1365	1374	1378	1104	1277	0	0	0	0	0	0	0 1242 1300 1057 244
8	1294	1332	1317	1317	1079	1259	0	0	0	0	0	0	0 1312 1378 1166 271
9	1117	1144	1124	1114	487	1004	0	0	0	0	0	0	0 1267 1332 1079 253
10	1201	1111	1185	1205	1117	1165	0	0	0	0	0	0	0 1095 1134 947 147
11	1441	1404	1411	1471	1134	1379	0	0	0	0	0	0	0 1176 1205 1117 17
12	1441	1417	1401	1455	1129	1390	0	0	0	0	0	0	0 1375 1471 1138 333
13	1441	1417	1401	1434	1074	1284	0	0	0	0	0	0	0 1372 1455 1122 333
14	1474	1472	1414	1424	1074	1314	0	0	0	0	0	0	0 1271 1338 1076 262
15	1474	1472	1472	1472	1134	1344	0	0	0	0	0	0	0 1304 1420 1070 340
16	1444	1444	1444	1444	1114	1344	0	0	0	0	0	0	0 1472 1637 1156 481
17	1444	1444	1444	1444	1114	1344	0	0	0	0	0	0	0 1349 1407 1114 293
18	1444	1444	1444	1444	1114	1344	0	0	0	0	0	0	0 1153 1317 982 335
19	1444	1444	1444	1444	1114	1344	0	0	0	0	0	0	0 1048 1096 923 172
20	1444	1444	1444	1444	1114	1344	0	0	0	0	0	0	0 1162 1378 967 411
21	1444	1444	1444	1444	1114	1344	0	0	0	0	0	0	0 1340 1402 1056 434
22	1444	1444	1444	1444	1114	1344	0	0	0	0	0	0	0 1266 1392 1026 366
23	1444	1444	1444	1444	1114	1344	0	0	0	0	0	0	0 1267 1542 1015 527
24	1444	1444	1444	1444	1114	1344	0	0	0	0	0	0	0 1478 1665 1131 534
25	1444	1444	1444	1444	1114	1344	0	0	0	0	0	0	0 1459 1580 1140 440

Figure 73. Temperature Spread Factor.

NOTES:

1. Combustor inlet temperature = 90°F
2. Combustor inlet pressure = 5 psig
3. Fuel = JP-5

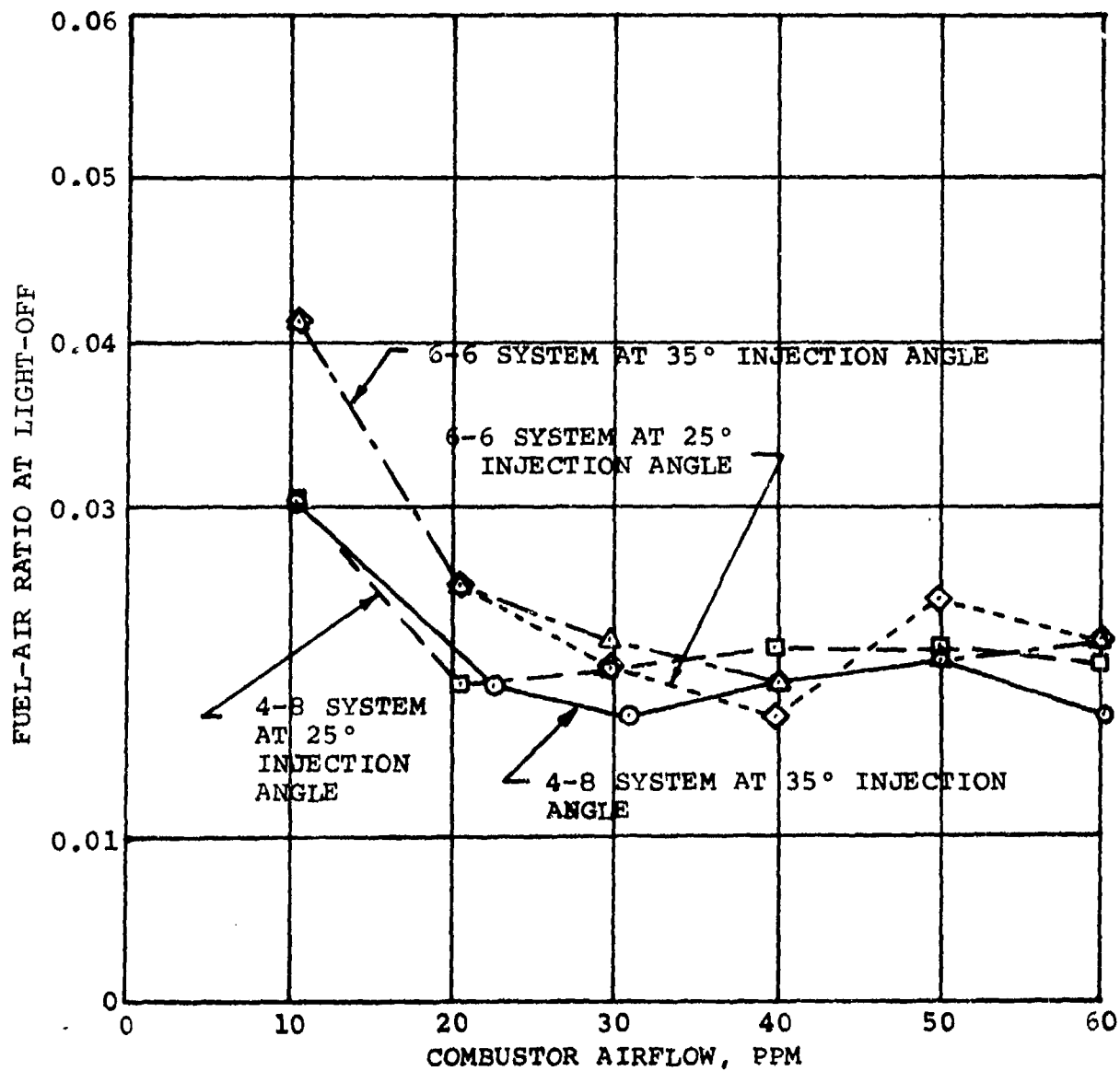


Figure 74. Sea-Level Ignition Characteristics.

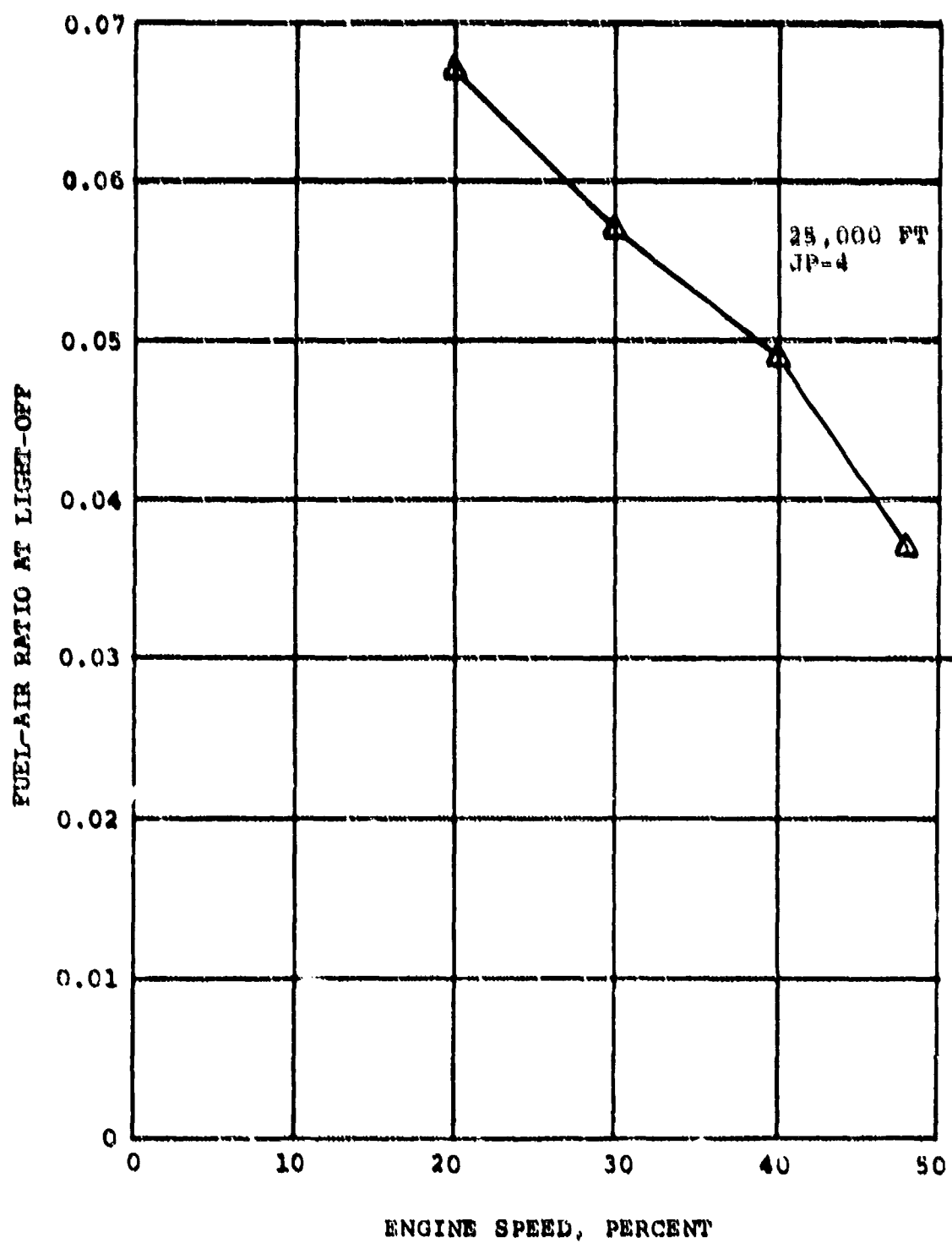


Figure 75. 25,000-Ft Altitude Ignition Characteristics.

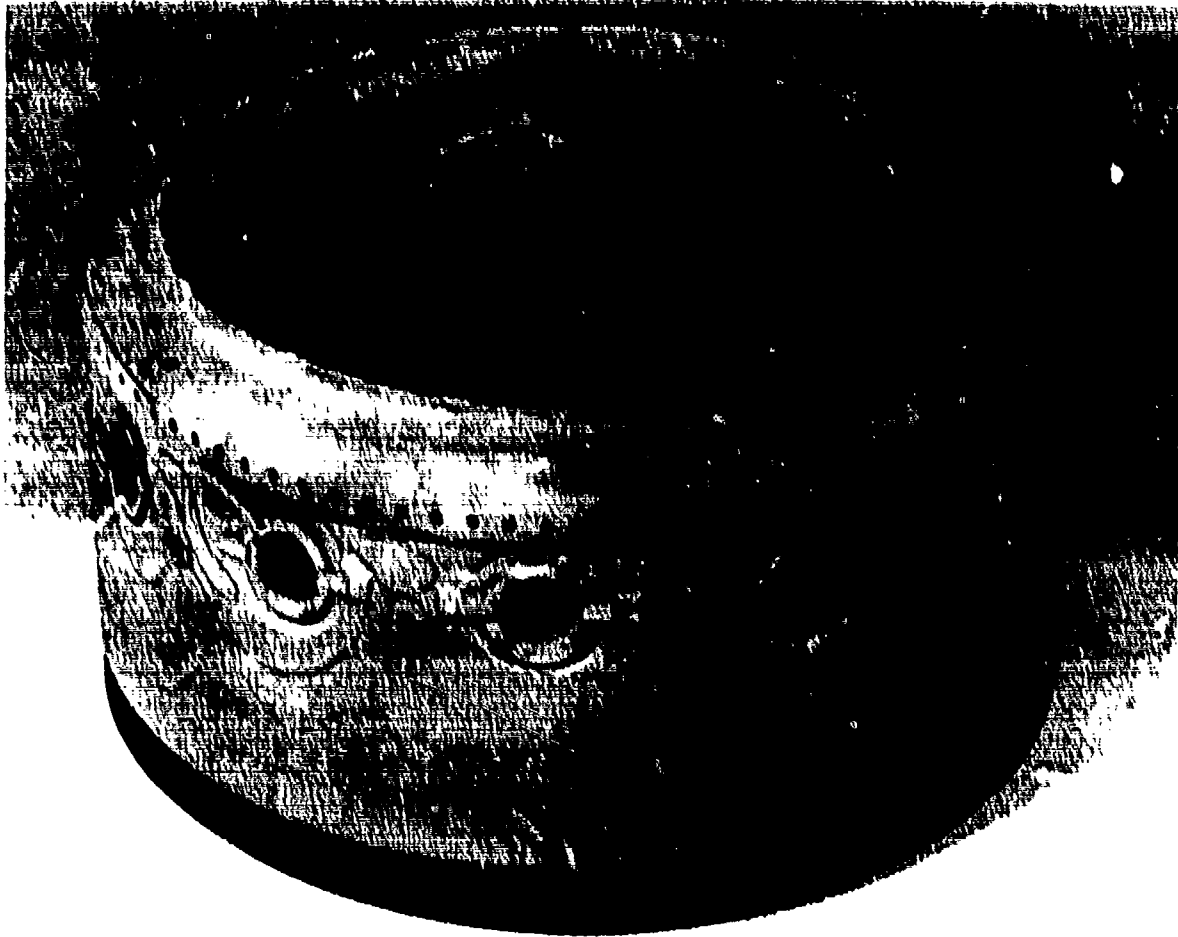


Figure 76. Combustor.

SECTION V

TURBINE DESIGN AND DEVELOPMENT

The basic design philosophy of the turbine section was to determine the smallest configuration that would exhibit an acceptable level of efficiency and would require a minimum cooling airflow rate.

Turbine analyses were conducted using three basic turbine wheel arrangements for both the single-shaft and the free-turbine APU configurations. The smallest configuration was for a two-stage axial turbine. The high-pressure ratio across the first-stage wheel dictated a very high Mach number within the turbine blading. The predicted efficiency of this type of power loading was less than that for a radial turbine wheel of similar loading.

A three-stage axial wheel turbine section was analyzed, with the first two stages replacing the high-work first-stage of the two-stage axial configuration. The efficiency of this general design was much better than that of the two-stage axial wheel, but the overall length is greater, which could cause the overall length of the APU to exceed the design goal.

Turbine configurations consisting of a radial inflow first stage and one or two axial stages proved to be the most efficient. The higher efficiency radial-inflow stage replaces either the high-work single-axial or the first two stages. Therefore, a radial first stage and an axial second stage formed the basis for the reference design.

Turbine analyses were conducted for two basic shaft speeds-- 80,860 and 89,000 rpm. The higher speed is more desirable for best aerodynamic efficiency and minimum size, but the lower speed gives a

lower stress. The analyses assumed that the tip clearance was 0.015 in. and the turbine exit diffuser recovery factor* was 0.50.

Designing the APU for maximum power required an 8 percent increase in turbine flowpath dimensions to accommodate the increased flow and power at the final design speed of 81,800 rpm. The stress levels in the turbine rotating components would not be exceeded since the final rotating speed was lower than the original design speed of 89,000 rpm.

The design-point work split between the first (radial) and the second (axial) stage was established at 2:1. The radial turbine was sized for a corrected flow of 0.474 lb/sec (with cooling) and the axial stage for 1.736 lb/sec. The efficiency goals for the two turbines were 89.7 percent (total-to-total) for the radial stage and 80 percent (inlet total-to-diffuser exit static) for the axial stage and a calculated combined efficiency of 86 percent. The calculated or rig test efficiencies for the radial turbine do not include the effects of cooling. The effect of cooling air is handled as a leakage to the ambient atmosphere in overall engine performance.

Table XI summarizes the aerodynamic goals of the turbine section. The radial turbine vector diagrams (Figures 77 and 78) and the axial turbine vector diagrams (Figure 79) were used to determine these goals.

1. RADIAL STAGE

In the design of a radial turbine, certain aerodynamic trade-offs are required because of thermal and mechanical considerations. The maximum number of blades and splitters is determined by disk stresses, boundary layer losses, and manufacturing capabilities. The minimum

*Diffuser recovery factor is defined as the ratio of the static pressure recovery through the diffuser to the velocity head pressure at the turbine exit.

TABLE XI
TURBINE AERODYNAMIC DESIGN GOALS

Parameters	Radial Turbine	Axial Turbine
$T'_{in}, ^\circ R$	2659.7	1967.9
$T'_{out}, ^\circ R$	2006.1	1660.4
$H'_{in}, \text{Btu/lb}$	712.89	508.19
$H'_{out}, \text{Btu/lb}$	519.95	421.32
$(P_{in}/P_{out})_{T-T}$	4.167	2.275
$W\sqrt{\theta}/\delta, \text{lb/sec}$	0.447*	1.736
$N/\sqrt{\theta}, \text{rpm}$	36,123.9	41,996.2
$\Delta H/\theta$	37.62	44.6
θ	5.128	3.794
δ	10.503	2.470
η_{T-T}	89.66	91.72
η_{T-S}	86.43	86.38
N, rpm	81,800	81,800
N_s	65.5	195.6
Cooling flow, W_c/W_1	0.06	0
*Cooling flow not included.		

$$N_s = 65.5$$

$$F_v = 0.9296$$

$$U_T = 2190 \text{ FT/SEC}$$

NOZZLE EXIT $R = 3.1599 \text{ IN.}$ 19 VANES

$$T_1' = 2659.7^\circ\text{R}$$

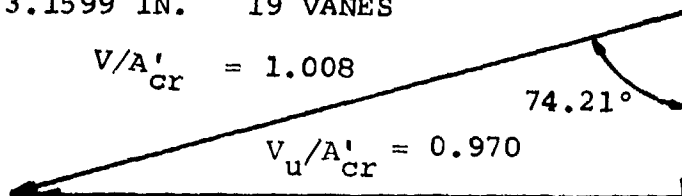
$$V/A_{cr}' = 1.008$$

$$A_{cr1}' = 2273.58 \text{ FT/SEC}$$

$$V_u/A_{cr}' = 0.970$$

$$74.21^\circ$$

$$V_x/A_{cr}' = 0.274$$



ROTOR TIP

$R = 3.0679 \text{ IN.}$

$$T_2' = 2659.7^\circ\text{R}$$

$$T_2'' = 2332.6^\circ\text{R}$$

$$\Delta T = 327.1^\circ$$

$$A_{cr2}' = 2273.58$$

$$A_{cr2}'' = 2129.20 \text{ FT/SEC}$$

$$W/A_{cr}' = 0.3063$$

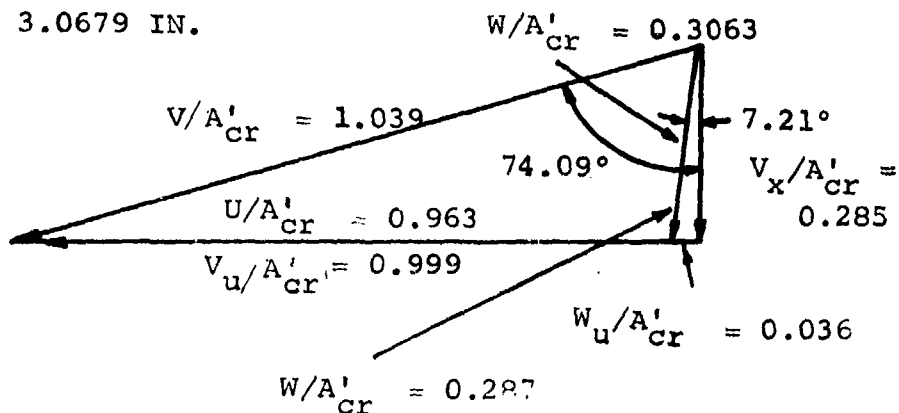
$$V/A_{cr}' = 1.039$$

$$U/A_{cr}' = 0.963$$

$$V_u/A_{cr}' = 0.999$$

$$74.09^\circ$$

$$V_x/A_{cr}' = 0.285$$



ROTOR EXIT HUB

$R = 1.2500 \text{ IN.}$

$$T_3' = 1986.42^\circ\text{R}$$

$$T_3'' = 2040.0^\circ\text{R}$$

$$A_{cr3}' = 1964.83$$

$$A_{cr3}'' = 1991.16$$

$$\beta_3 = 55.2^\circ$$

$$\frac{W_e}{W_I} = 1.697$$

$$V_x/A_{cr}' = 0.334$$

$$W/A_{cr}'' = 0.556$$

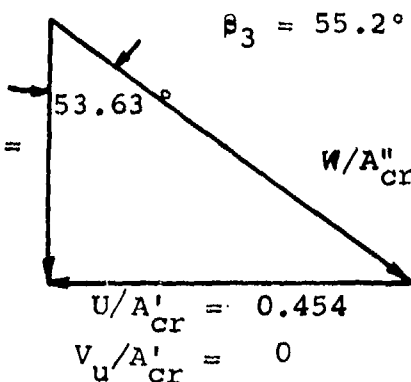


Figure 77. Radial Turbine Vector Diagram.

MEAN LINE R = 1.75 IN.

$$T_3' = 1986.42^\circ\text{R}$$

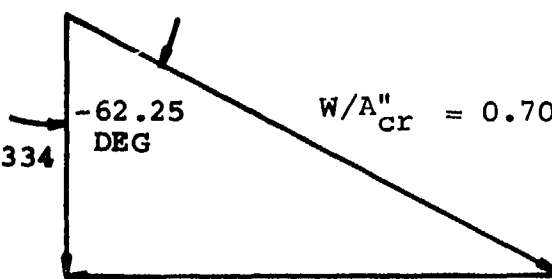
$$T_3'' = 2091.87^\circ\text{R}$$

$$A_{cr3}'' = 1964.83$$

$$A_{cr3}' = 2016.31$$

$$V_f/A_{cr}' = 0.334$$

$$\beta_b = -62.5 \text{ DEG}$$



$$U/A_{cr}' = 0.636$$

$$V_u/A_{cr}' = 0$$

ROTOR EXIT TIP R = 2.183 IN.

$$T_3' = 1986.42^\circ\text{R}$$

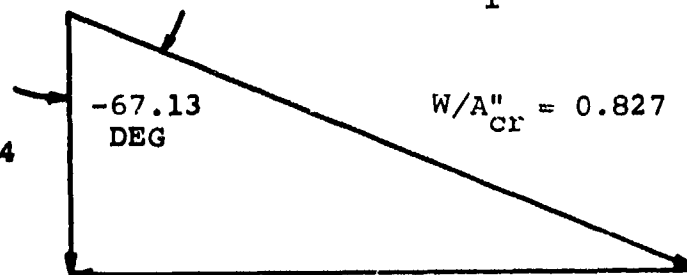
$$T_3'' = 2150.58^\circ\text{R}$$

$$A_{cr3}' = 1964.93$$

$$A_{cr3}'' = 2044.40$$

$$V_f/A_{cr}' = 0.334$$

$$\beta_b = 67.6 \text{ DEG}, \frac{W_e}{W_1} = 2.591$$



$$V/A_{cr}' = 0.793$$

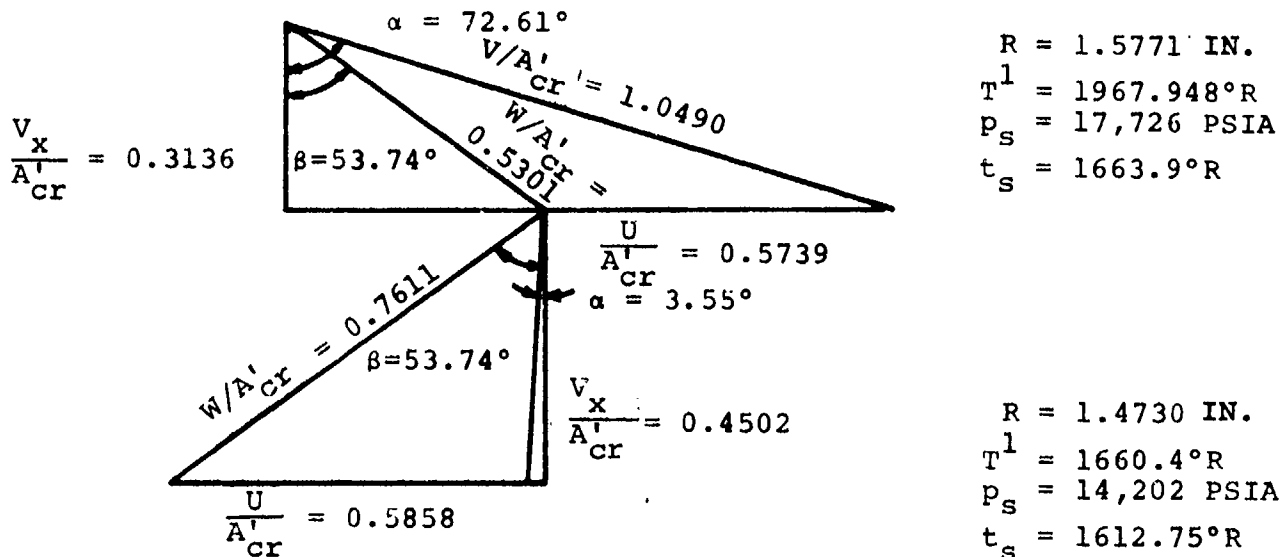
$$V_u/A_{cr}' = 0$$

$$\frac{N}{\sqrt{A}} = 36,123.9 \text{ RPM}$$

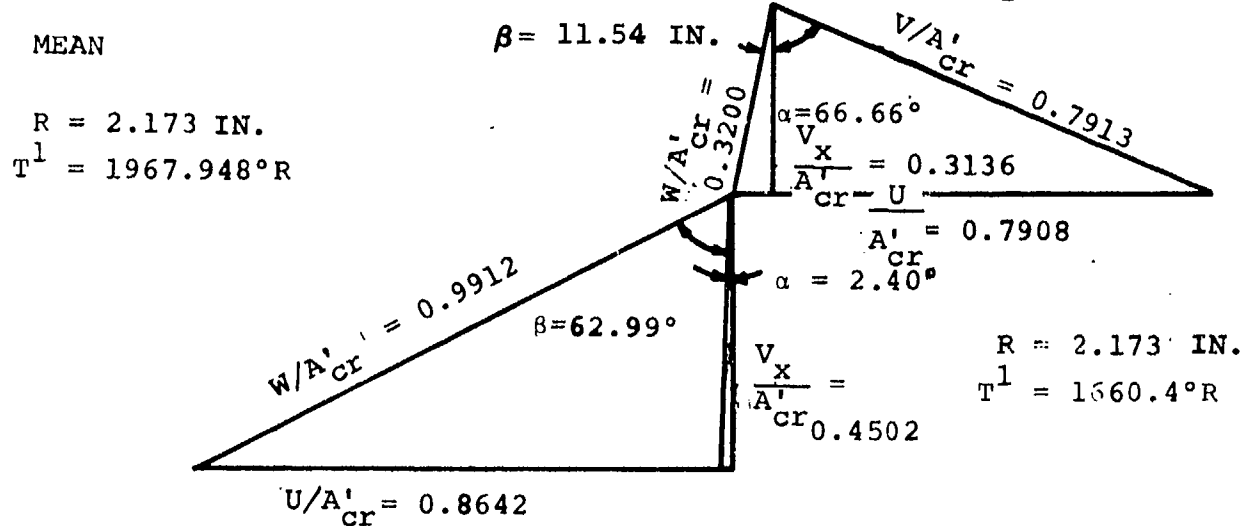
$$P_{rT-T} = 4.167$$

Figure 78. Radial Turbine Vector Diagrams, Rotor Exits.

HUB



MEAN



TIP

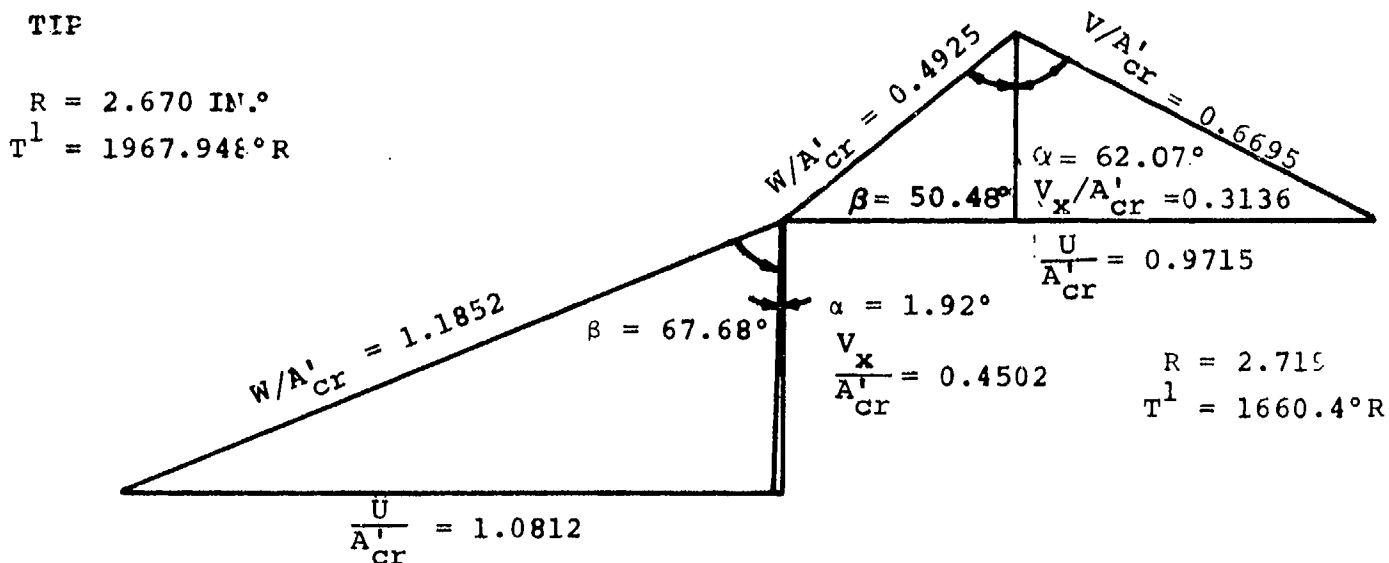


Figure 79. Axial Turbine Vector Diagrams

number of blades is generally determined by aerodynamic blade loading, which increases as the number of blades decreases. Current practice has been to design radial turbines with as many blades and splitters as practical from a mechanical viewpoint. This allows the blade loading to be reduced to the point where separation of the flow from the suction surface of the blade will not occur. However, the analytical techniques available do not permit a clear definition of the efficiency penalty incurred by decreasing the number of blades.

Stress analysis of the radial turbine in the GTCP305 has indicated that the turbine life could be improved with fewer blades. A three-dimensional, finite difference, analytical technique was developed to determine the effect of blade number on turbine efficiency. The reference radial turbine was analyzed, and the conclusion was that the number of blades and splitters could be reduced from 10 to 8 each, with approximately two to three points decrease in efficiency. To determine the possible efficiency penalty, the splitters were removed from the reference turbine wheel and tested. This reduced the efficiency 1.7-percentage points instead of the predicted 2 to 3.

The radial turbine was designed for a work output of 193 Btu/lb, with a total-to-total pressure ratio across the stage of 4.167. The wheel was designed with 20 blades (10 full + 10 splitters) and a tip speed of 2190 ft/sec. The vector diagrams for this stage were determined for a mean-line rotor reaction ratio (ratio of exit to inlet absolute velocities at mean line) of 1.808 and the following design considerations:

- (a) A rotor exit hub diameter for the flow passage of 2.50 in.
- (b) A stator-to-rotor radial clearance of 0.092 in.
- (c) An 8-in. OD on the turbine nozzle vane assembly.

- (d) The rotor was sized to pass 3 percent more flow than the stator, to allow for the cooling flow through the rotor itself.
- (e) The specific speed of the radial turbine was $65.5 \text{ (rpm-ft}^{3/4}\text{) / sec}^{1/2}$, which places the turbine in the high-efficiency range.

The radial turbine nozzle is an uncooled, 19-blade design. The aerodynamic vane shape was determined to satisfy the vector diagram requirements and to fit between an inner radius of 3.16 in. and an outer radius of 3.95 in. The trailing edge of the vane has a 0.030-in. thickness (0.015 rad), which is a practical minimum for high-temperature materials.

2. AXIAL STAGE

2.1 Preliminary Design

Following the design-point selection, an investigation was made to determine the lowest exit axial velocity compatible with the following mechanical design limitations:

- (a) Blade Centrifugal Stress - A value of 60,000 psi is considered a reasonable upper limit for cast materials. (The initial selection of the vector diagram produced a stress level of 61,668.9 psi and a life of 36,163 hr, based on the material properties of IN 713LC.)
- (b) Rotor Blade Tip Radius - To maintain an overall package maximum diameter of 10 in. and provide space for the annular combustor and containment ring, the rotor blade tip radius had to be kept within acceptable limits.

- (c) Manufacturing Consideration - The blading selection from the velocity diagrams should be such that construction will give predictable results.

Based on the above considerations at the axial rotor exit, the critical velocity ratio of $V_x/A_{cr} = 0.45$ was chosen as the best compromise. This also fixed the rotor exit blade tip radius at $R_{tip} = 2.7187$ in., since the rotor exit hub radius had originally been chosen at $R_{hub} = 1.473$ in. This choice of rotor exit hub radius was based on a stage work coefficient of $\lambda = 2$ at the hub.

2.2 Exhaust Diffuser

The selection of a rotor exit critical velocity ratio, $V_x/A_{cr} = 0.45$, placed on the exhaust diffuser the recovery of this exit kinetic energy before the final "dump" to the atmosphere. To achieve this goal, the design of the exhaust diffuser was based on a combination of experiences from other AiResearch units and current available literature. In-house experience has indicated the diffuser shroud recovers proportionately more static pressure than the hub, where the ratio of hub to shroud recovery is on the order of 2:3.

2.3 Stage Efficiency and Off-Design Performance

After completion of the detailed stage design, the anticipated stage efficiency was computed, and the stage off-design performance maps were generated. During the initial analysis, the attainable stage efficiency was determined by a parametric study aiming at the optimum geometry for this design and was achieved by accounting for the profile losses and the end wall effects.

3. AERODYNAMIC DEVELOPMENT

3.1 Two-Stage Testing

To determine the overall and stage performance of the GTCP305 turbine section, a cold-air test rig was designed and fabricated. Incorporated into this basic rig was the GTCP305 radial and axial turbine with the same rear bearing as used in the engine.

The most significant feature was the high-speed operation. The design engine speed was 81,800 rpm, corresponding to a corrected design speed of 36,124 rpm. The cold-air mapping test required speeds to 60,000 rpm. Multiple gearboxes were necessary and any available torquemeters for verification of turbine temperature drop were excluded. The difficulty of high-speed operation was aptly demonstrated early in the test, when the 2:1 gearbox, purchased primarily for this test program, failed because of a faulty coupling. However, this particular problem of the test rig was overcome, and valid data were obtained.

From Test 1, low speed test data were obtained to allow an evaluation of the mechanical integrity of the test rig with minimum risk. The APU-size turbine section (Figure 80) was used as the test specimen. The test configuration clearances for the radial stage were 0.021 in. axial and 0.014 in. radial. The axial-stage radial and the back shroud clearances were both 0.076 in. Testing was completed through 115-percent speed.

The design-point efficiency was exceeded by 0.5 points while the design flow of $W\sqrt{\theta} \delta = 0.4604$ was exceeded by 18 percent. The reasons for the excessive flow were:

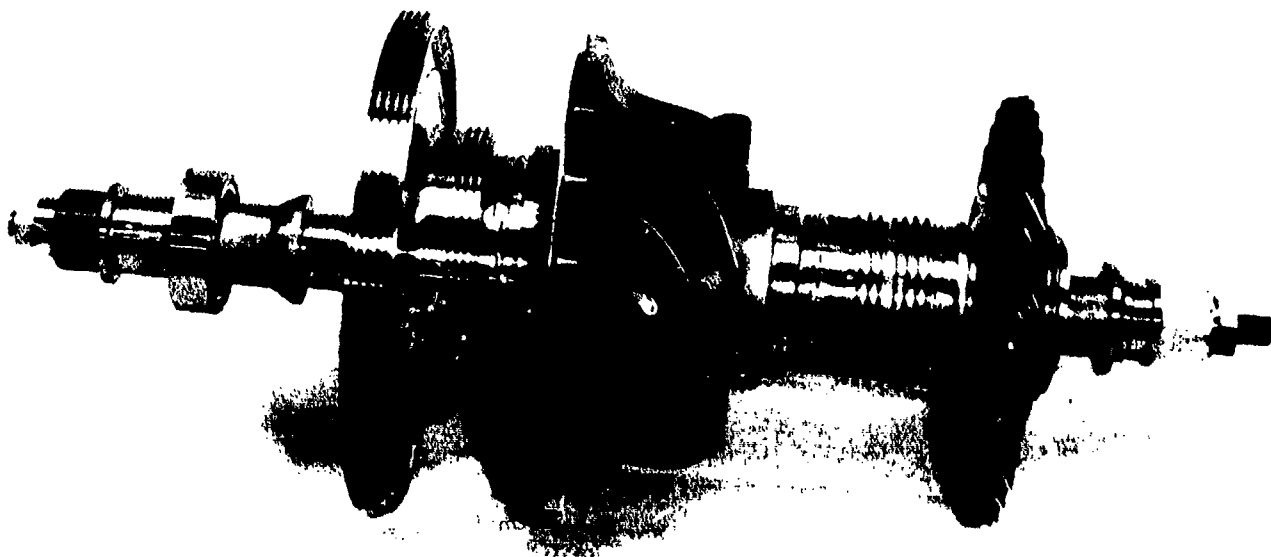
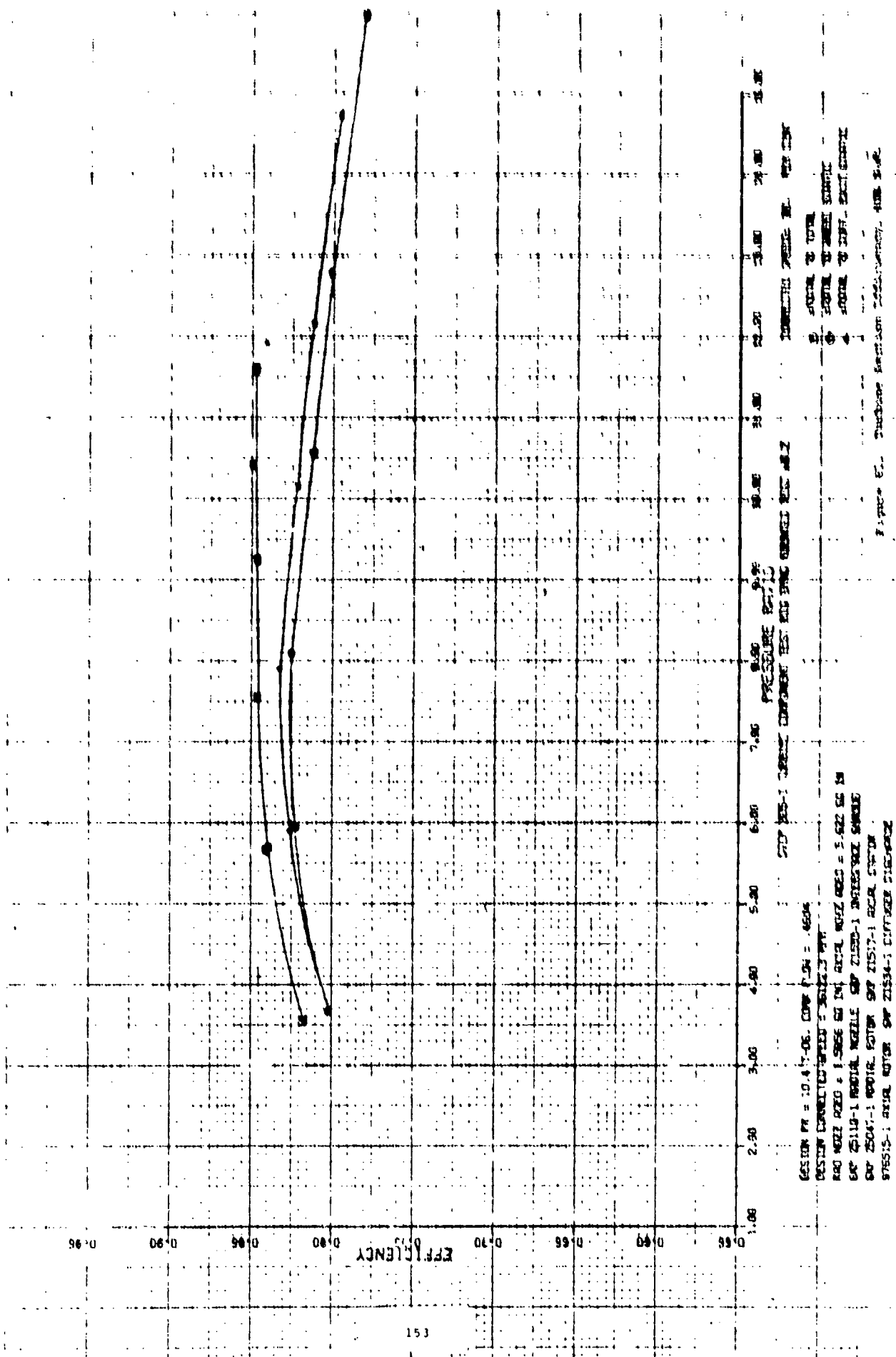


Figure 80. Scalloped Radial Wheel and Axial Turbine Assembly.

- (a) The nozzle "b" width was increased by 6.1 percent in the cold air test rig, to ensure the correct rotor flow since the cooling scheme was not duplicated in the test rig.
- (b) The nozzle flow coefficient was 0.995 rather than the 0.95 assumed in the design calculations; this is equivalent to opening the nozzle by 4.5 percent.
- (c) The nozzles were designed first in the axial plane and then transformed to the radial plane. During this transformation, the throat was inadvertently opened 5 percent.
- (d) The variation in the ratio of specific heats between the engine operating temperature and the cold air rig was equivalent to opening the nozzle 1.7 percent.

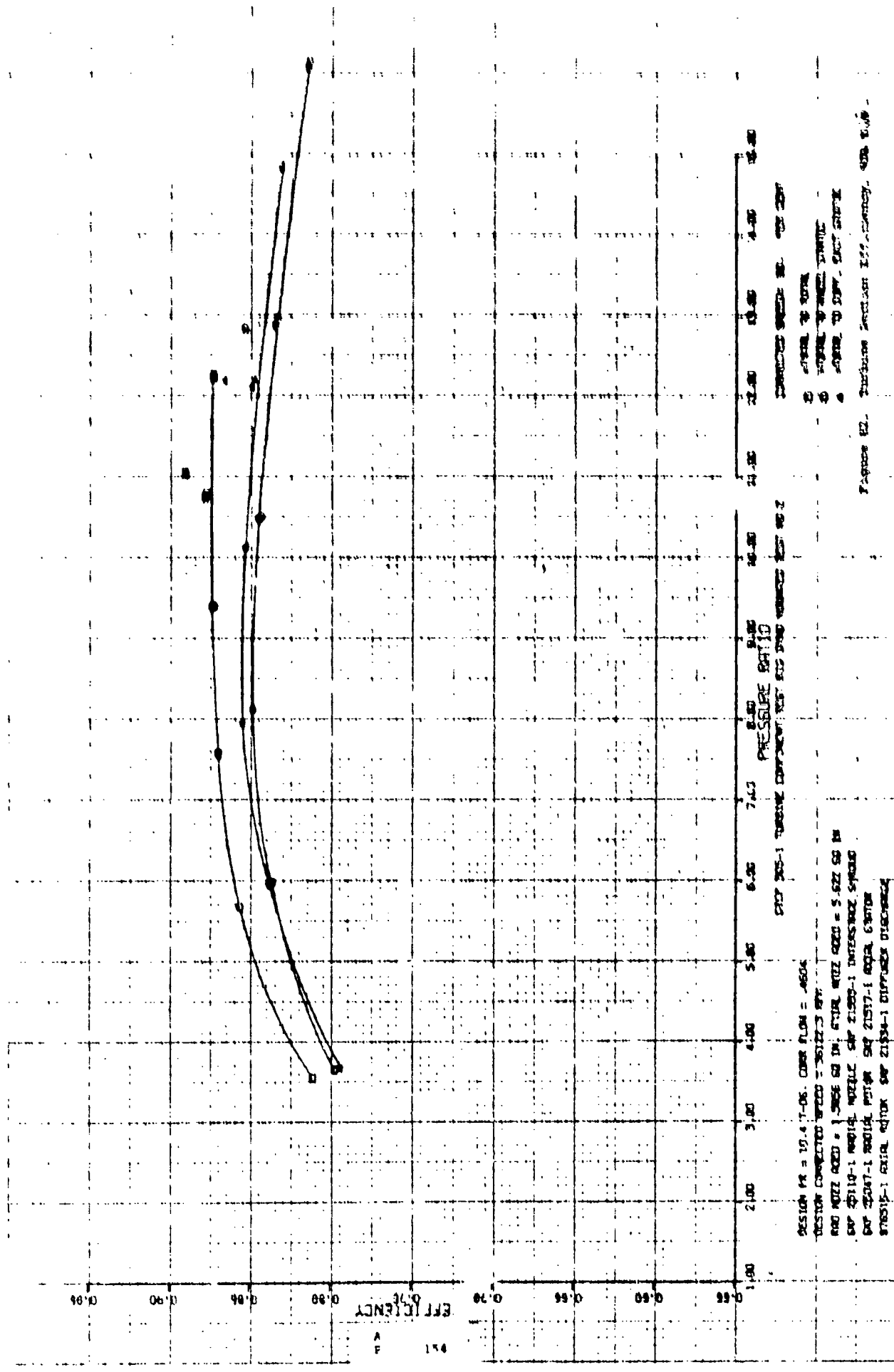
The results of these effects can account for 17.3 percent of the flow discrepancy. The remaining 0.7 percent could be either an accounting error or the result of leakage past the nozzle along the end plate. For the nozzle "b" width, an opening of only 0.002 in. could account for 0.7 percent flow. In fact, during Test 1, when the downstream pressure was reduced to increase the turbine pressure ratio, the large diameter adaptor at the discharge had enough of a cross-pressure differential to induce a bending moment in the radial turbine front shroud sufficiently large to warrant a modification of the rig to include tension ties between the front shroud (P/N 21532) and the exhaust adaptor (P/N 21520).

Figures 81 through 86 present the overall results of Test 2 from 80 through 115 percent of corrected design speed ($N/\sqrt{\theta} = 36,124$ rpm). Operation at higher speeds was abandoned due to the appearance of a predicted critical frequency of the test rig at 120-percent speed.



DESIGN PR = 10.4:1-06. COMP P.04 = 4504
 DESIGN CORRECTION FACTOR = 0.9223
 RAO WZ 020 = 1.9856 SQ IN. RAO WZ 020 = 1.922 SQ IN
 SQ 05119-1 RAO WZ 020 21533-1 RAO WZ 020 21533-1
 SQ 25047-1 RAO WZ 020 21533-1 RAO WZ 020 21533-1
 21533-1 RAO WZ 020 21533-1 RAO WZ 020 21533-1

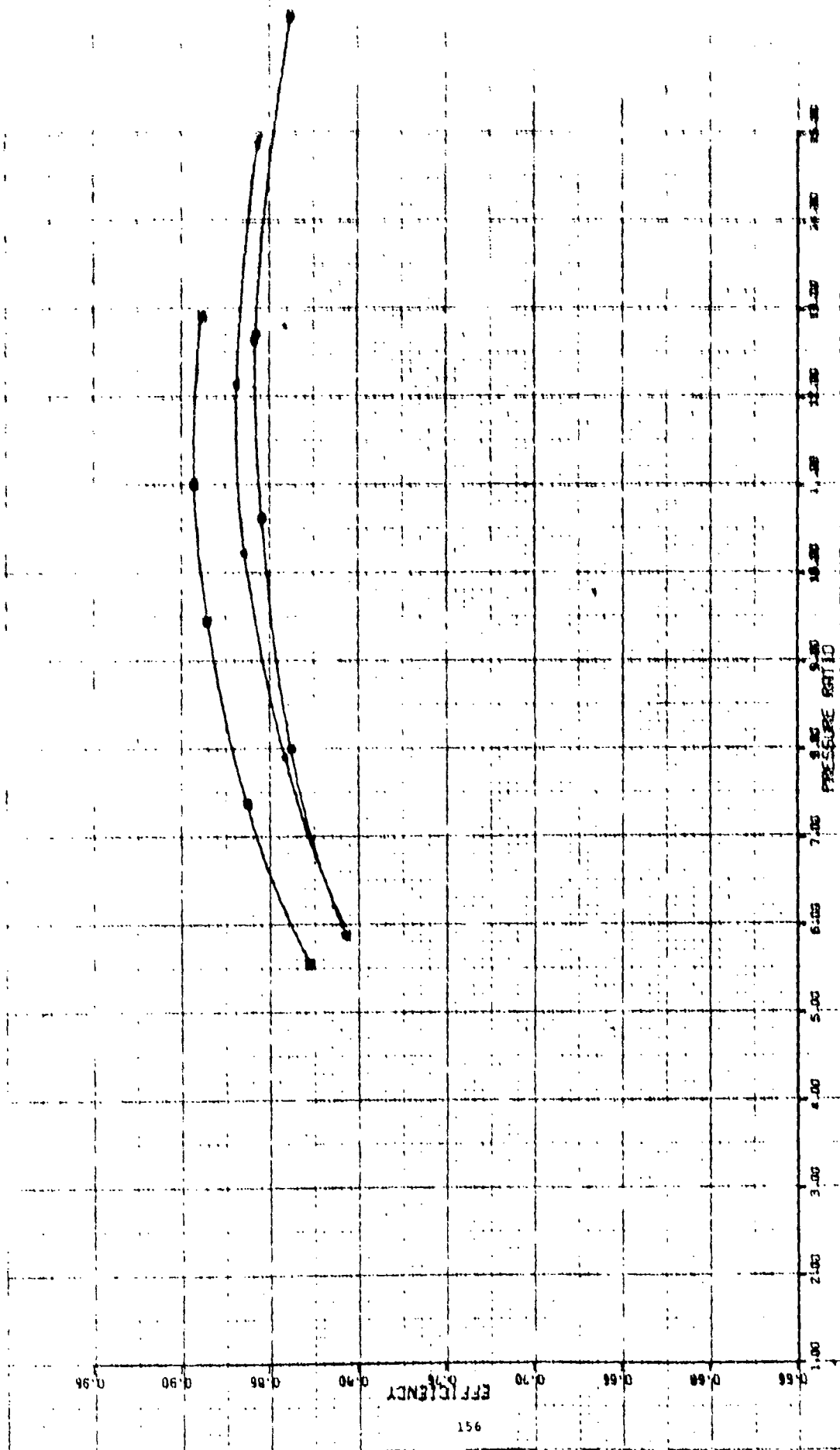
EFFICIENCY
 PRESSURE RATIO
 2.50 3.00 4.00 5.00 6.00 7.00 8.00 9.00 10.00 11.00 12.00 13.00 14.00 15.00
 0.86 0.88 0.90 0.92 0.94 0.96 0.98 1.00
 1.00 0.98 0.96 0.94 0.92 0.90 0.88 0.86
 0.84 0.82 0.80 0.78 0.76 0.74 0.72 0.70 0.68 0.66 0.64 0.62 0.60 0.58 0.56 0.54 0.52 0.50 0.48 0.46 0.44 0.42 0.40 0.38 0.36 0.34 0.32 0.30 0.28 0.26 0.24 0.22 0.20 0.18 0.16 0.14 0.12 0.10 0.08 0.06 0.04 0.02 0.00



DESIGN PR = 10.4:1-06. CORR. FLOW = .0604
 DESIGN CORRECTED SPEED = 30122.5 RPM
 R00 NOZZ ORDN = 1.0656 OR IN. 67102. NOZZ ORDN = 5.622 60 IN
 OR 21110-1 NOZZLE ORDN 21100-1 INTERNOZ SYNOLO
 OR 21047-1 NOZZLE ORDN 21017-1 ORDN 67102
 87815-1 AXIAL ORDN OR 21134-1 DISPOSED DISCHARGE

DESIGN PR = 10.4:1-06. CORR. FLOW = .0604
 DESIGN CORRECTED SPEED = 30122.5 RPM
 R00 NOZZ ORDN = 1.0656 OR IN. 67102. NOZZ ORDN = 5.622 60 IN
 OR 21110-1 NOZZLE ORDN 21100-1 INTERNOZ SYNOLO
 OR 21047-1 NOZZLE ORDN 21017-1 ORDN 67102
 87815-1 AXIAL ORDN OR 21134-1 DISPOSED DISCHARGE

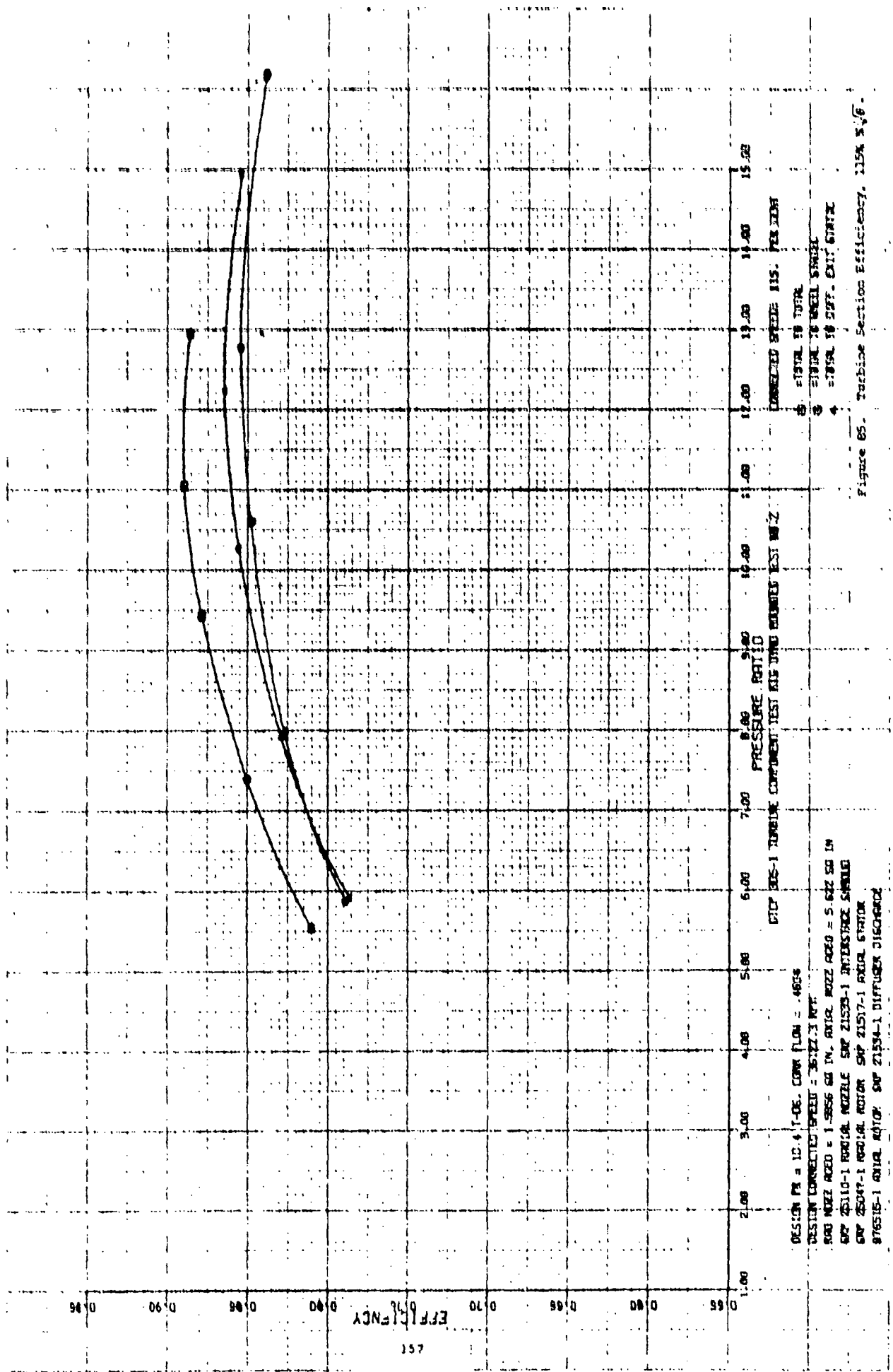
Figure 12. Turbine Section Efficiency vs. Pressure Ratio



DESIGN PR = 10.4 PSIA, CORR P.05 = .6504
 DESIGN CORRECTED SPEED = 3612.3 RPM
 NOZ NOZZ AXES = 1.5856 IN, AXIAL NOZZ AXES = 5.622 IN
 CAP 28110-1 NOZZLE NOZZLE CAP 21503-1 INTERMEDIATE SANGUIC
 CAP 25047-1 NOZZLE NOZZLE CAP 21517-1 NOZZLE SANGUIC
 976515-1 AXIAL NOZZLE CAP 21534-1 DIFFUSER 0.000000

DESIGN SPEED = 130 PER CENT
 1. AXIAL NOZZLE
 2. AXIAL NOZZLE SANGUIC
 3. AXIAL NOZZLE SANGUIC

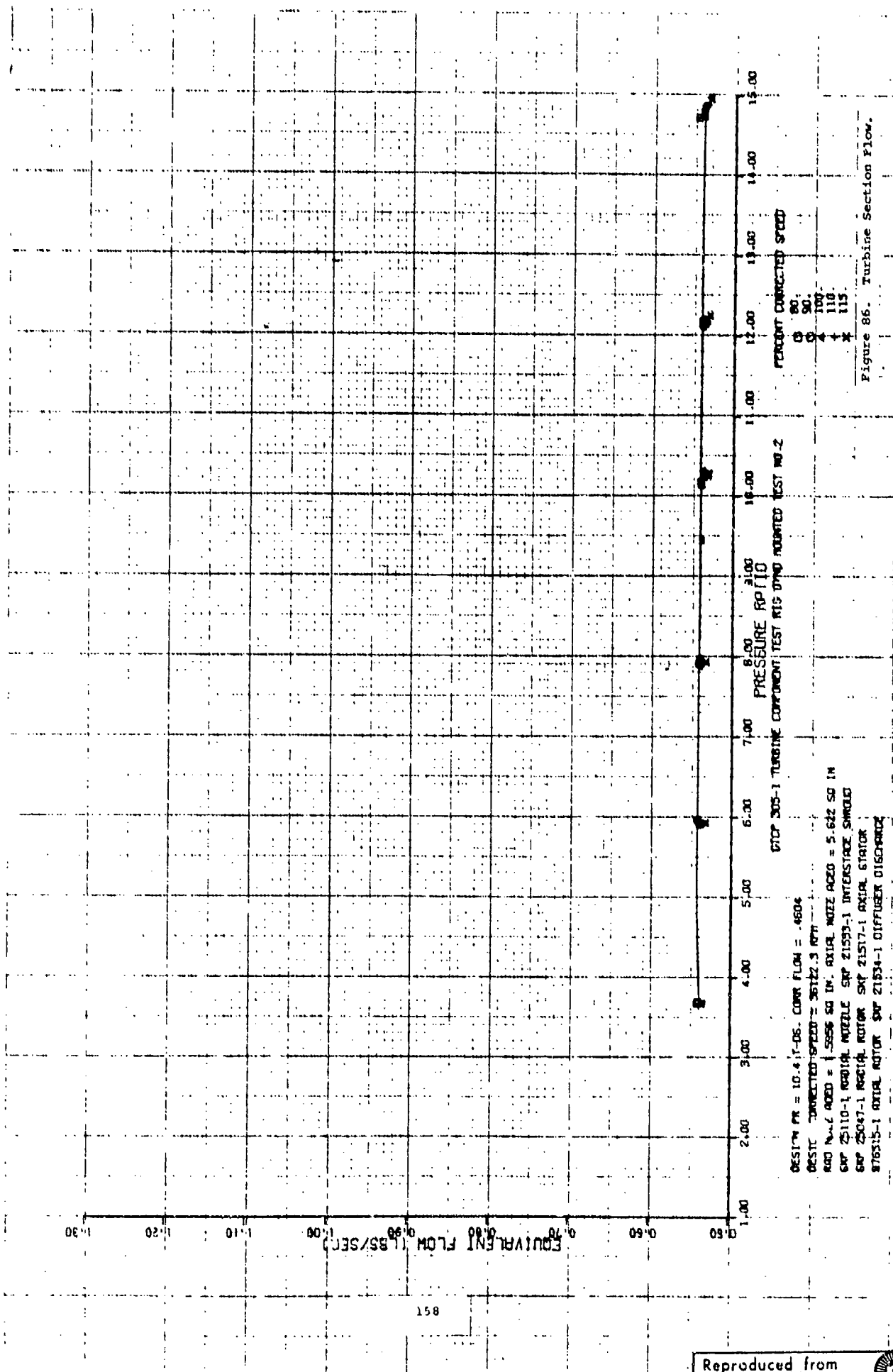
Figure 54. Turbine Section Efficiency, 1000 RPM



DESIGN PM = 12.4 T-05. CORN FLOW = .4675
 DESIGN CORRECTED SPEED = 36,227 RPM
 800 NOZZ A200 = 1.5856 IN. AXIAL NOZZ A200 = 5.622 SQ IN
 807 25110-1 RADIAL NOZZLE 807 21533-1 INTERMEDIATE SHAFT
 807 25047-1 RADIAL ROTOR 807 21517-1 AXIAL STATION
 876515-1 AXIAL ROTOR 807 21534-1 DIFFUSER DISCHARGE

CONVERTED SPEED 115. PERIOD
 1. 21517 TO 21533
 2. 21533 TO 21547
 3. 21547 TO 21561

Figure 65. Turbine Section Efficiency, 115% $\sqrt{6}$.



An analysis of the interstage data indicated that, due to the higher-than-design flow rate, the design-pressure ratio across the radial stage was not achieved; therefore, the remaining interstage data were not reduced. However, the radial survey data at several points of interest were reduced to aid in isolating possible stage interaction effects. Figure 87 presents the survey results at the discharge of the radial turbine at a constant pressure ratio of $PR_{T-T} = 3.9$ across the radial stage for 90- through 110-percent corrected design speed. From these data, the primary problem with the radial stage seemed to be the accumulation of low energy fluid near the shroud (upper 40 percent of the blade height), possibly caused by the strong centrifugal field created in the rotor. This effect and the normal tip leakage result in an efficiency profile for the radial turbine (Figure 87). The design efficiency at zero clearance and at a normal operating clearance of 0.015 in. is superimposed for comparison. The results of the radial survey for the overall two-stage turbine is presented in Figure 88.

3.2 Radial-Stage Testing

Following the completion of the two-stage test, the radial wheel was removed from the turbine rig and the fully back-shrouded wheel was installed in its place. The axial stator and rotor were removed, and a dummy stator was installed to provide the required hub contour at the discharge of the radial stage. With a nozzle throat area of 1.5956 in.² and a rotor throat area of 4.3 in.², a performance map from 80- to 120-percent design speed was generated for a range of pressure ratios at a clearance of 0.015 in. both radially and axially. The back shroud clearance was a nominal 0.032 in.

The overall performance maps are presented in Figures 89 through 94 for the operating range of this test. Figure 95 is a carpet plot presentation of the measured mean exit swirl angle as a function of percent corrected-speed and total-to-total pressure ratio for the mean

GTCP 305-1 TWO STAGE TURB TEST 2 PROBE S/W 1072
 RADIAL ROTOR DISCHARGE SURVEY 90.16" .110 PCT SPD
 PRT-DS-10-4 SCANS 28-24-21-22-51-52 PR RAL 3.8

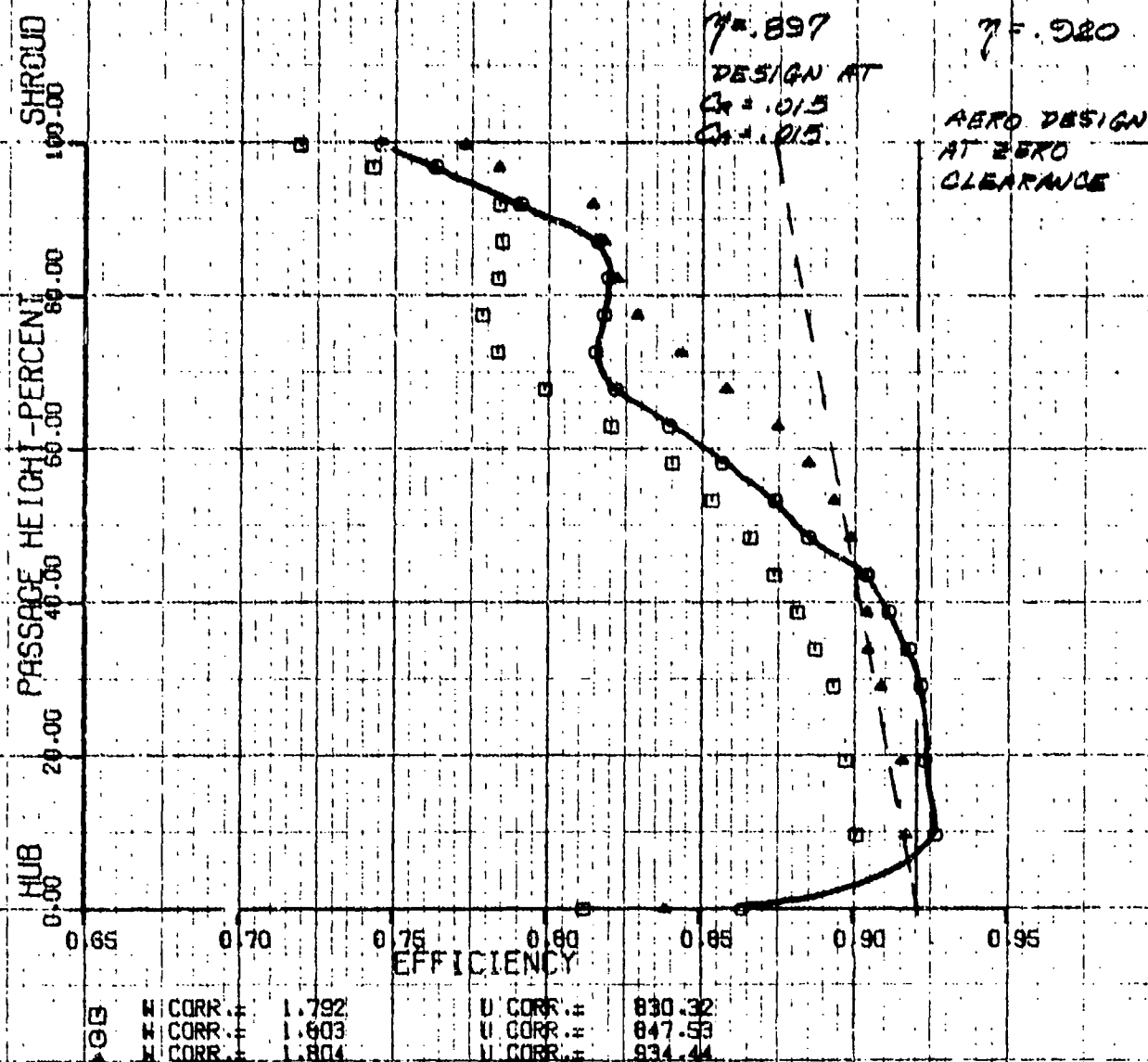


Figure 87. Radial Rotor Efficiency Survey Design Pressure Ratio.

GICP 305-1 TWO STAGE TURB TEST 2 PROBE S/N 1078
 100 PCT SPD AT 8.9, 8.10.4 AND 12.5 PRT-DS
 SCANS 73-74, 75-76, 21-22, 29-30 AXIAL TURB DISCH

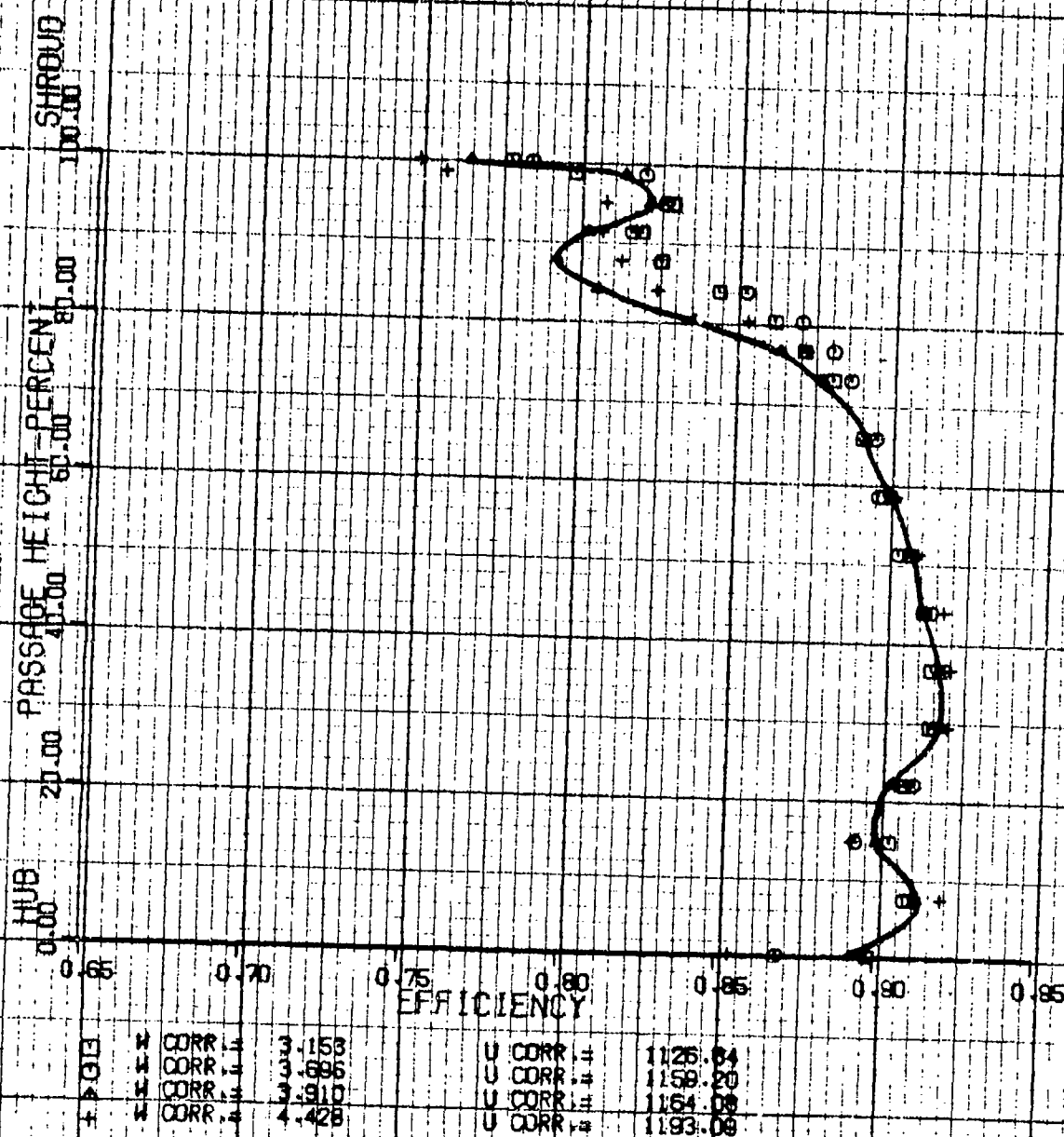


Figure 88. Radial Turbine Efficiency Survey Design Speed.
 (From Turbine Section Test)

0.95

0.90

0.85

0.80

EFFICIENCY

163

0.75

0.65

0.60

0.55

8.00

CORRECTED SPEED = 60. PER CENT

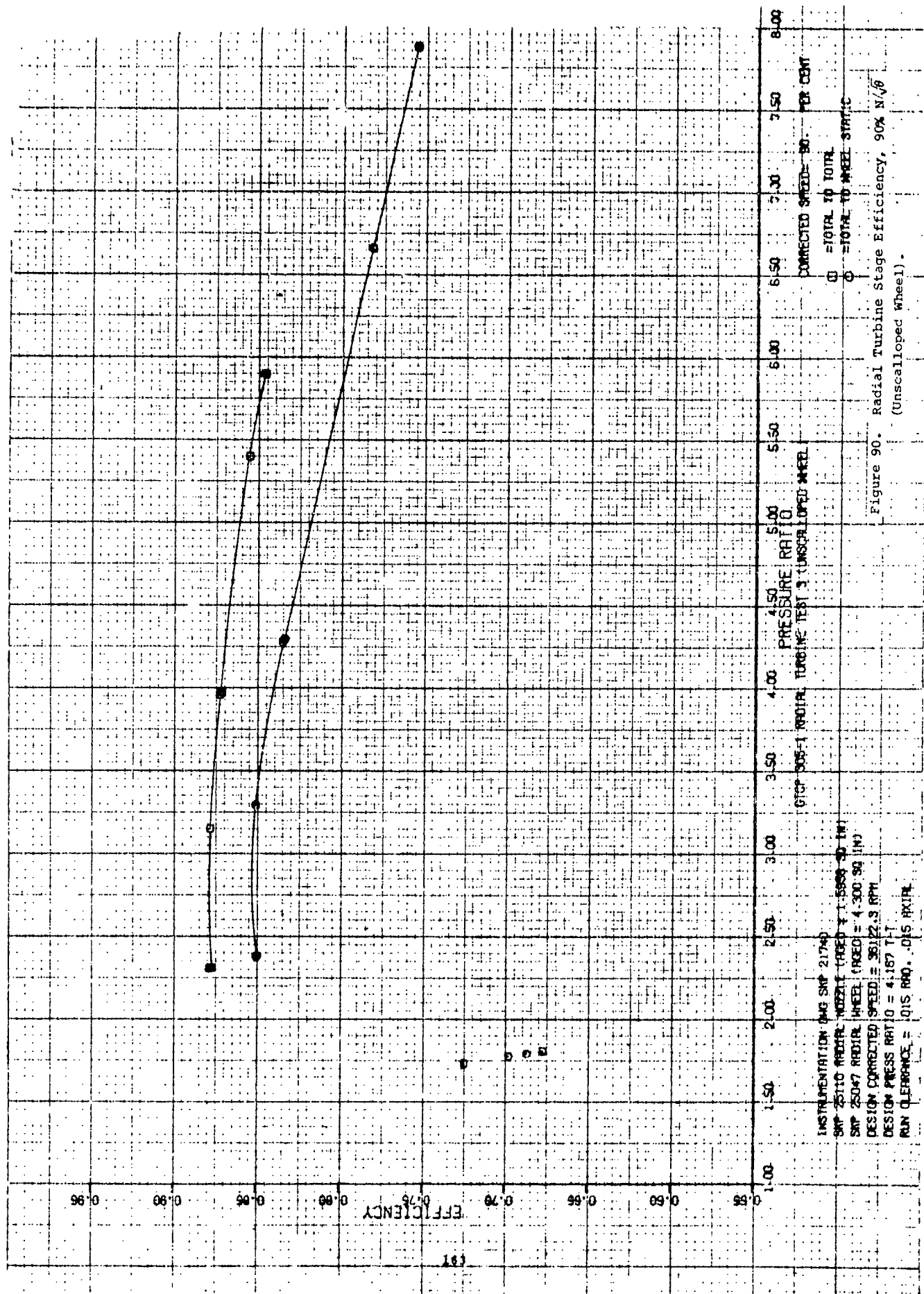
PRESSURE RATIO

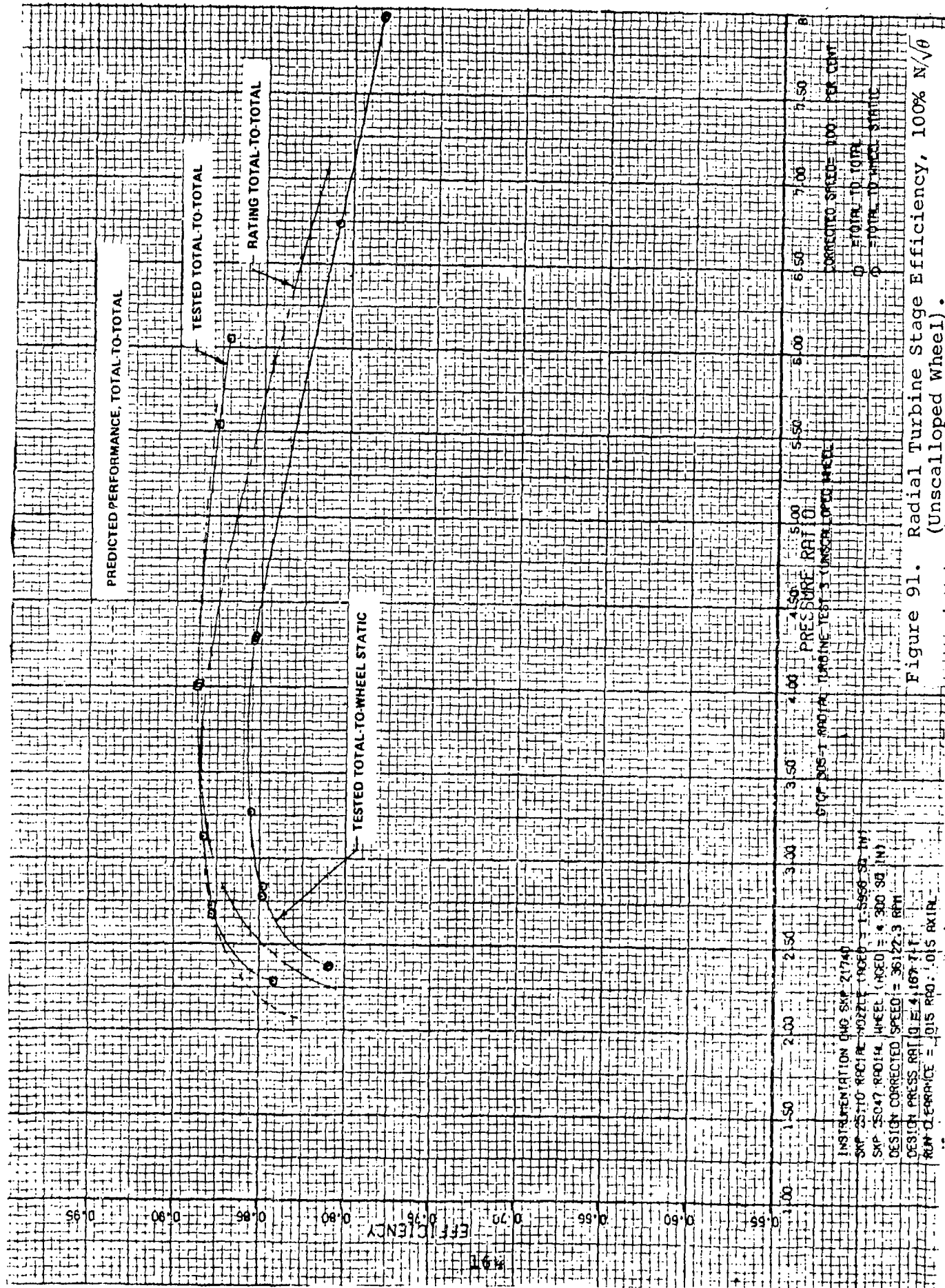
GTCP 305-1 RADIAL TURBINE TEST 3 UNSCALLOPED WHEEL

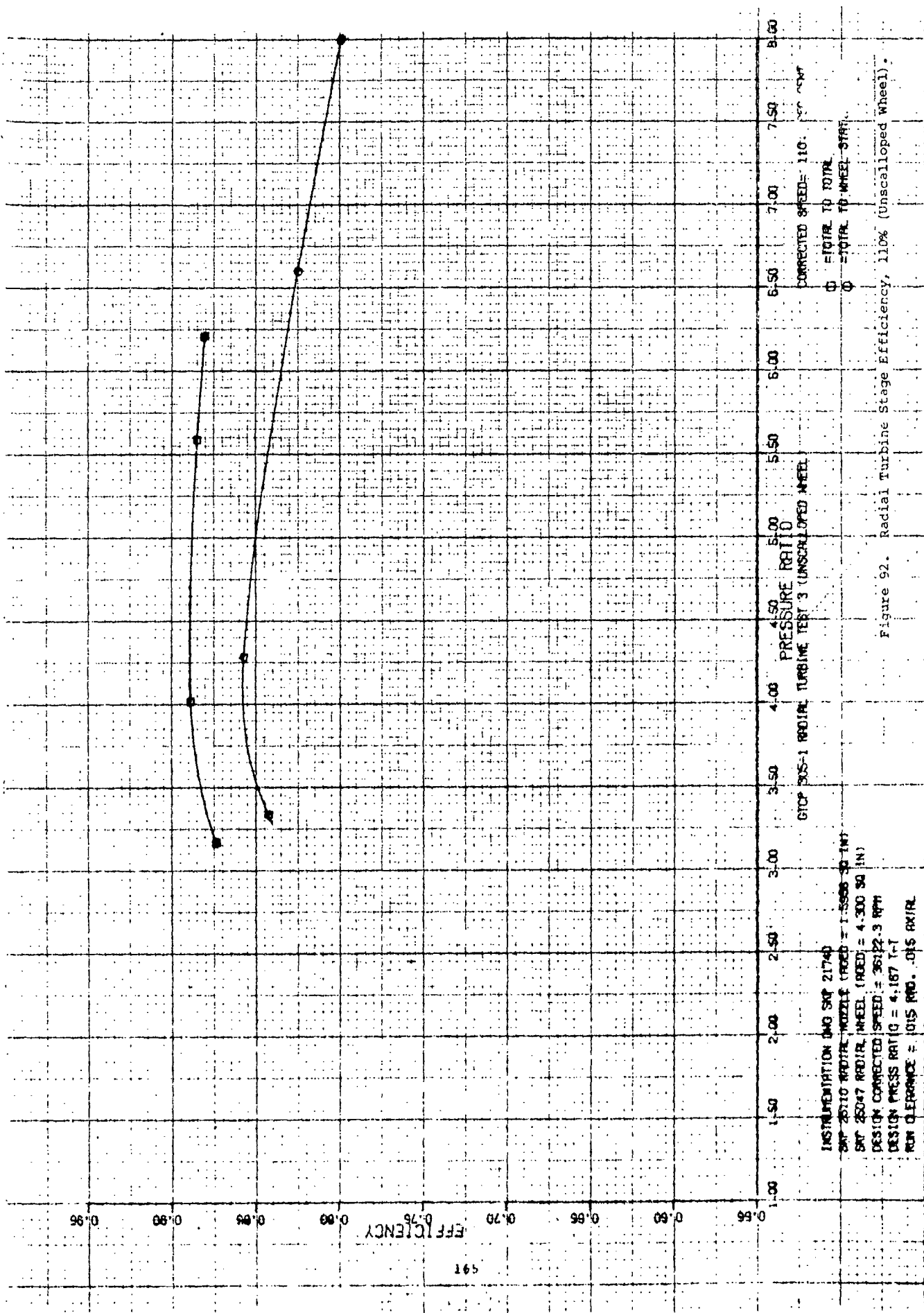
INSTRUMENTATION DAG SKP 21740
 SKP 25110 RADIAL NOZZLE (RATED = 1.5956 SQ IN)
 SKP 25047 RADIAL WHEEL (RATED = 4.300 SQ IN)
 DESIGN CORRECTED SPEED = 36122.3 RPM
 DESIGN PRESS RATIO = 4.167 T-T
 RUN CLEARANCE = .015 RAD. .015 AXIAL

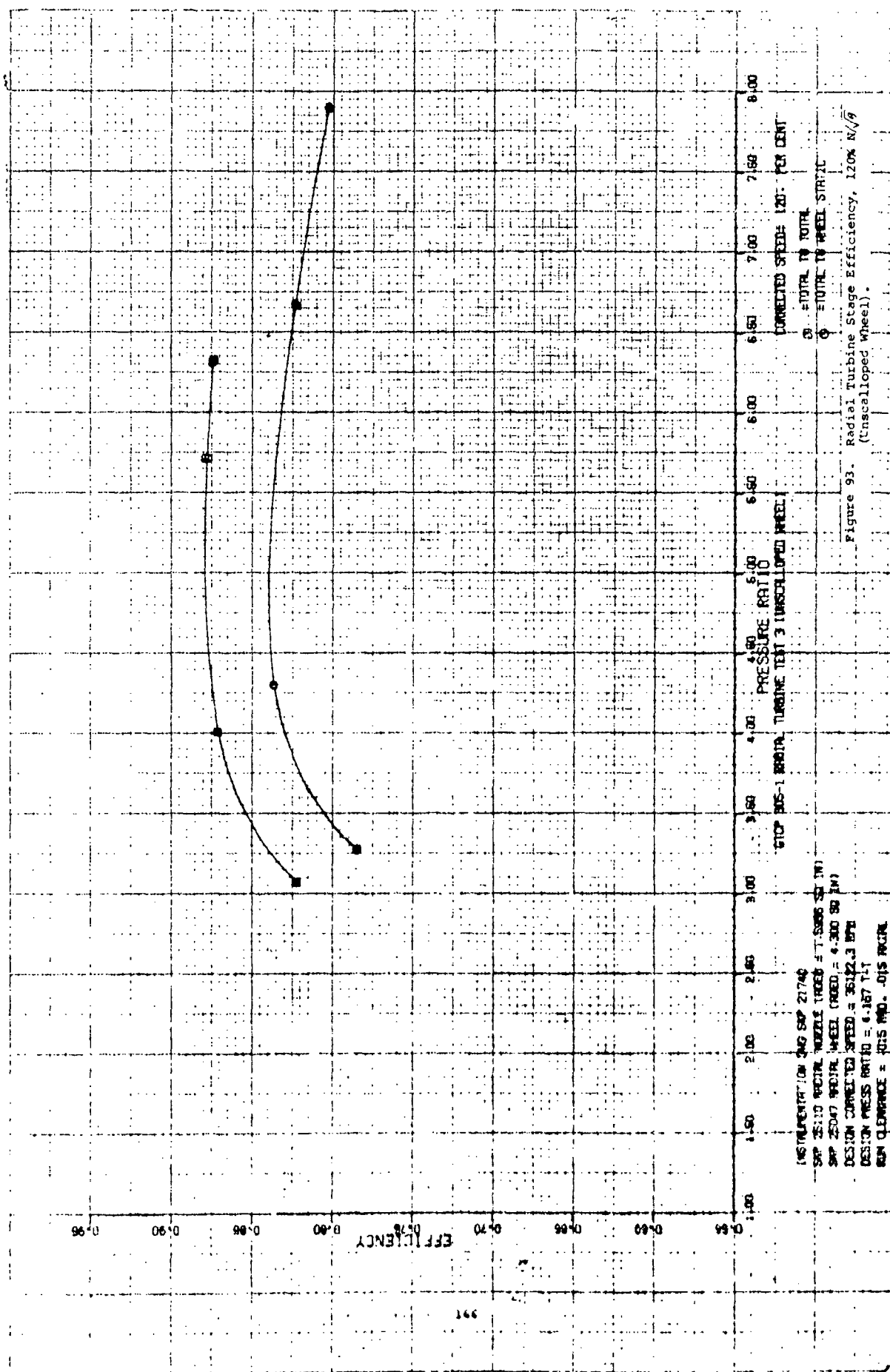
① = TOTAL TO TOTAL
 ② = TOTAL TO WHEEL STATIC

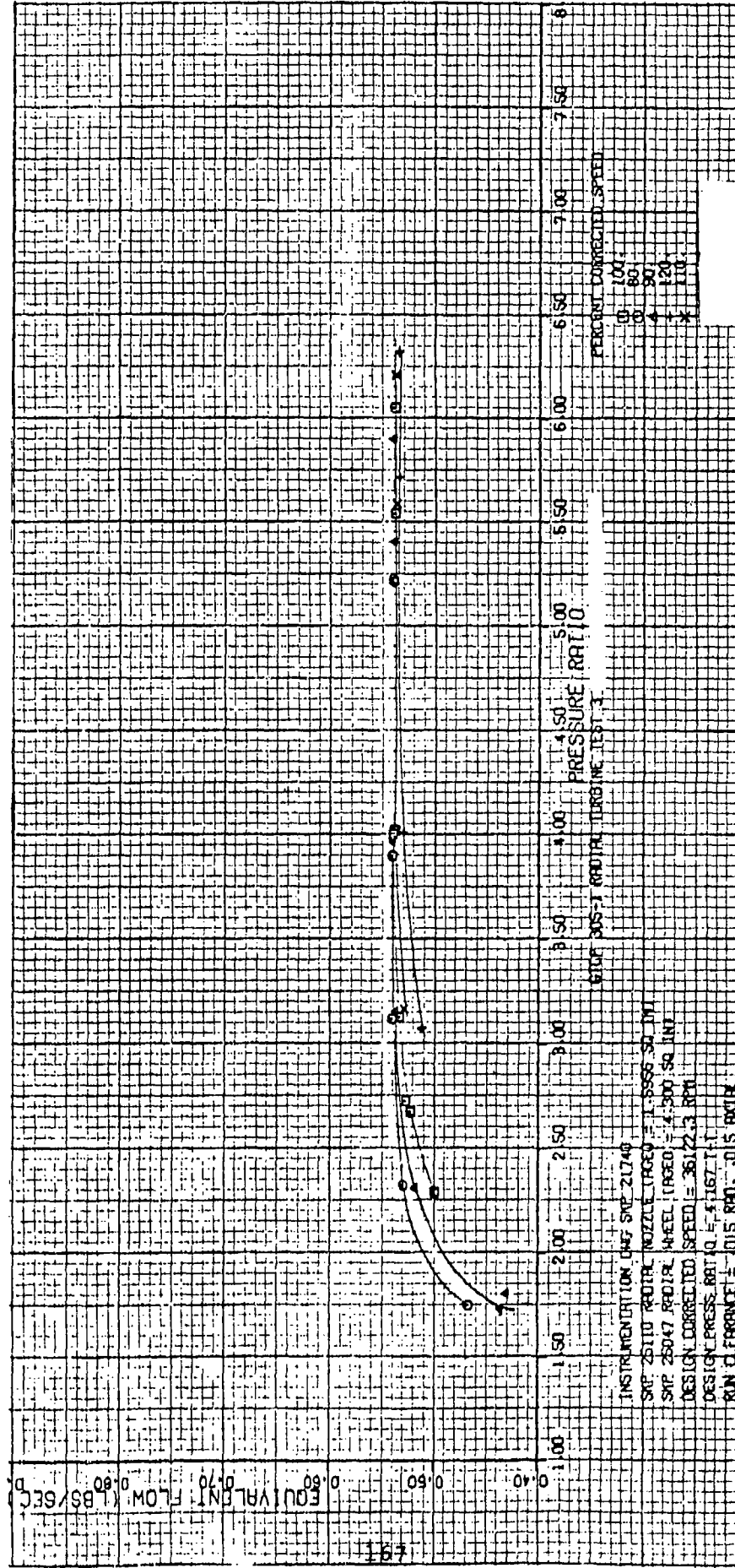
Figure 89. Radial Turbine Stage Efficiency, 80% N/B.











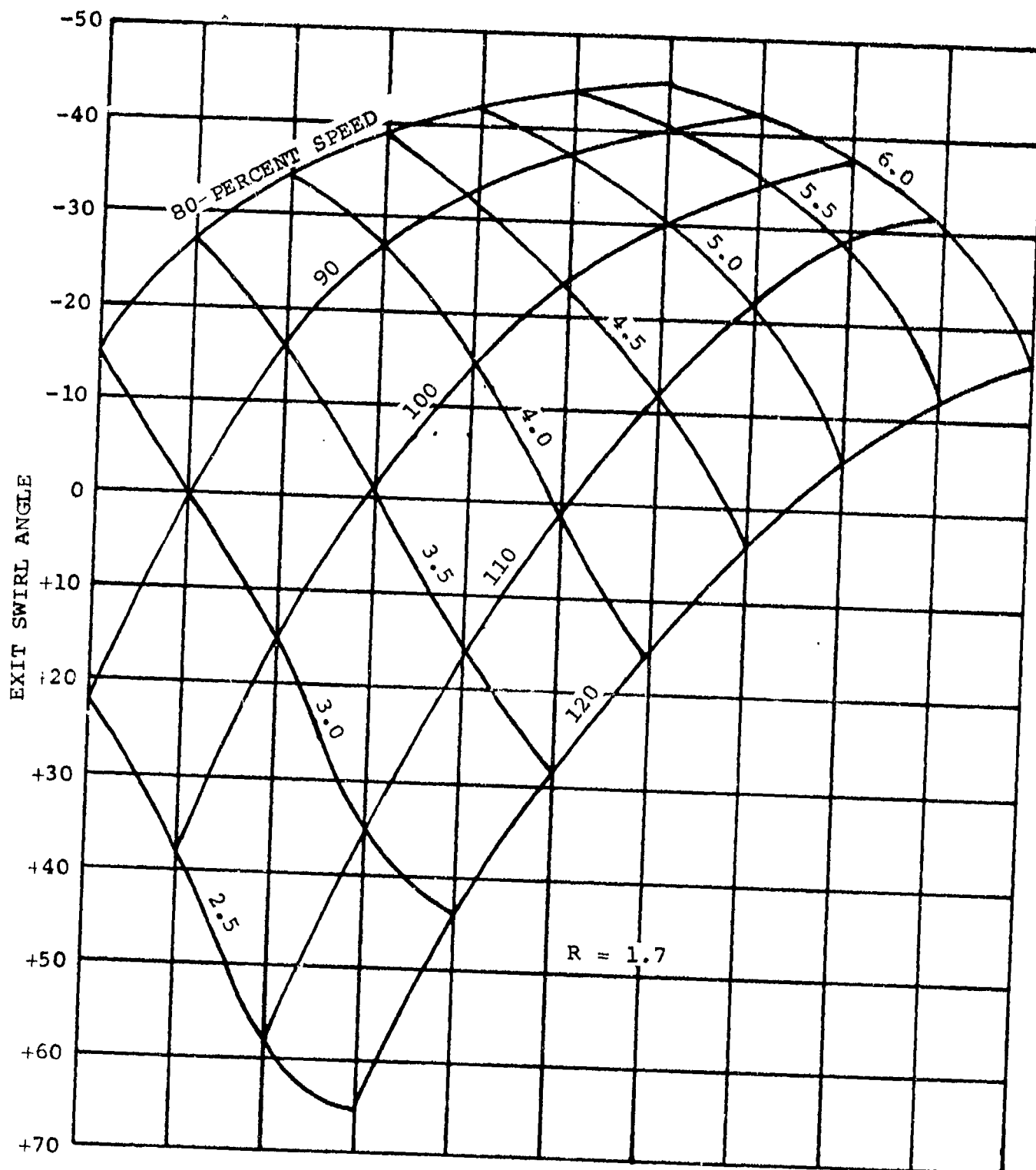


Figure 95. Radial Turbine Mean Exit Swirl Angle.

station at the discharge of the radial stage. Except for the flow, the performance of this stage follows design objectives with respect to efficiency attained.

The static pressure along the shroud of the radial turbine is compared to the design in Figure 96, showing good agreement between the design and test results. The absence of any sudden static pressure changes is evident for all but the very high overall pressure ratios.

Figures 97 through 100 present the results of the radial survey taken at the exit of the rotor near the design pressure ratio at 80-through 120-percent turbine corrected speed. The radial variation of efficiency (Figure 97) is the most significant result of the test. There is an obvious performance deficiency in the upper 50 percent of the blade height that, if recovered, could improve the overall turbine efficiency by 2.5 points. However, a detailed analysis of this rotor operating at these design-point conditions revealed very high suction, surface relative Mach numbers existing in a very strong centrifugal field. These high-Mach-number levels exist in the tip region where shroud clearance is an important factor. There are no available in-house data on the effects of shroud clearance on the performance of a radial in-flow turbine. Until recently, the available data⁽³⁾ report enough scatter to make it questionable. NASA has recently tested a lightly loaded radial turbine to determine the effects of clearance on turbine performance. If these results can be relied upon for highly loaded turbines, the performance of the GTCP305 radial turbine is about three points below attainable efficiency level and is in approximate agreement with the 2.5-points deficiency noted above.

In an effort to determine the effect of a more highly loaded radial turbine wheel, the contractor built and tested a wheel based on the GTCP305 radial turbine wheel with the splitters removed. The advantages of a more highly loaded turbine wheel are mainly mechanical,

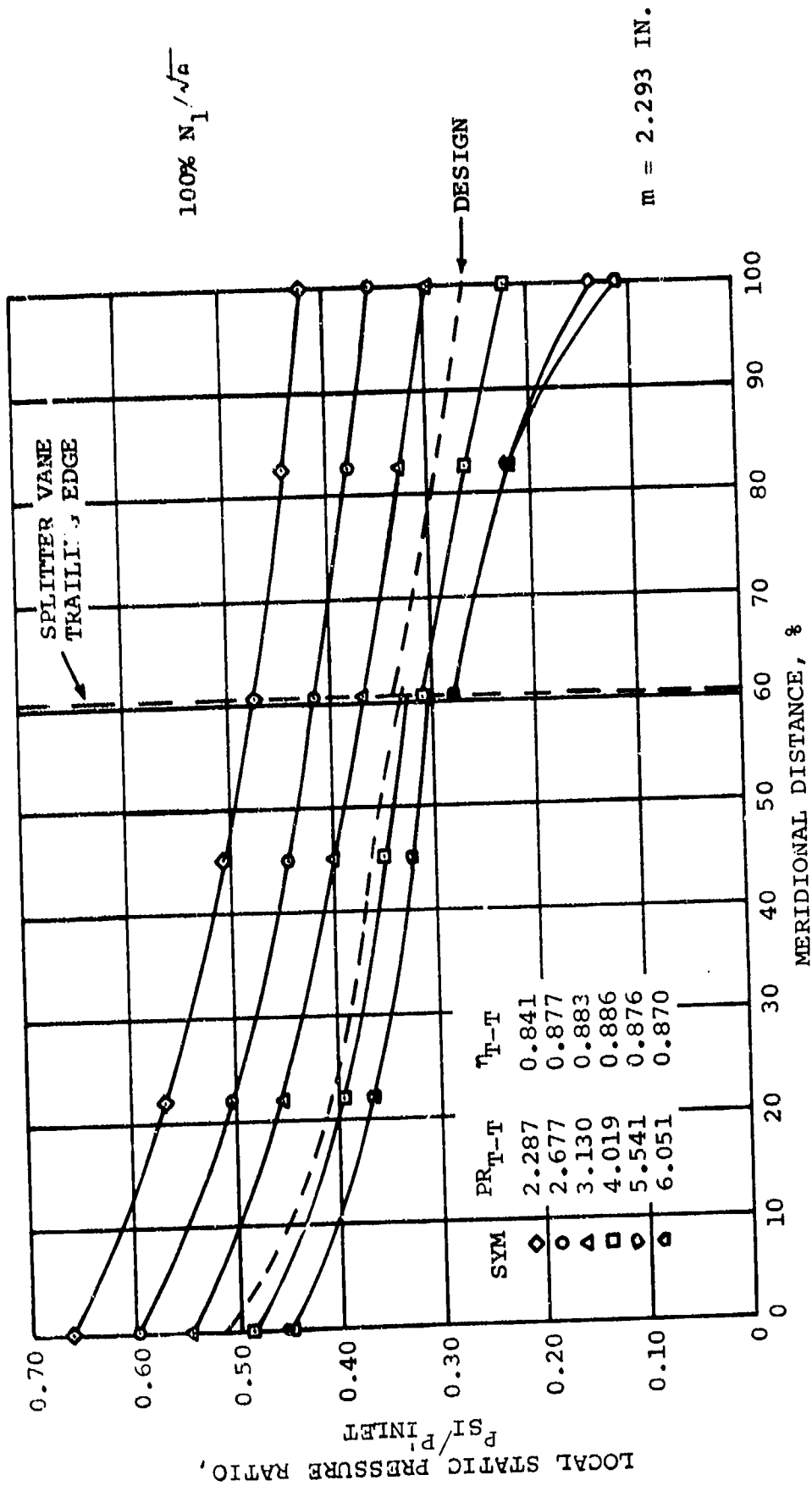


Figure 96. Radial Turbine Shroud Pressure Loading.

GTCP 305 RADIAL TURB TEST 3 PROBE S/N 1079

80. 90. 100. 110. 120 PCT SPD AT PR = 4.3 T-W/S

CLEARANCE CR = .015. CR = .018

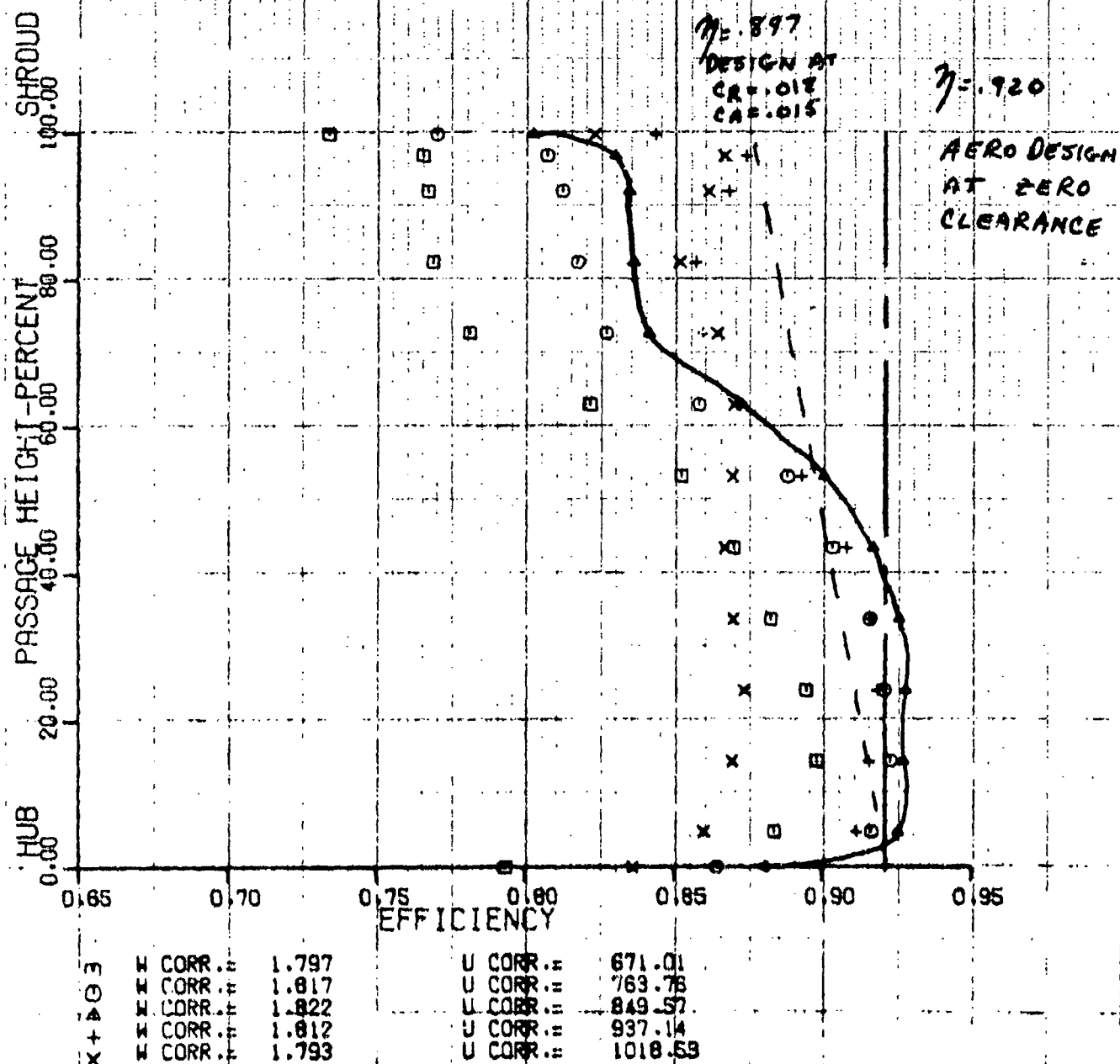
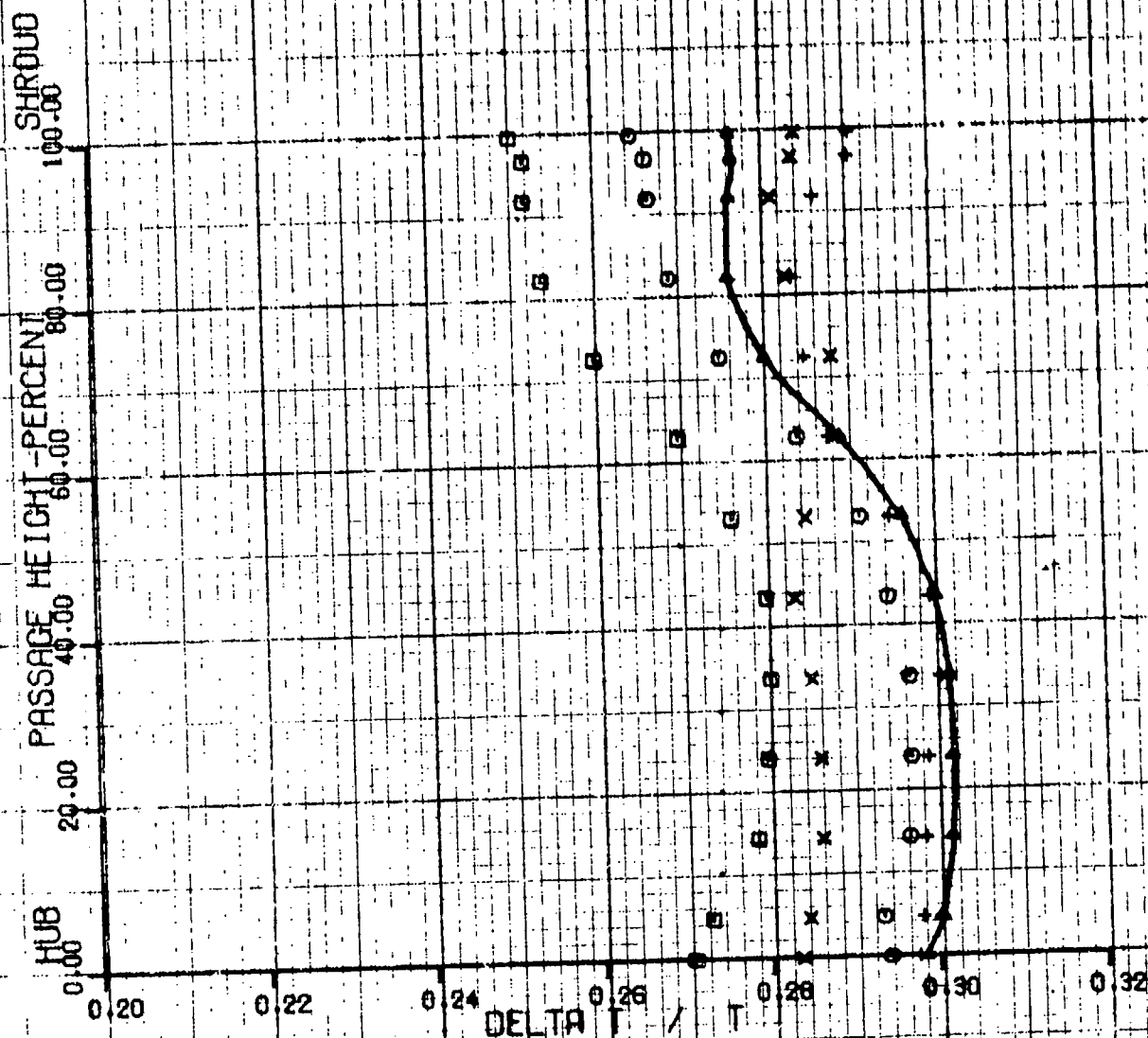


Figure 97. Radial Turbine Efficiency Survey.

GTCP 305 RADIAL TURB TEST 3 PROBE S/N 1009
 80, 90, 100, 110, 120 ACT SPD AT PR = 4.3 1-1/2
 CLEARANCE CA = .015, OR = .018



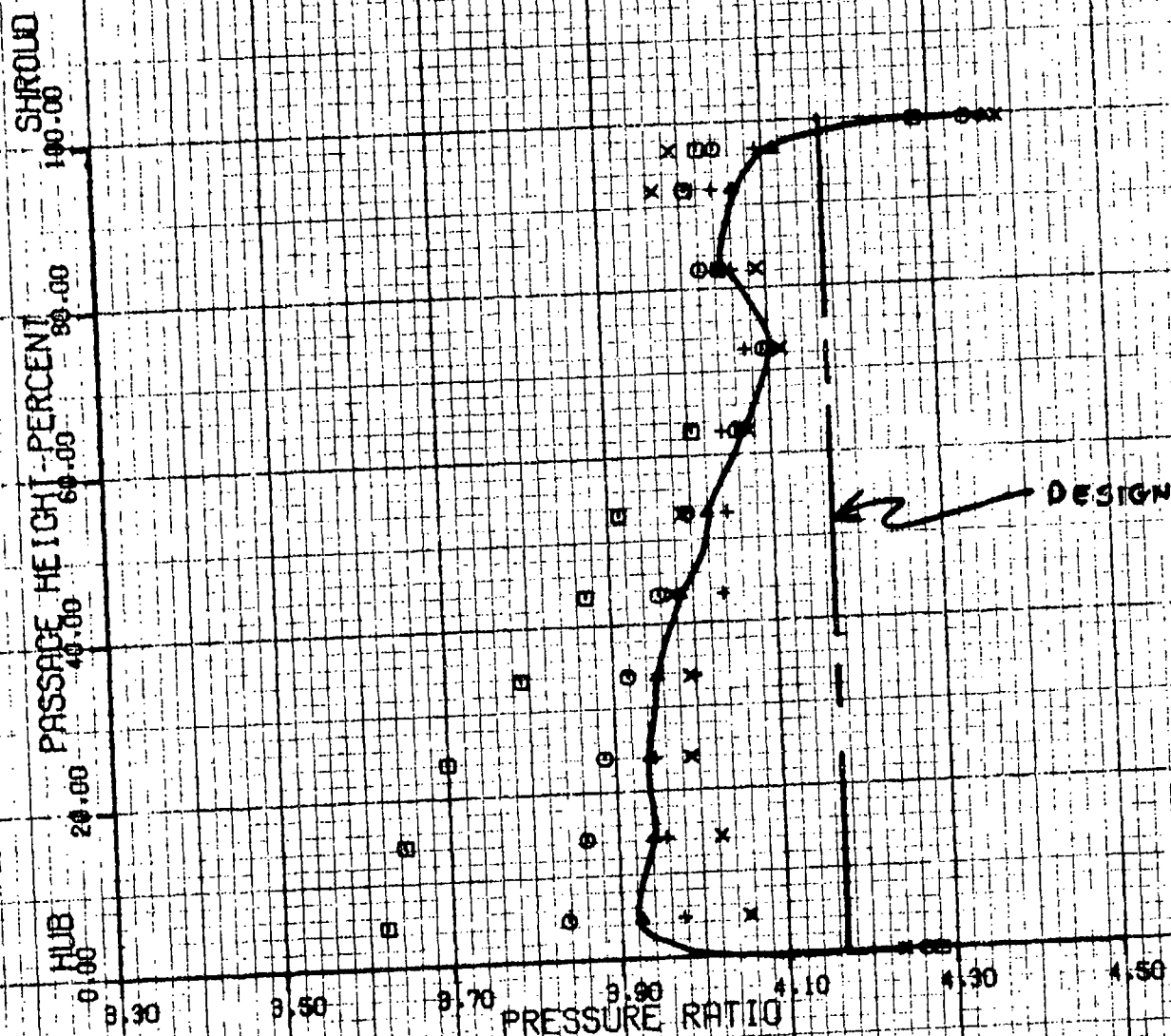
W CORR.:	1.797	U CORR.:	571.01
W CORR.:	1.817	U CORR.:	763.78
W CORR.:	1.822	U CORR.:	849.57
W CORR.:	1.812	U CORR.:	937.14
W CORR.:	1.793	U CORR.:	1018.53

Figure 98. Radial Turbine Delta T/T Survey.

GTCP 305 RADIAL TURB TEST 3 PROBE S/N 1009

80. 90. 100. 110. 120 PCT SPD AT PR = 4.3 T-W 5

CLEARANCE CR = .015. CR = .018



W CORR. =	1.797	U CORR. =	671.01
W CORR. =	1.817	U CORR. =	783.76
W CORR. =	1.822	U CORR. =	849.57
W CORR. =	1.812	U CORR. =	897.14
W CORR. =	1.793	U CORR. =	1018.53

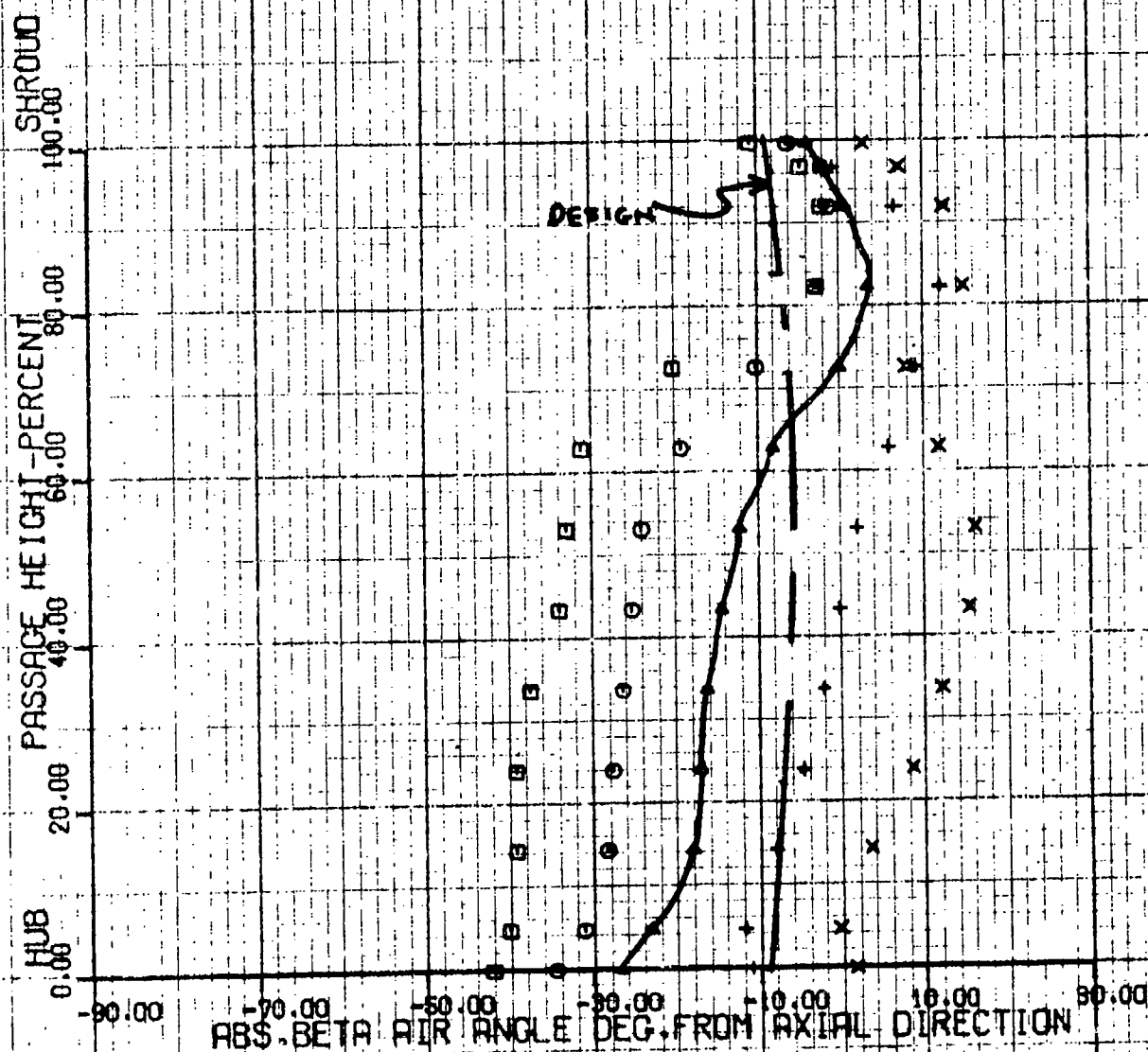
Figure 99. Radial Turbine Pressure Ratio Survey.

GTCP 305 RADIAL TURB TEST 3 PROBE S/N 1079

80, 90, 100, 110, 120 PCT SPD AT PR = 4.3 T-W/S

CLEARANCE CR = .015, OR = .018

AIR ANGLE DISTRIBUTION



X + 405	W CORR. =	1.797	U CORR. =	571.01
	W CORR. =	1.817	U CORR. =	763.76
	W CORR. =	1.822	U CORR. =	849.57
	W CORR. =	1.812	U CORR. =	897.14
	W CORR. =	1.793	U CORR. =	1018.53

Figure 100. Radial Turbine Swirl Angle Survey.

i.e., they require less cooling, are less susceptible to cracking due to greater allowable thickness, have lower centrifugal stresses at the blade roots and hub, and are easier and cheaper to manufacture. The adiabatic total-to-total efficiency for the 10-bladed wheel was approximately 1.8-percentage points less than that for the 20-bladed wheel throughout the flow range.

3.3 Axial-Stage Performance

When the radial and axial turbines were tested together as a two-stage turbine, sufficient instrumentation was provided to determine the individual performance of each stage with reasonable accuracy. Reliable instrumentation, capable of operating over a wide range of flow conditions, determined the performance of the individual stage as accurately as possible. However, stage interaction effects were present, creating an unknown amount of conservative error in the axial stage. These data were used to estimate the performance of the axial stage.

The performance of this turbine is represented in Figures 101 through 105 for efficiency as a function of pressure ratio at constant speed. Figure 106 shows the turbine corrected-flow as a function of pressure ratio for all speeds.

3.4 Predicted Radial Stage Off-Design Performance

Following the successful completion of the two-stage and the single-stage radial tests, the experimental data from the radial turbine test were computer-processed with the off-design performance prediction program. Experimental results were matched with the computer program by varying the stator and rotor loss coefficients and the power factors on rotor incidence. This analysis, at the design speed, is presented in Figure 107, which compares the analytical prediction with the experimental results. The stator viscous loss (which includes the vaneless space), the rotor incidence loss, the rotor viscous loss,

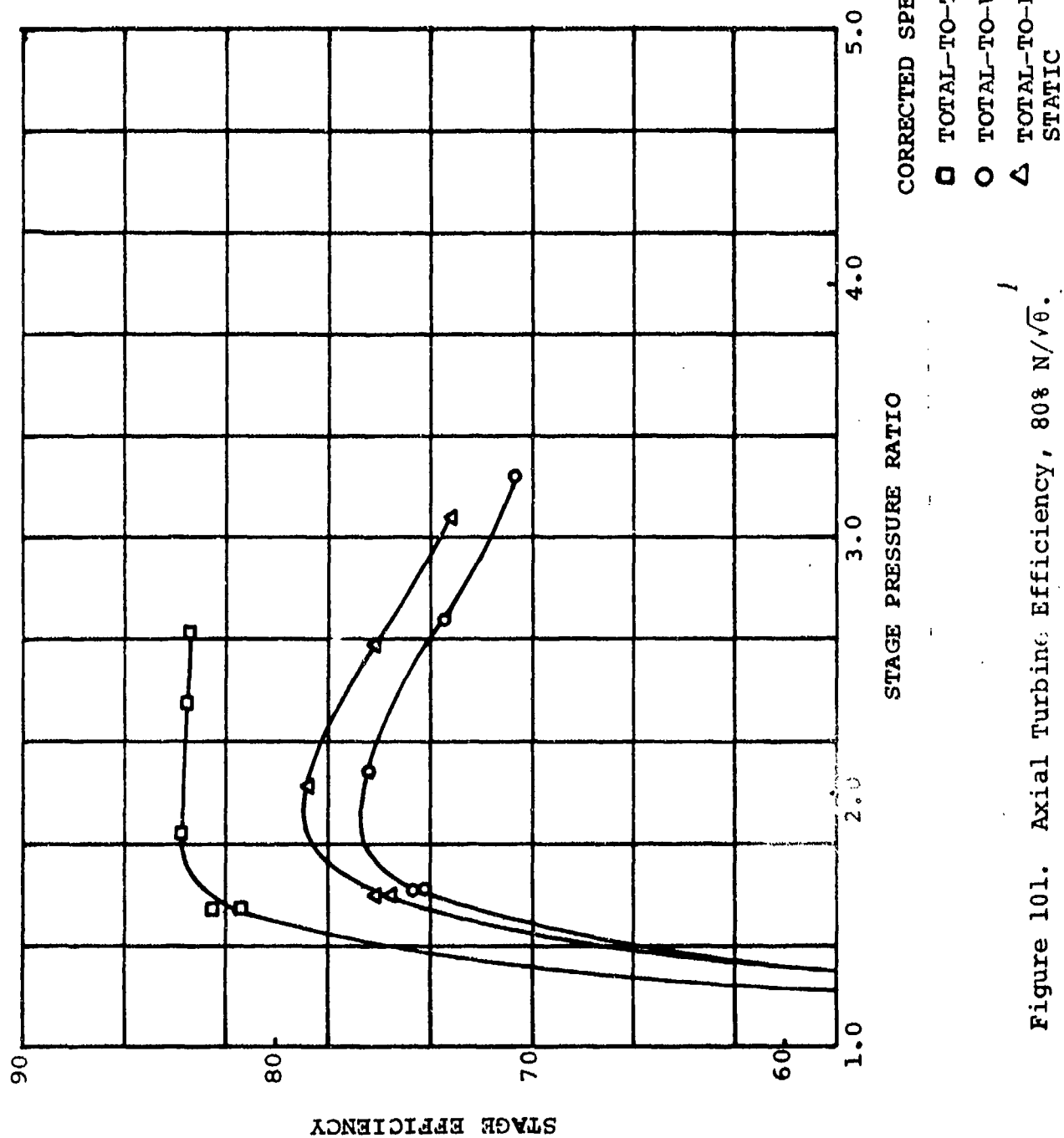


Figure 101. Axial Turbine Efficiency, 80% $N/\sqrt{\theta}$.

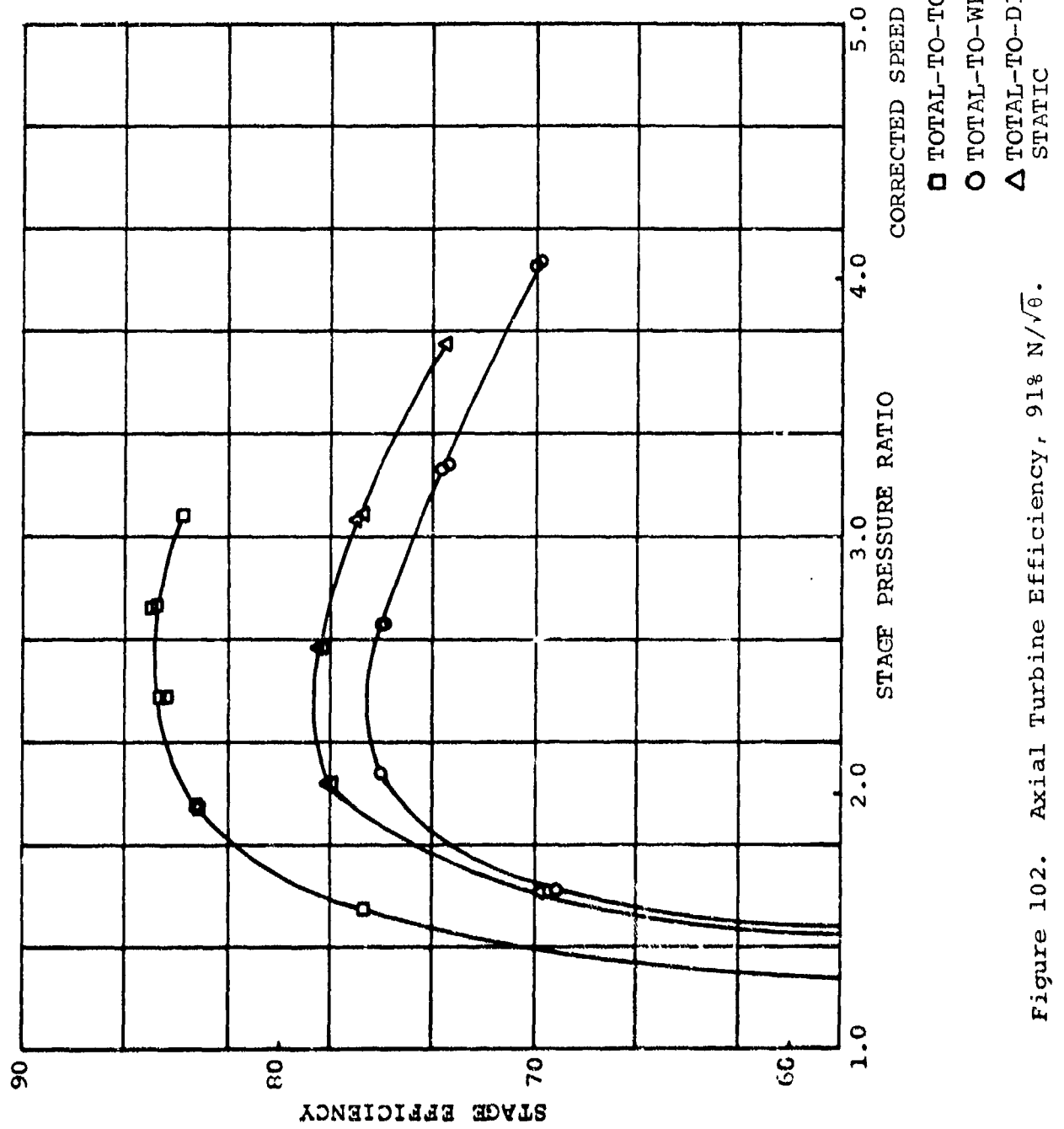


Figure 102. Axial Turbine Efficiency, 91% $N/\sqrt{\theta}$.

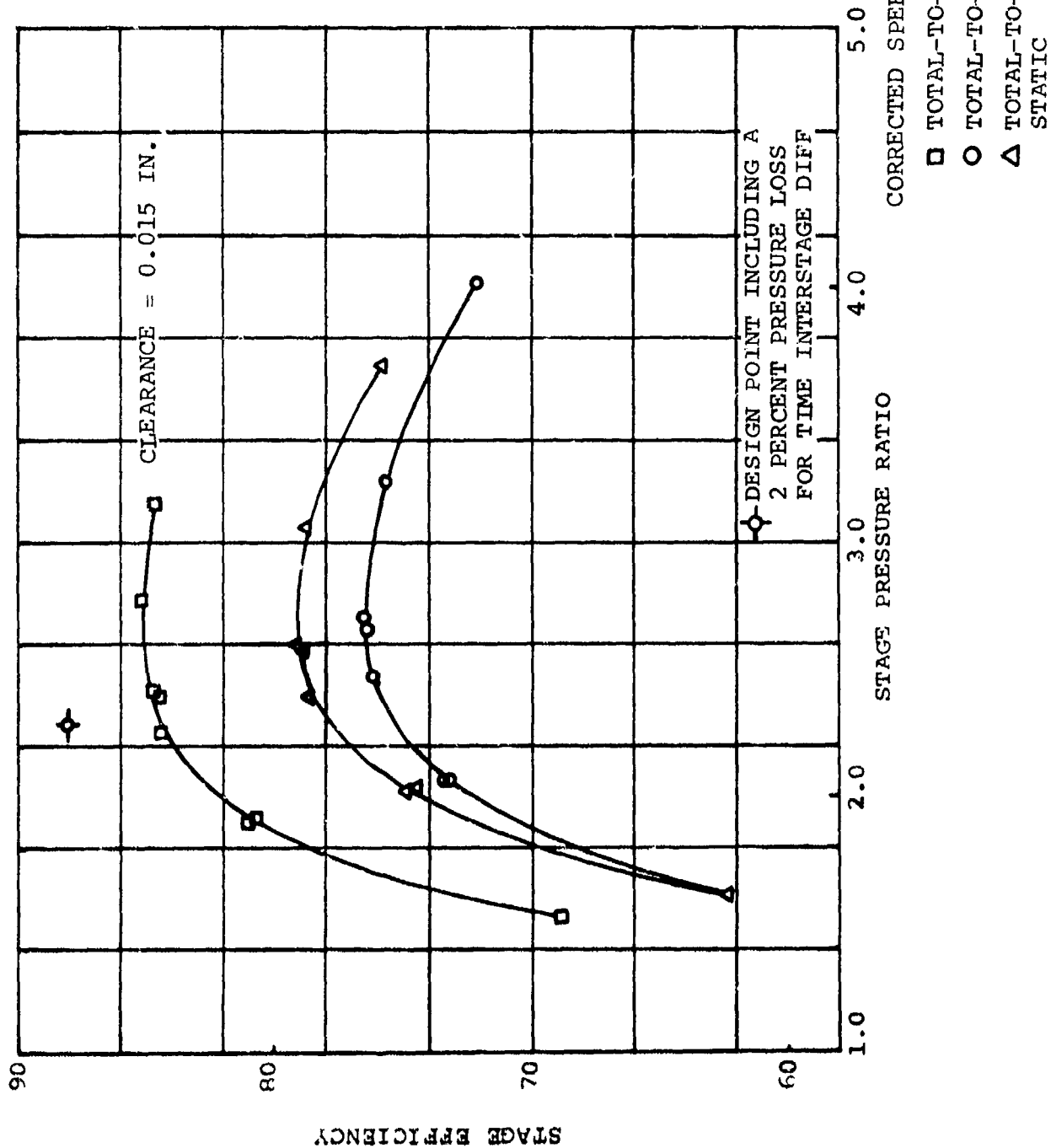
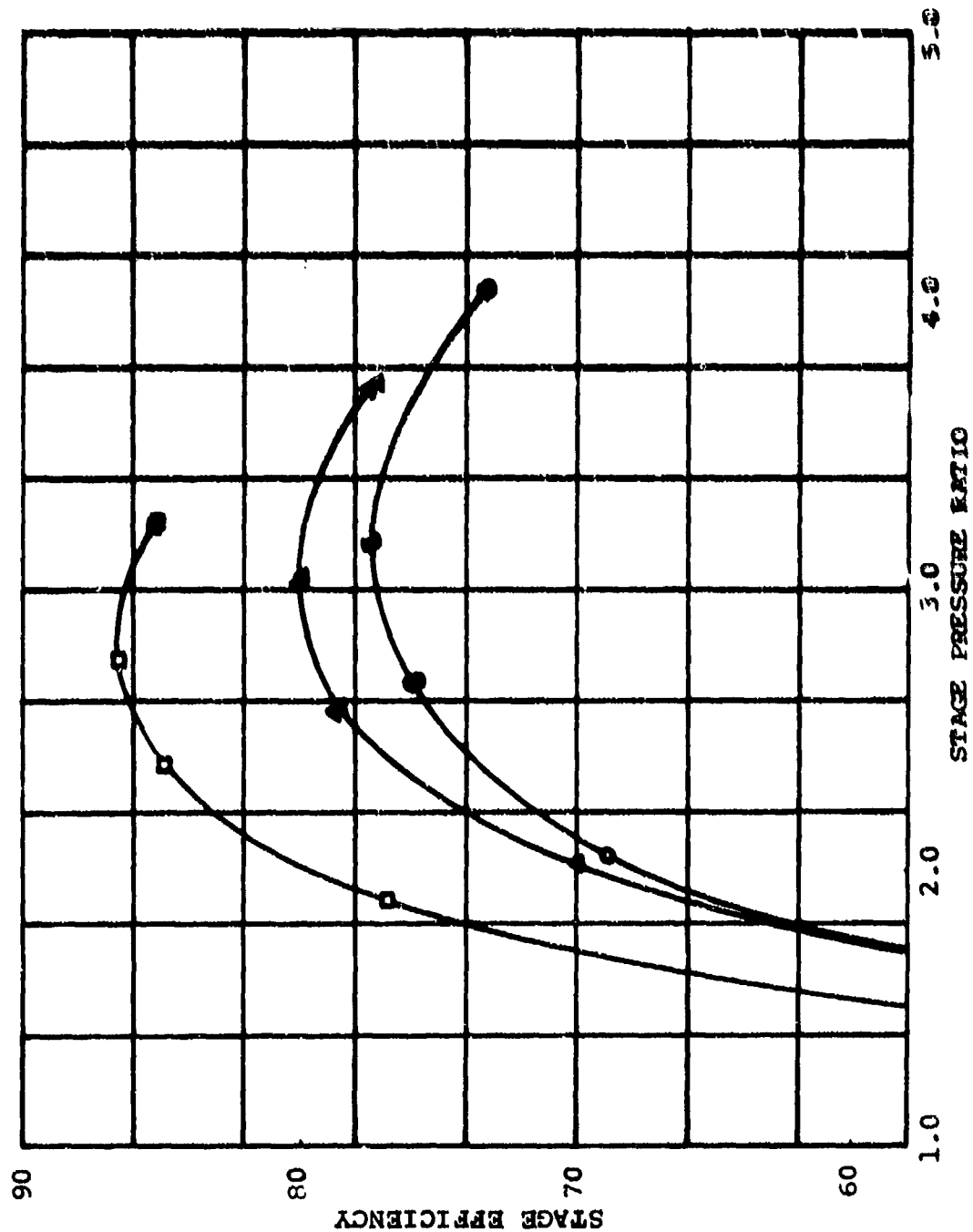


Figure 103. Axial Turbine Efficiency, $101\frac{1}{2} N/\sqrt{\theta}$.



CORRECTED SPEED = 101%
 □ TOTAL-TO-TOTAL
 ○ TOTAL-TO-STATIC
 △ TOTAL-TO-DIFFERENCE
 STATIC

Figure 104. Axial Turbine Efficiency, 1124 N/√L.

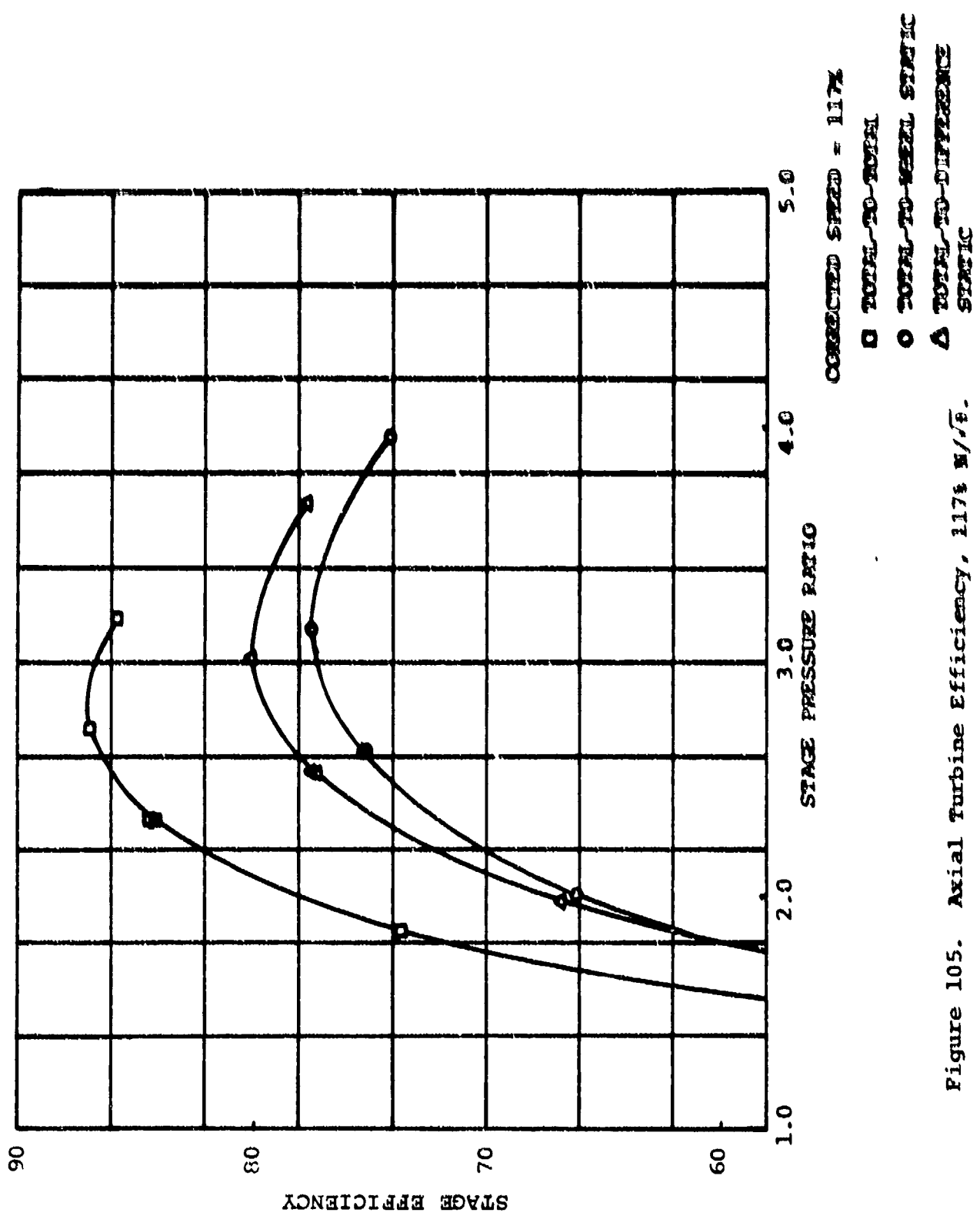


Figure 105. Axial Turbine Efficiency, 117% N/\sqrt{r} .

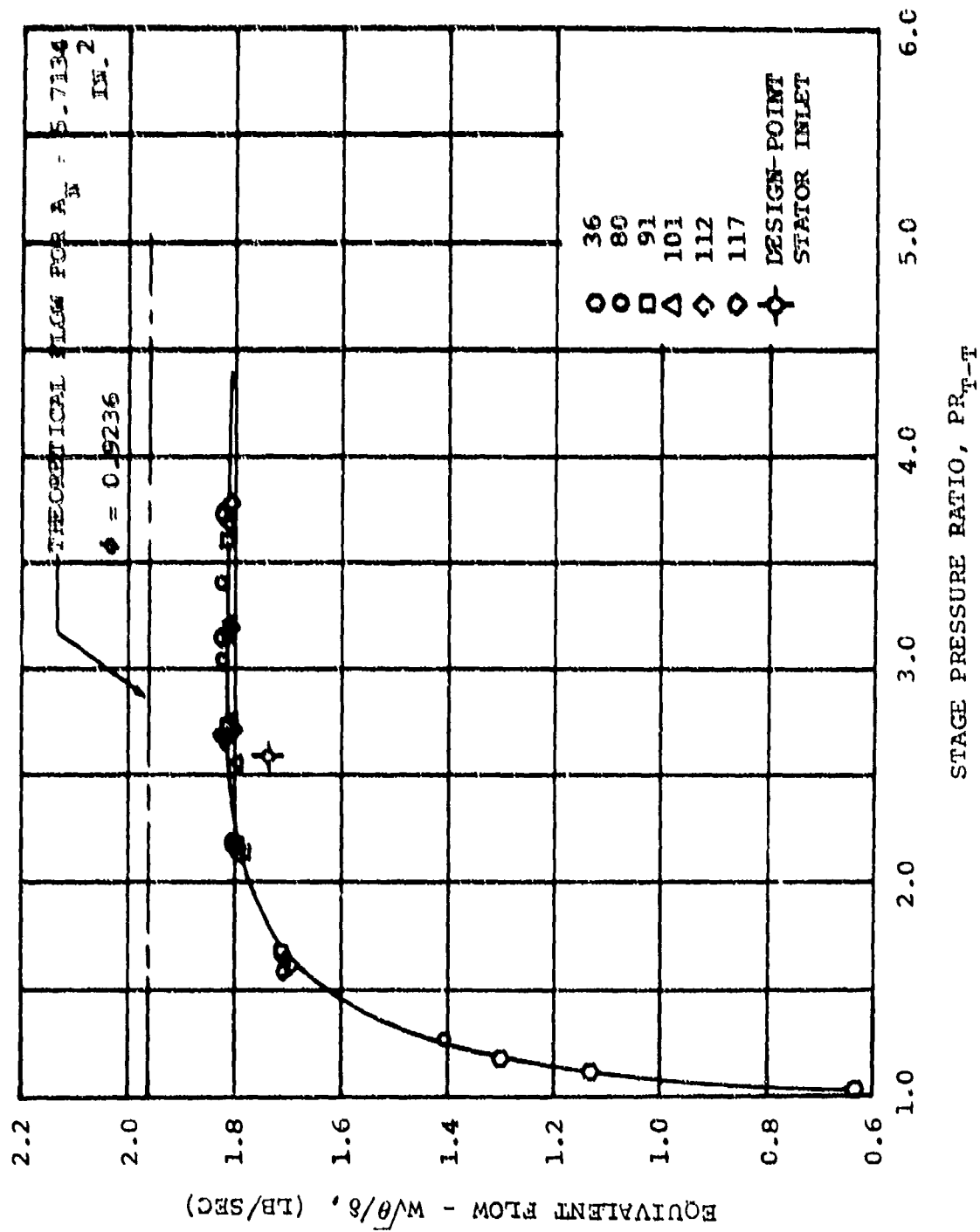


Figure 106. Axial Turbine Efficiency.

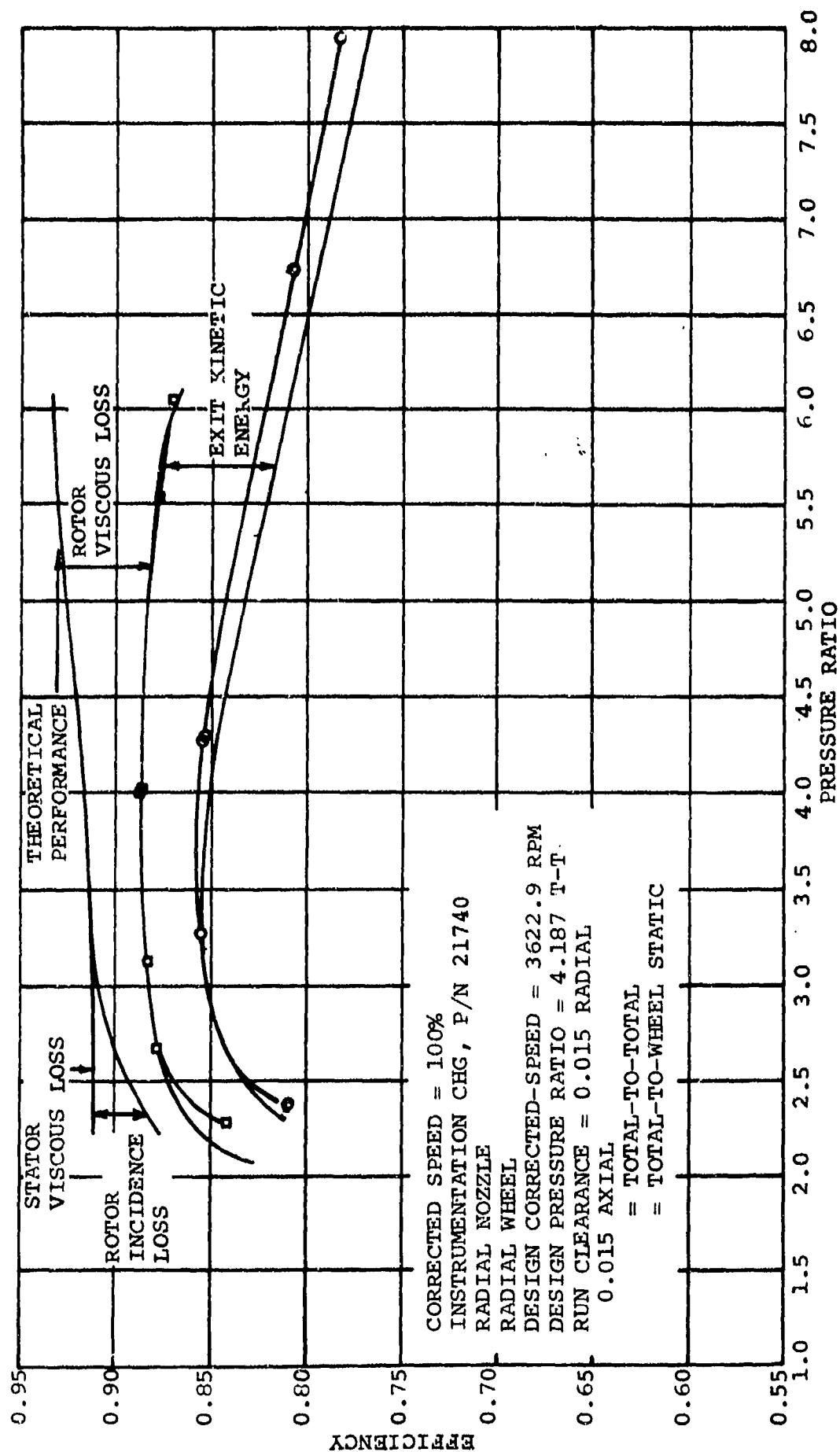


Figure 107. Radial Turbine Test 3 (Unscalloped Open Wheel) and Predicted Turbine Performance Comparison

and finally the rotor exit kinetic energy loss are presented so that the relative importance of each may be seen in terms of overall turbine performance. At low-pressure ratios, the predominate loss is negative rotor incidence, while at the high-pressure ratios the predominate loss is the rotor exit kinetic energy.

The advantage of matching the mathematical model of turbine performance to test data is that changes in geometry can be quickly evaluated. In addition, the computer model can be used to extrapolate the turbine operating characteristics to both higher and lower operating speeds. However, experience has shown that turbines of poor performance are difficult to match with the computer model and, therefore, the extrapolated results are less accurate.

The velocity vector diagram that resulted from the test data match at the reference design pressure ratio and speed is shown in Figure 108. The interesting feature of this vector diagram is that the slip factor (V_u/U) is 0.89, while the ideal Stannitz slip factor ($1 - 2/Z$, where Z = number of blades) for this impeller is 0.9, indicating rotor operation at almost shockless entry. This is in contrast to the original design slip factor of 1.04.

4. MECHANICAL DESIGN AND DEVELOPMENT

4.1 Uncooled Turbine Nozzle

An uncooled nozzle configuration was selected to conserve the use of cooling airflow. (The cooled nozzles were considered the backup configuration.)

Two high-temperature materials were tested in a cascade test rig to choose a material capable of operation at temperatures to 2400°F. Vane shapes were fabricated from silicon nitride and a silicide-coated columbium alloy (WC-3015). Silicon nitride was chosen as it appeared

$R = 3.068 \text{ IN.}$

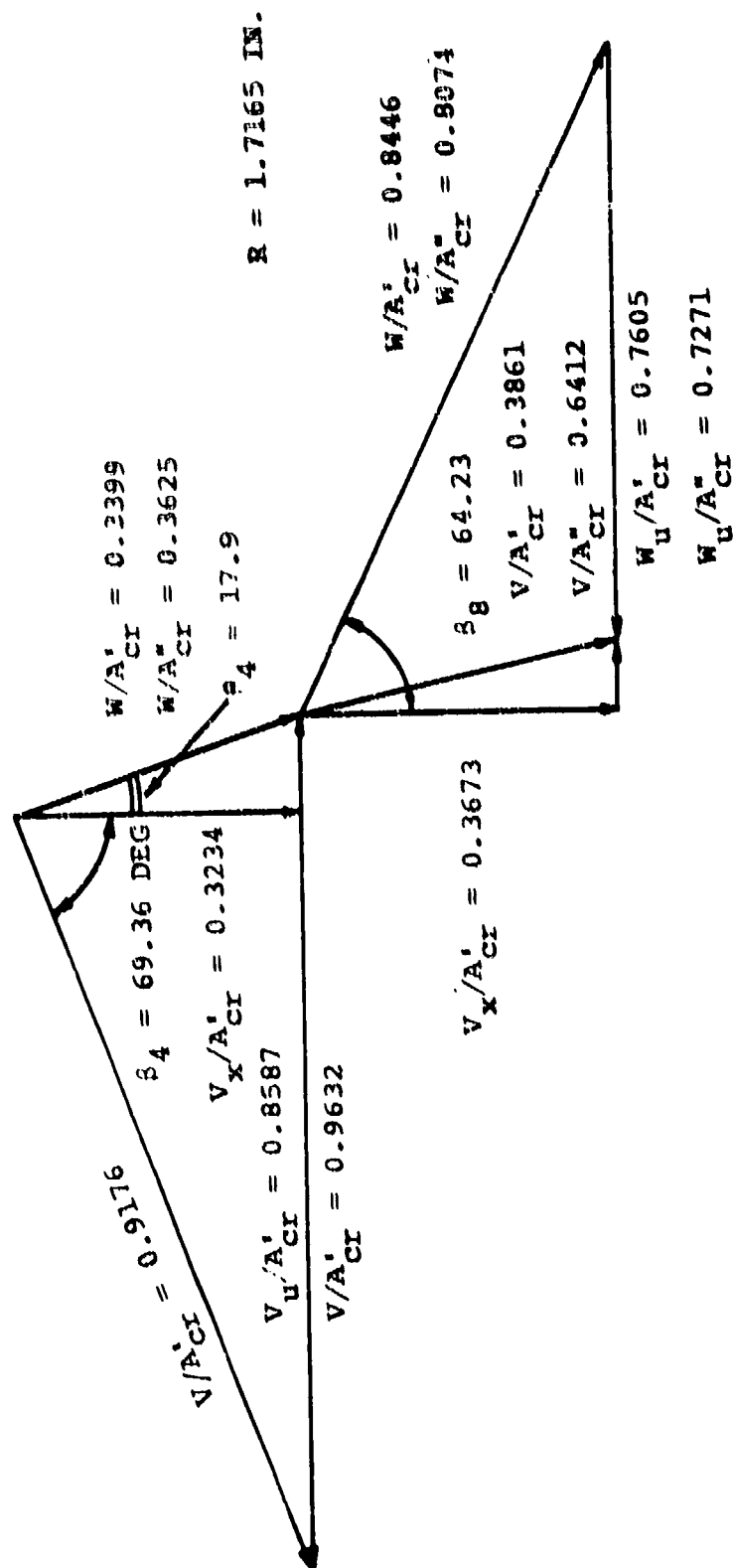


Figure 108. Radial Turbine Test Data Match.

to be the most promising ceramic and would require no coating. The remaining problem was the assembly of the vanes into a nozzle box. WC-3015 was selected as the best columbium alloy available, from the standpoint of oxidation resistance. The silicon nitride vanes were diamond-ground from a slip-cast plate, and the columbium vanes were machined from a forged plate.

Both sets of vanes were subjected to combustion gases at 2400°F for 8 hr in the test rig (Figure 109) and visually inspected for corrosion. Following the endurance run, the vanes were subjected to a minimum of 100 thermal cycles from ambient to 2400°F in approximately 15-sec half-cycles. A system of pneumatically actuated valves controlled the air and fuel flows so that the temperature profile simulated that of an actual engine start, plus a 200°F increase to allow for temperature variation. The test summary is presented in Table XII.

Based on the results of the tests, the WC-3015 Columbium Alloy was chosen. Although the coating was damaged in some areas, there was only slight oxidation of the base metal, and the vanes could have continued in the test rig considerably longer. To avoid possible fabrication problems, the nozzle was made as an assembly of vanes and side plates bolted together. Machining was accomplished by modifying existing super alloy techniques without requirements for exotic tooling or processes.

The engine operation of the nozzle was less than satisfactory, due to assembly and design techniques rather than failure of the alloy. Apparently the low expansion of columbium, compared to the A-286 iron-base alloy used for the bolts and many other parts of the nozzle assembly, allowed leakage between the vanes and side plates, severely reducing the turbine efficiency.

TABLE XII
UNCOOLED TURBINE NOZZLE TESTS

Test No.	Configuration	Purpose	Test Conditions	Results	Comments
1	Silicon Nitride	Endurance	2400°F inlet temperature	Slight glazing of surface, no visible oxidation or corrosion	Mechanical rig problems; some blades replaced
2	Silicon Nitride	Thermal Shock	Simulated APU starting cycle	Unable to complete	Rig problems prevented completion
3	Silicide-coated Columbium	Endurance	2400°F inlet temperature	8-hr endurance completed, slight visible oxidation	Rig problems corrected; some coating may have been scraped away by rig--believed cause of oxidation
4	Silicide-coated Columbium	Thermal Shock	Simulated APU starting cycle	100 cycles completed	Thermal shock resistance apparently excellent

20

19

18

17

16

H

G

F

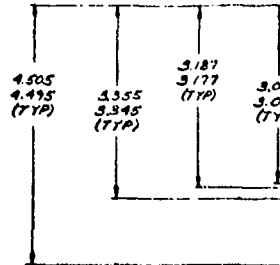
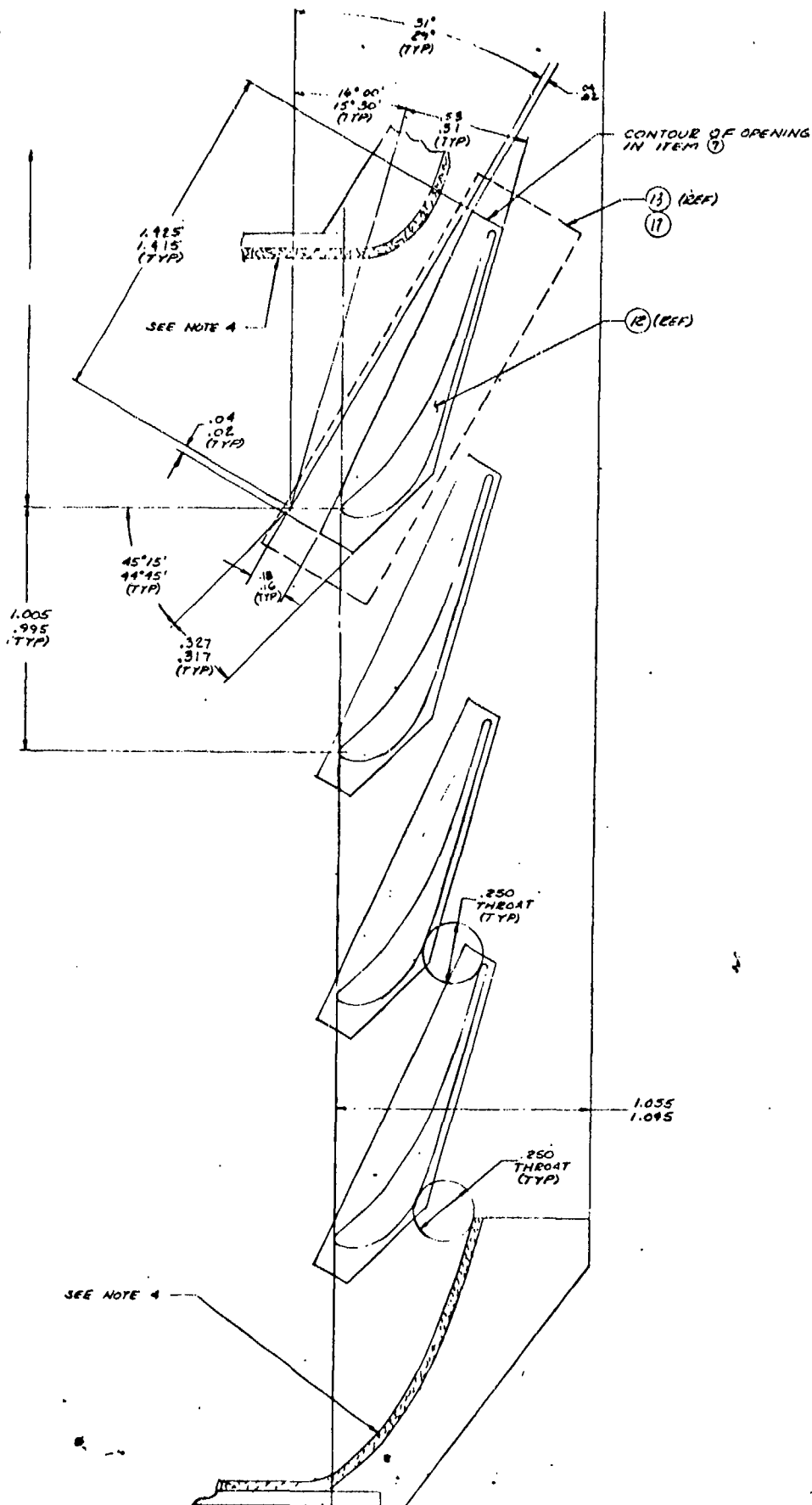
E

D

C

B

A



SECTION 13-13
SCALE: 5/1

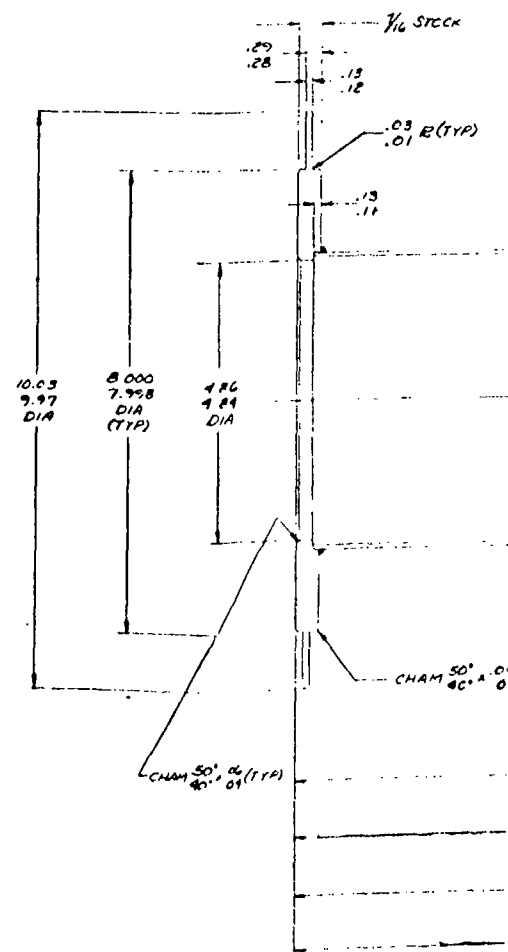
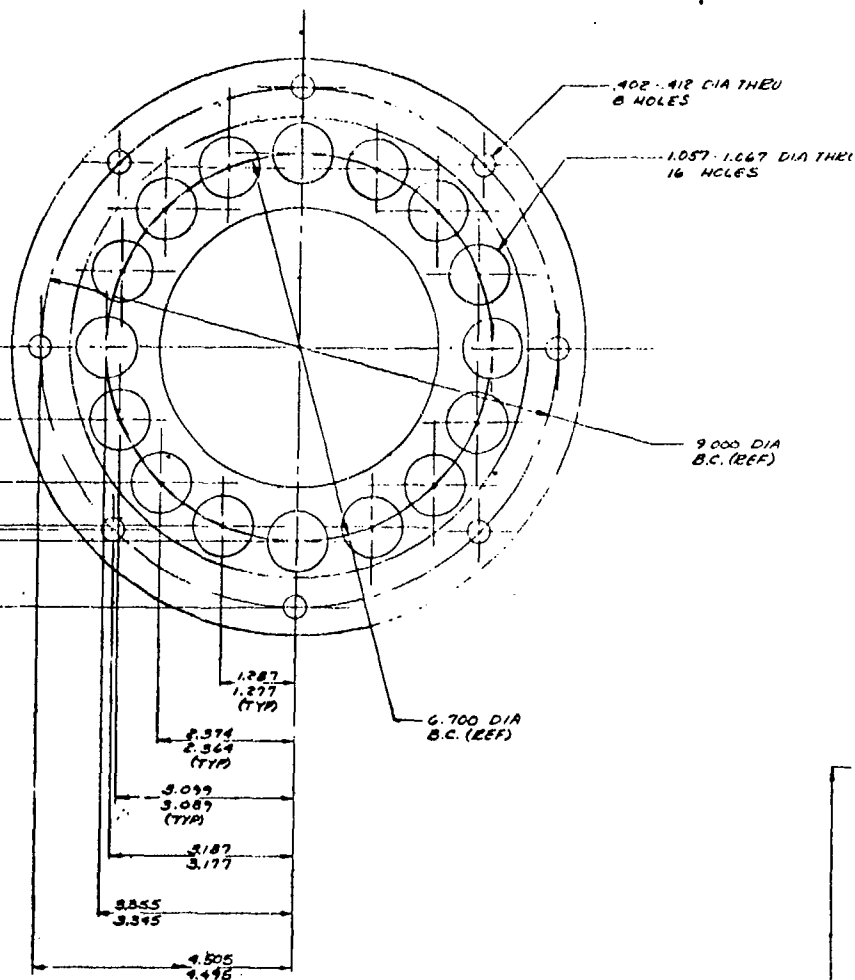
15

14

13

12

11



SKP25032

Provisions for future design should compensate for this difference in expansion to minimize the potential leak paths. A two-piece, machined, and bolted nozzle proved feasible by the successful operation of the Inconel 713LC nozzle assembly in the final demonstration run.

4.2 Structural Heat-Transfer Analysis

4.2.1 Cooled Radial Turbine Nozzles

While the primary radial turbine nozzle design is an uncooled columbium alloy, a conventionally cooled, nickel-base alloy design has been analyzed as a backup. The need for such a secondary design was prompted by the fact that columbium has not been used extensively in a turbine application; fabrication, thermal shock, and/or corrosion problems could preclude its use.

External boundary conditions and aerodynamic shape dictate cooling requirements for the radial turbine nozzle (Figure 110). The level of main-stream gas temperature requires cooling over the entire vane. High surface velocities, relative to the pressure surface, require significantly more cooling on the suction surface. The nozzle trailing edge requires extensive cooling and is too thin for internal cooling passages.

The nozzle design shown in Figure 111 is expected to achieve overall vane cooling and overcome the difficulties mentioned above. To achieve the desired cooling-flow split between suction and pressure surface, cooling gas for each side is independently metered through the insert-bolt caps. The desired internal cooling has been accomplished by adjusting the insert-to-vane-wall spacing. These flows join at the rear of the vane cavity to supply cooling air for the film-cooled trailing edge.

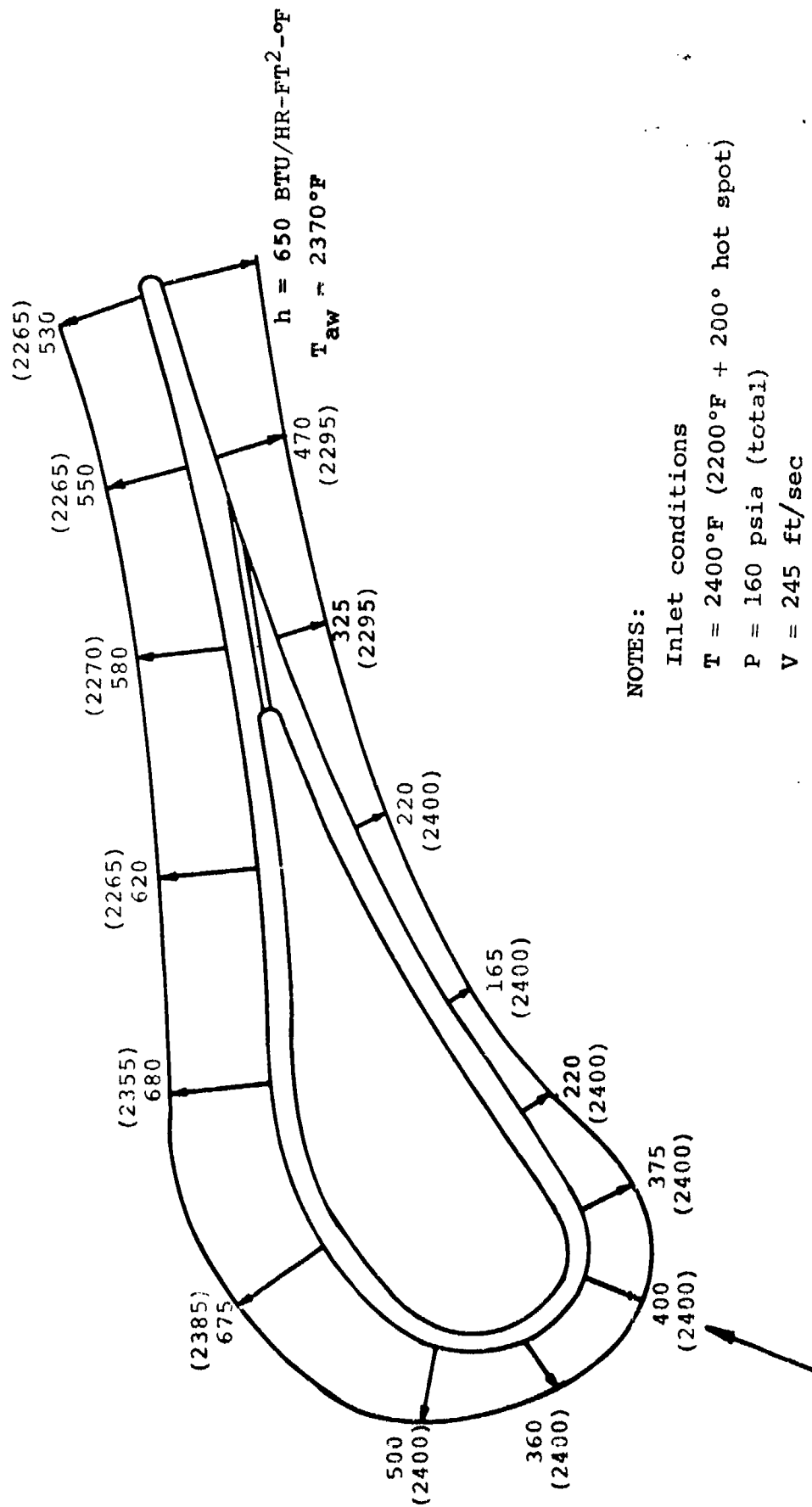


Figure 110. Design Boundary Conditions, Cooled Turbine Nozzles.

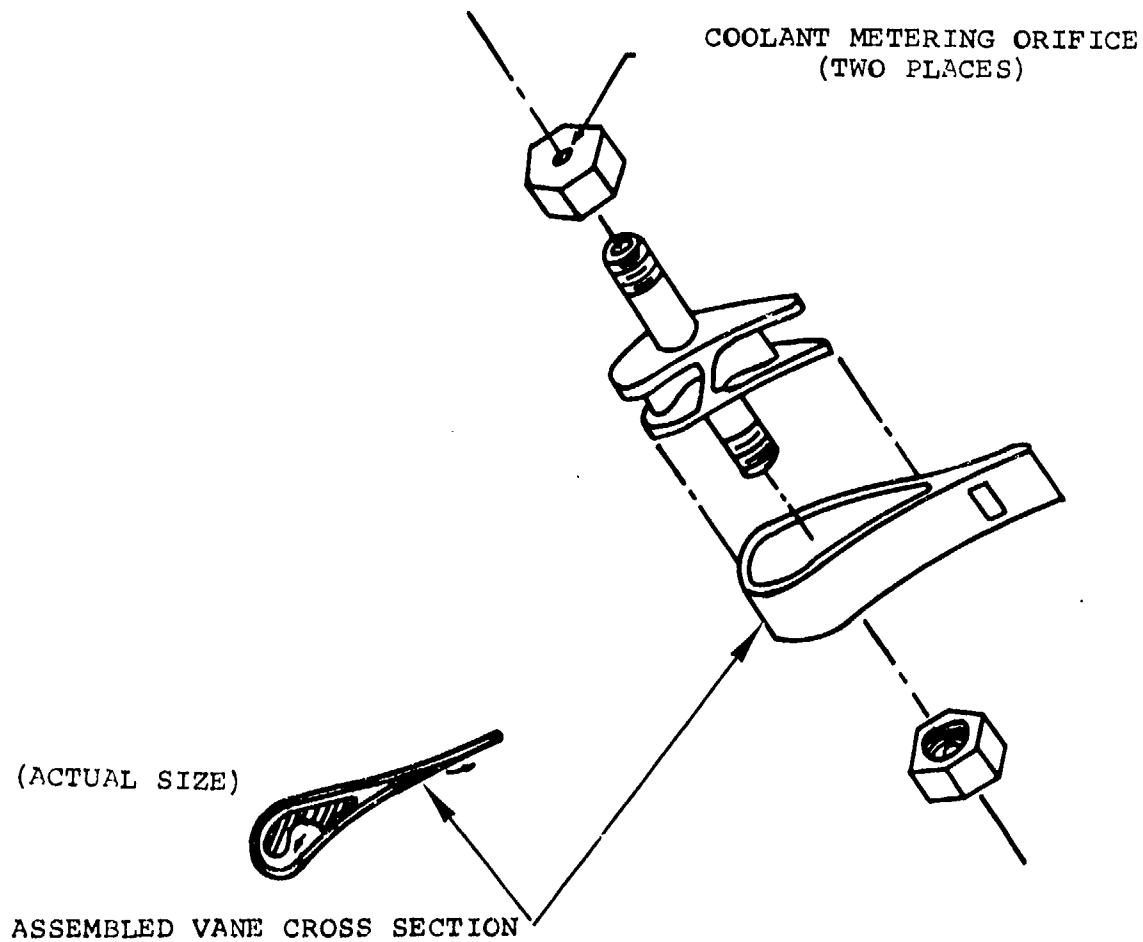


Figure 111. Cooled Turbine Nozzle Configuration.

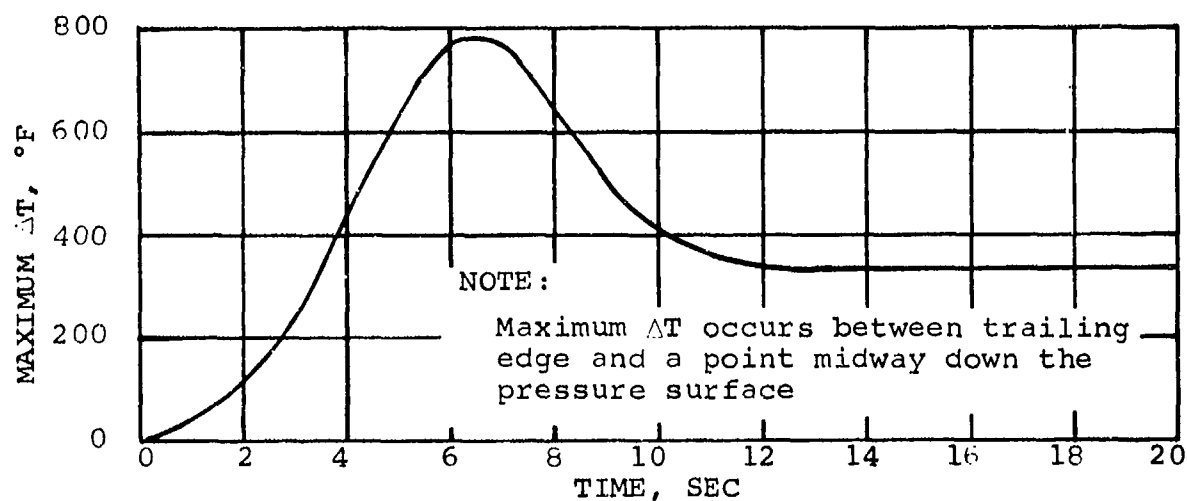
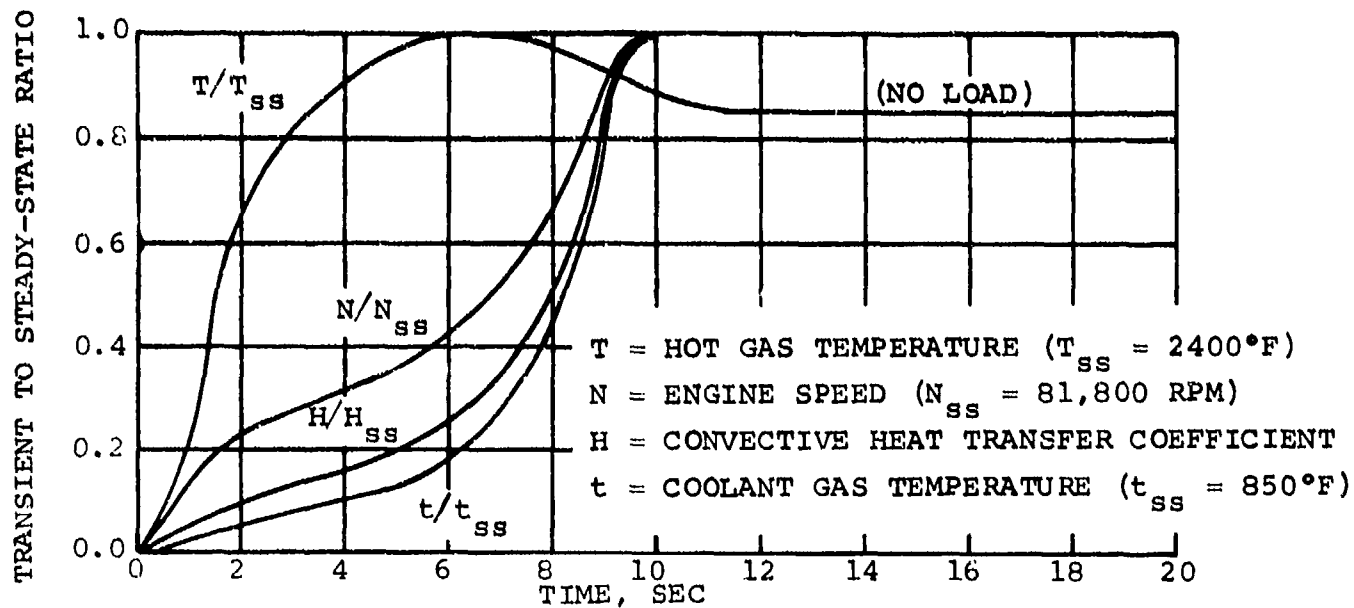
In addition to accomplishing the suction- to pressure-side flow split in a simple way, the design also has another desirable feature: the pressure drop is regulated at a point other than the vane film-cooling slot. Regulating through a film-cooling slot is difficult, because a realistic slot width (0.020 in.) results in excessive coolant flow to obtain a reasonable drop of 5 to 10 psi. In this design, a relatively large pressure drop is taken across the metering caps, ensuring a relatively invariant film-cooling flow at all times.

For a 2400°F hot spot, the cooling flow rate is dictated by the amount required for trailing edge film-cooling. It is 4-percent of the turbine through-flow (2.115 lbm/sec) for this design (0.020-in. slot width). Steady-state temperatures are shown in Figure 112. One disadvantage of the design is the high flow rate required for trailing-edge cooling; this leads to overcooling the vane pressure surface near the exit of the film-cooling slot. Transient temperature and stress analyses results on the vane for the engine-start condition are shown in Figure 113a. Maximum temperature difference in the vane is shown in Figure 113b. The resulting maximum stress occurs at approximately 7 sec (Figure 113c). For the maximum stress of 90,000 psi, a minimum low-cycle fatigue life of 10^5 cycles is predicted; however, a severe stress concentration created by the film-cooling slot and an increased stress range created by stress reversals at engine shutdown will undoubtedly reduce the predicted cycle-life.

Barring corrosion and oxidation, the primary causes of any blade failure, the blade should have sufficient life to withstand the duty-cycle goal of 2500 hr and 1500 starts.

4.2.2 Nozzle Support Structure and Radial Turbine Shroud

The assembled radial nozzle support structure and radial turbine shroud are shown in Figure 114. This configuration, which will accept either the uncooled or cooled vanes, has uncooled columbium nozzle



(b) Maximum Temperature Difference

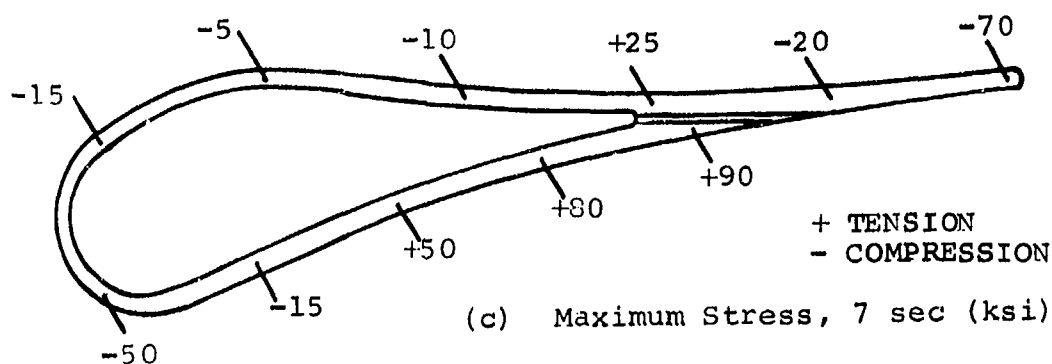
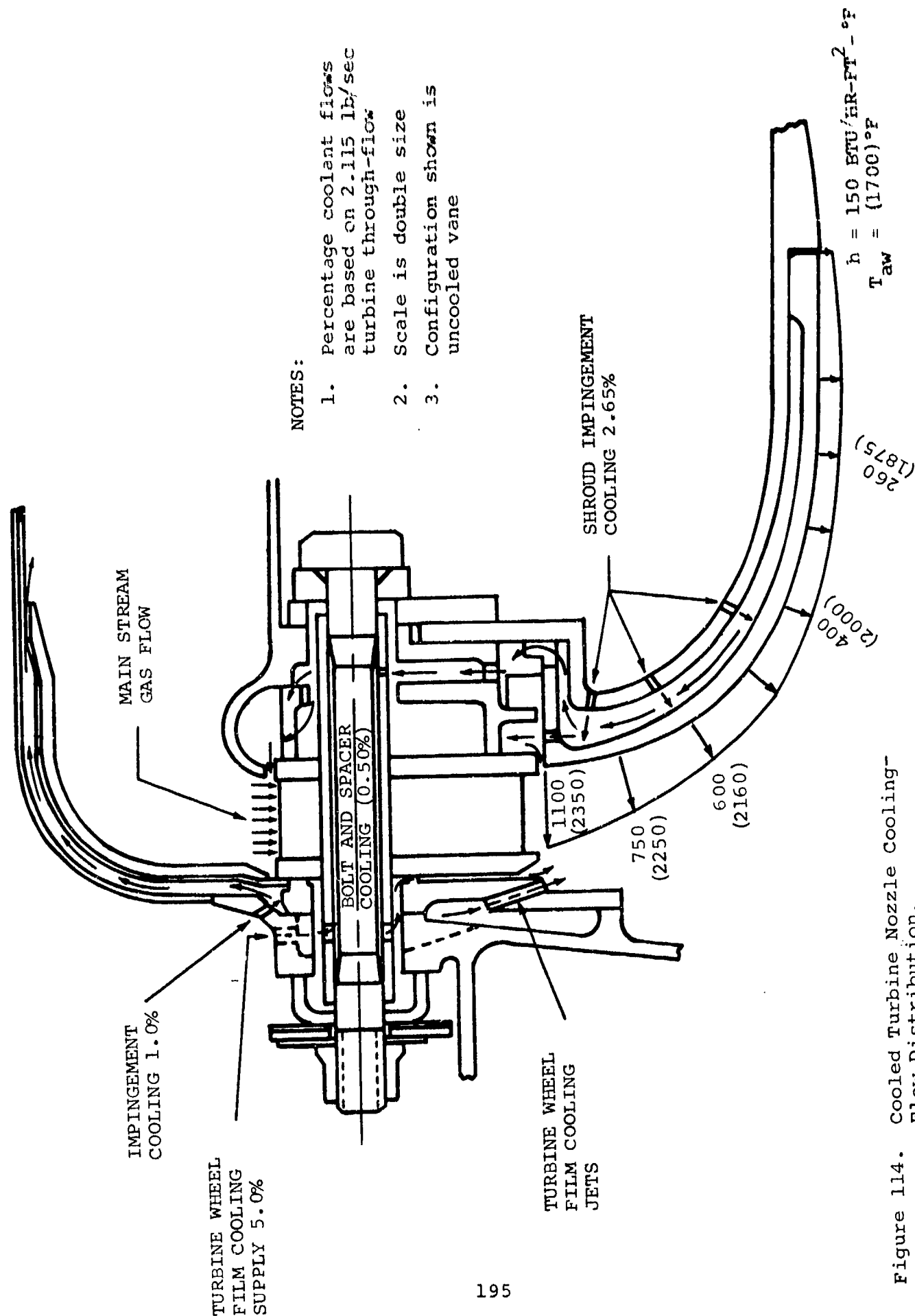


Figure 113. Cooled Turbine Nozzle Transient Temperatures.



NOTES:

1. Percentage coolant flows are based on 2.115 lb/sec turbine through-flow
2. Scale is double size
3. Configuration shown is uncooled vane

Figure 114. Cooled Turbine Nozzle Cooling-Flow Distribution.

vanes (used in the APU configuration), with the surrounding structure being fabricated from Hastalloy X, Inco 713LC, and Inconel 718.

While the columbium alloy can withstand temperatures above 2000°F without cooling, the nickel-base alloys must be cooled to levels of 1900°F or less. Coolant flow paths and rates are shown in Figure 114. To limit conduction into the structure, contact between the nickel-base alloys and the columbium bands was minimized by making local contact instead of continuous rings wherever possible. Where continuous rings were required to provide seals, impingement cooling was used.

Boundary conditions on the nozzle bands are essentially an average of those on the vane suction and pressure surfaces (Figure 110). External boundary conditions on the radial turbine shroud are illustrated in Figure 114. Because of the severe shroud boundary conditions, impingement cooling has been selected as the cooling scheme.

Average metal temperatures predicted for a 2400°F hot spot are shown in Figure 115. Circumferential conduction, to regions outside of the hot spot, was not considered.

As shown in Figure 115, the nozzle band temperatures are considerably higher than the surrounding structure. To allow the bands to grow (relative to their support structure), the bolt hole in the support structure is actually a slot that allows radial movement of the bolt and bands.

To minimize compressive loading on the nozzle vane as it heats and begins to expand, a spring (Figure 114 under the bolt lock nut) has been designed to hold the structure together. During operation, pressure forces hold the structure intact. This allows a relatively light load on the vane and should significantly decrease compressive nozzle stresses, whereas the nozzle is held rigidly between bands in the conventional structural design.

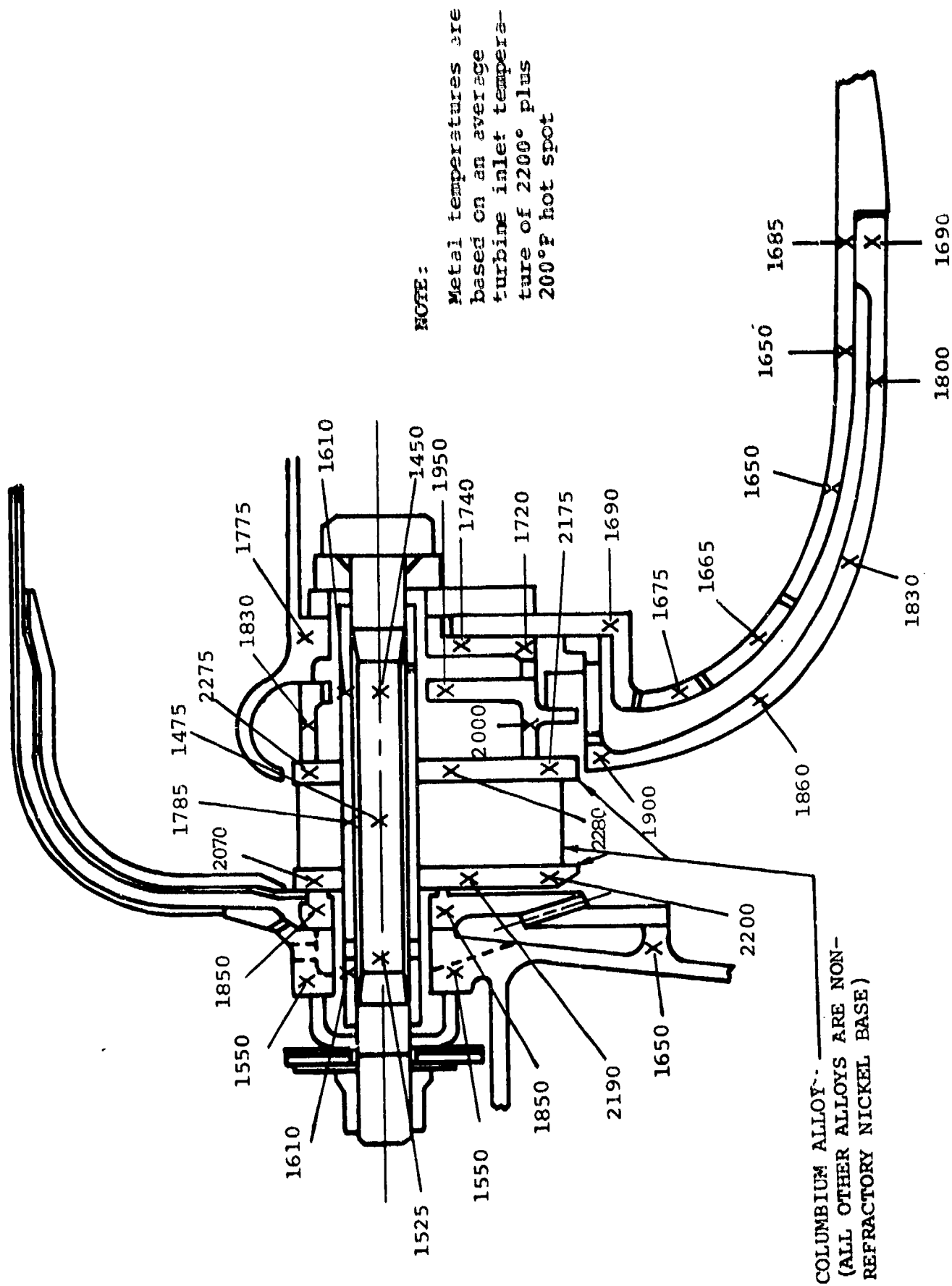


Figure 115. Cooled Turbine Nozzle Temperature Distribution.

One major disadvantage of this configuration is that metal-to-metal contact is relied upon to provide seals. With high-pressure drops found at several points in the structure (60 to 80 psi), small clearances created by tolerances or warping will allow large quantities of leakage--most likely, cooling air that will not cause catastrophic failure but will penalize engine performance.

4.2.3 Shroud Stress Analysis

Stress analysis of the impingement-cooled radial turbine shroud, designed to operate at a maximum turbine inlet temperature of 1900°F, was conducted for the following operating conditions:

- (a) Steady state at 1900°F and maximum bleed pressures
- (b) Transient maximum thermal gradient

The Inco 713 shroud analyzed has a maximum steady-state metal temperature of 1750°F, with 1 percent impingement cooling. This produces a minimum creep life (0.1 percent) of less than 1000 hr. Maximum stresses are due to thermal gradients, occur 8.9 sec after light-off, and yield an average low-cycle fatigue life of less than 5000 cycles. In an attempt to control blade tip-shroud clearance, the shroud was designed to compensate for the adverse axial growths of the supporting structure. This was accomplished with a double-walled shroud. A cool outer shroud and its supporting structure grows aft, while the hot inner shroud grows forward, resulting in a net shroud axial motion very near zero. This condition allows the flexibility necessary to closely control the blade tip-shroud clearances existing during steady-state operation.

Several locations around the shroud (Figure 116) are analyzed for maximum steady-state pressure stresses (Table XII), maximum steady-state combined pressure and thermal stresses (Table XIII), and maximum transient thermal stresses (Table XIV).

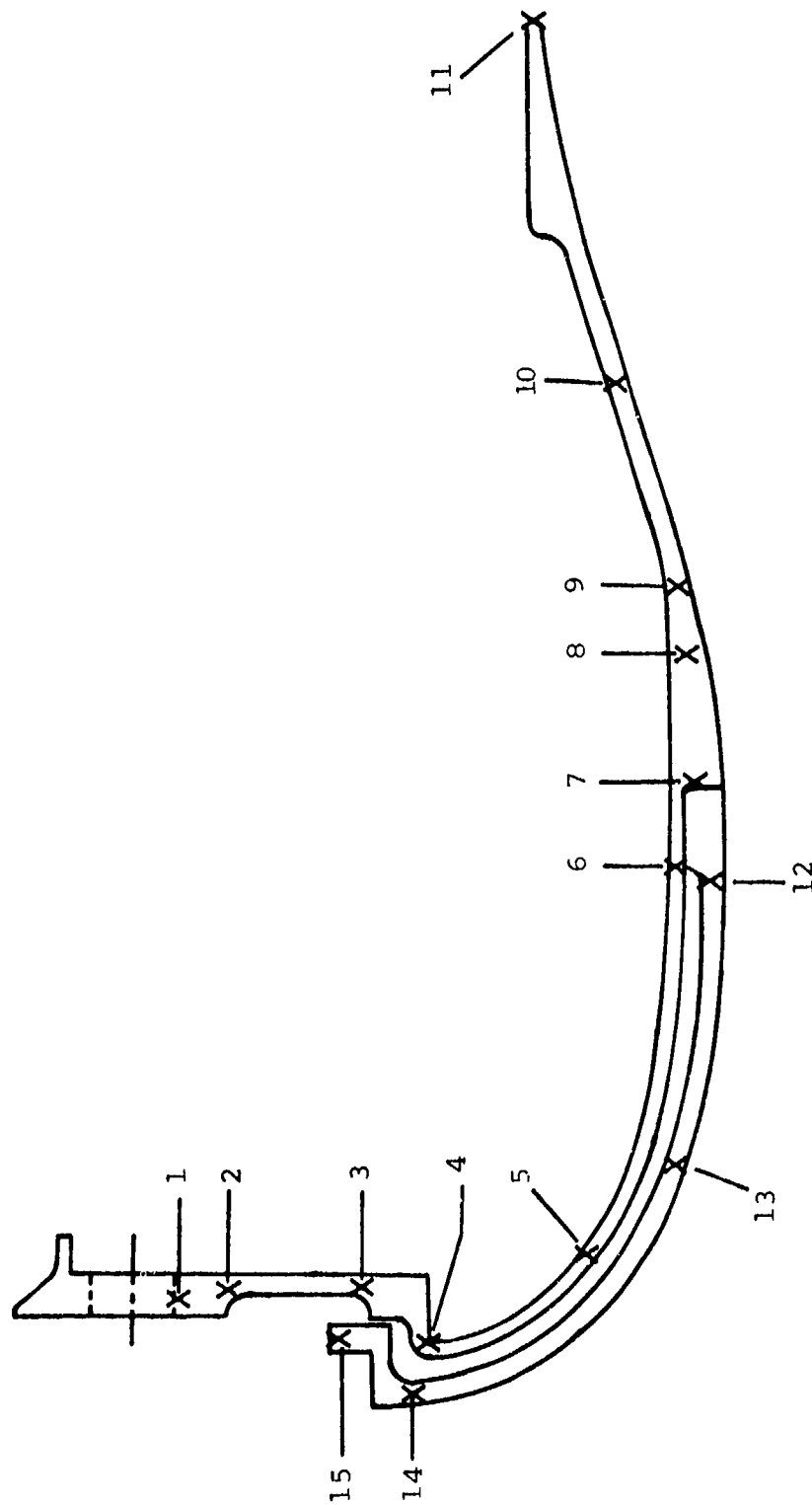


Figure 116. Turbine Shroud Maximum Calculated Stress Locations.

TABLE XIII

EFFECTIVE TURBINE SHROUD STRESSES DUE TO
STEADY-STATE PRESSURES

On Figure 92	Stress, psi	Temperature, °F	0.1 Percent Creep, min hr
1	30,400	1384	600
2	32,000	1360	900
3	41,900	1005	10^5
4	46,800	1005	
5	30,500	1025	
6	2,280	1155	
7	2,750	1200	
8	5,390	1230	
9	6,025	1245	
10	6,630	1279	
11	5,050	1270	
12	5,600	1273	
13	3,020	1563	10^5
14	5,070	1750	850
15	170	1700	10^5

TABLE XIV

EFFECTIVE TURBINE SHROUD STRESSES DUE TO STEADY-STATE
PRESSURE AND TEMPERATURE

On Figure 92	Stress, psi	Temperature, °F	Minimum 0.2 Percent Yield Strength, psi
1	68,750	1384	95,000
2	63,290	1360	95,200
3	34,740	1005	
4	51,290	1005	
5	27,600	1025	
6	41,760	1155	
7	7,690	1200	
8	9,079	1230	
9	6,600	1245	
10	8,740	1279	
11	5,050	1270	
12	49,100	1273	95,500
13	11,900	1563	80,000
14	17,920	1750	47,500
15	9,900	1700	54,000

4.3 Radial Turbine Wheel

4.3.1 Design Considerations

To achieve the desired limit of performance and efficiency, the GTCP305 was designed to operate at turbine inlet temperatures and tip speeds that represent a substantial increase in the state of the art for small auxiliary power units. The duty-cycle life goal of 2500 hr, with turbine inlet temperatures to 2200°F, makes the high-temperature, cast, nickel-base alloys a desirable choice because of the good stress-rupture properties. However, the operating tip speed of 2190 ft/sec demands higher tensile strength (found in the forged nickel-base alloys) to achieve adequate burst margin.

For these reasons, an alloy recently developed for the U.S. Air Force by the Universal Cyclops Company (AF2-1DA) was chosen. Test specimen from this alloy showed tensile strengths superior to the strongest wrought materials available, with stress-rupture strength equivalent to the cast alloys.

Although the projected material properties for AF2-1DA are excellent, the high temperature and speed-operating regime of the GTCP305 requires cooling the radial turbine, to maintain an adequate burst margin and stress-rupture life. Several cooling methods were considered, with the two schemes (Figure 117) receiving primary consideration.

As the design of the wheel progressed, aerodynamic efficiency and performance requirements dictated an increase in wheel size (Figure 118). The resulting analysis reflected a significant increase in stress, resulting in values that were considered limiting without the added stress concentration of internal cooling passages. In addition to this limitation, data published by United Aircraft of Canada on a similar internally cooled wheel showed a serious degradation in

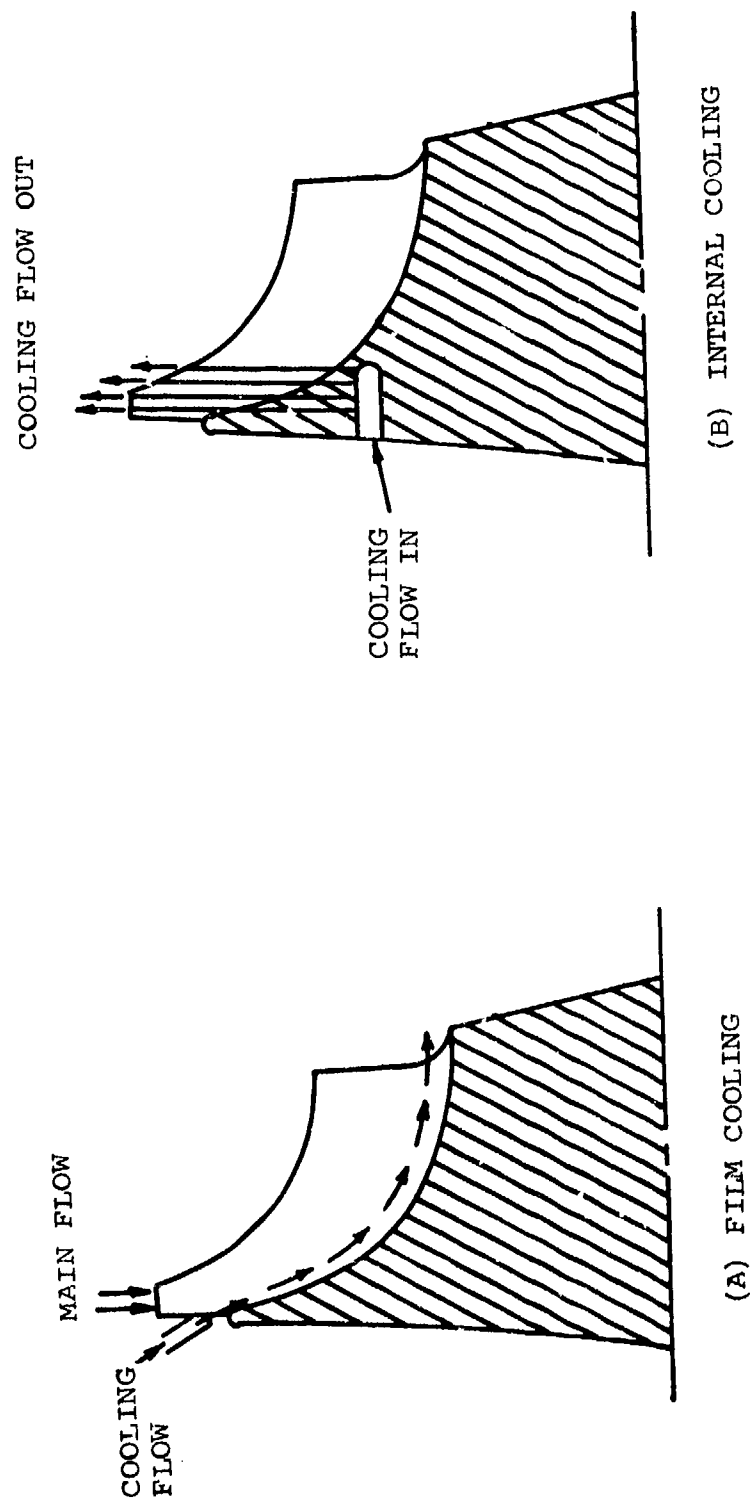


Figure 117. Film and Internal Cooling Schemes for Radial Turbine Wheel.

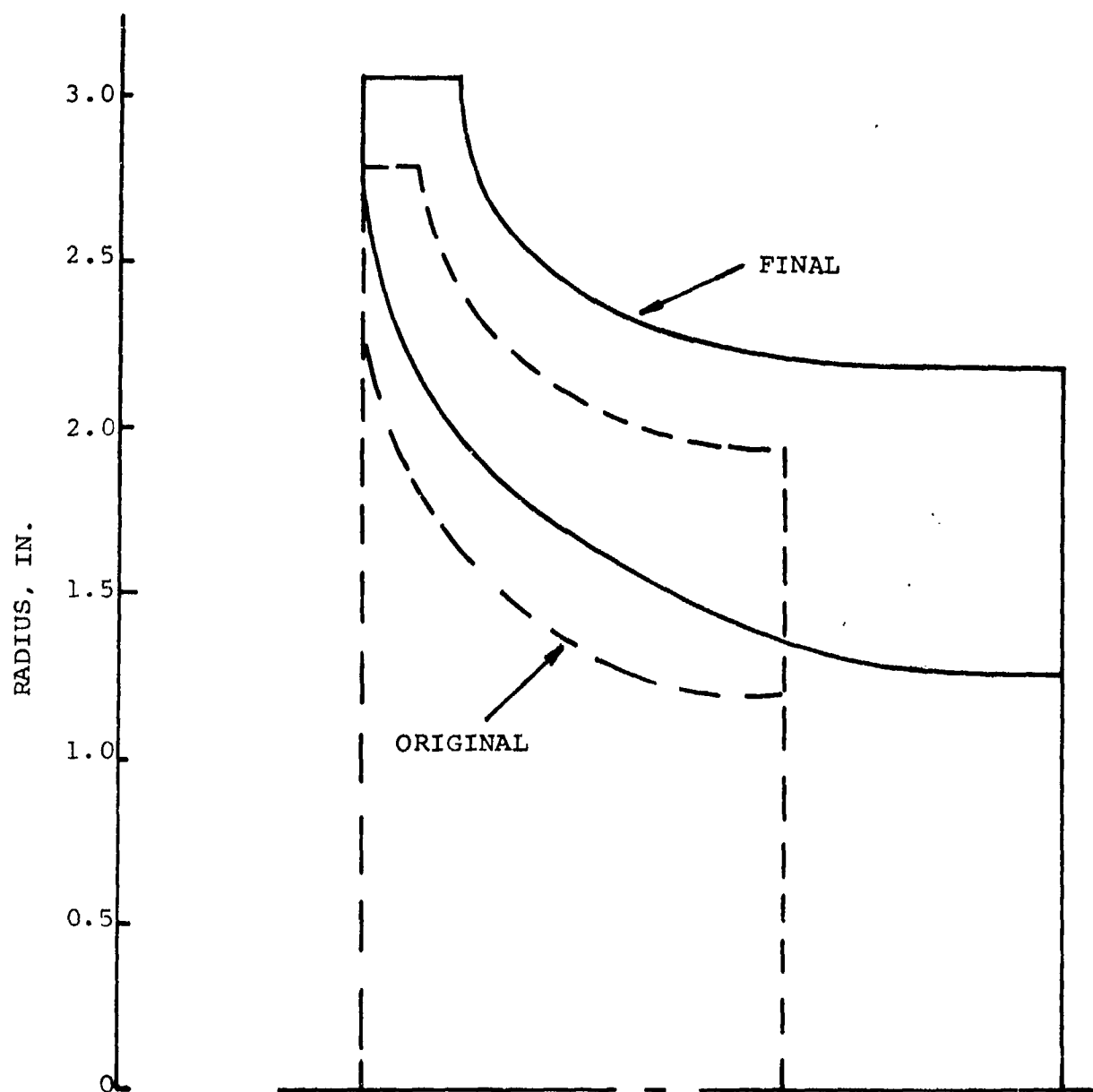


Figure 118. Progression of Radial Turbine Aerodynamic Configuration.

aerodynamic performance, due to cooling air being ejected at the blade tips. For these and other reasons, film-cooling was chosen as the primary cooling scheme for the radial turbine wheel.

4.3.2 Heat-Transfer Analysis

The film-cooling technique appears to be a natural method of cooling the radial turbine wheels. With this method, cooling flow is injected at a point on the wheel where cooling requirements are most stringent and flows in the direction of mainstream gas, with cooling efficiency diminishing as the cooling requirements lessen. This cool film of air also serves to insulate the turbine disk from the hot gases. The additional heat conduction from the blades decreases blade metal temperatures. This cooling scheme eliminates internal cooling passages, which are costly and difficult to locate accurately, thus significantly simplifying the design.

At the present, no proven state of the art--analytical or empirical correlations--in film-cooling radial turbine wheels is available for general design use. The studies reported in the literature on this method have resulted in the prediction of average (not local) heat-transfer effects and the measurement of temperatures in applications, which cannot be readily applied to the high-speed, high-temperature GTCP305 radial turbine engine.

The feasibility of the technique was demonstrated in a film-cooling test of the turbine wheel for the AiResearch Model GTCP85-98CK Gas Turbine Engine. This turbine wheel has a 9.75-in. diam (compared to the 6.136-in. diam GTCP305 wheel), normally operates at 1600 ft/sec (compared to 2190 ft/sec for the GTCP305 wheel), was not as highly loaded as the GTCP305 wheel, and was of a different design. Temperature reductions to 150°F in the radial turbine wheel were observed for cooling flows to 3 percent of the turbine flow (Figure 119).

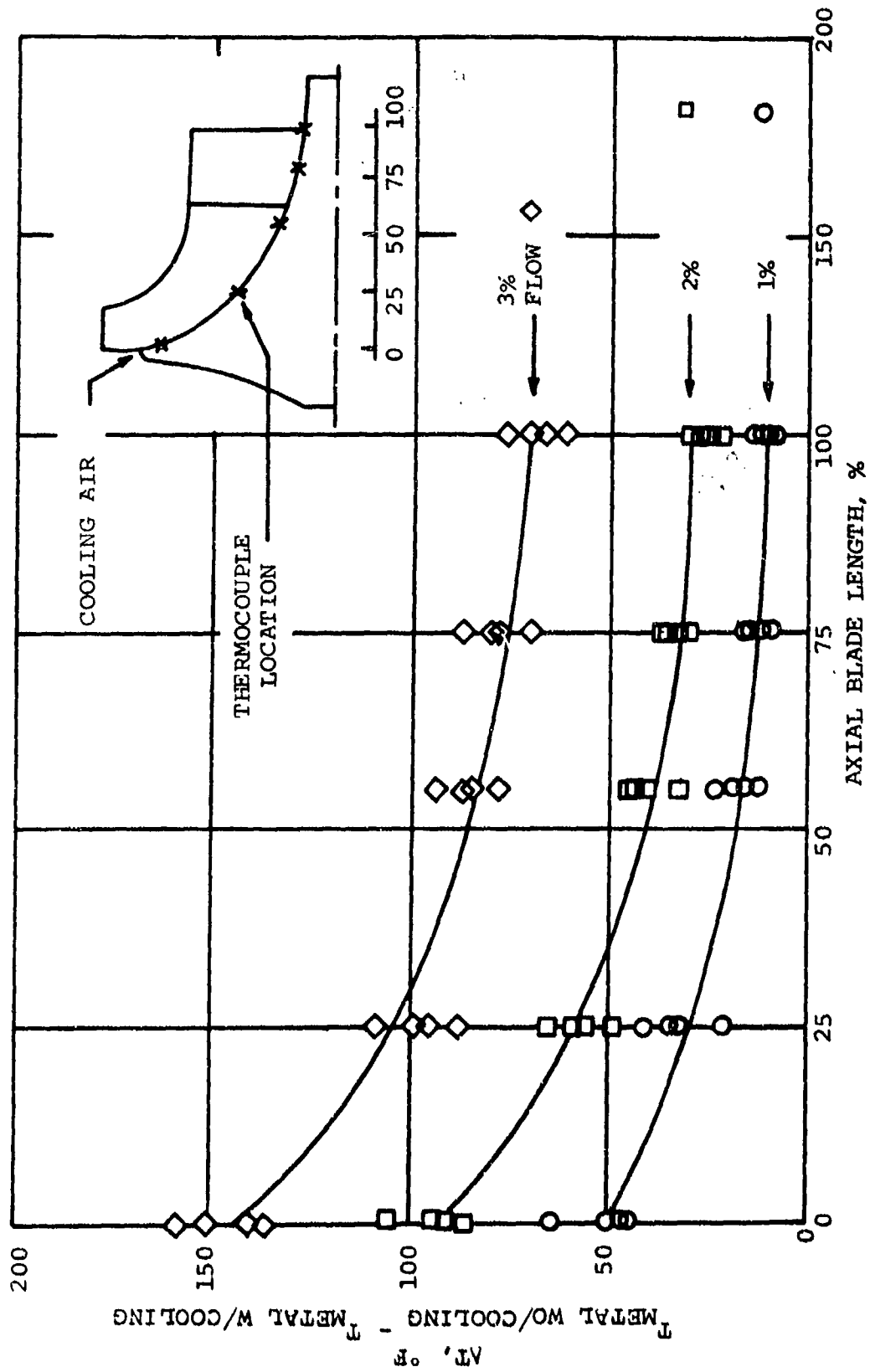


Figure 119. Radial Turbine Film-Cooling Test Results.

Proven analytical techniques did not exist, and the engine design would not permit tests on the radial wheel itself. Therefore, the design of the APU film-cooling system was completed, using the GTCP85 test data, on a conservative 6-percent flow rate. Also, an uncooled wheel model (Figure 120) was chosen for the life analysis, to ensure conservative results.

4.3.3 Stress Analyses

Stresses and deflections due to rotation (Figures 121 through 123 and Table XV) are combined with those of temperature for Figure 124 and Table XVI. The thermal effects are based on a typical operating point in the duty cycle (1900°F) but are representative of all operating conditions, since the thermal gradients do not change significantly. All stresses shown were computed on an elastic basis (i.e., no stress relaxation due to creep effects was considered).

AiResearch experience with turbine wheels has shown that burst speed can be correlated with the average tangential stress of the wheel. Based on the GTCP305 radial turbine average tangential stress of 80,450 psi and an assumed minimum material strength of 137.5 ksi at an average disk temperature of 1400°F (2200°F inlet), the minimum burst speed of the wheel is estimated as 17-percent above the operating speed of 81,800 rpm. Although this is below the normal AiResearch production design standard of 25 percent, film cooling should result in a lower average disk temperature than that of the conservative thermal model, without considering the effect of cooling.

Transient temperatures and stresses have also been estimated on the basis of the assumed engine start characteristic shown in Figure 125. Two critical locations of these elastically computed transient stresses (Figure 126) are important in estimating the wheel low-cycle fatigue life.

NOTES:

1. Temperature in °F
2. Twice-size scale
3. 2200°F inlet temperature

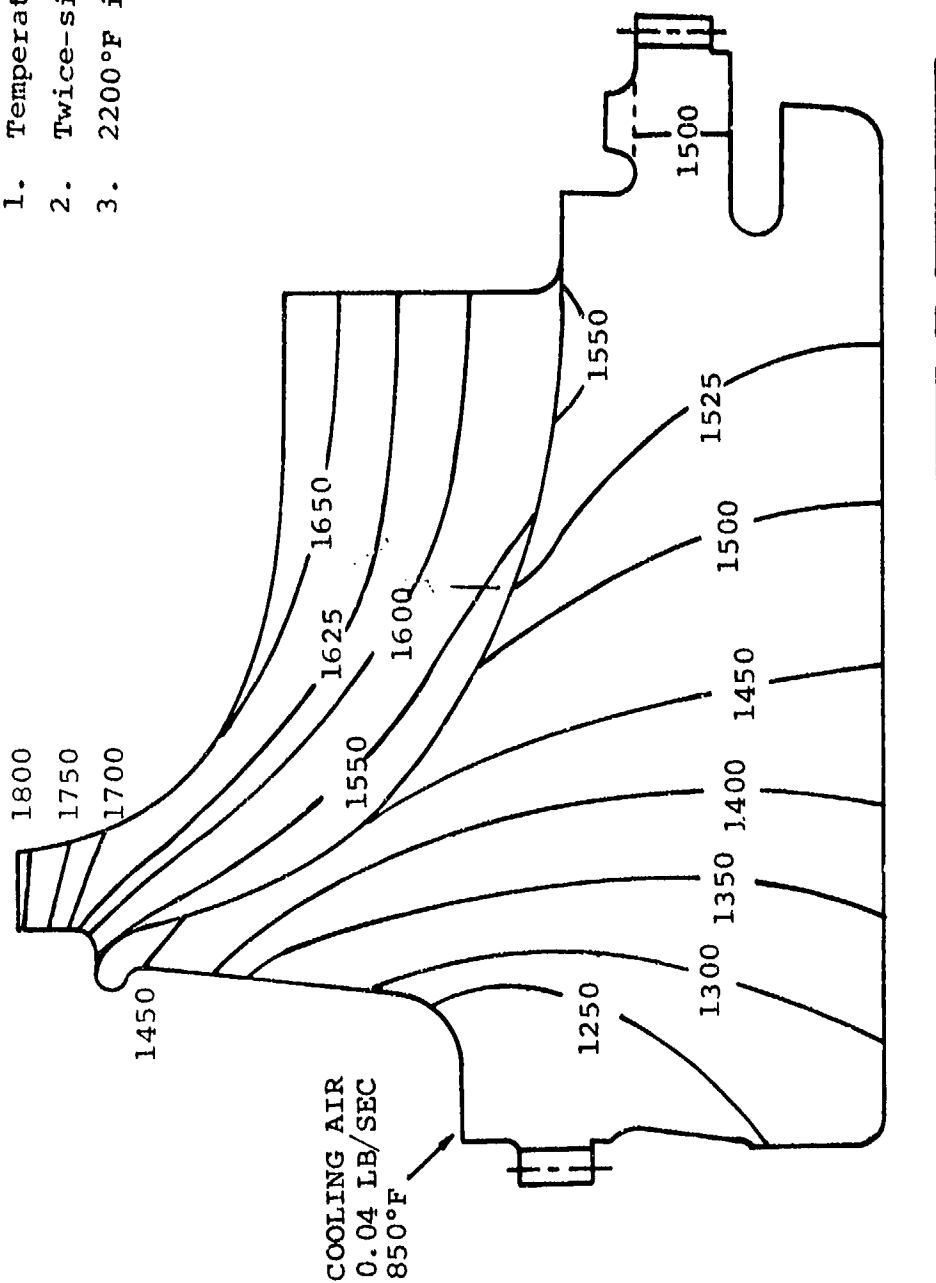


Figure 120. Radial Turbine Wheel Temperature Distribution.

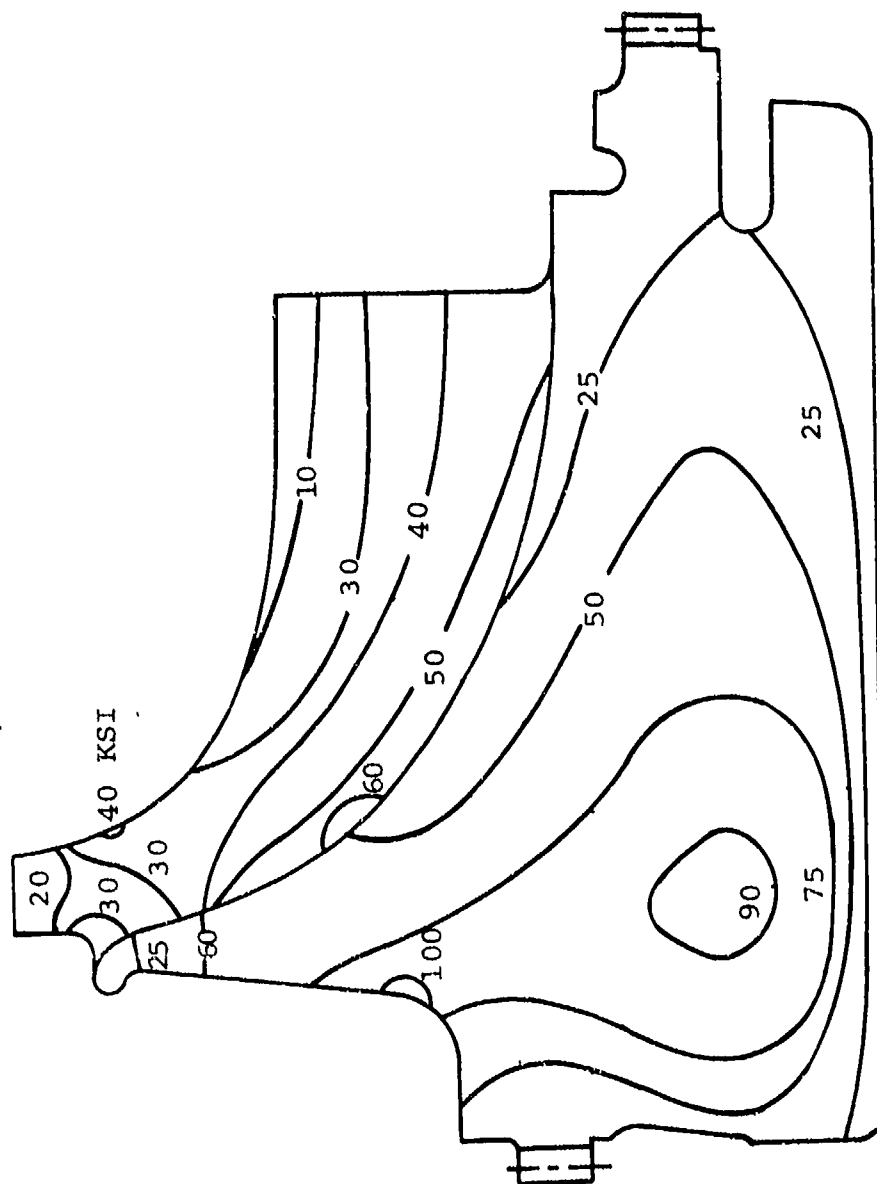


Figure 121. Radial Turbine Wheel Radial Stress.

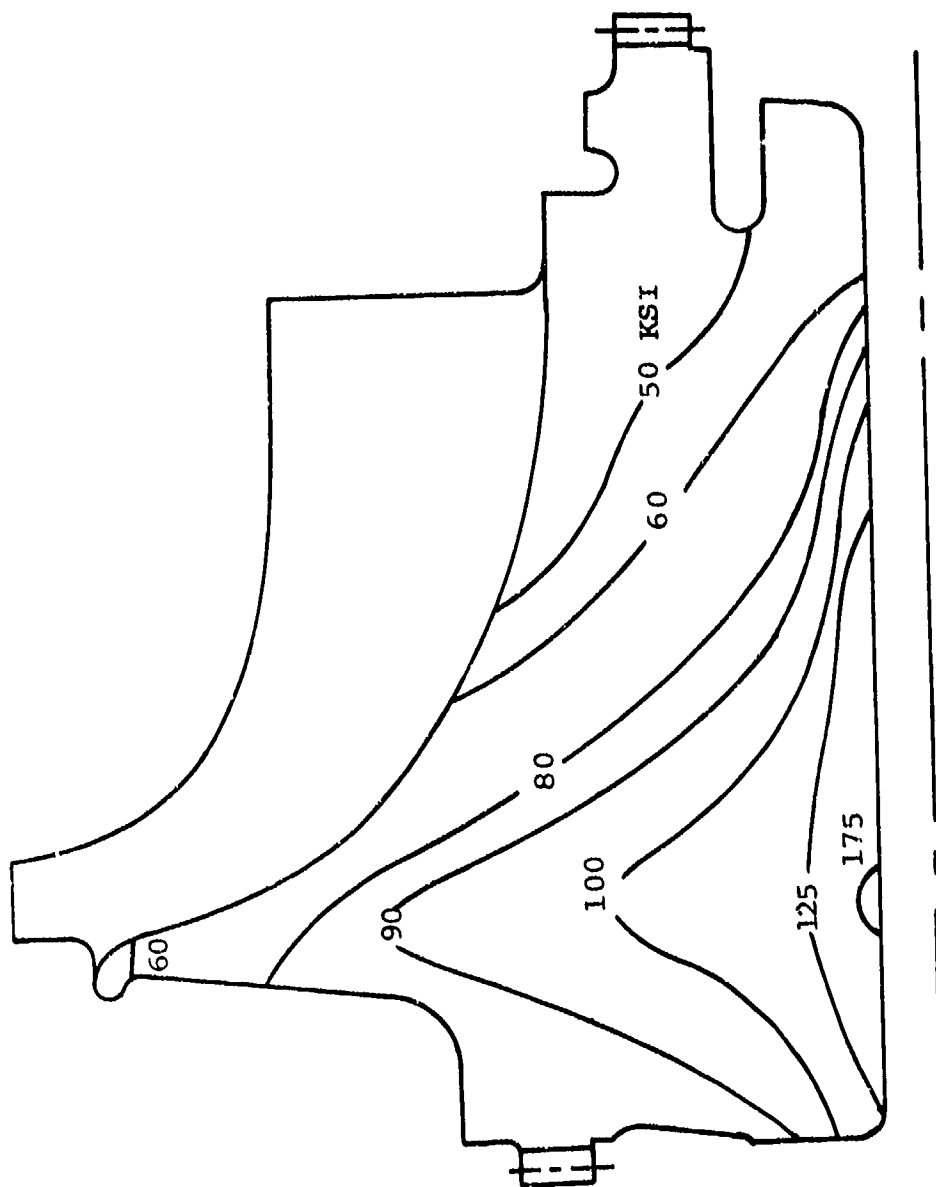


Figure 122. Radial Turbine Wheel Tangential Stress.

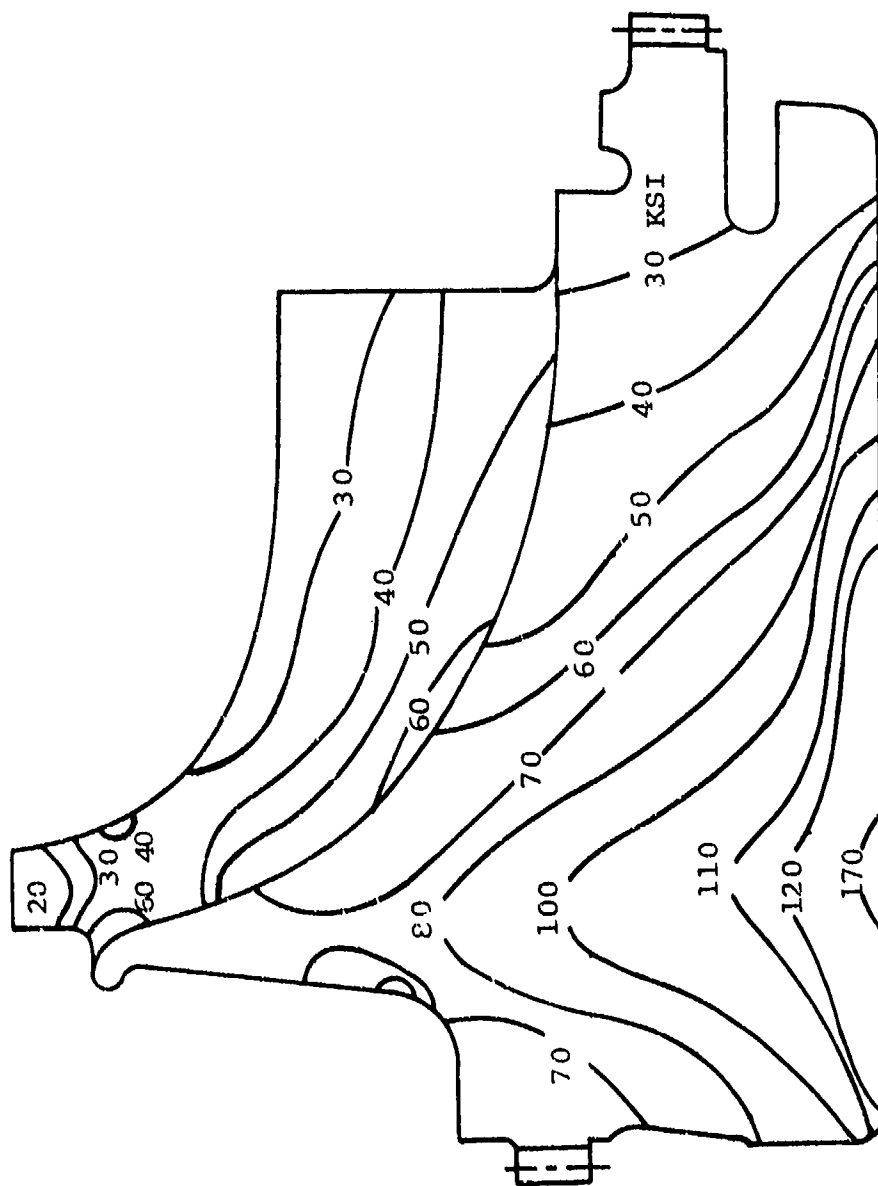


Figure 123. Equivalent Stress.

NOTES:

1. Material is Unitemp AF2-10A ($\sigma = 0.299$ lb/in.³)
2. Wheel speed = 81,000 rpm
3. Average tangential stress = 80,450 psi
4. Thermal effects based on 1900°F TIT

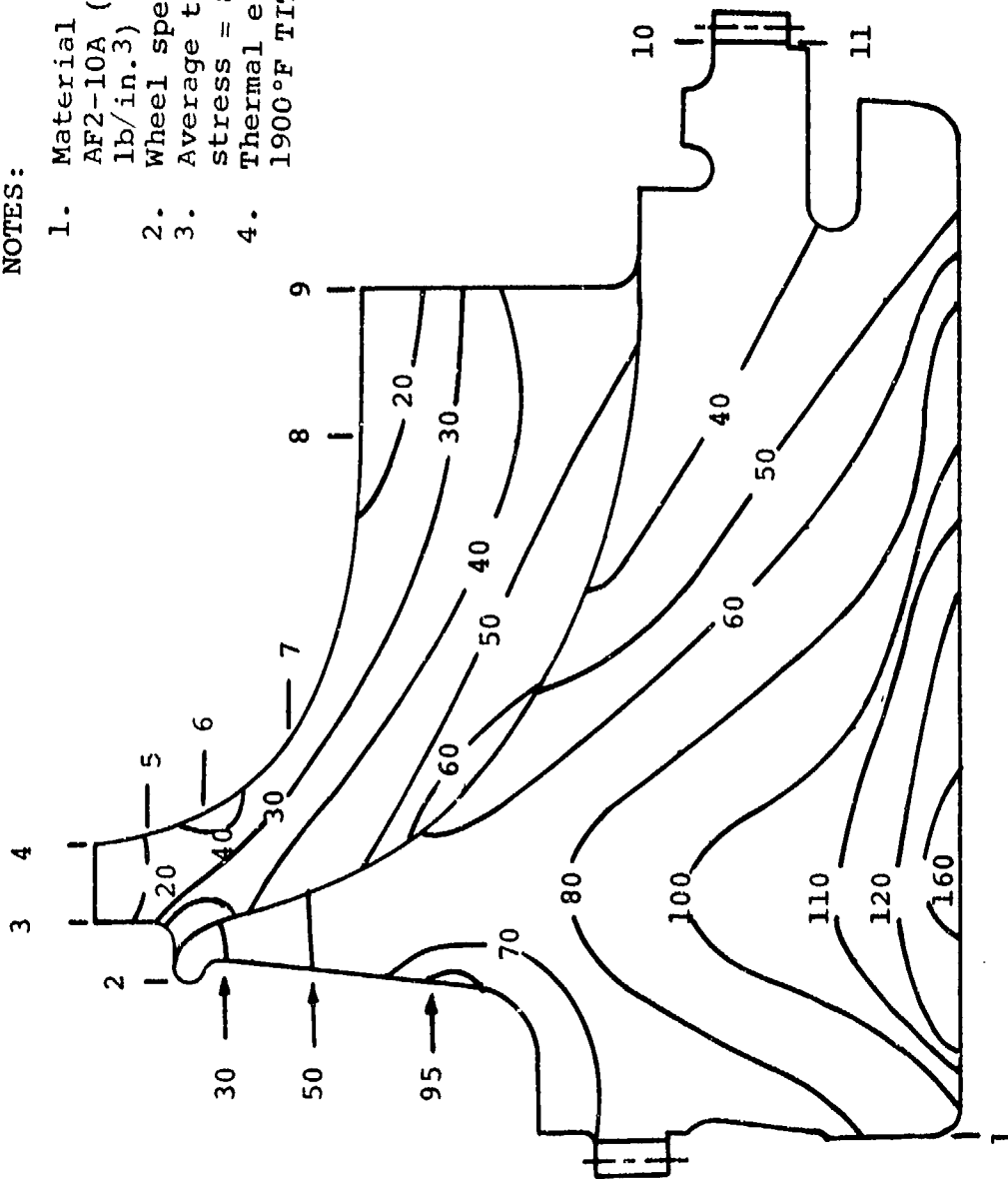


Figure 124. Radial Turbine Wheel Combined Centrifugal and Thermal Stresses and Deflections.

TABLE XV

TRANSIENT TURBINE SHROUD THERMAL EFFECTIVE STRESSES
(8.9 SEC AFTER LIGHT-OFF)

On Figure 116	Stress, psi	Temperature, °F	Typical Life Cycles
1	270	80	10^4
2	180	80	
3	150	85	
4	620	↓	
5	835	↓	10^4
6	77,980	168	4600
7	14,830	315	10^4
8	3,880	340	
9	7,740	405	
10	2,673	↓	
11	140	↓	
12	62,720	↓	
13	9,230	945	
14	28,500	1280	
15	21,430	950	10^4

TABLE XVI

RADIAL TURBINE WHEEL CENTRIFUGAL DEFLECTIONS

Point	Location		Radial Deflection, in.	Axial* Deflection, in.
	R, in.	Z, in.		
1	0.175	-0.675	0.00089	0.0000
2	2.800	-0.200	0.00452	-0.00068
3	3.068	0.000	0.00459	-0.00094
4	3.068	0.275	0.00462	-0.00094
5	2.900	0.310	0.00452	-0.00093
6	2.700	0.375	0.00422	-0.00100
7	2.400	0.625	0.00350	-0.00139
8	2.183	1.570	0.00229	-0.00228
9	2.183	2.100	0.00180	-0.00237
10	1.000	2.965	0.00074	-0.00427
11	0.680	2.965	0.00084	-0.00417
*Point 1 is the location of zero axial reference.				

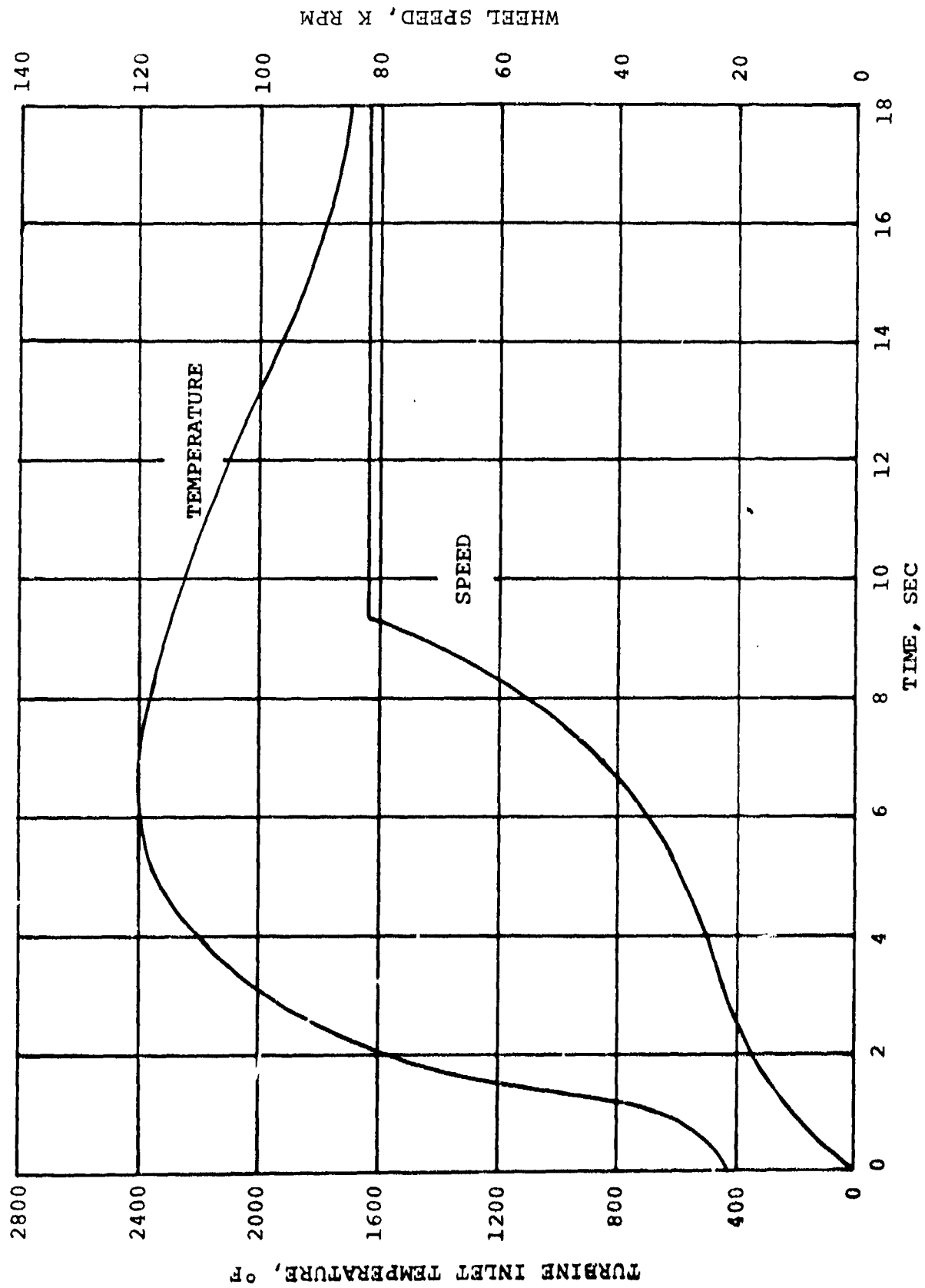


Figure 125. Engine Start Transients, Radial Turbine Inlet Temperature and Wheel Speed.

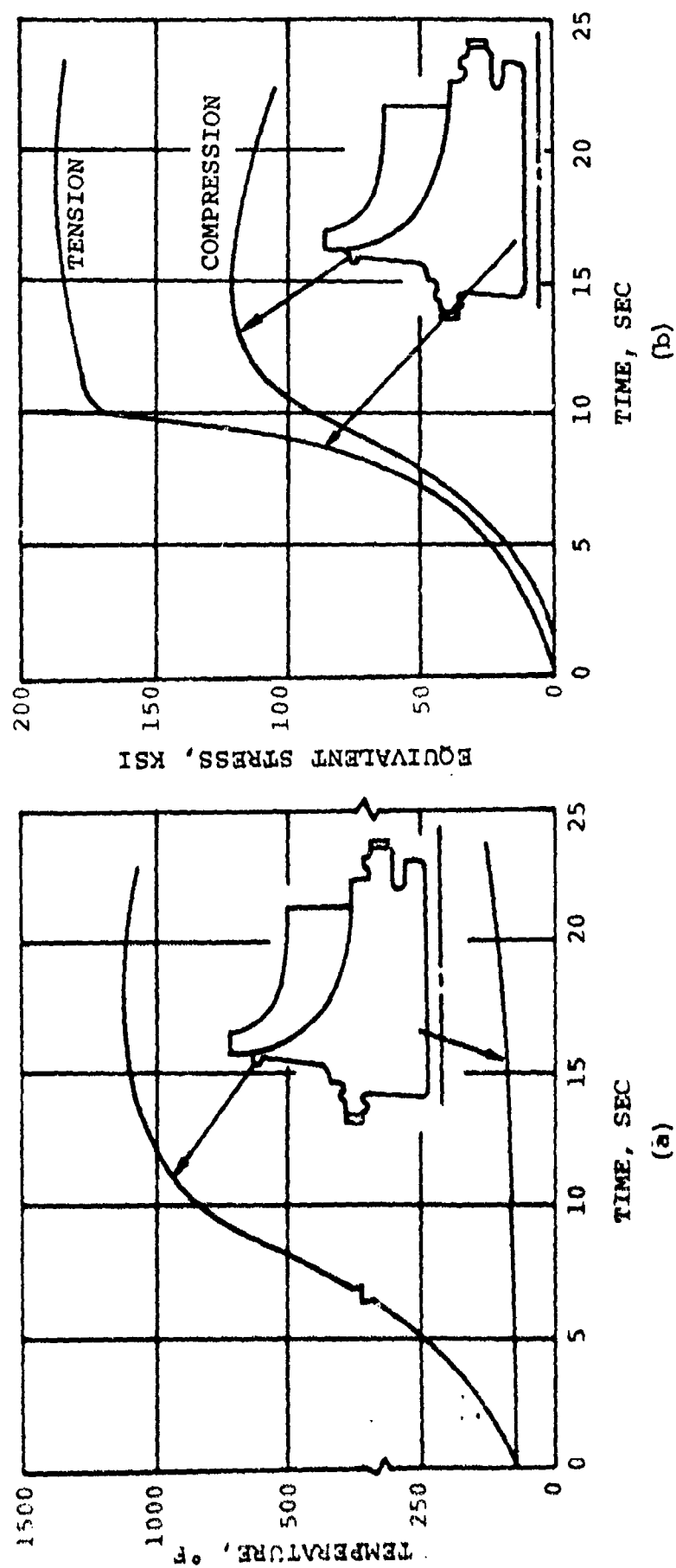


Figure 126. Radial Turbine Wheel Maximum Temperature and Stress Transients, Engine Start.

4.3.4 Stress-Rupture Life Analysis

Component failure in the stress-rupture mode results from a combination of stress and time-at-temperature operation. Generally in turbine wheels, this combination is most severe in the turbine blade inlet region where temperatures are the highest.

When all factors influencing stress are considered, computation of an absolute value for stress-rupture life becomes complicated. Stresses are influenced not only by rotational forces, but by temperature gradients, blade tolerance, and stacking. Also, in the case of the almost fully shrouded GTCP305 radial turbine, additional forces are imposed on the blade by the turbine disk. A further complication is the creep that, over a period of time, diminishes the effects of the thermal and bending stresses.

The design procedure established at AiResearch for determining stress-rupture life in turbine blades is based on an average stress at a critical radius, with a 20-percent increase to account for tolerance and stacking effects. However, this procedure was for application to blade stresses that are relatively unaffected by disk effects, as in the case of axial wheels and most partially shrouded radial turbines. Because stresses in the critical blade region of the GTCP305 radial turbine are influenced by disk stresses, a more conservative approach has been taken to estimate minimum stress-rupture life. Local values of stress have been used with a 20-percent increase to account for tolerance and stacking effects. AiResearch design procedure also calls for factors of safety applied to computed metal temperature, to account for variation in turbine inlet temperature, inaccuracies in the computation, and on material stress-rupture strength (minimum strength values are assumed to be three standard deviations below average values).

Based on this procedure, a blade stress-rupture estimate was made using the stress distribution shown in Figure 124 and the duty cycle on Table XVII. Stress-rupture life throughout the blade is shown in Figure 127, in terms of total life fraction. The effect of each operating point at the critical location is shown on Table XVII.

For a given duty cycle, life fraction is defined as

$$\text{Life fraction} = \sum_{i=1}^n \frac{\text{time}_i}{\text{life}_i}$$

where

time_i = required operating time at point i in the duty cycle

life_i = stress-rupture life at point i in the duty cycle

The reciprocal of the life fraction indicates the percent of duty-cycle life attainable. On this basis, the minimum life predicted is approximately 400 hr of duty-cycle life. As previously stated, this analysis is conservative, since it is based on an uncooled wheel, and the stress relief due to creep has not been taken into account.

Because stresses and temperatures in the disk are significantly high, the critical rupture point in the wheel could not be safely assumed to occur in the blade; hence, an estimate of creep-rupture life in the disk was necessary. Computation of rupture life in the disk bore region is meaningless if based on elastically computed stresses, as in the blade. Creep effects play a significant role in allowing stress redistribution in the disk and must be considered for a meaningful analysis. Therefore, the rupture life estimate for the disk was made on the basis of a creep analysis.

TABLE XVII
RADIAL TURBINE WHEEL CENTRIFUGAL AND
THERMAL DEFLECTIONS

Point	Location		Radial Deflection, in.	Axial* Deflection, in.
	R, in.	Z, in.		
1	0.175	-0.275	0.00190	0.00000
2	2.400	-0.200	0.02390	-0.00523
3	3.068	0.000	0.02760	-0.00700
4	3.067	0.275	0.02979	-0.00399
5	2.900	0.310	0.02805	-0.00242
6	2.700	0.375	0.02600	-0.00057
7	2.400	0.625	0.02343	0.00296
8	2.183	1.570	0.02190	0.01212
9	2.183	2.100	0.02160	0.01721
10	1.000	2.965	0.00907	0.02238
11	0.680	2.965	0.00659	0.02239
*Point 1 is the location of zero axial reference.				

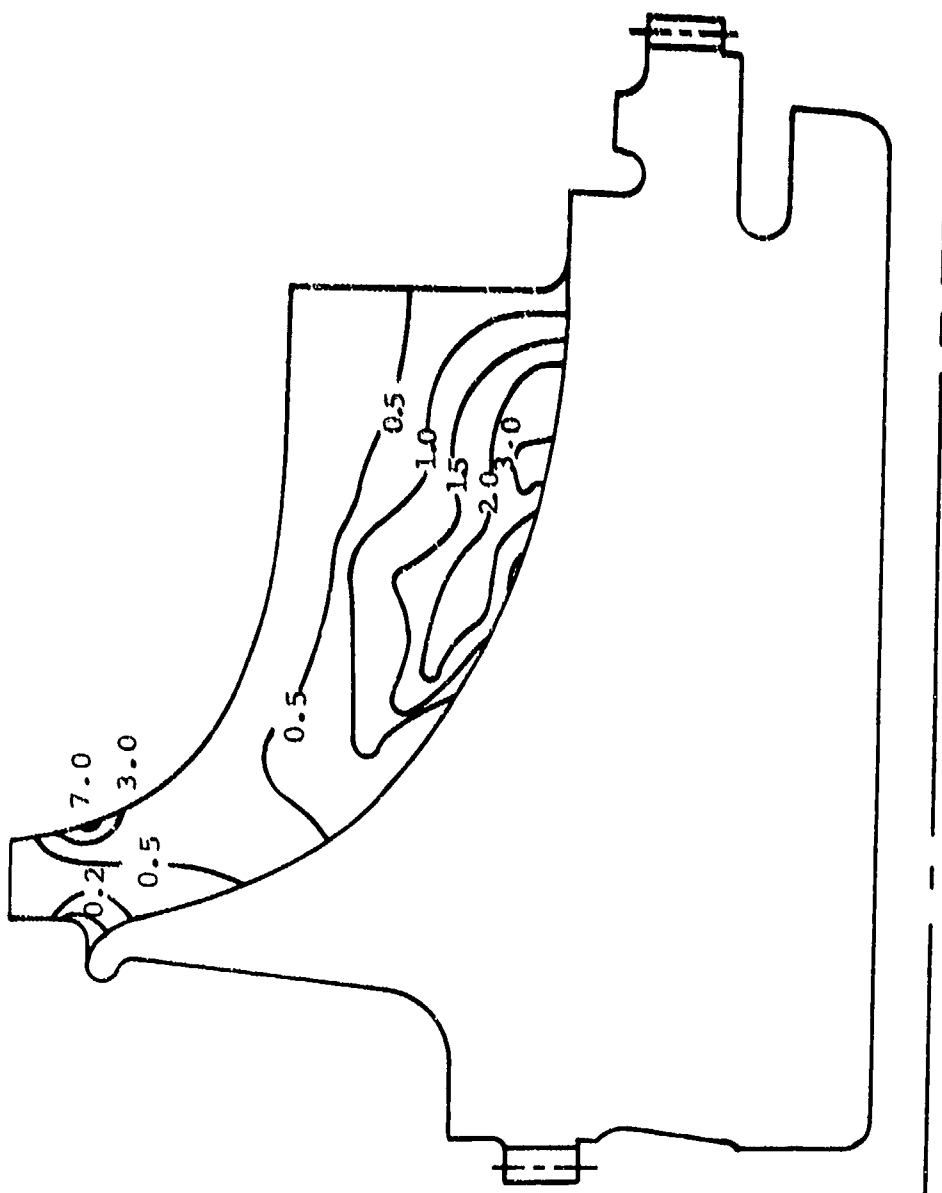


Figure 127. Radial Turbine Wheel, Life Fraction Distribution.

The analysis was based on nominal creep data from test bars supplied by the manufacturer (Figure 128). Rupture apparently occurred at 0.50-percent creep. No safety factors were added to the computed stresses or temperatures. The results of this analysis (which included the turbine blade) indicate the point of failure will be the disk bore (Figure 129). The effect of the cycle point on the bore is tabulated in Table XVIII.

Figure 129 shows that the blade entry and exducer sections reveal only 0.10-percent creep, whereas the results based on an elastic stress analysis (Figure 127 and Table XVII) showed the entry region as the most critical. These conflicting results arise from the fact that the creep analysis allows redistribution of bending stresses in the entry region; thus, local maximum stresses are relieved. Stresses in the exducer are primarily tensile, resulting from centrifugal loading, and do not relax. In an elastic analysis, no allowance is made for relaxation, and life predictions are based on local values. While the creep solution may more closely approximate reality, it does not represent a conservative approach to estimating minimum life and has not been verified sufficiently at AiResearch by experiment to be used as a design tool.

4.3.5 Low-Cycle Fatigue

Repetitive cycling of stresses above the yield strength, in a local region of a material, can result in a low-cycle fatigue failure. The cyclic centrifugal and thermal stresses imposed on certain components of a gas turbine engine, during start and shutdown, are often sufficient to cause low-cycle fatigue failure.

Based on the transient start characteristics shown in Figure 125 and the assumption that AF2-1DA has a low-cycle fatigue strength equivalent to Waspaloy, the bore fatigue life is estimated as 3350 cycles (Figure 130).

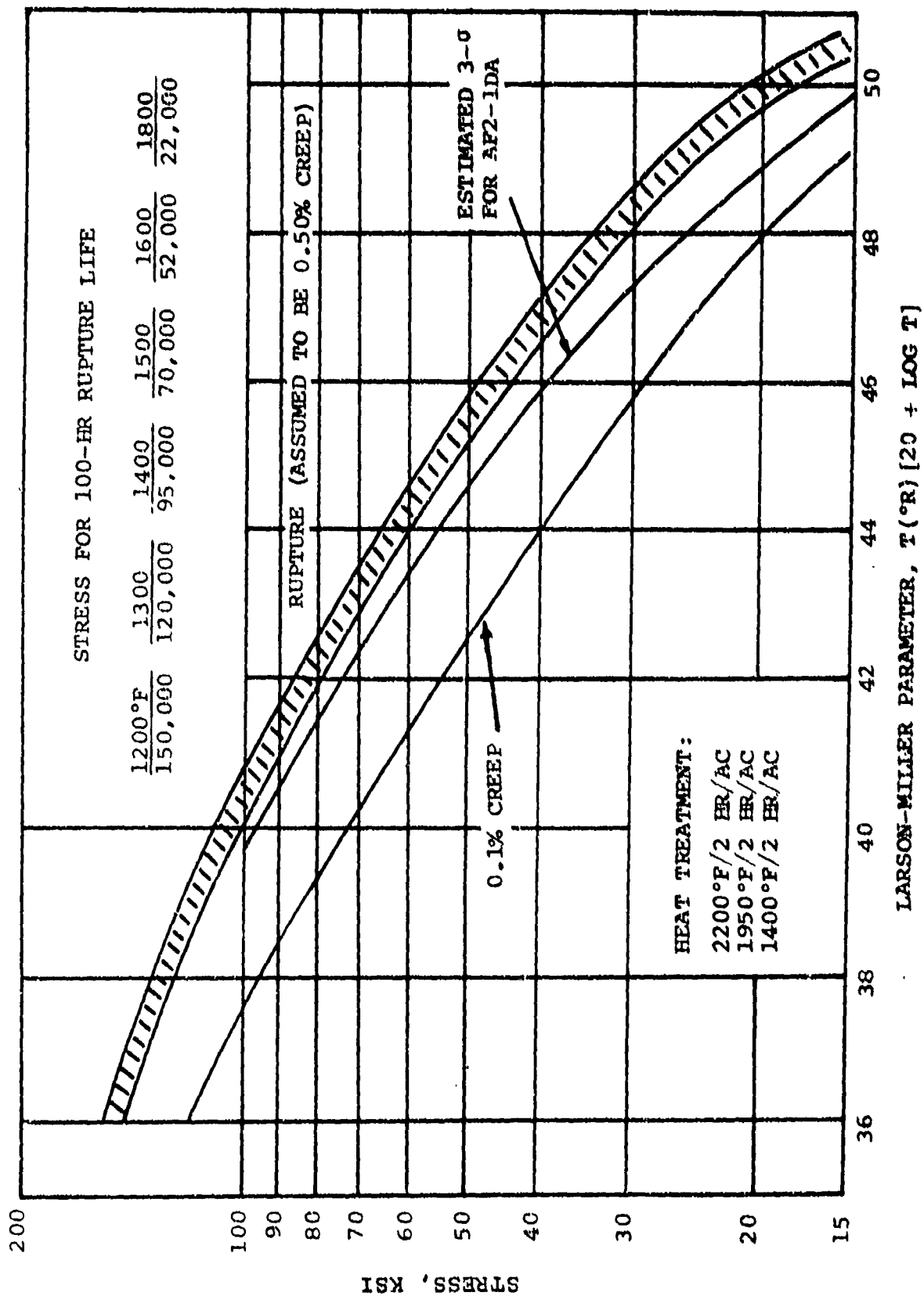


Figure 128. Manufacturer's Stress-Rupture Properties of Unitemp AF2-1DA.

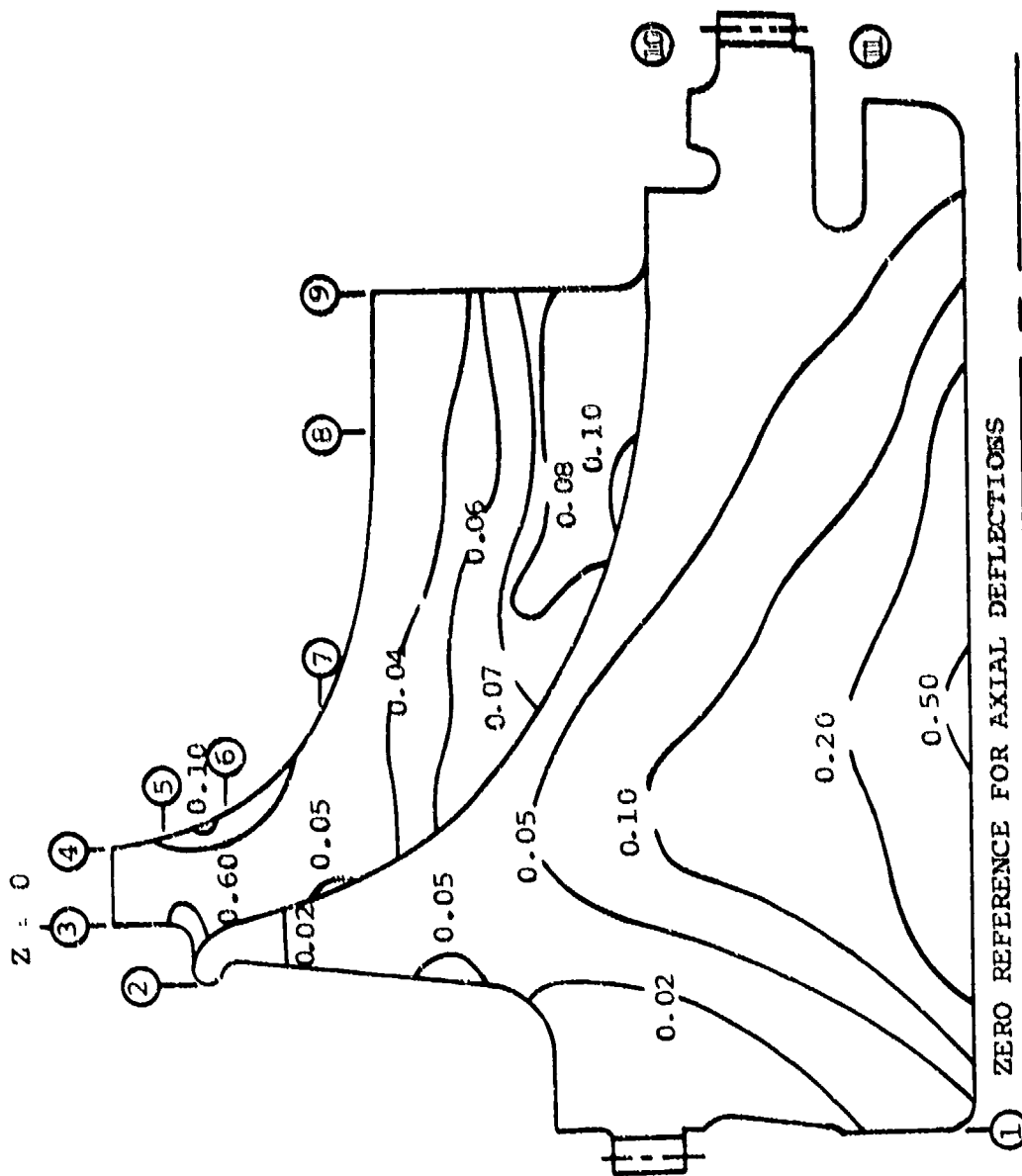


Figure 129. Radial Turbine Wheel 2500-Hr Creep Distribution.

TABLE XVIII

MAXIMUM RADIAL TURBINE WHEEL LIFE FRACTION SUMMATION

Time, hr	T ₄ , °F	Max Life Fraction
36	1950	0.225
72	1925	0.360
119	1900	0.305
226	1820	0.121
2040	1862	2.443
5	2120	0.673
3	2050	0.122
5	2200	2.430
2506		6.679

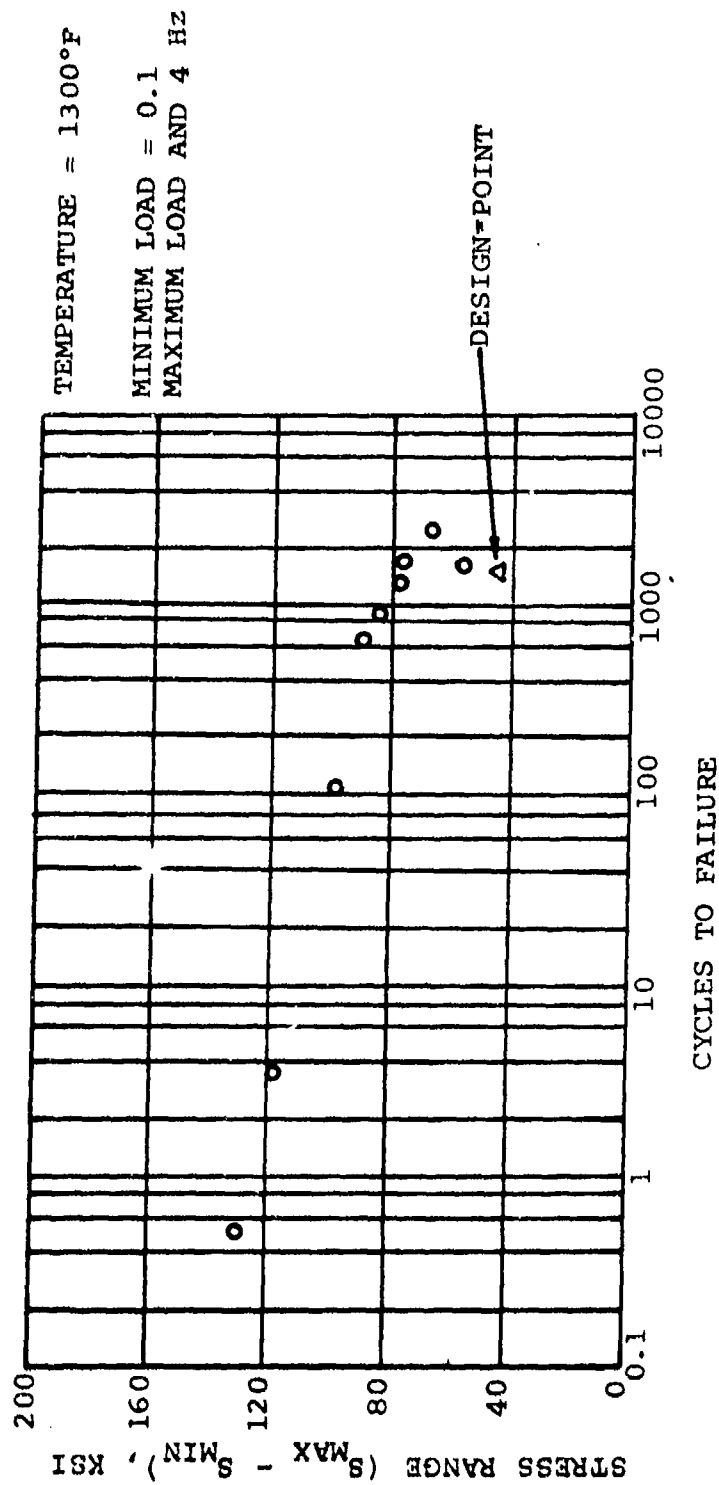


Figure 130. Low-Cycle Fatigue Test for Inertia Welded AF2-1DA Wheel and Inconel 718.

Generally, radial turbine cracks appear first in the disk saddle area or, as in the GTCP85, at the intersection of the blade exducer and hub, according to AiResearch experience. There are two probable reasons: (a) the engine shutdown transients cause local stresses to reverse, thus increasing the stress range (estimated 30 to 50 percent), and (b) stress concentration factors, not accounted for in the elastic stress analysis, increase stress levels. Accurate analytical fatigue-life predictions are quite difficult for these areas. Thus, regular inspections of the wheel should be made.

4.4 AF2-1DA Radial Turbine Wheel Material

Stress and design analyses revealed high levels of internal stress on the wheel, particularly in the center hub portion where high tensile strength is required to prevent wheel burst. A survey showed that AF2-1DA, developed by Universal Cyclops under Air Force contract, was the only material commercially available with adequate elevated temperature and stress-rupture properties for a 2200°F burner. The material was obtained from Universal Cyclops and forged by Wyman Gordon, Grafton, Mass.

In hot-rolling the material for extrusion billets, Universal Cyclops found that the can, used to clad the billet to prevent oxidation, did not reduce as much as expected. This left the billets undersized and required rework of the forging dies. These billets were used for forging development and evaluation pieces, and a second heat of bar was ordered for the forged wheel.

When forging operations were conducted on the evaluation billets, numerous surface bursts necessitated extensive grinding after each of the five forging operations scheduled. From the forging tensile data, (Tables XIX and XX), the strength, and in particular the elongation in the test bars, was quite low. The experimental heat-treat cycles are included on Table XXI. Metallography showed large carbide

TABLE XIX

INFLUENCE OF DUTY CYCLE ON RADIAL TURBINE DISC BORE CREEP

Turbine Inlet Temperature, °F	Time, hr	Creep, %
1950	36	0.122
1925	72	0.145
1900	119	0.155
1820	226	0.155
1862	2040	0.176
2120	1	0.206
2050	3	0.216
2200	1	0.300
↓	2	0.387
	3	0.464
	4	0.534
	5	0.598

TABLE XX

ROOM TEMPERATURE TENSILE PROPERTIES OF
AF2-1DA FROM VARIOUS FORGINGS

Forging and Heat Treat	Heat Treat Cycle*	Number of Tests	0.2 % YS, ksi	UTS, ksi	Elongation %
First Engineering Evaluation	A	2	130	157	5
First Production (re-heat treat as 1/4 forging)	B	2	148	155	2
Second Production Forging	B	4	144	159.5	5
Cookie-Cutter Rim Portion	D	2	141.7	177.8	9.5
Heat Treat as Test Bar	E	2	138.4	176.6	10.5
	F	2	139.3	172.2	8.5
Cookie-Wheel Forging	D	8	137.8	178.8	12
Astroloy		4	141	186	16
*Heat treat cycles delineated in Table XVII.					

TABLE XXI

1400°F TENSILE PROPERTIES OF AF2-1DA FROM VARIOUS FORGINGS

Forging and Heat Treat	Heat Treat Cycle*	Number of Tests	0.2 % YS, ksi	UTS, ksi	Elongation %
Engineering Evaluation	A	2	128	145	2.5
Re-heat treat as tensile bar	A	2	146	152	1.5
First Production	C	2	136.5	149	2.5
	A	↓	142.5	154	3.5
Re-heat treat as 1/4 forging	B		148	155	2
Second Production	B		140	151	4.5
Cookie-Cutter Rim Portion	D		144.7	159.2	12.2
Heat treated as test bars	E		141.1	154.8	12.5
	F	↓	144.0	154.0	10.2
Cookie-Cutter Wheel Blank	D	8	135.6	151.5	11.5
Re-heat treat as tensile bar	D	2	142.3	156.7	7.5
	E	↓	144.5	161.2	7
Astrolloy Wheel			134	147	12
*Heat treat cycle delineated in Table XVII.					

agglomerations in the material, accounting for the low strengths and ductilities at both room and elevated temperatures. In addition, lower strengths were shown in tensile bars tested by Universal Cyclops in the transverse direction in the billet, when compared to the longitudinal direction. A change in billet stock heat level resulted in better forgings and the accompanying properties, as reflected in Tables XIX and XX. Metallography showed a reduction in the carbide agglomeration size but the material still did not have an optimum dispersion. This is particularly demonstrated in the forging that was salt-quenched during heat treat, as the cracks uncovered by machining were found not only in notched areas, where quench-cracks could be expected, but also following carbide chains in areas where there was no severe notch (Figure 131). These properties were still not high enough for the wheel design and the "cookie-cutter" forging technique (a pancake forging large enough for several turbine wheel blanks) was proposed, as the technique offers a high degree of cold work and worked well with some previous Wyman Gordon Astroloy forgings.

During the initial period of work on the "cookie-cutter" forging, Universal Cyclops and AiResearch conducted independent studies on heat-treat cycles. The studies showed:

- (a) The solution treating cycle required close regulation. Too high a temperature and too long a time can result in poor properties as the incomplete solution treatment.
- (b) A three-step cycle is preferable to a four-step cycle, i.e., the 1600°F age immediately succeeding the 1400°F age reduces strength.
- (c) There does appear to be a definite mass effect, probably related to cooling rate from the solution treating temperature.



(a) Wheel Billet Forging Cracks



(b) Cross Section - 10X Enlargement

Figure 131, Typical AF2-1DA Forging Cracks.

detection of the heat treatment for the wheels was based on tests of rim scrap from the cookie-cutter pancake. The data (Tables XIX and XX) indicate that properties in the cookie-cutter rim portion were better than those in the closed die forgings, with a slight advantage in the yo-yo heat-treat cycle over the third-step cycle. The data also indicate that the variation in properties between the high and low temperatures for solution treating had little effect on the tensile properties. The tensile elongation of these bars (10 to 14 percent) was vastly superior to the closed die forgings (about 4 percent), which indicates a better carbide distribution over the previous billet stock and a more thorough working of the structure. This was confirmed by metallography.

One wheel blank was subjected to the yo-yo heat-treat cycle. The tensile results are on Tables XIX and XX and Figures 132 and 133 and the stress-rupture properties on Table XXII and Figure 134. Table XX also presents data on the yo-yo and three-step cycles taken from some test bars reheat-treated individually.

Tables XIX through XXII and Figure 134 show that the desired objective of the cookie-cutter method was not achieved. The yield strength at room temperature and 1400°F was still below the best closed-die data points, although improvement was gained in ultimate tensile strength. The notch sensitivity of the rupture samples is still apparent at 1400°F, although the effect is gone at 1500°F, and the data more closely approximates the published curve in AFML-TR-69-5. Comparison of the data (Table XXIII) to that derived from the Astroloy wheel forging indicates only a slight advantage in AF2-1DA tensile properties but a marked advantage in stress-rupture properties (Table XXIV).

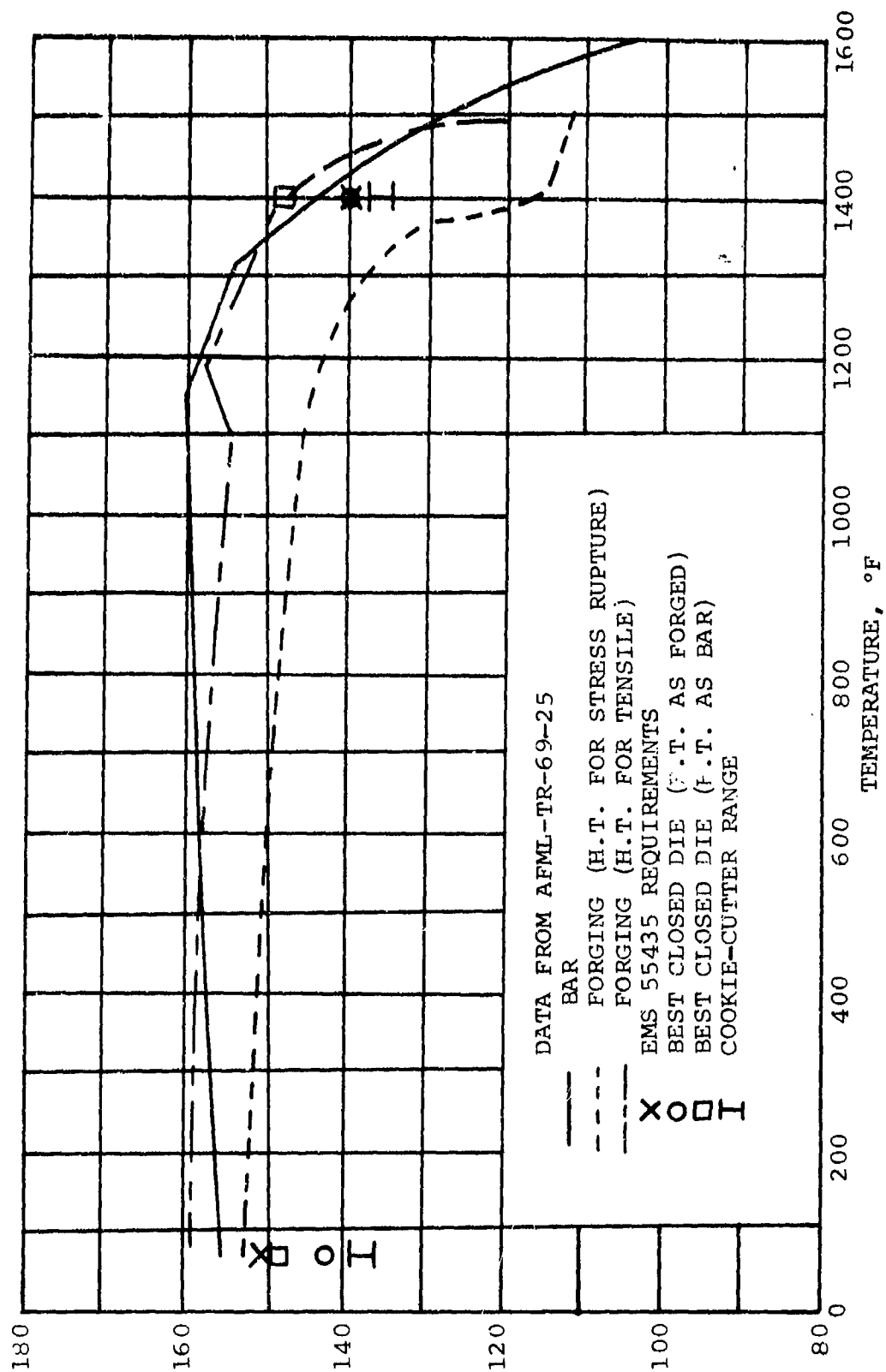


Figure 132. Yield Strength of AF2-1DA, 0.2%.

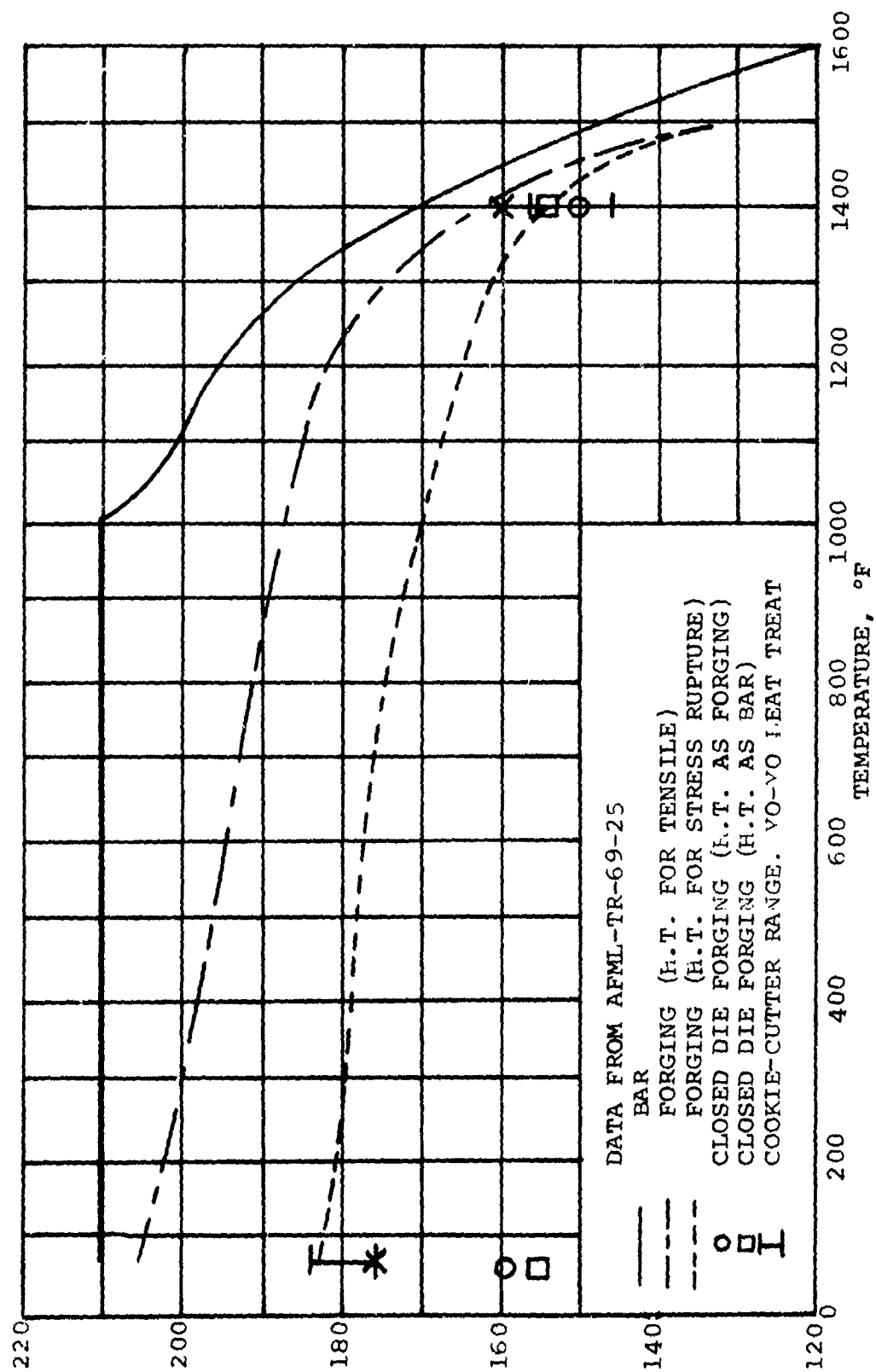


Figure 133. Ultimate Tensile Strength of AF2-1DA.

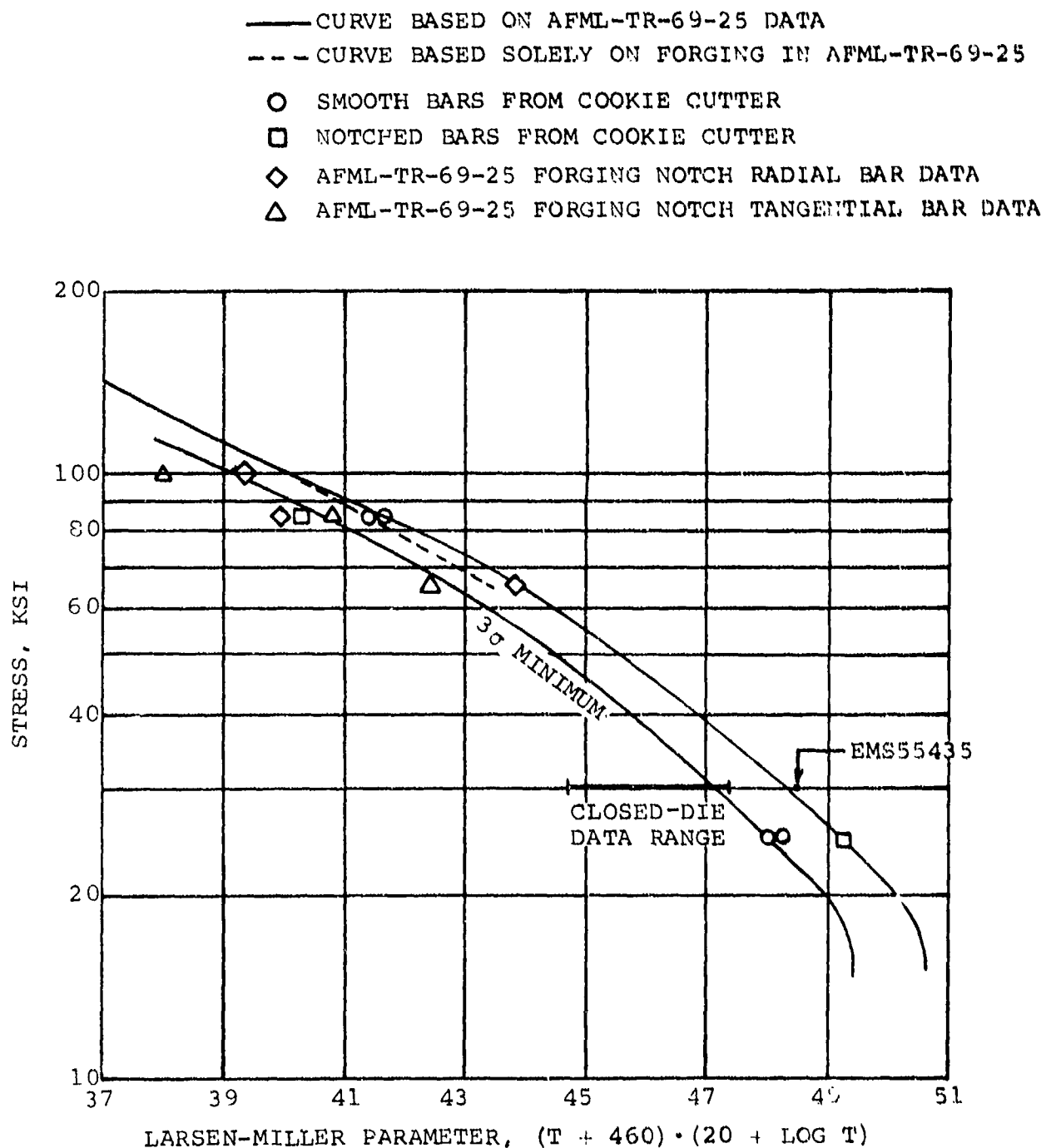


Figure 134. AF2-1DA Stress-Rupture Curve From AFML-TR-69-25, With AiResearch Data.

TABLE XXII
AP2-10A EXPERIMENTAL HEAT-TREAT CYCLES

Cycle	Temperature, °F	Time, hr	quenched
A	2175	8	Circulating Air
	1950	2	Circulating Air
	1600	24	Still Air
	1400	16	Still
B	2175	8	Circulating Air
	1950	4	Circulating Air
	1400	16	Still Air
C	2175	2	Circulating Air
	1600	24	Still Air
	1800	2	↓
	1400	16	
D*	2175	2	Circulating Air
	1600	16	Still Air
	1950	4	↓
	1400	16	
E	2175	2	Circulating Air
	1950	8	Circulating Air
	1400	16	Still Air
F	2225	2	Circulating Air
	1950	8	Circulating Air
	1400	16	Still Air
*Also called the yo-yo cycle.			

TABLE XXIII

STRESS-RUPTURE PROPERTIES OF AF2-1DA WHEEL FORGING,
USING THE COOKIE-CUTTER TECHNIQUE

Bar No.	Bar Type	Test Temperature, °F	Stress, ksi	Hours to Failure	Elongation, %	Location of Fracture (Comb. Bars)
B7	Smooth	1400	85	193.5	7.5	--
B10	Smooth	↓	↓	225.6	5.0	--
B8	Notch	↓	↓	50.9	--	--
B11	Notch	↓	↓	48.9	--	--
A1	Combination	1500	70	130.8	9.0	Smooth
A7	Combination	↓	↓	100.1	10.0	Smooth
A2	Smooth	↓	↓	80.6	6.0	--
A8	Smooth	↓	↓	105.8	11.0	--
A3	Combination	1600	55	43.0	13.0	Smooth
A9	Combination	↓	↓	48.1	10.0	Smooth
A4	Smooth	↓	↓	45.0	9.0	--
A10	Smooth	↓	↓	45.9	10.0	--
A5	Combination	1700	40	29.2	16.7	Smooth
A11	Combination	↓	↓	29.9	13.3	Smooth
A6	Smooth	↓	↓	21.4	12.0	--
A12	↓	↓	↓	28.0	17.5	--
B9	↓	1800	25	17.7	15.0	--
B12	↓	↓	↓	22.9	14.5	--
D1	Notch	↓	↓	69.5	--	--

TABLE XXIV

COMPARISON OF
AF2-1DA PUBLISHED, COOKIE-CUTTER, AND
ASTROLOY STRESS-RUPTURE DATA

Material	Hours to Rupture	
	1400°F 85 ksi	1800°F 20 ksi
Universal Cyclops Data	235	110
Cookie-Cutter "Average"	120	75
Astroloy	50.7	23.6

The work completed indicates that the material does show promise, and additional exploration and development of the forging and heat-treat cycles should successfully increase the tensile properties of AF2-1DA, with stress-rupture properties equivalent to those published in AFML-TR-69-25.

4.5 Axial Turbine Wheel

Although the 1935 ft/sec tip-speed of the second-stage axial turbine is normally a limiting condition for cast materials, the temperature drop through the radial wheel is sufficient to allow the use of a cast-metal base alloy. Inconel 713LC was chosen, because it exhibits a good combination of tensile and stress-rupture strength, is economical, and is readily available.

Aspects of the design summarized in this report are (a) elastic stresses and deflections (centrifugal and combined centrifugal and thermal), (b) blade stress-rupture and disk creep, (c) low-cycle fatigue, and (d) blade vibration.

4.5.1 Elastic Stresses and Deflections

Turbine disk elastic stress distributions, resulting from rotation only, are shown in Figure 135. Blade and pedestal elastic stresses are illustrated in Figure 136a. Area distribution and estimated metal temperatures are shown in Figures 136b and c, respectively. Equivalent stress distribution for combined thermal and centrifugal effects in the disk is in Figure 137.

Burst margin of the cast Inconel 713LC wheel is estimated as 23 percent above normal operating speed. Calculations were based on a $3\text{-}\sigma$ minimum material ultimate strength of 94,100 psi and a burst factor of 0.90. This is slightly below the normal design standard of 25 percent.

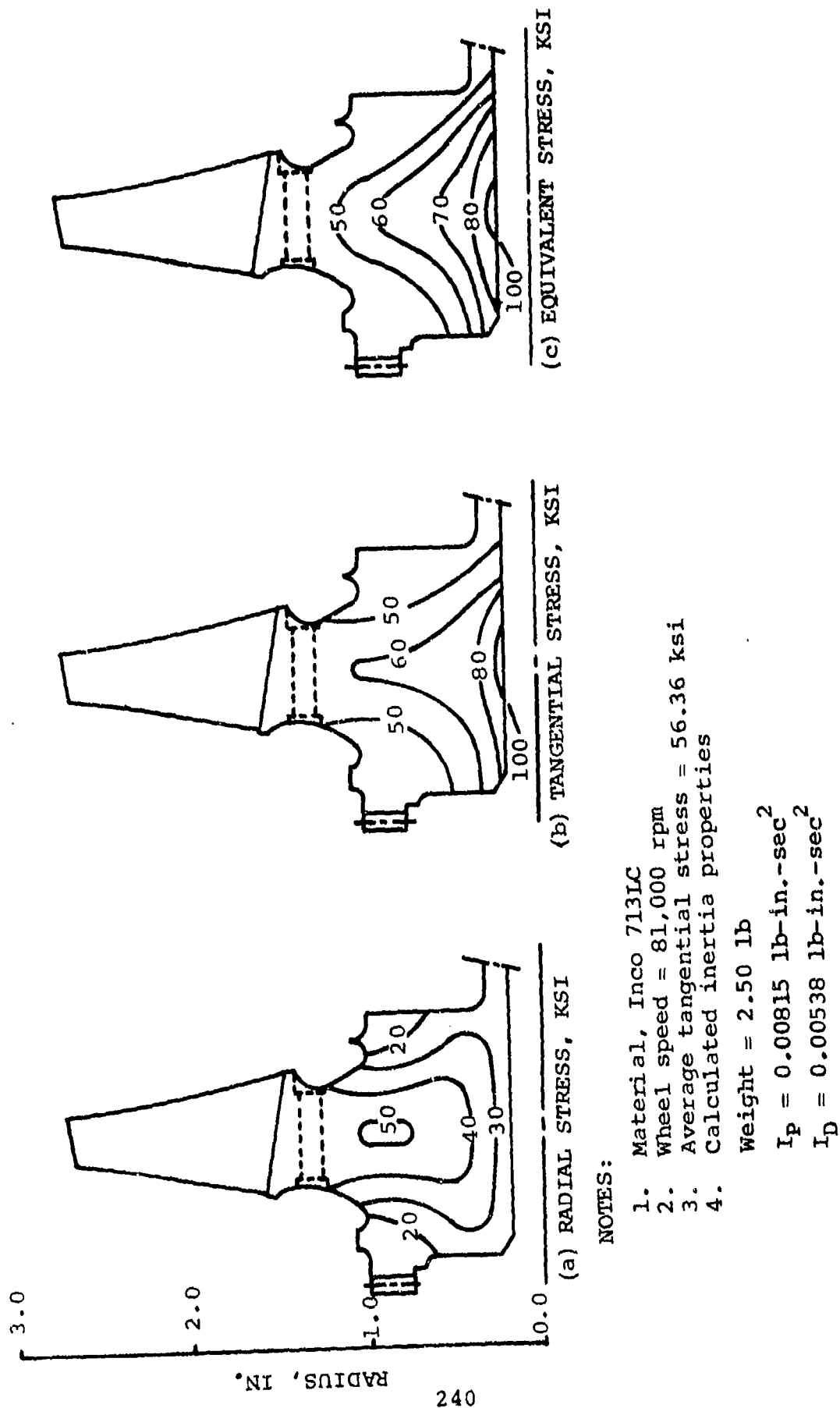
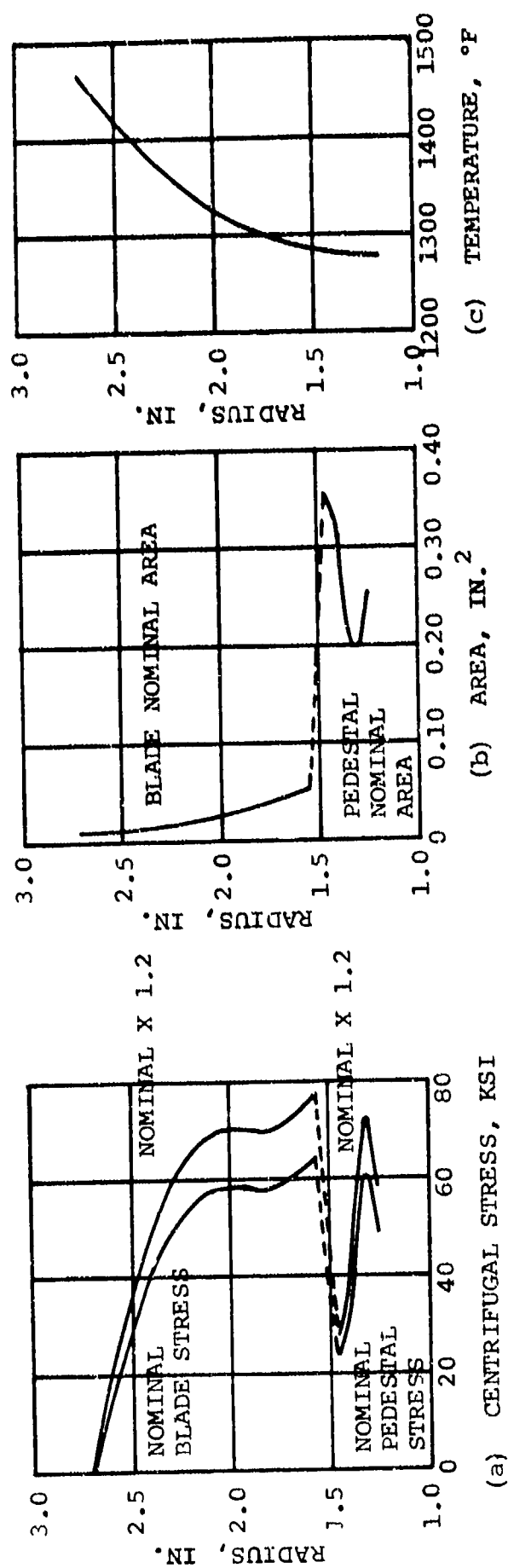


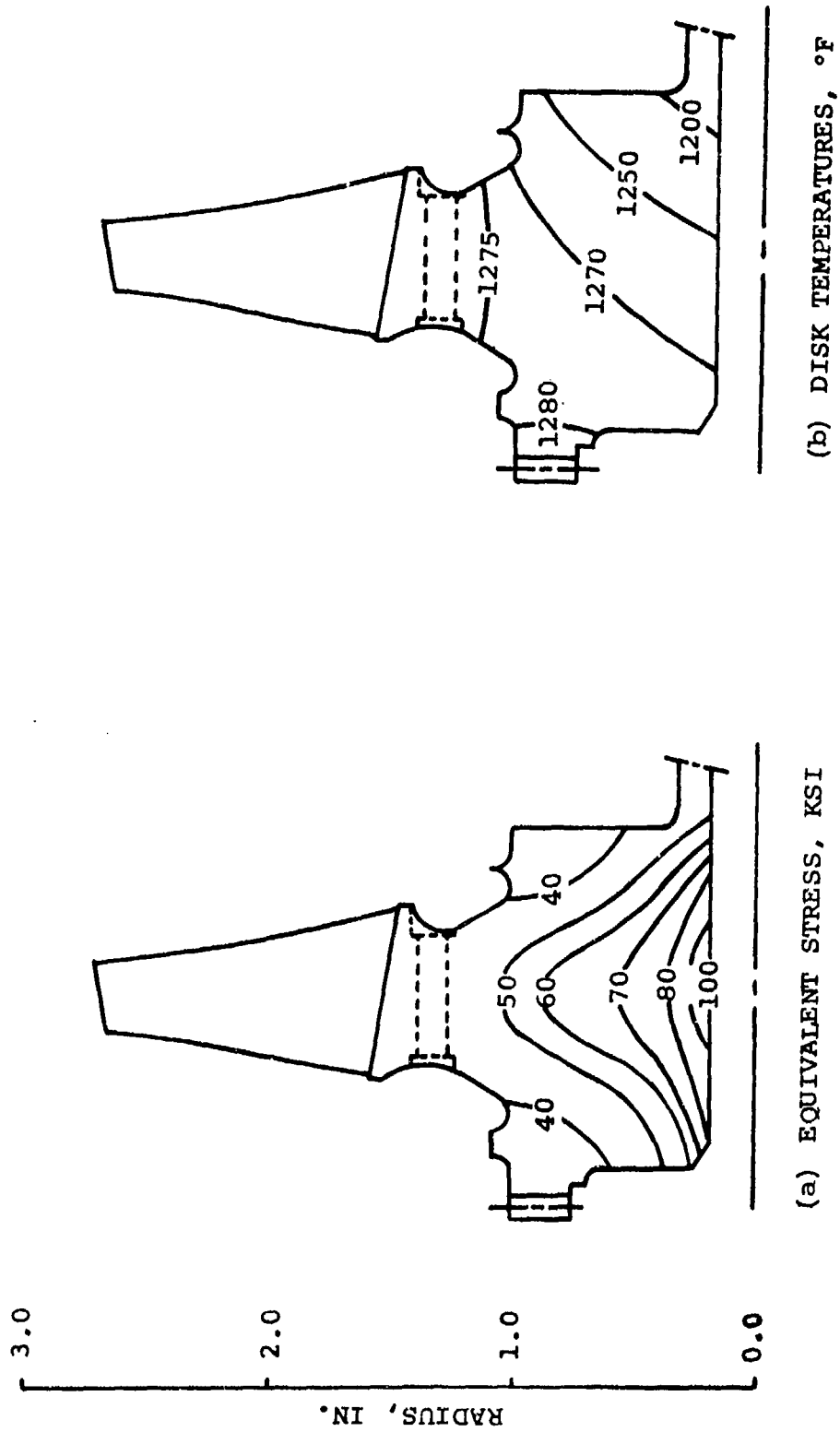
Figure 135. Axial Turbine Wheel Centrifugal Stress Distributions.



NOTES:

1. Material is Inco 713LC
2. Wheel Speed = 81,800 rpm
3. Temperatures Based on Radial Turbine Inlet Temperature of 2200°F

Figure 136. Axial Turbine Blade Characteristics.



NOTES:

1. Material, Inco 713LC
2. Wheel speed = 81,800 rpm
3. Average tangential stress = 56.36 ksi
4. Disk temperatures based on radial turbine inlet temperature of 2200°F

Figure 137. Axial Turbine Combined Thermal and Centrifugal Stress Distributions.

Mechanical and thermal growth values are listed below:

(a) Mechanical growth (radial):

Disk	0.0018
Platform	0.0003
Blade	<u>0.0019</u>
	0.0040 in.

(b) Thermal growth (radial)

Disk	0.0114
Platform	0.0024
Blade	<u>0.0121</u>
	<u>0.0259</u> in.

Total growth 0.0299 in. (thermal and mechanical)

Mechanical growth is based on a wheel speed of 81,800 rpm. Thermal growth is based on wheel temperatures resulting from an inlet of 2200°F to the radial turbine.

4.5.2 Turbine Life

Creep-rupture life estimates have been made, assuming the turbine operates over the duty cycle shown on Table XXV.

Life estimates for the blade and pedestal, using production design criteria, show a minimum life of 100,000 hr over the duty cycle. A disk creep analysis showed less than 0.05-percent creep after 2506 hr of duty-cycle operation.

TABLE XXV
RADIAL TURBINE DUTY CYCLE

Radial Turbine Inlet Temperature, °F	Required Operating Time, hr	Total Time, %
1950	36	1.44
1925	72	2.87
1900	119	4.75
1820	226	9.02
1862	2040	81.40
2120	5	0.20
2050	3	0.12
2200	5	0.20
TOTALS	2506	100.00

4.5.3 Low-Cycle Fatigue

The axial turbine wheel is subjected to low-cycle fatigue as a result of engine-start and shutdown transients. Transient stress estimates during an engine-start are based on the start characteristic in Figure 138. Resulting temperature and stress of the wheel are shown in Figure 139.

Although the nominal stress at the bottom of a rivet hole is much less than that of the disk bore, concentration factors, resulting from the presence of the hole, increase rim stress to a value exceeding bore stress. Because of the relatively large angular hole spacings (approximately 17 deg), the stress concentration at the bottom of the

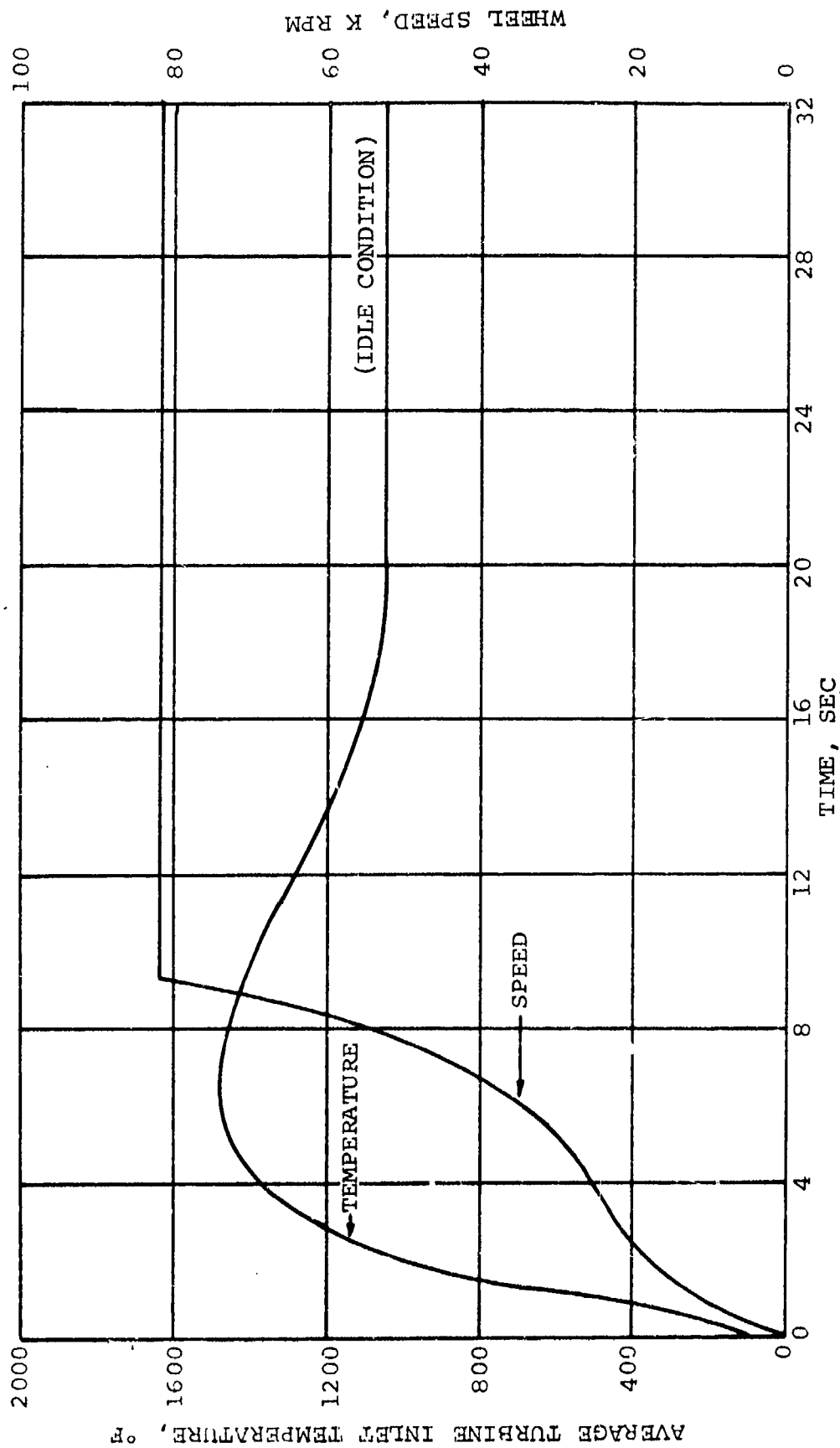


Figure 138. Axial Turbine Inlet Temperature and Wheel Speed Transients, Engine Start.

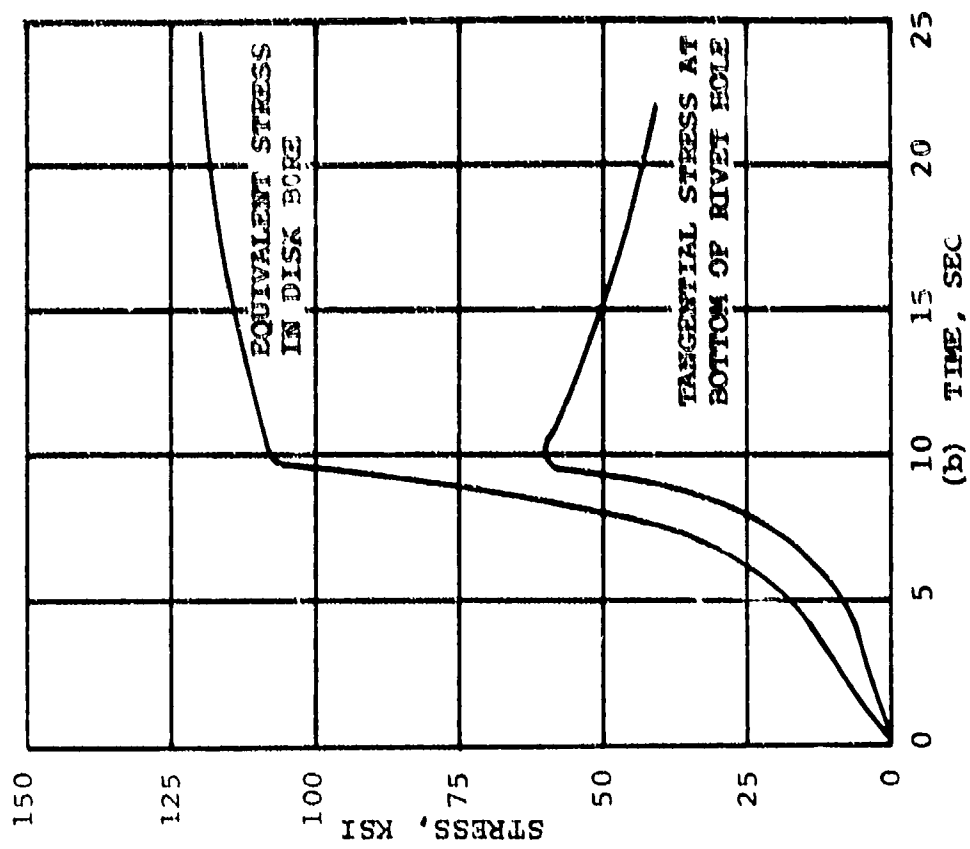
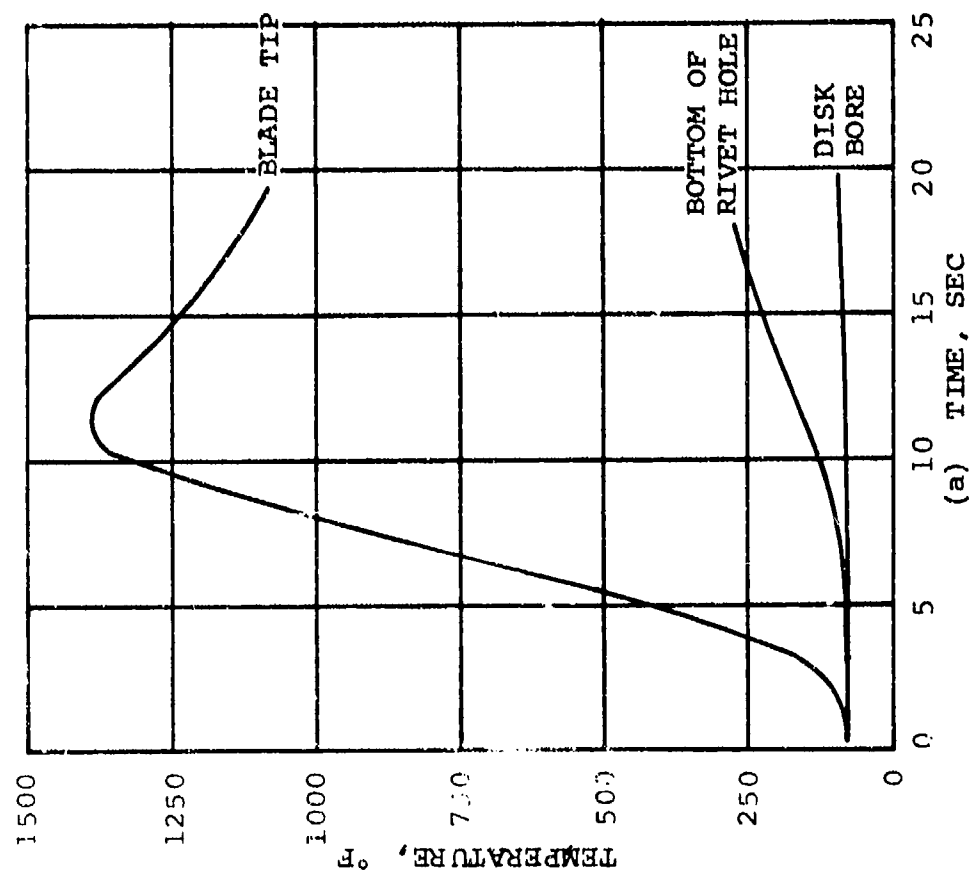


Figure 139. Axial Turbine Wheel Maximum Temperature and Stress Transients, Engine Start.

rivet hole may be as high as 5.0, causing a local maximum stress of 300 ksi. This stress could result in a minimum low-cycle fatigue-life of 200 cycles. However, the basis for determining stress concentration factors around rivet holes was not well substantiated with engine hardware.

Altering the fuel schedule to start the engine over a longer period of time (30 to 40 sec) should allow thermal gradients to induce compressive stress in the rim, before tensile stress caused by rotation reaches peak value. Reducing the number of blades would also increase fatigue life.

4.5.4 Blade Vibration

AIResearch design criteria, for a normal production design, limit centrifugal blade stress to allow a vibratory stress level of $\pm 10,000$ psi. However, the optimum aerodynamic design resulted in stresses that violated this design (Figure 140). Because the primary purpose of the GTCP305 is the demonstration of power, no corrective measures are planned for the present time. It is possible that exciting forces in the engine will not be strong enough to generate significant vibratory stresses in the blade. If engine operation reveals vibratory fatigue problems, blade frequencies could be changed by shortening blade height or redesigning the blade.

While nothing short of engine testing is sufficient to determine the pressure and magnitude of exciting forces, salt-pattern tests have been made to determine blade resonant frequencies. An interference diagram, constructed from these results, is shown in Figure 141. Areas of blade resonance at operating speed are possible due to first- and second-shaft speed harmonics and the six second-stage turbine diffuser struts.

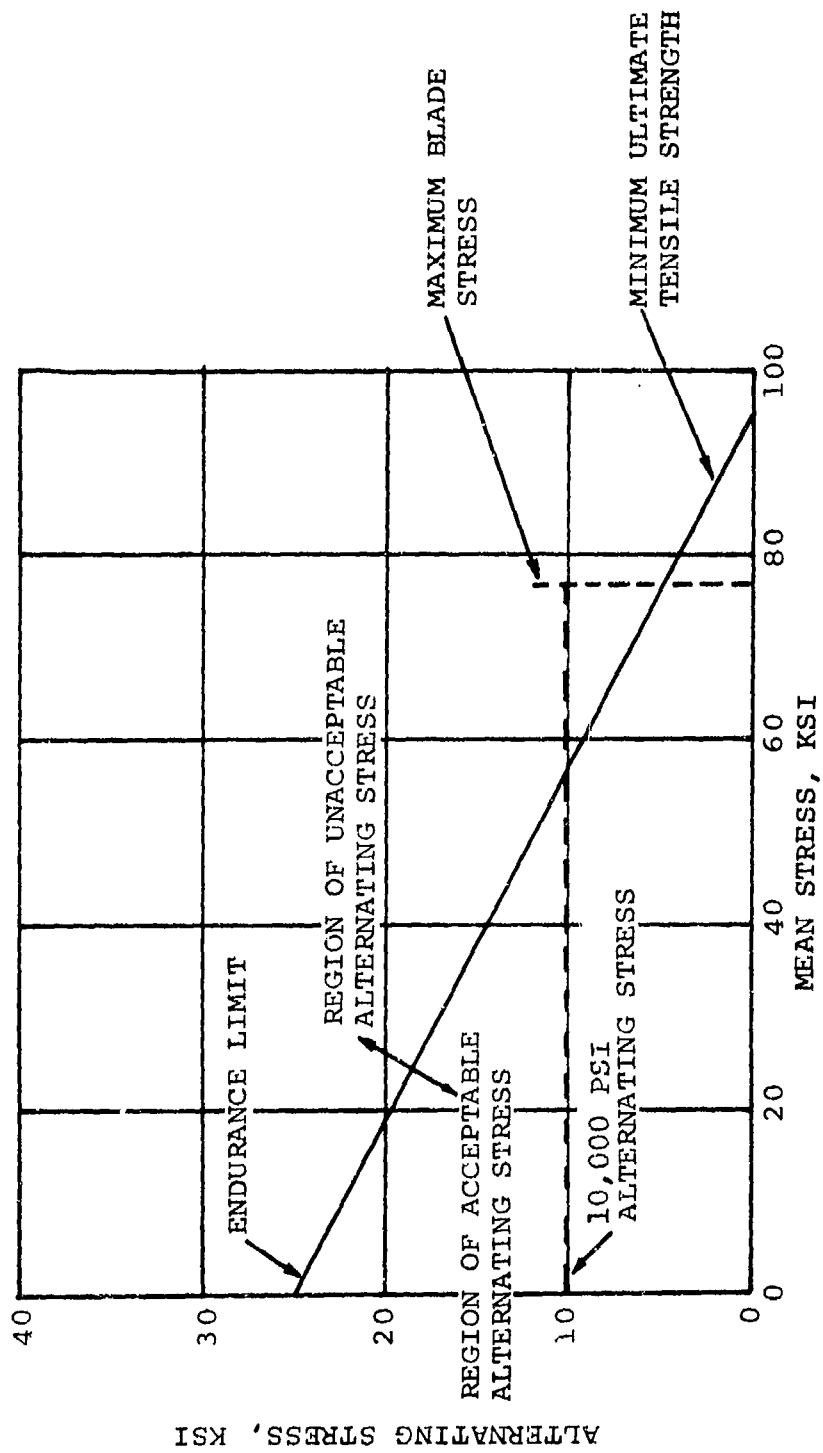


Figure 140. Axial Turbine, Modified Goodman Diagram.

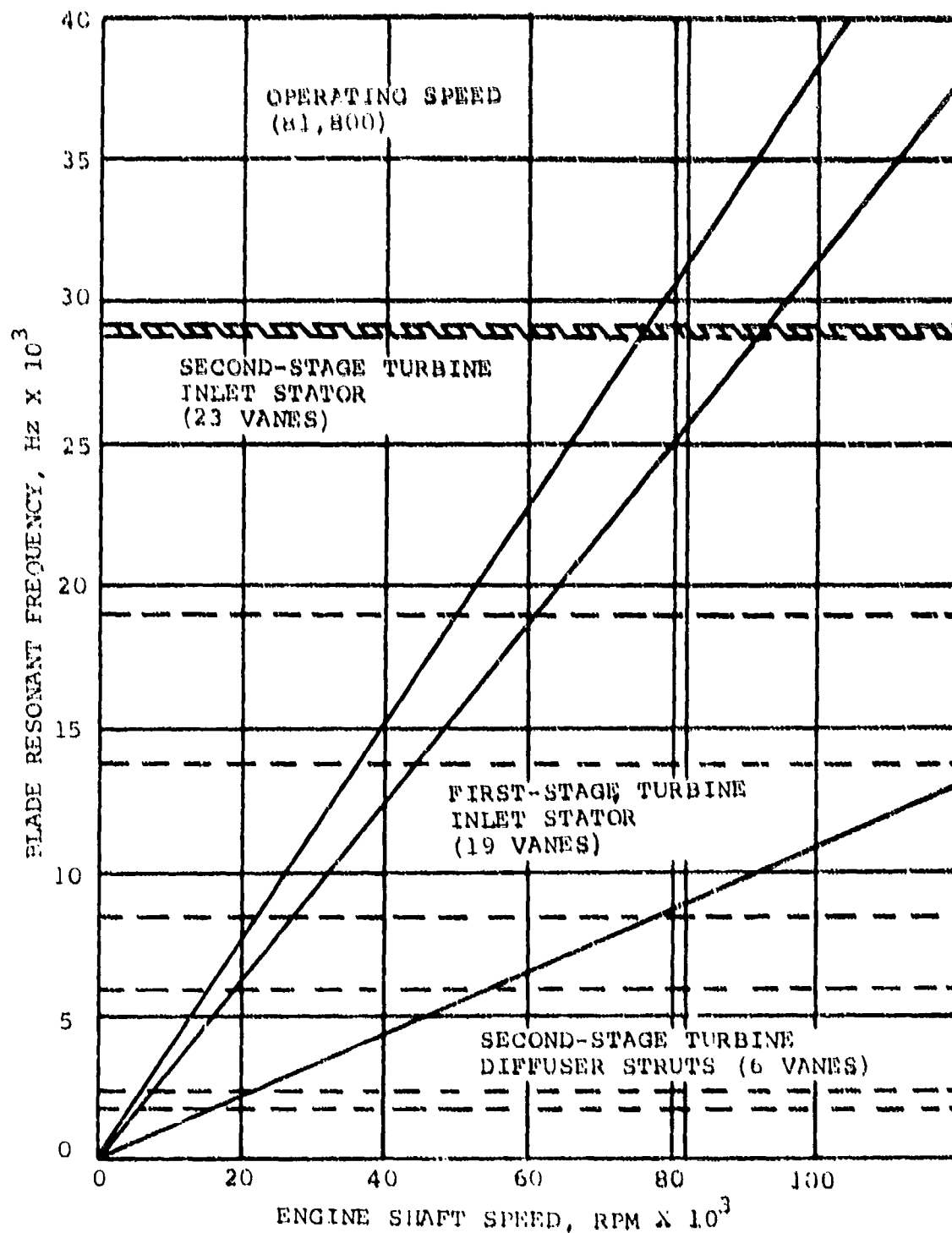


Figure 141. Axial Turbine, Interference Diagram

Two differences exist between the design and the actual rotor used to determine these frequencies:

- (a) The rotor disk was in the as-cast configuration. The excess stock alters the blade-to-disk mass ratio, which tends to increase the blade and disk natural frequencies.
- (b) The first rotor castings were delivered without blade root fillets. Subsequent rotors had fillets that increased the first bending frequency.

Other effects that made blade natural frequency at operating speed difficult to predict are centrifugal stiffening, manufacturing tolerances, and material stiffness changing with temperature.

SECTION VI

TORQUE CONVERTER

1. DESIGN GOALS

1.1 Program Goals

The original design goal of the Advanced APU Torque Converter was for a stall capacity of 280 hp at an input speed of 20,000 rpm. The four shapes and blade profiles for the impeller, turbine, and reactor were designed to achieve a stall torque ratio of 2.2 and a peak efficiency of 0.80. As a follow-on program, a lockup device was developed that clutched in the impeller and turbine, eliminating the inefficiency of the torque converter.

There are three main functions of the Advanced Auxiliary Power System that requires power to be transmitted by the torque converter. For a typical mission, the operation modes would be in the sequence listed below, and the transition from one to the other will be at APU governed-speed:

- (a) Checkout - The torque converter is filled with oil to transmit power to either a 22-kva generator or two hydraulic pumps. The checkout of individual hydraulic and electrical systems requires 35 to 39 hp from the APU without the lockup feature and lasts about 30 min.
- (b) Standby - The APU supplies 55 lb/min bleed-air for environmental control and powers a 3-kva generator. The torque converter is drained and, thus, acts as a disengaged clutch to prevent the auxiliary equipment from being driven. The time of the standby mode operation may vary from a few minutes to 8 hr.

- (c) Engine Starting - The torque converter is drained, stopping the output shaft. The main engine is then coupled to this shaft, and the torque converter is filled, initiating a main-engine start.

1.2 Lockup Device

A torque converter lockup device was an additional work item under the contract. It was designed, built, and tested as an integral part of the torque converter, to provide a method of changing the mode of power transmission from the torque converter (with a speed differential and a power loss) to no-speed differential (and consequently, no power loss) while under load. The lockup device was demonstrated on the torque converter test rig in the following manner:

- (a) The load was sufficient to maintain a speed ratio just below 0.9 at start of demonstration cycle.
- (b) The load was decreased until the actuation speed ratio of 0.9 was reached.
- (c) The clutch was actuated by oil pressure to bring the turbine speed to the impeller speed under constant load.
- (d) The lockup device was engaged.
- (e) Power absorption was increased to 280 shp.
- (f) The above procedure was performed 10 times.

2. DESIGN ANALYSES

2.1 Torque Converter Design

Five basic torque converter element arrangements were considered during the preliminary design phase. The configuration selected was a variable reactor vane torque converter with a fill-and-drain system for coupling and decoupling the power train. This design allows the APU to operate independently from the engine-driven pumps and generators. When filled, torque is transmitted to the engine shaft or, when this shaft is uncoupled, constant-speed power is transmitted to the gearbox components. An overrunning clutch was provided at the torque converter output shaft to prevent the main engine from driving the torque converter turbine. Separate oil pumps were utilized for the APU and gearbox, and oil cooling was accomplished by a separate unit.

Contour shapes and blade profiles were defined for the impeller, turbine, and reactor to achieve the design-stall torque ratio peak efficiency. The high rotational speed and geometrical constraints of the torque converter prevented direct scaling of any existing design. The preliminary geometry was determined by using data from a three-element torque converter designed by Jandasek^[4]. Data corrections were made for the differences in size and speed of the two torque converters. The density of the MIL-L-7808 oil used in the gearbox is the same as that of the torque converter.

Jandasek showed that the parameters affecting performance were primarily functions of speed ratio and impeller exit angle. Detailed analysis indicated that an impeller exit angle of 105 deg was desirable for best performance, and a gear ratio of 3.7 between the torque converter output shaft and the load was necessary for engine-starting requirements. Having established these conditions, the performance was predicted, using the Jandasek data (Figure 142).

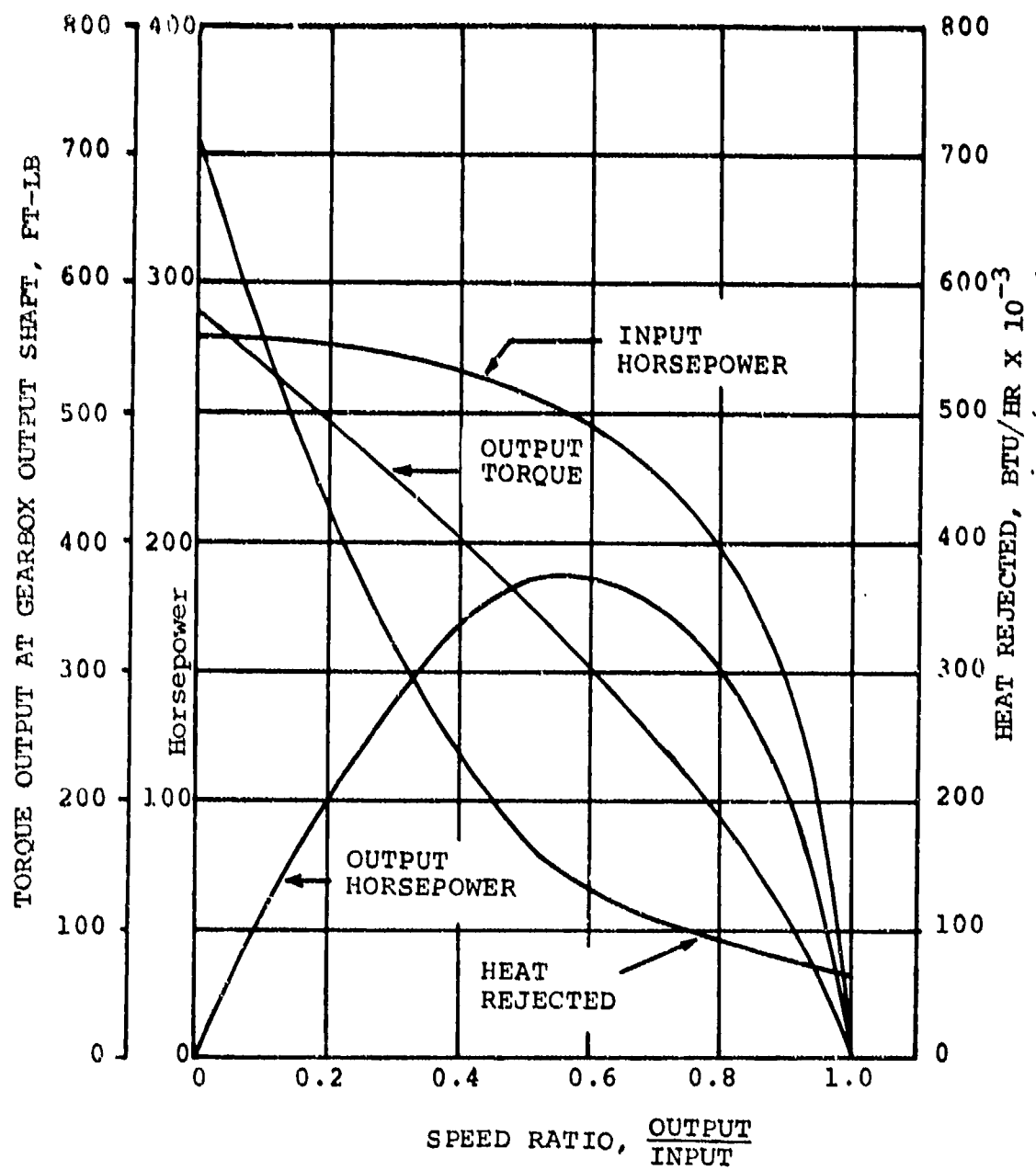


Figure 142. Estimated Torque Converter Performance at 20,000-rpm Impeller Speed.

An analysis of the velocity triangles along the design path showed that the desired design-point speed ratio was 0.7. The entrance angles to the components for various speed ratios are shown in Figure 143. The following design-point parameters evolved from the preliminary analysis:

(a) Input speed	20,000 rpm
(b) Maximum power input	280 hp
(c) Impeller exit angle	105 deg
(d) Torus diameter	3.74 in.
(e) Stall torque ratio	2.24
(f) Speed ratio	0.7
(g) Peak efficiency	0.80
(h) Gear ratio	3.7

2.1.1 Geometrical Shape

The meridional shape of the torque converter was determined, using a torus diameter of 3.74 in. The hub contour was chosen as a circular arc, to provide a smooth surface and reduce manufacturing problems. The shroud contour was determined so that the flow area throughout the circuit was approximately constant. The optimum toroidal flow area (based on the torus diameter) was made equal to 23 percent of the projected flow, as indicated by Jandasek. The reactor chord length at the design-point was selected as 0.6 in. at the mean radius. The torque converter was later elongated by 0.065 in. in the axial direction to accommodate the variable reactor position at off-design conditions. The final meridional shape is shown in Figure 144. Extensive use of existing AiResearch aerodynamic computer programs was made in performing the design analysis.

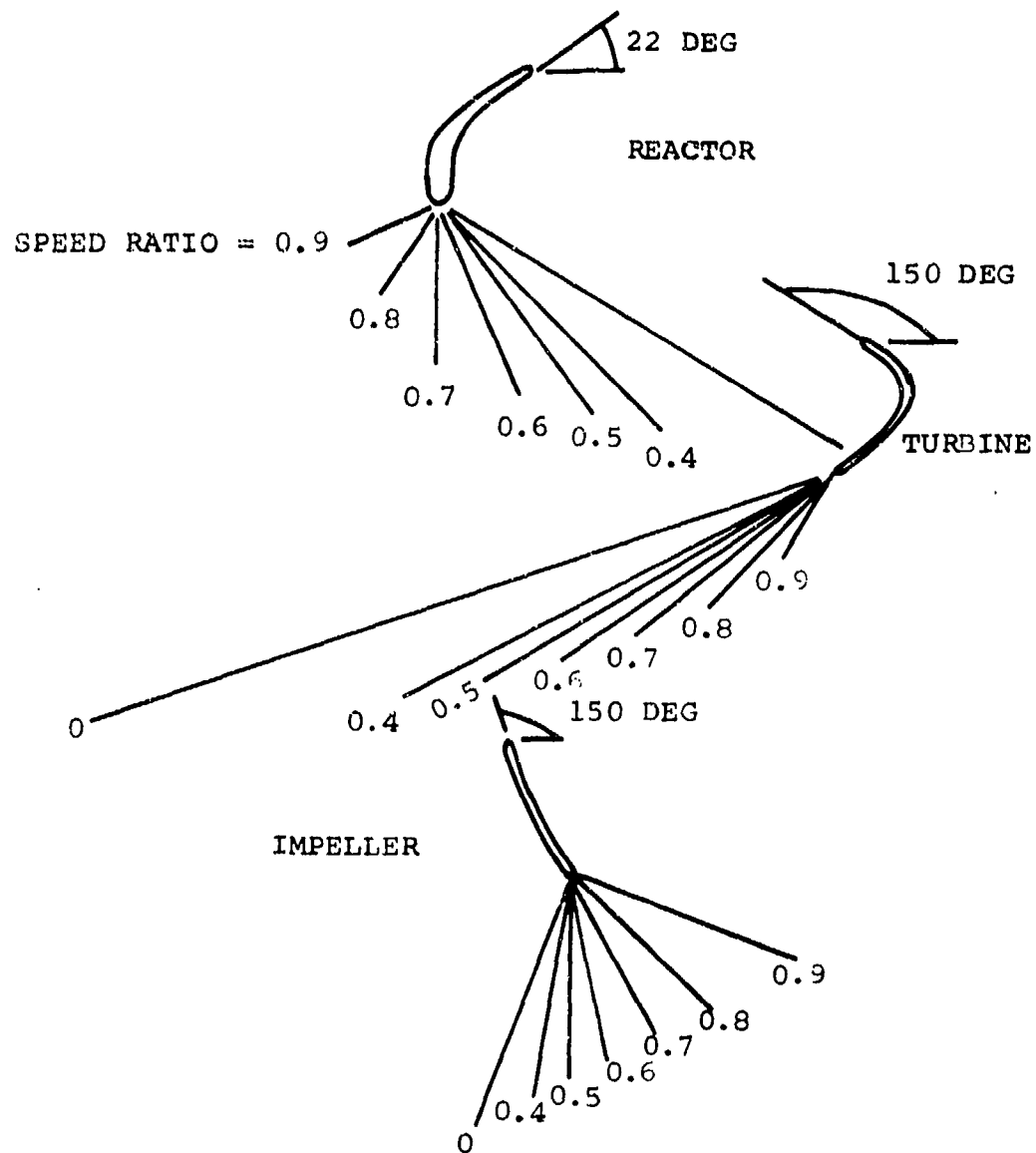


Figure 143. Torque Converter Design Vector Diagram.

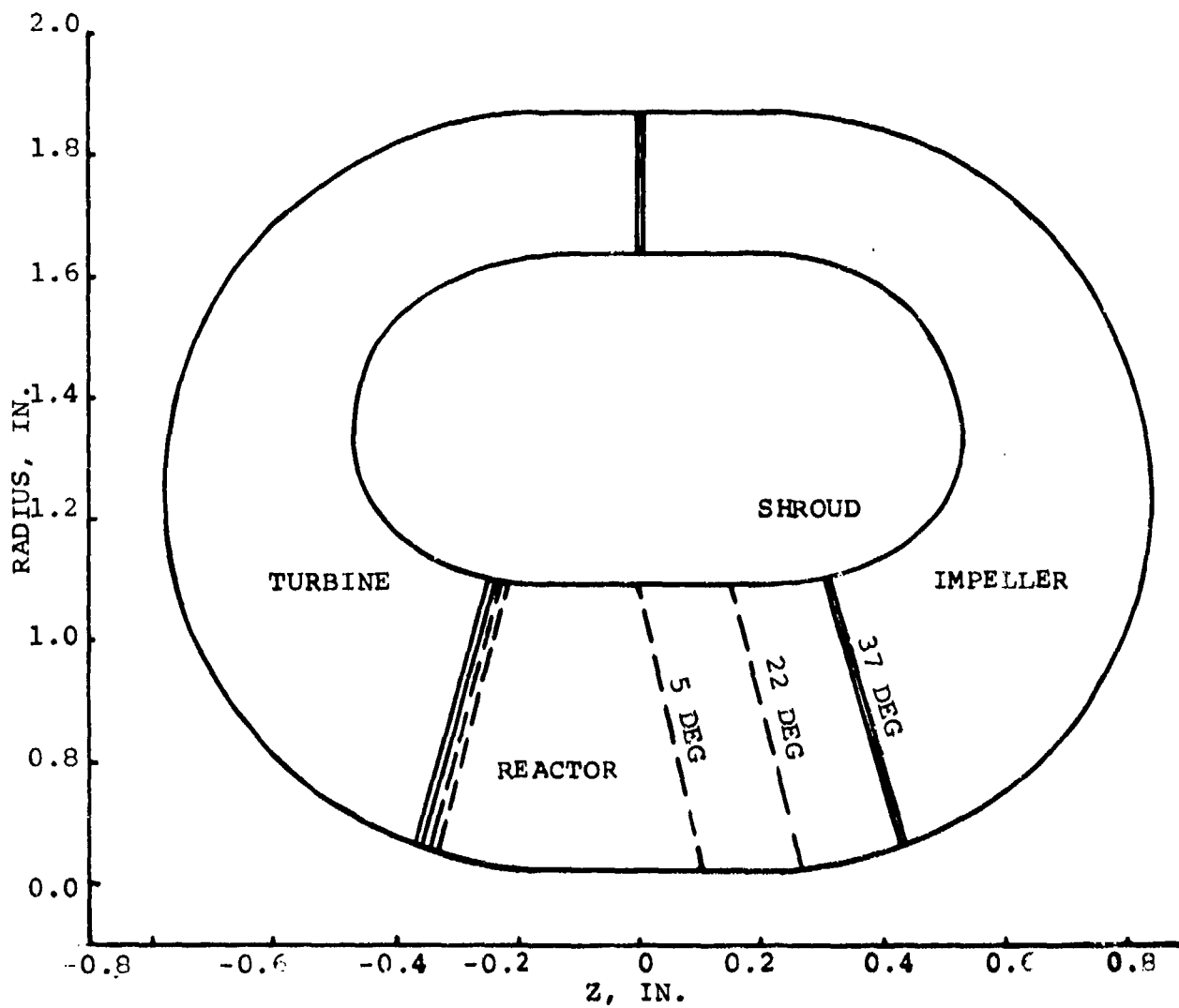


Figure 144. Advanced APU Torque Converter Final Meridional Shape.

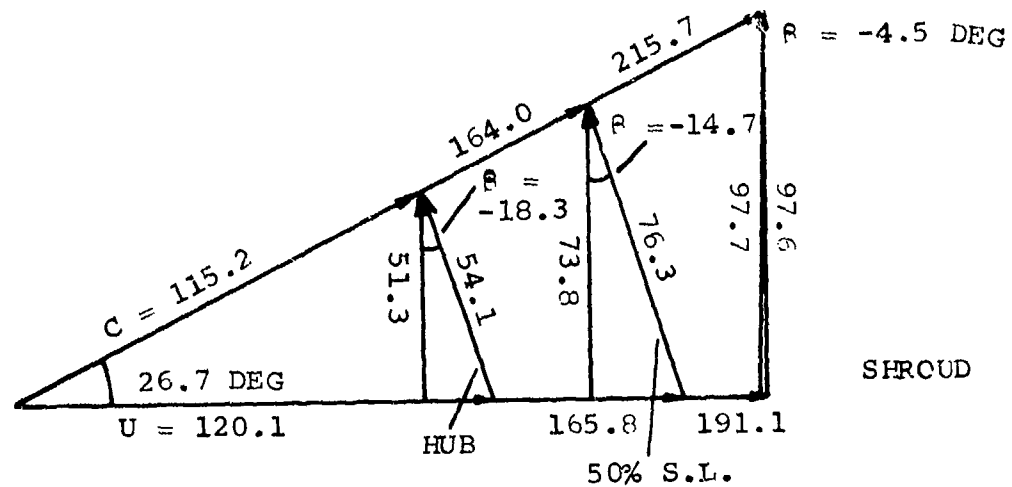
2.1.2 Velocity Triangles

An existing computer program generated the meridional velocity profiles throughout each element at various streamlines. The exit-flow angle was considered constant for each element. The corresponding leading-edge flow angles and subsequent velocity triangles (inlet and exit flow) were then established at the hub, shroud, and 50-percent streamline, as shown in Figures 145 through 147 for the impeller, turbine, and reactor, respectively.

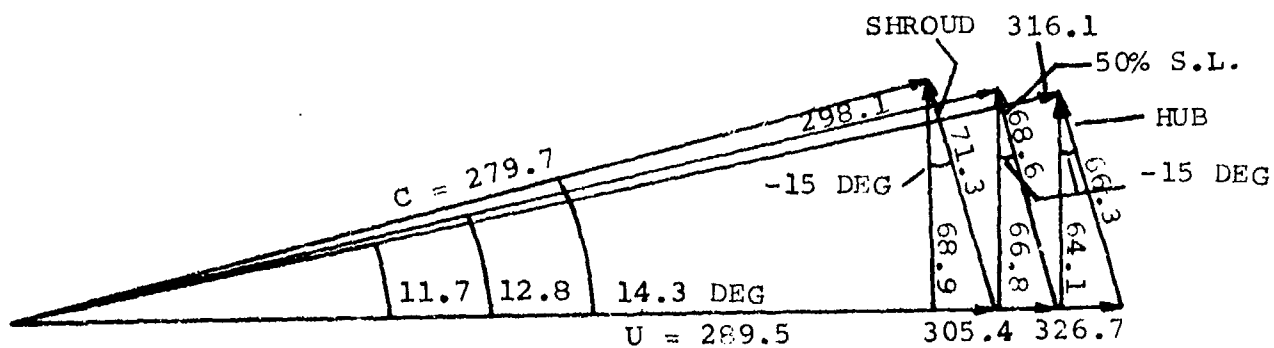
2.1.3 Calculation of Blade Shapes

The final blade shapes for the impeller and turbine were based on the assumption that along any straight-line element connecting the hub and shroud, $\tan \beta/R$ is a constant. Jandasek used this approach in the design of the torque converter. He also assumed that the $\Delta(RCu)$ through each element was divided into an equal number of increments and then calculated the blade angle at the design path (mean-line) from this value of RCu . The blade angle was calculated at the hub and shroud, using $\tan \beta/R =$ the constant along a straight-line element passing through the design-point and approximately normal to the mean-flow direction.

The Jandasek approach was modified slightly by neglecting the assumption that the $\Delta(RCu)$ could be divided into equal increments along the design path, as this assumption does not generally yield a satisfactory loading in the turbomachinery circuit. The procedure utilized the results obtained for the 50-percent streamline from an existing AiResearch computer program. Straight-line elements were drawn from the hub to the shroud through the mean streamline. The Beta-distribution on the 50-percent streamline was used to calculate $\tan \beta/R$ at the intersections of the straight-line elements with this mean path. Then invoking the assumption of constant $\tan \beta/R$, the

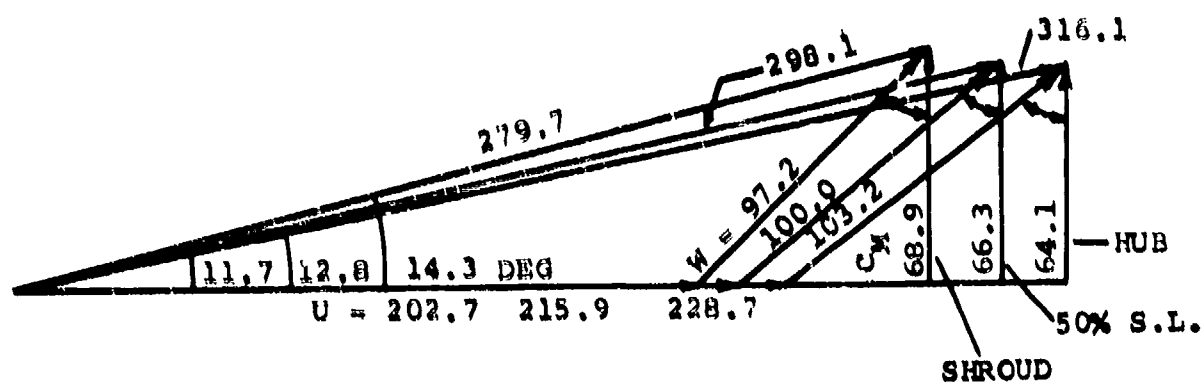


(a) PUMP INLET VELOCITY TRIANGLE, FLOW

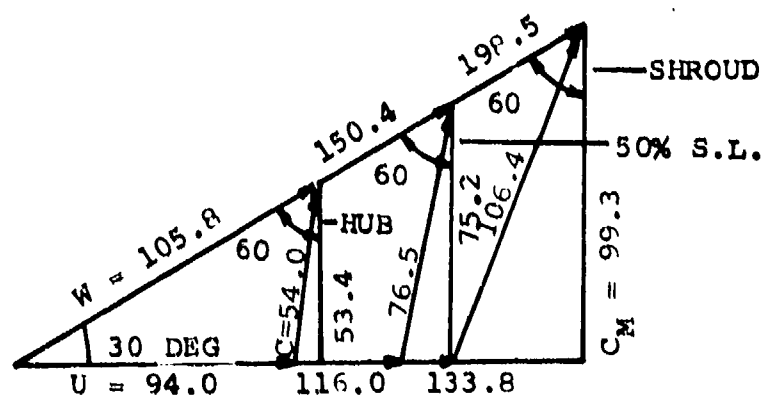


(b) PUMP EXIT VELOCITY TRIANGLE

Figure 145. Torque Converter Impeller Vector Diagram.

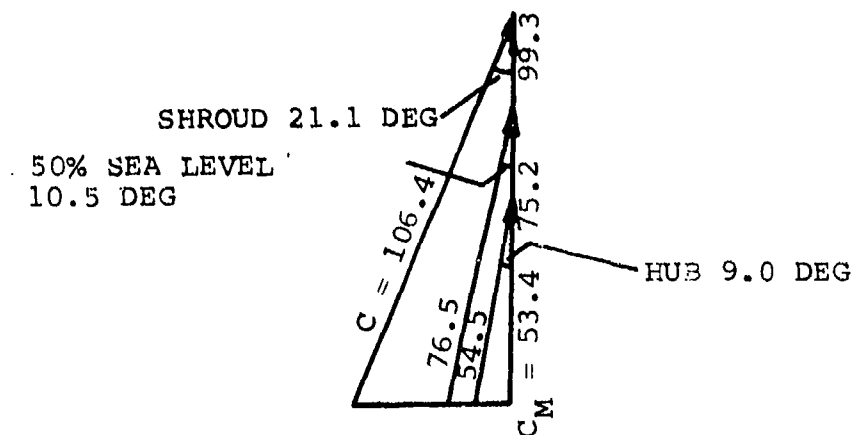


(a) TURBINE INLET VELOCITY TRIANGLE, FLOW

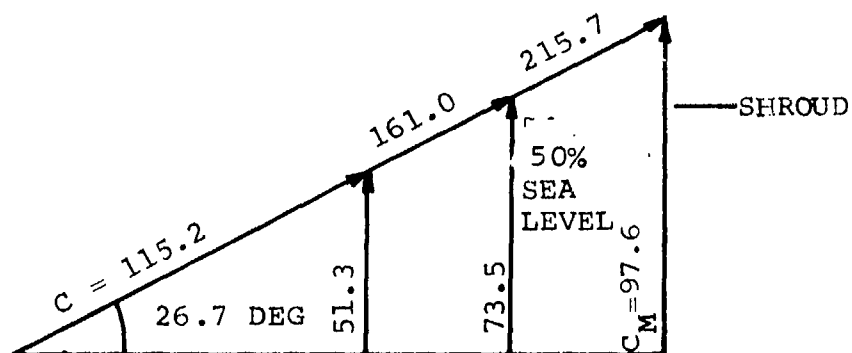


(b) TURBINE EXIT VELOCITY TRIANGLE

Figure 146. Torque Converter Turbine Vector Diagram.



(a) REACTOR INLET VELOCITY TRIANGLE, FLOW



(b) REACTOR EXIT VELOCITY TRIANGLE

Figure 147. Torque Converter Reactor Vector Diagram.

blade angle distributions along the hub and shroud were obtained. The blade loadings for these new β -distributions were checked on the computer and were satisfactory. The corresponding X-Y coordinates along the hub and shroud were then determined.

The vanes of the reactor are used to accelerate the flow from the turbine exit to the pump entrance and provide for torque multiplication. A computer program, which calculates the velocities and streamline paths for a cascade of blades, was used to determine a satisfactory vane shape. The blade shape at the 50-percent streamline was adjusted until a reasonable vane loading was obtained. Then the vane shapes at the hub and shroud were determined by scaling the mean blade shape by the ratio of the chord lengths and adjusting the inlet angles. The resulting profiles were stacked about their centers of gravity by another program, which also provided the necessary information to manufacture the vanes.

2.1.4 Final Impeller Design

There are 25 impeller blades. A greater number would have resulted in high friction losses, and less would not allow the impeller to absorb sufficient torque. The blade thickness was chosen as 0.030 in. throughout the blade, principally for ease of manufacturing.

2.1.5 Final Turbine Design

Twenty-nine blades were selected for the turbine. To facilitate manufacturing, the blade thickness was chosen as a constant 0.030 in.

2.1.6 Final Reactor Design

Twelve vanes were required in the reactor to accelerate the flow. The exit angle of the reactor vane at the design-point was 22 deg. The variable angle reactor vane was designed to have starting

capabilities at altitude, where the maximum input horsepower is limited. The capacity of the torque converter could be increased by increasing the reactor exit angle. Anticipated reactor vane rotation is from 5 to 27 deg. A mechanical stop is provided at 34.5 deg to prevent interference of the vane trailing edge with the pump blade leading edge. The effect of the varying reactor exit angle is shown in Figure 148.

2.1.7 Fabrication

The most complex parts to fabricate in the torque converter are the impeller, turbine, and reactor, because of subjection to possible cavitation damage. These parts are fabricated from Type 347 corrosion-resistant steel. The shafts and the sprag-type overrunning clutch housing are made of Type AISI 4340 chrome-moly steel. The special heat-treatment for these give a Rockwell "C" scale hardness of 54-50.

The links on the four master pivot reactor vanes contain hardened pins that slide in the slotted inner shaft. The slots in this shaft are surface treated to reduce friction. All of the antifriction bearings are aircraft Grade 5. The internal seals are a carbon-face pressure-balanced type that rub against hardened Type 430 stainless steel rotors that are flat within three helium light-bands.

The main torque converter support housing is machined from 6061 Aluminum bar stock, heat-treated to a T-6 (hardened) condition.

The gears are fabricated from AMS6260 forgings. Each gear is finished-ground, and the teeth are case-hardened by the carburizing process. The core hardness is Rockwell "C" 33-43.

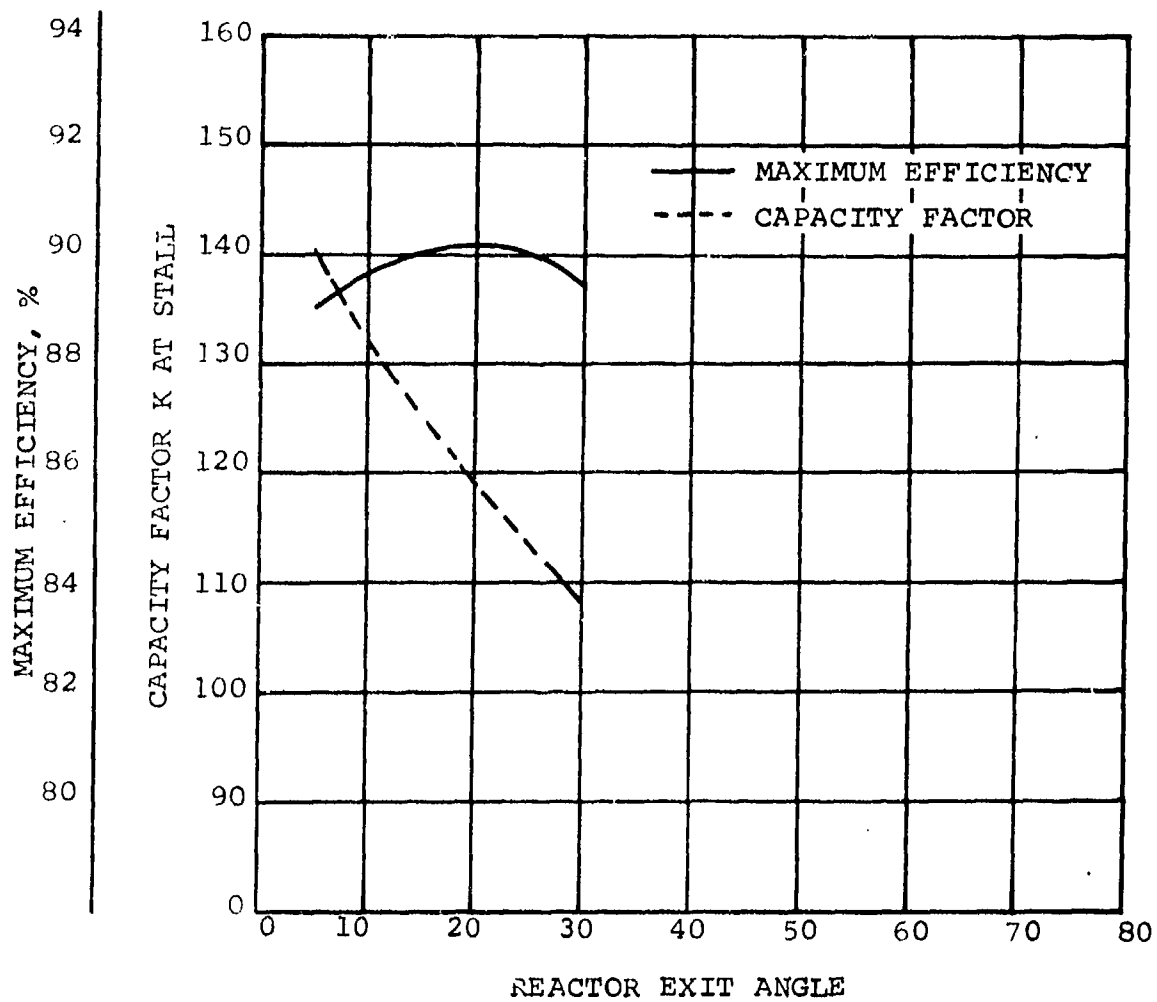


Figure 148. Effect of Varying Reactor Exit Angle.

The torque converter weighed approximately 8 lb, including the input and output gears and utilized an overrunning reactor clutch for optimum performance at the higher speed ratios. The torque converter assembly is shown in Figure 149, and the impeller and turbine are shown in Figure 150. A fixed-blade reactor (Figure 151) was fabricated to obtain baseline performance for the variable reactor (Figure 152).

2.2 Lockup Elements

The essential elements of the lockup torque converter (Figures 153 and 154) are the torque converter, disk clutch, a positive engagement mechanism that utilizes a dental clutch, and a control system. The disk clutch is in parallel with the dental clutch. When the disk clutch has synchronized the turbine and impeller, the dental clutch engagement is initiated and positively engages the load to the prime mover. After the splines have been engaged, continuous oil pressure is supplied to overcome the return-spring force, and power transmission is limited only by the strength of the shafts and splines.

The sequence of operation is in the following six stages:

- (a) When the impeller is at 100-percent speed and the turbine is at rest, only lubricating oil is in the torque converter, and the disk clutch and dental clutch actuating pistons are held in a neutral position by spring force, since there is no actuating oil pressure on the pistons.
- (b) When the turbine is at 90-percent speed, the 90-percent speed switch actuates. If the disk clutch arming switch is closed, the three-way valve solenoid is actuated, allowing oil pressure on the disk clutch piston to engage the clutch. The piston oil pressure increases from 0 to 100 percent in a few seconds, the actual time depending upon the accumulator displaced volume, orifice size, and supply oil pressure.

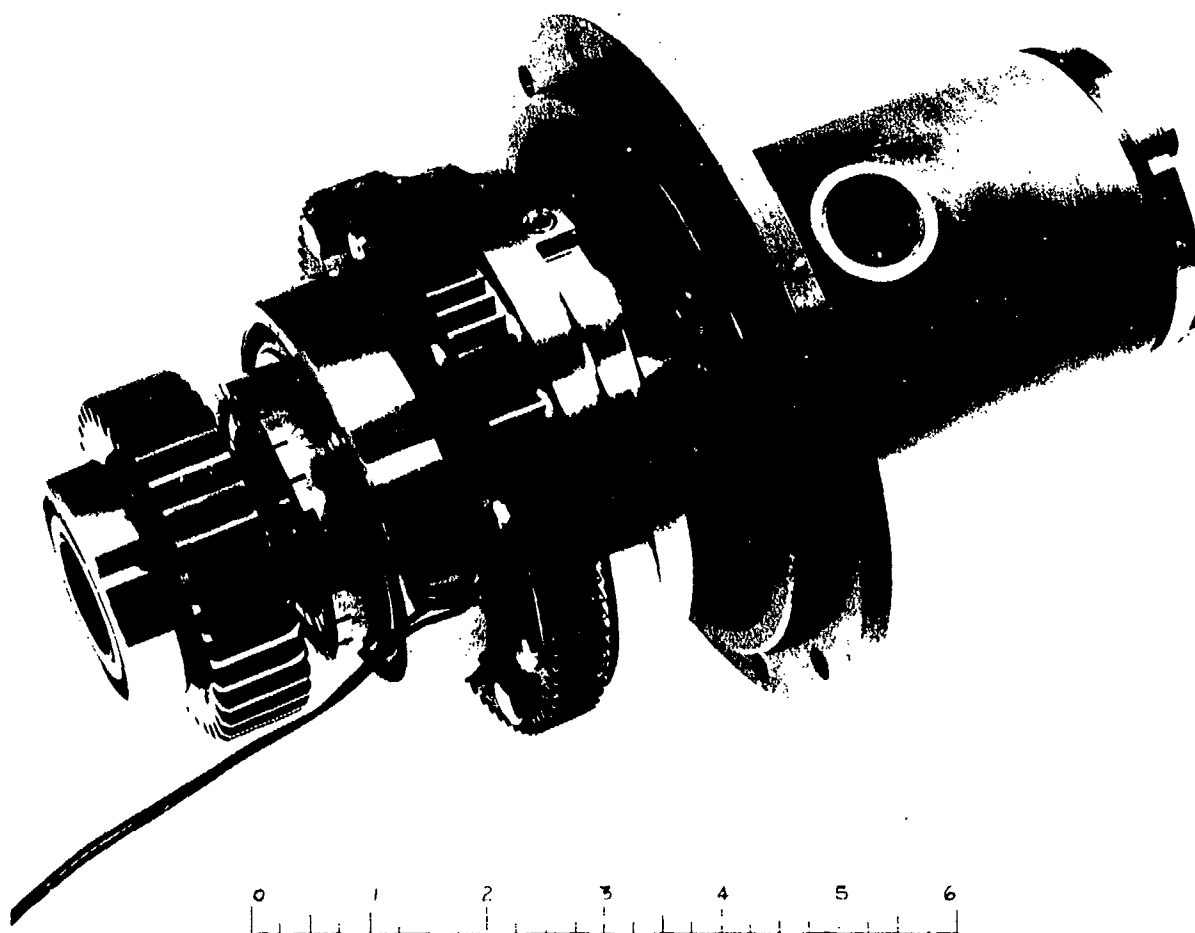


Figure 149. Torque Converter Configuration.

BREADBOARD TORQUE CONVERTER
ADVANCED TECHNOLOGY APU
AFSC CONTRACT F33615-69-C-1100

PHOTO NO. P-38705
AIRESEARCH MANUFACTURING COMPANY

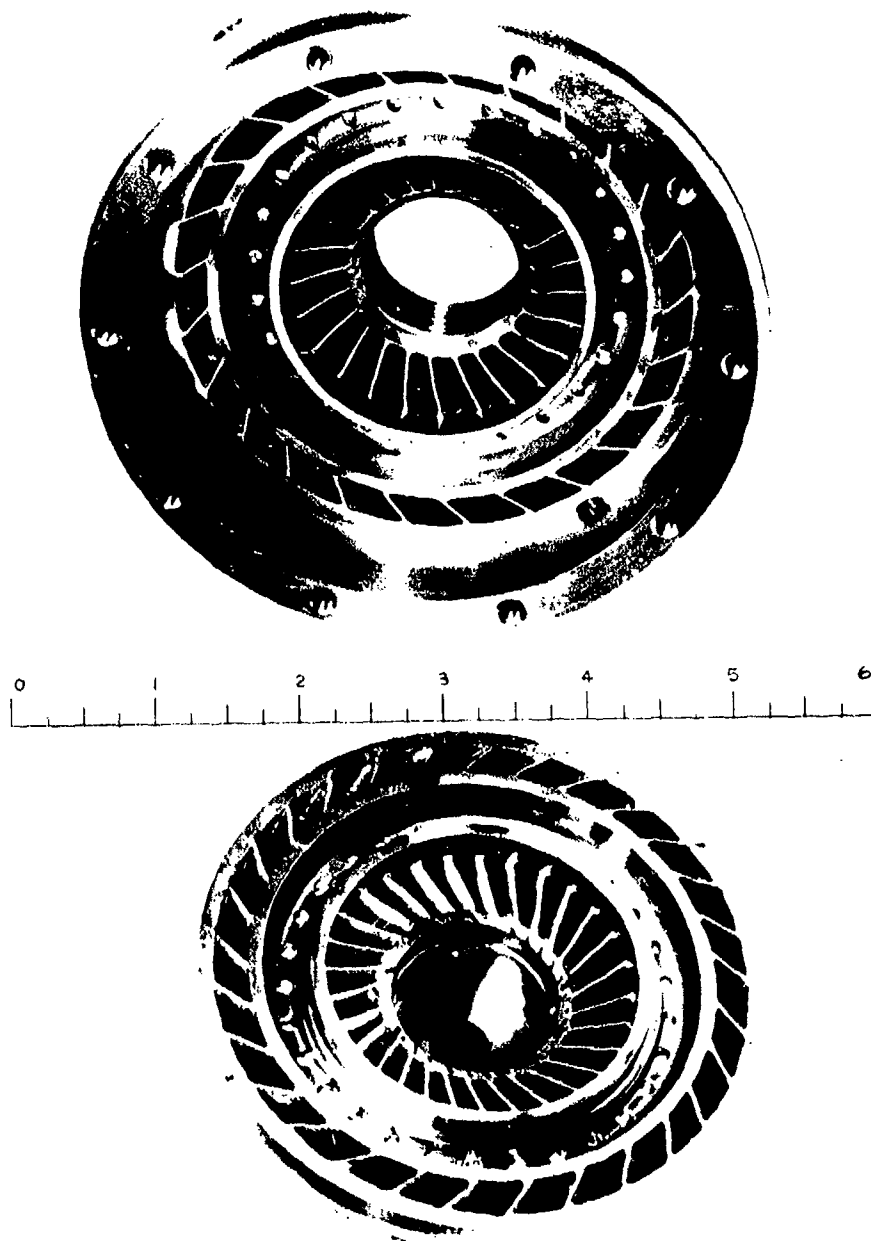


Figure 150. Torque Converter Impeller (Top)
and Turbine (Bottom).



Figure 151. Torque Converter Fixed Reactor.

BREADBOARD TORQUE CONVERTER
FIXED REACTOR BLADE ASSEMBLY
ADVANCED TECHNOLOGY AP
AFSC CONTRACT F11615-69-C-1100

PHOTO NO. F 38680-7
AIRESEARCH MANUFACTURING COMPANY

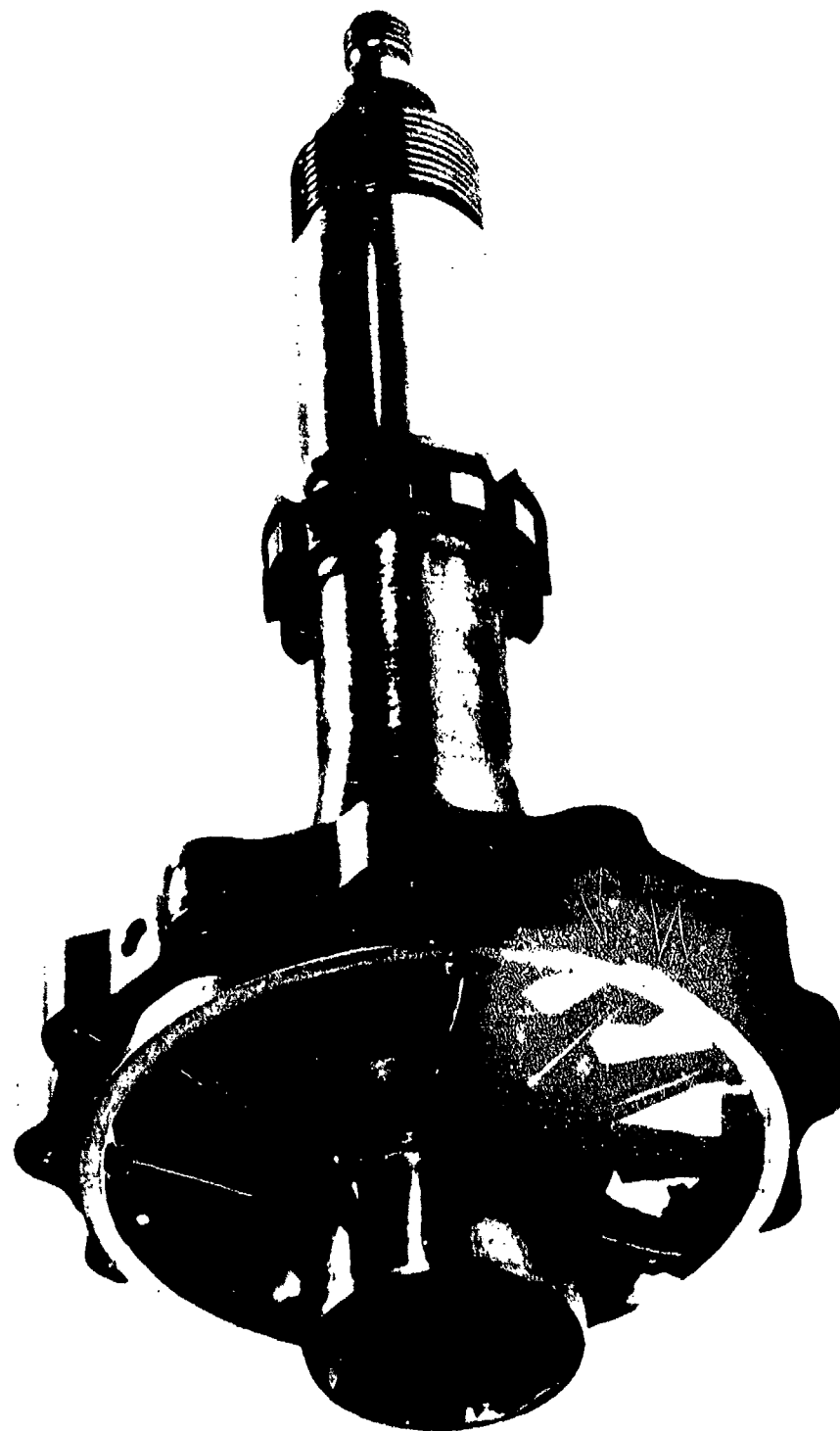


Figure 152. Torque Converter Variable Reactor.

XXXXXXXXXXXXXXXXXXXX
 See the following page
 for the full details
 XXXXXXXXXXXXXXXXXXXX

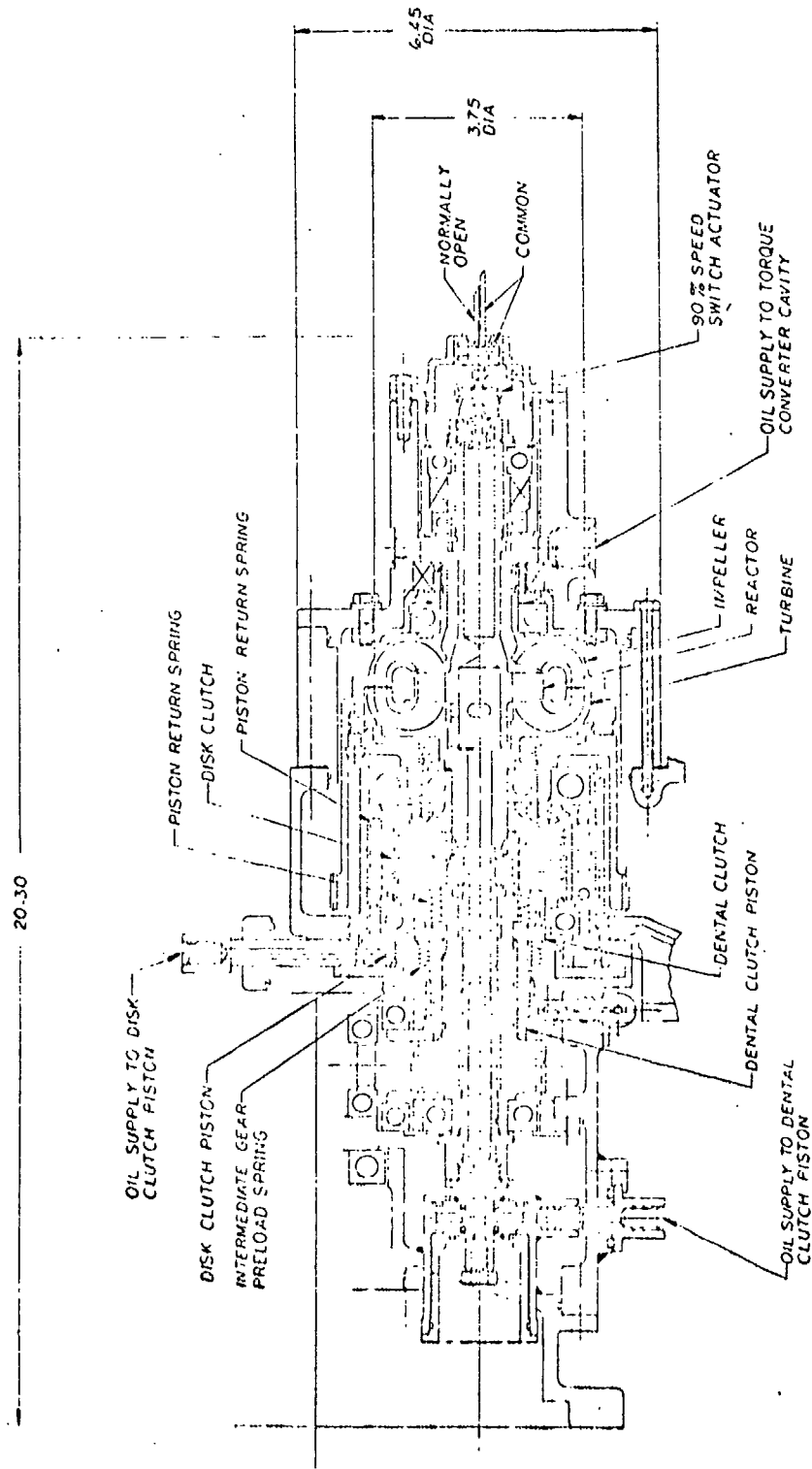


Figure 153. Lockup Clutch and Torque Converter Layout

Preceding page blank

Reproduced from
 Best available copy.

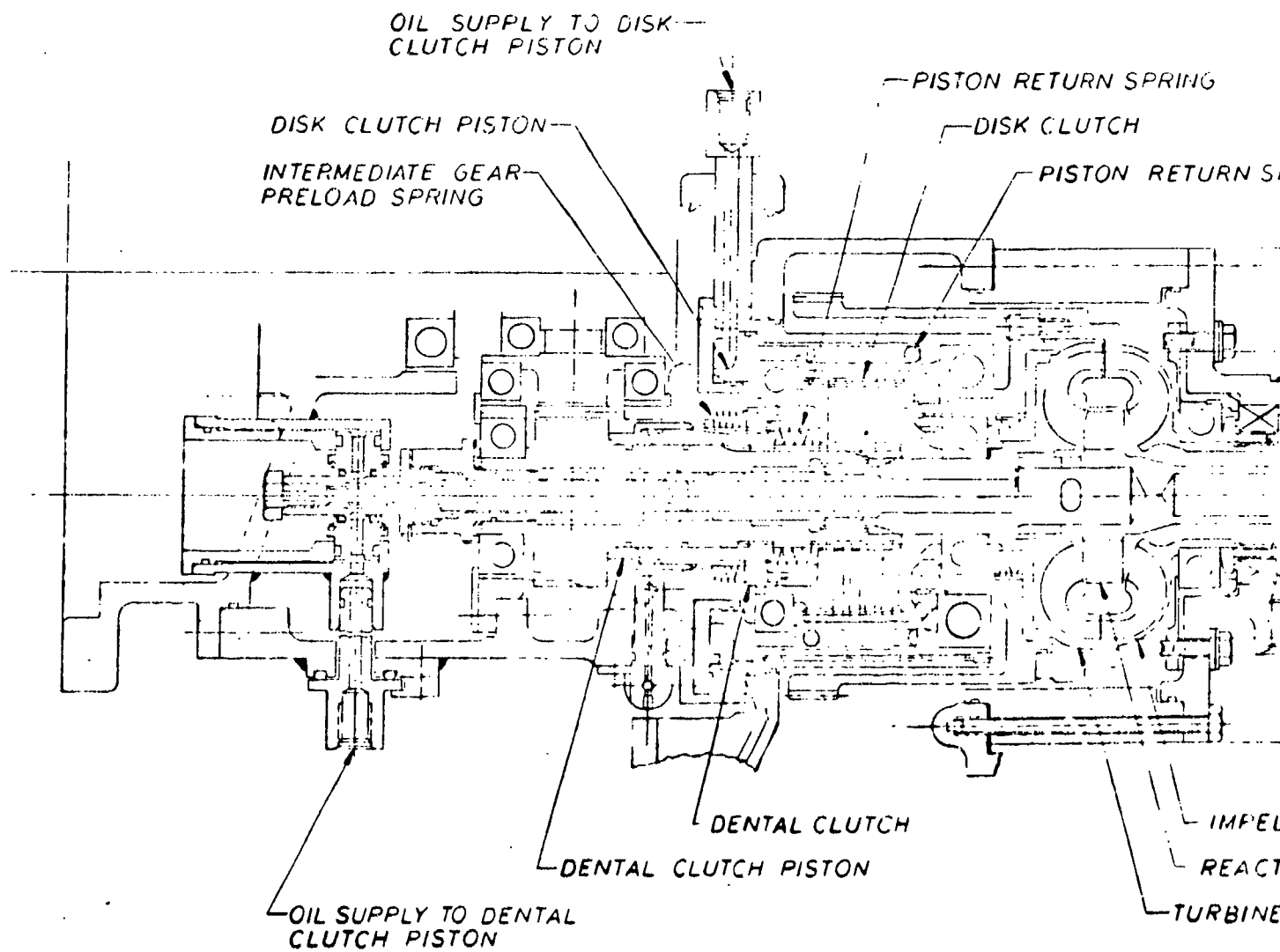


Figure 153.

Preceding page blank

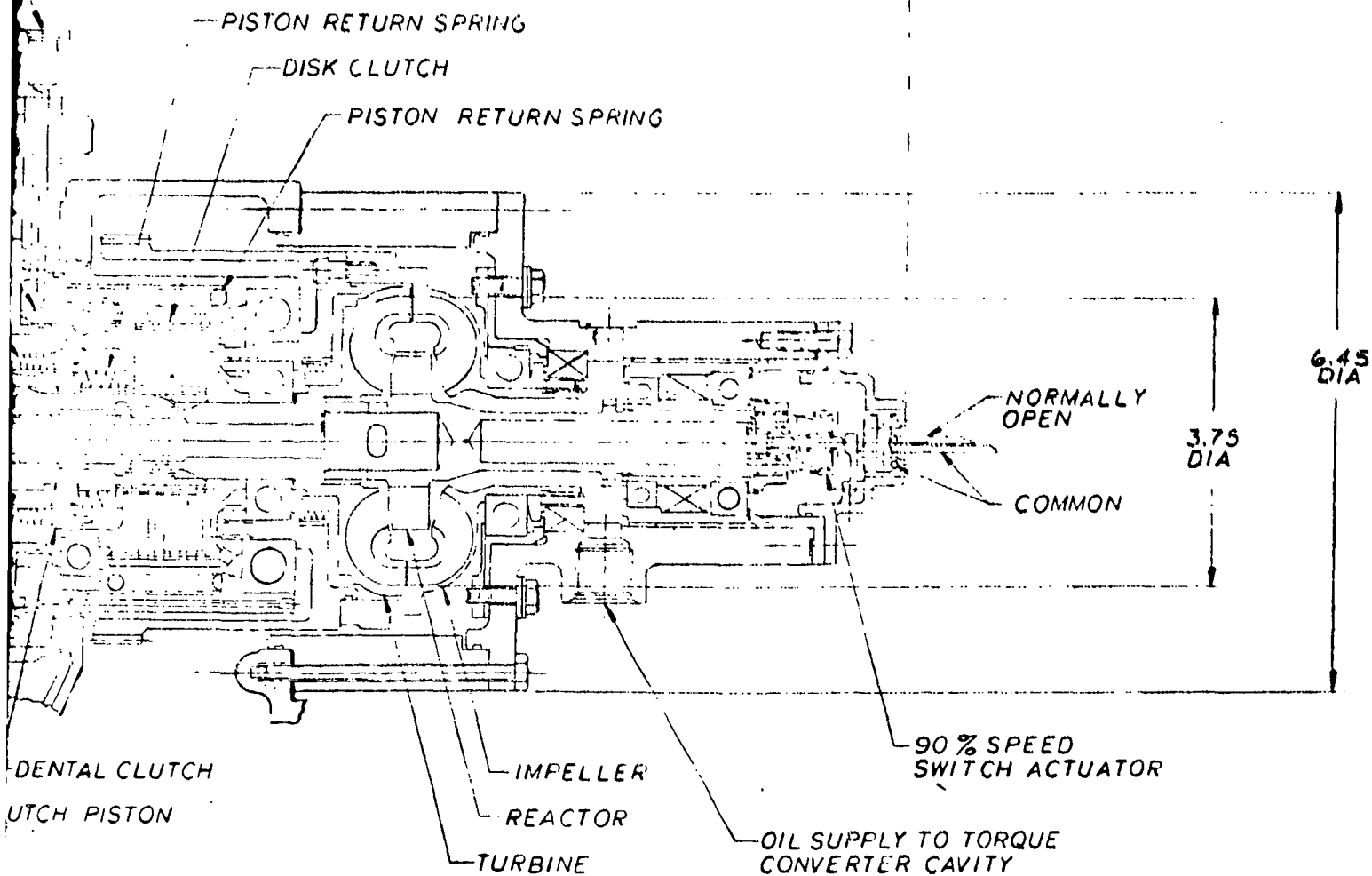


Figure 153. Lockup Clutch and Torque Converter Layout



B

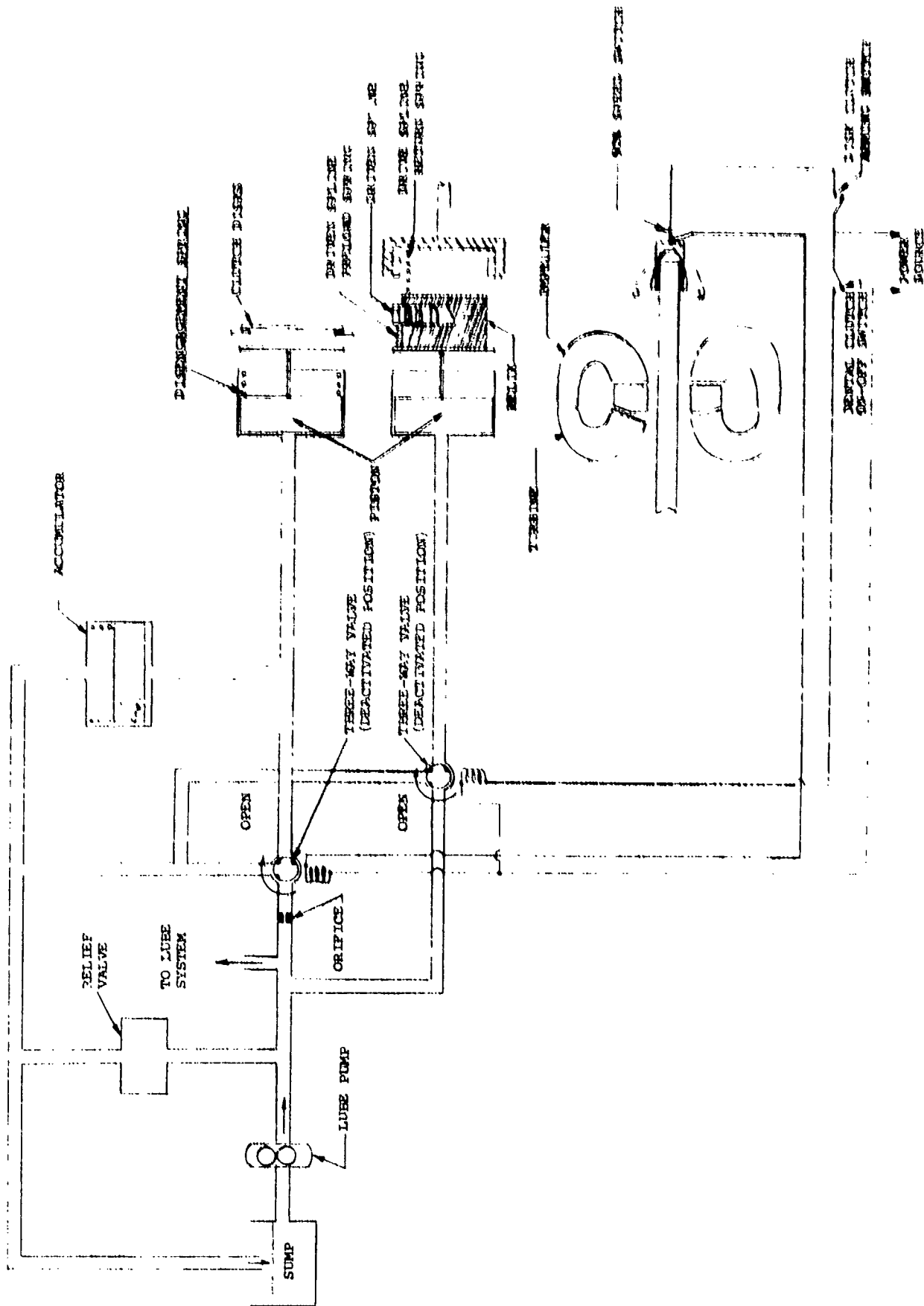


Figure 154. Lockup Clutch and Torque Converter Schematic.

Preceding page blank

- (c) When synchronization is achieved, the dental clutch is actuated by closing an on-off switch that energizes a three-way solenoid valve, allowing the piston to be actuated by oil pressure. The resultant force starts shifting the helix to the right (Figure 154), compressing the return spring.
- (d) The driven spline is displaced to the right the same amount as the helix, until the driven spline butts against the driving spline.
- (e) As the helix is moved farther to the right by the oil pressure acting on the piston, the driven spline is rotated by the helix teeth.
- (f) When the teeth of the driven spline are in line with the slots of the drive spline, the driven spline preload spring forces the driven spline into engagement with the drive spline.

The estimated performance curves for the lockup torque converter are shown in Figure 155. These curves summarize the results of a parametric study that predicted the size of the clutch and the number of rubbing surfaces for a 3-in. accumulator. Note that the clutch may have from four to eight rubbing surfaces, depending upon the driving horsepower available. The oil was supplied at pressures from 100 to 150 psig, depending upon the setting of the lube system pressure relief valve.

The test rig APU had sufficient power to utilize eight rubbing surfaces at 150-psig oil supply pressure. To minimize the power requirement for the APU, four rubbing surfaces at 125-psig oil pressure were recommended.

NOTES:

1. 100% speed = 17,922 rpm
2. Accumulator volume = 3.0 in.²
3. Clutch area = 3.885 in.²
4. Piston area = 7.45 in.²
5. Orifice diameter = 0.03125 in.

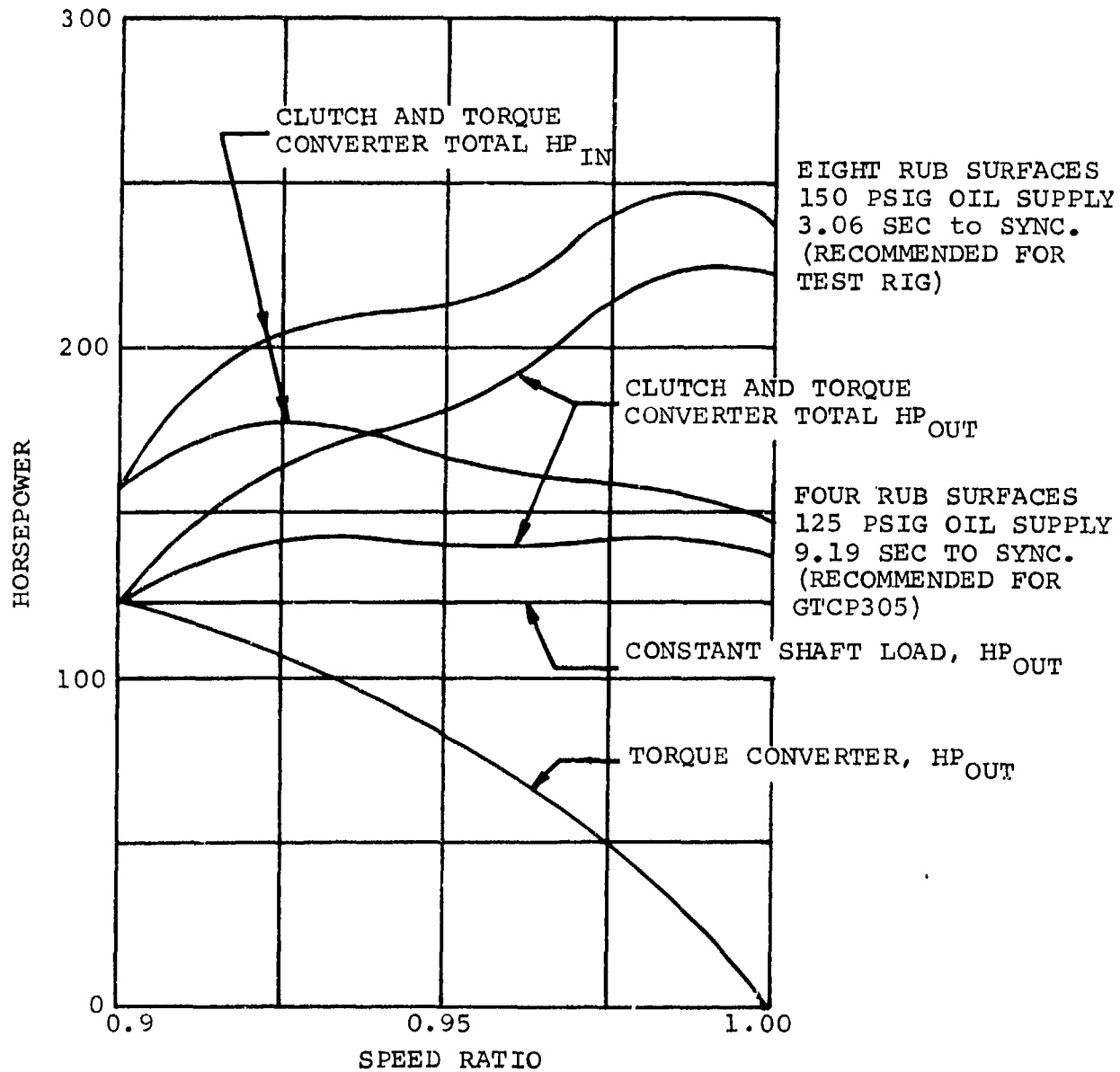


Figure 155. Estimated Performance Lockup Torque Converter.

The difference between the horsepower-in and -out curves was calculated, using the total efficiency curve of the torque converter-clutch system obtained by multiplying the clutch, gear train, bearing, and torque converter efficiencies together (Figure 156).

If the ratio of accumulator volume to orifice area remains constant, the piston pressure schedule remains constant. The pressure rise increases as the accumulator volume decreases, or the orifice area increases, or the time from initiation increases.

3. DEVELOPMENT

Three sets of turbine and impeller hardware were used throughout the development program, designated numbers 601, 602, and 603. Tests 1 through 7 were run with the 601 hardware, and Tests 8 through 12 were run with the 602 hardware. The turbine of the 602 hardware was cut back after several fatigue cracks were discovered at the exit. Tests 13 through 15 were run, using the modified 602 hardware. From Test 16 on, the 603 hardware was used. This hardware has the same hydrodynamic blade shapes, but the blade thickness on both the turbine and impeller was increased from 0.032 to 0.040 in. Also, the material for the 603 hardware was changed from CRES 347 to 17-4-PH for the housing and 17-7-PH for the blades.

Through Test 15, only two reactor shafts were used. One was the variable reactor of the original hydrodynamic design, and the other was the fixed reactor with a two-dimensional, 22-deg exit-angle blade with coordinates taken from the mean-streamline blade coordinates of the variable reactor.

Three additional fixed reactors were later fabricated to the same blade shape as the variable reactor with exit angles of 14, 22, and 30 deg (nominal). The variation in exit angle was obtained by rotating

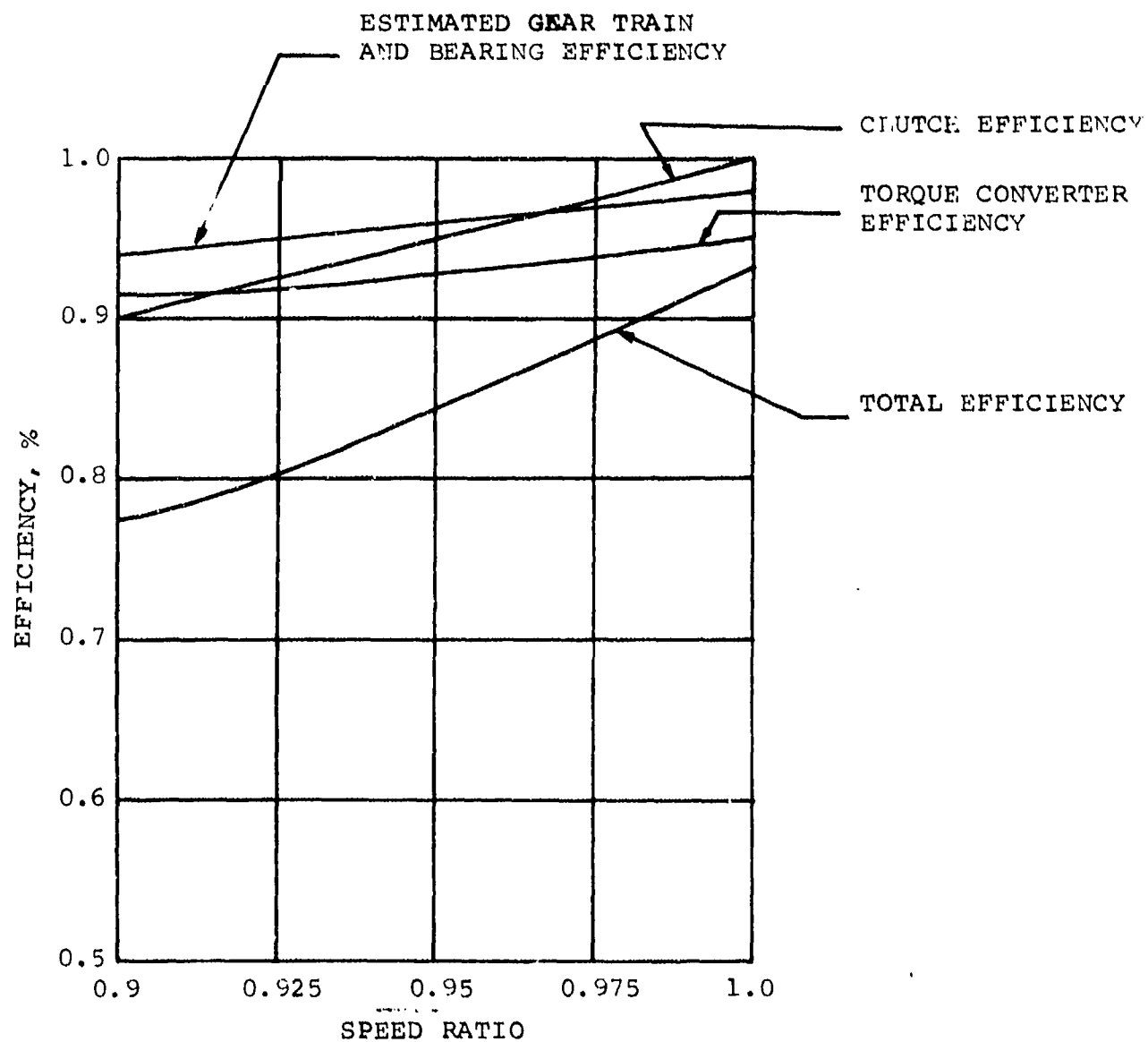


Figure 156. Estimated Lockup Torque Converter Efficiency.

the tooling about the blade-stacking axis. These three reactors were used with the 603 impeller and turbine hardware, from Test 16 on.

From Test 1 through 16, all output torques were calculated from the rate of speed change, as determined from the slope of the time-speed trace. After Test 16, a Lebow Torque Meter was installed on the output side of the torque converter, thereby measuring both input and output torque. Therefore, the results of Tests 17, 18, and 19 are considered the most accurate.

The following paragraphs describe the tests as they were conducted.

3.1 Tests 1, 2, 3

These tests were run with the fixed reactor and 12,000-rpm input speed to determine the mechanical integrity without danger of failure at high speed. The test results were as follows:

- (a) Performance Data - Performance data were not taken.
- (b) Cooling System - The cooling system exhibited an adequate safety margin.
- (c) Operating Charge Pressure - The operating charge pressure varied from 18 to 31 psia. The oil flow for cooling and the charge pressure were not independent (a higher charge pressure resulted in a correspondingly higher through-flow). Therefore, a flow circuit redesign was necessary.
- (d) Mechanical Integrity - There was no evidence of mechanical failure.

- (e) Fill-and-Drain System - A total of 115 start cycles were made by filling the torque converter with oil and accelerating a flywheel to the cutout speed (3750 rpm). The torque converter was then drained and the procedure repeated. The fill-time varied from 1 to 3 sec and the drain-time from 0.5 to 1.0 sec.

3.2 Tests 4, 5, 6

These tests utilized the fixed reactor, and the input speed was changed to 20,000 rpm. The test results were as follows:

- (a) Performance Evaluation - Parasitic losses were determined so that gearing, bearing, and windage losses could be considered when reducing the performance data. Some data were recorded, but disassembly revealed that several turbine blades had cracked and broken off. Thus, the data were suspect and were not used.
- (b) Cooling System - The cooling system proved to be adequate.
- (c) Operating Charge Pressure - The operating charge pressure varied from 20 to 155 psia. The oil through-flow (cooling flow) could not yet be adjusted and maintained independently of charge pressure.
- (d) Mechanical Integrity - Several turbine blades were broken at the trailing edges. Apparently, a combination of bad brazing and vibration caused the failures. A new impeller and turbine were made and their natural frequencies of vibration were determined by a shake table, with vibration pickups attached to the blades. A preliminary interference diagram was constructed to include all possible impulse forces that might have caused the failure. For Test 5, the old hardware

was re-installed to get vibrational traces without risking any new parts. Vibrational traces were recorded on a tape recorder and analyzed to determine the prominent excitation frequencies. Analysis revealed that the exciting frequencies were coming from the gears between the torque converter and the dynamometer. Knowing these exciting frequencies, an interference diagram could be constructed to indicate the critical speeds.

The new hardware was installed for 12,000 rpm running (Test 6). The unit was run quickly from stall to high-speed ratio and then shut down. Transient data were recorded on a multichannel oscillograph recording.

The final results of this test are shown in Figure 157. The circled areas indicate critical vibrational regions, where hazardous conditions may exist if the torque converter were operated at these critical speeds.

- (e) Fill-and-Drain System - No fill and drain tests were conducted.

3.3 Test 7

The torque converter was run at 12,000 rpm with the variable reactor. The test results were as follows:

- (a) Performance Evaluation - The variable reactor configuration showed more than a 10-percent reduction in torque ratio than the theoretical performance, and the fixed reactor performance gave results close to the theoretical. Reducing the reactor angle reduced the capacity with a small reduction in torque ratio.

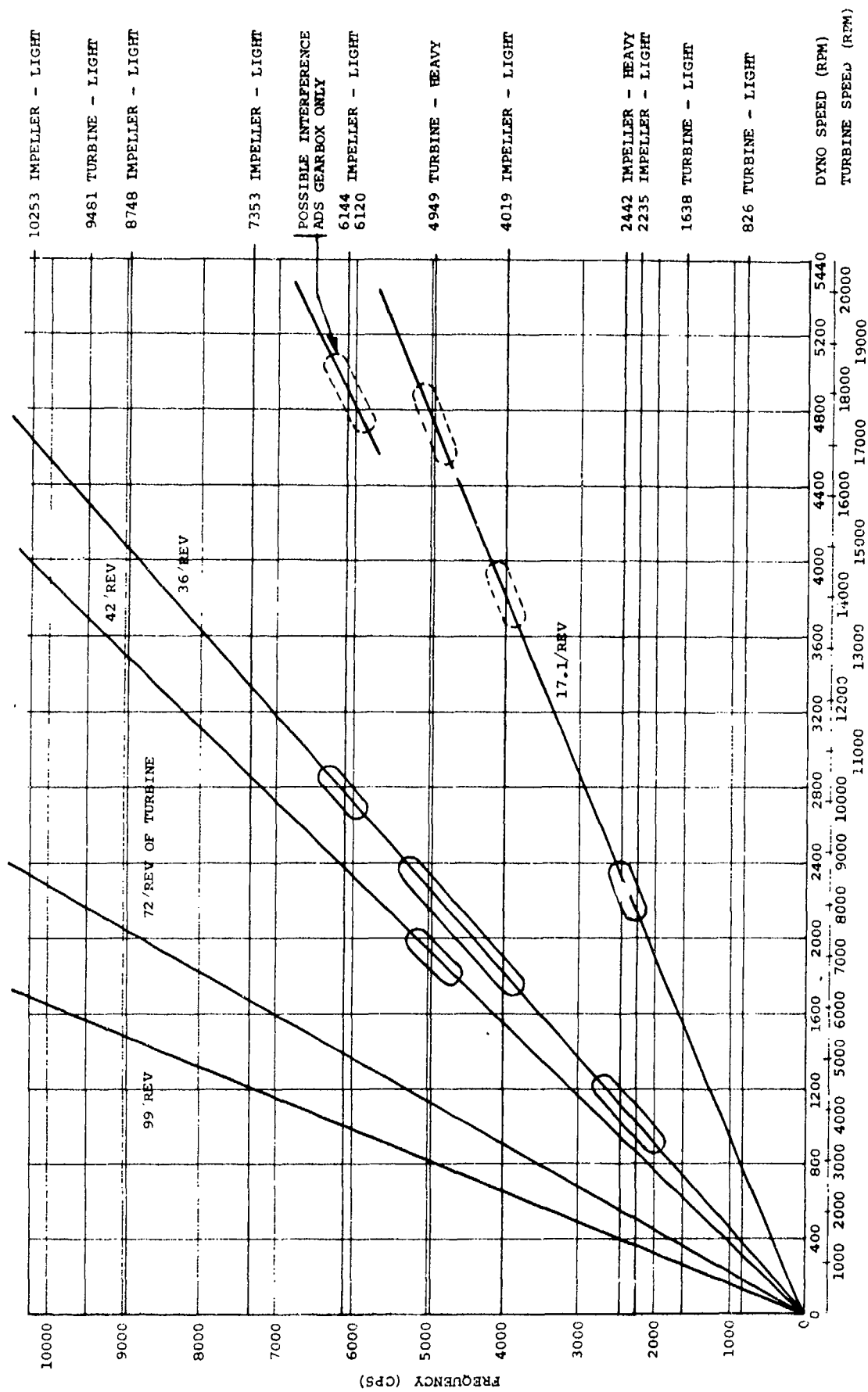


Figure 157. Torque Converter Reactor Interference Diagram.

- (b) Cooling System - The cooling system was adequate.
- (c) Operating Charge Pressure - Charge pressures were varied from 50 to 400 psia. Changes in capacity were noted. Higher charge pressures yielded higher capacities. The charge pressure was varied independently from cooling flow.
- (d) Mechanical Integrity - Upon disassembly, the blades of the turbine were inspected in detail. There was no evidence of fatigue cracks or wear.

3.4 Test 8

This test utilized the fixed reactor at 12,000 rpm input speed. The test results are as follows:

- (a) Performance Evaluation - The efficiency was slightly better and the torque ratio was slightly less than the theoretical. The power input capacity was lower than the variable reactor, a factor attributable to the inefficiencies of the flow around the variable reactor blades at the vane-end openings.
- (b) Cooling System - The cooling system was adequate.
- (c) Operating Charge Pressure - The operating charge pressure was 200 psi.
- (d) Mechanical Integrity - All parts functioned well.

3.5 Test 9 (Steady State)

The torque converter was assembled with the fixed reactor and operated at 20,000 rpm. Steady-state data were taken at high-speed ratios and various charge pressures. The results (Figure 158) of the

IMPELLER SPEED = 20,000 RPM
 INLET PRESSURE
 300 PSIG
 250 PSIG
 150 PSIG
 50 PSIG

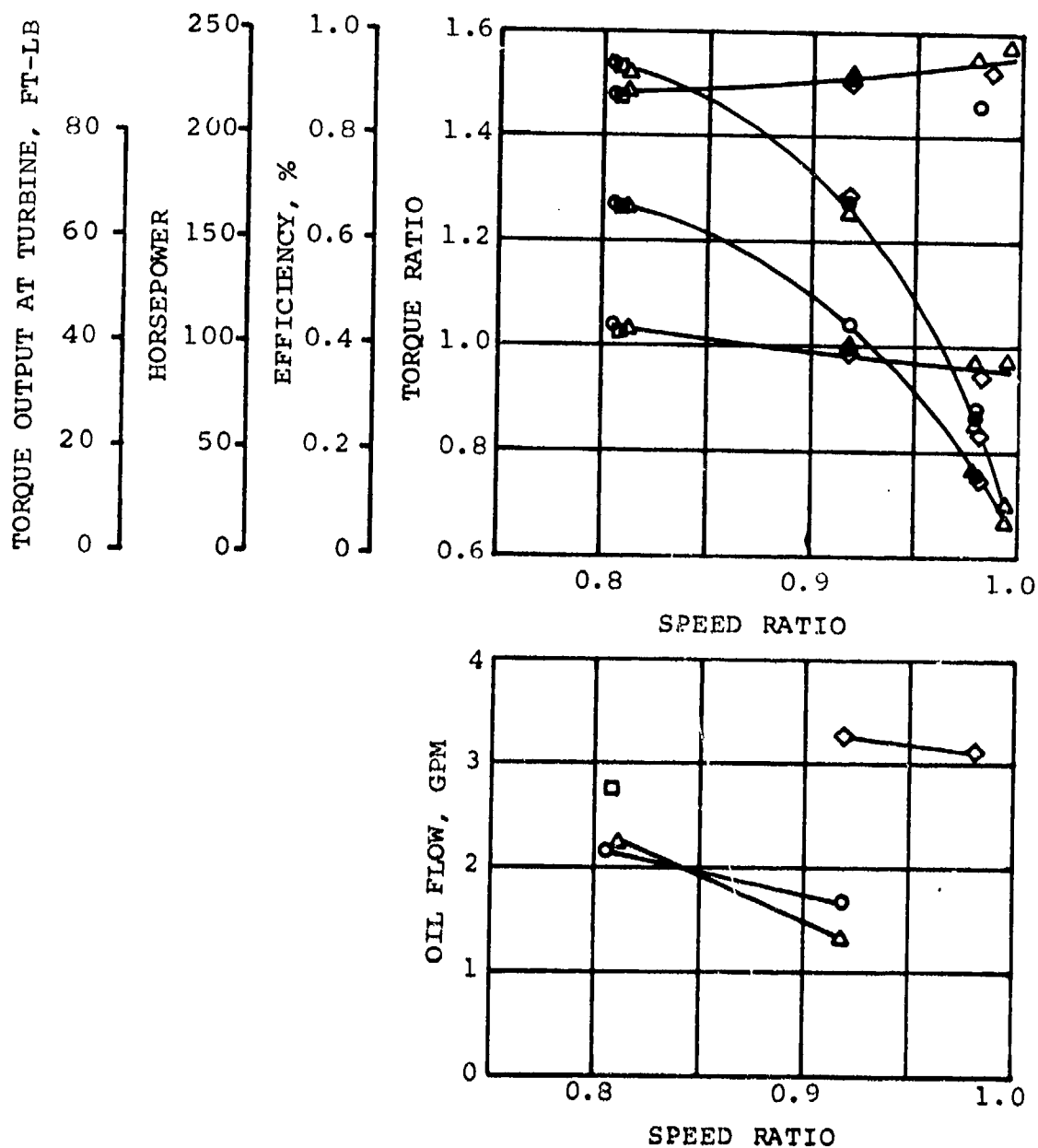


Figure 158. Steady-State Torque Converter Performance.

test show that charge-pressure variations have little or no influence on capacity or efficiency at high-speed ratios. Steady-state data at low-speed ratios were not obtained, due to the inability of the test rig to dissipate the rejected heat.

3.6 Test 10 (Acceleration)

The acceleration tests were run at arbitrary charge pressures set during steady-state conditions, prior to start initiation. Some selected results of these tests show that for the first few seconds after the start of the test run, the torque converter pumped the oil through the unit at a rate sufficient to keep the inlet pressure low. During this time, the torque converter capacity was low, resulting in a variable-fill type of test.

3.7 Test 11 (Acceleration)

The results of the Test 10 acceleration tests indicated excessive cooling flows through the unit. In an effort to reduce this flow and provide a faster fill-time, the inlet flow control valve was removed and two exit lines (9 and 2 gpm, respectively) were inserted in parallel with the relief valve. At approximately 0.5 speed ratio, the 9-gpm line was shut off to decrease the oil through-flow.

The results of Test 11 showed that, if the oil flow rate is decreased as the speed ratio increases, a higher efficiency will result. To obtain the best efficiency, the cooling-oil flow rate should be proportional to the heat-rejection rate.

3.8 Test 12 (Steady State)

Test 12 was intended to expand the steady-state information obtained from Test 9 to lower speed ratios. Vibrational amplitude experienced during steady-state operation at lower speed ratios precluded further testing.

3.9 Test 13 (Acceleration)

Test 13 was performed only as a check-run after the replacement of a bearing in the test rig gearbox.

3.10 Test 14 (Acceleration)

The oil flow passages within the torque converter were redesigned to approximate the ideal flow schedule (discussed under Test 11). The flow restriction devices external to the torque converter on the outlet side are eliminated, and the oil ports in the hollow turbine shaft are sized orifices. This allows high oil flows at the low-speed ratios, caused by the high exit turbine pressures, and low oil flows at the high-speed ratios, caused by the low turbine exit pressures and the centrifugal force of the oil at the orifice.

The test results at 100-psig charge pressure are compared with those of Test 10 in Figure 159.

3.11 Test 15 (Acceleration)

Test 15 was performed to evaluate the effect of flow control orifice size on performance (Figure 160).

Since previous testing had shown that the variable reactor blade design gave lower performance, due to leakage around the ends of the blades and the fixed reactor blading was neither twisted nor tapered, three new units were fabricated for further testing. The first was a 22-deg reactor that had the same blade shape as the variable reactor. Two other units with exit angles of 14 and 26 deg were fabricated.

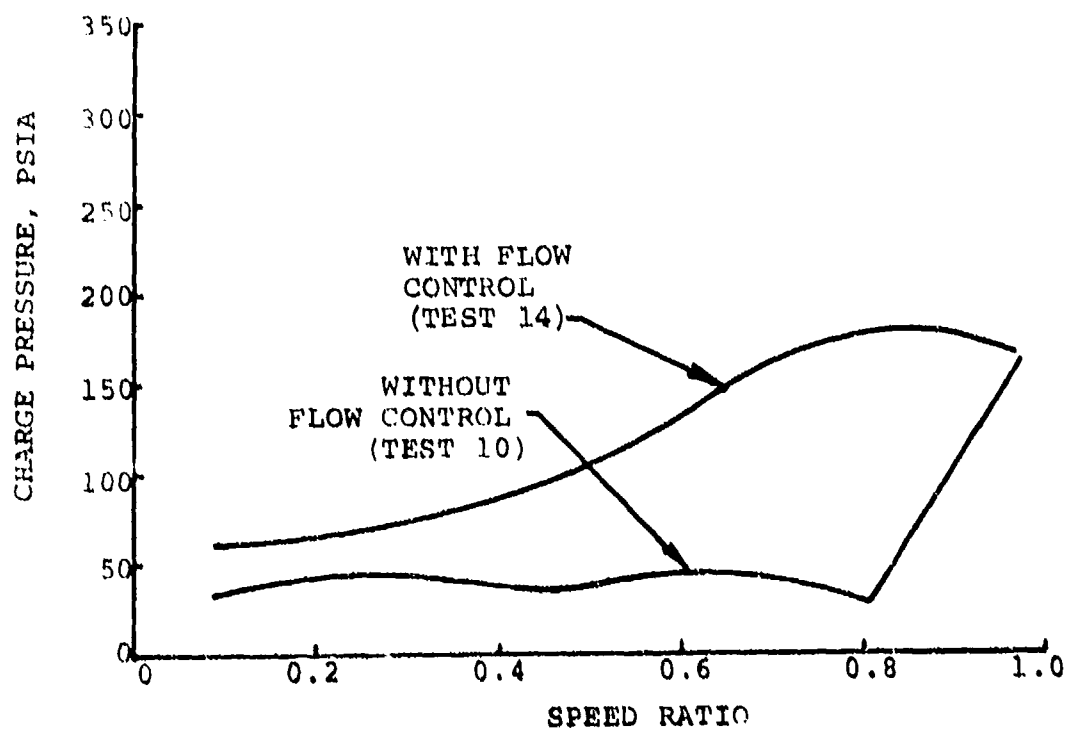
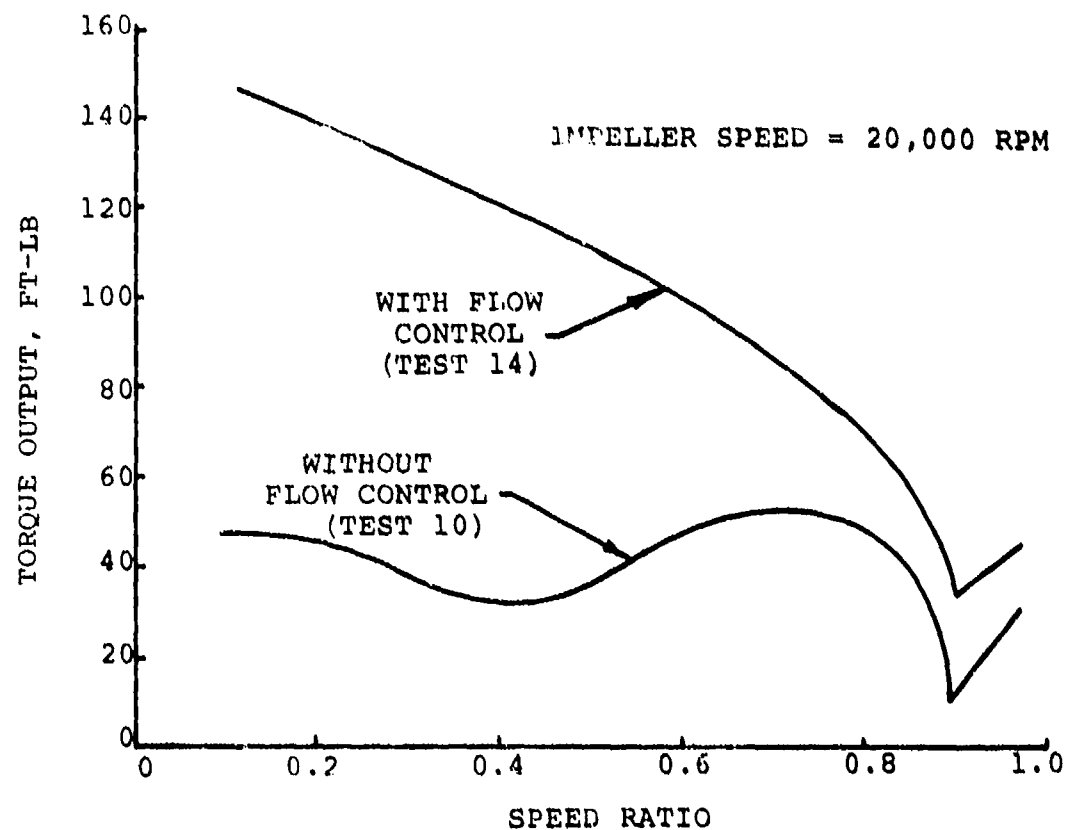


Figure 159. Comparison of Torque Converter Tests 10 and 14 at 100 psig Charge Pressure.

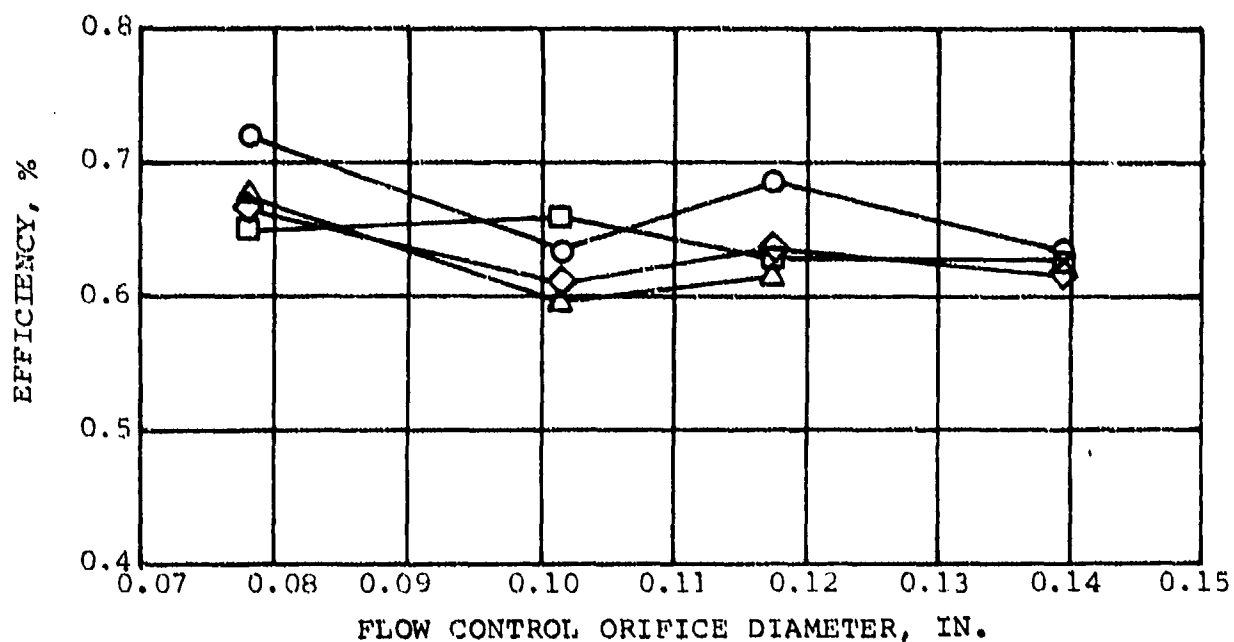
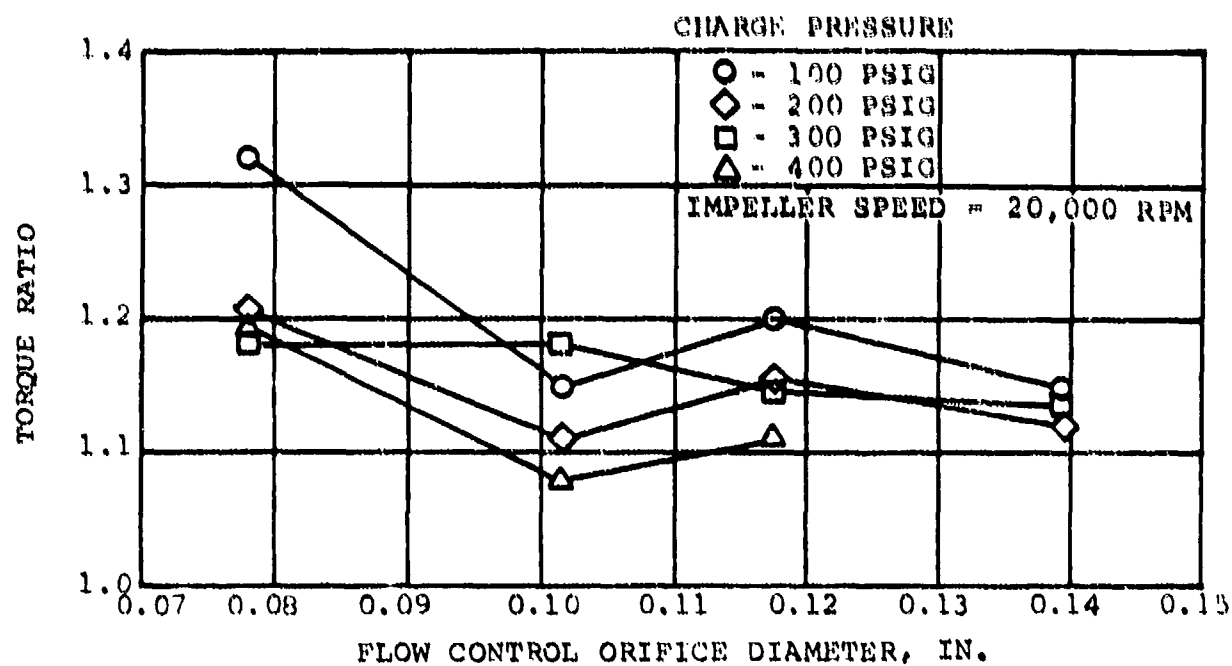


Figure 160. Performance Comparison of Torque Converter Flow Control Orifice Sizes at 0.5 Speed Ratio.

The maximum power absorption of the torque converter, as tested, is approximately 330 hp at 20,000 rpm. To more nearly match the torque required to start the main engine and to match the power available from the breadboard APU, several methods were considered.

- (a) Reduction of the reactor blade angle
- (b) Altering the flow area of the impeller and turbine by changing the torus core contour
- (c) Scaling down the existing design
- (d) Changing number of blades and/or angles
- (e) Reduction of the torque converter speed

The selected approach to match the APU output capability was to reduce the design speed from 20,000 to 17,922 rpm.

3.12 Test 16

The torque converter was assembled with the 14-deg reactor and the new impeller and turbine. The maximum horsepower absorbed by this torque-converter build during these tests was 270, compared to 330 from tests using the 22-deg reactor.

3.13 Tests 17, 18, 19

Tests 17, 18, and 19 were similar to Test 16, except that the 22-, 14-, and 30-deg reactors, respectively, were installed. Figure 161 shows the torque ratio, and the capacity factor is shown in Figure 162. Curves of the average test results are compared to the theoretical performance. The efficiency may be obtained as the product of the torque ratio and speed ratio.

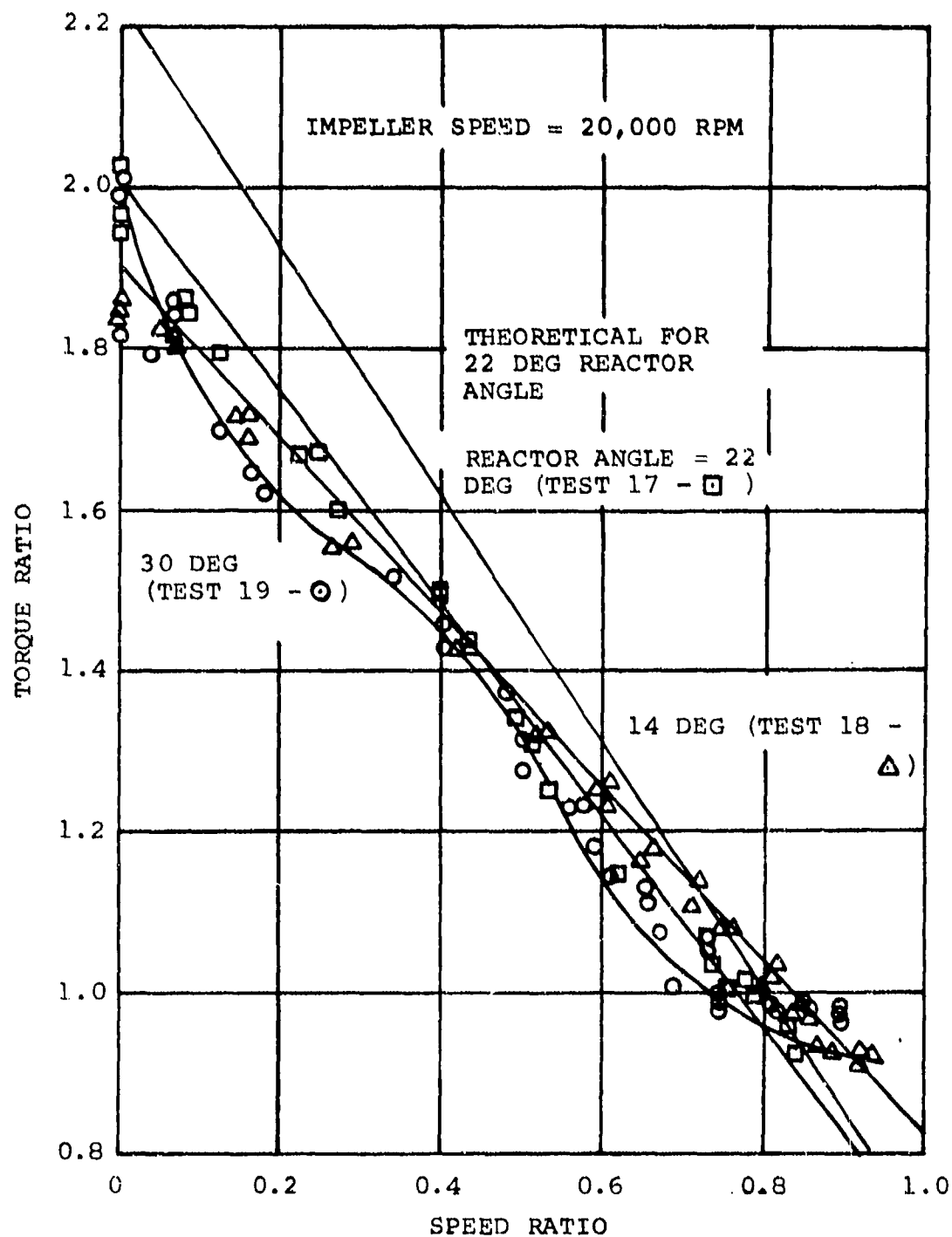


Figure 161. Final Torque Converter Test Results.

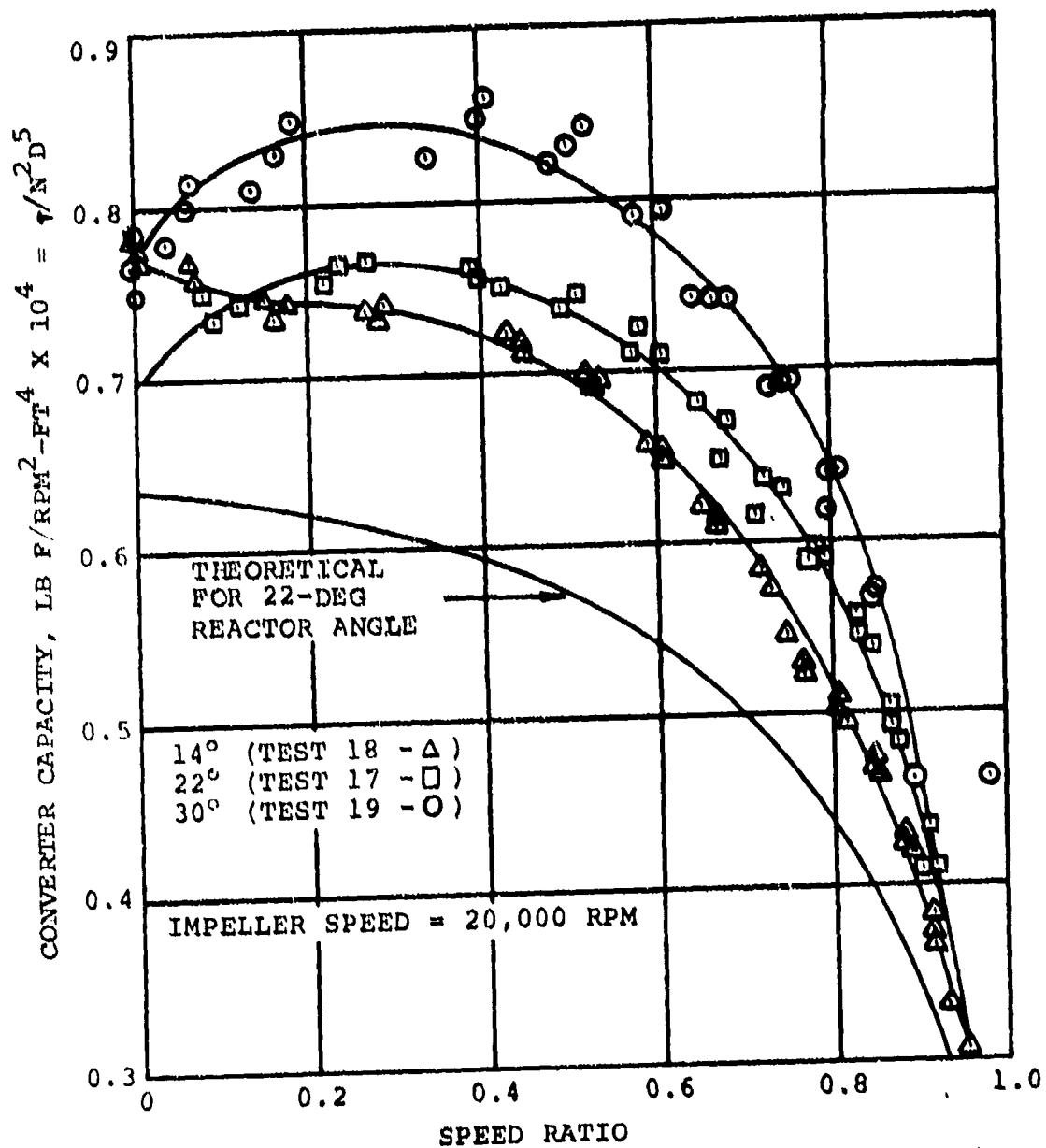


Figure 162. Capacity Factor Final Torque Converter Test Results.

Demonstration of the lockup torque converter in the test rig was successfully completed at speeds of 18,000 and 20,000 rpm. A typical test data trace is on the attached foldouts.

45,000 RPM

ENGINE SPEED

35,000 RPM

5000 RPM

DYNAMOMETER SPEED

3000 RPM

2500 IN.-LB

ENGINE TORQUE

0 IN.-LB

0 IN.-LB

DYNAMOMETER TORQUE

5000 IN.-LB

500 PSIG

CLUTCH PRESSURE

0 PSIG

500 PSIG

LOCKUP MECHANISM PRESSURE

0 PSIG

ON SPEED

BEGIN TORQUE CONVERT

Preceding page blank

BL

TORQUE CONVERTER FILL

1 SEC

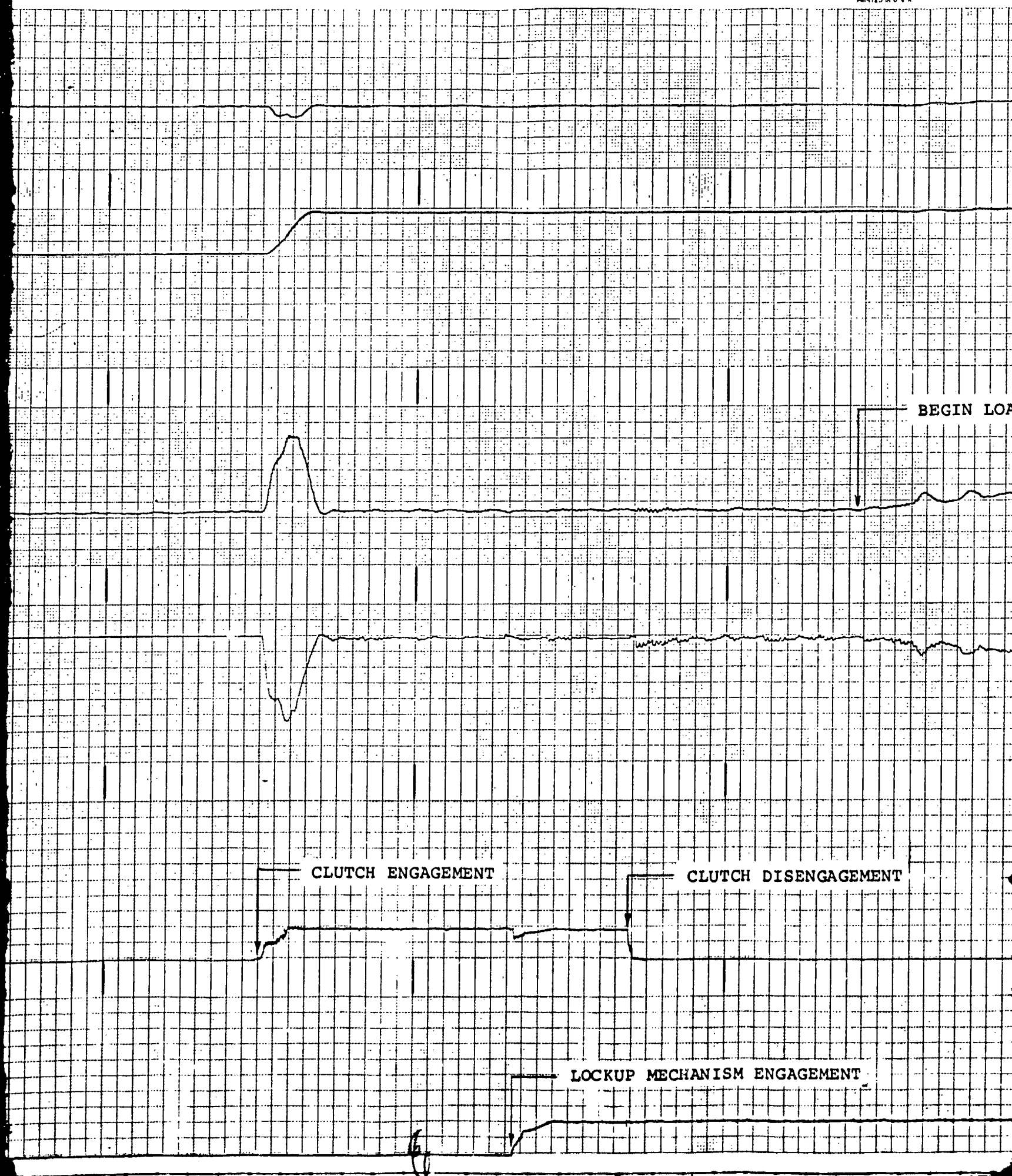
Blank

B

291-6

BEGIN LOADING

OUTPUT STABILIZED AT 0.9 SPEED RATIO

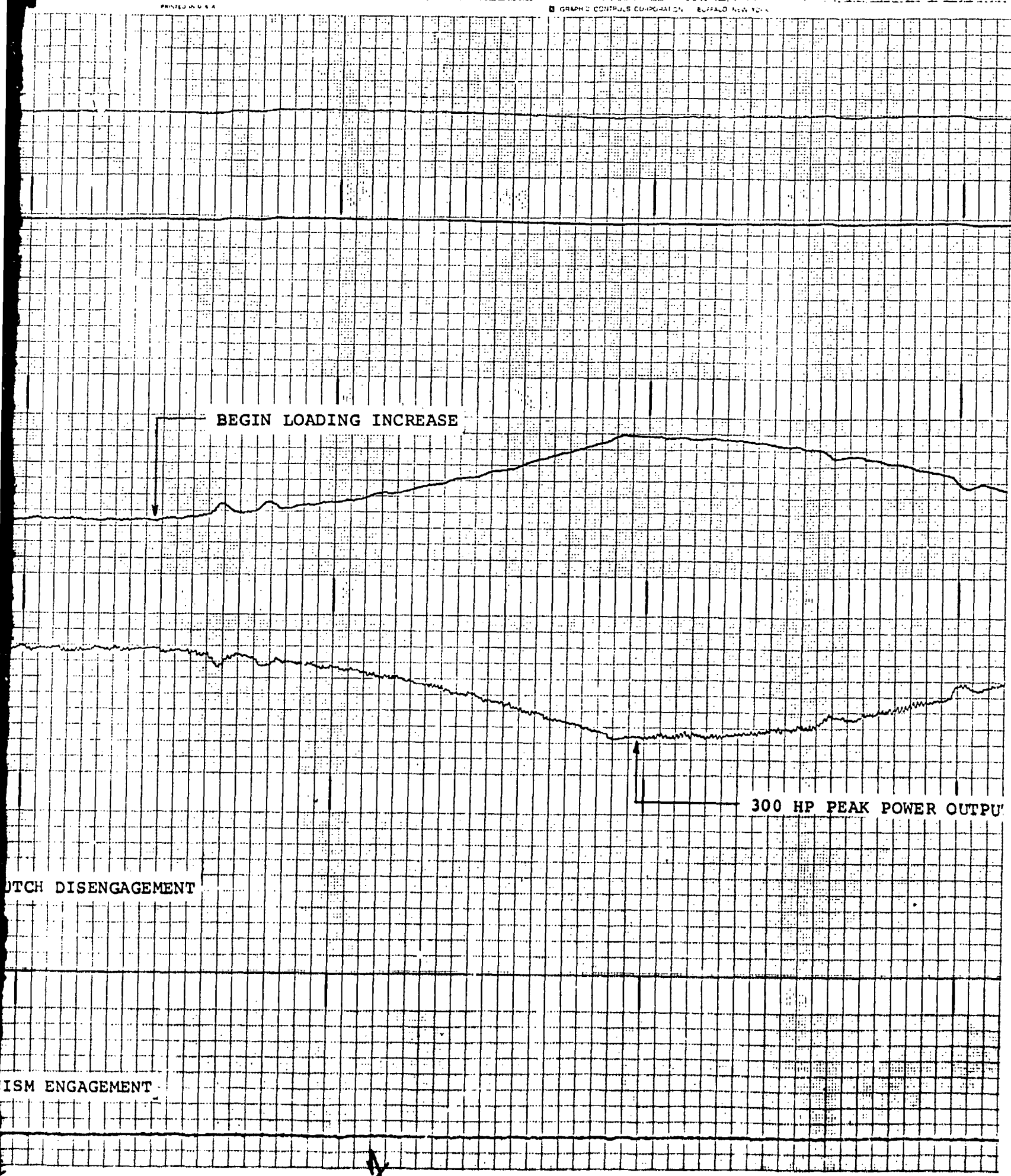


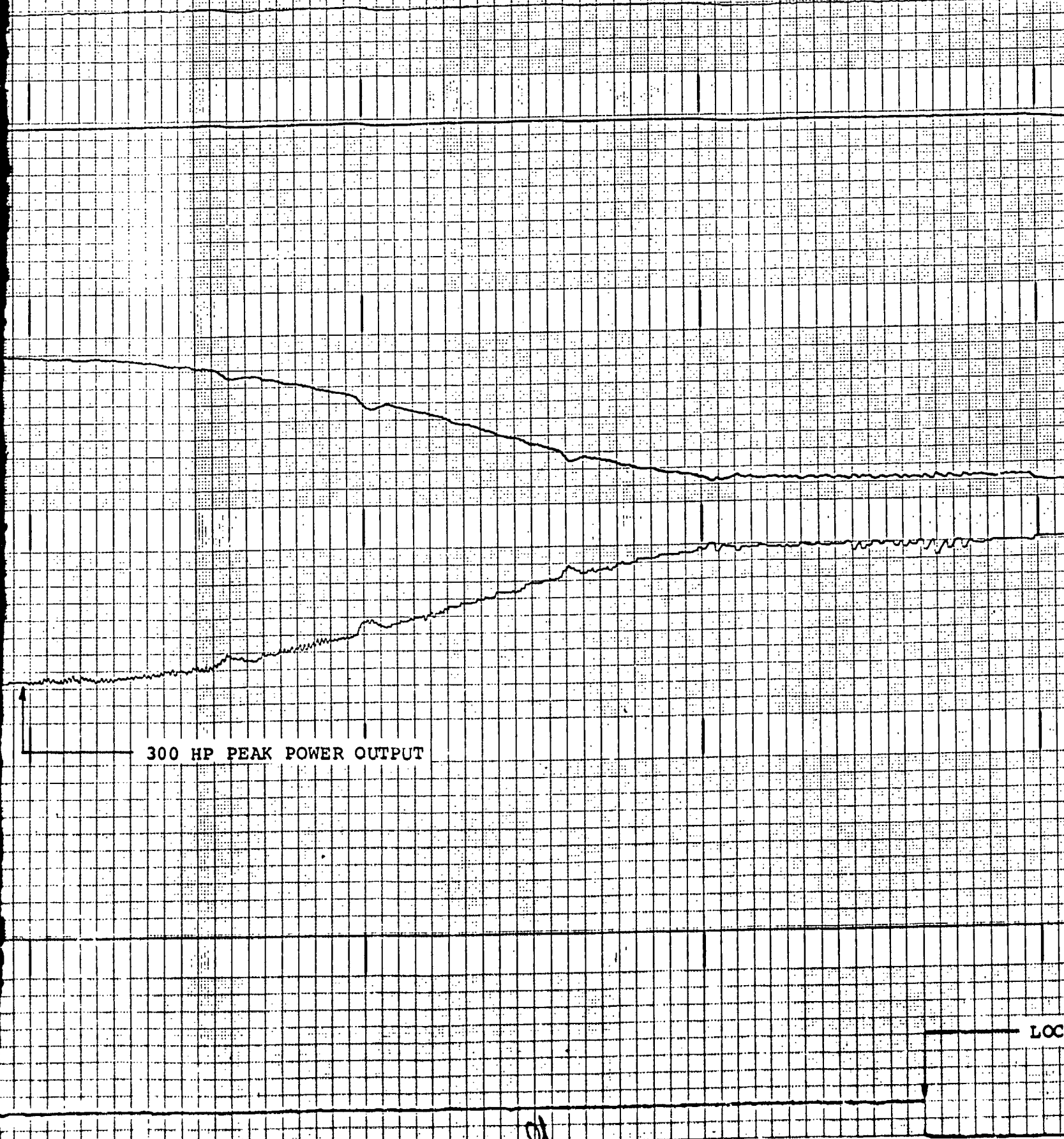
BEGIN LOADING INCREASE

300 HP PEAK POWER OUTPUT

CLUTCH DISENGAGEMENT

CLUTCH ENGAGEMENT





300 HP PEAK POWER OUTPUT

LOCK

91

ENG

NOTE: 39,000 RPM ENGI
TO 18,036 RPM T
IMPELLER SPEED.
SPEED EQUIVALEN
CONVERTER TURBI

LOCKUP MECHANISM DISENGAGEMENT

18,000 R

TEST DAT

ENGINE SHUTDOWN

NOTE: 39,000 RPM ENGINE SPEED EQUIVALENT
TO 18,036 RPM TORQUE CONVERTER
IMPELLER SPEED. 4930 RPM DYNAMOMETER
SPEED EQUIVALENT TO 18,036 RPM TORQUE
CONVERTER TURBINE SPEED.

LOCKUP MECHANISM DISENGAGEMENT

18,000 RPM LOCKUP TORQUE CONVERTER
TEST DATA RECORDINGS

45,000 RPM

ENGINE SPEED

ON SPEED

35,000 RPM

6000 RPM

DYNAMOMETER SPEED

3500 RPM

0 IN.-LB

BEGIN TORQUE CONVERTER FILL

ENGINE TORQUE

250 IN.-LB

0 IN.-LB

DYNAMOMETER TORQUE

5000 IN.-LB

250 PSIG

CLUTCH PRESSURE

0 PSIG

250 PSIG

LOCKUP MECHANISM PRESSURE

0 PSIG

1 SEC

X

B

BEGIN LOADING

OUTPUT STABILIZED AT 0.9 SPEED RATIO

0 50000 00000

BEGIN

CLUTCH ENGAGEMENT

CLUTCH DISENGAGEMENT

CLUTCH MECHANISM ENGAGEMENT

BEGIN LOADING INCREASE

300 HP PEAK POWER OUT

H ENGAGEMENT

CLUTCH DISENGAGEMENT

LOCKUP MECHANISM ENGAGEMENT

BEGIN TORQ

300 HP PEAK POWER OUTPUT

LOCKUP MECHANISM DISENGAGEMENT

Same as Rec. Eng. Recorder

ENGINE SHUTDOWN

BEGIN TORQUE CONVERTER DRAIN

NOTE: 39,000 RPM ENGINE SPEED EQUIVALENT TO
20,000 RPM TORQUE CONVERTER IMPELLER
SPEED. 5475 RPM DYNAMOMETER SPEED
EQUIVALENT TO 20,000 RPM TORQUE
CONVERTER TURBINE SPEED.

MECHANISM DISENGAGEMENT

20,000 RPM LOCKUP TORQUE CONVERTER
TEST DATA RECORDINGS

SECTION VII

CONTROL SYSTEM

1. AUTOMATIC CONTROL SYSTEMS DESIGNS

An automatic control system, suitable as a production unit for the APU and gearbox systems, has the basic functions of governing speed, preventing compressor surge, scheduling compressor inlet guide vane position, providing overspeed and overtemperature protection, and scheduling other switching functions relative to APU starting and various system operating modes. These functions are integrated into a complete automatic system as a part of the overall APU and gearbox assembly, with certain command signal inputs, to permit these components to perform in the various operating modes required.

An overall control system diagram is shown in Figure 163. This diagram depicts the single-shaft, integral-bleed APU system with the addition of control subsystems applicable to the other candidates considered in Section II.2. Each of the subsystems is identified by separate drawings, which are included to show system details. Each drawing contains a logic diagram in addition to the schematic presentation of system components. The logic portion represents the electronics of the control system.

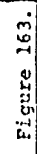
1.1 Speed Control Systems

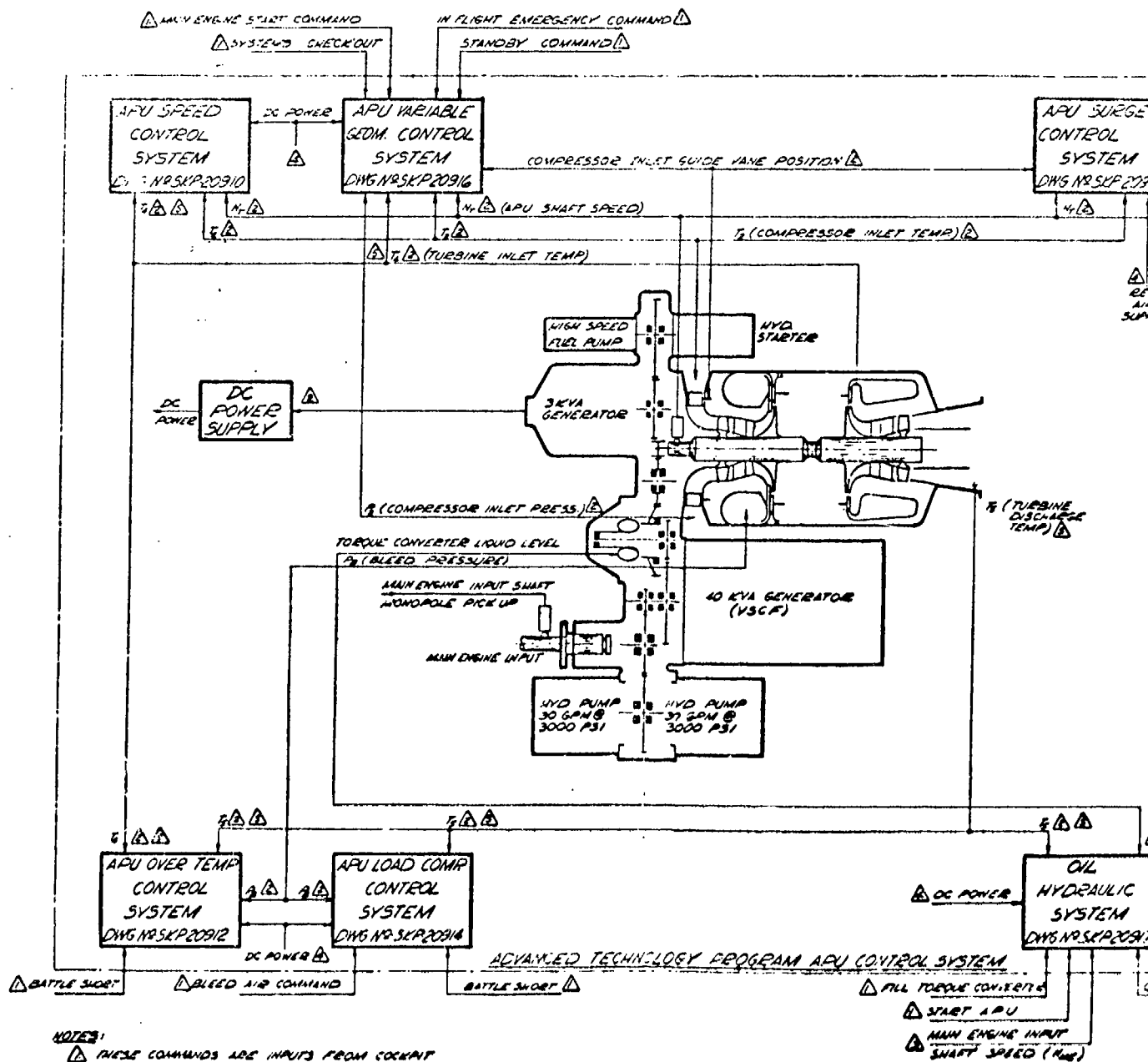
The single-shaft speed-control system and the free-turbine gas generator speed-control system incorporate a closed-loop turbine inlet temperature scheduling control. Figure 164 illustrates a typical electronic control system for controlling the APU from start to governed-speed.

The control system senses engine speed (N_T) [gas generator speed in the case of the free-turbine (N_{GG})], compressor inlet temperature (T_2), and turbine inlet temperature (T_4). Directly sensing the turbine inlet temperature is being considered so that performance and engine life can be optimized. The input goes to an electronic component, which generates a desired schedule of corrected turbine inlet temperature (T_4/θ) as a function of physical speed. A speed signal is fed into another circuit, and a nominal value of torque motor current is generated as a function of speed. The generated T_4 is compared to that actually measured. The resulting error is an input to the proportional-plus-rate control. The output of this control is added to or subtracted from the nominal. The desired current value is thereby achieved and sent to the torque motor in the metering valve. This approach will more effectively permit droop-control during acceleration. If the output of the proportional control is subtracted from a fixed maximum limit of torque motor current, the droop would be excessively large throughout the low end of the acceleration speed regime.

The rate feature is added to compensate for the inherently slow response of the temperature-sensing device at low mass flows. The rate current senses the rate of change of the turbine inlet temperature and prevents temperature overshoots during start until the temperature sensing device can function with adequate response, to fulfill the needs of the system.

At 95-percent speed, the switching system cuts out the closed-loop temperature-scheduling control and switches in the electronic proportional-plus-integral governed-speed control that functions from a speed-error signal. At the same time, the 95-percent switching function turns on the minimum fuel circuit, thus preventing lean-fuel blow-out in the combustor.





NOTES:

- △ THESE COMMANDS ARE INPUTS FROM COCKPIT
- △ THESE PARAMETERS ARE INPUTS FROM THE APU/AOS SYSTEM
- △ THIS PARAMETER IS AN INPUT FROM THE MAIN ENGINE
- △ THIS PARAMETER IS AN INPUT GENERATED BY THE CONTROL SYSTEM
- △ T1 OR T2 WILL BE USED
- △ ENERGIZE APU HYDRAULIC STARTER SQUENCH

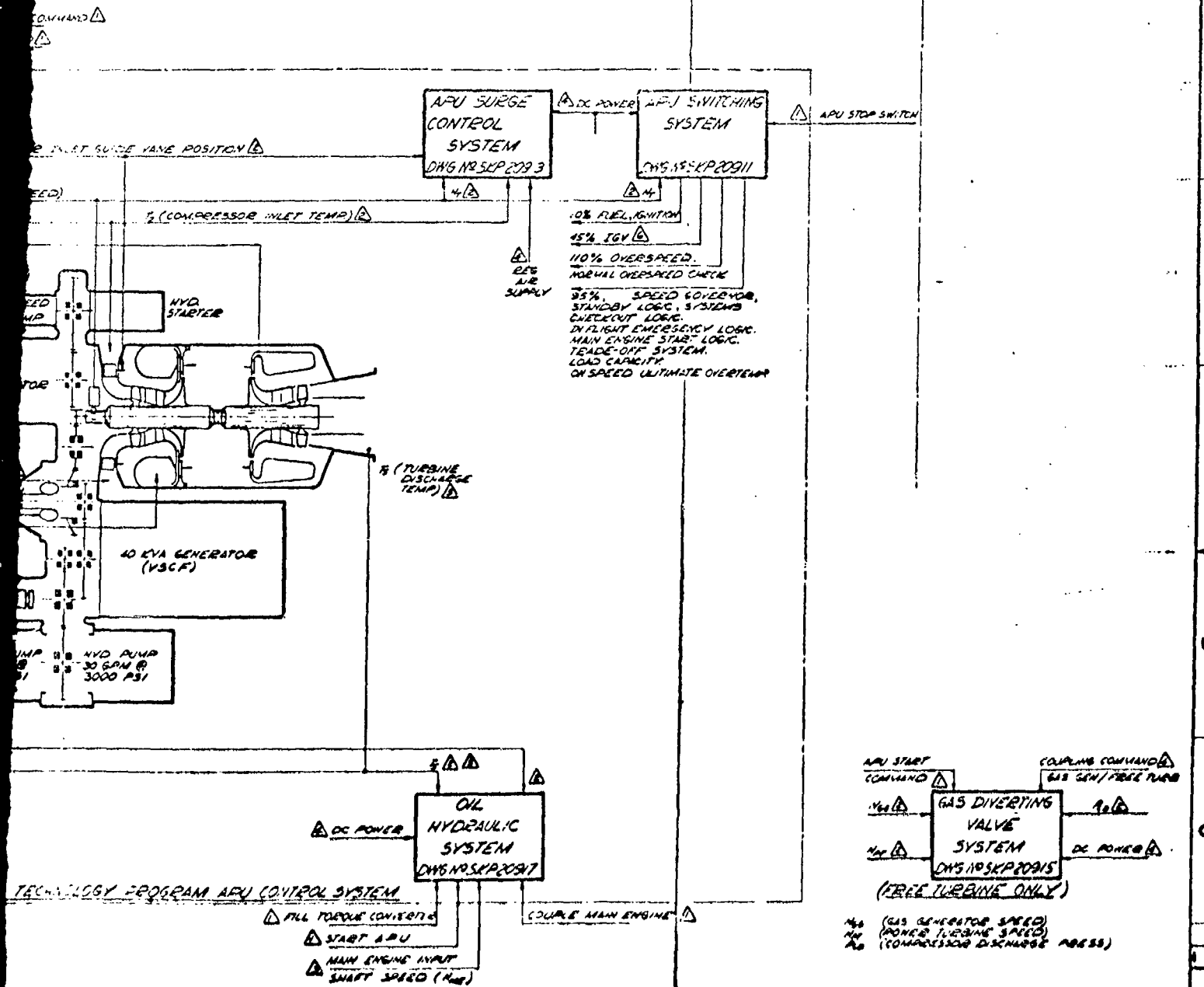
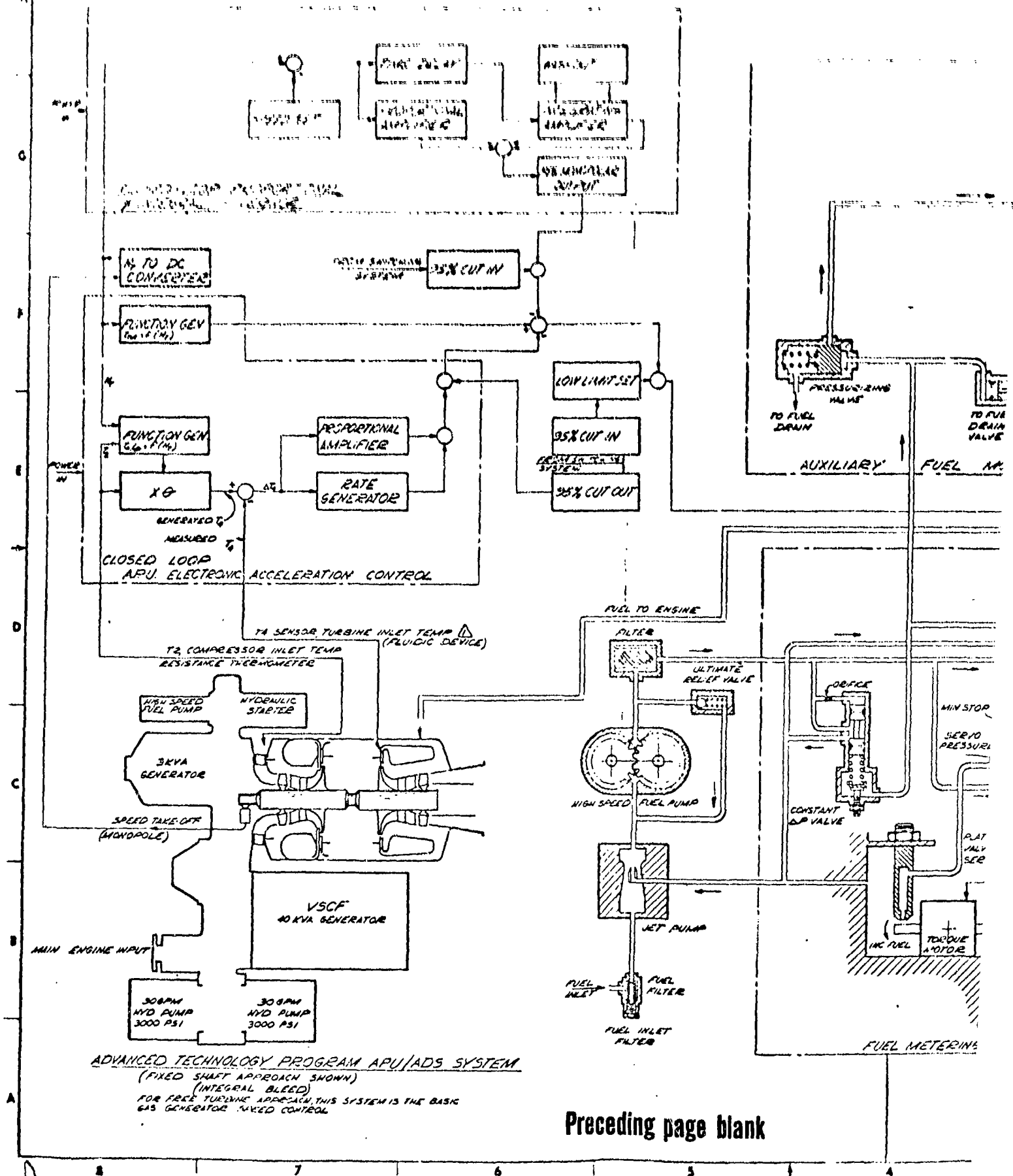


Figure 163.

DATE	DESCRIPTION	BY	CHKD	APPROVED
1993-09-10	REVISION 1
1993-09-10	REVISION 2
1993-09-10	REVISION 3
1993-09-10	REVISION 4
1993-09-10	REVISION 5
1993-09-10	REVISION 6
1993-09-10	REVISION 7
1993-09-10	REVISION 8
1993-09-10	REVISION 9
1993-09-10	REVISION 10

B



For a free-turbine version, the previously described operation applies to the gas generator speed control only. There is a system requirement to drive a 3-kva electrical generator from the gas generator gearbox, and the frequency output of the 3 kva has to be held within close tolerances during all gas generator, governed-speed operation. The normal mode, therefore, of allowing free-turbine gas generator speed to float, to control power turbine speed, is not allowable. Restrictions imposed on the overall system weight permit only a generator which produces 400-cycle ac power directly. The free-turbine power section speed control is discussed with the operation of a gas diverting valve.

The signal that is generated by the electronic acceleration control, or the electronic-governing control, goes to an electromechanical device known as a torque motor (flapper-type) that positions a metering valve. This metering valve, in conjunction with a constant differential pressure valve, allows correct fuel flow to the combustor nozzle system.

Fuel flows to the metering valve through the hydromechanical portion of the subsystem from the aircraft fuel system and passes through the APU fuel inlet filter. From the filter, it flows through the jet-boost pump, which has been included in the system to prevent cavitation at the inlet of the gear pump. A high-speed gear pump is used to help reduce gearbox weight. Fuel flows into this pump and is delivered at high pressure to the metering valve section. An ultimate relief valve is used to prevent overpressurizing the fuel system. The differential pressure valve maintains a constant ΔP across the metering valve, so that the metered fuel is a function of the valve area only and is not influenced by system inlet fuel and compressor discharge pressure changes or fuel pressure changes caused by plugged fuel nozzles.

In the system schematically illustrated, a constant pressure regulator is needed to get correct servo-valve operation over the range of pump discharge pressures.

Fuel leaving the metering section flows through the pressurizing valve that back-pressures the metering valve servo during the low pump-discharge pressure regime (low pump-speed) of the acceleration mode and through the fuel shut-off solenoid to the combustor nozzles. The fuel drain valve is added to the system to drain the fuel manifold on shutdown. In annular combustor engines where the manifold is wrapped around the turbine plenum, draining the manifold on shutdown to prevent fuel varnishing and coking is desirable..

1.2 Speed Switching Control and DC Power Supply

Figure 165 shows the schematic representation of the speed-switching control and the dc power supply. AC power coming from the 3-kva generator is fed into the dc power supply, which has to rectify and regulate the desired dc levels for the various electronic control circuits and the electronic speed switch.

This electronic speed switch receives a signal from the APU monopole pickup and transmits signals to various APU peripheral equipment at the desired speed level over the entire operating speed range of the engine.

1.3 APU Overtemperature Control System

Figure 166 illustrates the bleed/shaft power trade-off with the shaft priority overtemperature protection system for the APU. The system incorporates a variable and a fixed upper-temperature limit that is not a function of ambient temperature.

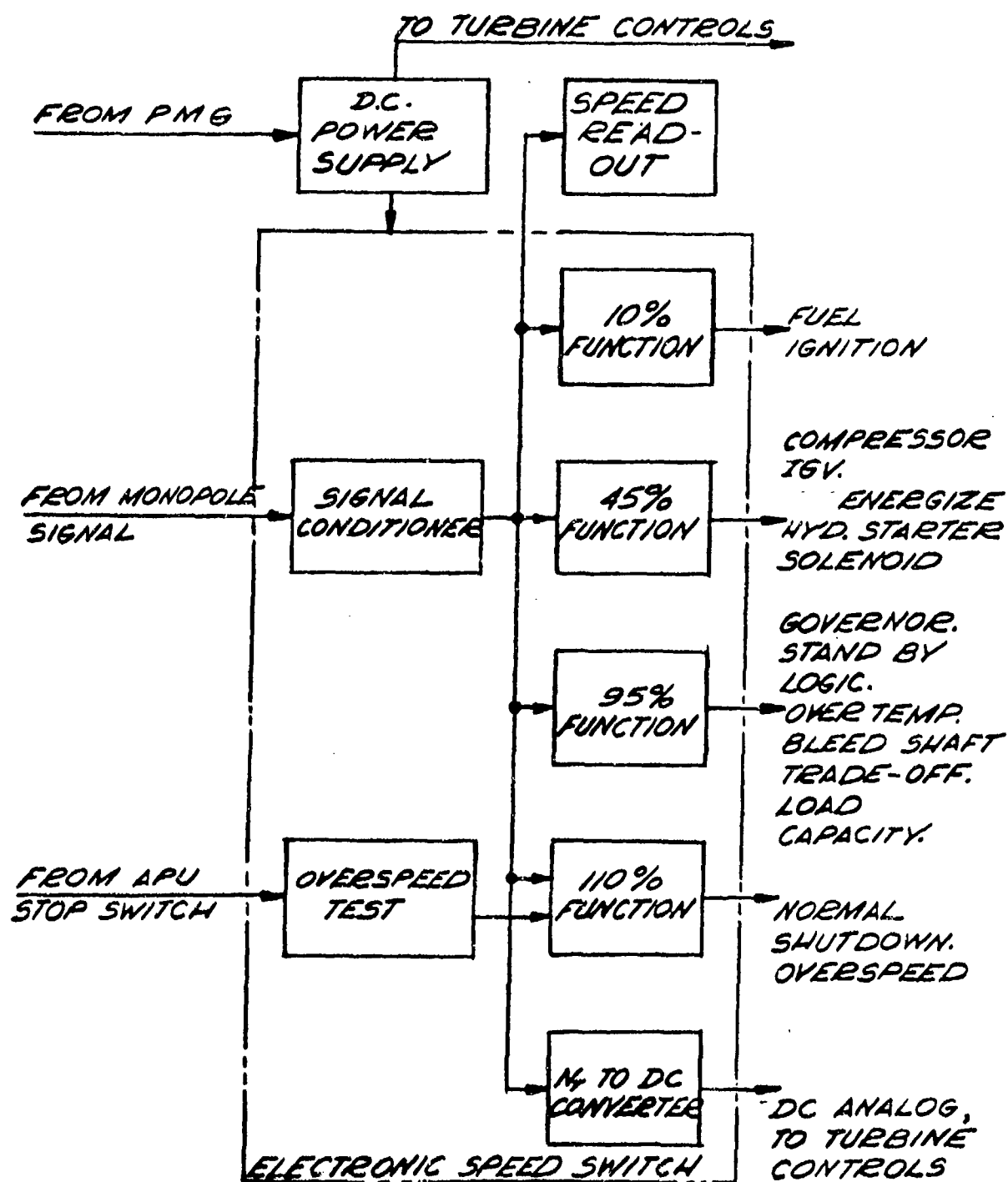


Figure 165. Power Supply and Switching Schematic (APU/ADS System) Single-Shaft Version.

If the turbine inlet temperature reaches this upper limit (variable during acceleration and fixed during governed-speed operation), the APU will be shut down by the fail-safe system. The cockpit contains a battle-short command switch that overrides these shutdown features. This system is applicable to both the single-shaft and free-turbine versions.

If an overload causes an APU overtemperature condition, the trade-off system throttles the bleed-air delivered, in order to maintain a safe turbine temperature while retaining the required shaft load.

This system uses thermocouple rakes or a fluidic temperature sensor at the turbine discharge (T_5) or turbine inlet (T_4). The sensed T_5 (or T_4) signal is compared to a reference, and the error is an input to a proportional-plus-integral control, which sends the desired signal to the bleed-air throttling device. In the integral-bleed version, this is a load-control valve that is a servo-operated, pneumatically powered butterfly. This is used as a tight shut-off valve, when no bleed-air is demanded from the APU. When bleed-air is demanded, the load control valve opens wide and remains in that position unless the overtemperature set-point is exceeded. When the load-control valve torque motor receives an overtemperature signal from the system, the valve servo-system bleeds the actuator until the temperature error disappears. The bleed load is thus reduced sufficiently to lower the T_5 temperature below the set-point. If the aircraft system demands more bleed-air, causing the engine to once again go overtemperature, or if more shaft load is added with the same effect, the valve will throttle to a more closed position. This type of operation will continue with increased load until the maximum shaft load level is reached. If a full-bleed shock load is suddenly applied to the APU, the valve will close rapidly.

If the T_5 exhaust gas signal is lost completely, due to a failure of the sensing circuit, the signal-loss detector will activate the fail-safe circuit and shut down the APU. A battle-short command signal will override this shutdown feature.

1.4 Surge Control System

Figure 167 shows the APU acceleration surge control system for the single-shaft and free-turbine versions and the on-speed surge prevention system for both the single-shaft and free-turbine, integral-bleed machines.

The APJ surge protection on acceleration will be accomplished by utilizing a spring-loaded open surge valve and modulating the VIGVs.

This system requires sensing speed and compressor inlet temperature and sending signals to an electronic control, which generates an inlet guide vane (IGV) position signal as a function of corrected speed. An angular position-measuring device, such as a rotary variable-differential transducer, would measure the actual IGV position and allow the use of a closed-loop system with the position as the closed-loop variable.

On APU shutdown, the first-stage IGVs will go to the full-closed spring-loaded position. On start-up, the vanes will remain in this position until approximately 45-percent corrected speed. At this point, a signal is given to begin modulating the IGVs through the generated schedule toward the full-open position. The IGVs will be in the full-open position by 95-percent speed and will be modulated toward a closed position, as the bleed-flow rate is decreased.

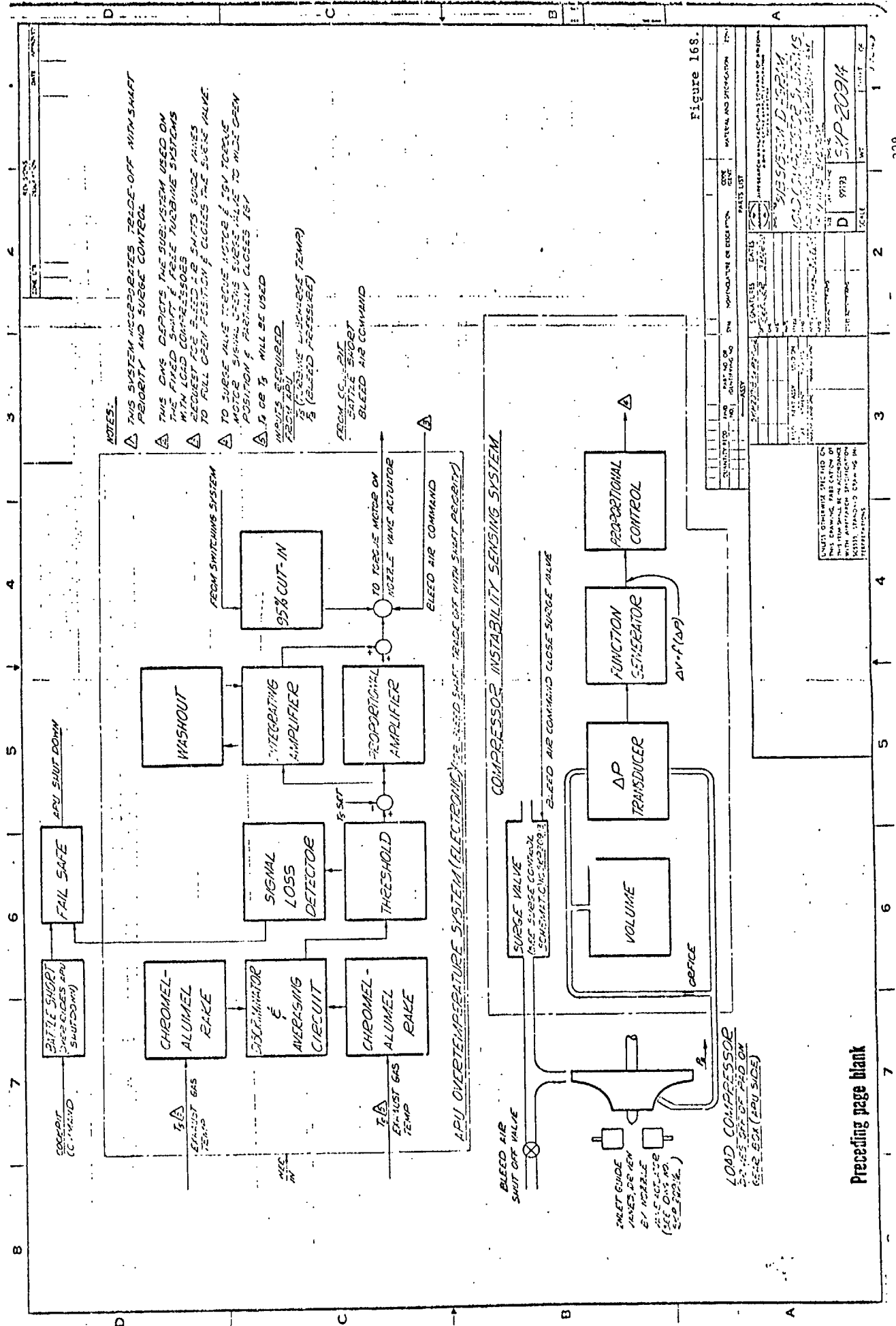
If on-speed surge protection for the integral bleed machines is needed, it will be accomplished by incorporating a boost venturi airflow sensor in the bleed-airflow ducting located downstream from the

surge-valve tee but upstream from the load-control valve. This minimum bleed-flow system restricts the bleed-flow drop to a set value, during on-speed conditions. If the bleed flow is suddenly reduced, the flow sensor reacts to this and, at a predetermined level, opens the surge valve. The surge valve is a servo-operated, pneumatically actuated butterfly valve. It would provide a minimum leakage shutoff during other than low bleed-flow conditions, during on-speed operation.

1.5 Load Compressor Systems

In order to have a trade-off system with shaft priority for APU overtemperature protection while using a load compressor, some method, other than throttling, is necessary to regulate the bleed-flow. Throttling limits the range of flows from 75 to 90 percent of the maximum to avoid surge. Variable inlet or diffuser guide vanes may be used advantageously to modulate the flow. The variable vanes may be closed almost completely, the opening depending upon the airflow required for cooling. Variable diffuser guide vanes have the advantage of modulating the flow with a relatively constant pressure ratio. The variable swirl angle would be insignificant, since there is no need for a constant exit velocity vector profile.

Figure 168 shows the single-shaft or free-turbine load compressor control systems. The surge system, for preventing on-speed surge from a load compressor to supply bleed-air, would use the technique of sensing a sudden drop in the delivered bleed-pressure as an indication of imminent surge. The ΔP -transducer would sense the pressure drop across the orifice and send a signal to the function generator. When the differential voltage signal, which is proportional to the delta-pressure signal, reaches predetermined trip-level, the control sends a signal to the surge valve, causing a wide-open position. Simultaneously, a signal to the inlet guide vanes is received, causing them to close.



The load compressor trade-off overtemperature system is almost identical to that of the integral-bleed. The difference is that the output of the proportional-plus-integral control goes to the guide vane torque motor instead of the load-control valve torque motor.

Systems utilizing a clutch to separate the load compressor from the APU output shaft in lieu of guide vanes were investigated, and it was established that a trade-off system with shaft priority for overtemperature would also be required. The guide vane system would still be necessary.

During APU starting, the load compressor guide vanes would be in a spring-loaded, full-closed position. The surge valve would be spring-loaded to the open position and would close when a bleed-air command was received from the cockpit. The load compressor system would also have to incorporate a bleed-air shut-off valve.

1.6 Gas-Diverting Valve System

Figure 169 shows the gas-diverting valve control system applicable only to a free-turbine APU. Because the requirement for a tight frequency band on the output of the 3-kva electrical generator driven by the gas generator eliminates the normal floating-gas-generator-speed approach to power turbine speed control, the gas-diverting valve is added to the system to dissipate the excess gas from the constant-speed gas generator at low power-turbine demand. In this system, the power turbine speed is sensed and compared to its speed reference. The generated error signal is the input to a proportional-plus-integral control which positions the gas-diverting valve. The correct amount of flow from the gas generator is routed through the power turbine to maintain the proper speed. The excess gas is diverted into the APU tail pipe.

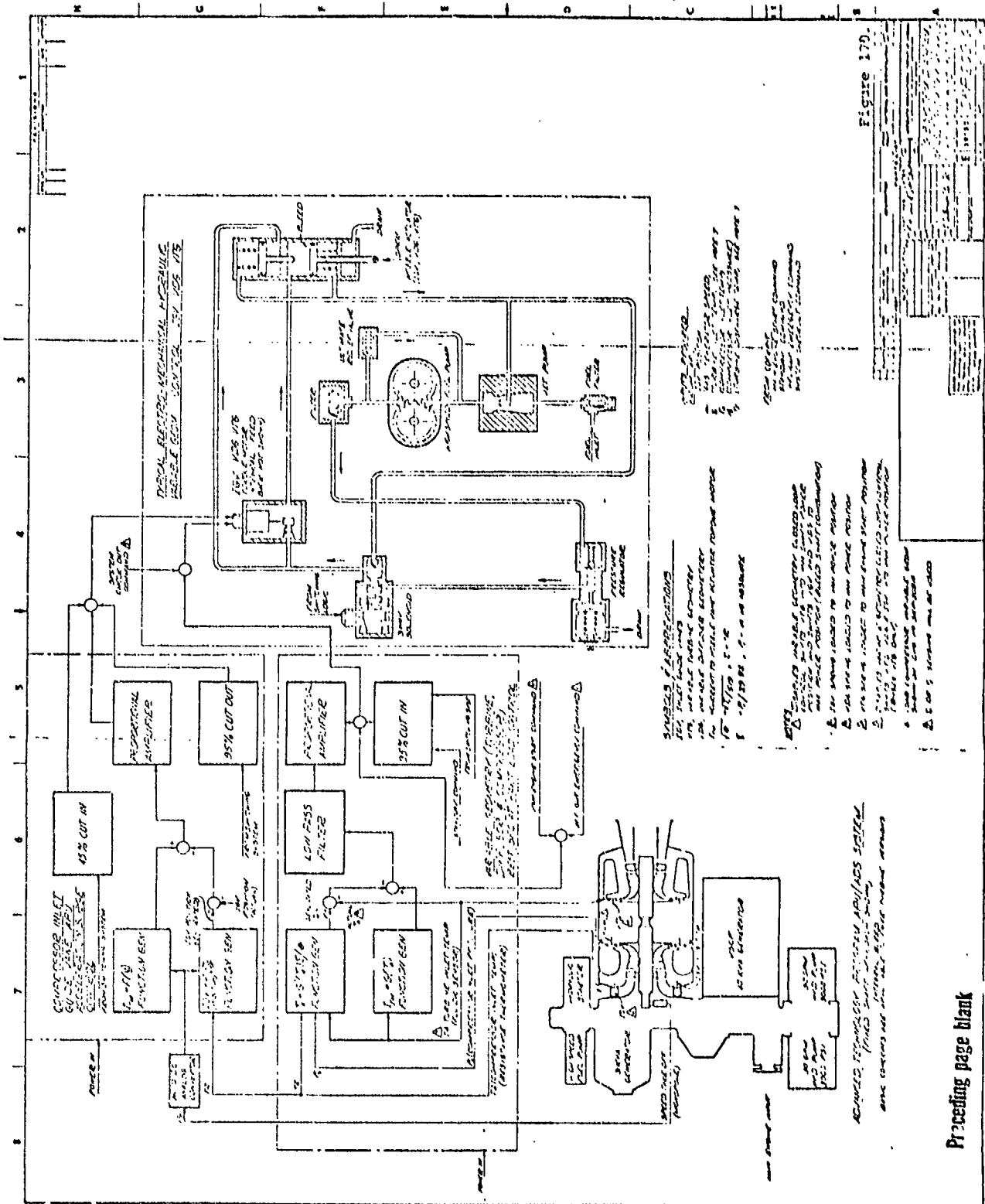
A gas generator speed-override system is added as a soft coupling control for mode transitioning. Very rapid closure of the diverting-valve caused by a system check-out command or a main-engine-start command would result in a drastic droop of gas generator speed. This droop is brought about by imposing a sudden large back-pressure against the gas generator. In order to avoid speed droop, which is not allowable because of the 3-kva electrical generator requirements, the override system is necessary. If the gas generator speed drops below a certain value (i.e., 96 percent), the override prevents the gas-diverting valve from closing and holds its position fixed until the gas generator speed comes back to nominal value. The system logic would send a coupling command to the override network that would warn the system of a need for mode transitioning. This coupling command would then activate the override.

During APU starting, the gas-diverting valve would be biased to the full-open position. The failure mode would be spring-loaded in the closed position, which corresponds to the main-engine starting mode. Because of its proximity to the high-temperature engine plenum, the gas-diverter valve configuration would have to use bellows and pistons instead of diaphragms.

1.7 Variable Geometry Control System

Figure 170 shows the schematic of the variable geometry actuation control system. This control concerns variable compressor geometry (diffuser or IGV) or variable turbine nozzles. The details of operation and function of these control components and their interrelating effects have not been included, since the degree of variable geometry in the single-shaft APU system will be confined to two stages of IGV in the compressor. The drawing, however, includes a control system component schematic and logic diagrams representative of an all-variable system.

Preceding page blank



Preceding page blank

1.8 Oil Hydraulic System

The final APU design incorporates a hydraulic start system. The hydraulic motor receives high-pressure hydraulic fluid from an accumulator. A manually opened, electrically closed valve initiates the APU-start. This system includes a manually operated emergency pump that may be used to recharge the system if it bleeds down while idle. At the termination of starter assist, a speed-sensitive switch activates the hydraulic shut-off valve circuit. The accumulator is refilled from the 3000-psig aircraft system.

The engine decoupler actuator system works in conjunction with the low-pressure gearbox-driven lube pump. A three-way solenoid, spring-loaded to the vent position when de-energized, ports the oil to the shaft coupler. When the solenoid is energized, the coupler is decoupled, thus the coupled position is fail-safe.

The torque converter control system was designed for a fill-and-drain torque converter with a modulated liquid oil level and/or variable reactor vanes to vary its capacity. As shown in Figure 171, the liquid level is sensed, giving a capacity indication. The temperature at the turbine inlet (T_4) or exit (T_5) will be used to control the torque converter capacity, so that the engine cannot be lugged down when a large load requirement tends to overload the engine.

2. APS DEMONSTRATOR CONTROL SYSTEM

The demonstrator APS utilized a predominantly manual control system comprised of modified existing hardware (Figure 172). This was necessary due to the experimental nature of the APS and the lack of accurate performance predictions.

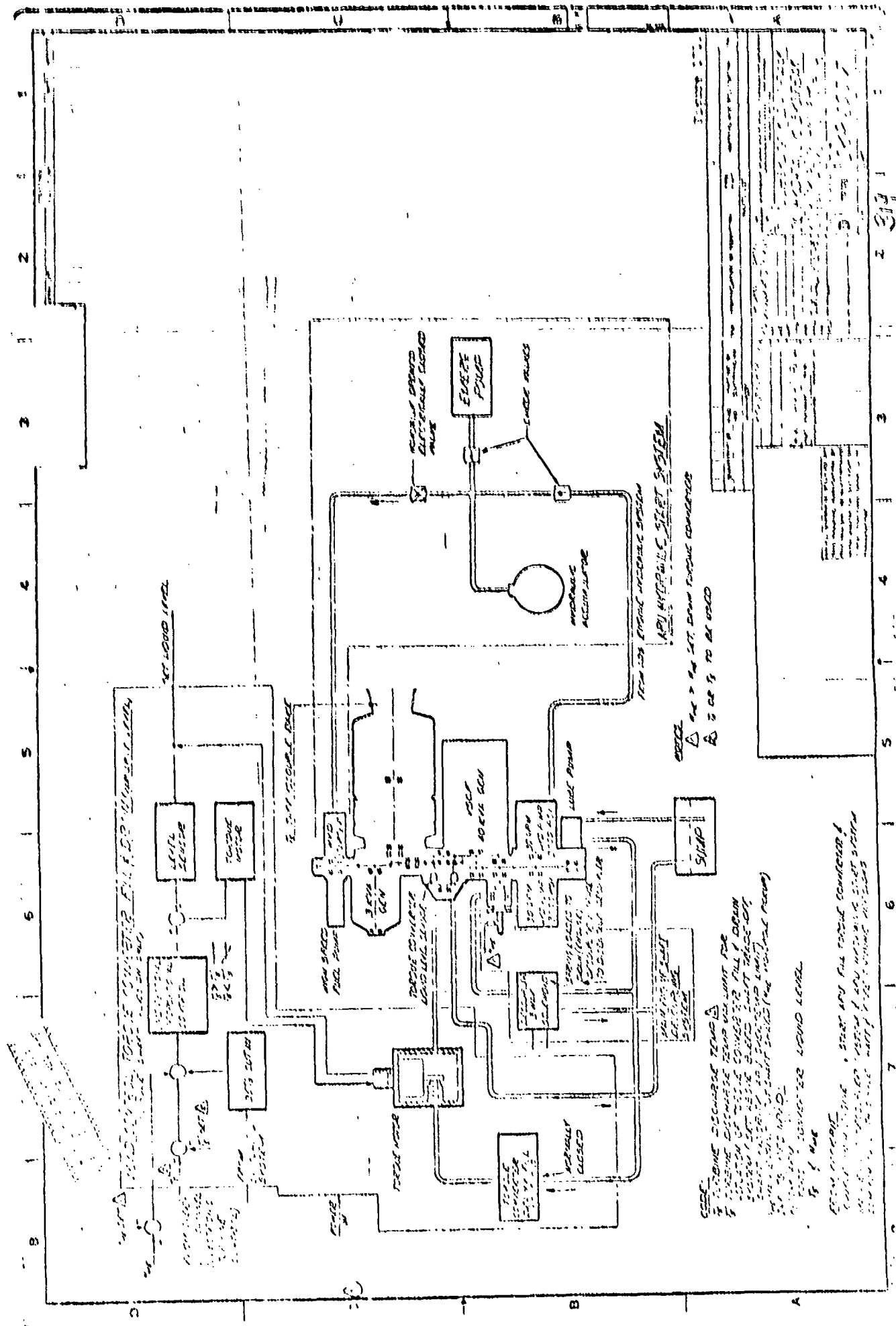
2.1 Control Components

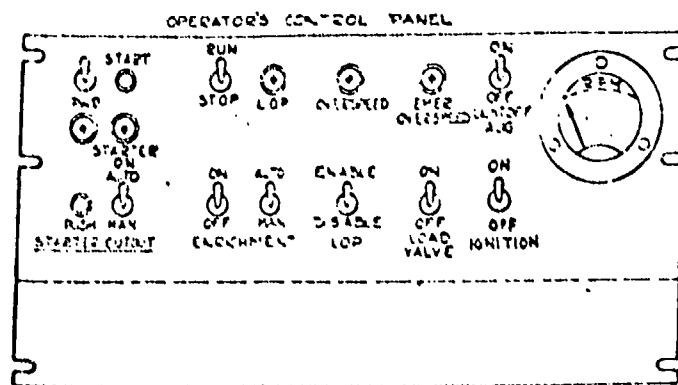
The control system comprises three subsystems: the fuel control, surge and bleed (pneumatic) control, and the electronic control. The components comprising these subsystems and the operation of the system are summarized in the following paragraphs.

2.1.1 Fuel Control

The fuel control consists of six components described briefly as follows:

- (a) Fuel Pump - Constant displacement gear-type. Includes bypass relief valve to prevent overpressure.
- (b) Fuel Filter - Forty micron, full flow.
- (c) Fuel-Scheduling Valve - Meters fuel flow to the fuel nozzles during acceleration. When used in an automatic control system, fuel is metered in proportion to compressor discharge pressure or APU airflow, according to a predetermined fuel-air ratio during start. Direct manual control of fuel flow, obtained by regulating cell air pressure, was used to actuate the valve in place of compressor discharge pressure for the demonstrator APU.
- (d) Mechanical Governor - Flyball-type droop governor to maintain steady-state within a 3-percent speed increment.
- (e) Fuel Solenoid Shutoff Valve - Opens for light-off and closes to shut down the APU.
- (f) Fuel Solenoid Enrichment Valve - Opens at 95-percent governed-speed, creating a new fuel schedule line.





CELL
NEED
VALVE
CONTROL

24VDC
CELL POWER

ELECTRONIC
CONTROL

VOLTAGE
REGULATOR

SPEED
SWITCH

RESTRICTOR

REGULATED
AIR OR GN₂
SUPPLY

AIR
POSITION
CONTROL

CONTROL ROOM

FUEL FILTER

ROTAMETER

FUEL
BOOST
PUMP

RELIEF
VALVE

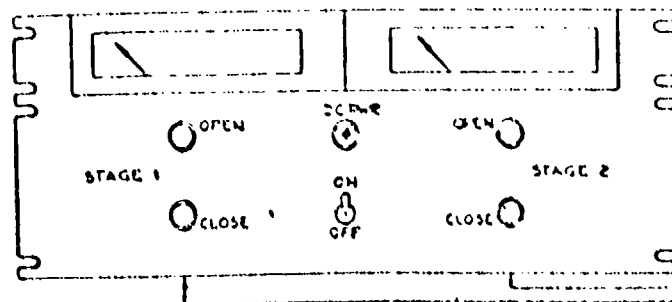
SHUT OFF
VALVE

CELL
FUEL

RESTRICTOR

REGULATED
AIR OR GN₂
SUPPLY

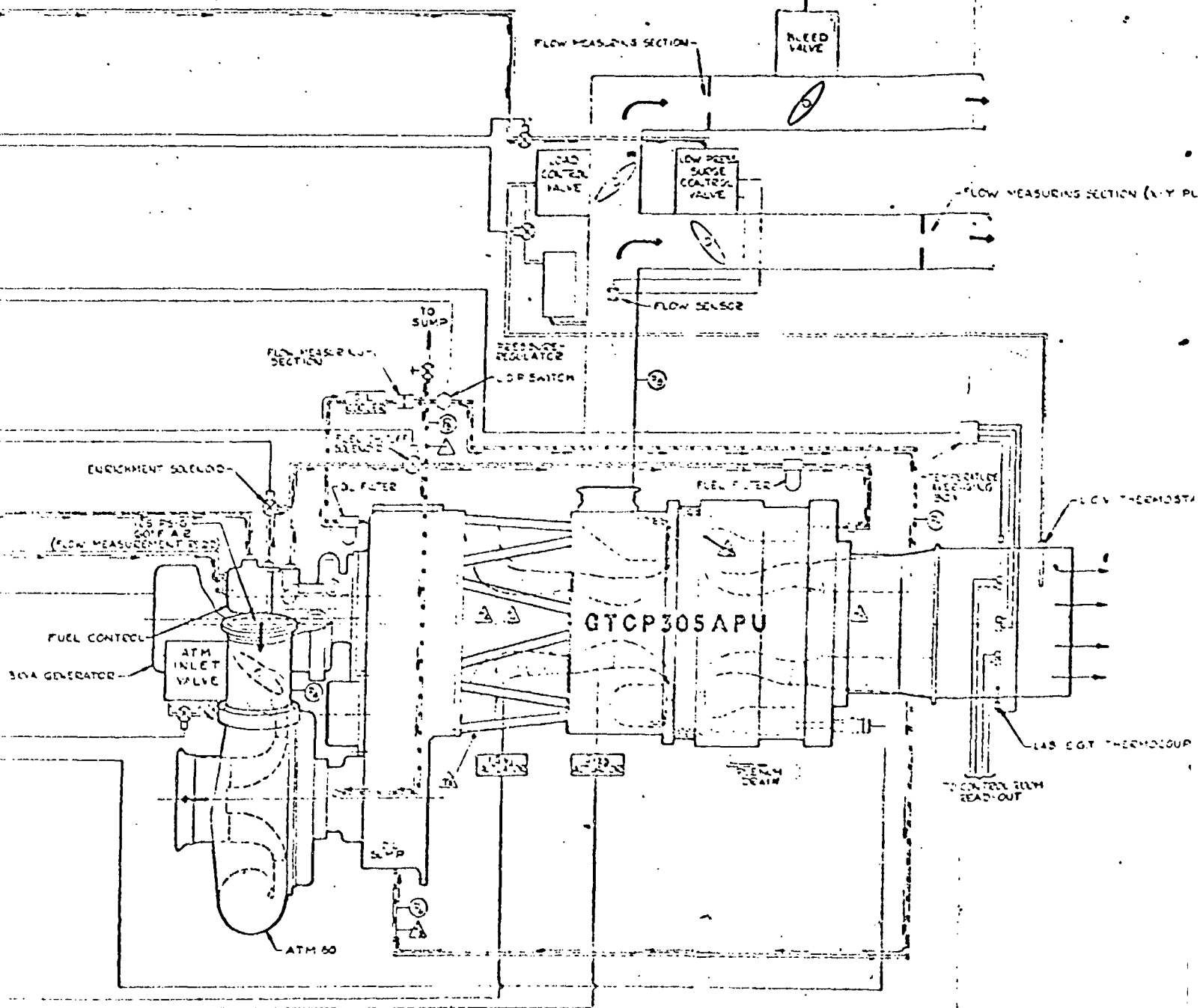
GUIDE VANE CONTROL PANEL



MANUAL
CONTROL

MANUAL
VALVE
CONTROL

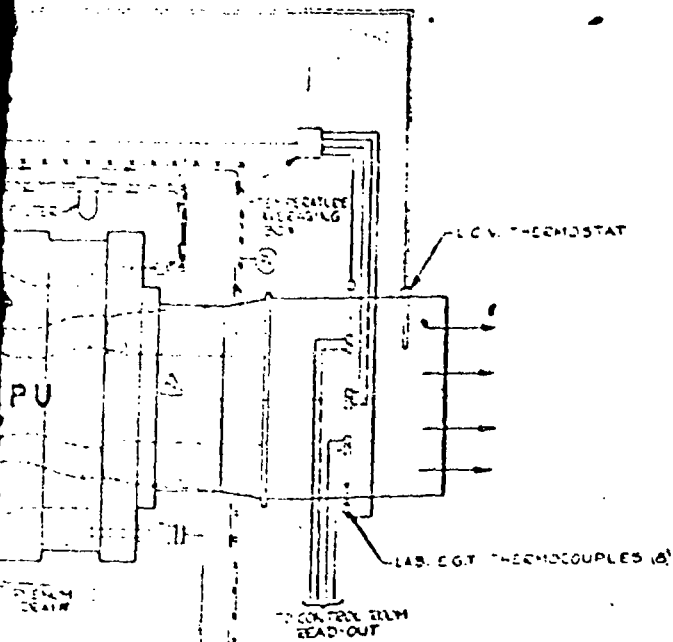
Preceding page blank



PA364824

NEED VALVE

LOW MEASURING SECTION (X-Y PLOTTER)



CONTROL ROOM MOUNTED INSTRUMENTATION		
SYMBOL	PARAMETER	RANGE/UNIT
P ₁	FUEL CONTROL VALVE PRESSURE	0-50 PSIG E11
P ₂	L.P. OIL CONTROL PRESSURE	0-50 PSIG G1
P ₃	FUEL CONTROL DAP-1000 PRESSURE	0-75 PSIG E11
P ₄	ATM. INLET PRESSURE	0-35 PSIG D6
P ₅	LUBE PUMP DISCHARGE PRESSURE	0-40 PSIG F7
P ₆	WATER OIL PRESSURE	0-25 PSIG C7
P ₇	TURBINE BEARING OIL PRESSURE	0-25 PSIG E5
P ₈	NEED PRESSURE	0-40 PSIG F6
T ₁	LUBE PUMP DISCHARGE TEMPERATURE	0-200°F E7
T ₂	WATER OIL TEMPERATURE	0-400°F D7
T ₃	WATER OIL TEMPERATURE	0-200°F C7
T ₄	COMPRESSION BEARING TEMPERATURE	0-200°F E7
T ₅	TURBINE OIL TEMPERATURE	0-250°F E6
T ₆	TURBINE BEARING TEMPERATURE	0-200°F E7
T ₇	TURBINE BEARING TEMPERATURE	0-400°F E5

LEGEND

- AIR LINE
- FUEL LINE
- HIGH PRESSURE LUBE OIL
- LOW PRESSURE LUBE OIL

Reproduced from
best available copy.

Figure 172.

APU DEMONSTRATOR
CONTROL SYSTEM

J11111 PA364024

2.1.2 Pneumatic System

The pneumatic system comprises the surge and bleed control components:

- (a) Low-Pressure Surge Control Valve - For automatic operation, a flow sensor sensing total low-pressure bleed-flow would modulate the surge valve to maintain a minimum bleed to keep the APU compressor out of surge. Since specific surge line data were not available, the surge valve was operated manually, simulating the flow sensor signal from test cell air pressure. The valve normally remained full-open and was modulated only at 100-percent APU speed to reduce bleed-flow. A solenoid in this line opened the surge valve automatically on APU shutdown through the breadboard electronic control.
- (b) Load-Control Valve - This unit was designed to modulate bleed-flow at 100-percent APU speed to maintain a constant exhaust gas temperature. A thermostat in the tail pipe was designed to bleed-off the valve actuation pressure and close the load valve when the thermostat set-point was exceeded. However, during testing of the APU, the thermostat was not connected, keeping the load valve closed. The low-pressure surge valve was used to modulate bleed flow.

2.1.2 Breadboard Electronic Control

The following portions of the electronic control were utilized:

- (a) Variable Light-off Speed Potentiometer - This potentiometer adjustment was used to vary the opening of the fuel solenoid to the selected light-off speed.

- (b) Ignition Circuit - The ignition unit on and off actuation could be initiated manually or at a preselected speed and could be de-activated at 95-percent APU speed.
- (c) PMG Speed Circuit - This circuit was used to indicate APU speed. It also contained 35-, 95-, and 110-percent (over-speed shutdown) speed switch-points. The 35- and 95-percent switch function was normally overridden.
- (d) Emergency Overspeed - This was a 110-percent overspeed circuit connected to a monopole speed sensor, sensing speed from the APU shaft.
- (e) Starter Control - The ATM inlet valve was opened by depressing the start button. Operation was always in the manual mode, and the starter cutout button closed the valve.
- (f) Enrichment Solenoid - Manual operation permitted this solenoid to be opened for operation on the fuel control governor.
- (g) Guide Vane Controls - The first- and second-stage guide vanes were positioned by a manually operated electric motor drive.
- Overtemperature Protection - The electronic control contained an overtemperature shutdown circuit actuated by exhaust gas thermocouples.
- (i) Power Supply - A 24-vdc cell power supply was used to power the breadboard electronic control.

2.2 Control System Operation

The desired light-off speed was selected and the light-off speed potentiometer adjusted to that setting. The light-off fuel flow was selected by an adjustment of the corresponding fuel control air pressure (simulated compressor discharge pressure). The guide vanes were adjusted to the desired settings.

The ATM inlet valve was then opened and the ATM inlet pressure increased until the APU reached light-off speed. The unit was then accelerated to the desired speed by manually varying fuel flow, ATM inlet pressure, surge control valve position, and guide vane position.

The manual fuel control system (Figure 173) allowed adjustment of the fuel control at any speed. The operation of the fuel system is dependent upon the estimated characteristics of the components (Figure 174) and the manner in which they are used as a system. The nominal pump output is always higher than would ever be required. The excess flow is bypassed by the acceleration-scheduling valve as a function of the control air pressure (supplied from a manually controlled, pressure-regulating valve from the test cell air system). This manual method enabled the APU to be run at any speed on the required-to-run line, provided the maximum tail-pipe temperature was not exceeded.

For an automatic control system, as the APU approached governed-speed, the enrichment solenoid valve was opened by a speed switch. The actual delivered limit was reached when the fuel enrichment was activated. As the speed increased, the APU operation entered the droop-governor operating regime, and the governor assumed control. The manually operated demonstration unit was similar, except that no load was reached under manual control before the enrichment valve was opened.

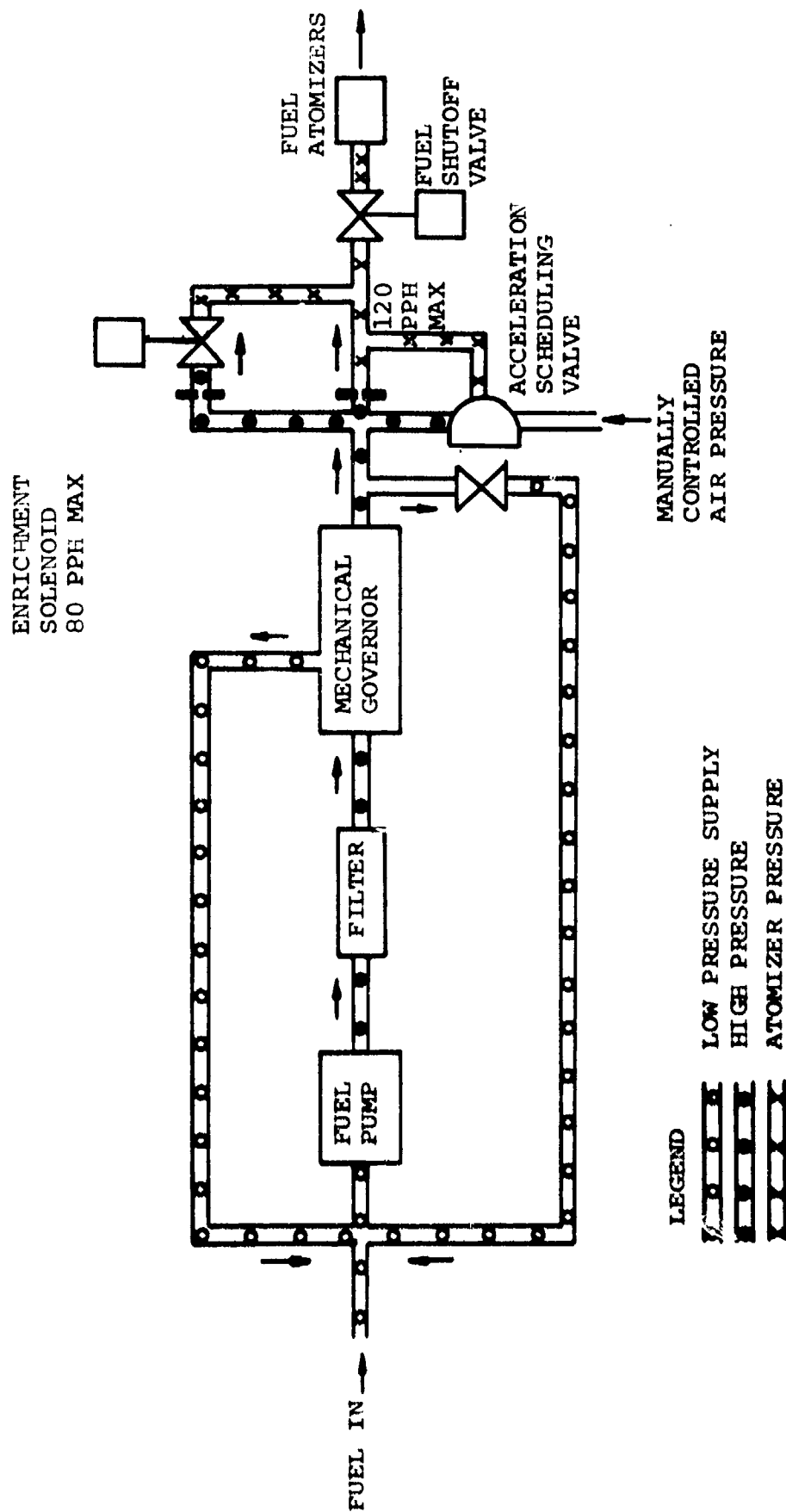


Figure 173. APU Demonstrator Fuel Control System.

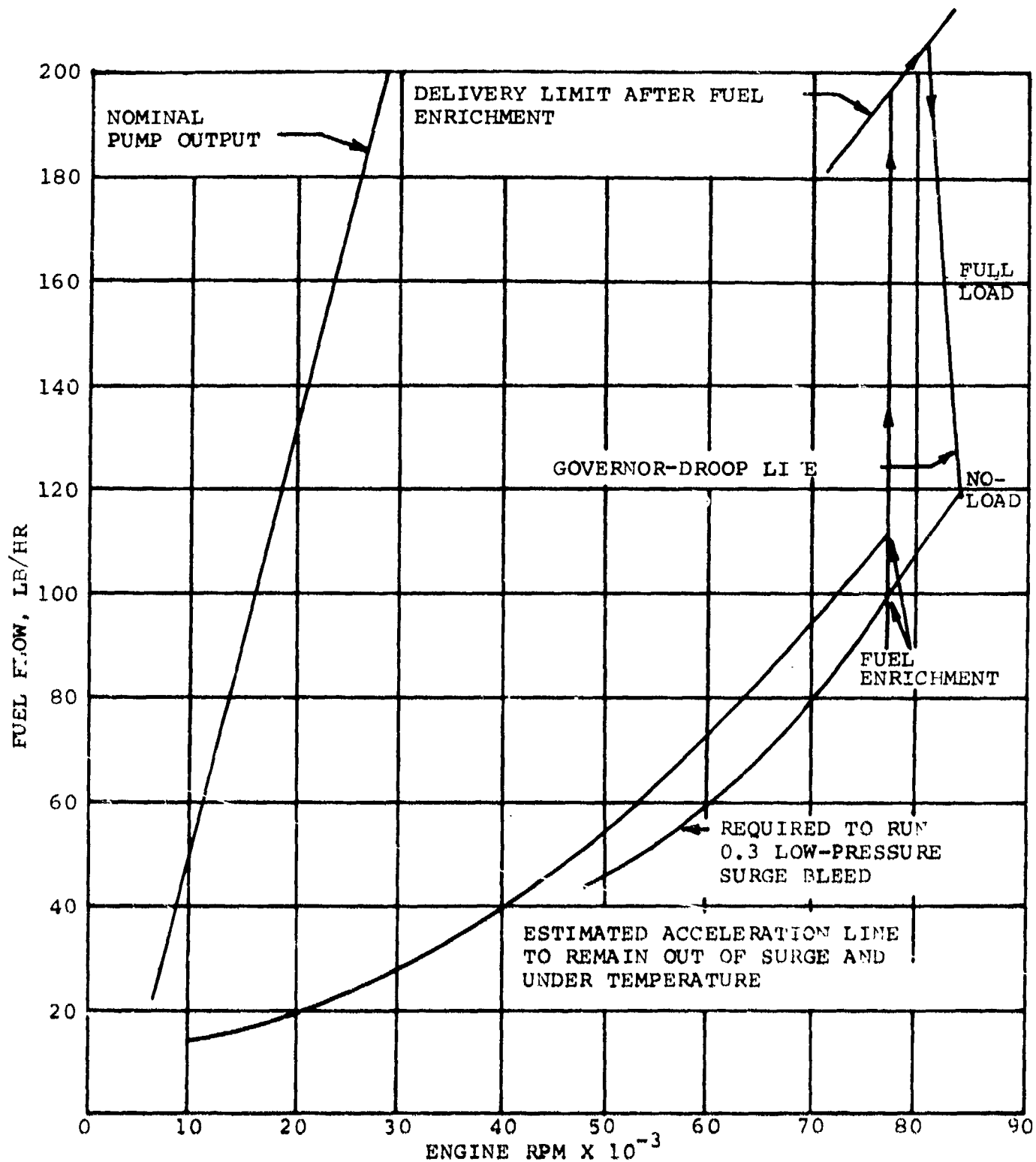


Figure 174. APU Demonstrator, Fuel Control System Characteristics.

SECTION VIII

APU DESIGN ANALYSIS

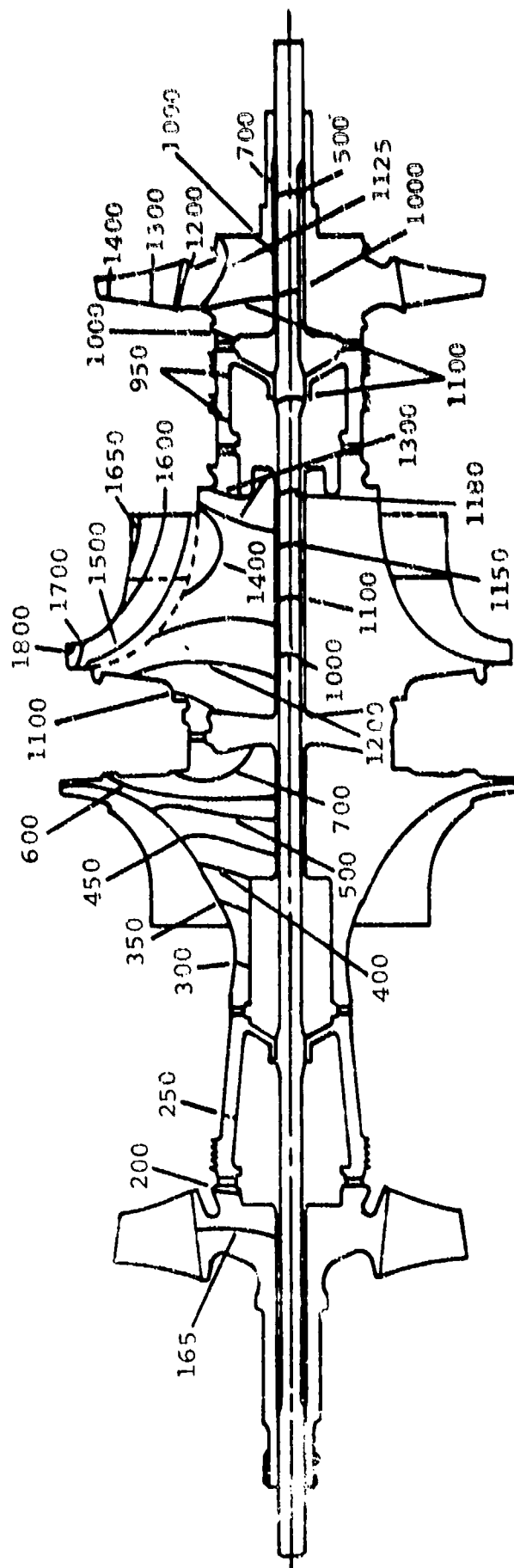
The optimum APU design (used as a test vehicle for technological advancement) was the result of an iterative process directed toward optimizing engine components through a detailed analysis involving thermal, relative displacement, stress, dynamic, test data, and dimensional considerations. The design of the compressor and turbine wheels and their surrounding structure has been discussed in previous sections.

1. THERMAL ANALYSIS OF ROTATING GROUP

The steady-state temperature distribution for the rotating group is shown on Figure 175. These temperatures were computed for a turbine inlet temperature of 2200°F, with cooling flow distributed as follows:

- (a) Film-cooling flow (850°F) on the radial turbine equivalent to 5 percent of the turbine through-flow.
- (b) Two percent cooling (850°F) supplied to the radial turbine wheel back shroud.
- (c) One-half percent (850°F) supplied to buffer the seals between the turbine stages.

Temperatures, compared with the preliminary calculations, have increased in the coupling between the turbine stages approximately 150°F, due to an assumed 200°F increase in air temperature used to buffer the seals. This design assumption, with the change to a hollow-wheel turbine design, caused disk temperatures to rise by approximately 50°F under the blade exducer but did not significantly affect the disk integrity. Reduction of the radial turbine back shroud outer radius



and the resultant removal of cooling in the immediate blade-tip area caused temperatures to increase in the test area.

2. RELATIVE DISPLACEMENT ANALYSES

Relative axial and radial displacement analyses were conducted for engine start-up, steady-state operation, and shutdown. Figure 176 depicts the qualitative relative axial displacement of the seal rotor and housing during an engine cycle.

3. ROTATING GROUP DYNAMIC ANALYSIS

The compressor and turbine rotors are coupled with the central tie-bolt to form a series of masses that respond as an integral assembly. In a turbine engine, this system is supported by bearings, which in turn are supported at engine mount-points through static structure. The bearings and supporting structure add elements of flexibility to the systems.

The flexibly mounted rotating group represents a system capable of several distinct modes of vibration. The most important are:

- (a) The linear mode (cylindrical), corresponding to linear displacement of the mass center in a direction perpendicular to the shaft
- (b) The angular mode (conical), corresponding to an angular displacement of the rotor body with respect to the shaft axis
- (c) The bending mode, corresponding to a bending displacement along the shaft

DISPLACEMENT FROM INSTALLED DIMENSION AT BUILD

SEAL
COMPRESSION

SEAL
RELAXATION

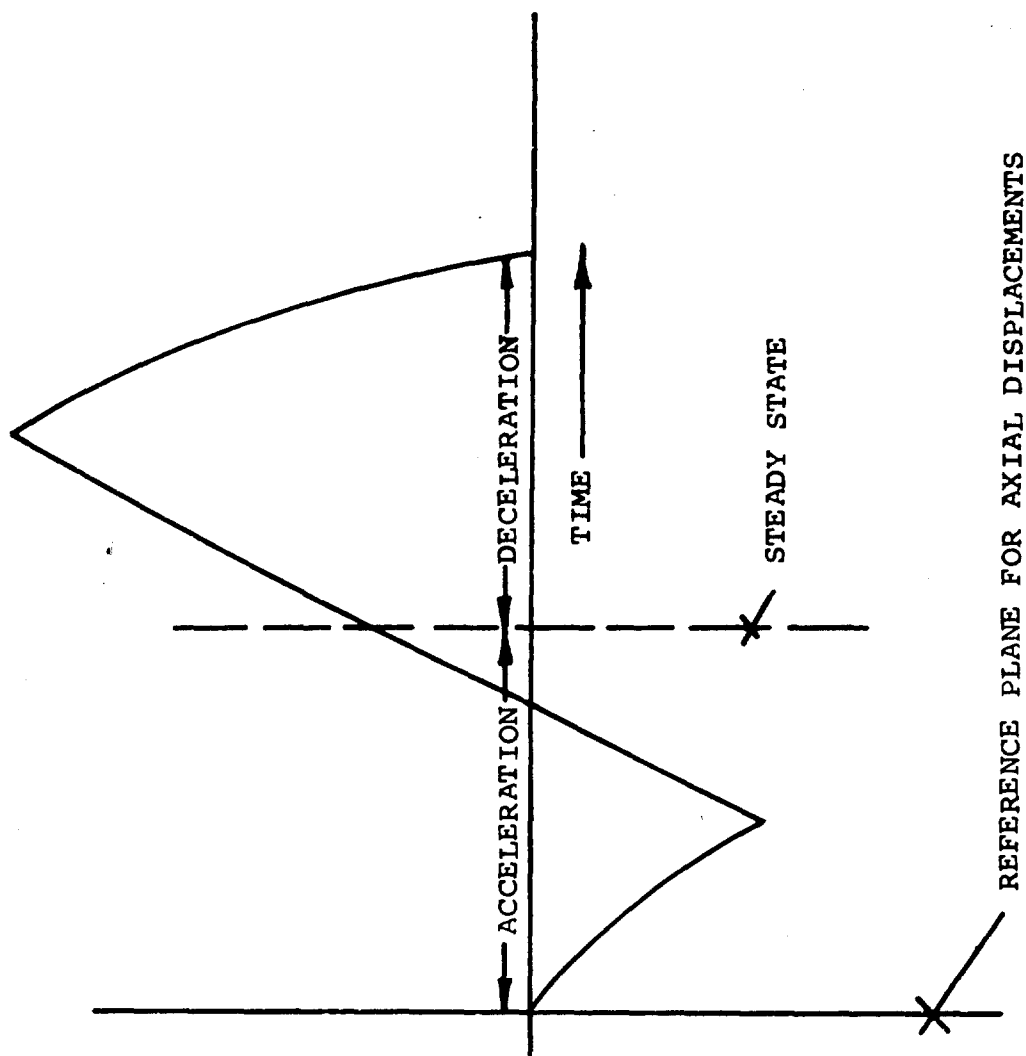


Figure 176. Seal Displacement During Transient Operation.

The spring-mass model, representing the rotor group system, and the results of the dynamic analysis are shown in Figure 177. Spring rates K_1 and K_2 represent the stiffness of the bearings and bearing support structure. In addition, the compressor and turbine end bearings are hydraulically mounted (spring rate varies with speed). Spring rates K_3 , K_5 , K_7 , and K_8 represent the tie-bolt flexibility.

The first, second, and third critical speed points (Figure 177) represent the linear, angular, and first bending modes of vibration, respectively. The rotor system has been designed to operate between the second and third critical speeds with a 70-lb compressor bearing-load and a 20-lb turbine bearing-load. The bearing loads at critical speed points are unrealistically high, as damping is not included in the analysis. The squeeze-film action at the bearings sufficiently damps the rotor vibration at the critical speeds and at operating speed for smooth running.

4. ROTATING GROUP TIE-BOLT

The rotating group of the APU is formed by the coupled turbine and compressor rotor sections locked together with a central tie-bolt, which is designed to maintain rotor group integrity, i.e., prevent separation at the curvic coupling joints throughout the life of the engine. The factors which tend to cause separation at the curvic coupling are:

- (a) Dynamic unbalance of the rotor
- (b) Differential thermal expansion of the rotor and tie-bolt
(both transient and steady-state)
- (c) Poisson's contraction of the disk due to tangential and radial disk stresses

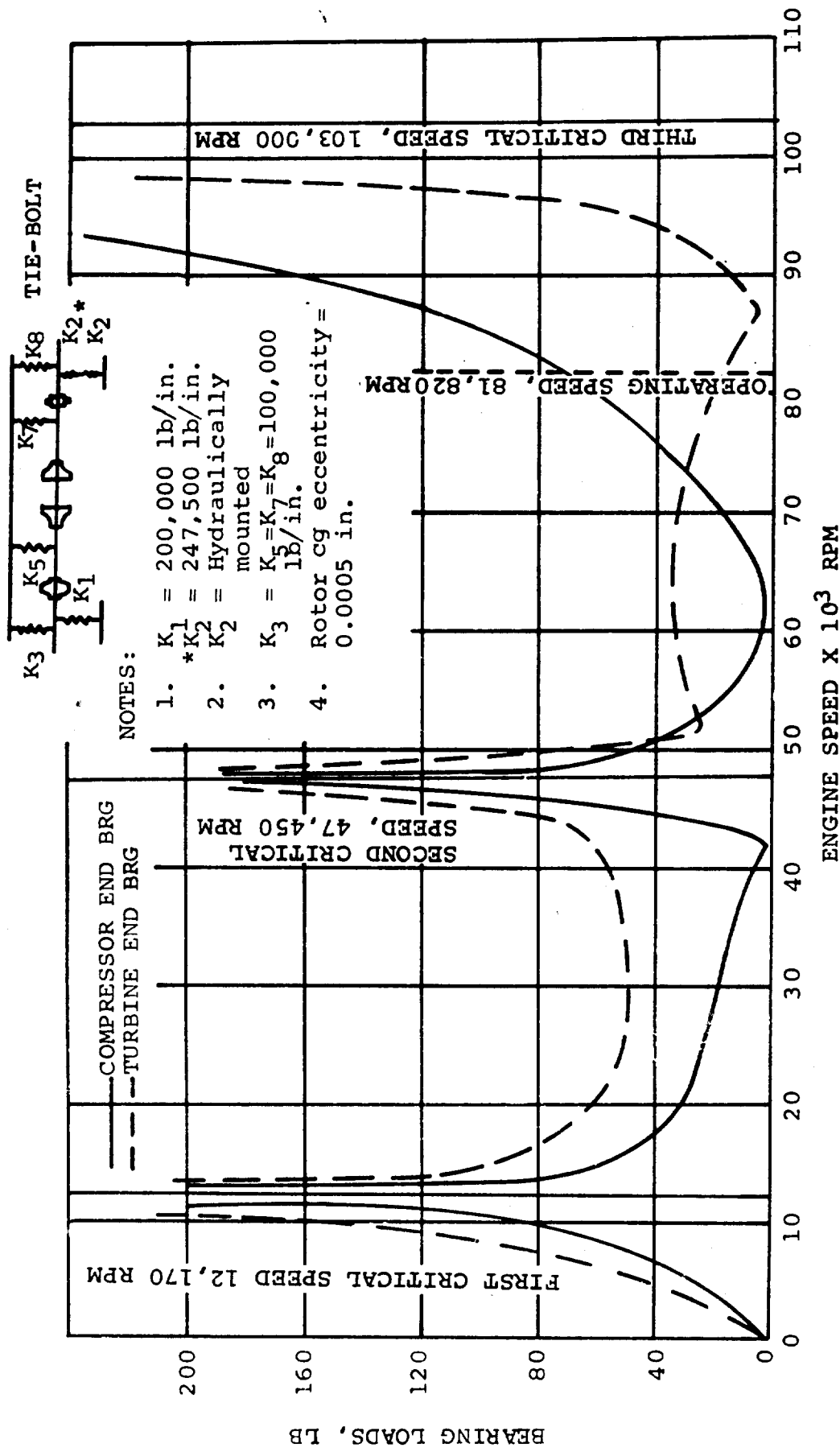


Figure 177. Bearing Loads vs Engine Speed.

- (d) Pressure forces on the face of the rotor disks and blading
- (e) Transmission of transient and steady-state torque through curvic couplings

Tie-bolt preload is normally selected in the following manner:

- (a) The worst combination of transient and steady-state conditions is determined from the separating factors listed above.
- (b) The preload is selected so that a minimum margin of 20-percent load exists above the maximum separating load.
- (c) With the preload selected, the tie-bolt stress range is defined by the following criteria:
 - (1) Tie-bolt stress range must not exceed the low-cycle fatigue strength of the material for the engine design-life.
 - (2) The steady-state stress at various operating conditions must not result in a relaxation of tie-bolt load exceeding 5 percent over the full design-life.
 - (3) The maximum steady-state stress in the tie-bolt under any condition must not exceed 80 percent of the ultimate tensile strength of the material.

During the design phase, two engine configurations were investigated. One has a central hole in the radial turbine wheel, with the tie-bolt running the length of the engine (Figure 178). The second configuration has a solid radial turbine wheel with two tie-bolts inertially welded to the wheel (Figure 179).

The configurations discussed in the following paragraph were analyzed according to the above design criteria. Although the test strengths of the welds exceeded the maximum design requirement, the engine was ultimately designed using a tie-bolt and curvic coupling, since this is a proven method with a high reliability. For the single-bolt design, an initial load of 12,000 lb is expected to maintain rotor integrity while meeting the design requirements.

4.1 Hollow Radial Turbine Tie-Bolt Configuration

Limiting values for the hollow radial turbine tie-bolt configuration are:

- (a) Low-cycle fatigue strength for 1500 cycles at 1200°F, 150,000 psi stress range (Figure 180)
- (b) Initial steady-state tie-bolt load, resulting in 5.0-percent load relaxation, 8900 lb
- (c) Eighty percent of ultimate tensile strength (based on Inconel 718 specification minimums), 148,000 psi at room temperature, 116,000 psi at 1200°F

The ultimate strength requirement at room temperature is the limiting value and sets the initial bolt load at 12,000 lb for the 0.322- to 0.325-in.-diam bolt. The resulting steady-state operating load for this initial value is estimated as 8100 lb and the maximum stress range as 148,000 psi. For a 12,000-lb preload, a separating moment during the second critical speed of 8.0 times the steady-state operating moment (based on rotating group cg eccentricities of 0.0005 in.) can probably be tolerated. The calculated tie-bolt load relaxation characteristics are shown in Figure 181.

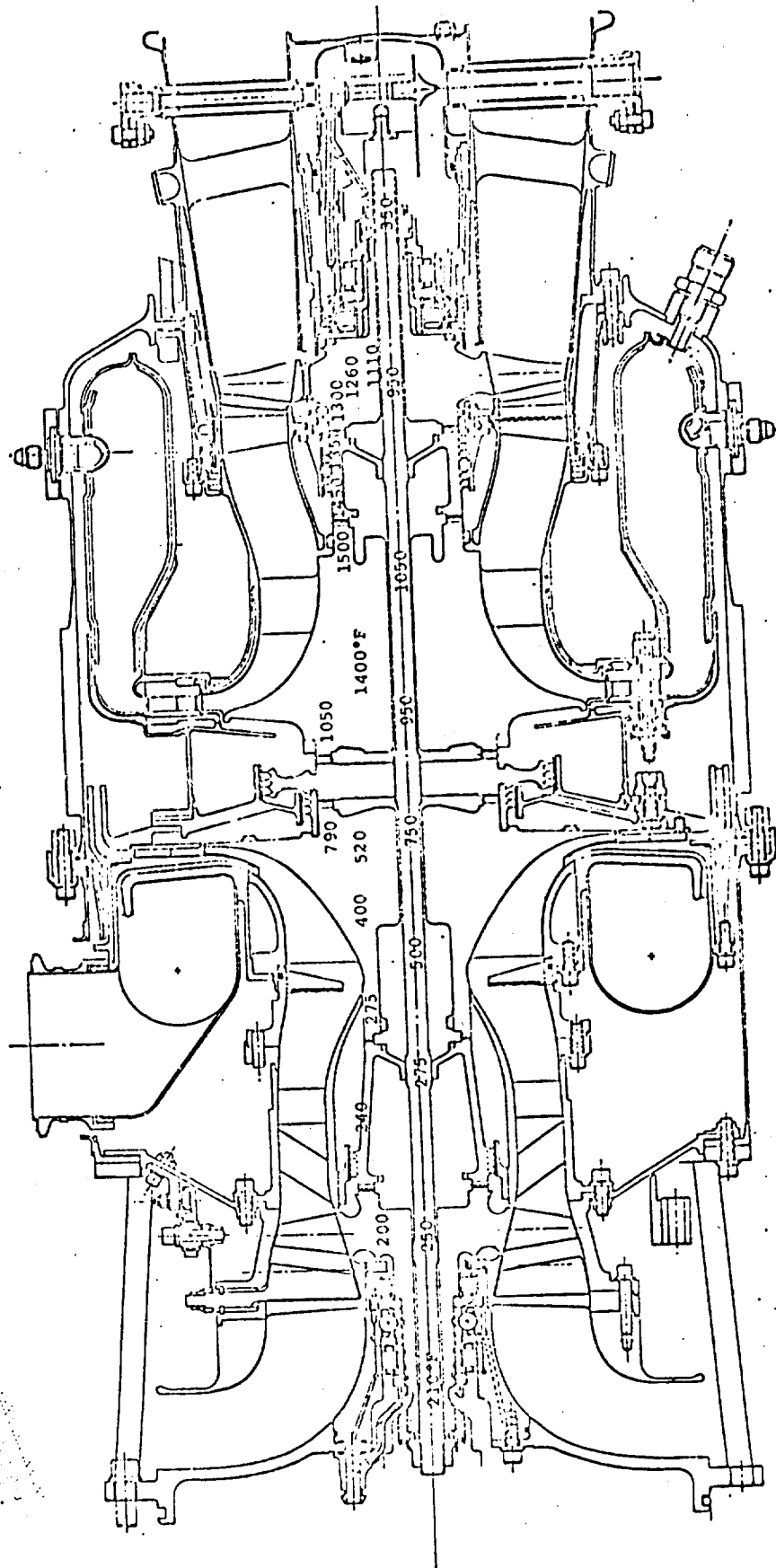


Figure 178. Hollow Radial Turbine Configuration, APU Temperature Distribution.

REPRODUCTION OF
 ORIGINAL DRAWING
 BY THE NATIONAL
 ARCHIVES

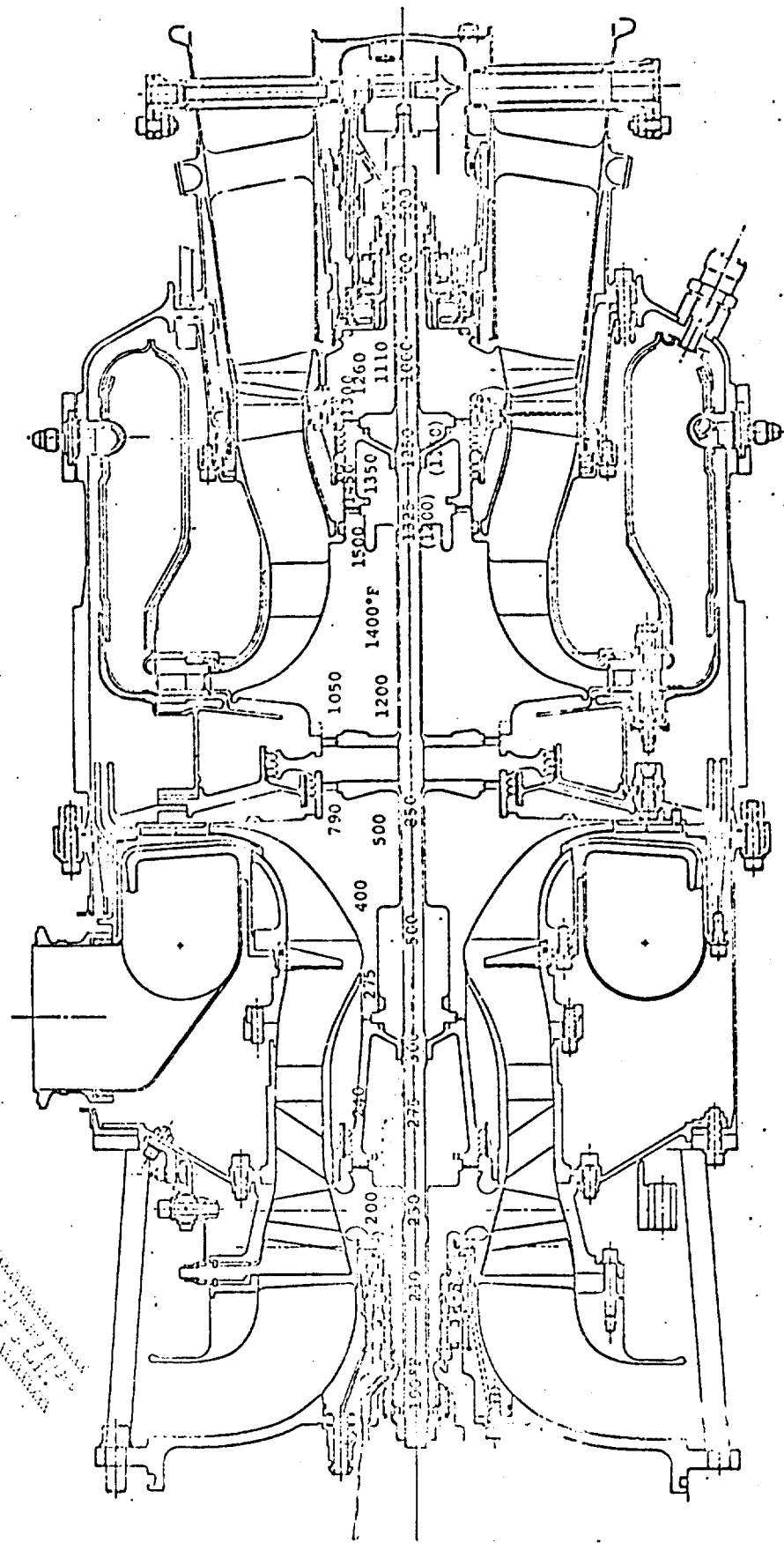
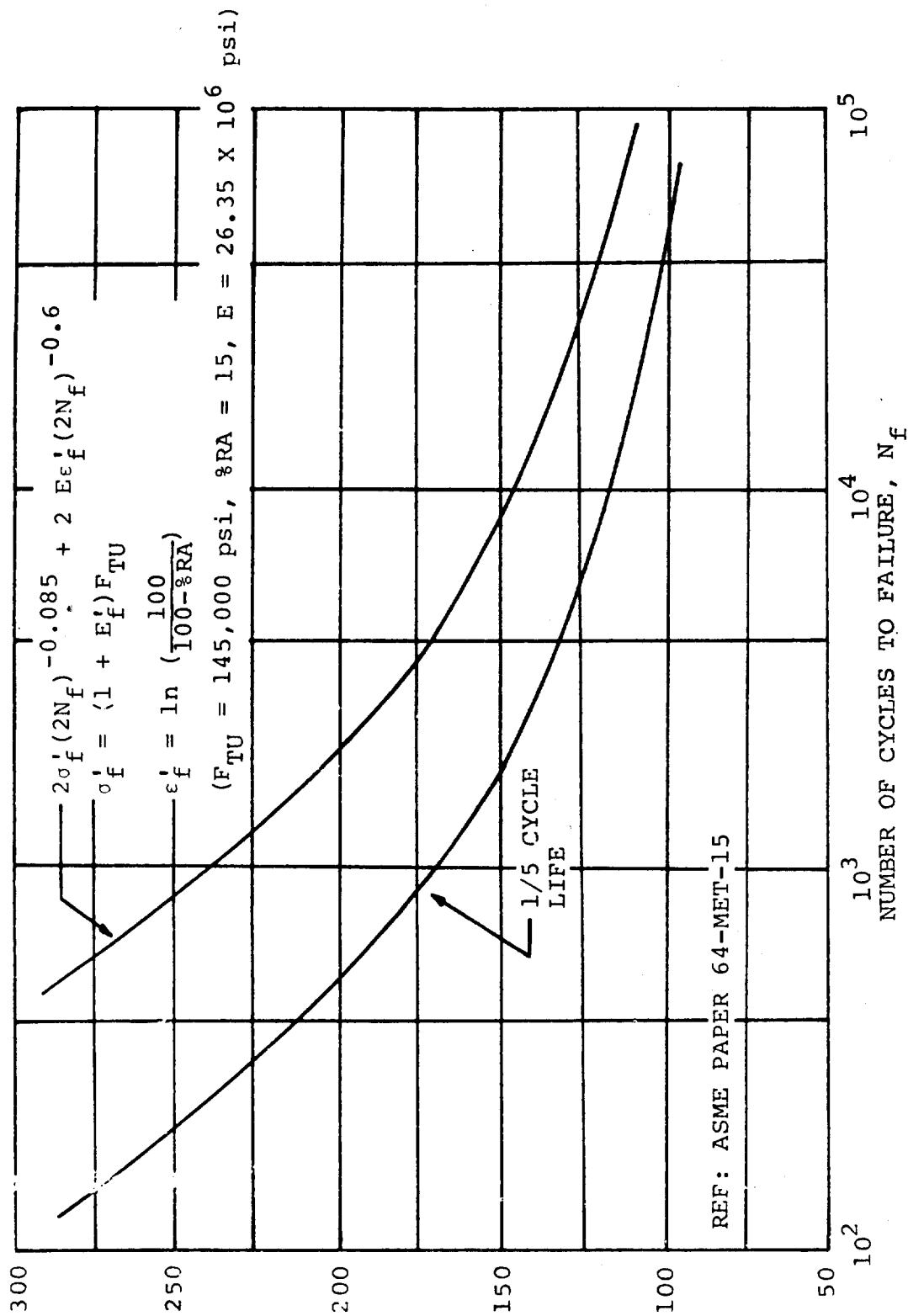


Figure 179. Solid Radial Turbine Configuration, APU Temperature Distribution.



NOTE: Current design practice is to use 1/5 the calculated cycle-life to account for scatter in the data.

Figure 180. Low-Cycle Fatigue for Inconel 718 at 1200°F.

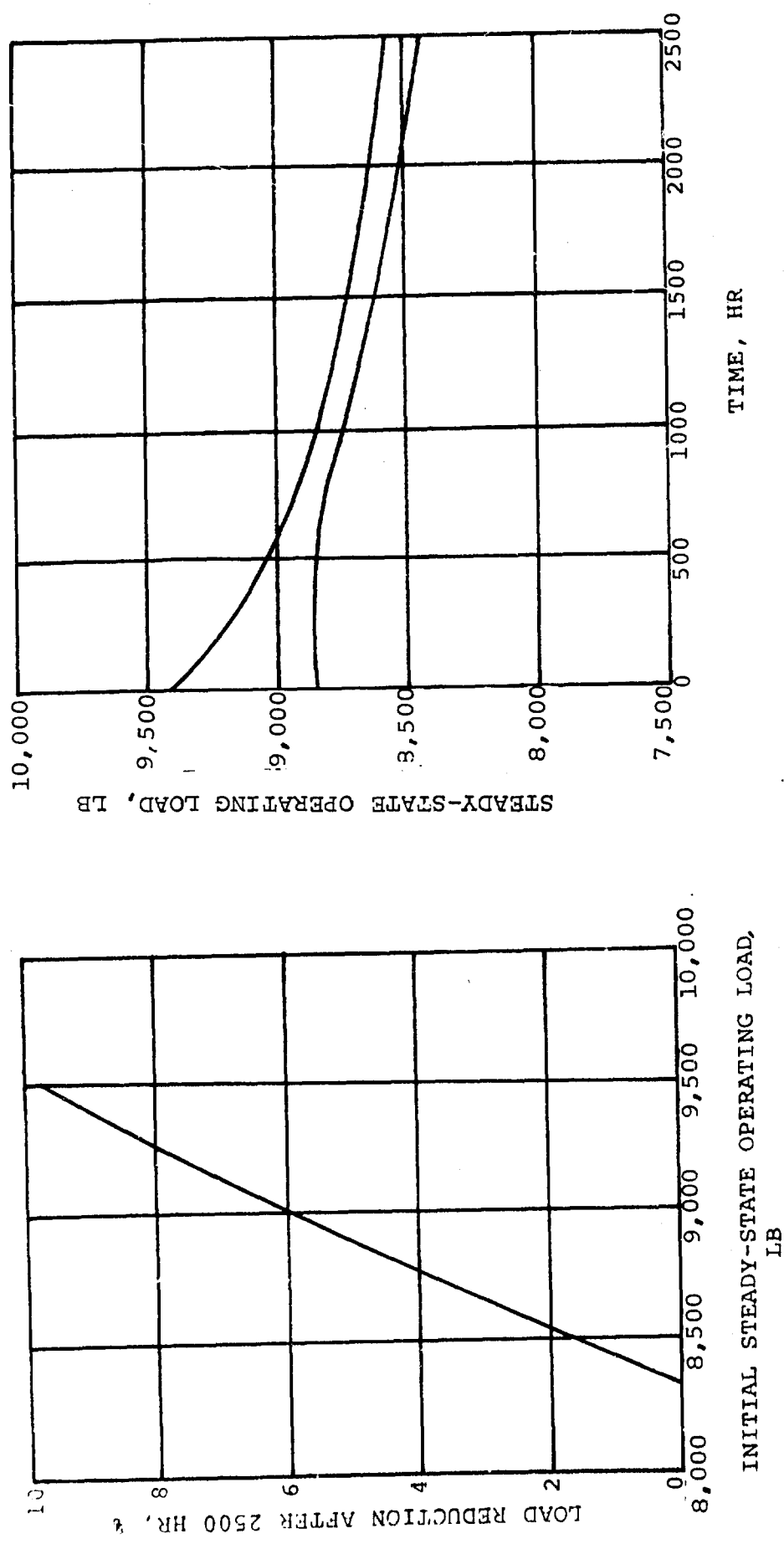


Figure 181. Tie-Bolt Load Relaxation, Hollow Radial Turbine Configuration.

Steady-state thermal expansion values were based on the calculated temperature distribution (Figure 178). Since the effect of film cooling on radial turbine disk temperature has not been determined experimentally nor has there been a computation technique designed, no cooling was included in computing the temperatures. Effects of cooling air on the coupling between the turbine stages and the axial turbine wheel have also been omitted. These elements will probably reduce the steady-state operating load by a 15-percent maximum.

4.2 Solid Radial Turbine Tie-Bolt Configuration

The analyses revealed two problem areas in the solid radial turbine tie-bolt configuration, both with the turbine end of the tie-bolt. The first problem (Figure 182) is that when a cold-engine start is made, the axial turbine and coupling heat much more rapidly than the tie-bolt. Thermal expansion of these components, while the bolt is cool, increases the tie-bolt stress. Assuming the worst-case, when the turbine and coupling reach steady-state before the tie-bolt makes any response, the initial tie-bolt stress would be increased by 261,000 psi (based on elastic calculation). This stress increase, combined with the decrease from initial stress at steady-state, gives a bolt-stress range of 295,000 psi, as compared to a 1500-cycle fatigue strength of 150,000 psi for Inconel 718.

In reality, the stress-range would not reach this maximum value because the tie-bolt will react thermally to a small degree, while the turbine and coupling are responding. However, the stress range will probably not be less than 150,000 psi, since this would require the tie-bolt to react at least half as fast as the rotor components. This will not happen if the thermal response shown in Figure 182 is correct. A second factor that would increase the fatigue-life is that all engine starts will not be made from a cold condition. The number of cold-engine starts is, however, not defined, so the analysis must be based on the conservative assumption that all starts will be cold.

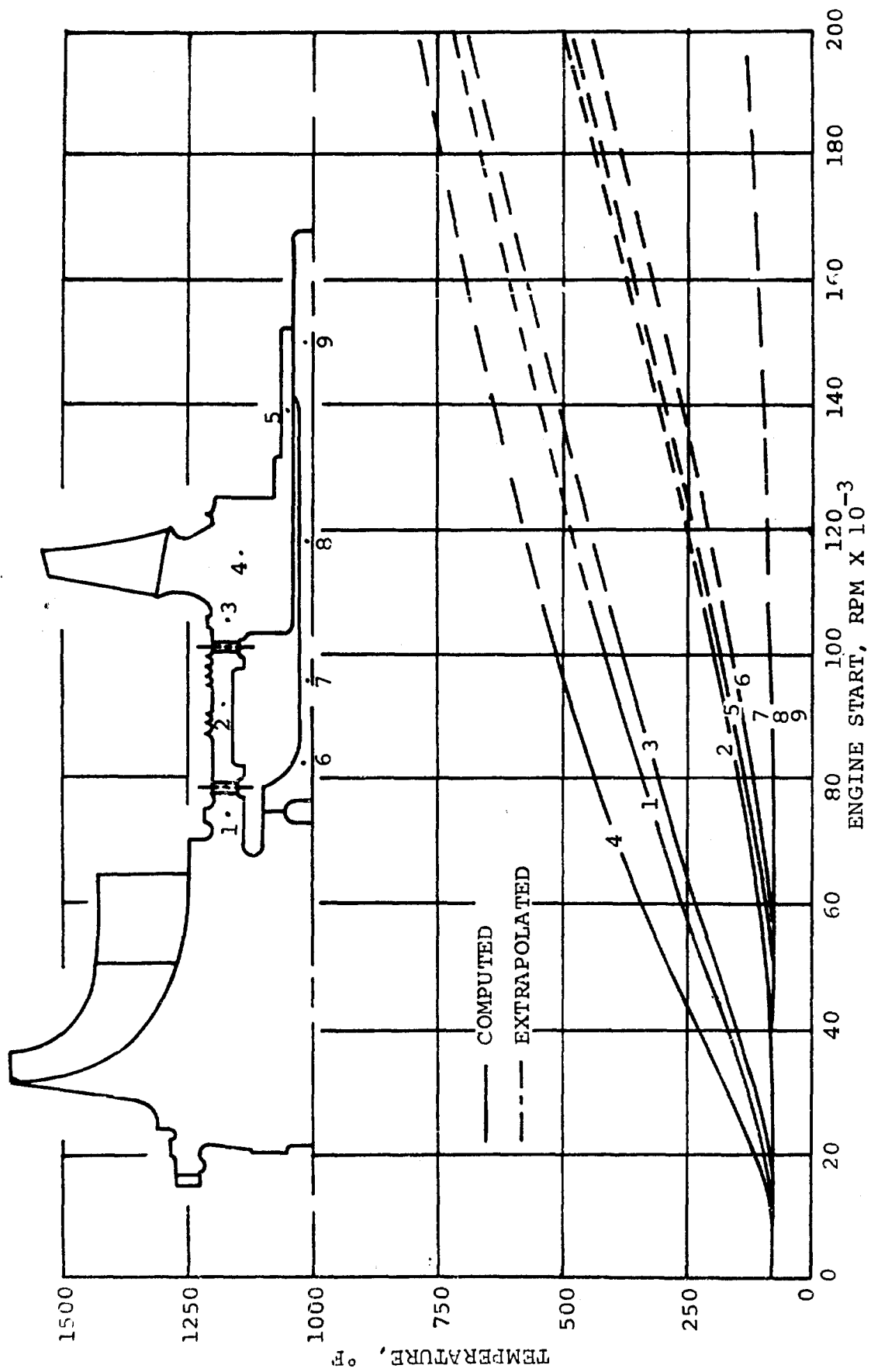


Figure 182. Turbine Transient Temperature Response.

The second turbine end tie-bolt problem is load relaxation. The maximum allowable initial load for 5-percent load relaxation is 8775 lb. With this, the resulting steady-state operating load is 6000 lb or enough to resist 6.0 times the steady-state bending moment (based on rotating group cg eccentricities of 0.0005 in.). It is doubtful if this load would maintain rotor integrity. (The stress required to produce 5-percent load relaxation was based on the tie-bolt temperatures shown in Figure 178, because the majority of operating time occurs at turbine inlet temperatures around 1900°F.) Relaxation characteristics of both turbine and compressor end tie-bolts are shown in Figure 183.

5. BEARING SYSTEM

5.1 APU Main Shaft

A three-bearing mounting system was used for the APU main shaft, with a ball and roller bearing combination at the compressor end and a single roller bearing at the turbine end. This type of mounting was used instead of the simpler two-bearing system, because high dynamic loads at the compressor end caused by shaft imbalance would have resulted in very short ball-bearing life.

All three bearings are 104-size (20-mm bore, 43-mm OD, and 12-mm wide) and at 82,000 rpm operate at 1.64×10^6 DN. At this high speed, cooling the bearing is extremely critical; therefore, the lubrication system was designed to provide oil-flow first to the bearing ID to cool the inner race and then radially outward through holes in the bearing inner rings to lubricate the bearings.

The bearing system functioned reliably throughout the program, with no catastrophic failures. Two problems were noted: the lubrication of the turbine end roller bearing was inadequate in early test unit builds, and the compressor-end bearings ran excessively hot. The

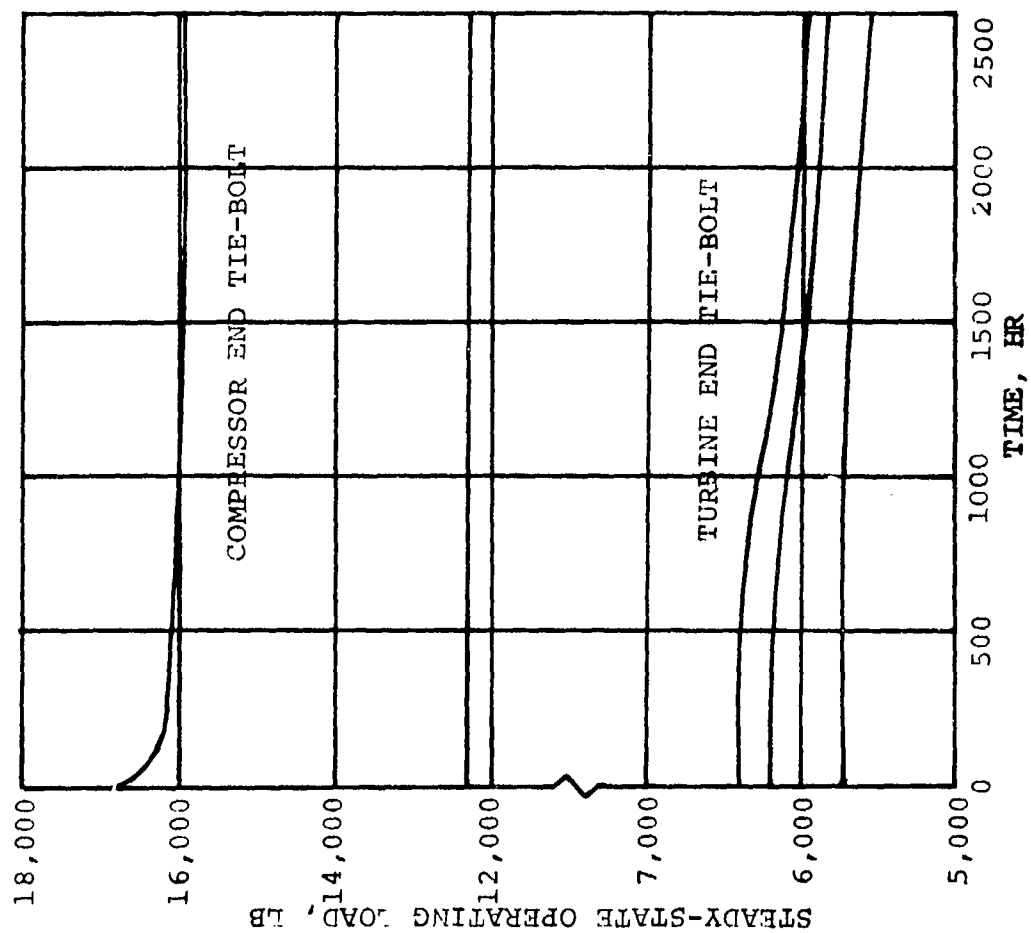
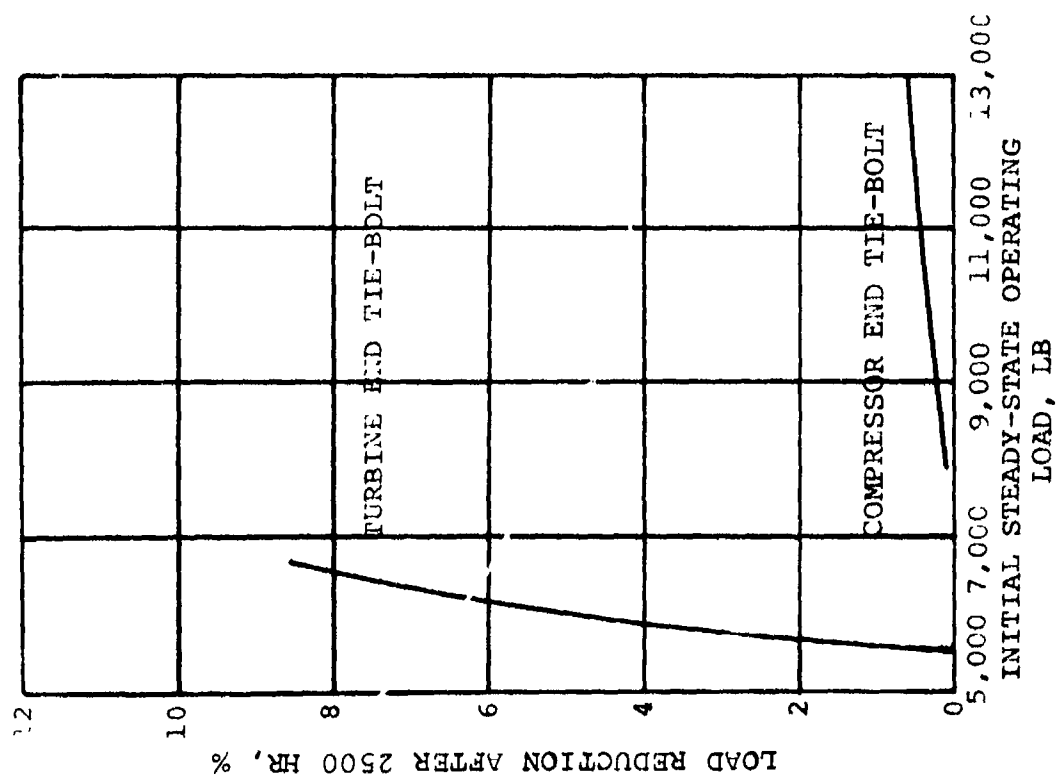


Figure 183. Tie-Bolt Load Relaxation Solid Radial Turbine.

lubrication of the turbine-end bearing was improved by more accurately locating the oil jet.

High bearing temperatures at the compressor end have not yet been resolved. Apparently, they were due to lubricant being churned by the slinger between the two bearings and by an excessively high face seal load. The slinger was removed in Build 5, and the face seal load reduced. Although compressor bearing temperatures decreased, further reductions will be necessary. Further test evaluation of variation effects in lubricant flow rate and increased bearing cavity drainage was expected to result in reduced bearing temperatures.

Prior to Build 5, a bearing test rig (Figure 184) was designed and built to verify that the changes incorporated into the hardware, subsequent to Build 4 testing, would result in a lower compressor bearing temperature. Figure 185 compares the results of the rig testing to that of Build 4. A significant decrease in bearing temperature is shown.

5.2 Accessory Drive Gearbox

The bearings in the accessory drive gearbox were designed to achieve a B_1 fatigue life of 2000 hr at maximum speed and load.

The operating speeds of most of the bearings were well within normal gearbox ranges. The high-speed pinion bearings, however, are required to run at a main-shaft speed of 82,000 rpm. This is equivalent to 1.64×10^6 DN in the 1904-size (20-mm bore, 37-mm OD, 9-mm wide) bearings used. As on the main shaft, cooling the high-speed pinion bearings was extremely critical. Adequate bearing cooling and lubrication was provided by a positive impingement jet on each bearing combined with oil jetted into the shaft ID. The adequacy of this system was proven by reliable operation of these bearings in the test unit.

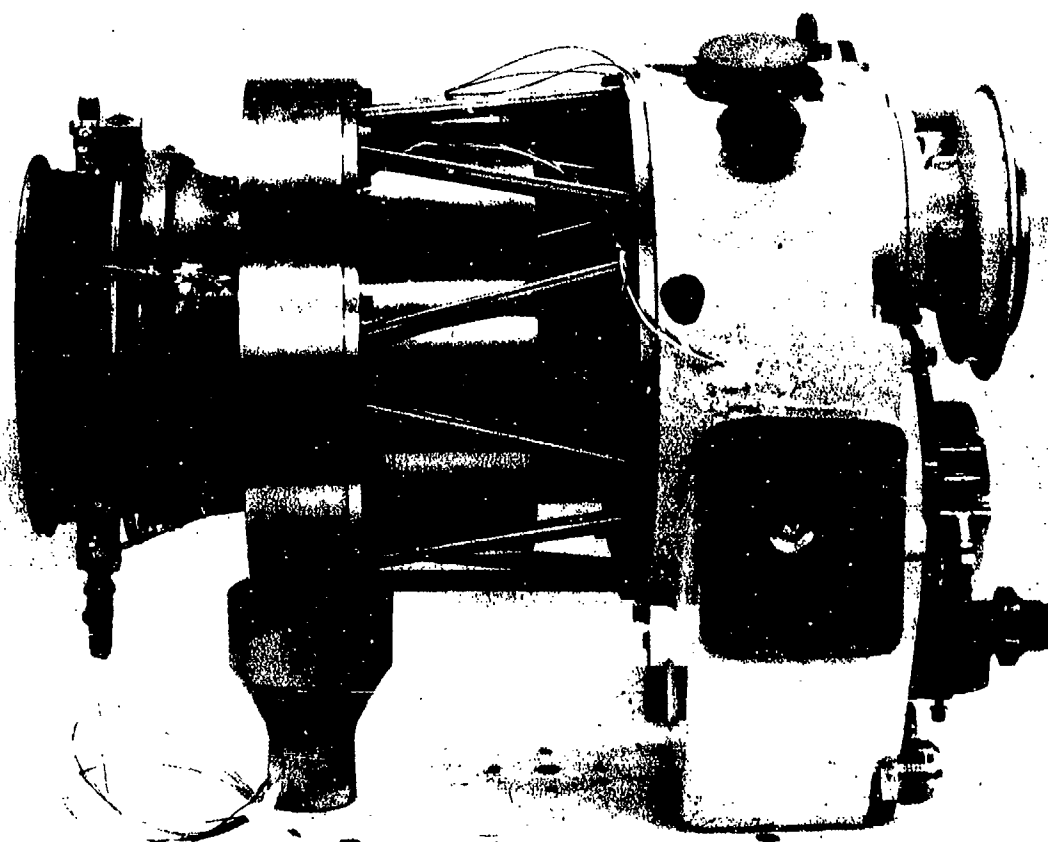
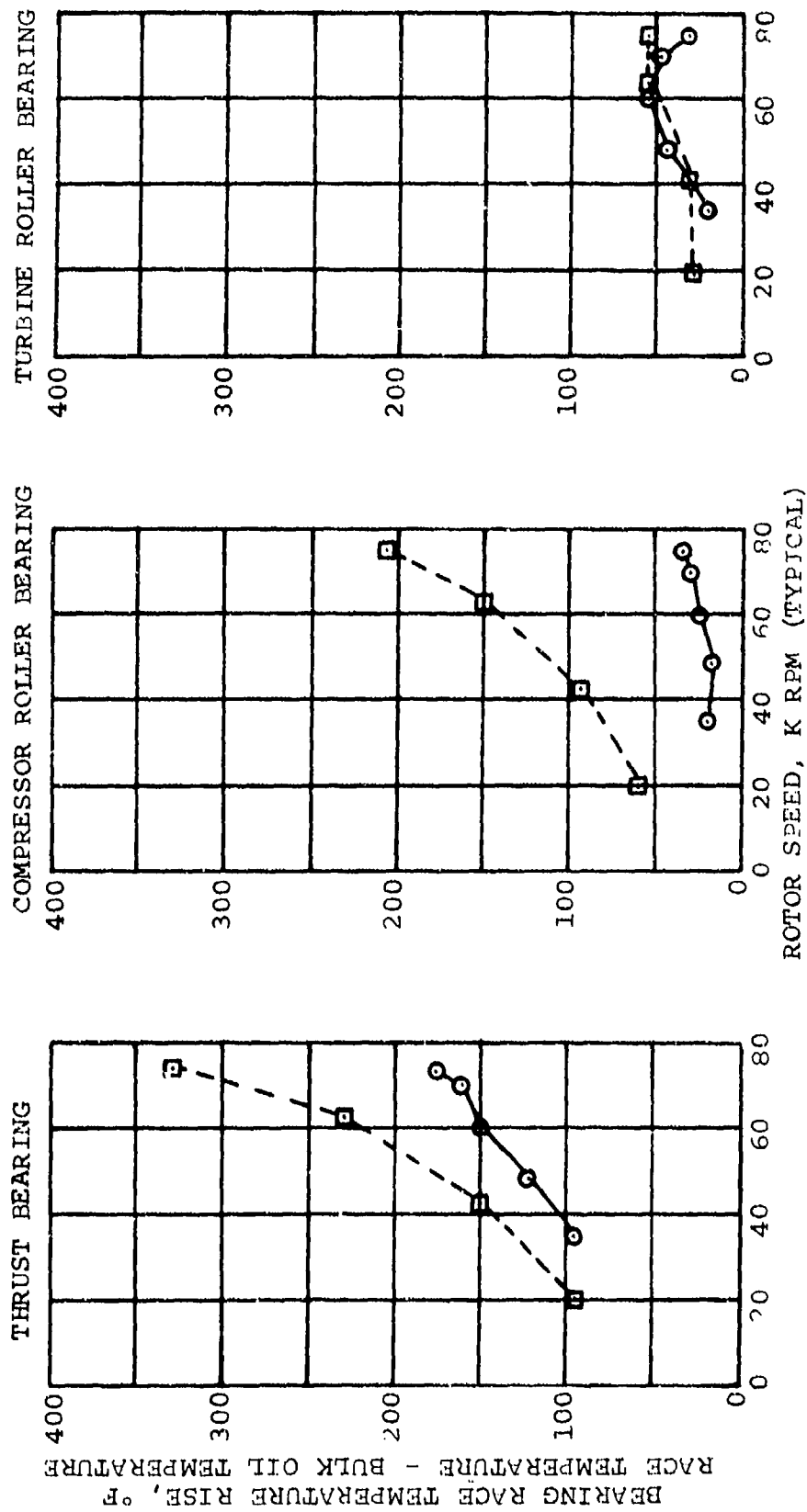


Figure 184. Bearing Test Rig.



□ BUILD 4 ENGINE TEST
 ○ BEARING RIG TEST AND
 MOTORING CHECK-OUT

Figure 185. Comparison of Bearing Rig Tests and APU Tests.

6. SEALS

6.1 Compressor Bearing Cavity

The pressure, speed, and temperature requirements for the compressor section of the GTCP305 fell within the realm of a rotating carbon face seal.

The long-life requirement of 3000 hr necessitated a light seal face load (5 to 8 psi); hence, a narrow carbon nose was designed to minimize the spring load (0.66 to 1.17 lb).

The secondary sealing member was made from a nonelastomeric material (Teflon), to reduce the hysteresis and to provide compatibility with all lubricating oils at elevated temperature. The antirotation device and seal case were designed for simple construction techniques and low cost (Figure 186).

A Bellows seal was used in the first three builds. During the fourth build, the spring-load in a new secondary sealing-member vendor seal was too high, causing excessive power losses and bearing cavity heating. For the fifth build, the spring-load was changed to give a 1.9-lb face load.

During initial Build 5 engine runs, the carbon ring hung up on the antirotation tang of the seal case. The seal was removed and replaced with a conventional face seal, as in Build 4, but with a reduced face load.

6.2 Rotating Knife Labyrinth Seals

The labyrinth seals performed well, but developed minimum problems with knife wear and/or the abradable material.

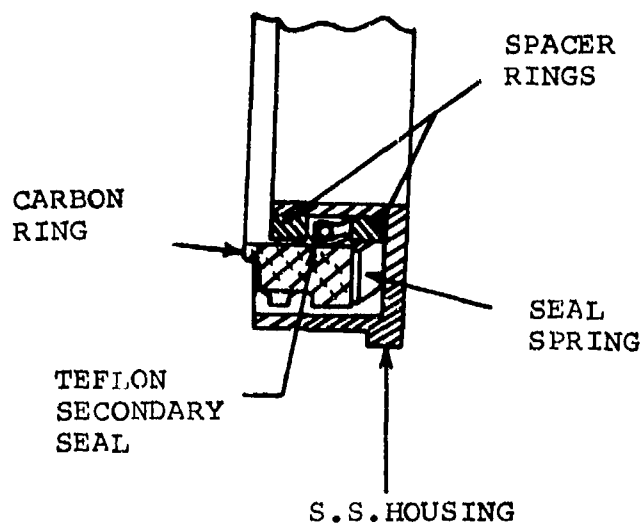


Figure 186. Compressor Face Seal Assembly.

6.3 Turbine Bearing Cavity

For the existing GTCP305 Engine, the bellows-type rubbing face seal has proven adequate. The response of the bellows to pressure could have been improved to reduce carbon nose wear. In future versions of the engine, the bellows-type seal could be replaced with a gas film face seal (Figure 187). This type would require some development work but would provide the advantages of increased tolerance to temperature, misalignment, and minimum wear.

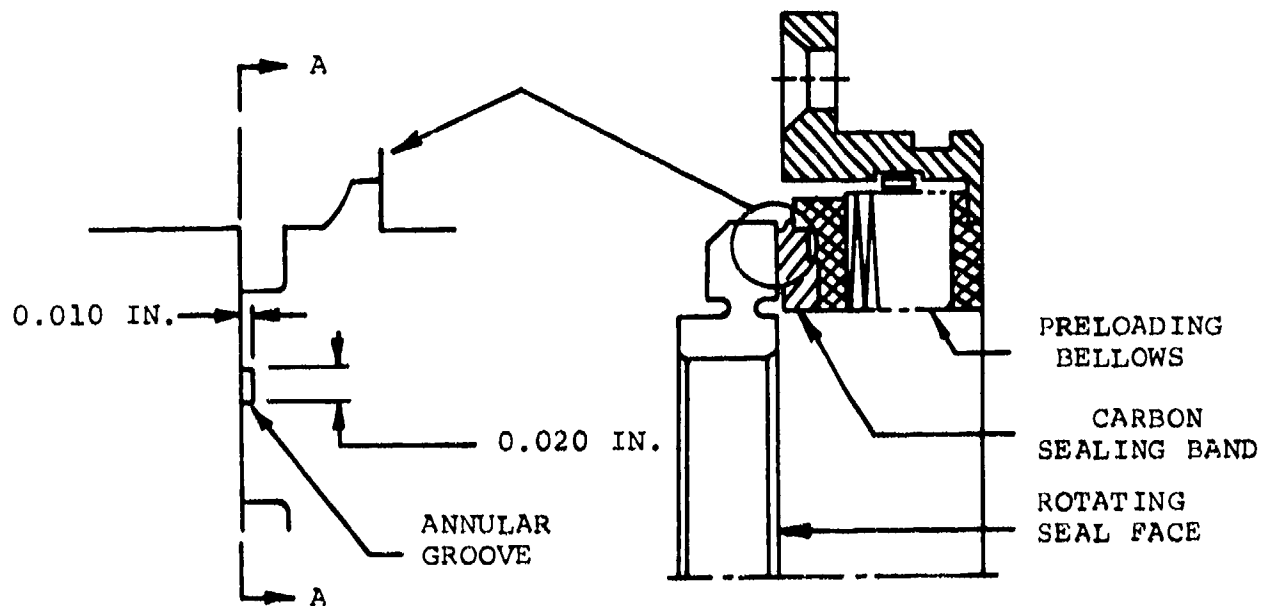
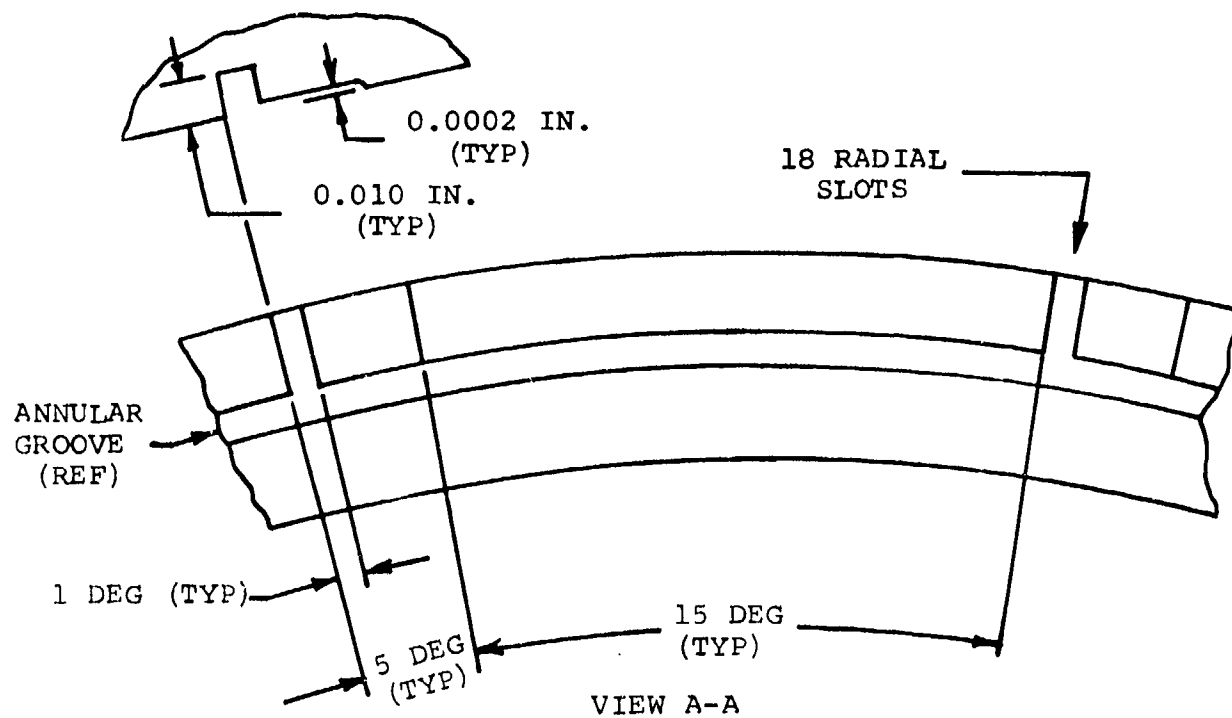


Figure 187. Typical Hydrodynamic Seal.

SECTION IX
GEARBOX DEVELOPMENT

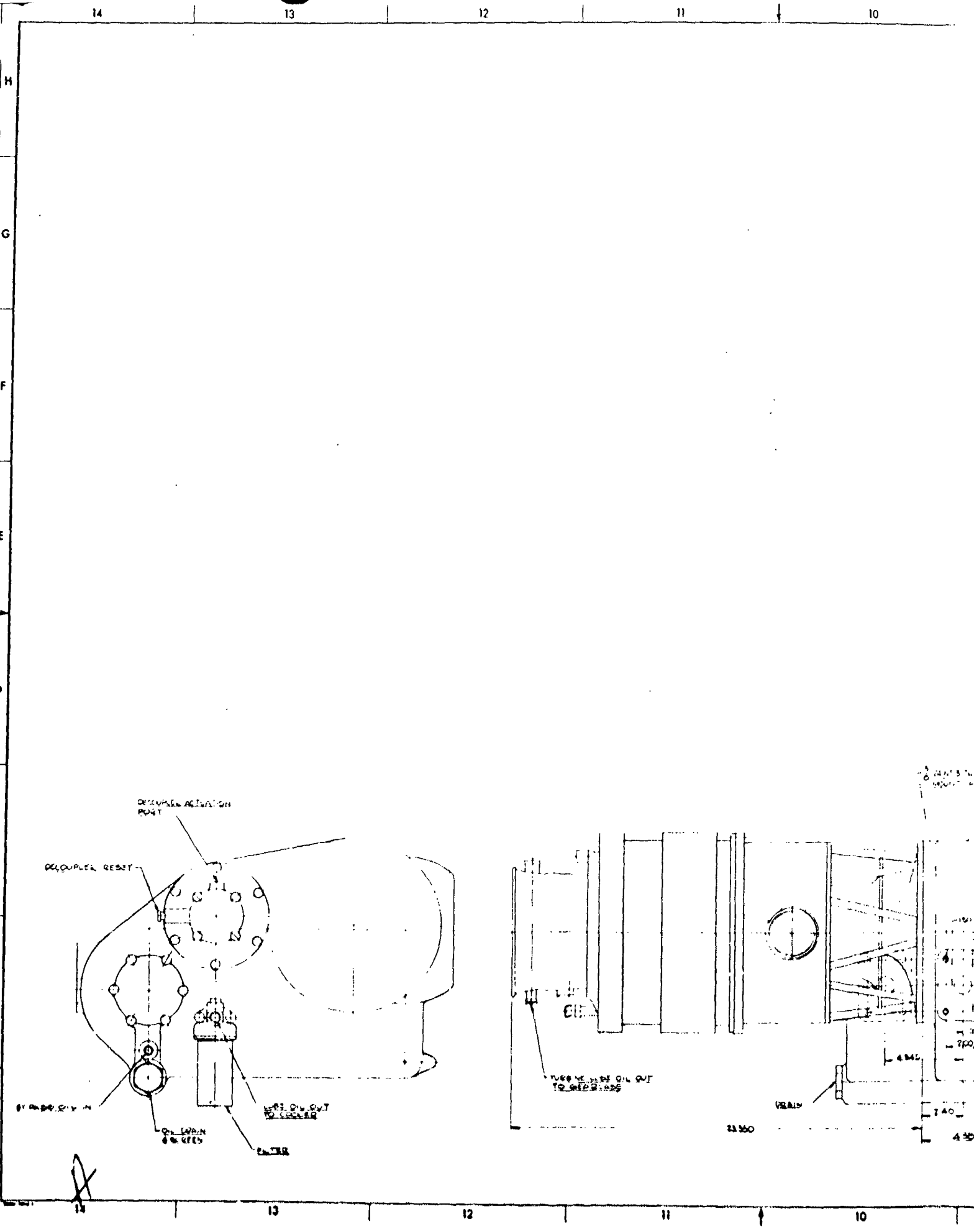
1. GENERAL DESIGN

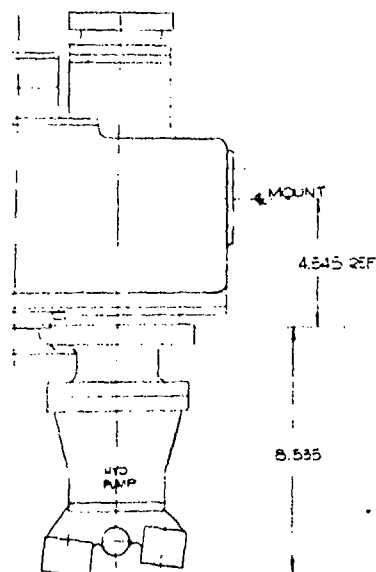
Figure 188 shows the installation of the accessories and the gearbox design, which consists of two separate gearboxes coupled by a torque converter. The first (APU gearbox) is coupled to the APU shaft and contains the APU starter motor shaft, accessories, and the torque converter drive. The second (ADS gearbox) is coupled to the main engine input and drives the hydraulic pumps, the lube pump, and the VSCF generator. The main-engine drive is coupled to the torque converter output through an overrunning clutch, which starts the main engine with APU shaft power but does not allow the main engine to drive the APU. When the engine speed exceeds the torque point, the APU may continue to operate or may be shut down, if not required for another purpose, since it no longer furnishes power to the engine or accessories. With the main engine decoupled, the APU would be capable of driving the main engine accessories at a speed corresponding to engine-idle. The gearing schematic and the APS component design data are illustrated on Table XXVI and Figure 189.

The APS gearbox was designed to provide an operational service-life of 30,000 hr with 5000 hr between overhauls. The design provided gears that incorporated the latest developments in precision aircraft gear-tooth design, such as a 25-deg pressure angle for increased load-carrying capability, but omitted weight reducing refinements in the shafts, webs, and rims.

TABLE XXVI
COMPONENT DESIGN DATA

Comment	APU Drive Nominal, rpm	Engine Drive Nominal, rpm	Design, shp
1. APU	81,820	--	280
2. Main Engine Input	4,915	8,200	246
3. VSCF	10,998	17,650	124
4. Hydarulic Pumps (two each)	3,609	6,000	55
5. Generator, 3 kva	11,974	--	5
6. APU Starter	12,000 (50%)		(400 in.-lb max torque at stall)
7. Lube Pump, APU Side	6,502	--	4
8. Lube Pump, Engine Side	3,609	6,000	4
9. Torque Converter In	17,922	--	195 max
10. Torque Converter Out	17,922	--	580 ft-lb at stall
11. PMG	40,040	--	1





~~ENGINE NO. 4~~

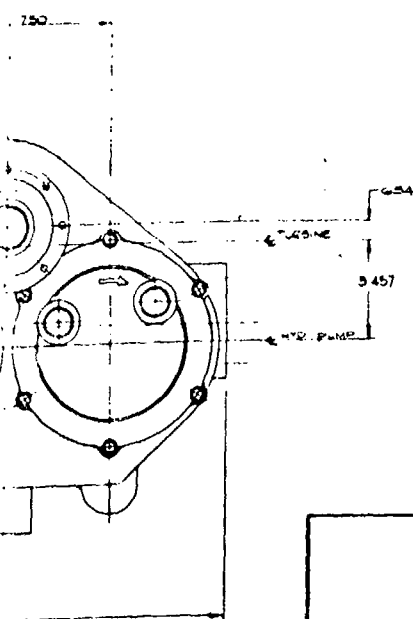


Figure 188.

[illegible]

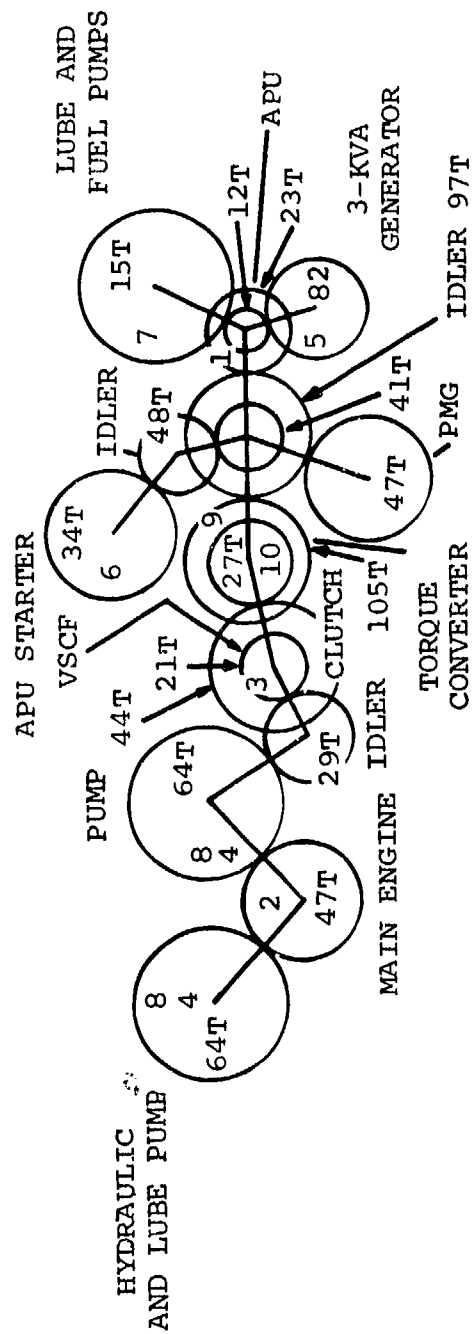


Figure 189. APS Gear Schematic.

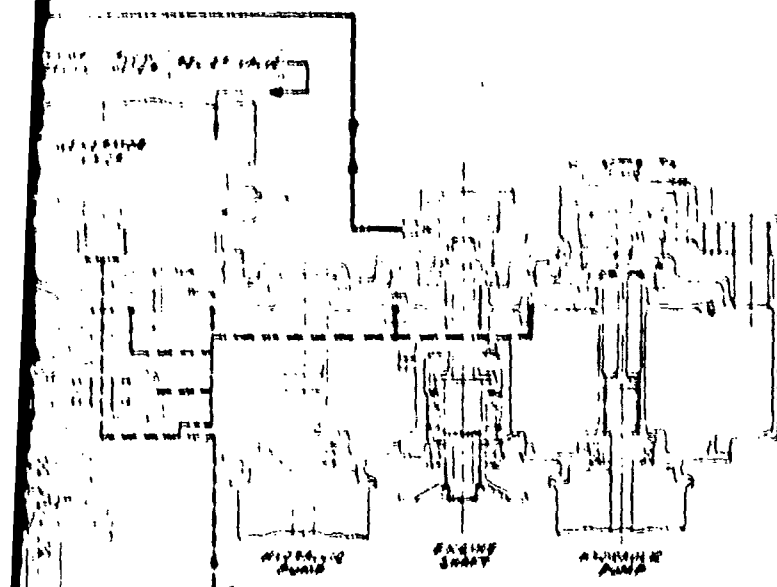
The material selected for the gears was AISI 9310 per AMS6260. The gear and spline teeth were carburized to provide a minimum surface hardness of Rockwell C-60 and the bearing journals and abutment faces of Rockwell C-57. The gear-tooth profiles were finish-ground to obtain the required precision in tooth profile and surface finish for the breadboard APS gearbox. No special processing was required for the raw material. For the engine gearbox, forgings and CEVM 9310 per AMS 6265 were specified for certain highly loaded gears, to maintain the load capability with lightweight gears.

Rolling element bearings were selected, and shaft and housing fits established. The initial design objective was for a B_1 fatigue life of 2000 hr at maximum speed and load of the prototype APS. Therefore, the bearing lives should significantly exceed the overhaul life of 5000 hr under the actual load and speed conditions that the unit would experience. To ensure a minimum cost gearbox, commensurate with the demands of the demonstration unit, bearings from AiResearch stock will be utilized, resulting in a lower actual B_1 fatigue-life.

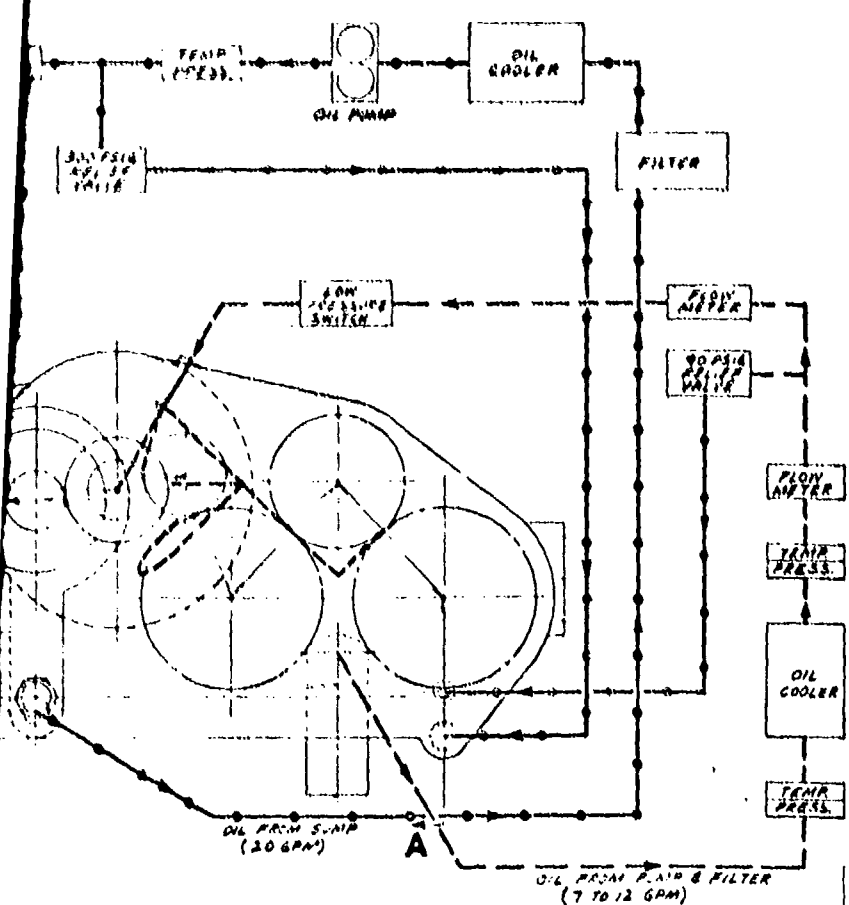
With the exception of the APU high-speed drive pinion, all bearings in the gearbox were within normal operating speed ranges. The pinion bearings must be capable of operation at speeds to 84,320 rpm (1.64×10^6 DN). At this speed, special precautions, such as with oil jets impinging onto the shaft as well as the bearing, were taken to cool the bearings. Prototype cooling provisions may include pressure jets from inside the shaft.

2. LUBRICATION SYSTEM

Lubrication of the gearbox (Figure 190) was accomplished with a Gerotor pump on each side of the torque converter. All bearings were pressure-lubricated, and the heavily loaded gear meshes were lubricated from oil jets. Lightly loaded gear meshes were splash-and-mist



SECTION A-A



Reproduced from
best available copy.

Figure 190.

- APU LEAKS & LUBRICATION SYSTEM
- ACCESSORY LEAKS & LUBRICATION SYSTEM
- TEMP. CONVERTER CHARGE SYSTEM
- SCAVENGE OIL RETURN SYSTEM

REV.	DATE	DESCRIPTION	CODE	MATERIAL AND SPECIFICATION
1	10/1/53	INITIAL DESIGN		
2	10/1/53	REVISION		
3	10/1/53	REVISION		
4	10/1/53	REVISION		
5	10/1/53	REVISION		
6	10/1/53	REVISION		
7	10/1/53	REVISION		
8	10/1/53	REVISION		
9	10/1/53	REVISION		
10	10/1/53	REVISION		

APPROVED: *[Signature]* DATE: 10/1/53

DESIGNED BY: *[Signature]* DATE: 10/1/53

CHECKED BY: *[Signature]* DATE: 10/1/53

FLOW DIAGRAM (SCHEMATIC),
OIL, GAS TURBINE ENGINE
ACCESSORY DRIVE

SKP 25530

lubricated. The gearboxes were cooled by the lubricating oil pumped through external coolers.

3. ACCESSORIES

The gearbox accessories included those required for the APU and the main engine. The accessories discussed in this section do not include the APU fuel pump and PMG, since these items are part of the combustion and control systems. These accessories include the VSCF generator and the variable displacement hydraulic pumps on the main engine side of the gearbox, and the 3-kva ac generator and APU hydraulic starter motor on the APU side.

3.1 Standby Generator

This was a small ac generator being developed by the Bendix Corporation for the F-14 Aircraft. The ac rating is 5 kva, 120/208 v, from 0.75-lagging to unity power factor at 400 Hz and a speed of 12,000 rpm. Twenty-eight amperes of dc power is available at 28 v. These ratings are higher than required, but the generator is representative of the state of the art in small generators, and some weight and size savings may be expected from lower capacity units. The generator weighs 12.75 lb.

The generator mounts onto the gearbox with a quick disconnect flange and is driven from a spline connection in the center of the flange. Lubrication and cooling is obtained from the gearbox lube system, through mating ports in the gearbox and the generator mounting pads. The ac voltage output must be regulated for use in the aircraft system by an external voltage regulator, and the frequency is a function of the speed.

3.2 Main Engine Generator

This is a General Electric VSCF (variable speed, constant frequency) generator. The generator system (including the converter/control unit) is rated at 75-kva intermittent and 60-kva continuous power at a speed range of 10,000 to 20,000 rpm.

The VSCF generator was mounted on the gearbox with a quick-disconnect flange and driven by a splined shaft. It contains its own sump, pump and forced lubrication and cooling system. However, for a prototype APS, the oil can be supplied from, and returned to, the gearbox through mating ports in the mounting pad. For the demonstration APS, the VSCF oil supply was contained in a separate closed-loop system to enable heat-rejection rates to be measured.

3.3 Hydraulic Pumps

Two Vickers variable-displacement hydraulic pumps now in production for the A-7A and A-7D Aircraft were used. The pumps have a maximum displacement of 1.15 in.³/rev and the rated continuous speed is 5650 rpm. They contain an integral pressure control system that controls the outlet pressure from 2975 \pm 25 psi at full-flow to 3075 \pm 25 psi at zero-flow. Although the pump weight is 13.29 lb, it is a production pump, and some weight reduction could be expected from an advanced design for a prototype APS.

3.4 Starter Motor

The starter motor to be used on the demonstration APS was to be a 0.367-in.³/rev hydraulic motor. This particular motor is used on production engines and has a weight of 5.5 lb, which can probably be reduced for a prototype APS. Also, the preliminary starting analyses showed that a slightly larger motor may give better results with no

lubricated. The gearboxes were cooled by the lubricating oil pumped through external coolers.

3. ACCESSORIES

The gearbox accessories included those required for the APU and the main engine. The accessories discussed in this section do not include the APU fuel pump and PMG, since these items are part of the combustion and control systems. These accessories include the VSCF generator and the variable displacement hydraulic pumps on the main engine side of the gearbox, and the 3-kva ac generator and APU hydraulic starter motor on the APU side.

3.1 Standby Generator

This was a small ac generator being developed by the Bendix Corporation for the F-14 Aircraft. The ac rating is 5 kva, 120/208 v, from 0.75-lagging to unity power factor at 400 Hz and a speed of 12,000 rpm. Twenty-eight amperes of dc power is available at 28 v. These ratings are higher than required, but the generator is representative of the state of the art in small generators, and some weight and size savings may be expected from lower capacity units. The generator weighs 12.75 lb.

The generator mounts onto the gearbox with a quick disconnect flange and is driven from a spline connection in the center of the flange. Lubrication and cooling is obtained from the gearbox lube system, through mating ports in the gearbox and the generator mounting pads. The ac voltage output must be regulated for use in the aircraft system by an external voltage regulator, and the frequency is a function of the speed.

3.2 Main Engine Generator

This is a General Electric VSCF (variable speed, constant frequency) generator. The generator system (including the converter/control unit) is rated at 75-kva intermittent and 60-kva continuous power at a speed range of 10,000 to 20,000 rpm.

The VSCF generator was mounted on the gearbox with a quick-disconnect flange and driven by a splined shaft. It contains its own sump, pump and forced lubrication and cooling system. However, for a prototype APS, the oil can be supplied from, and returned to, the gearbox through mating ports in the mounting pad. For the demonstration APS, the VSCF oil supply was contained in a separate closed-loop system to enable heat-rejection rates to be measured.

3.3 Hydraulic Pumps

Two Vickers variable-displacement hydraulic pumps now in production for the A-7A and A-7D Aircraft were used. The pumps have a maximum displacement of 1.15 in.³/rev and the rated continuous speed is 5650 rpm. They contain an integral pressure control system that controls the outlet pressure from 2975 \pm 25 psi at full-flow to 3075 \pm 25 psi at zero-flow. Although the pump weight is 13.29 lb, it is a production pump, and some weight reduction could be expected from an advanced design for a prototype APS.

3.4 Starter Motor

The starter motor to be used on the demonstration APS was to be a 0.367-in.³/rev hydraulic motor. This particular motor is used on production engines and has a weight of 5.5 lb, which can probably be reduced for a prototype APS. Also, the preliminary starting analyses showed that a slightly larger motor may give better results with no

lubricated. The gearboxes were cooled by the lubricating oil pumped through external coolers.

3. ACCESSORIES

The gearbox accessories included those required for the APU and the main engine. The accessories discussed in this section do not include the APU fuel pump and PMG, since these items are part of the combustion and control systems. These accessories include the VSCF generator and the variable displacement hydraulic pumps on the main engine side of the gearbox, and the 3-kva ac generator and APU hydraulic starter motor on the APU side.

3.1 Standby Generator

This was a small ac generator being developed by the Bendix Corporation for the F-14 Aircraft. The ac rating is 5 kva, 120/208 v, from 0.75-lagging to unity power factor at 400 Hz and a speed of 12,000 rpm. Twenty-eight amperes of dc power is available at 28 v. These ratings are higher than required, but the generator is representative of the state of the art in small generators, and some weight and size savings may be expected from lower capacity units. The generator weighs 12.75 lb.

The generator mounts onto the gearbox with a quick disconnect flange and is driven from a spline connection in the center of the flange. Lubrication and cooling is obtained from the gearbox lube system, through mating ports in the gearbox and the generator mounting pads. The ac voltage output must be regulated for use in the aircraft system by an external voltage regulator, and the frequency is a function of the speed.

3.2 Main Engine Generator

This is a General Electric VSCF (variable speed, constant frequency) generator. The generator system (including the converter/control unit) is rated at 75-kva intermittent and 60-kva continuous power at a speed range of 10,000 to 20,000 rpm.

The VSCF generator was mounted on the gearbox with a quick-disconnect flange and driven by a splined shaft. It contains its own sump, pump and forced lubrication and cooling system. However, for a prototype APS, the oil can be supplied from, and returned to, the gearbox through mating ports in the mounting pad. For the demonstration APS, the VSCF oil supply was contained in a separate closed-loop system to enable heat-rejection rates to be measured.

3.3 Hydraulic Pumps

Two Vickers variable-displacement hydraulic pumps now in production for the A-7A and A-7D Aircraft were used. The pumps have a maximum displacement of 1.15 in.³/rev and the rated continuous speed is 5650 rpm. They contain an integral pressure control system that controls the outlet pressure from 2975 \pm 25 psi at full-flow to 3075 \pm 25 psi at zero-flow. Although the pump weight is 13.29 lb, it is a production pump, and some weight reduction could be expected from an advanced design for a prototype APS.

3.4 Starter Motor

The starter motor to be used on the demonstration APS was to be a 0.367-in.³/rev hydraulic motor. This particular motor is used on production engines and has a weight of 5.5 lb, which can probably be reduced for a prototype APS. Also, the preliminary starting analyses showed that a slightly larger motor may give better results with no

significant weight increase. For the demonstration unit, the hydraulic starter motor was replaced by an air turbine motor (AiResearch Model ATM80). This allowed motoring to high speeds and provided additional torque for the APU to full speed.

SECTION X
APU TEST HISTORY

The APU was tested through five builds. This section describes these builds, teardown inspections, reworks, and performance. The APS gearbox and accessories (less the 60-kva generator) are shown in Figure 191, the APU in Figure 192, and the Build 5 APS on the test stand in Figure 193.

1. BUILD 1

Build 1 (Figure 194, with exceptions noted on Table XXVII) was motored to 30 percent to determine the drag torque, check the mechanical integrity of the APU, determine burner in-flows, surge bleed-flow requirements, and optimum setting of the inlet guide vanes to the axial (first-stage) compressor. No usable aerodynamic data were recorded, and the APU was torn down to incorporate light-off configuration components.

2. BUILD 2

2.1 Configuration

Further changes from Build 1 were:

(a) To obtain higher performance, the clearances were reduced to the following design values:

- (1) Axial compressor - 0.0145 to 0.018 in.
- (2) Radial compressor - 0.029 to 0.0336
- (3) Radial turbine - 0.014 to 0.018 (axial at tip)
- (4) Radial turbine - 0.0115 to 0.0185 (radial at exducer)
- (5) Axial turbine - 0.015 to 0.018

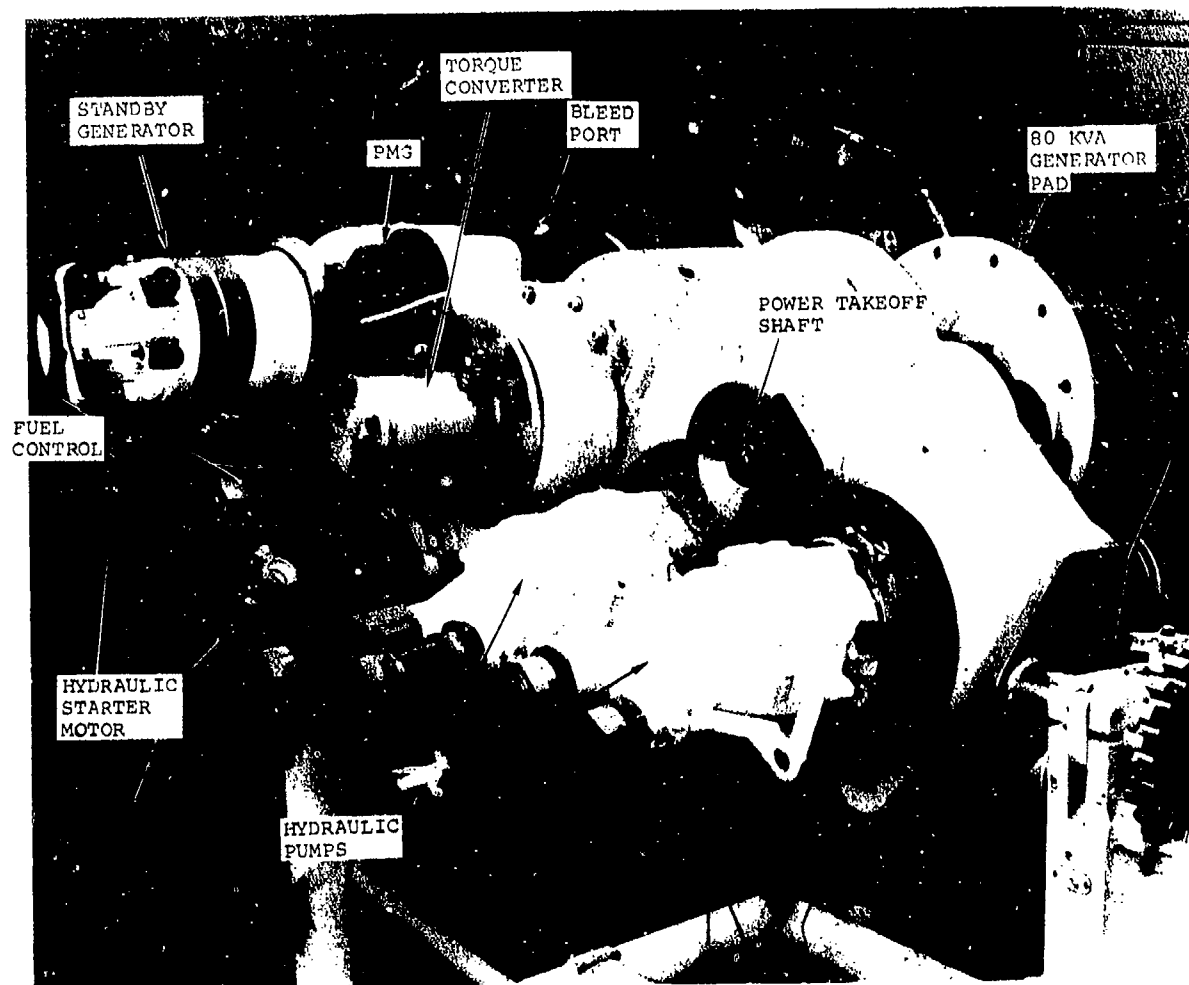


Figure 191. APS Gearbox and Accessories.

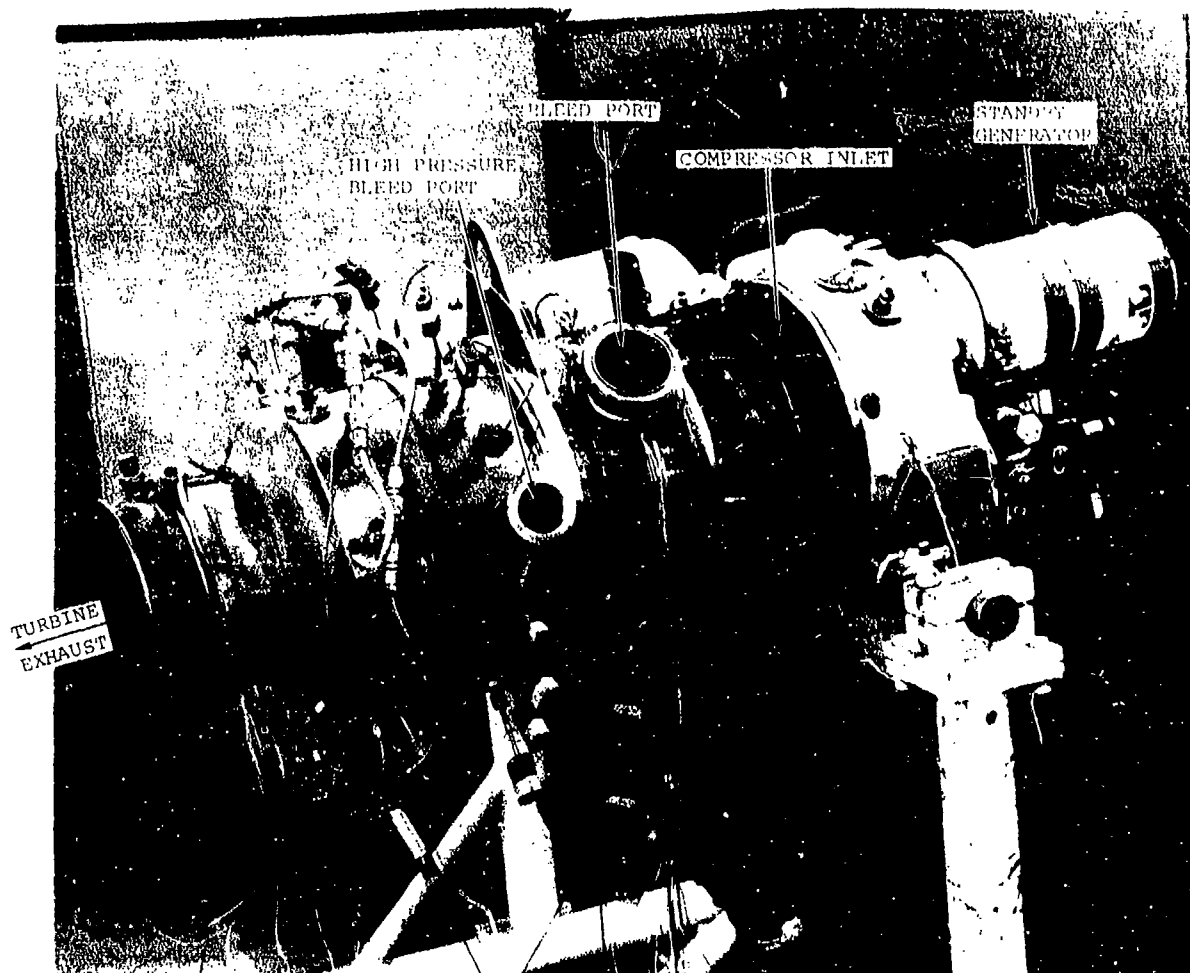


Figure 192. APU and Gearbox.

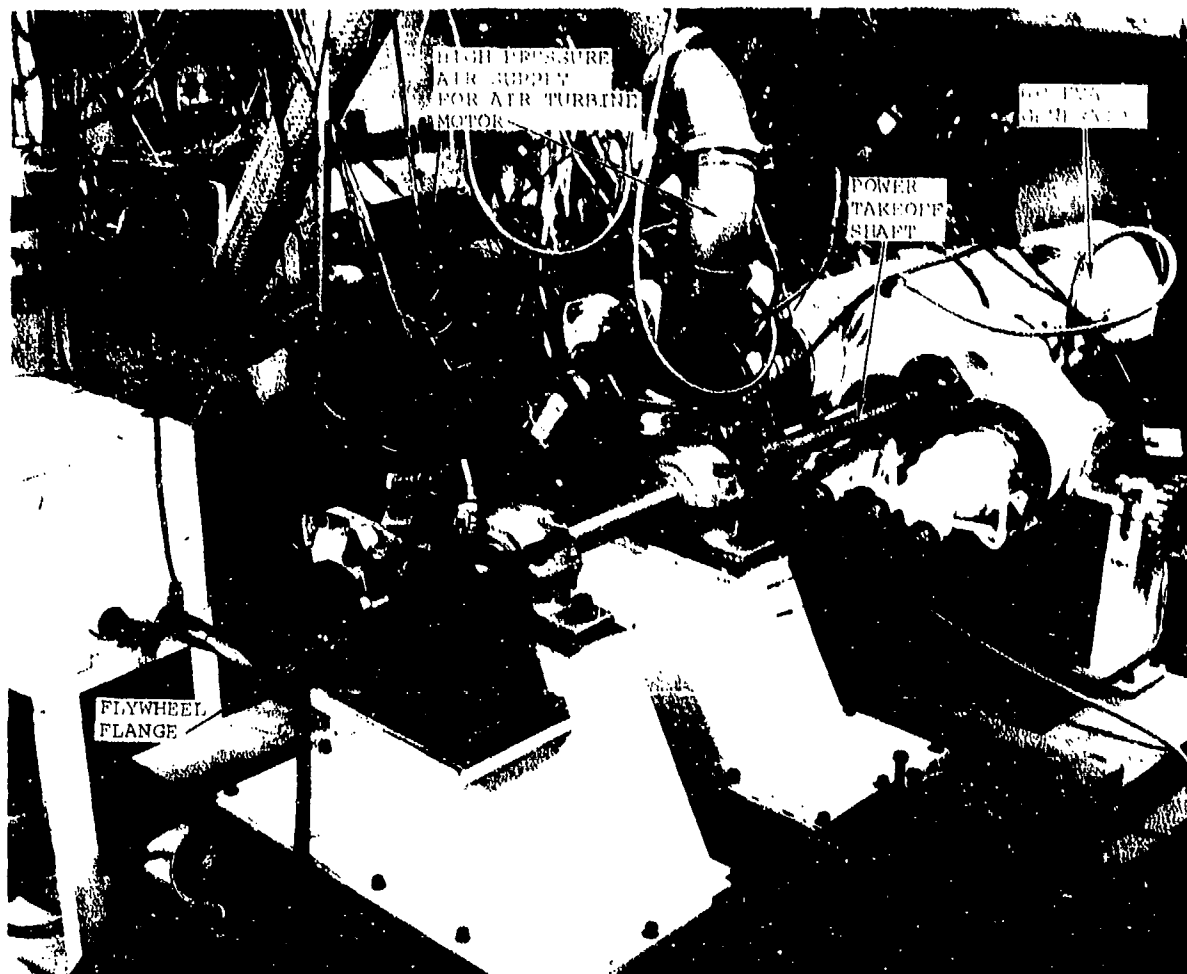
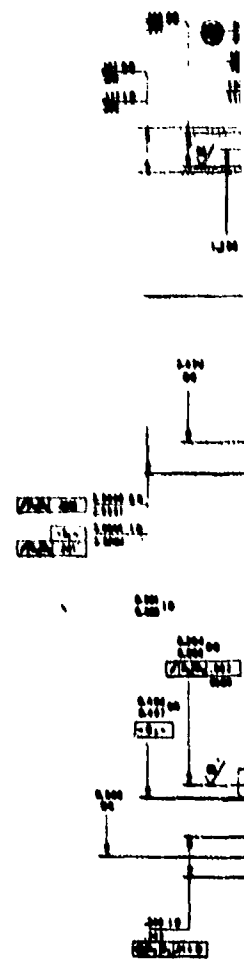
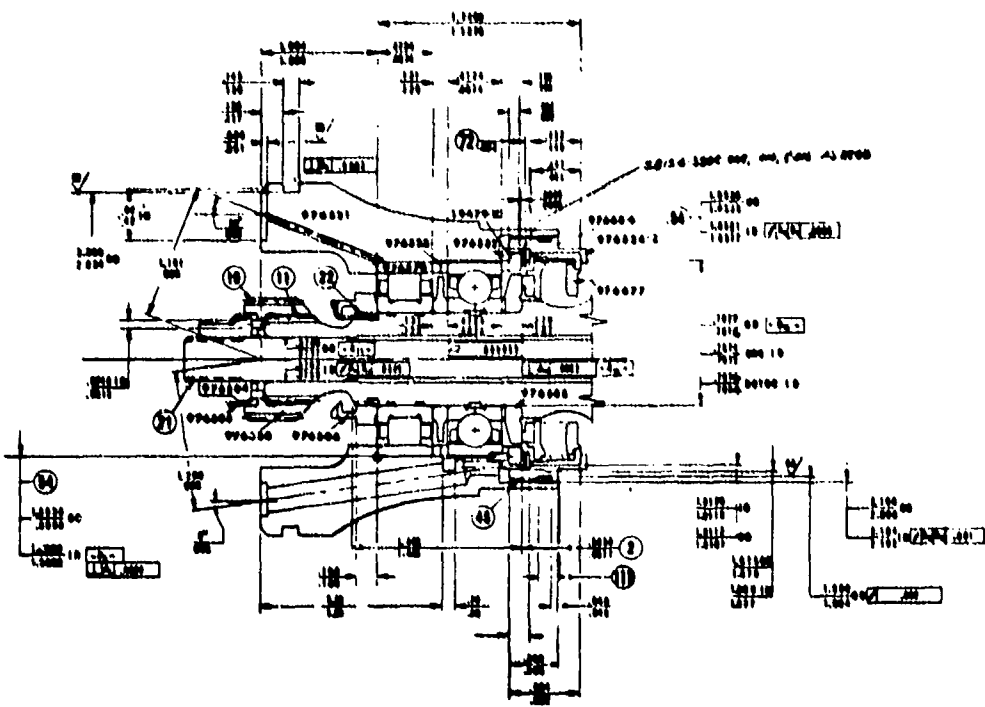
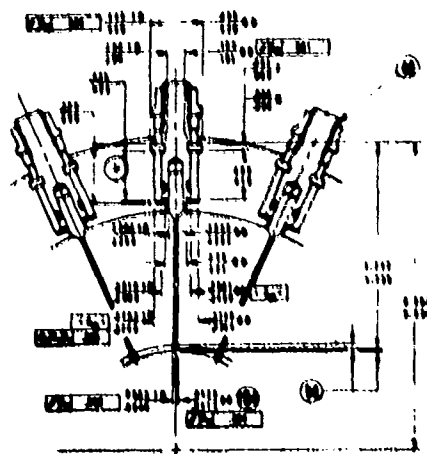
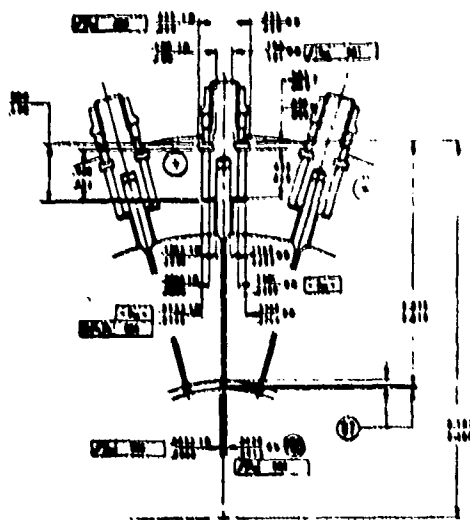
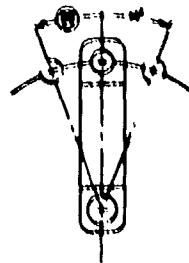
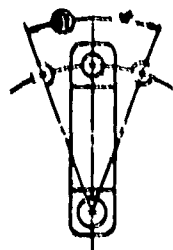


Figure 193. APS Test Setup





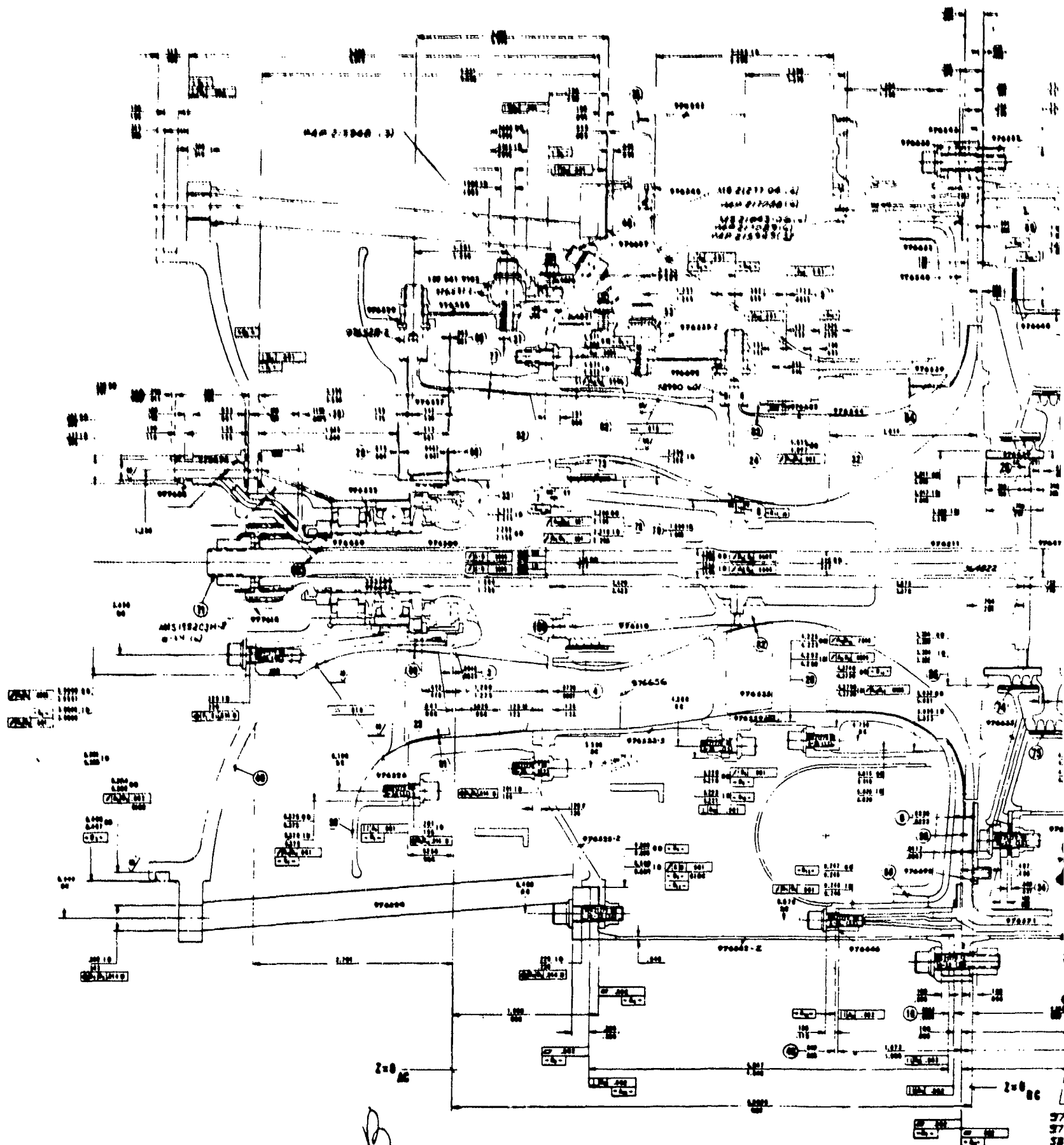




TABLE XXVII

EXCEPTIONS TO GTCP305 ASSEMBLY P/N 380977-1, REV. A, BUILD 1

Part Number	Part Substituted Into Build 1	Remark
976505	PAP216102	R/W for interference
976521	PAP216105	R/W to match contour
976523	PAP220357	Incorporates thrust measurement
976693	PAP216106	Notch for thrust ring antirota- tion
976542	PAP216101	Reloaates bleed plenum
976563	PAP216104	12-point nut
976511	PAP220352	Opened radial clearance (P/N 976511-2 inducer cutback)
SKP25159	P/N 976536	
976533	PAP216107	Open ID to clear rotor

- (b) The turbine plenum and tail-pipe assembly was replaced with a new part to the TIT thermocouple instrumentation ports and rematched to the structural assembly.
- (c) To prevent thermal binding of the squeeze-film hydraulic mount assembly, the axial end clearance was increased from 0.0005 to 0.002-0.003 in.
- (d) The rotor balance was improved over the previous build from 0.00025- to 0.00018-in. cg eccentricity, in obtaining a better balance on the radial impeller.
- (e) The compressor end roller bearing was replaced. The previous bearing had some scratches and marks on the separator, caused by the assembly tool for the shaft nut. This tool has subsequently been reworked.
- (f) The radial turbine stator assembly was modified slightly to provide a more consistent and repeatable preload on the bolt-leaf-spring assembly. The modification centered each leaf-spring over the bolts with a single preloading bolt for each leaf-spring assembly instead of two bolts. This provided the required repeatability, after carefully determining the preloading of each bolt by measuring and recording the deflection with a dial gauge indicator.
- (g) The oil drainage from the turbine bearing seal cavity was modified slightly to improve the drainage around the squeeze-film mount. However, a short run at low speeds indicated the squeeze-film may have been affected since a high vibration at 1/rev was apparent. The APU was partially disassembled to change the assembly back to the original configuration. The repeat test indicated the vibration at 1/rev was again low and satisfactory for engine testing.

TABLE XXVII

EXCEPTIONS TO GTCP305 ASSEMBLY P/N 380977-1, REV. A, BUILD 1

Part Number	Part Substituted Into Build 1	Remark
976505	PAP216102	R/W for interference
976521	PAP216105	R/W to match contour
976523	PAP220357	Incorporates thrust measurement
976693	PAP216106	Notch for thrust ring antirotation
976542	PAP216101	Reloaates bleed plenum
976563	PAP216104	12-point nut
976511	PAP220352	Opened radial clearance (P/N 976511-2 inducer cutback)
SKP25159	P/N 976536	
976533	PAP216107	Open ID to clear rotor

- (b) The turbine plenum and tail-pipe assembly was replaced with a new part to the TIT thermocouple instrumentation ports and rematched to the structural assembly.
- (c) To prevent thermal binding of the squeeze-film hydraulic mount assembly, the axial end clearance was increased from 0.0005 to 0.002-0.003 in.
- (d) The rotor balance was improved over the previous build from 0.00025- to 0.00018-in. cg eccentricity, in obtaining a better balance on the radial impeller.
- (e) The compressor end roller bearing was replaced. The previous bearing had some scratches and marks on the separator, caused by the assembly tool for the shaft nut. This tool has subsequently been reworked.
- (f) The radial turbine stator assembly was modified slightly to provide a more consistent and repeatable preload on the bolt-leaf-spring assembly. The modification centered each leaf-spring over the bolts with a single preloading bolt for each leaf-spring assembly instead of two bolts. This provided the required repeatability, after carefully determining the preloading of each bolt by measuring and recording the deflection with a dial gauge indicator.
- (g) The oil drainage from the turbine bearing seal cavity was modified slightly to improve the drainage around the squeeze-film mount. However, a short run at low speeds indicated the squeeze-film may have been affected since a high vibration at 1/rev was apparent. The APU was partially disassembled to change the assembly back to the original configuration. The repeat test indicated the vibration at 1/rev was again low and satisfactory for engine testing.

2.2 Testing

Sixty-three data scans (pressure, temperature, acceleration, clearance, rpm, and flow data at a constant speed) were taken from tests of Builds 1 and 2 for a total running time of 14 hr 44 min. Performance data were obtained for variations of inlet guide vane settings, bleed-airflow rates, and high-pressure surge bleed-flow rates. Test data from Scans 57, 59, and 61 are shown on Table XXVIII. The series of tests determined that high pressure surge bleed was not required. Testing was terminated when a high vibration was observed at low speeds.

In addition to audible indications of stall and surge, the reduced performance data indicated the following:

- (a) The bypass ratio (BPR) at which stall occurred was approximately 0.33, rather than 0.25, as determined from the reference rig tests.
- (b) The bleed-pressure ratio was lower than design.
- (c) The APU cycle pressure ratio was lower than expected.
- (d) The turbine cooling airflow was approximately 20 percent of the radial compressor through-flow, compared to the design flow rate of 6 percent.
- (e) The VIGVs for the radial compressor did not give the APU a performance advantage.

2.3 Teardown Inspection

The APU was disassembled on April 17, 1971. Following is a summary of observations in order of teardown sequence:

TABLE XXVIII

GTCP305 LIGHT-OFF TESTS, BUILD 2A, TEST 2, RUN 46, SCANS 56-63 4/14/71

	SCAN NUMBER	57.00	59.00	61.00
	PCT PHYS SPEED	90.89	92.41	94.31
	IGV1 DEGR CLOSED	31.00	28.00	30.00
	IGV2 DEGR CLOSED	0.00	0.00	0.00
AXIAL	**PCT CORR SPEED	88.33	89.50	90.85
COMPR	* CORR FLOW, LB/SEC	2.626	2.558	2.436
(C1)	* TOTAL PRESS RATIO	1.369	1.436	1.434
	**EFFICIENCY	.646	.674	.636
RAD COMPRESSOR	CORR PCT SPEED	94.707	99.314	100.414
	**CORR FLOW, LB/SEC	.645	.528	.464
BLEED	* STAGE P/P	1.397	2.433	2.623
RADIAL	* ROTOR P/P	3.219	3.096	3.165
COMPR	* EFFICIENCY, STAGE	.210	.604	.652
(C2)	* EFFICIENCY, ROTOR	.831	.795	.801
	**ROTOR EXIT MACH NO	1.052	.959	.912
	**CORR FLOW, LB/SEC	1.408	1.392	1.374
ENGINE	* STAGE P/P	4.470	4.371	4.448
RADIAL	* ROTOR P/P	3.951	4.092	4.145
COMPR	* EFFICIENCY, STAGE	.687	.654	.636
(C3)	* EFFICIENCY, ROTOR	.619	.618	.600
	**ROTOR EXIT MACH NO	1.761	1.815	1.823
BLEED	* LB/MIN (COR TO INL)	49.534	42.215	36.873
PORT	* GPH (W(C2)/W(C3))	.459	.379	.337
	**P(PORT)/P(ATM)	1.911	3.494	3.761
HI PR SURGE FLOW, LB/SEC		0.000	0.000	0.000
	**COMPR DISCH TEMP, F	645.089	682.621	724.121
	* CALC BURN TEMP, F	1633.851	1648.598	1694.520
	* TSF BASED ON ABOVE	.116	.120	.123
	* AVE MEAS BURN T, F	1482.163	1520.321	1562.317
	* TSF BASED ON ABOVE	.318	.291	.300
BURNER	* MAX MEAS BURN T, F	1743.465	1764.486	1813.883
	* CALC TURB IN T, F	1450.868	1465.524	1531.519
	* FUEL FLOW, LB/HR	74.000	74.000	75.000
	* EFFICIENCY	.997	.998	1.000
	* FUEL/AIR RATIO	.015	.015	.015
	**PRESSURE RATIO	.941	.940	.940
	**CORR FLOW AT NOZZLE	.497	.497	.497
	* NOZZLE P/P DISCHG	5.758	5.900	5.993
	* W(COOL)/W(C3)	.192	.196	.174
	* CORR FLOW AT WHEEL	.604	.608	.593
TURBINE	* PCT CORR SPD AT WHL	107.236	108.621	108.996
	* WHEEL PRESS/P DISCH	5.595	5.726	5.834
	* EFF AT WHEEL	.743	.741	.756
	* MEAS TDT, F	957.281	963.883	1000.019
	* TDT BASED ON ATM HP	966.976	970.756	1019.562
	**TURBINE HORSEPOWER	324.763	338.938	352.964
	**APU CALC SHP	-107.053	-111.564	-103.201
	* BLEED HP (BHP)	98.716	87.686	79.338
PERFORM-	* APU EQUIV HP (EHP)	-8.337	-23.878	-23.863
	**APU CYCLE P/P	6.117	6.275	6.378

- (a) The turbine bearing carrier (P/N 976521) had rotated approximately 20 deg opposite the direction of rotation. This rotation sheared the hydraulic mount oil supply tube integral with P/N 976564.
- (b) A slight tip rub occurred between the axial turbine wheel (P/N 976515) and the shroud (P/N 976553). Both parts were reusable.
- (c) All labyrinth seal running surfaces were deeply grooved, requiring replacement.
- (d) Fretting occurred on curvic coupling teeth between the radial turbine wheel (P/N 976513) and interstage coupling (P/N 976514).
- (e) The radial turbine wheel rubbed the shroud (P/N 976548), producing a hole in one area at the knee.
- (f) The radial compressor wheel lost portions of two adjacent blades in the inducer region. Blade pieces were lodged in the bleed diffuser.
- (g) The bleed-flow splitter (P/N 976540) was rubbed, by radial excursion of the compressor wheel, on its inner edge and rubbed slightly on its aft surface by the tip of the compressor wheel. Radial cracks at the inner edge were caused by fatigue.
- (h) Second-stage inlet guide vanes were rubbed by the compressor wheel hub and coupling (P/N 976510) along the inner ends.
- (i) Axial compressor had a slight tip rub at the leading edge.

(j) On the first-stage variable inlet guide vane (P/N 976526), the fixed leading edges were cracked at the hub. Polishing the failure surface caused by vibration during APU operation precluded identification of the failure mode.

(k) The tie-bolt (P/N 364822) length increased by 0.012 in.

2.4 Teardown Failure Analysis

Review of APU operating conditions and metallurgical investigation of components revealed that the APU failure was initiated by fatigue in the radial compressor, followed by the tensile failure of two adjacent inducer blades. Fatigue cracks were initiated at some time during the test, due to a combination of the following environments:

- (a) Stall and surge encountered during aerodynamic and performance testing
- (b) A high frequency resonance at part-speed excited by the second-stage inlet guide vanes (15/rev)

Either of these conditions would produce areas of high vibratory stress near the blade hub where the fatigue cracks originated. The remaining failures observed during APU teardown were secondary to blade fatigue and were due to the resulting high unbalance in the rotating group and to low oil pressure.

3. BUILD 3

3.1 Configuration

The third APU build was initiated in April and incorporated the following changes derived from the performance and teardown data of Build 2:

- (a) The second-stage variable inlet guide vanes were removed.
- (b) The bleed diffuser forward wall was recontoured to increase the diffuser width.
- (c) The high-pressure compressor radial diffuser passage width was increased about 4 1/2 percent, and the compressor wheel blade height increased 15 percent.
- (d) The radial turbine nozzle area was reduced by 13 percent.
- (e) The combustor incorporated high-pressure atomization nozzles and improved sealing at the turbine nozzle interface to prevent leakage of compressor discharge air.

3.2 Testing

Prior to light-off, the APU was motored at various speeds to ensure mechanical integrity. Although the maximum average burner exit temperature was predicted as 1900°F at self-sustaining operation, the maximum average temperature reached 2044°F (Table XXIX, Scan 82). The temperature spread factors for Scans 82 and 83 were 0.146 and 0.159, respectively. Maximum self-sustaining speed was 84.1-percent corrected-speed (86.4-percent actual speed) with the BPR reduced to 0.404 (Scan 83) from 0.532 (Scan 82). The calculated APU bleed horsepower was 86.9 and 77.1 for Scans 82 and 83, respectively. Since the shaft horsepower was zero, these power levels are also the eshp (equivalent shaft horsepower). Table XXIX shows some selected Build 3 performance data. There were some problems associated with leakage at the turbine nozzles, causing the calculated cooling flow, flow function, and turbine efficiency to be erroneous.

TABLE XXIX

SELF-SUSTAINING RUNS, GTCP305, BUILD 3, TEST 2, 5/24/71

SCAN NUMBER	82.00	83.00
PCT PHYS SPEED	84.56	86.37
PHYS SPEED, RPM	69168.00	70651.20
INLET TEMP, DEG F	87.56	86.84
CORR SPEED, RPM	67339.09	68828.19
IGV1 DEGR CLOSED	0.00	0.00
IGV2 DEGR CLOSED	0.00	0.00
AXIAL **PCT CORR SPEED	82.32	84.14
COMPR * CORR FLOW, LB/SEC	2.440	2.542
(C1) * TOTAL PRESS RATIO	1.319	1.343
**EFFICIENCY	.734	.725
COMPRESSOR INTRST DUCT P/P	1.000	1.000
RAD COMPRESSOR CORR PCT SPEED	93.350	95.022
**CORR FLOW, LB/SEC	.680	.577
BLEED * STAGE P/P	1.415	2.251
RADIAL * ROTOR P/P	3.007	2.953
COMPR * EFFICIENCY, STAGE	.243	.601
(C2) * EFFICIENCY, ROTOR	.861	.878
**ROTOR EXIT MACH NO	1.115	.972
**CORR FLOW, LB/SEC	1.287	1.427
ENGINE * STAGE P/P	4.993	5.353
RADIAL * ROTOR P/P	5.529	6.106
COMPR * EFFICIENCY, STAGE	.782	.788
(C3) * EFFICIENCY, ROTOR	.845	.867
**ROTOR EXIT MACH NO	.984	1.010
BLEED **LB/MIN	47.701	41.042
PORT * BPR (W(C2)/W(C3))	.529	.404
**P(PORT)/P(AMB)	1.866	3.023
**COMPR DISCH TEMP, F	592.441	619.418
*AIR MASS FLOW, LB/SEC	1.211	1.350
* AVE MEAS BURN T, F	2043.679	1940.889
* TSF BASED ON ABOVE	.146	.159
BURNER * MAX MEAS BURN T, F	2255.728	2150.843
* FUEL FLOW, LB/HR	99.000	103.000
* EFFICIENCY	.788	.809
* FUEL/AIR RATIO	.030	.027
**PRESSURE RATIO	.959	.957
**CORR FLOW AT NOZZLE	.339	.361
* NOZZLE P/P DISCHG	6.314	6.880
* W(COOL)/W(C3)	.378	.345
TURBINE * PCT CORR SPD	87.157	90.912
* EFFICIENCY	1.079	1.014
* MEAS TOT, F	1108.531	1053.839
**TURBINE HORSEPOWER	358.749	399.057
**APU CALC SHP	0.000	0.000
* BLEED HP (BHP)	86.871	77.086
PERFORM. * APU EQUIV HP (ESHP)	86.871	77.086
**APU CYCLE P/P	6.584	7.190

The third build was motored for 3 hr 15 min. It was started five times and run hot for 1 hr 45 min. Nineteen data scans were recorded. Cumulative running time through Build 3 was 25 hr 29 min, of which 6 hr 38 min were with APU light-off. Twenty-eight starts were accumulated through Build 3.

3.3 Teardown Inspection

Teardown inspection of Build 3 was completed during May 1971. Following is a summary observations in order of teardown sequence:

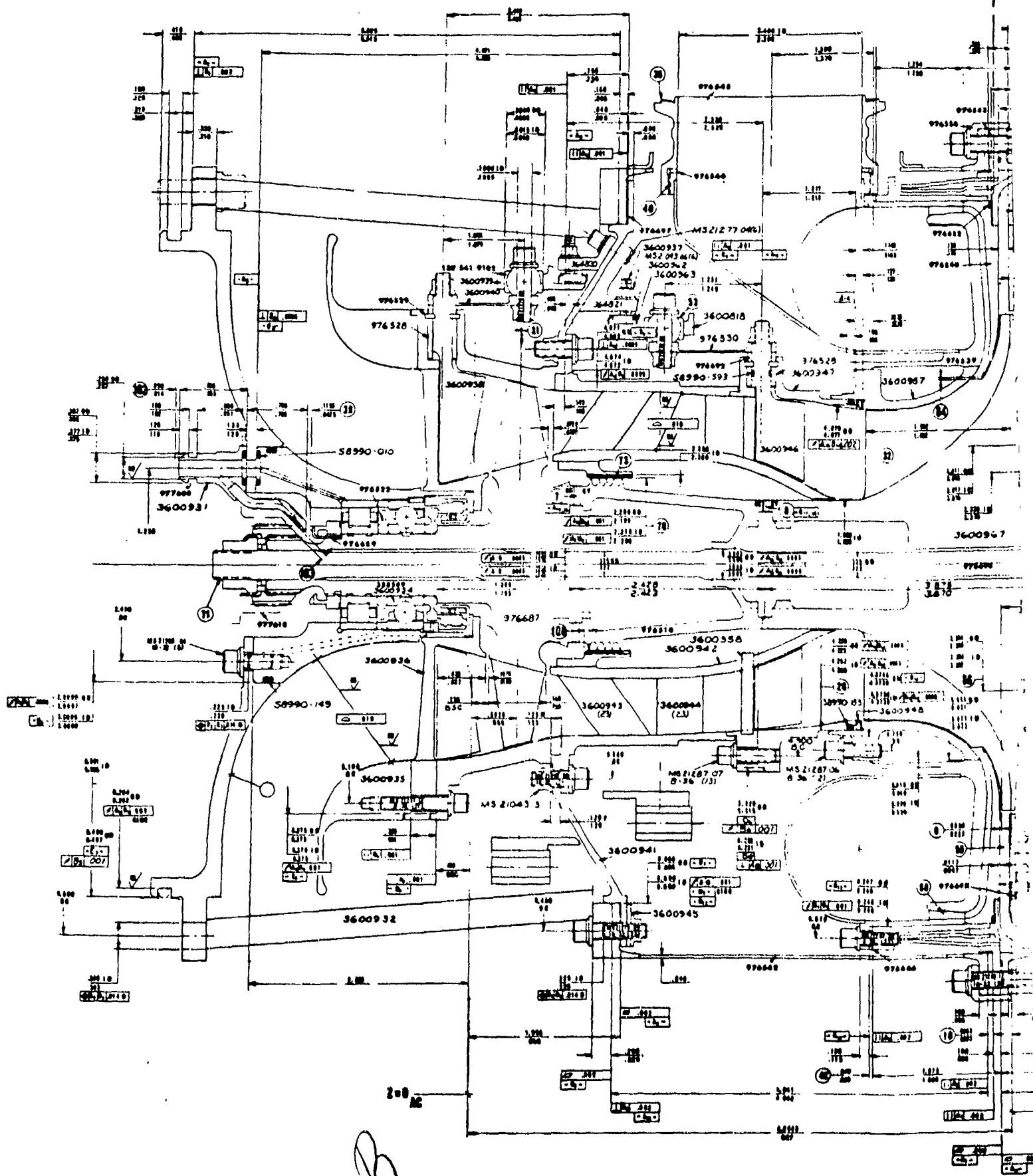
- (a) The radial turbine wheel rubbed the shroud (P/N 976548) in a 1-in.² area near the knee.
- (b) The nickel graphite seal running material in P/N 976633 was broken out of the larger diameter seal but intact in the smaller diameter seal.
- (c) The bleed-airflow splitter (P/N 976540) had a number of radially oriented cracks at the inner edge.
- (d) The combustor liner (P/N SKP25549) (interium configuration) showed evidence of thermal distress, particularly on the inner liner transition.
- (e) The turbine roller bearing was heat-discolored, due to heat soak-back after shutdown.

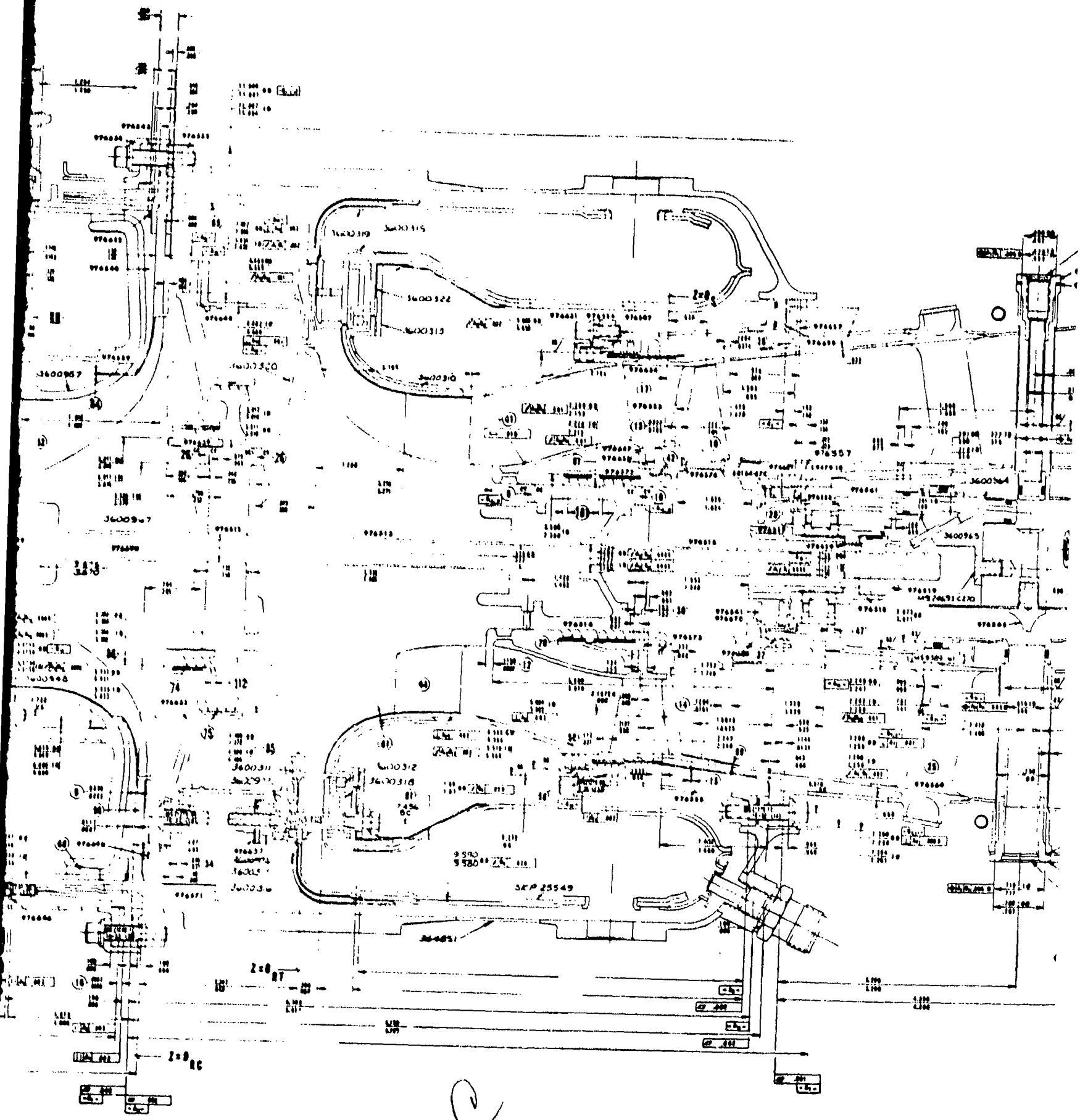
4. BUILD 4

4.1 Configuration

The fourth build was initiated in June 1971 and incorporated the following major changes in the APU hardware (Figure 195):

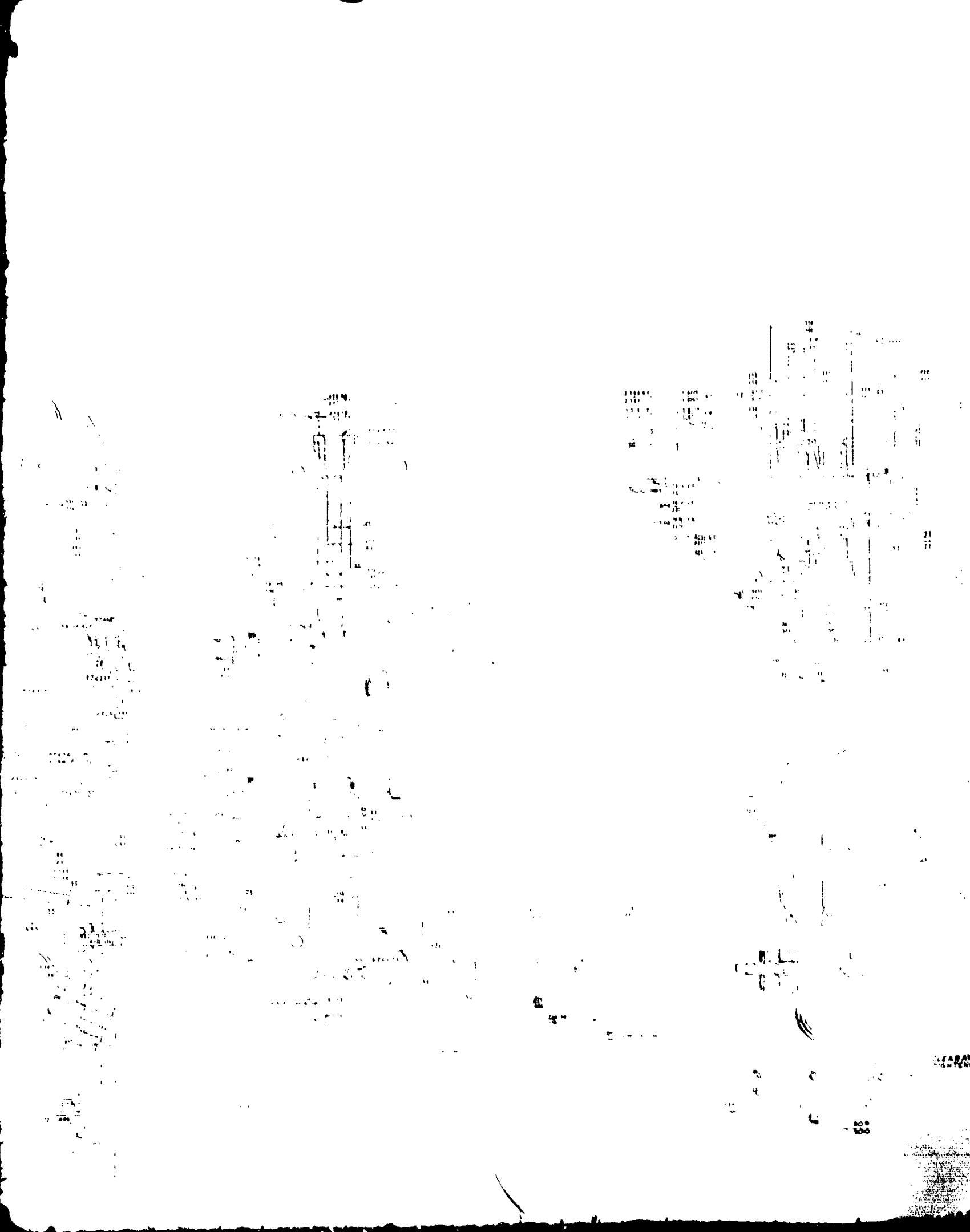
- (a) A new axial compressor rotor (-3 design) was incorporated.
- (b) A new two-stage axial compressor stator vane assembly, with a swept first-stage and rectilinear second stage, was installed.
- (c) A recontoured splitter (P/N 976540) and diffuser (P/N 976539) were incorporated.
- (d) The high-temperature columbium turbine nozzle assembly P/N 3600316) was incorporated.
- (e) Felt-metal abradable material was used on the P/N 976633 Interstage Seal Carrier.
- (f) An antirotation feature was installed on the P/N 976651 Turbine Bearing Carrier.
- (g) The exhaust housing assembly (P/N) 976560) was detuned to eliminate undesirable frequency responses.
- (h) The second-stage inlet guide vanes were omitted, as in the previous build.
- (i) The radial compressor wheel (P/N 976511-3, S/N 102) from Build 3 was re-used.
- (j) The bleed diffuser cross-sectional area was increased by shifting the forward wall and bleed plenum forward 0.070 in. and recontouring the knee. Enlarged passages were machined through the deswirl vanes to assure that no downstream flow limitation would occur.
- (k) Total and static pressure instrumentation was installed near the rotor notch to measure rotor performance.

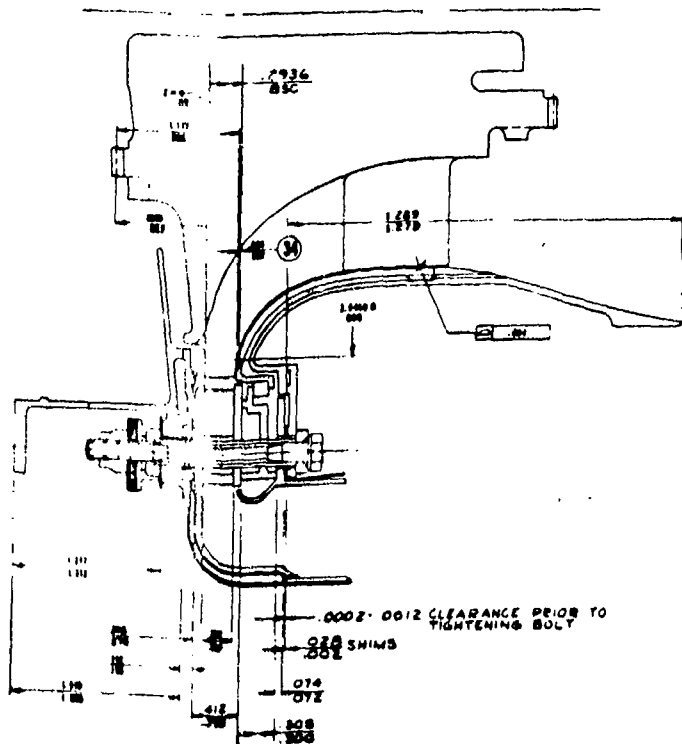
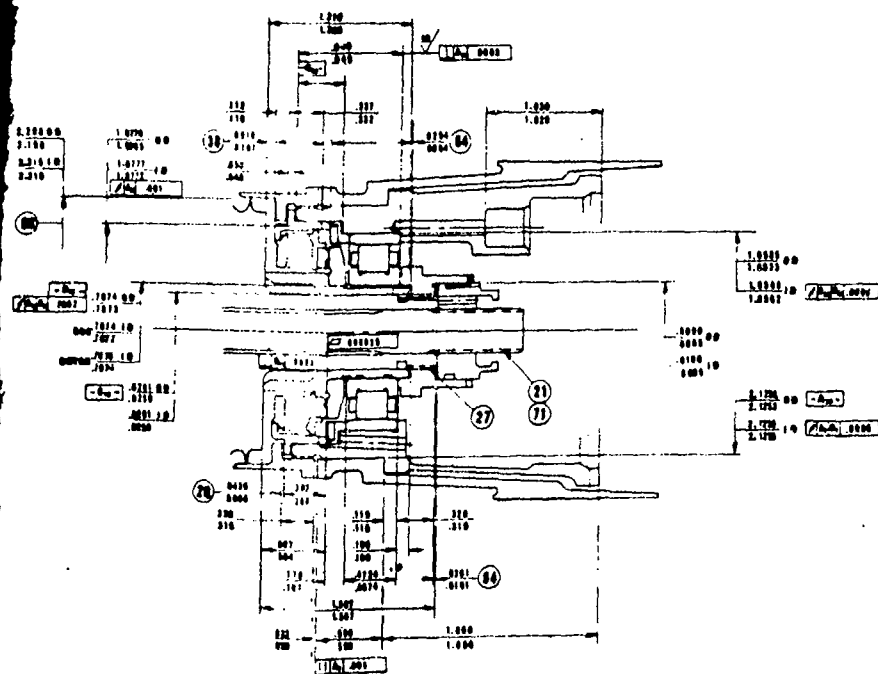




9

9 2 7





Filed as L687991

Figure 195

PREPARED BY DESIGNED BY CHECKED BY APPROVED BY DATE	2X 67CP 385-1	LAYOUT 3010-4 ADVANCED APU DIMENSIONAL LAYOUT	AL 7000379 4 25 2
---	------------------	---	----------------------

The APU was installed in the test cell with the following system hardware:

- (a) APU gearbox
- (b) Accessory gearbox
- (c) Torque converter
- (d) Hydraulic pumps (2)
- (e) VSCF generator
- (f) 5-kva generator

Provisions were made for loading the hydraulic pumps to 15 gpm and 3000 psi and the VSCF generator to 22 kva. A separately driven 20-gpm, 300-psi oil pump was provided for torque converter charging. An adapter was installed on the APU gearbox at the starter pad to mount an air turbine motor (ATM 80) for motoring and starting the APU.

4.2 Testing

The first motoring run was conducted on July 17, 1971. Twelve light-offs were made to check the APU performance and to attempt to make the APU self-sustaining. Efforts to attain these conditions were hampered by excessive thrust-bearing temperature (in the compressor bearing cavity) and a requirement to limit turbine inlet temperature to 2000°F.

The fourth build was motored for 3 hr 34 min. The APU was started 12 times and run hot for 1 hr 17 min. Twenty-six data scans were recorded, and representative data for Scans 108 and 109 are shown on Table XXX. Self-sustaining operation was not achieved. Analyses of the test data indicated a high leakage flow past the turbine nozzles and the possibility of nozzle-area increase, necessitated by vane distortion. The Build 4 first-stage nozzle consisted of individual

TABLE XXX

HOT RUNS, GTCP305, BUILD 4, 7/26/71

	SCAN NUMBER	108.00	109.00
	PCT PHYS SPEED	69.34	90.09
	PHYS SPEED, RPM	56721.60	73689.60
	INLET TEMP, DEG F	86.34	96.19
	CORR SPEED, RPM	55283.08	71182.17
	IGV1 DEGR CLOSED	0.00	0.00
	IGV2 DEGR CLOSED	0.00	0.00
AXIAL	**PCT CORR SPEED	67.58	87.02
COMPR	* CORR FLOW, LB/SEC	1.839	3.071
(C1)	* TOTAL PRESS RATIO	1.232	1.666
	**EFFICIENCY	.699	.796
	COMPRESSOR INTSTG DUCT P/P	1.000	1.000
RAD COMPRESSOR	CORR PCT SPEED	77.478	95.112
	**CORR FLOW, LB/SEC	.753	.756
BLEED	* STAGE P/P	1.155	1.277
RADIAL	* ROTOR P/P	2.756	3.458
COMPR	* EFFICIENCY, STAGE	.143	.153
(C2)	* EFFICIENCY, ROTOR	0.000	.896
	**ROTOR EXIT MACH NO	1.291	1.506
	**CORR FLOW, LB/SEC	.804	1.261
ENGINE	* STAGE P/P	3.050	3.337
RADIAL	* ROTOR P/P	3.202	4.925
COMPR	* EFFICIENCY, STAGE	.765	.543
(C3)	* EFFICIENCY, ROTOR	.804	.762
	**ROTOR EXIT MACH NO	.827	1.000
BLEED	**LB/MIN	49.728	63.729
PORT	* APR (W(C2)/W(C3))	.937	.599
	**P(PORT)/P(AMB)	1.423	2.127
	**COMPR DISCH TEMP, F	422.048	693.885
	*AIR MASS FLOW, LB/SEC	.802	.991
	* CALC BURN TEMP, F	1502.736	2320.078
	* TSF BASED ON ABOVE	.342	-.094
	* AVE MEAS BURN T, F	1589.064	1864.896
	* TSF BASED ON ABOVE	.243	.259
BURNER	* MAX MEAS BURN T, F	1872.384	2167.839
	* FUEL FLOW, LB/HR	48.000	96.500
	* EFFICIENCY	.979	.994
	* FUEL/AIR RATIO	.017	.027
	**PRESSURE RATIO	.954	.957
	**CORR FLOW AT NOZZLE	.463	.463
	* NOZZLE P/P DISCHG	3.579	5.424
	* W(COOL)/W(C3)	.073	.429
TURBINE	* PCT CORR SPD	80.725	88.117
	* EFFICIENCY	1.074	1.501
	* MEAS TOT, F	931.426	951.379
	**TURBINE HORSEPOWER	196.943	1009.974
	**APU CALC SHP	26.195	477.918
	* BLEED HP (RHP)	62.516	153.129
PERFORM.	* APU EQUIV HP (ESHP)	88.711	631.047
	**APU CYCLE P/P	3.759	5.559

nozzle vanes clamped between relatively thin end plates and restrained by a light spring-load through bolts. The high leakage and flow distortion at the inducer of the centrifugal stage would not permit self-sustaining operation at the rated maximum turbine inlet temperature.

Cumulative running time for all builds was 29 hr 3 min, of which 7 hr 55 min were with APU light-off. Forty cumulative starts were made through Build 4.

4.3 Teardown Inspection

Teardown inspection was completed July 30, 1971. Following is a summary of the observations:

- (a) The track of one knife edge of the P/N 976572 Seal was not running in the abradable material. An axial stack check revealed the seal was improperly assembled.
- (b) The P/N 3600314 Bolts showed discoloration at the cooling air inlet of the P/N 3600317 Sleeves.
- (c) Medium rub was evident in the area near the knee of the P/N 3600310 Turbine Shroud.
- (d) The P/N 976513 Radial Turbine Wheel had rub indications on all blades near the knee area, also on all blades at the tip of the forward face. Tips showed oxidation and/or erosion.
- (e) Slight fretting was evident on the radial compressor curvic teeth (P/N 976551).
- (f) The P/N 3600930 Seal ran with a portion of the carbon face over the relief groove of the seal rotor (P/N 3600955).

- (g) The bearing seat of the P/N 3600933 Bearing Carrier had indications of heavy fretting.
- (h) The P/N 3600934 Thrust Bearing was discolored on the aft side.
- (i) A very light rub was evident between the splitter (P/N 976540) and the wheel (P/N 976511).
- (j) All labyrinth seal hardware was in excellent condition.

5. BUILD 5

5.1 Configuration

The final Build 5 (Figure 196) incorporated the following design change improvements:

- (a) The compressor bearing carrier (P/N 3601751) was redesigned to provide increased oil drainage capacity and positive retention of the carbon seal.
- (b) Compressor inlet seal (P/N 3600930) was redesigned with reduced face load and seal rotor (P/N 976508).
- (c) The oil slinger, between the roller and ball bearing, was replaced with a cylindrical spacer.
- (d) The flow path contour between the axial-stage stator discharge and the radial compressor inlet was modified. A screen (P/N 3601771) was installed in the same area to improve the flow distribution as an interim fix.
- (e) The bleed diffusion passage was the same as the original Build 3 configuration.
- (f) The flow splitter (P/N 976540) inside diameter was increased 0.054 in., resulting in a thicker edge which maintained the

nozzle vanes clamped between relatively thin end plates and restrained by a light spring-load through bolts. The high leakage and flow distortion at the inducer of the centrifugal stage would not permit self-sustaining operation at the rated maximum turbine inlet temperature.

Cumulative running time for all builds was 29 hr 3 min, of which 7 hr 55 min were with APU light-off. Forty cumulative starts were made through Build 4.

4.3 Teardown Inspection

Teardown inspection was completed July 30, 1971. Following is a summary of the observations:

- (a) The track of one knife edge of the P/N 976572 Seal was not running in the abradable material. An axial stack check revealed the seal was improperly assembled.
- (b) The P/N 3600314 Bolts showed discoloration at the cooling air inlet of the P/N 3600317 Sleeves.
- (c) Medium rub was evident in the area near the knee of the P/N 3600310 Turbine Shroud.
- (d) The P/N 976513 Radial Turbine Wheel had rub indications on all blades near the knee area, also on all blades at the tip of the forward face. Tips showed oxidation and/or erosion.
- (e) Slight fretting was evident on the radial compressor curvic teeth (P/N 976551).
- (f) The P/N 3600930 Seal ran with a portion of the carbon face over the relief groove of the seal rotor (P/N 3600955).

- (g) The bearing seat of the P/N 3600933 Bearing Carrier had indications of heavy fretting.
- (h) The P/N 3600934 Thrust Bearing was discolored on the aft side.
- (i) A very light rub was evident between the splitter (P/N 976540) and the wheel (P/N 976511).
- (j) All labyrinth seal hardware was in excellent condition.

5. BUILD 5

5.1 Configuration

The final Build 5 (Figure 196) incorporated the following design change improvements:

- (a) The compressor bearing carrier (P/N 3601751) was redesigned to provide increased oil drainage capacity and positive retention of the carbon seal.
- (b) Compressor inlet seal (P/N 3600930) was redesigned with reduced face load and seal rotor (P/N 976508).
- (c) The oil slinger, between the roller and ball bearing, was replaced with a cylindrical spacer.
- (d) The flow path contour between the axial-stage stator discharge and the radial compressor inlet was modified. A screen (P/N 3601771) was installed in the same area to improve the flow distribution as an interim fix.
- (e) The bleed diffusion passage was the same as the original Build 3 configuration.
- (f) The flow splitter (P/N 976540) inside diameter was increased 0.054 in., resulting in a thicker edge which maintained the

M

D

E

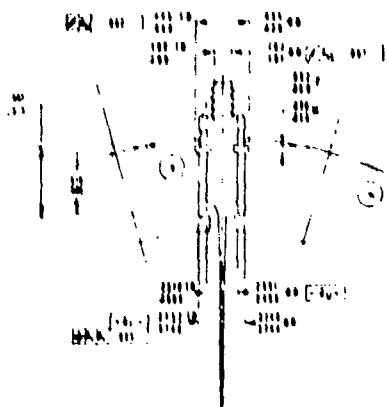
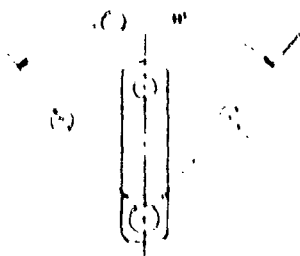
E

D

C

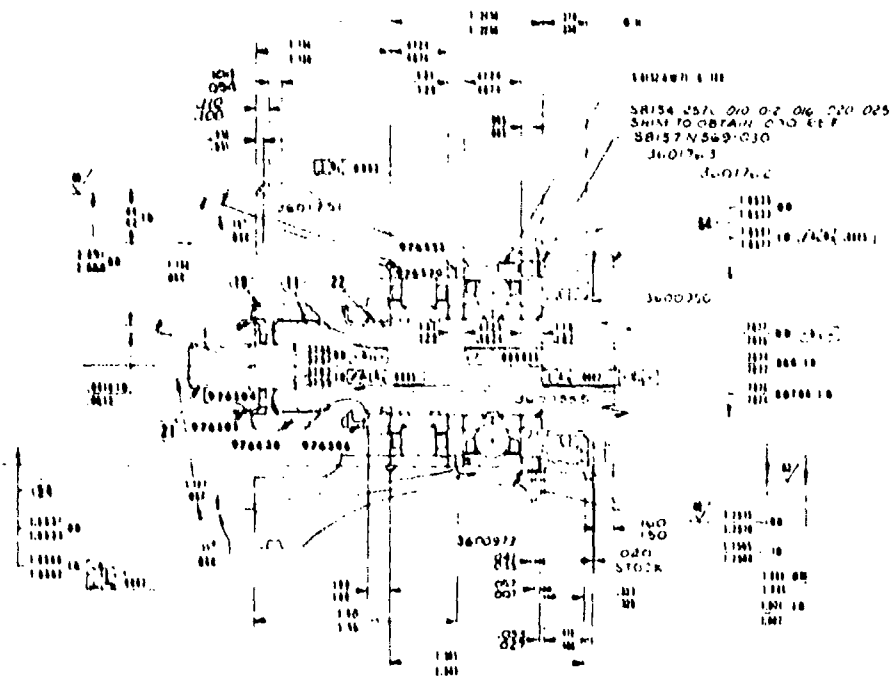
B

A



1.00

1.00



DATA 100 100
100 100

[Handwritten signature]

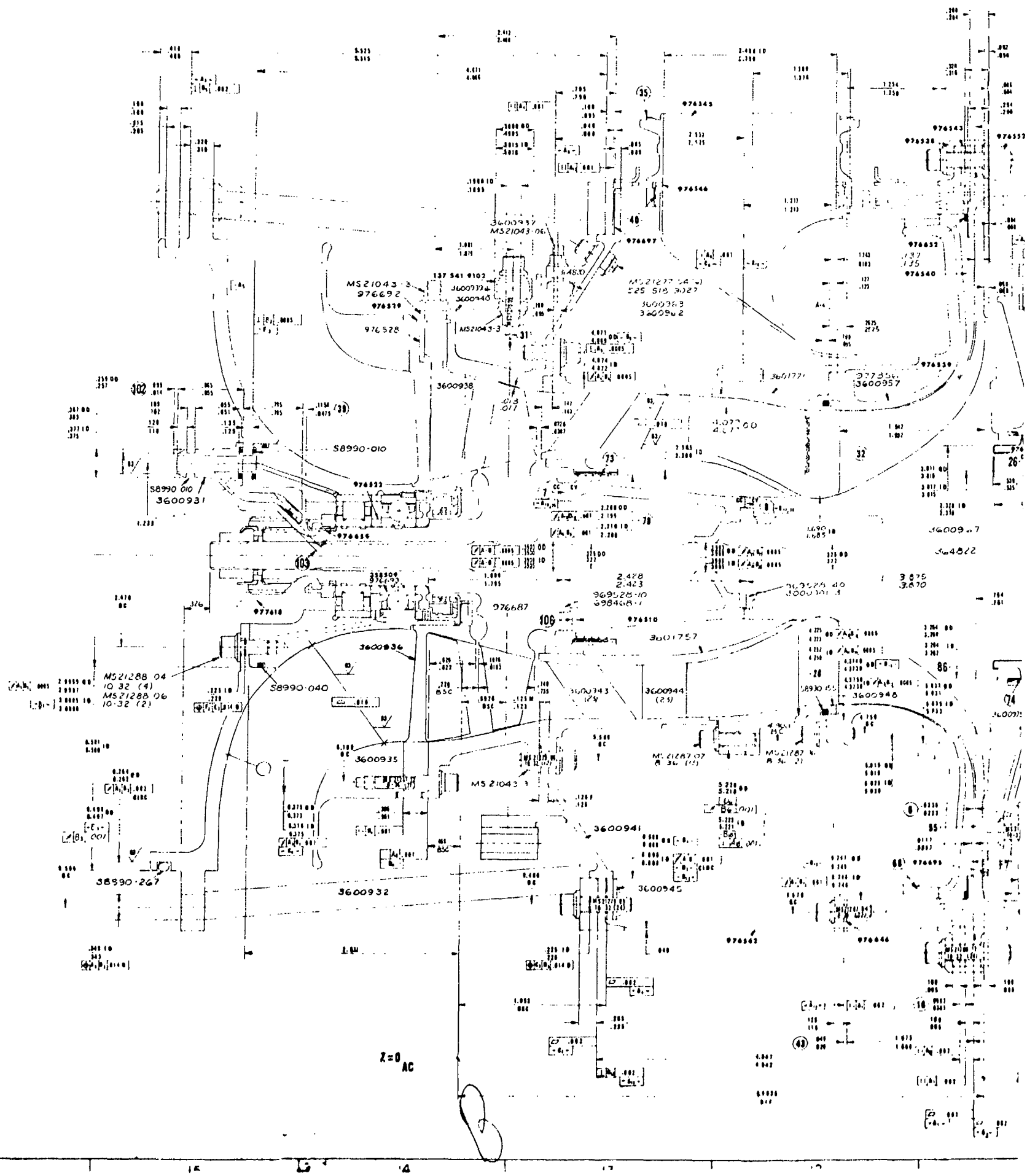
20

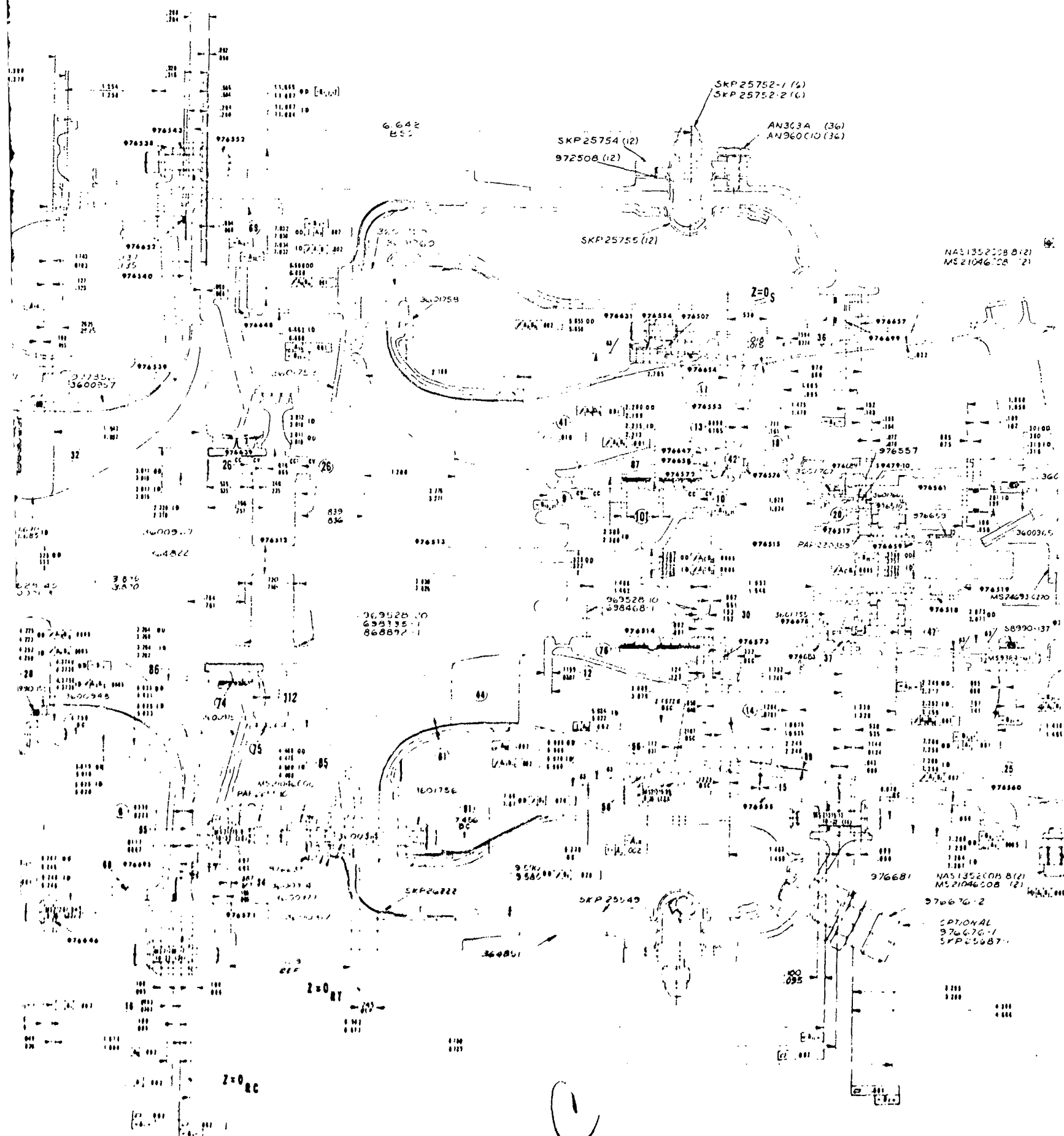
19

18

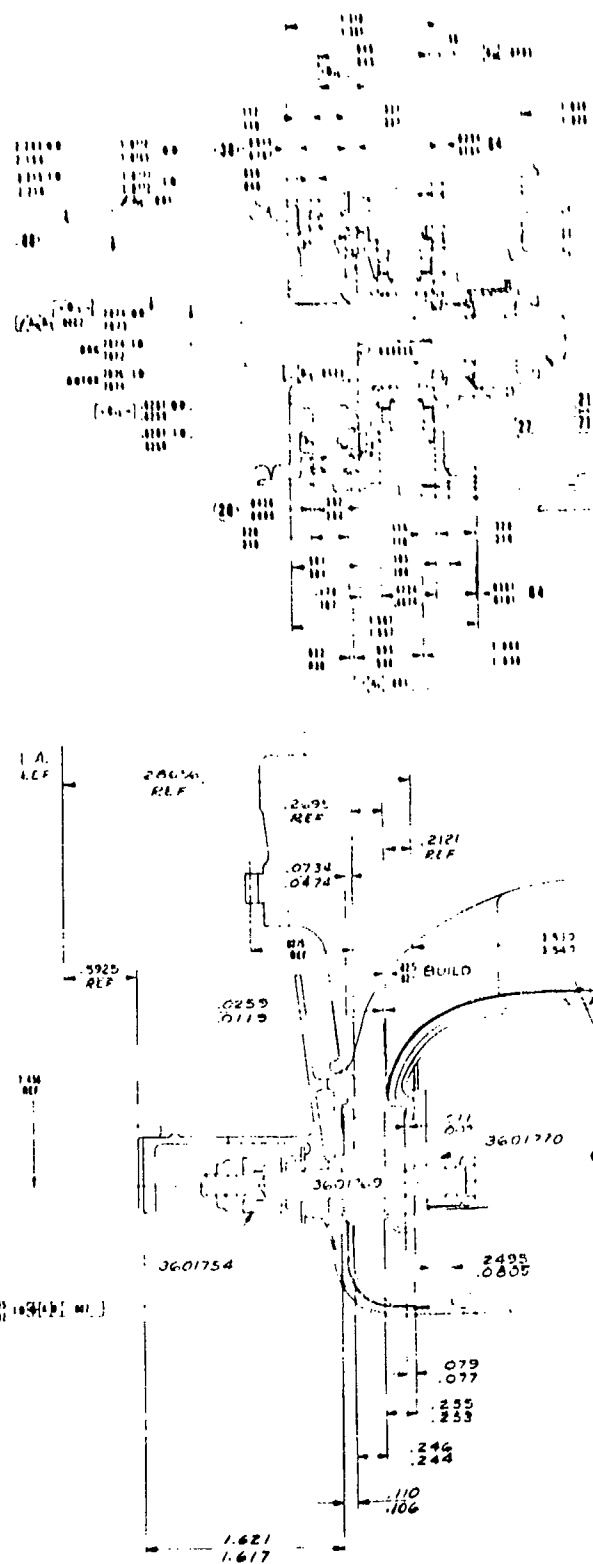
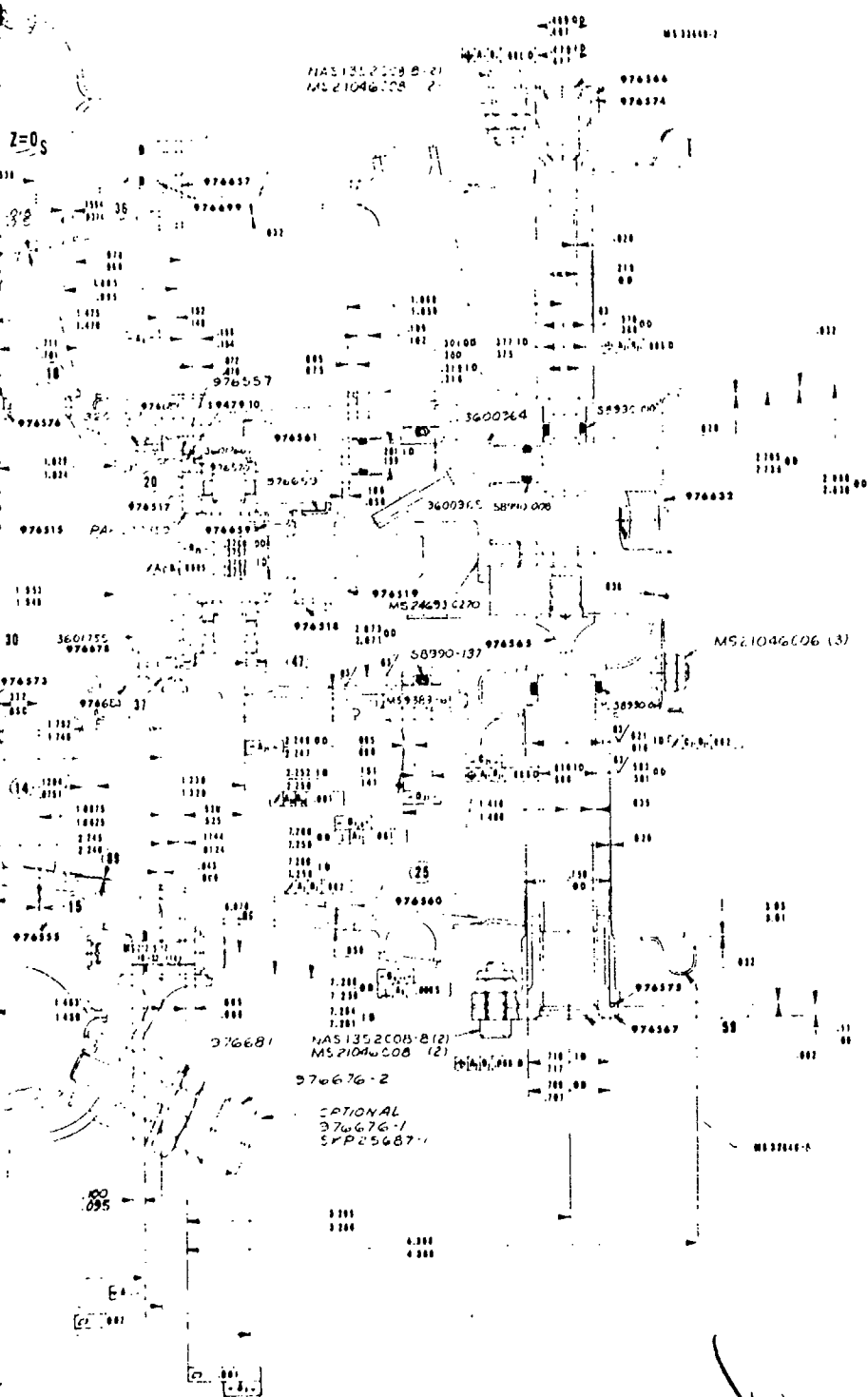
17

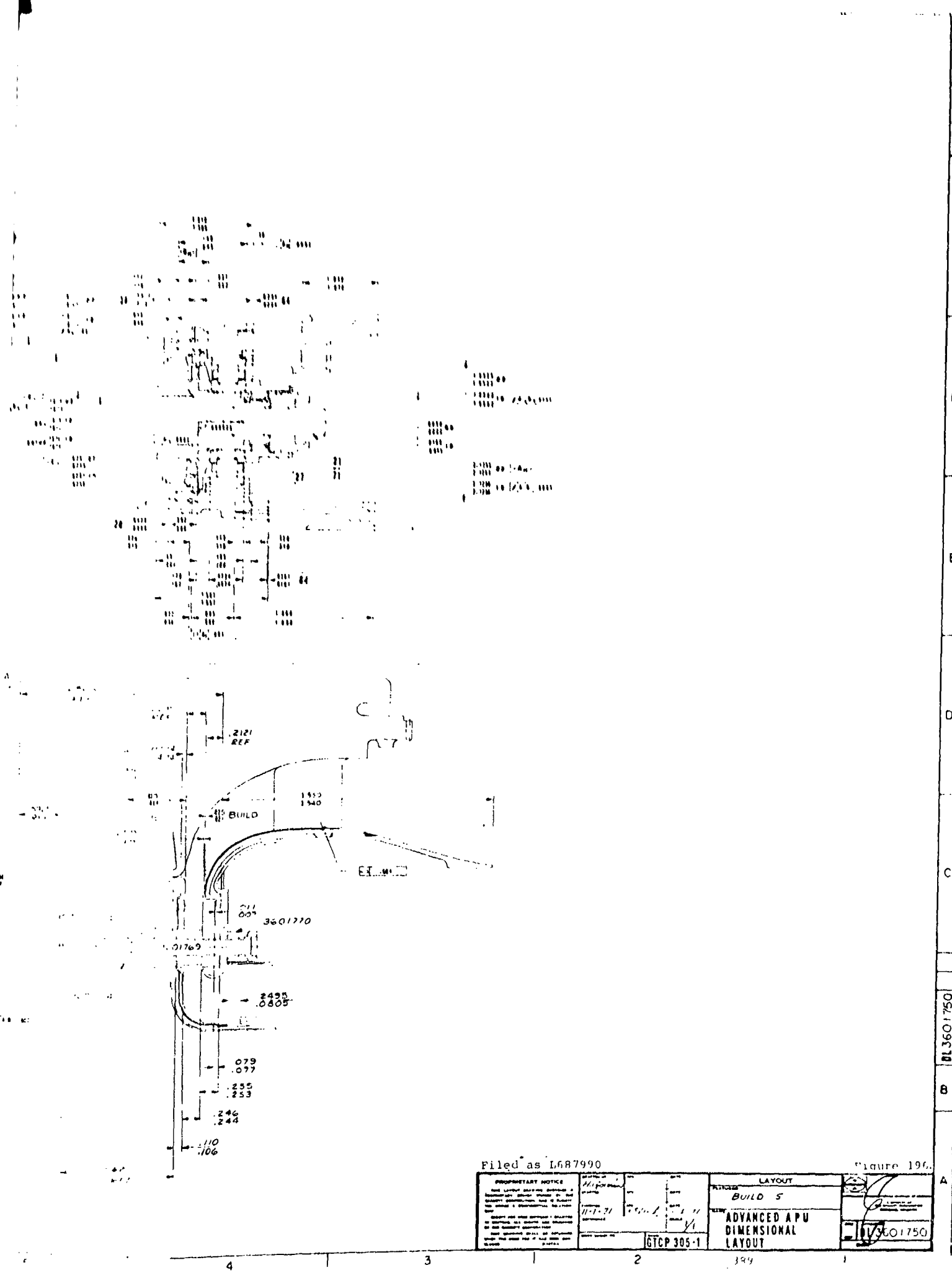
16





AN3634 4.3
AN3600 (1.1.1.1)





H
G
F
E
D
C
B
A

Filed as L687990

Figure 196.

PROPRIETARY NOTICE This layout drawing contains a proprietary design. It is not to be reproduced, copied, or otherwise used in any way without the written consent of the owner.	DATE OF DESIGN 11-1-71	DATE OF LAYOUT 11-1-71	DATE OF CHECK 11-1-71	LAYOUT BUILD 5	3601750
	GTCP 305-1			ADVANCED APU DIMENSIONAL LAYOUT	

original aerodynamic contour. The edge was finished to a full radius.

- (g) The radial compressor wheel (P/N 3600967) was modified to provide increased inducer blade thickness.
- (h) The radial turbine nozzle was modified to minimize leakage. Nozzle vanes were integral with one side plate, and intermediate side plates were eliminated. A redundant nozzle-bolting configuration was used. Nine of the 19 bolts were designed to operate in thermal transients without spring-preload, and the remainder were preloaded with springs identical to those of previous builds. The spring preloaded bolts contained 10 springs each and provided a total clamping load equivalent to previous builds. All turbine nozzle and wheel cooling passages were eliminated.
- (i) The turbine bearing carbon seal was antirotated.

5.2 Instrumentation

Aerodynamic and mechanical safety instrumentation, used in Build 5, is shown schematically in Figure 197. The instrumentation (similar to that used in previous builds) is described in the following paragraphs.

5.2.1 Aerodynamic Instrumentation

Aerodynamic instrumentation is comprised of the following five components:

- (a) First-Stage Compressor controls the following characteristics.
 - (1) Inlet Temperature (Items 300 through 307) - Four pairs of thermocouples, attached to inlet screen at four 90-deg locations

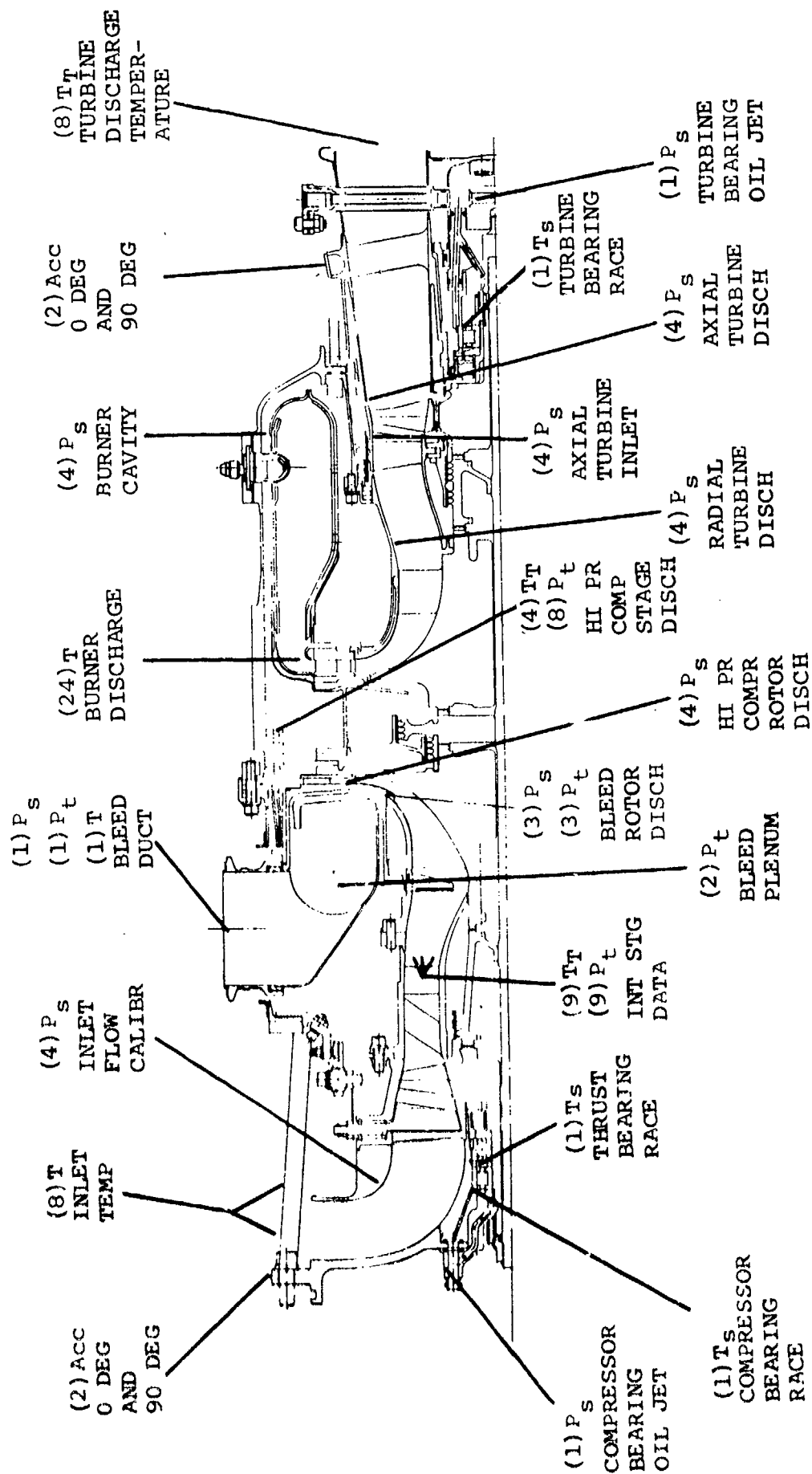


Figure 197. Build 5 APU Instrumentation.

- (2) Inlet Air Flow (Items 115 through 118 and 224) - One total pressure (KIEL) probe and four shroud wall static-pressure taps ahead of inlet guide vanes and calibrated for flow measurement prior to APU assembly
 - (3) Discharge Temperature and Pressure (Items 216 through 224 and 400 through 408) - Three element total-temperature and total-pressure rakes located at rectilinear stator discharge
- (b) Interstage Duct distributes the static pressure through the following taps:
- (1) Shroud Static Pressure Taps (Items 170 through 180) - For distribution at 45-deg circumferential position from rectilinear stator trailing edge to radial compressor notch
 - (2) Hub Static Pressure Taps (Items 181 through 185) - For distribution at 45-deg circumferential position from rectilinear stator trailing edge to radial compressor inlet.
- (c) Bleed is controlled by thermocouples, a discharge duct, and to specific flow measurements:
- (1) Bleed Plenum Temperature (Items 429 through 432) - Four thermocouples at 90-deg spacing in low velocity plenum
 - (2) Discharge Duct Total Pressure (Item 249) - One lab total-pressure probe in slave discharge duct ahead of load control and surge valve

- (3) Flow Measurement - Lab orifice P_1 = Item 153, P_2 = Item 54, Temperature = Item 334
- (d) Compressor Discharge is controlled by the following pressures:
- (1) Rotor Static Pressure (Items 146 through 149) - Four aft wall static taps at 90-deg spacing
 - (2) Stage Total Pressure (Items 228 through 235) - Four dual-element, total-pressure rakes at approximately 90-deg spacing (midway between pairs of axial diffuser vanes)
 - (3) Stage Total Temperature (Item 412 through 415) - Four single-element, total-temperature rakes at approximately 90-deg spacing (midway between pairs of axial diffuser vanes)
 - (4) Stage Static Pressure (Items 160 through 163) - Four static taps in outer wall at 90-deg spacing
- (e) Turbine elements are governed by the following factors:
- (1) Fuel Flow - By lab rotometer
 - (2) Turbine Inlet Temperature (Items 601 through 623) - Twenty-three platinum thermocouples of 10-percent rhodium-aspirated at 15-deg spacing, in measure temperature at combustor discharge pitch streamline.
 - (3) Axial Turbine Stator Shroud Static Pressure (Items 100 through 103) - Four shroud static taps at 90-deg spacing stator discharge

- (4) Axial Turbine Rotor Exit Shroud Static Pressure (Items 104 through 107) - Four shroud static taps at 90-deg spacing rotor discharge
- (5) Turbine Exit Temperature (Items 420 through 427) - Four dual-element total-temperature rakes of 90-deg spacing in lab tail pipe.

5.2.2 Mechanical Safety Instrumentation

The mechanical safety instrumentation involves the following four parameters and the precise characteristics of each.

(a) Oil Pressure:

- (1) Compressor Oil Jet Pressure (Item 150) - Measured at APU fitting
- (2) Turbine Oil Jet Pressure (Item 136) - Measured at APU fitting

(b) Bearing Temperature:

- (1) Compressor Roller Bearing Outer Race (Item 333) - Mounted in bearing carrier touching outer race forward edge
- (2) Thrust Bearing Outer Race (Items 309 and 339) - Welded to forward edge and race OD near aft edge
- (3) Turbine Roller Bearing Outer Race (Item 308) - Mounted in bearing carrier touching outer race aft edge

(c) APU Vibration:

- (1) APU/Gearbox Interface (Items 402 and 403) - Two accelerometers mounted on gearbox adjacent to APU mounting flange, 0- and 90-deg positions
- (2) Turbine Exhaust Duct - Two accelerometers mounted on strut support ring, 0- and 90-deg positions

(d) Surge Warning Detection:

- (1) First-Stage Compressor High-Response Thermocouple (Item 341) - Near shroud ahead of Stage 1 rotor
- (2) Second-Stage Compressor High-Response Thermocouple (Item 340) - Near shroud ahead of Stage 2 rotor.

5.3 Testing

The APU was installed on the system demonstration stand on January 3, 1972. Mechanical check runs, motoring for light-off data, and self-sustaining running were completed on January 28, 1972. Build 5 accumulated 8 hr 40 min of rotating time, of which 3 hr 36 min was hot running; 36 digital data scans were recorded. Total cumulative rotating time on all APU builds was 37 hr 43 min of which 11 hr 31 min were hot operation; 162 data scans were recorded. To provide an adequate stress margin for the Build 5 APU with the backup Astroloy turbine wheel, turbine inlet temperatures were limited to a maximum of 2000°F rather than design inlet temperature of 2200°F. The corresponding performance goal for the demonstration test was 162 eshp.

The APU was first motored for mechanical integrity, then to obtain optimum light-off parameters and optimum variable IGV settings. The setting that gave sufficient surge margin, commensurate with maximum shaft

power at speeds above 95 percent, was +15 deg (closed) at a full-open bleed-valve position.

The starting sequence was manually controlled to 95-percent speed, where control automatically reverted to the governor. Prior to start initiation, the axial compressor VIGVs were closed to 40 deg, the ignition was turned on, the bleed-air valve was opened, and the high-pressure surge valve was opened. The high-pressure surge valve was required, since the normal bleed valve was not large enough to pass enough bleed-air to keep the axial compressor out of surge during low-speed operation. An automatic control would normally sequence the first-stage IGVs closed to reduce or eliminate the requirement of surge bleed; however, for the test bed engine, a conservative manual control approach was followed to ensure a safe, cool start. An air turbine motor was utilized to motor and start the APU in order to provide a maximum of experimental flexibility with a minimum of risk to the APU.

Table XXXI shows selected performance data from the final Build 5 APU performance testing. Scan 147 data show an equivalent shaft horsepower of 162.7 at the corrected conditions corresponding to a 130°F sea-level day. The performance goal at these conditions was 162 eshp. Analysis of the data shows the axial compressor efficiency was significantly lower than predicted and the centrifugal compressor efficiency slightly lower than predicted. Although the build incorporated a significant amount of interstage instrumentation for this size engine, insufficient valid data were available for any final conclusions on APU compressor performance. Turbine efficiency was slightly higher than predicted, and the data showed evidence of first-stage turbine nozzle erosion or leakage around the combustor lip seal, resulting in an effective area (flow) reduction. The combustor temperature spread factor was higher than predicted and appeared to increase as testing progressed, an indication that the lip seal at the outlet of the combustor had developed leakage that resulted in a temperature higher than normal.

TABLE XXXI

SELF-SUSTAINING RUN, GTP405, BUILD 5, 1-21, 1-24, and 2-17-72

	SCAM POWER	137.00	144.00	149.00	147.00
	PCT ADVQ SPEED	84.95	94.81	94.84	93.96
	DIFFS SPEED, RPM	71126.84	77067.25	77044.99	76775.04
	INLET TEMP, DEG F	74.95	74.44	74.83	77.40
	CORR SPEED, RPM	69920.87	74945.19	75945.64	75444.71
	IOV1 DRGT CLOSED	35.00	15.00	15.00	15.00
	IOV2 DRGT CLOSED	0.00	0.00	0.00	0.00
AXIAL	COMPCT CORR SPEED	85.49	92.84	92.84	92.24
COMPR	• CORR FLOW, LB/SEC	2.273	2.748	2.748	2.809
(C1)	• TOTAL PRESS RATIO	1.403	1.648	1.648	1.631
	• EFFICIENCY	.897	.902	.901	.879
	COMPRESSION INTRIN DUCT P/P	.962	.948	.958	.955
MAN COMPRESSOR	CORR PCT SPEED	94.511	100.324	100.301	99.832
	• CORR FLOW, LB/SEC	.668	.684	.684	.692
BLEED	• STAGE P/P	2.711	2.754	2.752	2.615
RADIAL	• ROTOR P/P	3.404	3.404	3.409	3.402
COMPR	• EFFICIENCY, STAGE	.904	.947	.944	.923
(C2)	• EFFICIENCY, ROTOR	.943	.773	.773	.782
	• ROTOR EXIT MACH NO	1.193	1.230	1.231	1.265
	• CORR FLOW, LB/SEC	1.154	1.272	1.272	1.300
ENGINE	• STAGE P/P	5.232	5.468	5.464	5.538
RADIAL	• ROTOR P/P	5.858	6.207	6.204	6.189
COMPR	• EFFICIENCY, STAGE	.791	.749	.748	.751
(C3)	• EFFICIENCY, ROTOR	.859	.810	.804	.813
	• ROTOR EXIT MACH NO	.964	.995	.994	.994
BLEED	• LB/MIN	47.229	53.278	53.292	55.447
PORT	• RPM (W(C2)/W(C3))	.575	.514	.514	.533
	• P(PORT)/P(AMB)	3.659	4.149	4.346	4.075
	• CORR DISCH TEMP, F	635.493	729.092	730.401	728.450
	• AIR MASS FLOW, LB/SEC	1.437	1.744	1.742	1.724
	• AVE HEAS BURN T, F	1978.401	1992.410	1994.344	2056.745
	• TSF BASED ON ABOVE	.208	.260	.242	.255
BURNER	• MAX HEAS BURN T, F	2254.720	2321.514	2326.020	2394.866
	• FUEL FLOW, LB/HR	115.400	136.100	136.300	139.400
	• EFFICIENCY	.830	.857	.860	.862
	• FUEL/AIR RATIO	.026	.024	.024	.025
	• PRESSURE RATIO	.949	.944	.946	.947
	• CORR FLOW AT NOZZLE	.420	.443	.445	.445
	• NOZZLE P/P DISCH	6.784	8.419	8.409	8.298
	• W(COOL)/W(C3)	.084	.054	.050	.084
TURBINE	• PCT CORR SPD	90.809	98.116	98.114	96.491
	• EFFICIENCY	.866	.858	.864	.878
	• MEAS TOT, F	1219.361	1153.147	1156.720	1194.433
	• TURBINE HORSEPOWER	391.379	562.448	563.409	566.442
	• APU CALC SHP	0.000	0.000	0.000	0.000
	• BLEED HP (RHP)	116.623	156.932	157.311	161.423
PERFORM.	• APU EQUIV HP (ESHP)	116.623	156.932	157.311	161.423
	• APU CYCLE P/P	7.061	8.791	8.787	8.630

SECTION XI

CONCLUSIONS

The overall results of this program show the potential, through experimental development, of achieving high horsepower per unit volume and per unit weight. Significant achievements were made in small gas turbine component technology, utilizing an advanced auxiliary power unit gas turbine and power system test bed as vehicles for development.

Technological advancements applicable to small gas turbines, in general, were made in the following areas:

- (a) High-work radial inflow turbine aerodynamics
- (b) Uncooled combustor
- (c) High-work axial compressor with variable geometry
- (d) Short radius ratio centrifugal compressor/diffuser combination
- (e) High-speed torque converter

Areas requiring further effort for general technological application center around matching the small compressors for bleed and power machines and turbine material work, specifically AF2-1DA. In addition, controls, accessories, and gearbox functions, not covered under this contract, are recommended for consideration.

To validate the results of Experimental Development component technological efforts, as applicable to small gas turbines, a much broader spectrum of effort is recommended, involving the total system. Consideration should also be given to gas turbine life and life-cycle cost, pertaining to advanced small auxiliary power units.

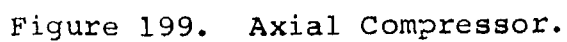
REFERENCES

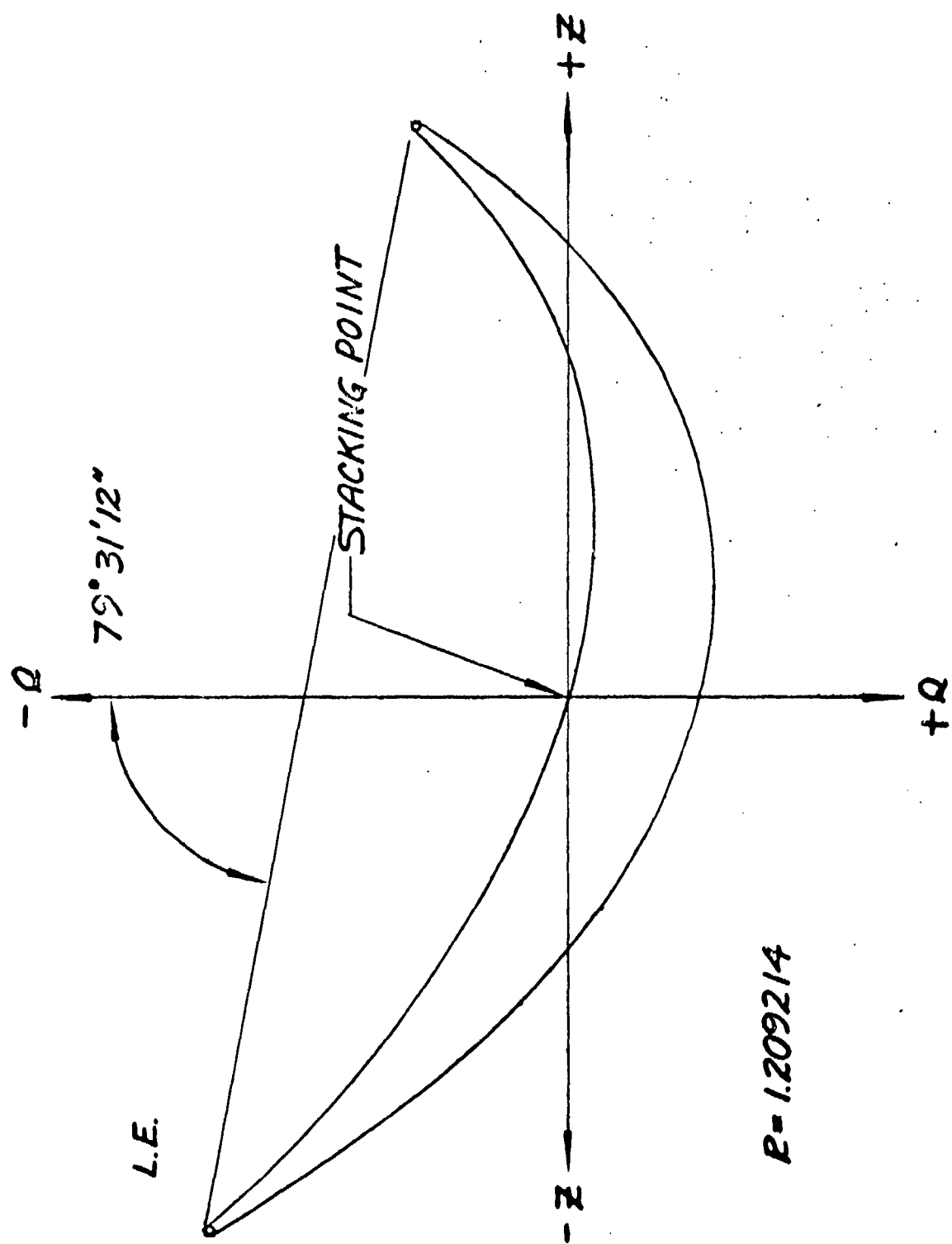
1. NASA Reports, NASA CR-72562 and NASA CR-72694,
2. Morgan, P. G., "Fluid Flow Through Screens of Low Solidity," Journal of the Aeronautical Society, Vol. 66, January 1962.
3. Penny, N., "Power Case History of Small Gas Turbines," Paper 634A, Automotive Engineering Congress, January 1963.
4. Jandasek, V. J., "The Design of a Single-Stage Three-Element Torque Converter," SAE Advances in Engineering, Vol. 1, 1962 pp. 154-174.

APPENDIX

Illustrations and Their Tabular Coordinates
for the
Technologically Advanced
Auxiliary Power System Program

Preceding page blank





P-1209214

Figure 200. Axial Compressor Blade Stacking.

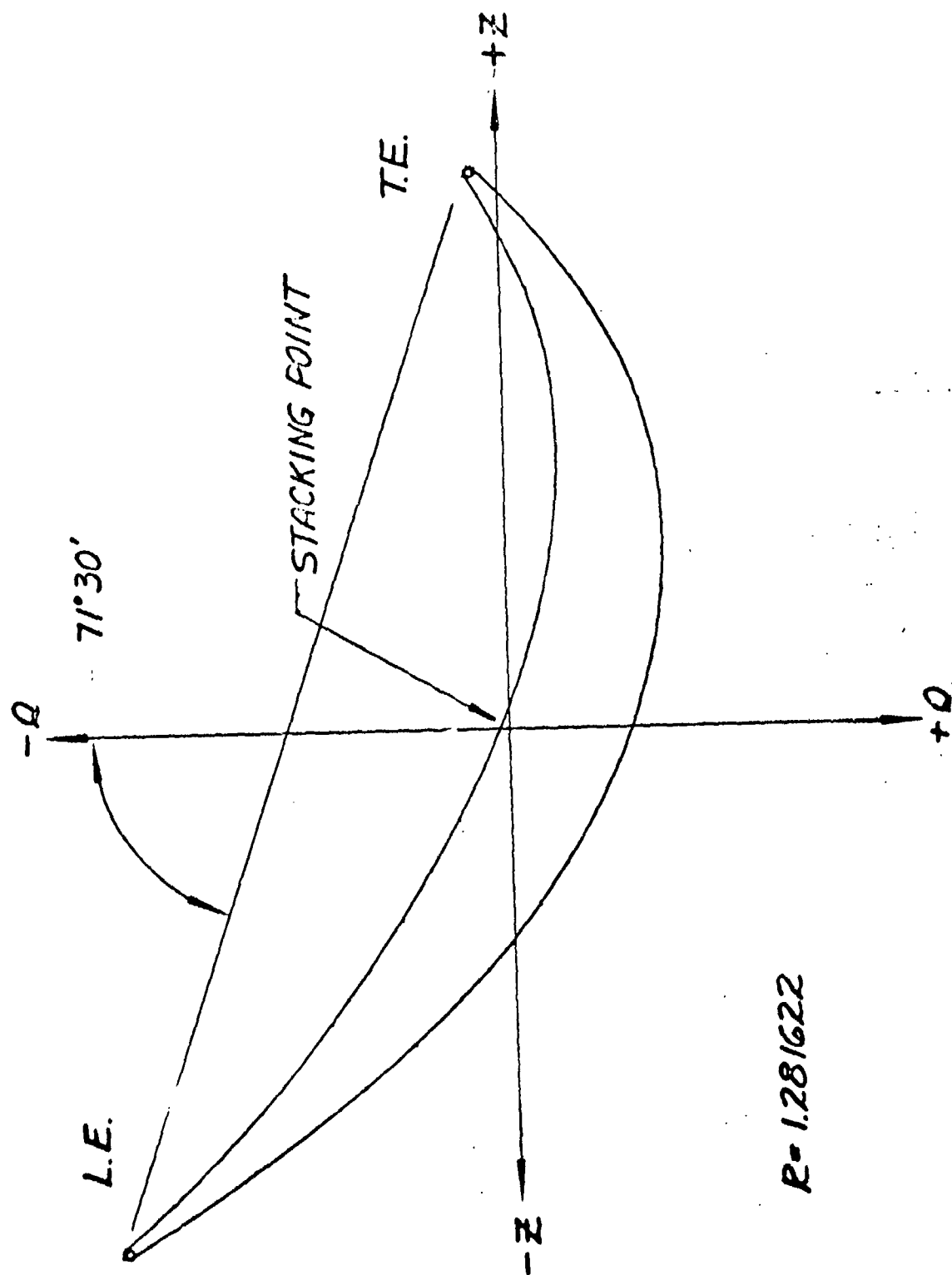
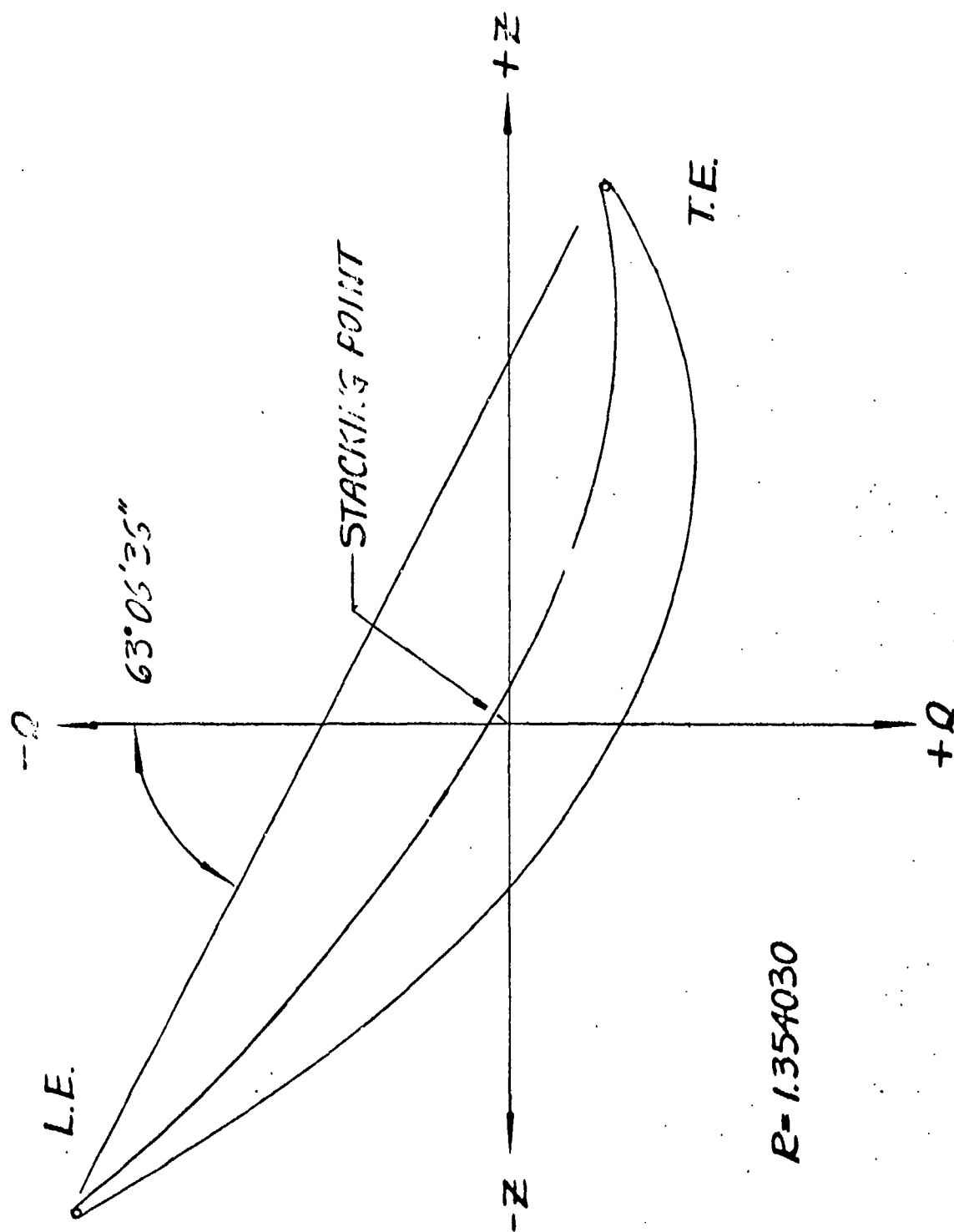


Figure 201. Axial Compressor Blade Stacking.



$R=1.354030$

Figure 202. Axial Compressor Blade Stacking.

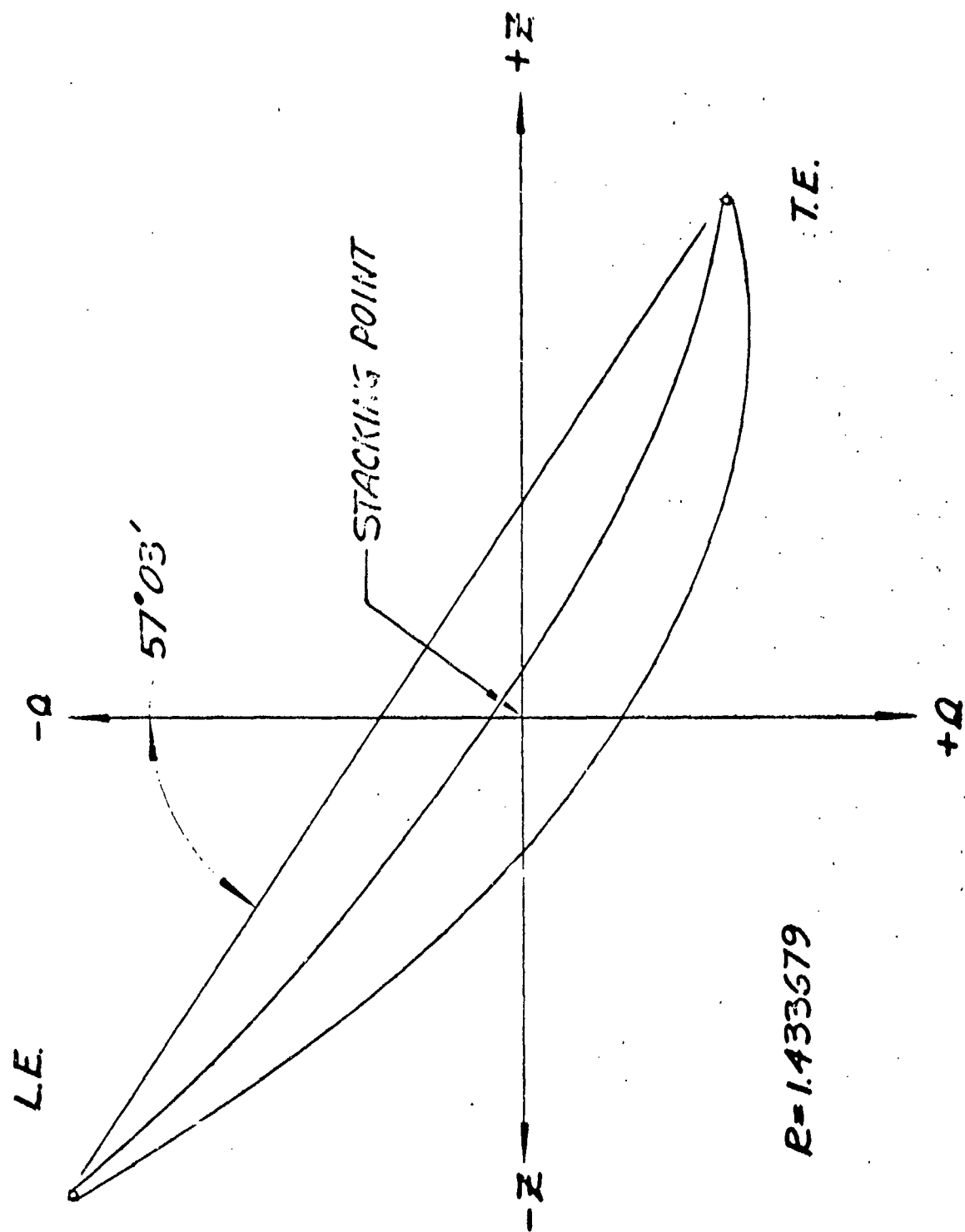


Figure 203. Axial Compressor Blade Stacking.

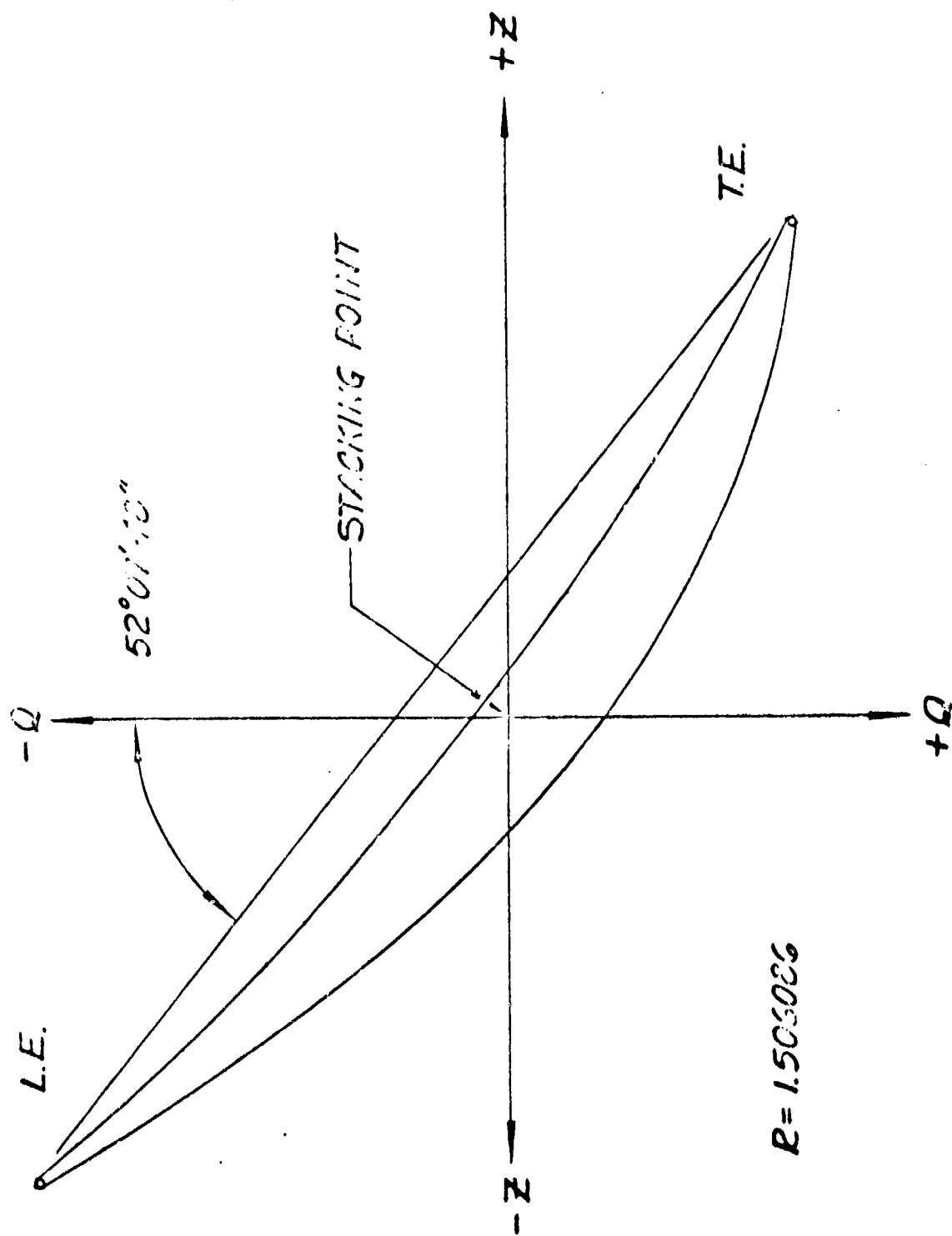


Figure 204. Axial Compressor Blade Stacking.

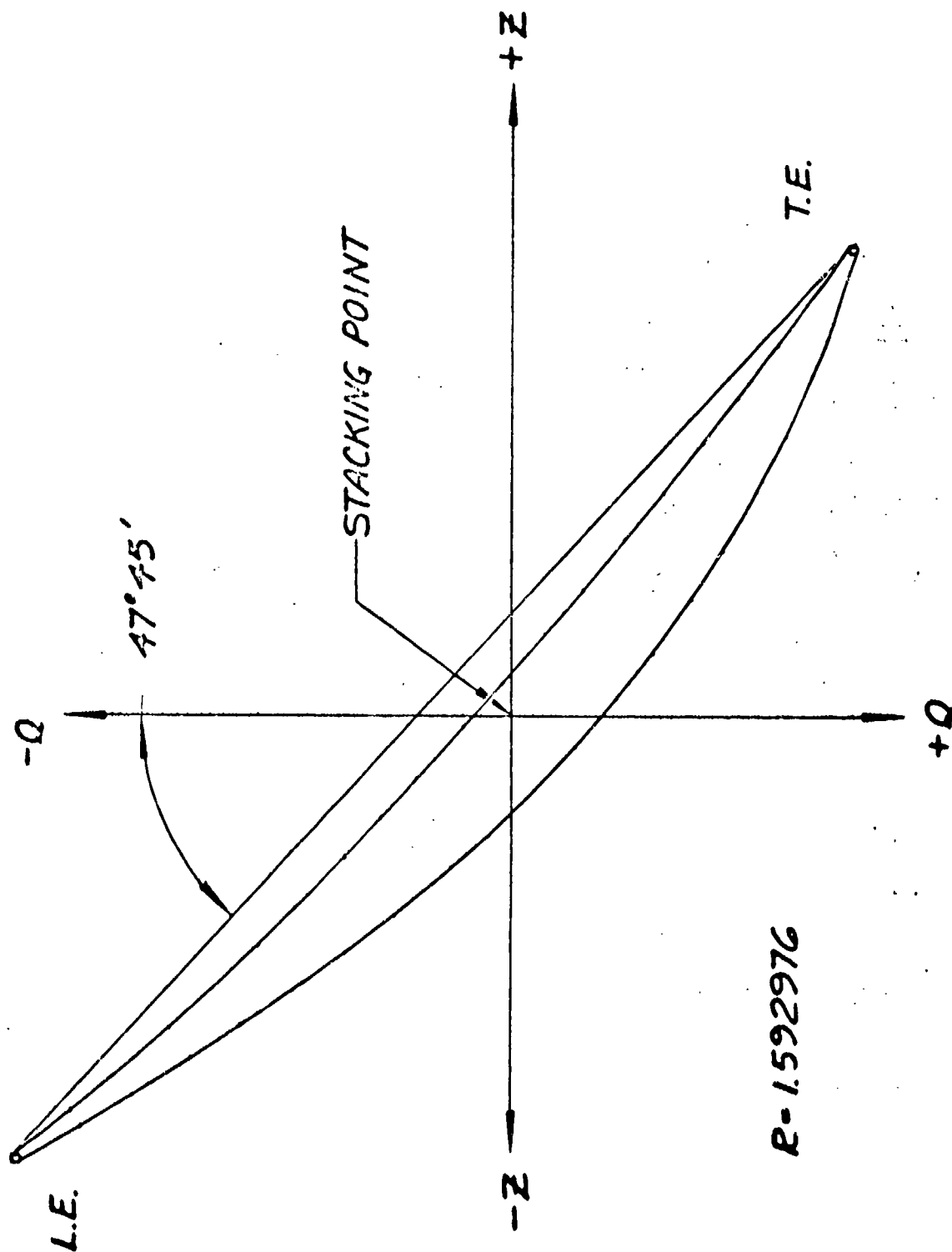


Figure 205. Axial Compressor Blade Stacking.

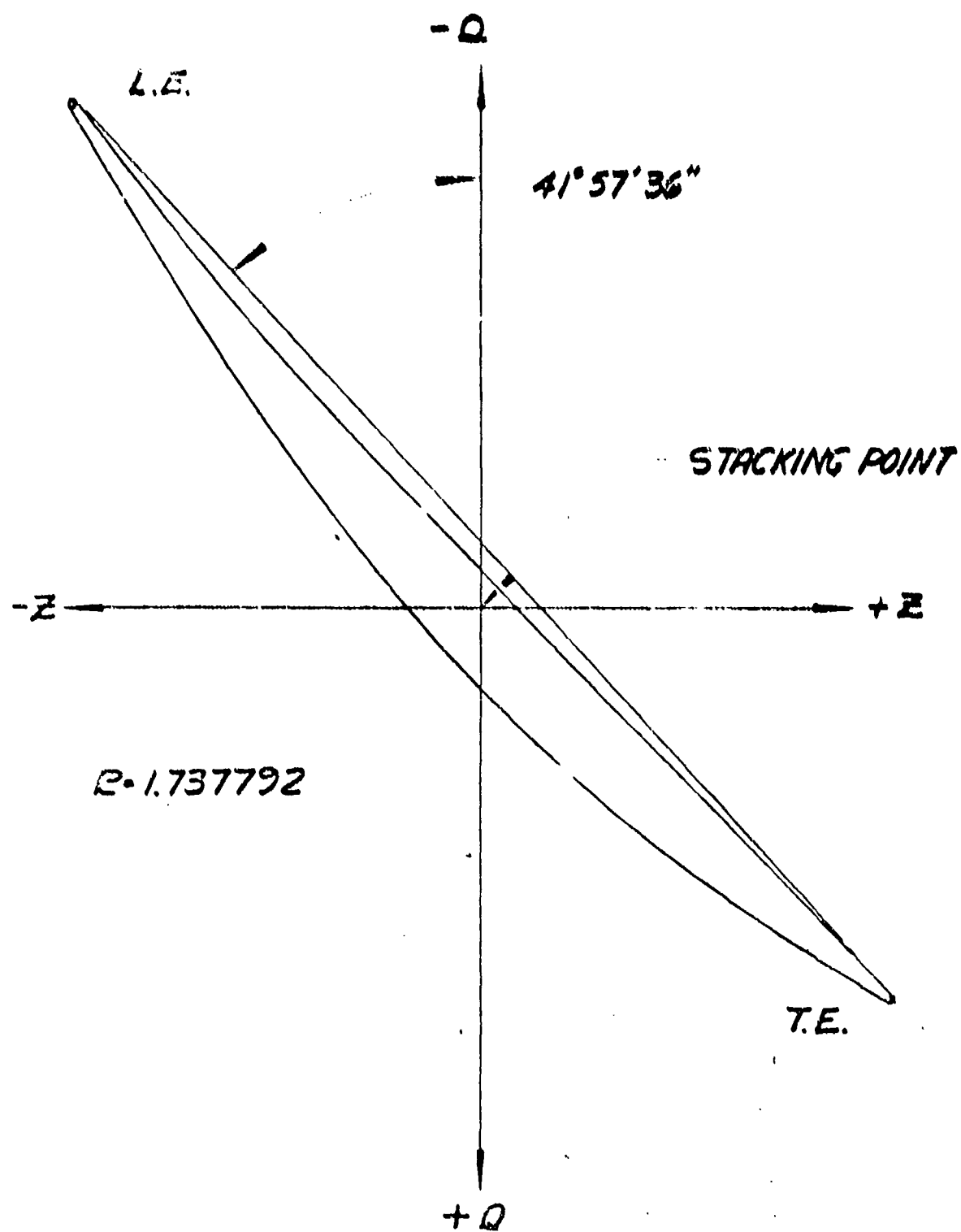


Figure 206. Axial Compressor Blade Stacking.

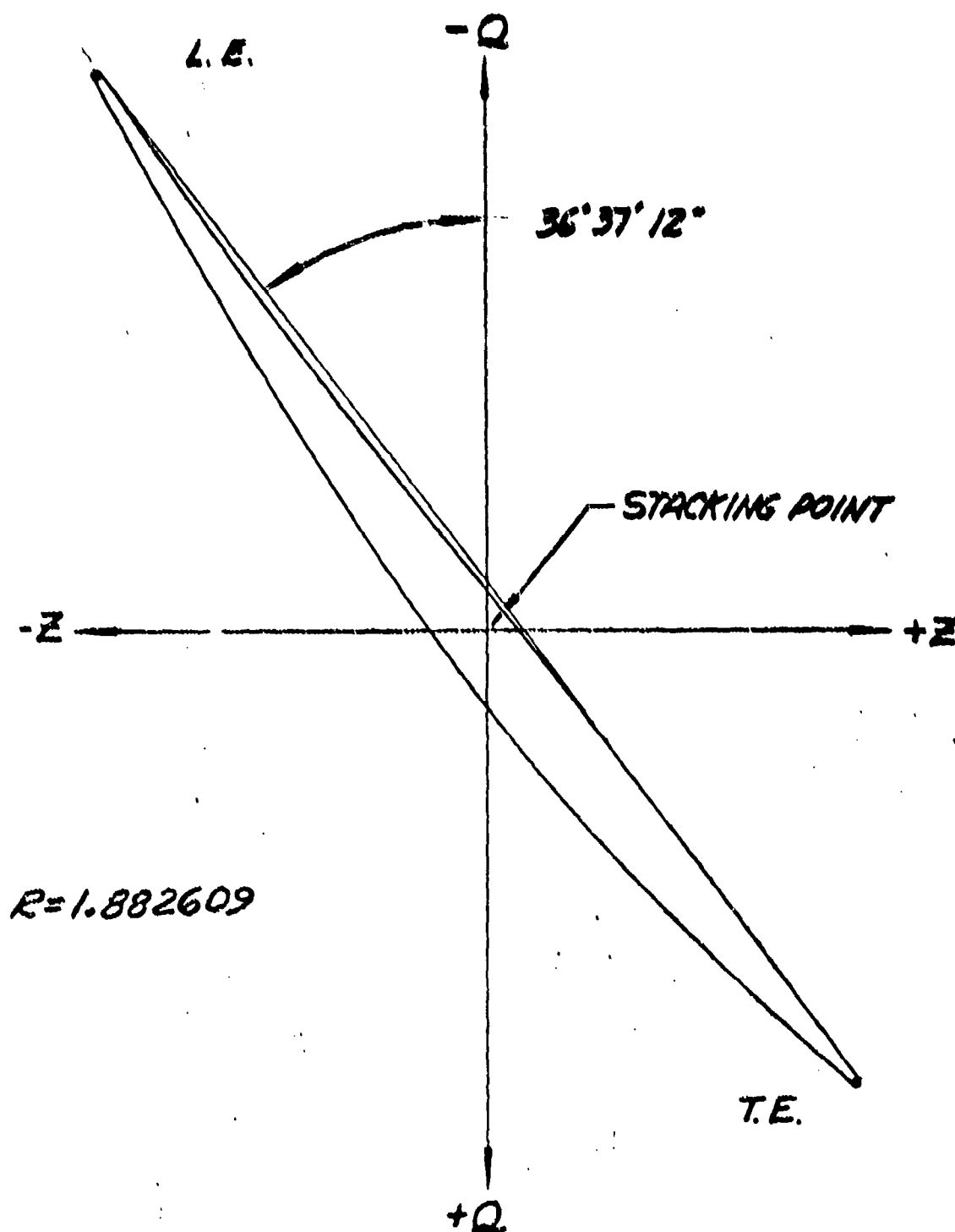


Figure 207. Axial Compressor Blade Stacking.

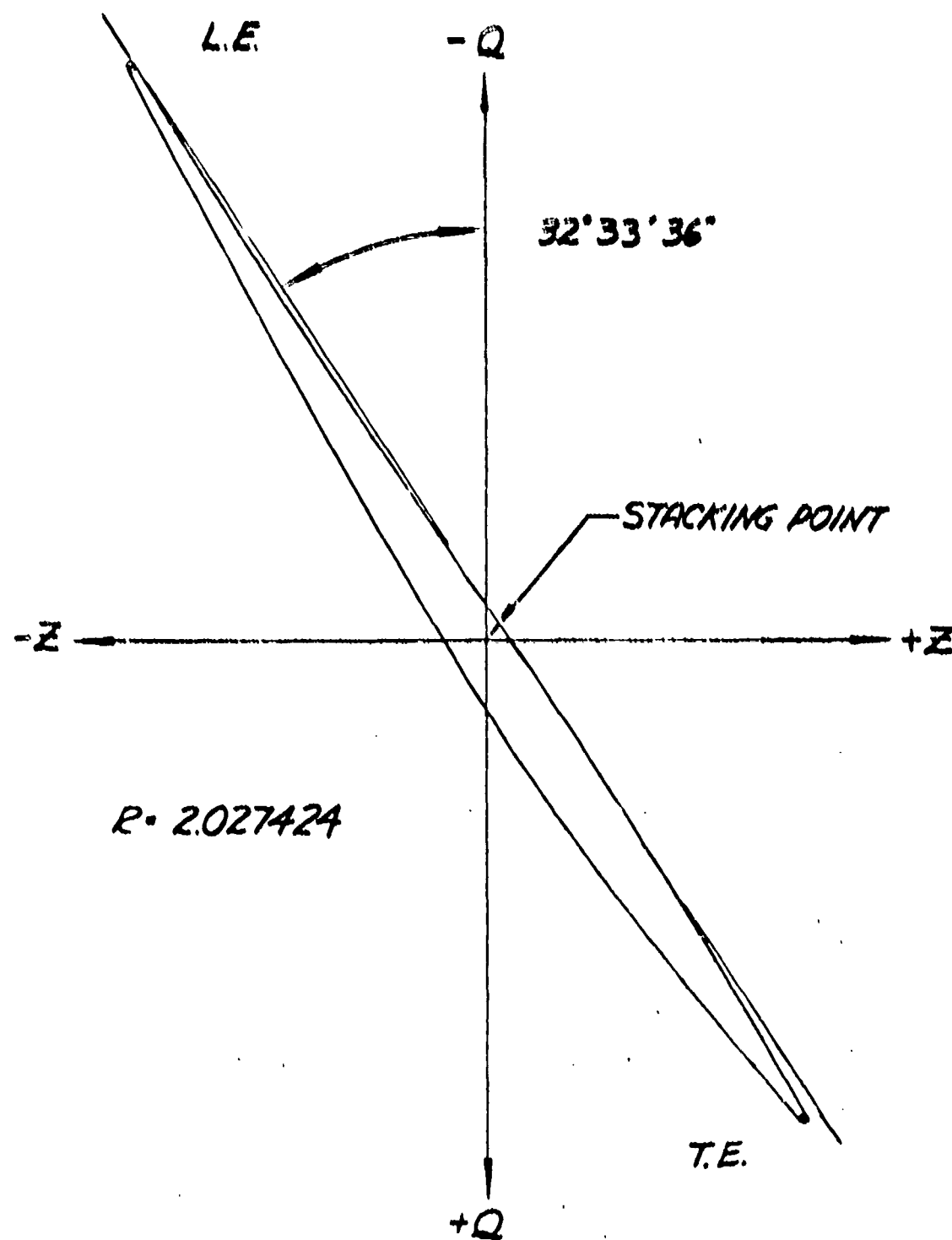


Figure 208. Axial Compressor Blade Stacking.

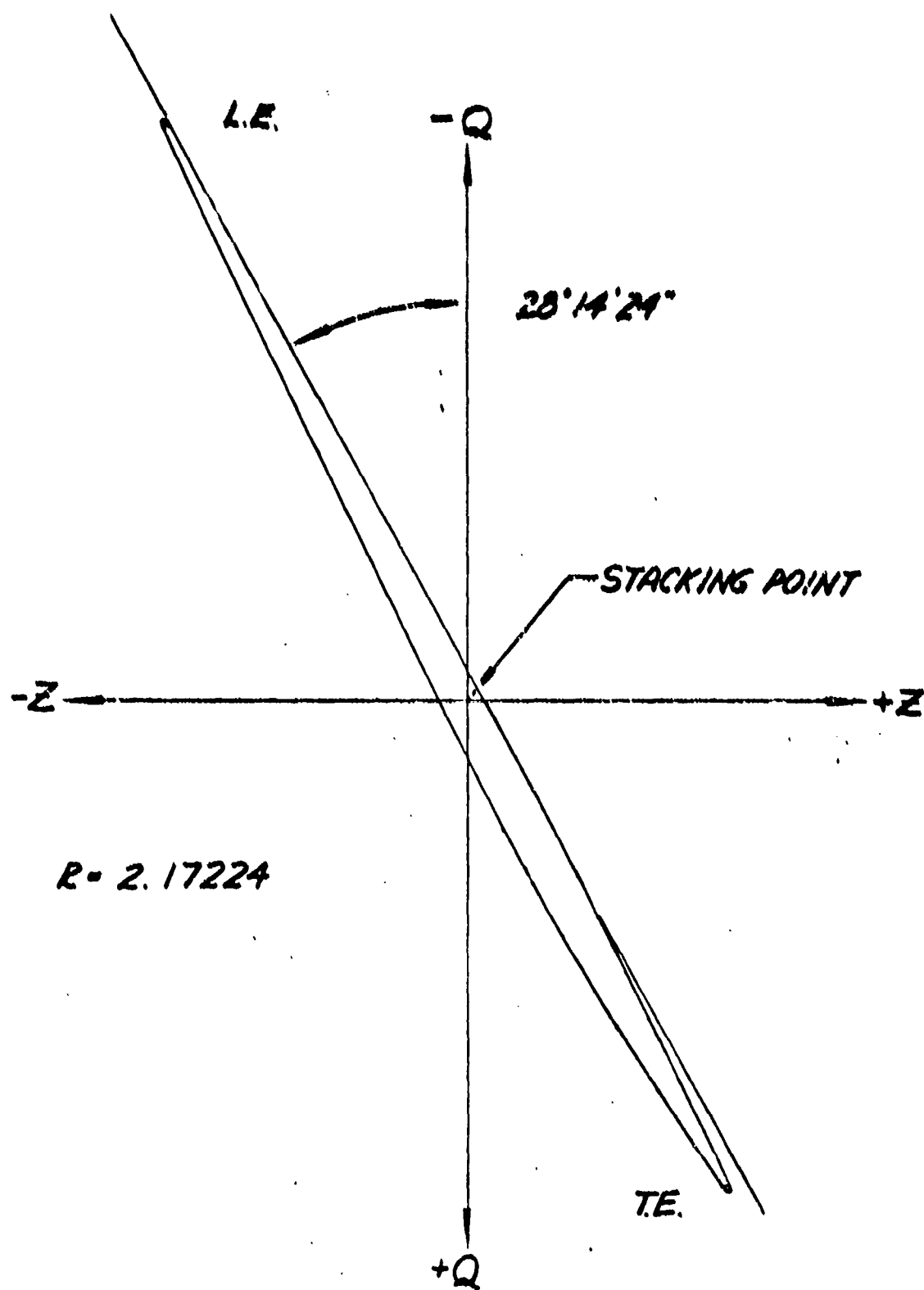


Figure 209. Axial Compressor Blade Stacking.

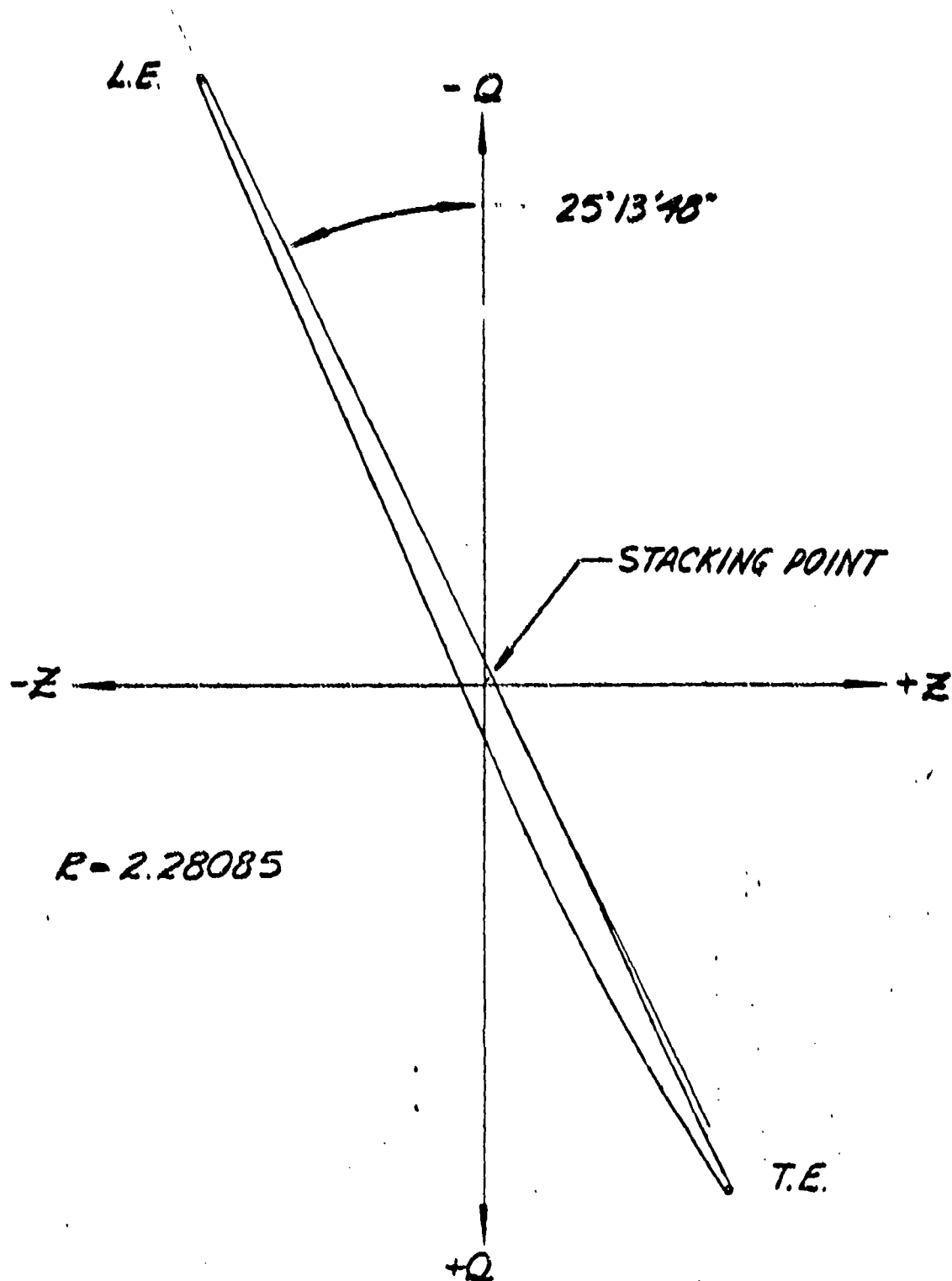


Figure 210. Axial Compressor Blade Stacking.

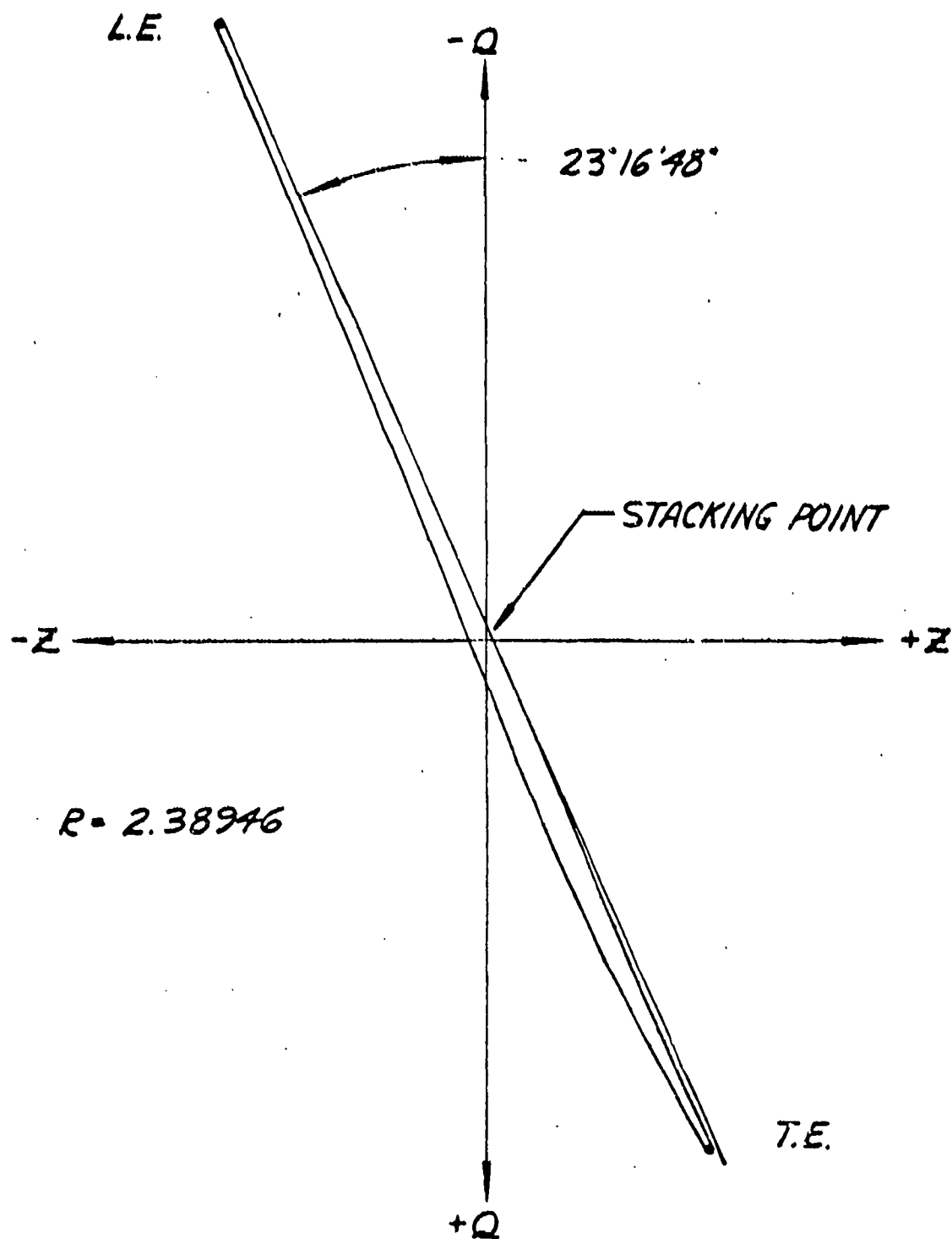


Figure 211. Axial Compressor Blade Stacking.

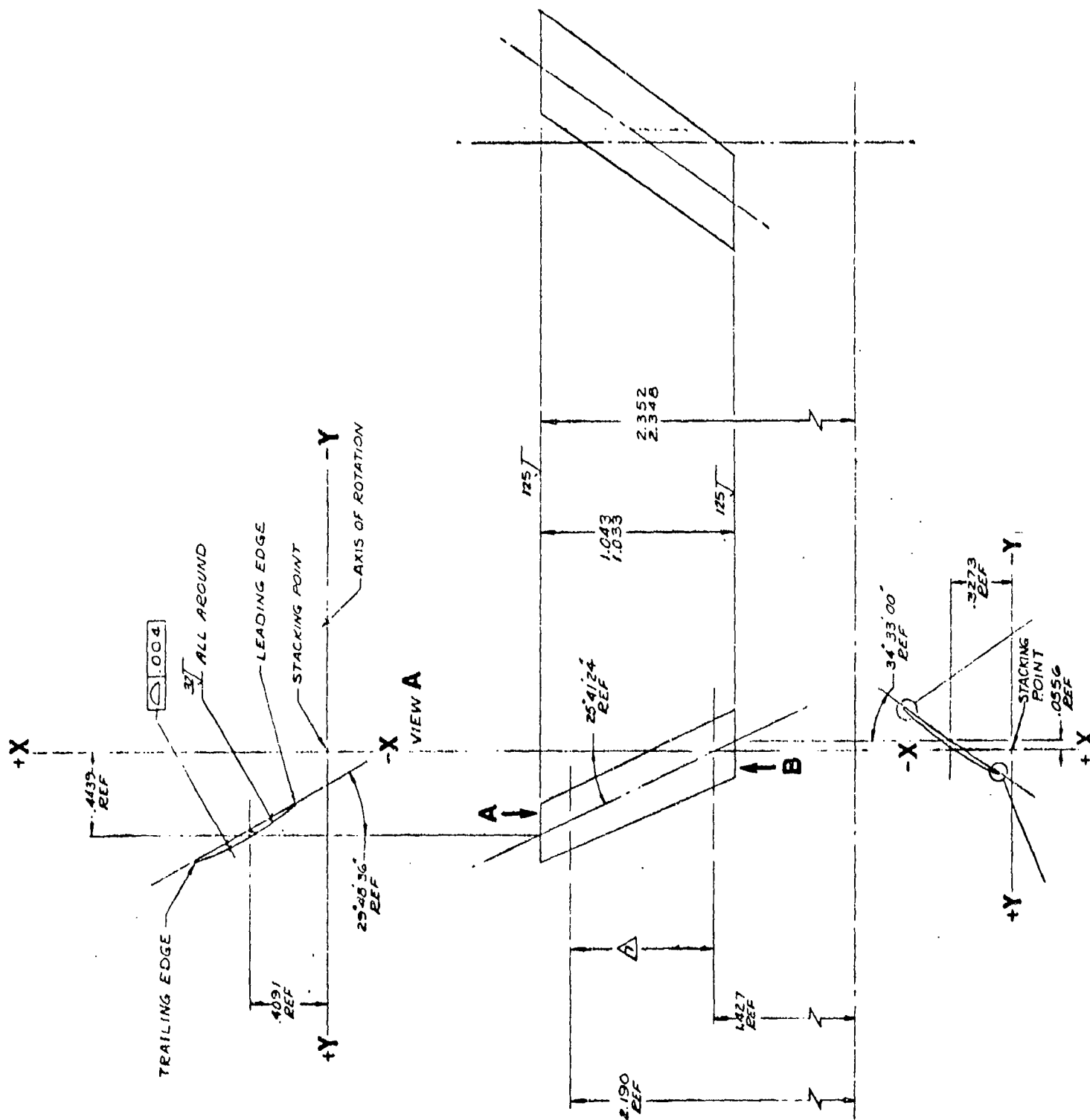


Figure 212. Swept Inlet Stator.

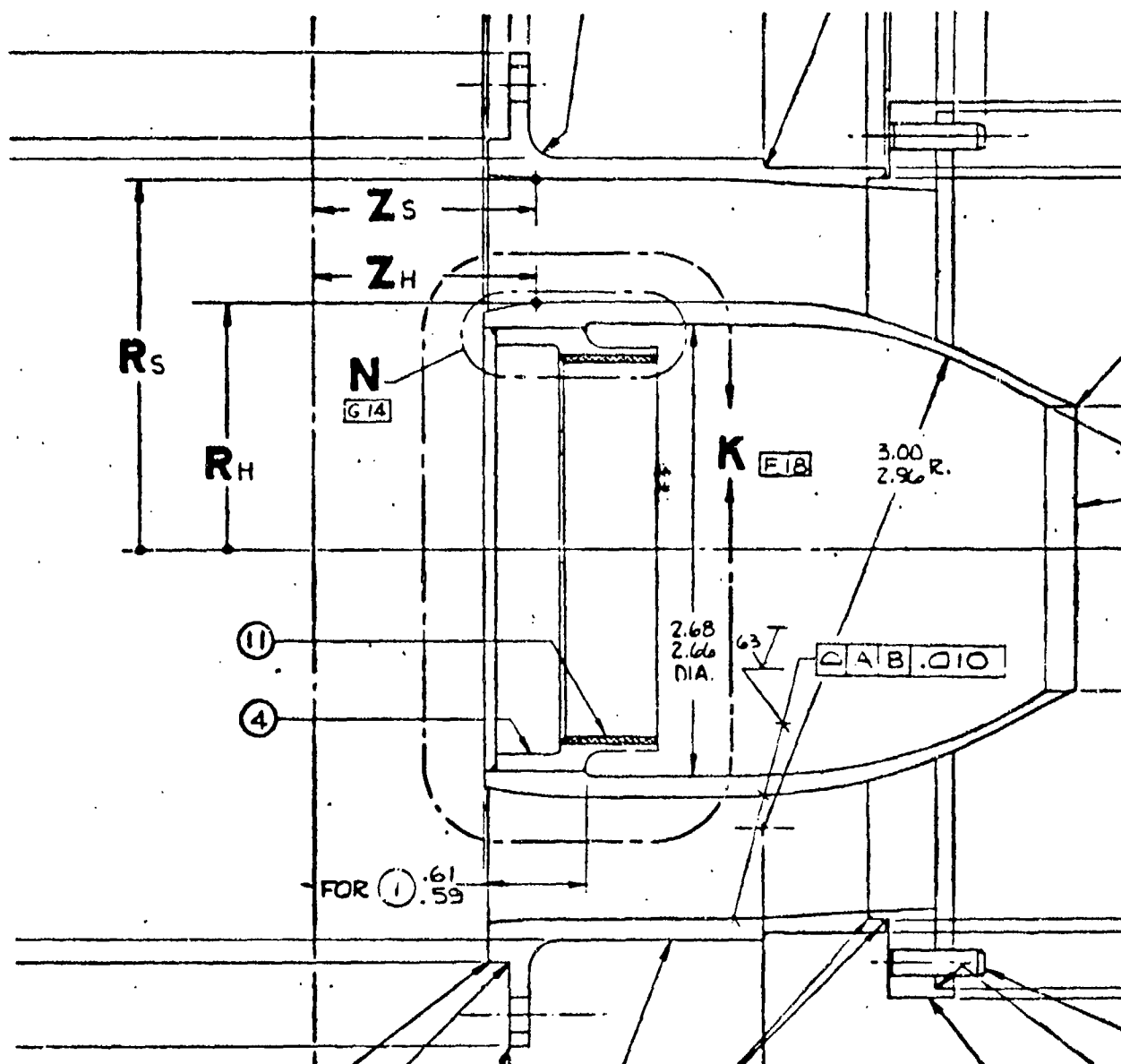


Figure 213. Duct Assembly, Diffuser, Interstage.

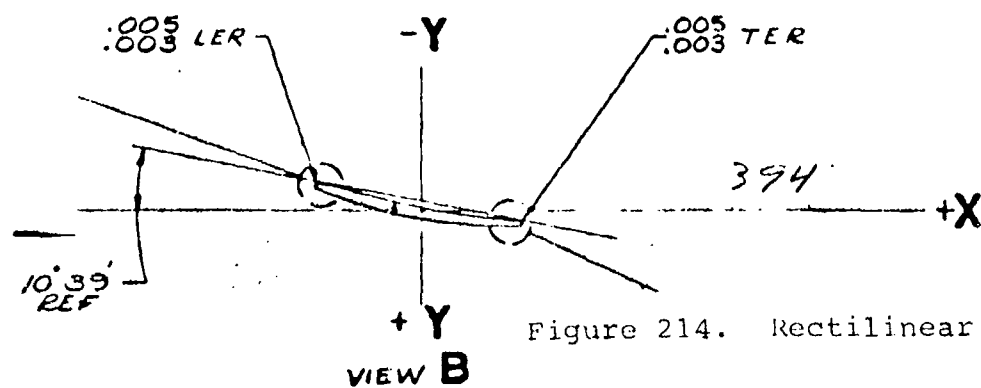
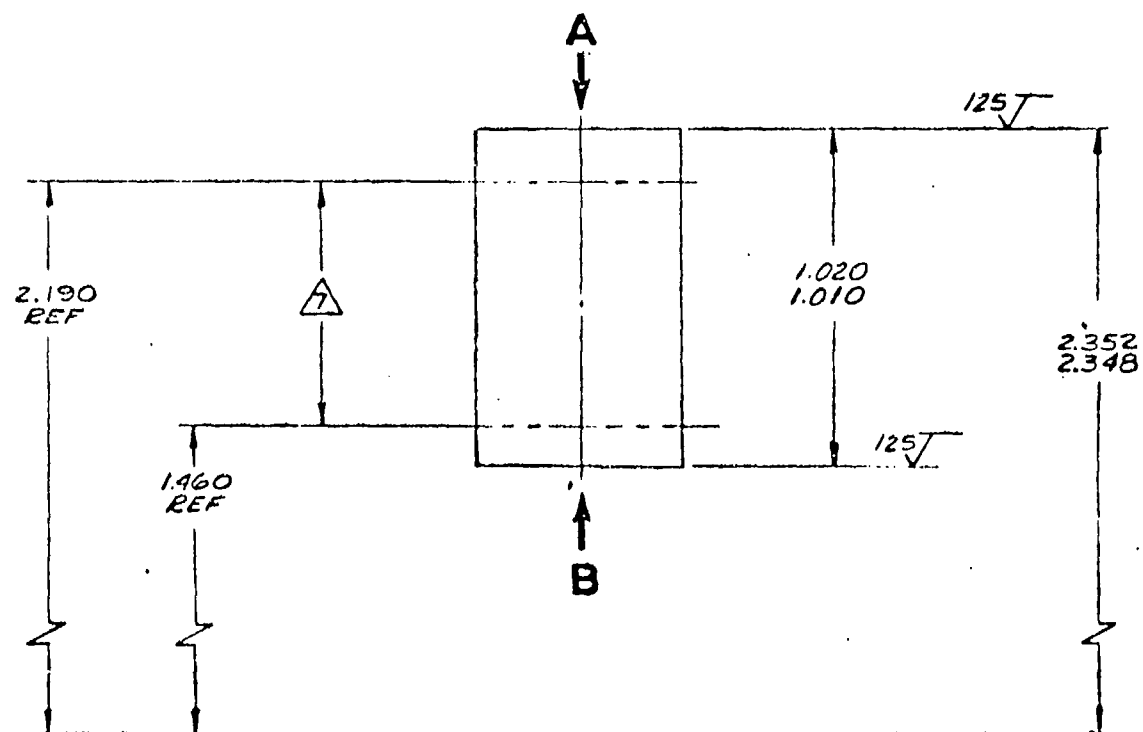
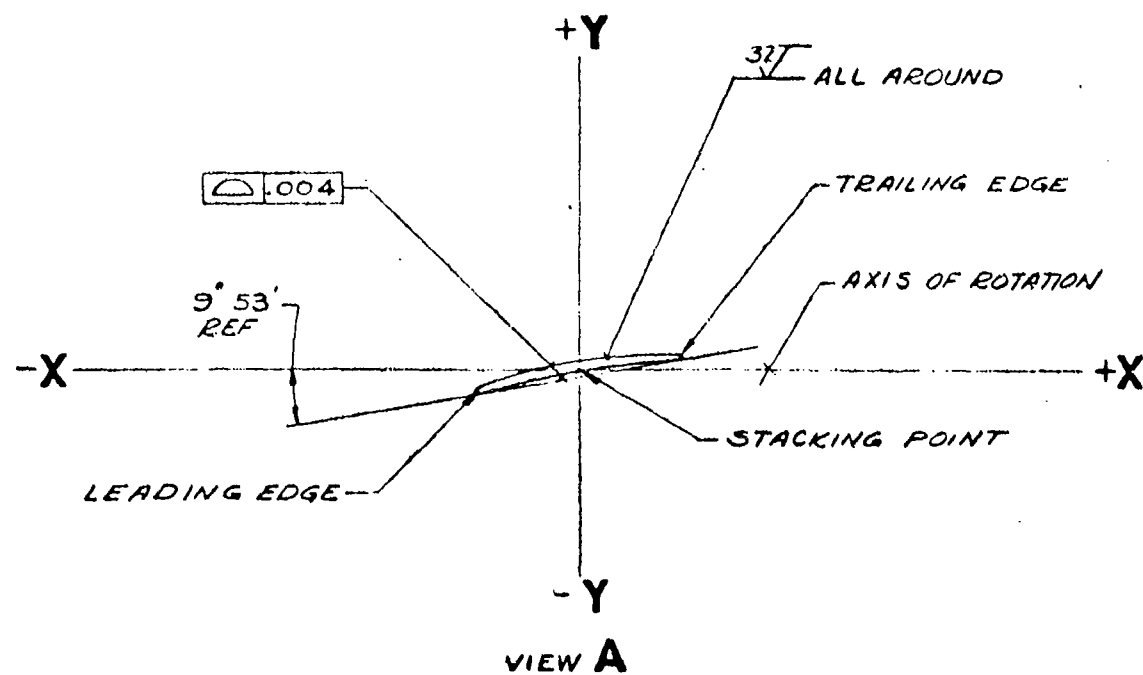


Figure 214. Rectilinear Stator.

TABLE I

BASIC COORDINATES			
HUB		SHROUD	
Z _H	R _H	Z _S	R _S
* 1.000	1.399	1.000	2.237
1.050	1.412	1.050	2.227
1.100	1.423	1.100	2.218
1.150	1.433	1.150	2.211
1.200	1.441	1.200	2.204
1.250	1.448	1.250	2.195
1.300	1.453	1.300	2.190
1.350	1.457	1.350	2.190
1.400	1.459	1.400	2.190
1.450	1.460	1.450	2.190
1.500	1.460	1.500	2.190
1.550	1.460	1.550	2.190
1.600	1.460	1.600	2.190
1.700	1.460	1.700	2.190
1.800	1.460	1.800	2.190
1.900	1.460	1.900	2.190
2.000	1.460	2.000	2.188
2.200	1.460	2.200	2.181
2.300	1.460	2.300	2.176
2.400	1.460	2.400	2.171
2.500	1.460	2.500	2.165
2.600	1.460	2.600	2.161
2.700	1.460	2.700	2.157
2.800	1.457	2.800	2.154
2.900	1.452	2.900	2.151
3.000	1.443	3.000	2.147
3.100	1.428	3.100	2.143
3.200	1.406	3.200	2.137
3.300	1.380	3.300	2.130
3.400	1.350	3.400	2.119
3.500	1.317		
3.600	1.280		
3.700	1.241		
3.800	1.199		
3.900	1.155		
4.000	1.109		
SEE CONTINUATION OF THIS COLUMN ABOVE RIGHT			

TABLE I (CONTINUED)

BASIC COORDINATES			
HUB		SHROUD	
Z _H	R _H	Z _S	R _S
4.100	1.061		
4.200	1.008		
4.300	.955		
4.400	.903		
4.500	.858		
4.600	.822		

* - FOR TOOLING PURPOSES ONLY.

Figure 215. Coordinates for Figure 202.

COORDINATES VIEW A	
X	Y
2980	0750
2050	0639
2375	0623
2072	0559
1771	0497
1473	0437
1176	0379
0882	0324
0585	0270
0286	0217
0005	0164
0276	0117
0575	0070
0866	0023
1156	0022
1447	0006
1739	0109
2029	0150
2321	0191
2615	0230
2910	0269
3204	0312
3494	0350
3780	0392
4069	0435
4354	0477
4644	0525
4930	0570
5217	0601
5508	0643
5794	0689
6084	0732
6375	0775
6666	0816
6957	0857
7248	0898
7539	0939
7830	0980
8121	1021
8412	1062
8703	1103
8994	1144
9285	1185
9576	1226
9867	1267
10158	1308
10449	1349
10740	1390
11031	1431
11322	1472
11613	1513
11904	1554
12195	1595
12486	1636
12777	1677
13068	1718
13359	1759
13650	1800
13941	1841
14232	1882
14523	1923
14814	1964
15105	2005
15396	2046
15687	2087
15978	2128
16269	2169
16560	2210
16851	2251
17142	2292
17433	2333
17724	2374
18015	2415
18306	2456
18597	2497
18888	2538
19179	2579
19470	2620
19761	2661
20052	2702
20343	2743
20634	2784
20925	2825
21216	2866
21507	2907
21798	2948
22089	2989
22380	3030
22671	3071
22962	3112
23253	3153
23544	3194
23835	3235
24126	3276
24417	3317
24708	3358
25000	3399
25291	3440
25582	3481
25873	3522
26164	3563
26455	3604
26746	3645
27037	3686
27328	3727
27619	3768
27910	3809
28201	3850
28492	3891
28783	3932
29074	3973
29365	4014
29656	4055
29947	4096
30238	4137
30529	4178
30820	4219
31111	4260
31402	4301
31693	4342
31984	4383
32275	4424
32566	4465
32857	4506
33148	4547
33439	4588
33730	4629
34021	4670
34312	4711
34603	4752
34894	4793
35185	4834
35476	4875
35767	4916
36058	4957
36349	4998
36640	5039
36931	5080
37222	5121
37513	5162
37804	5203
38095	5244
38386	5285
38677	5326
38968	5367
39259	5408
39550	5449
39841	5490
40132	5531
40423	5572
40714	5613
41005	5654
41296	5695
41587	5736
41878	5777
42169	5818
42460	5859
42751	5900
43042	5941
43333	5982
43624	6023
43915	6064
44206	6105
44497	6146
44788	6187
45079	6228
45370	6269
45661	6310
45952	6351
46243	6392
46534	6433
46825	6474
47116	6515
47407	6556
47698	6597
47989	6638
48280	6679
48571	6720
48862	6761
49153	6802
49444	6843
49735	6884
50026	6925
50317	6966
50608	7007
50899	7048
51190	7089
51481	7130
51772	7171
52063	7212
52354	7253
52645	7294
52936	7335
53227	7376
53518	7417
53809	7458
54100	7499
54391	7540
54682	7581
54973	7622
55264	7663
55555	7704
55846	7745
56137	7786
56428	7827
56719	7868
57010	7909
57301	7950
57592	7991
57883	8032
58174	8073
58465	8114
58756	8155
59047	8196
59338	8237
59629	8278
59920	8319
60211	8360
60502	8401
60793	8442
61084	8483
61375	8524
61666	8565
61957	8606
62248	8647
62539	8688
62830	8729
63121	8770
63412	8811
63703	8852
63994	8893
64285	8934
64576	8975
64867	9016
65158	9057
65449	9098
65740	9139
66031	9180
66322	9221
66613	9262
66904	9303
67195	9344
67486	9385
67777	9426
68068	9467
68359	9508
68650	9549
68941	9590
69232	9631
69523	9672
69814	9713
70105	9754
70396	9795
70687	9836
70978	9877
71269	9918
71560	9959
71851	9999

COORDINATES VIEW B	
X	Y
2937	0881
2640	0772
2376	0670
2074	0575
1775	0486
1478	0404
1182	0327
0883	0256
0586	0190
0284	0123
0013	0072
0278	0023
0578	0023
0883	0065
1183	0101
1440	0134
1731	0161
2024	0185
2317	0203
2612	0218
2908	0227
3202	0229
3492	0237
3789	0248
4080	0261
4375	0274
4676	0283
4972	0287
5267	0293
5562	0303
5857	0316
6152	0330
6447	0344
6742	0358
7037	0372
7332	0387
7627	0401
7922	0416
8217	0431
8512	0446
8807	0461
9102	0476
9397	0491
9692	0506
9987	0521
10282	0536
10577	0551
10872	0566
11167	0581
11462	0596
11757	0611
12052	0626
12347	0641
12642	0656
12937	0671
13232	0686
13527	0701
13822	0716
14117	0731
14412	0746
14707	0761
15002	0776
15297	0791
15592	0806
15887	0821
16182	0836
16477	0851
16772	0866
17067	0881
17362	0896
17657	0911
17952	0926
18247	0941
18542	0956
18837	0971
19132	0986
19427	1001
19722	1016
20017	1031
20312	1046
20607	1061
20902	1076
21197	1091
21492	1106
21787	1121
22082	1136
22377	1151
22672	1166
22967	1181
23262	1196
23557	1211
23852	1226
24147	1241
24442	1256
24737	1271
25032	1286
25327	1301
25622	1316
25917	1331
26212	1346
26507	1361
26802	1376
27097	1391
27392	1406
27687	1421
27982	1436
28277	1451
28572	1466
28867	1481
29162	1496
29457	1511
29752	1526
30047	1541
30342	1556
30637	1571
30932	1586
31227	1601
31522	1616
31817	1631
32112	1646
32407	1661
32702	1676
33000	1691

Figure 216. Coordinates for Figure 202.

COORDINATES VIEW A		COORDINATES VIEW B	
X	Y	X	Y
.1584	.2840	-.5681	-.2179
.1530	.3047	-.5432	-.1969
.2178	.3250	-.5240	-.1761
.2129	.3447	-.5015	-.1557
.2732	.3639	-.4787	-.1357
.2938	.3824	-.4555	-.1161
.3195	.4004	-.4319	-.0968
.3456	.4178	-.4081	-.0780
.3717	.4344	-.3837	-.0599
.3983	.4500	-.3590	-.0425
.4249	.4657	-.3347	-.0253
.4515	.4798	-.3097	-.0084
.4783	.4941	-.2840	.0081
.5049	.5087	-.2587	.0249
.5315	.5212	-.2330	.0396
.5553	.5334	-.2070	.0549
.5753	.5448	-.1810	.0685
.6130	.5557	-.1548	.0821
.6407	.5659	-.1284	.0953
.6672	.5755	-.1020	.1079
.6942	.5846	-.0756	.1207
.7260	.5933	-.0493	.1350
.7533	.6014	-.0231	.1493
.7847	.6092	-.0083	.1635
.8190	.6160	-.0038	.1778
.8534	.6220	-.0025	.1920
.8877	.6272	-.0017	.2062
.9219	.6317	-.0010	.2204
.9560	.6355	-.0006	.2346
.9900	.6388	-.0003	.2488
.1020	.6417	-.0002	.2630
.1140	.6442	-.0001	.2772
.1260	.6464	0.0000	.2914
.1380	.6483	0.0000	.3056
.1500	.6499	0.0000	.3198
.1620	.6512	0.0000	.3340
.1740	.6522	0.0000	.3482
.1860	.6530	0.0000	.3624
.1980	.6536	0.0000	.3766
.2100	.6540	0.0000	.3908
.2220	.6542	0.0000	.4050
.2340	.6543	0.0000	.4192
.2460	.6543	0.0000	.4334
.2580	.6542	0.0000	.4476
.2700	.6539	0.0000	.4618
.2820	.6534	0.0000	.4760
.2940	.6527	0.0000	.4902
.3060	.6518	0.0000	.5044
.3180	.6507	0.0000	.5186
.3300	.6494	0.0000	.5328
.3420	.6478	0.0000	.5470
.3540	.6460	0.0000	.5612
.3660	.6440	0.0000	.5754
.3780	.6417	0.0000	.5896
.3900	.6392	0.0000	.6038
.4020	.6364	0.0000	.6180
.4140	.6334	0.0000	.6322
.4260	.6302	0.0000	.6464
.4380	.6268	0.0000	.6606
.4500	.6232	0.0000	.6748
.4620	.6194	0.0000	.6890
.4740	.6154	0.0000	.7032
.4860	.6112	0.0000	.7174
.4980	.6068	0.0000	.7316
.5100	.6022	0.0000	.7458
.5220	.5974	0.0000	.7600
.5340	.5924	0.0000	.7742
.5460	.5872	0.0000	.7884
.5580	.5818	0.0000	.8026
.5700	.5762	0.0000	.8168
.5820	.5704	0.0000	.8310
.5940	.5644	0.0000	.8452
.6060	.5582	0.0000	.8594
.6180	.5518	0.0000	.8736
.6300	.5452	0.0000	.8878
.6420	.5384	0.0000	.9020
.6540	.5314	0.0000	.9162
.6660	.5242	0.0000	.9304
.6780	.5168	0.0000	.9446
.6900	.5092	0.0000	.9588
.7020	.5014	0.0000	.9730
.7140	.4934	0.0000	.9872
.7260	.4852	0.0000	.1000
.7380	.4768	0.0000	.1000
.7500	.4682	0.0000	.1000
.7620	.4594	0.0000	.1000
.7740	.4504	0.0000	.1000
.7860	.4412	0.0000	.1000
.7980	.4318	0.0000	.1000
.8100	.4222	0.0000	.1000
.8220	.4124	0.0000	.1000
.8340	.4024	0.0000	.1000
.8460	.3922	0.0000	.1000
.8580	.3818	0.0000	.1000
.8700	.3712	0.0000	.1000
.8820	.3604	0.0000	.1000
.8940	.3494	0.0000	.1000
.9060	.3382	0.0000	.1000
.9180	.3268	0.0000	.1000
.9300	.3152	0.0000	.1000
.9420	.3034	0.0000	.1000
.9540	.2914	0.0000	.1000
.9660	.2792	0.0000	.1000
.9780	.2668	0.0000	.1000
.9900	.2542	0.0000	.1000
.1000	.2414	0.0000	.1000

Figure 217. Coordinates for Figure 200.

Z=.0387				Z=.0774				Z=.1162				
X _S	Y _S	X _P	Y _P	X _S	Y _S	X _P	Y _P	X _S	Y _S	X _P	Y _P	X _S
.3740	2.1930	.3350	2.5000	.2680	2.1020	.3620	2.4900	.1950	2.0140	.9720	2.4780	.13
.4050	2.2210	.3300	2.4900	.3020	2.1290	.3200	2.4800	.2210	2.0470	.9420	2.4700	.16
.4360	2.2410	.3250	2.4800	.3360	2.1550	.2800	2.4710	.2570	2.0780	.9110	2.4610	.20
.4660	2.2510	.3200	2.4700	.3690	2.1800	.2400	2.4620	.2930	2.1070	.8810	2.4520	.24
.4960	2.2790	.3150	2.4600	.4020	2.2030	.2000	2.4530	.3290	2.1340	.8520	2.4430	.27
.5250	2.2950	.3100	2.4500	.4340	2.2230	.1600	2.4440	.3650	2.1600	.8230	2.4340	.31
.5540	2.3130	.3050	2.4400	.4660	2.2440	.1200	2.4350	.3950	2.1850	.7940	2.4250	.35
.5820	2.3290	.3000	2.4300	.4970	2.2630	.0800	2.4260	.4290	2.2070	.7660	2.4160	.38
.6110	2.3430	.2950	2.4200	.5270	2.2810	.0400	2.4170	.4620	2.2230	.7370	2.4070	.42
.6390	2.3570	.2900	2.4100	.5580	2.2980	.0000	2.4080	.4960	2.2330	.7090	2.3980	.45
.6680	2.3710	.2850	2.4000	.5870	2.3140		2.3990	.5290	2.2430	.6810	2.3890	.48
.6970	2.3850	.2800	2.3900	.6160	2.3300		2.3900	.5630	2.2530	.6530	2.3800	.52
.7250	2.3990	.2750	2.3800	.6440	2.3430		2.3810	.5930	2.2630	.6230	2.3710	.55
.7540	2.4110	.2700	2.3700	.6720	2.3560		2.3720	.6130	2.2730	.5930	2.3620	.58
.7860	2.4230	.2650	2.3600	.7000	2.3690		2.3630	.6430	2.2830	.5620	2.3530	.61
.8170	2.4350	.2600	2.3500	.7280	2.3820		2.3540	.6730	2.2930	.5310	2.3440	.65
.8490	2.4450	.2550	2.3400	.7570	2.3940		2.3450	.7030	2.3030	.5000	2.3350	.68
.8800	2.4570	.2500	2.3300	.7860	2.4060		2.3360	.7340	2.3130	.4690	2.3260	.71
.9120	2.4670	.2450	2.3200	.8150	2.4170		2.3270	.7640	2.3230	.4380	2.3170	.73
.9450	2.4770	.2400	2.3100	.8450	2.4280		2.3180	.7940	2.3330	.4070	2.3080	.76
.9780	2.4880	.2350	2.3000	.8750	2.4390		2.3090	.8250	2.3430	.3760	2.2990	.79
.9900	2.4990	.2300	2.2900	.9060	2.4490		2.3000	.8550	2.3530	.3450	2.2900	.82
.9510	2.4800	.2250	2.2800	.9370	2.4580		2.2910	.8850	2.3630	.3140	2.2810	.85
.9560	2.4810	.22320	2.2320	.9630	2.4670		2.2820	.9150	2.3730	.2830	2.2720	.88
.9630	2.4820	.3540					2.2480	.9450	2.3830	.2520	2.2630	.91
								.9750	2.3930	.2210	2.2530	.93
								.9940	2.4030	.1900	2.2440	.95
									2.4130	.1600	2.2350	.98
									2.4230	.1300	2.2260	.99

TABLE II BLADE COORDINATES

SEE L3600

Z=.1549					Z=.1859				Z=.5422				
Y _P	X _S	Y _S	X _P	Y _P	X _S	Y _S	X _P	Y _P	X _S	Y _S	X _P	Y _P	X _S
2.4780	1.1300	1.9430	1.3870	2.4710	1.0930	1.9030	1.3390	2.4650	0.8110	1.5040	1.1270	2.0580	0.6040
2.4700	1.1690	1.9850	1.3950	2.4630	1.1320	1.9440	1.3470	2.4570	0.8110	1.5040	1.1270	2.0580	0.6040
2.4610	1.2050	2.0210	1.4030	2.4550	1.1700	1.9850	1.3550	2.4490	0.8110	1.5040	1.1270	2.0580	0.6040
2.4520	1.2410	2.0540	1.4110	2.4470	1.2080	2.0210	1.3630	2.4410	0.8110	1.5040	1.1270	2.0580	0.6040
2.4420	1.2760	2.0860	1.4190	2.4390	1.2460	2.0540	1.3710	2.4330	0.8110	1.5040	1.1270	2.0580	0.6040
2.4320	1.3140	2.1190	1.4270	2.4310	1.2840	2.0860	1.3790	2.4250	0.8110	1.5040	1.1270	2.0580	0.6040
2.4220	1.3500	2.1430	1.4350	2.4230	1.3220	2.1150	1.3870	2.4170	0.8110	1.5040	1.1270	2.0580	0.6040
2.4110	1.3850	2.1690	1.4430	2.4150	1.3600	2.1430	1.3950	2.4090	0.8110	1.5040	1.1270	2.0580	0.6040
2.4000	1.4200	2.1930	1.4510	2.4070	1.3980	2.1700	1.4030	2.4010	0.8110	1.5040	1.1270	2.0580	0.6040
2.3890	1.4550	2.2160	1.4590	2.3990	1.4360	2.1930	1.4110	2.3930	0.8110	1.5040	1.1270	2.0580	0.6040
2.3780	1.4890	2.2380	1.4670	2.3910	1.4740	2.2160	1.4190	2.3850	0.8110	1.5040	1.1270	2.0580	0.6040
2.3670	1.5230	2.2590	1.4750	2.3830	1.5120	2.2380	1.4270	2.3770	0.8110	1.5040	1.1270	2.0580	0.6040
2.3560	1.5570	2.2790	1.4830	2.3750	1.5500	2.2590	1.4350	2.3690	0.8110	1.5040	1.1270	2.0580	0.6040
2.3450	1.5910	2.2990	1.4910	2.3670	1.5880	2.2800	1.4430	2.3610	0.8110	1.5040	1.1270	2.0580	0.6040
2.3340	1.6250	2.3190	1.4990	2.3590	1.6260	2.3020	1.4510	2.3530	0.8110	1.5040	1.1270	2.0580	0.6040
2.3230	1.6590	2.3390	1.5070	2.3510	1.6640	2.3240	1.4590	2.3450	0.8110	1.5040	1.1270	2.0580	0.6040
2.3120	1.6930	2.3590	1.5150	2.3430	1.7020	2.3460	1.4670	2.3370	0.8110	1.5040	1.1270	2.0580	0.6040
2.3010	1.7270	2.3790	1.5230	2.3350	1.7400	2.3680	1.4750	2.3290	0.8110	1.5040	1.1270	2.0580	0.6040
2.2900	1.7610	2.3990	1.5310	2.3270	1.7780	2.3900	1.4830	2.3210	0.8110	1.5040	1.1270	2.0580	0.6040
2.2790	1.7950	2.4190	1.5390	2.3190	1.8160	2.4120	1.4910	2.3130	0.8110	1.5040	1.1270	2.0580	0.6040
2.2680	1.8290	2.4390	1.5470	2.3110	1.8540	2.4340	1.4990	2.3050	0.8110	1.5040	1.1270	2.0580	0.6040
2.2570	1.8630	2.4590	1.5550	2.3030	1.8920	2.4560	1.5070	2.2970	0.8110	1.5040	1.1270	2.0580	0.6040
2.2460	1.8970	2.4790	1.5630	2.2950	1.9300	2.4780	1.5150	2.2890	0.8110	1.5040	1.1270	2.0580	0.6040
2.2350	1.9310	2.4990	1.5710	2.2870	1.9680	2.5000	1.5230	2.2810	0.8110	1.5040	1.1270	2.0580	0.6040
2.2240	1.9650	2.5190	1.5790	2.2790	2.0060	2.5220	1.5310	2.2730	0.8110	1.5040	1.1270	2.0580	0.6040
2.2130	2.0000	2.5390	1.5870	2.2710	2.0440	2.5440	1.5390	2.2650	0.8110	1.5040	1.1270	2.0580	0.6040
2.2020	2.0340	2.5590	1.5950	2.2630	2.0820	2.5660	1.5470	2.2570	0.8110	1.5040	1.1270	2.0580	0.6040
2.1910	2.0680	2.5790	1.6030	2.2550	2.1200	2.5880	1.5550	2.2490	0.8110	1.5040	1.1270	2.0580	0.6040
2.1800	2.1020	2.5990	1.6110	2.2470	2.1580	2.6100	1.5630	2.2410	0.8110	1.5040	1.1270	2.0580	0.6040
2.1690	2.1360	2.6190	1.6190	2.2390	2.1960	2.6320	1.5710	2.2330	0.8110	1.5040	1.1270	2.0580	0.6040
2.1580	2.1700	2.6390	1.6270	2.2310	2.2340	2.6540	1.5790	2.2250	0.8110	1.5040	1.1270	2.0580	0.6040
2.1470	2.2040	2.6590	1.6350	2.2230	2.2720	2.6760	1.5870	2.2170	0.8110	1.5040	1.1270	2.0580	0.6040
2.1360	2.2380	2.6790	1.6430	2.2150	2.3100	2.6980	1.5950	2.2090	0.8110	1.5040	1.1270	2.0580	0.6040
2.1250	2.2720	2.6990	1.6510	2.2070	2.3480	2.7200	1.6030	2.2010	0.8110	1.5040	1.1270	2.0580	0.6040
2.1140	2.3060	2.7190	1.6590	2.1990	2.3860	2.7420	1.6110	2.1930	0.8110	1.5040	1.1270	2.0580	0.6040
2.1030	2.3400	2.7390	1.6670	2.1910	2.4240	2.7640	1.6190	2.1850	0.8110	1.5040	1.1270	2.0580	0.6040
2.0920	2.3740	2.7590	1.6750	2.1830	2.4620	2.7860	1.6270	2.1770	0.8110	1.5040	1.1270	2.0580	0.6040
2.0810	2.4080	2.7790	1.6830	2.1750	2.5000	2.8080	1.6350	2.1690	0.8110	1.5040	1.1270	2.0580	0.6040
2.0700	2.4420	2.7990	1.6910	2.1670	2.5380	2.8300	1.6430	2.1610	0.8110	1.5040	1.1270	2.0580	0.6040
2.0590	2.4760	2.8190	1.6990	2.1590	2.5760	2.8520	1.6510	2.1530	0.8110	1.5040	1.1270	2.0580	0.6040
2.0480	2.5100	2.8390	1.7070	2.1510	2.6140	2.8740	1.6590	2.1450	0.8110	1.5040	1.1270	2.0580	0.6040
2.0370	2.5440	2.8590	1.7150	2.1430	2.6520	2.8960	1.6670	2.1370	0.8110	1.5040	1.1270	2.0580	0.6040
2.0260	2.5780	2.8790	1.7230	2.1350	2.6900	2.9180	1.6750	2.1290	0.8110	1.5040	1.1270	2.0580	0.6040
2.0150	2.6120	2.8990	1.7310	2.1270	2.7280	2.9400	1.6830	2.1210	0.8110	1.5040	1.1270	2.0580	0.6040
2.0040	2.6460	2.9190	1.7390	2.1190	2.7660	2.9620	1.6910	2.1130	0.8110	1.5040	1.1270	2.0580	0.6040
1.9930	2.6800	2.9390	1.7470	2.1110	2.8040	2.9840	1.6990	2.1050	0.8110	1.5040	1.1270	2.0580	0.6040
1.9820	2.7140	2.9590	1.7550	2.1030	2.8420	3.0060	1.7070	2.0970	0.8110	1.5040	1.1270	2.0580	0.6040
1.9710	2.7480	2.9790	1.7630	2.0950	2.8800	3.0280	1.7150	2.0890	0.8110	1.5040	1.1270	2.0580	0.6040
1.9600	2.7820	2.9990	1.7710	2.0870	2.9180	3.0500	1.7230	2.0810	0.8110	1.5040	1.1270	2.0580	0.6040
1.9490	2.8160	3.0190	1.7790	2.0790	2.9560	3.0720	1.7310	2.0730	0.8110	1.5040	1.1270	2.0580	0.6040
1.9380	2.8500	3.0390	1.7870	2.0710	3.0000	3.0940	1.7390	2.0650	0.8110	1.5040	1.1270	2.0580	0.6040
1.9270	2.8840	3.0590	1.7950	2.0630	3.0400	3.1160	1.7470	2.0570	0.8110	1.5040	1.1270	2.0580	0.6040
1.9160	2.9180	3.0790	1.8030	2.0550	3.0800	3.1380	1.7550	2.0490	0.8110	1.5040	1.1270	2.0580	0.6040
1.9050	2.9520	3.0990	1.8110	2.0470	3.1200	3.1600	1.7630	2.0410	0.8110	1.5040	1.1270	2.0580	0.6040
1.8940	2.9860	3.1190	1.8190	2.0390	3.1600	3.1820	1.7710	2.0330	0.8110	1.5040	1.1270	2.0580	0.6040
1.8830	3.0200	3.1390	1.8270	2.0310	3.2000	3.2040	1.7790	2.0250	0.8110	1.5040	1.1270	2.0580	0.6040
1.8720	3.0540	3.1590	1.8350	2.0230	3.2400	3.2260	1.7870	2.0170	0.8110	1.5040	1.1270	2.0580	0.6040
1.8610	3.0880	3.1790	1.8430	2.0150	3.2800	3.2480	1.7950	2.0090	0.8110	1.5040	1.1270	2.0580	0.6040
1.8500	3.1220	3.1990	1.8510	2.0070	3.3200	3.2700	1.8030	2.0010	0.8110	1.5040	1.1270	2.0580	0.6040
1.8390	3.1560	3.2190	1.8590	2.0000	3.3600	3.2920	1.8110	1.9930	0.8110	1.5040	1.1270	2.0580	0.6040
1.8280	3.1900	3.2390	1.8670	1.9920	3.4000	3.3140	1.8190	1.9850	0.8110	1.5040	1.1270	2.0580	0.6040
1.8170	3.2240	3.2590	1.8750	1.9840	3.4400	3.3360	1.8270	1.9770	0.8110	1.5040	1.1270	2.0580	0.6040
1.8060	3.2580	3.2790	1.8830	1.9760	3.4800	3.3580	1.8350	1.9690	0.8110	1.5040	1.1270	2.0580	0.6040
1.7950	3.2920	3.2990	1.8910	1.9680	3.5200	3.3800	1.8430	1.9610	0.8110	1.5040	1.1270	2.0580	0.6040
1.7840	3.3260	3.3190	1.8990	1.9600	3.5600	3.4020	1.8510	1.9530	0.8110	1.5040	1.1270	2.0580	0.6040
1.7730	3.3600	3.3390	1.9070	1.9520	3.6000	3.4240	1.8590	1.9450	0.8110	1.5040	1.1270	2.0580	0.6040
1.7620	3.3940	3.3590	1.9150	1.9440	3.6400	3.4460	1.8670	1.9370	0.8110	1.5040	1.1270	2.0580	0.6040
1.7510	3.4280	3.3790	1.9230	1.9360	3.6800	3.4680	1.8750	1.9290	0.8110	1.5040	1.1270	2.0580	0.6040
1.7400	3.4620	3.3990	1.9310	1.9280	3.7200	3.4900	1.8830	1.9210	0.8110	1.5040	1.1270	2.0580	0.6040
1.7290	3.4960	3.4190	1.9390	1.9200	3.7600	3.5120	1.8910	1.9130	0.8110	1.5040	1.1270	2.0580	0.6040
1.7180	3.5300	3.4390	1.9470	1.9120	3.8000	3.5340	1.8990	1.9050	0.8110	1.5040	1.1270	2.0580	0.6040
1.7070	3.5640	3.4590	1.9550	1.9040	3.8400	3.5560	1.9070	1.8970	0.8110	1.5040	1.1270	2.0580	0.6040
1.6960	3.5980	3.4790	1.9630	1.8960	3.8800	3.5780	1.9150	1.8890	0.8110	1.5040	1.1270	2.0580	0.6040
1.6850	3.6320	3.4990	1.9710	1.8880	3.9200	3.6000	1.9230	1.8810	0.8110	1.5040	1.1270	2.0580	0.6040
1.6740	3.6660	3.5190	1.9790	1.8800	3.9600	3.6220	1.9310	1.8730	0.8110	1.5040	1.1270	2.0580	0.6040
1.6630	3.7000	3.5390	1.9870	1.									

S

SEE L3600949

Z = .5422				Z = .9296				Z = 1.2395				Z = 1.5493		
Y_S	X_P	Y_P		X_S	Y_S	X_P	Y_P	X_S	Y_S	X_P	Y_P	X_S	Y_S	X_P
.5040	1.1270	2.0580		0.6040	1.1890	0.6090	1.9290	0.4390	1.0700	0.5760	2.0180	0.2148	0.9251	0.2056
.5430	1.1050	2.0310		0.6210	1.2600	0.7350	1.8780	0.4520	1.1810	0.5550	1.9390	0.2135	0.9859	0.2013
.5820	1.0820	2.0030		0.6380	1.3290	0.7550	1.8260	0.4660	1.2670	0.5360	1.8590	0.2126	1.0477	0.1972
.6240	1.0600	1.9740		0.6560	1.3990	0.7440	1.7710	0.4810	1.3500	0.5170	1.7730	0.2118	1.1077	0.1932
.6630	1.0370	1.9450		0.6740	1.4610	0.7230	1.7150	0.4360	1.4830	0.4390	1.6850	0.2114	1.1659	0.1893
.6990	1.0150	1.9140		0.6920	1.5250	0.7030	1.6590	0.5110	1.5840	0.4790	1.5950	0.2112	1.2250	0.1856
.7350	0.9930	1.8830		0.7100	1.5850	0.6820	1.5930	0.5270	1.6760	0.4610	1.5010	0.2119	1.2824	0.1821
.7710	0.9710	1.8510		0.7290	1.6450	0.6620	1.5390	0.5440	1.7650	0.4430	1.4030	0.2116	1.3390	0.1789
.8070	0.9490	1.8190		0.7480	1.7050	0.6420	1.4760	0.5610	1.8500	0.4250	1.3020	0.2122	1.3937	0.1756
.8430	0.9270	1.7850		0.7670	1.7610	0.6230	1.4110	0.5780	1.9330	0.4090	1.1970	0.2130	1.4497	0.1727
.8790	0.9050	1.7500		0.7870	1.8160	0.6030	1.3450	0.5960	2.0130	0.3930	1.0870	0.2140	1.5037	0.1699
.9130	0.8830	1.7140		0.8060	1.8700	0.5840	1.2770					0.2153	1.5570	0.1674
.9440	0.8620	1.6780		0.8260	1.9220	0.5650	1.2070					0.2167	1.6094	0.1650
.9730	0.8400	1.6400										0.2184	1.6611	0.1629
.9930	0.8190	1.6020										0.2203	1.7120	0.1610
.0210	0.7980	1.5630										0.2224	1.7622	0.1593
.0430	0.7770	1.5220										0.2247	1.8116	0.1578
												0.2271	1.8593	0.1566
												0.2298	1.9082	0.1557
												0.2327	1.9555	0.1550

493		Z=1.8592			
X _P	Y _P	X _S	Y _S	X _P	Y _P
0.2056	1.9583	-0.2527	0.7917	-0.2859	1.9879
0.2013	1.9115	-0.0733	0.8521	-0.2769	1.9020
0.1972	1.8639	-0.0991	0.9112	-0.2673	1.8147
0.1932	1.8157	-0.1120	1.0731	-0.2571	1.7261
0.1893	1.7668	-0.1201	1.1754	-0.2461	1.6363
0.1856	1.7171	-0.1274	1.2707	-0.2345	1.5453
0.1821	1.6665	-0.1340	1.3649	-0.2222	1.4531
0.1789	1.6154	-0.1399	1.4590	-0.2092	1.3598
0.1756	1.5634	-0.1455	1.5499	-0.1955	1.2652
0.1727	1.5105	-0.1505	1.6407	-0.1811	1.1696
0.1699	1.4569	-0.1553	1.7333	-0.1660	1.0729
0.1674	1.4024	-0.1597	1.8199	-0.1501	0.9746
0.1650	1.3471	-0.1636	1.9059	-0.1334	0.8750
0.1629	1.2909	-0.1662	1.9918	-0.1159	0.7741
0.1610	1.2339				
0.1593	1.1761				
0.1578	1.1174				
0.1563	1.0578				
0.1549	0.9973				
0.1530	0.9360				

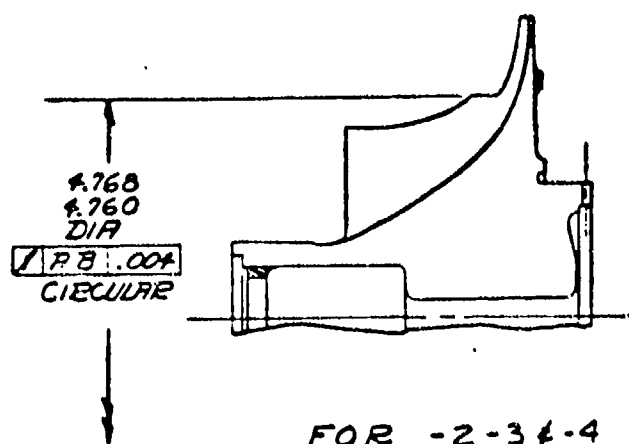
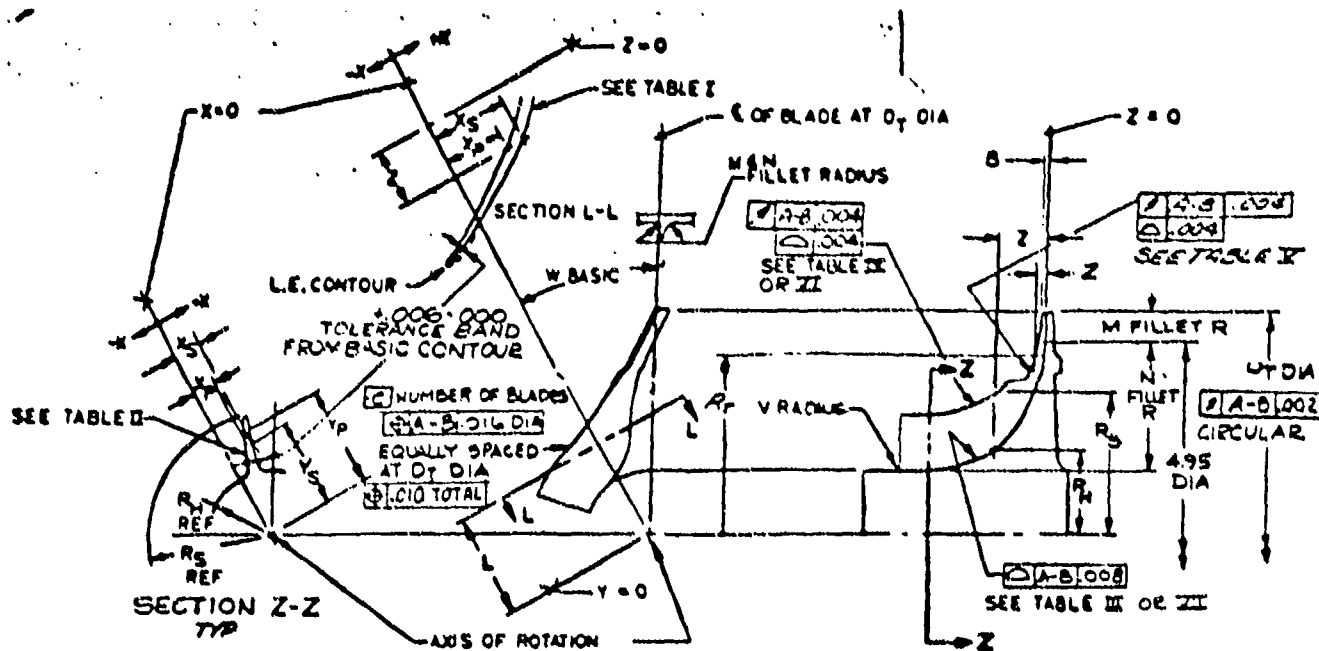


Figure 218. Centrifugal Compressor Ref. Figure 207.

L-1.C

Xs Z

0.0000	0.0000
0.0001	0.0001
0.0002	0.0002
0.0003	0.0003
0.0004	0.0004
0.0005	0.0005
0.0006	0.0006
0.0007	0.0007
0.0008	0.0008
0.0009	0.0009
0.0010	0.0010
0.0011	0.0011
0.0012	0.0012
0.0013	0.0013
0.0014	0.0014
0.0015	0.0015
0.0016	0.0016
0.0017	0.0017
0.0018	0.0018
0.0019	0.0019
0.0020	0.0020
0.0021	0.0021
0.0022	0.0022
0.0023	0.0023
0.0024	0.0024
0.0025	0.0025
0.0026	0.0026
0.0027	0.0027
0.0028	0.0028
0.0029	0.0029
0.0030	0.0030
0.0031	0.0031
0.0032	0.0032
0.0033	0.0033
0.0034	0.0034
0.0035	0.0035
0.0036	0.0036
0.0037	0.0037
0.0038	0.0038
0.0039	0.0039
0.0040	0.0040
0.0041	0.0041
0.0042	0.0042
0.0043	0.0043
0.0044	0.0044
0.0045	0.0045
0.0046	0.0046
0.0047	0.0047
0.0048	0.0048
0.0049	0.0049
0.0050	0.0050
0.0051	0.0051
0.0052	0.0052
0.0053	0.0053
0.0054	0.0054
0.0055	0.0055
0.0056	0.0056
0.0057	0.0057
0.0058	0.0058
0.0059	0.0059
0.0060	0.0060
0.0061	0.0061
0.0062	0.0062
0.0063	0.0063
0.0064	0.0064
0.0065	0.0065
0.0066	0.0066
0.0067	0.0067
0.0068	0.0068
0.0069	0.0069
0.0070	0.0070
0.0071	0.0071
0.0072	0.0072
0.0073	0.0073
0.0074	0.0074
0.0075	0.0075
0.0076	0.0076
0.0077	0.0077
0.0078	0.0078
0.0079	0.0079
0.0080	0.0080
0.0081	0.0081
0.0082	0.0082
0.0083	0.0083
0.0084	0.0084
0.0085	0.0085
0.0086	0.0086
0.0087	0.0087
0.0088	0.0088
0.0089	0.0089
0.0090	0.0090
0.0091	0.0091
0.0092	0.0092
0.0093	0.0093
0.0094	0.0094
0.0095	0.0095
0.0096	0.0096
0.0097	0.0097
0.0098	0.0098
0.0099	0.0099
0.0100	0.0100



Preceding page blank

49	TABLE III		TABLE IV		TABLE V		TABLE VI		TABL
3	HUB CONTOUR COORDINATES		OUTSIDE EDGE CONTOUR COORDINATES		OUTSIDE EDGE CONTOUR COORDINATES		OUTSIDE EDGE CONTOUR COORDINATES		HUB CO. COOR
KP Z	Z	R _H	Z	R _s	Z	R _r	Z	R _s	Z
.0112	.2831		2.0925	1.9745	.4094	2.3143	.517	2.355	2.4500
.0137	.3132		1.9920	1.9635	.3643	2.3695	.580	2.293	2.3600
.0142	.3457		1.8930	1.9580	.3448	2.3971	.640	2.242	2.2750
.0123	.3739		1.7740	1.9580	.3261	2.4265	.700	2.199	2.2000
.0085	.4128		1.5900	1.9580	.3087	2.4547	.750	2.167	2.1250
.0027	.4456		1.4600	1.9580	.2712	2.5211	.800	2.139	2.0500
.0000	.4793		1.3130	1.9720	.2510	2.5624	.871	2.104	1.9925
.0000	.5109		1.1660	1.9960	.2327	2.6039	.950	2.070	1.9367
.0000	.5435		1.0180	2.0350	.2216	2.6313	1.050	2.034	1.8399
.0000	.5751		.8710	2.0910	.2068	2.6726	1.150	2.006	1.7431
.0000	.6066		.7530	2.1500	.1935	2.7140	1.250	1.985	1.6785
.0000	.6412		.6060	2.2490	.1782	2.7664	1.350	1.970	1.6139
.0000	.6735		.4890	2.3550	.1706	2.7966	1.460	1.960	1.5494
.0000	.7055		.3860	2.4820	.1642	2.8242	1.590	1.958	1.4526
.0000	.7373		.3070	2.6200	.1558	2.8655	1.774	1.958	1.3880
.0000	.7723		.2480	2.7770	.1489	2.9068	1.937	1.958	1.2911
.0000	.8052		.2130	2.9580	.1435	2.9435			1.1943
.0000	.8382		.2040	3.0850	.1375	3.0000			1.0652
.0000	.8713		.2030	3.1680	.1320	3.0711			.9361
.0000	.9044				.1300	3.0990			.8392
.0000	.9375				.1285	3.1685			.7424
.0000	.9709								.6456
.0000	1.0043								.5717
.0000	1.0402								.4915
.0000	1.0743								.4263
.0000	1.1094								.3595
.0000	1.1445								.2996
.0000	1.1796								.2518
.0000	1.2147								.2039
.0000	1.2498								.1619
.0000	1.2849								.1257
.0000	1.3200								.0981
.0000	1.3551								.0718
.0000	1.3902								.0504
.0000	1.4253								.0349
.0000	1.4604								.0215
.0000	1.4955								.0119
.0000	1.5306								.0060
.0000	1.5657								.0020
.0000	1.6008								.0002
.0000	1.6359								.0000
.0000	1.6710								.0000
.0000	1.7061								.0000
.0000	1.7412								.0000
.0000	1.7763								.0000
.0000	1.8114								.0000
.0000	1.8465								.0000
.0000	1.8816								.0000
.0000	1.9167								.0000
.0000	1.9518								.0000
.0000	1.9869								.0000
.0000	2.0220								.0000
.0000	2.0571								.0000
.0000	2.0922								.0000
.0000	2.1273								.0000
.0000	2.1624								.0000
.0000	2.1975								.0000
.0000	2.2326								.0000
.0000	2.2677								.0000
.0000	2.3028								.0000
.0000	2.3379								.0000
.0000	2.3730								.0000
.0000	2.4081								.0000
.0000	2.4432								.0000
.0000	2.4783								.0000
.0000	2.5134								.0000
.0000	2.5485								.0000
.0000	2.5836								.0000
.0000	2.6187								.0000
.0000	2.6538								.0000
.0000	2.6889								.0000
.0000	2.7240								.0000
.0000	2.7591								.0000
.0000	2.7942								.0000
.0000	2.8293								.0000
.0000	2.8644								.0000
.0000	2.8995								.0000
.0000	2.9346								.0000
.0000	2.9697								.0000
.0000	3.0048								.0000
.0000	3.0399								.0000
.0000	3.0750								.0000
.0000	3.1101								.0000
.0000	3.1452								.0000
.0000	3.1803								.0000
.0000	3.2154								.0000
.0000	3.2505								.0000
.0000	3.2856								.0000
.0000	3.3207								.0000
.0000	3.3558								.0000
.0000	3.3909								.0000
.0000	3.4260								.0000
.0000	3.4611								.0000
.0000	3.4962								.0000
.0000	3.5313								.0000
.0000	3.5664								.0000
.0000	3.6015								.0000
.0000	3.6366								.0000
.0000	3.6717								.0000
.0000	3.7068								.0000
.0000	3.7419								.0000
.0000	3.7770								.0000
.0000	3.8121								.0000
.0000	3.8472								.0000
.0000	3.8823								.0000
.0000	3.9174								.0000
.0000	3.9525								.0000
.0000	3.9876								.0000
.0000	4.0227								.0000
.0000	4.0578								.0000
.0000	4.0929								.0000
.0000	4.1280								.0000
.0000	4.1631								.0000
.0000	4.1982								.0000
.0000	4.2333								.0000
.0000	4.2684								.0000
.0000	4.3035								.0000
.0000	4.3386								.0000
.0000	4.3737								.0000
.0000	4.4088								.0000
.0000	4.4439								.0000
.0000	4.4790								.0000
.0000	4.5141								.0000
.0000	4.5492								.0000
.0000	4.5843								.0000
.0000	4.6194								.0000
.0000	4.6545								.0000
.0000	4.6896								.0000
.0000	4.7247								.0000
.0000	4.7598								.0000
.0000	4.7949								.0000
.0000	4.8300								.0000
.0000	4.8651								.0000
.0000	4.9002								.0000
.0000	4.9353								.0000
.0000	4.9704								.0000
.0000	5.0055								.0000
.0000	5.0406								.0000
.0000	5.0757								.0000
.0000	5.1108								.0000
.0000	5.1459								.0000
.0000	5.1810								.0000
.0000	5.2161								.0000
.0000	5.2512								.0000
.0000	5.2863								.0000
.0000	5.3214								.0000
.0000	5.3565								.0000
.0000	5.3916								.0000
.0000	5.4267								.0000
.0000	5.4618								.0000
.0000	5.4969								.0000
.0000	5.5320								.0000
.0000	5.5671								.0000
.0000	5.6022								.0000
.0000	5.6373								.0000
.0000	5.6724								.0000
.0000	5.7075								.0000
.0000	5.7426								.0000
.0000	5.7777								.0000
.0000	5.8128								.0000
.0000	5.8479								.0000
.0000	5.8830								.0000
.0000	5.9181								.0000
.0000	5.9532								.0000
.0000	5.9883								.0000
.0000	6.0234								.0000
.0000	6.0585								.0000
.0000	6.0936								.0000
.0000	6.1287								.0000
.0000	6.1638								.0000
.0000	6.1989								.0000
.0000	6.2340								.0000
.0000	6.2691								.0000
.0000	6.3042								.0000
.0000	6.3393								.0000
.0000	6.3744								.0000
.0000	6.4095								.0000
.0000	6.4446								.0000
.0000	6.4797								.0000
.0000	6.5148								.0000

TABLE IV	TABLE V	TABLE VI	TABLE VII
OUTSIDE EDGE CONTOUR COORDINATES	OUTSIDE EDGE CONTOUR COORDINATES	OUTSIDE EDGE CONTOUR COORDINATES	HUB CONTOUR COORDINATES
<div>Z</div> <div>Rs</div> <div>2.0925 1.9745</div> <div>1.9920 1.9635</div> <div>1.8930 1.9580</div> <div>1.7740 1.9580</div> <div>1.5900 1.9580</div> <div>1.4600 1.9580</div> <div>1.3130 1.9720</div> <div>1.1660 1.9960</div> <div>1.0180 2.0350</div> <div>.8710 2.0910</div> <div>.7530 2.1500</div> <div>.6060 2.2490</div> <div>.4290 2.3550</div> <div>.3860 2.4820</div> <div>.3070 2.6200</div> <div>.2480 2.7770</div> <div>.2130 2.9580</div> <div>.2040 3.0850</div> <div>.2030 3.1680</div>	<div>Z</div> <div>Rr</div> <div>.4094 2.3143</div> <div>.3643 2.3695</div> <div>.3448 2.3971</div> <div>.3261 2.4265</div> <div>.3087 2.4547</div> <div>.2712 2.5211</div> <div>.2510 2.5624</div> <div>.2327 2.6039</div> <div>.2216 2.6313</div> <div>.2068 2.6726</div> <div>.1935 2.7140</div> <div>.1782 2.7664</div> <div>.1706 2.7966</div> <div>.1642 2.8242</div> <div>.1558 2.8655</div> <div>.1489 2.9068</div> <div>.1435 2.9435</div> <div>.1375 3.0000</div> <div>.1320 3.0711</div> <div>.1300 3.0990</div> <div>.1285 3.1685</div>	<div>Z</div> <div>Rs</div> <div>.517 2.355</div> <div>.580 2.293</div> <div>.640 2.242</div> <div>.700 2.199</div> <div>.750 2.167</div> <div>.800 2.139</div> <div>.871 2.104</div> <div>.950 2.070</div> <div>1.050 2.034</div> <div>1.150 2.006</div> <div>1.250 1.985</div> <div>1.350 1.970</div> <div>1.460 1.960</div> <div>1.590 1.958</div> <div>1.774 1.958</div> <div>1.937 1.958</div>	<div>Z</div> <div>Rh</div> <div>2.4500 .8410</div> <div>2.3600 .8130</div> <div>2.2750 .7970</div> <div>2.2000 .7930</div> <div>2.1250 .7990</div> <div>2.0500 .8140</div> <div>1.9925 .8318</div> <div>1.9367 .8522</div> <div>1.8399 .8945</div> <div>1.7431 .9420</div> <div>1.6785 .9751</div> <div>1.6139 1.0076</div> <div>1.5494 1.0409</div> <div>1.4526 1.0925</div> <div>1.3880 1.1280</div> <div>1.2911 1.1833</div> <div>1.1943 1.2411</div> <div>1.0652 1.3229</div> <div>.9361 1.4109</div> <div>.8392 1.4818</div> <div>.7424 1.5579</div> <div>.6456 1.6403</div> <div>.5717 1.7084</div> <div>.4915 1.7887</div> <div>.4263 1.8600</div> <div>.3595 1.9402</div> <div>.2996 2.0204</div> <div>.2518 2.0917</div> <div>.2039 2.1719</div> <div>.1619 2.2521</div> <div>.1257 2.3323</div> <div>.0981 2.4036</div> <div>.0718 2.4838</div> <div>.0504 2.5640</div> <div>.0349 2.6353</div> <div>.0215 2.7156</div> <div>.0119 2.7957</div> <div>.0060 2.8671</div> <div>.0020 2.9473</div> <div>.0002 3.0275</div> <div>.0000 3.0809</div> <div>.0000 3.0899</div> <div>.0000 3.0988</div> <div>.0000 0.0000</div>
FOR -1 E-2	FOR -2-34-4	FOR -34-4	

FOR -4 ONLY

FOR -1 SEE L 687543
FOR -2 SEE L 687490
FOR -3 SEE L 687569
FOR -4 SEE L 687679

Figure 219. Centrifugal Compressor.

D _T	G	Z _G		Z _H	M	W	C	V
6.13	2.851	0.237-0.300		2.095-2.105	0.00	8.7406°	20	0.11
6.124					0.050			0.08

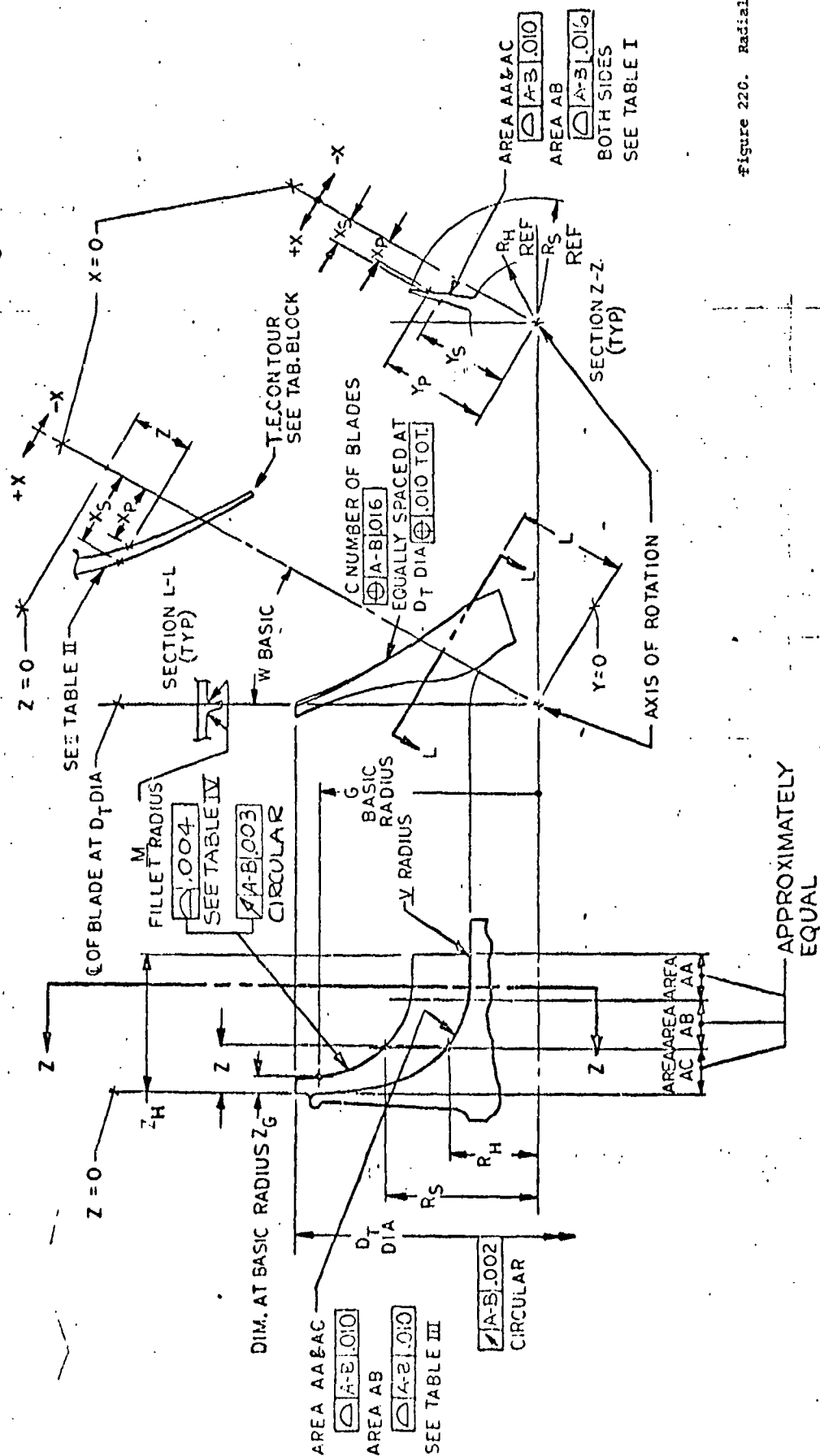


Figure 220. Radial Turbine.

'L' SECTION R = 1.3000			'L' SECTION R = 1.5200			
	SUCTION SIDE	PRESSURE SIDE		SUCTION SIDE	PRESSURE SIDE	
Z	YS	YP	Z	YS	YP	Z
0.0000	0.0000	0.0000	0.0000	0.0000	0.0000	0.0000
0.0375	0.0000	0.0000	0.0375	0.0000	0.0000	0.0375
0.0700	0.0000	0.0000	0.0700	0.0000	0.0000	0.0700
0.1500	0.0000	0.0000	0.1500	0.0000	0.0000	0.1500
0.2175	0.0000	0.0000	0.2175	0.0000	0.0000	0.2175
0.3000	0.0000	0.0000	0.3000	0.0000	0.0000	0.3000
0.3525	0.0000	0.0000	0.3525	0.0000	0.0000	0.3525
0.5000	0.0000	0.0000	0.5000	0.0000	0.0000	0.5000
0.6500	0.0000	0.0000	0.6500	0.0000	0.0000	0.6500
0.7725	0.0000	0.0000	0.7725	0.2909	0.1153	0.7725
0.9000	0.0000	0.0000	0.9000	0.2408	0.0874	0.9000
1.0350	0.0000	0.0000	1.0350	0.1704	0.0391	1.0350
1.1500	0.0000	0.0000	1.1500	0.0975	-0.0267	1.1500
1.2000	0.0000	0.0000	1.2000	0.0628	-0.0628	1.2000
1.2500	0.0000	0.0000	1.2500	0.0250	-0.1027	1.2500
1.3500	-0.0212	-0.1944	1.3500	-0.0563	-0.1927	1.3500
1.4600	-0.1179	-0.2897	1.4600	-0.1707	-0.3066	1.4600
1.6000	-0.2681	-0.4311	1.6000	-0.3483	-0.4713	1.6000
1.7100	-0.4114	-0.5620	1.7100	-0.5164	-0.6255	1.7100
1.8000	-0.5410	-0.6935	1.8000	-0.6688	-0.7787	1.8000
1.9000	-0.7120	-0.8646	1.9000	-0.8700	-0.9791	1.9000
1.9750	-0.8663	-1.0155	1.9750	-1.0498	-1.1573	1.9750
2.0500	-1.0503	-1.1922	2.0500	-1.2616	-1.3681	2.0500
2.1000	-1.1922	-1.3285	2.1000	-1.4222	-1.5344	2.1000

Preceding page blank

TABLE II BLADE COORDINATES

'L' SECTION R = 1.7400			'L' SECTION R = 1.8500			'L' SECTION R = 1.9600		
	SUCTION SIDE	PRESSURE SIDE		SUCTION SIDE	PRESSURE SIDE		SUCTION SIDE	PR
Z	YS	YP	Z	YS	YP	Z	YS	
000	0.0000	0.0000	0.0000	0.0000	0.0000	0.0000	0.0000	
075	0.0000	0.0000	0.0375	0.0000	0.0000	0.0375	0.0000	
100	0.0000	0.0000	0.0700	0.0000	0.0000	0.0700	0.0000	
100	0.0000	0.0000	0.1500	0.0000	0.0000	0.1500	0.0000	
175	0.0000	0.0000	0.2175	0.0000	0.0000	0.2175	0.0000	
200	0.0000	0.0000	0.3000	0.0000	0.0000	0.3000	0.3991	
225	0.0000	0.0000	0.3525	0.3840	0.1826	0.3525	0.3950	
300	0.3616	0.1700	0.5000	0.3694	0.1962	0.5000	0.3768	
300	0.3342	0.1772	0.6500	0.3410	0.2033	0.6500	0.3484	
325	0.2963	0.1670	0.7725	0.3015	0.1900	0.7725	0.3076	
400	0.2433	0.1339	0.9000	0.2463	0.1539	0.9000	0.2512	
450	0.1655	0.0751	1.0350	0.1658	0.0902	1.0350	0.1677	
500	0.0829	-0.0017	1.1500	0.0788	0.0075	1.1500	0.0763	
500	0.0432	-0.0414	1.2000	0.0365	-0.0365	1.2000	0.0293	
500	0.0000	-0.0889	1.2500	-0.0102	-0.0857	1.2500	-0.0178	
600	-0.0935	-0.1921	1.3500	-0.1132	-0.1943	1.3500	-0.1303	
600	-0.2241	-0.3229	1.4600	-0.2511	-0.3310	1.4600	-0.2754	
600	-0.4256	-0.5140	1.6000	-0.4623	-0.5373	1.6000	-0.4967	
600	-0.6137	-0.6953	1.7100	-0.6599	-0.7325	1.7100	-0.7033	
600	-0.7883	-0.8717	1.8000	-0.8444	-0.9216	1.8000	-0.8969	
700	-1.0168	-1.1038	1.9000	-1.0838	-1.1714	1.9000	0.0000	
750	-1.2176	-1.3137	1.9750	0.0000	0.0000	1.9750	0.0000	
800	0.0000	0.0000	2.0500	0.0000	0.0000	2.0500	0.0000	
800	0.0000	0.0000	2.1000	0.0000	0.0000	2.1000	0.0000	

ORDINATES

'L' SECTION R = 1.9600				'L' SECTION R = 2.0700			
SURE SIDE		SUCTION SIDE	PRESSURE SIDE		SUCTION SIDE	PRESSURE SIDE	
YP	Z	YS	YP	Z	YS	YP	Z
0000	0.0000	0.0000	0.0000	0.0000	0.0000	0.0000	0.0000
0000	0.0375	0.0000	0.0000	0.0375	0.0000	0.0000	0.0375
0000	0.0700	0.0000	0.0000	0.0700	0.0000	0.0000	0.0700
0000	0.1500	0.0000	0.0000	0.1500	0.0000	0.0000	0.1500
0000	0.2175	0.0000	0.0000	0.2175	0.4170	0.2170	0.2175
0000	0.3000	0.3991	0.2015	0.3000	0.4076	0.2266	0.3000
1826	0.3525	0.3950	0.2076	0.3525	0.4017	0.2338	0.3525
1962	0.5000	0.3768	0.2232	0.5000	0.3839	0.2496	0.5000
2033	0.6500	0.3484	0.2245	0.6500	0.3556	0.2543	0.6500
1700	0.7725	0.3076	0.2151	0.7725	0.3162	0.2379	0.7725
1539	0.9000	0.2512	0.1759	0.9000	0.2584	0.1913	0.9000
0902	1.0350	0.1677	0.1036	1.0350	0.1709	0.1157	1.0350
0075	1.1500	0.0763	0.0151	1.1500	0.0752	0.0215	1.1500
0365	1.2000	0.0293	-0.0293	1.2000	0.0266	-0.0266	1.2000
0857	1.2500	-0.0178	-0.0822	1.2500	-0.0265	-0.0792	1.2500
943	1.3500	-0.1303	-0.1957	1.3500	-0.1445	-0.2000	1.3500
310	1.4600	-0.2754	-0.3419	1.4600	-0.2969	-0.3553	1.4600
373	1.6000	-0.4967	-0.5629	1.6000	-0.5282	-0.5914	1.6000
325	1.7100	-0.7033	-0.7730	1.7100	0.0000	0.0000	1.7100
216	1.8000	-0.8969	-0.9744	1.8000	0.0000	0.0000	1.8000
714	1.9000	0.0000	0.0000	1.9000	0.0000	0.0000	1.9000
000	1.9750	0.0000	0.0000	1.9750	0.0000	0.0000	1.9750
000	2.0500	0.0000	0.0000	2.0500	0.0000	0.0000	2.0500
000	2.1000	0.0000	0.0000	2.1000	0.0000	0.0000	2.1000

Figure 221. Radia

'L' SECTION R = 2.0700			'L' SECTION R = 2.1800		
	SUCTION SIDE	PRESSURE SIDE		SUCTION SIDE	PRESSURE SIDE
Z	YS	YP	Z	YS	YP
0.0000	0.0000	0.0000	0.0000	0.0000	0.0000
0.0375	0.0000	0.0000	0.0375	0.0000	0.0000
0.0700	0.0000	0.0000	0.0700	0.0000	0.0000
0.1500	0.0000	0.0000	0.1500	0.4332	0.2349
0.2175	0.4170	0.2170	0.2175	0.4255	0.2427
0.3000	0.4076	0.2266	0.3000	0.4156	0.2548
0.3525	0.4017	0.2338	0.3525	0.4095	0.2610
0.5000	0.3839	0.2496	0.5000	0.3902	0.2769
0.6500	0.3556	0.2543	0.6500	0.3630	0.2794
0.7725	0.3162	0.2379	0.7725	0.3216	0.2603
0.9000	0.2584	0.1913	0.9000	0.2634	0.2103
1.0350	0.1709	0.1157	1.0350	0.1749	0.1271
1.1500	0.0752	0.0215	1.1500	0.0759	0.0259
1.2000	0.0266	-0.0266	1.2000	0.0258	-0.0258
1.2500	-0.0265	-0.0792	1.2500	-0.0298	-0.0816
1.3500	-0.1445	-0.2000	1.3500	-0.1544	-0.2085
1.4600	-0.2969	-0.3553	1.4600	0.0000	0.0000
1.6000	-0.5282	-0.5914	1.6000	0.0000	0.0000
1.7100	0.0000	0.0000	1.7100	0.0000	0.0000
1.8000	0.0000	0.0000	1.8000	0.0000	0.0000
1.9000	0.0000	0.0000	1.9000	0.0000	0.0000
1.9750	0.0000	0.0000	1.9750	0.0000	0.0000
2.0500	0.0000	0.0000	2.0500	0.0000	0.0000
2.1000	0.0000	0.0000	2.1000	0.0000	0.0000

Figure 221. Radial Turbine, Coordinates for Figure 208.

$Z = 0.0375$				$Z = 0.1175$				$Z = 0.2175$		
SUCTION SIDE		PRESSURE SIDE		SUCTION SIDE		PRESSURE SIDE		SUCTION SIDE		PR
X _S	Y _S	X _P	Y _P	X _S	Y _S	X _P	Y _P	X _S	Y _S	X _P
0.0932	2.5100	-0.0932	2.5100	0.1000	2.2325	-0.1000	2.2325	0.1040	2.0250	-0.1
0.0890	2.5604	-0.0890	2.5604	0.0941	2.3116	-0.0941	2.3116	0.0966	2.1237	-0.0
0.0864	2.5886	-0.0864	2.5886	0.0909	2.3536	-0.0909	2.3536	0.0925	2.1762	-0.0
0.0836	2.6167	-0.0836	2.6167	0.0878	2.3956	-0.0878	2.3956	0.0885	2.2286	-0.0
0.0807	2.6449	-0.0807	2.6449	0.0845	2.4376	-0.0845	2.4376	0.0845	2.2811	-0.0
0.0779	2.6731	-0.0779	2.6731	0.0813	2.4796	-0.0813	2.4796	0.0805	2.3335	-0.0
0.0749	2.7013	-0.0749	2.7013	0.0780	2.5217	-0.0780	2.5217	0.0766	2.3860	-0.0
0.0712	2.7295	-0.0712	2.7295	0.0746	2.5637	-0.0746	2.5637	0.0726	2.4384	-0.0
0.0681	2.7577	-0.0681	2.7577	0.0712	2.6057	-0.0712	2.6057	0.0687	2.4909	-0.0
0.0650	2.7859	-0.0650	2.7859	0.0675	2.6477	-0.0675	2.6477	0.0647	2.5433	-0.0
0.0619	2.8141	-0.0619	2.8141	0.0637	2.6897	-0.0637	2.6897	0.0606	2.5958	-0.0
0.0584	2.8423	-0.0584	2.8423	0.0598	2.7317	-0.0598	2.7317	0.0567	2.6483	-0.0
0.0548	2.8705	-0.0548	2.8705	0.0557	2.7738	-0.0557	2.7738	0.0527	2.7007	-0.0
0.0513	2.8987	-0.0513	2.8987	0.0516	2.8158	-0.0516	2.8158	0.0487	2.7532	-0.0
0.0468	2.9269	-0.0468	2.9269	0.0473	2.8578	-0.0473	2.8578	0.0447	2.8056	-0.0
0.0429	2.9551	-0.0429	2.9551	0.0431	2.8998	-0.0431	2.8998	0.0406	2.8581	-0.0
0.0388	2.9833	-0.0388	2.9833	0.0385	2.9418	-0.0385	2.9418	0.0366	2.9105	-0.0
0.0343	3.0115	-0.0343	3.0115	0.0340	2.9839	-0.0340	2.9839	0.0327	2.9630	-0.0
0.0296	3.0397	-0.0296	3.0397	0.0294	3.0259	-0.0294	3.0259	0.0288	3.0154	-0.0
0.0230	3.0800	-0.0230	3.0800	0.0220	3.0950	-0.0220	3.0950	0.0229	3.1000	-0.0

TABLE I BLADE COORDINATES

Z = 0.2175			Z = 0.3000				Z = 0.5000				SUC
ON	PRESSURE		SUCTION		PRESSURE		SUCTION		PRESSURE		S
E	SIDE		SIDE		SIDE		SIDE		SIDE		S
Y _S	X _P	Y _P	X _S	Y _S	X _P	Y _P	X _S	Y _S	X _P	Y _P	X _S
2.0250	-0.1040	2.0250	0.1012	1.9250	-0.1012	1.9250	0.0980	1.7250	-0.0970	1.7250	0.1200
2.1237	-0.0966	2.1237	0.0952	2.0193	-0.0952	2.0193	0.0915	1.8059	-0.0906	1.8059	0.1100
2.1762	-0.0925	2.1762	0.0913	2.0711	-0.0913	2.0711	0.0882	1.8457	-0.0872	1.8457	0.1065
2.2286	-0.0885	2.2286	0.0872	2.1228	-0.0872	2.1228	0.0849	1.8854	-0.0839	1.8855	0.1029
2.2811	-0.0845	2.2811	0.0831	2.1746	-0.0831	2.1746	0.0815	1.9252	-0.0804	1.9252	0.0999
2.3335	-0.0805	2.3335	0.0788	2.2263	-0.0788	2.2263	0.0783	1.9649	-0.0772	1.9650	0.0970
2.3860	-0.0766	2.3860	0.0748	2.2781	-0.0748	2.2781	0.0748	2.0047	-0.0737	2.0047	0.0942
2.4384	-0.0726	2.4384	0.0703	2.3299	-0.0703	2.3299	0.0712	2.0444	-0.0701	2.0445	0.0918
2.4909	-0.0687	2.4909	0.0663	2.3816	-0.0663	2.3816	0.0679	2.0842	-0.0667	2.0842	0.0893
2.5433	-0.0647	2.5433	0.0621	2.4334	-0.0621	2.4334	0.0641	2.1240	-0.0630	2.1240	0.0871
2.5958	-0.0606	2.5958	0.0577	2.4852	-0.0577	2.4852	0.0606	2.1637	-0.0594	2.1638	0.0849
2.6483	-0.0567	2.6483	0.0530	2.5369	-0.0530	2.5369	0.0568	2.2035	-0.0556	2.2035	0.0828
2.7007	-0.0527	2.7007	0.0489	2.5887	-0.0489	2.5887	0.0529	2.2432	-0.0517	2.2433	0.0808
2.7532	-0.0487	2.7532	0.0441	2.6405	-0.0441	2.6405	0.0492	2.2830	-0.0480	2.2830	0.0788
2.8056	-0.0447	2.8056	0.0400	2.6922	-0.0400	2.6922	0.0453	2.3228	-0.0440	2.3228	0.0769
2.8581	-0.0406	2.8581	0.0355	2.7440	-0.0355	2.7440	0.0416	2.3625	-0.0403	2.3625	0.0749
2.9105	-0.0366	2.9105	0.0320	2.7958	-0.0320	2.7958	0.0377	2.4023	-0.0364	2.4023	0.0730
2.9630	-0.0327	2.9630	0.0281	2.8475	-0.0281	2.8475	0.0338	2.4420	-0.0324	2.4420	0.0712
3.0154	-0.0288	3.0154	0.0250	2.8993	-0.0250	2.8993	0.0308	2.4818	-0.0294	2.4818	0.0693
3.1000	-0.0229	3.1000	0.0207	2.9950	-0.0207	2.9950	0.0257	2.5500	-0.0243	2.5500	0.0665

BLADE COORDINATES

Z=0.5000				Z=0.7725				Z=1.0350			
SUCTION SIDE		PRESSURE SIDE		SUCTION SIDE		PRESSURE SIDE		SUCTION SIDE		PRESSURE SIDE	
	Y _s	X _p	Y _p	X _s	Y _s	X _p	Y _p	X _s	Y _s	X _p	Y _p
980	1.7250	-0.0970	1.7250	0.1200	1.5209	-0.0600	1.5245	0.1970	1.3964	0.0375	1.4098
915	1.8059	-0.0906	1.8059	0.1100	1.6170	-0.0462	1.6201	0.1931	1.4793	0.0551	1.4909
882	1.8457	-0.0872	1.8457	0.1065	1.6568	-0.0411	1.6597	0.1919	1.5216	0.0633	1.5323
849	1.8854	-0.0839	1.8855	0.1029	1.6965	-0.0359	1.6992	0.1908	1.5638	0.0714	1.5738
815	1.9252	-0.0804	1.9252	0.0999	1.7362	-0.0314	1.7388	0.1901	1.6060	0.0791	1.6153
783	1.9649	-0.0772	1.9650	0.0970	1.7759	-0.0269	1.7784	0.1899	1.6482	0.0863	1.6568
748	2.0047	-0.0737	2.0047	0.0942	1.8156	-0.0226	1.8179	0.1897	1.6903	0.0935	1.6984
712	2.0444	-0.0701	2.0445	0.0918	1.8553	-0.0186	1.8575	0.1902	1.7324	0.1000	1.7399
679	2.0842	-0.0667	2.0842	0.0893	1.8950	-0.0145	1.8971	0.1906	1.7745	0.1066	1.7815
641	2.1240	-0.0630	2.1240	0.0871	1.9347	-0.0108	1.9367	0.1914	1.8166	0.1128	1.8232
606	2.1637	-0.0594	2.1638	0.0849	1.9744	-0.0070	1.9762	0.1924	1.8586	0.1188	1.8648
568	2.2035	-0.0556	2.2035	0.0828	2.0141	-0.0034	2.0158	0.1935	1.9007	0.1246	1.9064
529	2.2432	-0.0517	2.2433	0.0808	2.0538	0.0002	2.0554	0.1951	1.9427	0.1301	1.9481
492	2.2830	-0.0480	2.2830	0.0788	2.0935	0.0038	2.0950	0.1966	1.9847	0.1355	1.9898
453	2.3228	-0.0440	2.3228	0.0769	2.1332	0.0073	2.1346	0.1985	2.0267	0.1406	2.0315
416	2.3625	-0.0403	2.3625	0.0749	2.1729	0.0108	2.1742	0.2004	2.0687	0.1457	2.0732
377	2.4023	-0.0364	2.4023	0.0730	2.2126	0.0142	2.2138	0.2024	2.1106	0.1507	2.1150
338	2.4420	-0.0324	2.4420	0.0712	2.2523	0.0176	2.2534	0.2045	2.1526	0.1556	2.1567
298	2.4818	-0.0294	2.4818	0.0693	2.2920	0.0211	2.2929	0.2067	2.1946	0.1604	2.1984
257	2.5500	-0.0243	2.5500	0.0665	2.3561	0.0265	2.3569	0.2090	2.2365	0.1651	2.2402

Z=1.0350			Z=1.2000				Z=1.2100					
ACTION SIDE	PRESSURE SIDE		SUCTION SIDE		PRESSURE SIDE		SUCTION SIDE		PRESSURE SIDE			
	X _p	Y _p	X _s	Y _s	X _p	Y _p	X _s	Y _s	X _p	Y _p		
	1.3964	0.0375	1.4098	0.2709	1.2989	0.1318	1.3203	0.2917	1.2953	0.1240	1.3219	0.4
	1.4793	0.0551	1.4909	0.2826	1.4009	0.1512	1.4211	0.3017	1.3941	0.1450	1.4190	0.4
	1.5216	0.0633	1.5323	0.2864	1.4446	0.1608	1.4639	0.3055	1.4379	0.1550	1.4618	0.5
	1.5638	0.0714	1.5738	0.2894	1.4884	0.1711	1.5065	0.3091	1.4817	0.1651	1.5046	0.5
	1.6060	0.0791	1.6153	0.2924	1.5322	0.1813	1.5492	0.3116	1.5258	0.1764	1.5472	0.5
	1.6482	0.0863	1.6568	0.2952	1.5760	0.1919	1.5919	0.3148	1.5697	0.1870	1.5900	0.5
	1.6903	0.0935	1.6984	0.2984	1.6198	0.2019	1.6346	0.3177	1.6136	0.1979	1.6327	0.5
	1.7324	0.1000	1.7399	0.3012	1.6636	0.2124	1.6773	0.3203	1.6576	0.2090	1.6753	0.5
	1.7745	0.1066	1.7815	0.3049	1.7073	0.2221	1.7201	0.3227	1.7017	0.2204	1.7179	0.5
	1.8166	0.1128	1.8232	0.3083	1.7511	0.2319	1.7628	0.3251	1.7457	0.2317	1.7605	0.5
	1.8586	0.1188	1.8648	0.3124	1.7947	0.2411	1.8057	0.3278	1.7897	0.2427	1.8032	0.5
	1.9007	0.1246	1.9064	0.3166	1.8384	0.2503	1.8486	0.3308	1.8336	0.2535	1.8459	0.5
	1.9427	0.1301	1.9481	0.3212	1.8819	0.2589	1.8915	0.3344	1.8775	0.2637	1.8887	0.6
	1.9847	0.1355	1.9898	0.3261	1.9254	0.2674	1.9345	0.3384	1.9213	0.2735	1.9316	0.6
	2.0267	0.1406	2.0315	0.3313	1.9689	0.2754	1.9775	0.3427	1.9650	0.2829	1.9745	0.6
	2.0687	0.1457	2.0732	0.3373	2.0123	0.2828	2.0206	0.3474	2.0087	0.2920	2.0175	0.6
	2.1106	0.1507	2.1150	0.3427	2.0557	0.2907	2.0637	0.3526	2.0523	0.3005	2.0605	0.6
	2.1526	0.1556	2.1567	0.3490	2.0990	0.2976	2.1069	0.3588	2.0957	0.3081	2.1037	0.6
	2.1946	0.1604	2.1984	0.3556	2.1423	0.3044	2.1501	0.3656	2.1390	0.3150	2.1471	0.6
	2.2365	0.1651	2.2402	0.3618	2.1856	0.3115	2.1933	0.3722	2.1824	0.3222	2.1903	0.6

		Z=1.4600				Z=1.7100				Z=1.9000			
PRESSURE SIDE		SUCTION SIDE		PRESSURE SIDE		SUCTION SIDE		PRESSURE SIDE		SUCTION SIDE			
X _P	Y _P	X _S	Y _S	X _P	Y _P	X _S	Y _S	X _P	Y _P	X _S	Y _S	X _S	Y _S
240	1.3219	0.4657	1.1635	0.2943	1.2182	0.6679	1.0011	0.5094	1.0903	0.8488	0.8540		
450	1.4190	0.4891	1.2627	0.3326	1.3126	0.7140	1.1102	0.5787	1.1863	0.9073	0.9435		
550	1.4618	0.5000	1.3081	0.3501	1.3559	0.7333	1.1545	0.6066	1.2258	0.9348	0.9841		
651	1.5046	0.5106	1.3536	0.3678	1.3992	0.7527	1.1988	0.6344	1.2654	0.9620	1.0248		
764	1.5472	0.5210	1.3992	0.3857	1.4424	0.7727	1.2428	0.6616	1.3053	0.9900	1.0649		
870	1.5900	0.5315	1.4447	0.4035	1.4856	0.7927	1.2867	0.6889	1.3451	1.0178	1.1052		
979	1.6327	0.5420	1.4903	0.4213	1.5288	0.8131	1.3304	0.7156	1.3853	1.0462	1.1450		
1090	1.6753	0.5527	1.5358	0.4390	1.5720	0.8335	1.3742	0.7425	1.4254	1.0744	1.1849		
1204	1.7179	0.5633	1.5813	0.4567	1.6153	0.8543	1.4176	0.7688	1.4657	1.1031	1.2244		
1317	1.7605	0.5737	1.6269	0.4746	1.6585	0.8750	1.4612	0.7953	1.5061	1.1317	1.2640		
1427	1.8032	0.5841	1.6725	0.4926	1.7016	0.8964	1.5043	0.8211	1.5467	1.1609	1.3031		
1535	1.8459	0.5944	1.7181	0.5106	1.7448	0.9177	1.5475	0.8470	1.5874	1.1901	1.3422		
1637	1.8887	0.6049	1.7636	0.5284	1.7880	0.9396	1.5904	0.8722	1.6283	1.2198	1.3809		
1735	1.9316	0.6158	1.8090	0.5458	1.8314	0.9615	1.6333	0.8976	1.6693	1.2495	1.4196		
1829	1.9745	0.6275	1.8542	0.5625	1.8749	0.9837	1.6760	0.9225	1.7104	1.2795	1.4580		
1920	2.0175	0.6396	1.8992	0.5787	1.9187	1.0060	1.7186	0.9474	1.7516	1.3096	1.4963		
2005	2.0605	0.6520	1.9442	0.5946	1.9625	1.0291	1.7608	0.9716	1.7932	1.3405	1.5340		
2081	2.1037	0.6649	1.9890	0.6100	2.0065	1.0523	1.8030	0.9955	1.8350	1.3715	1.5716		
2150	2.1471	0.6783	2.0336	0.6249	2.0506	1.0762	1.8447	1.0188	1.8770	1.4032	1.6086		
222	2.1903	0.6923	2.0780	0.6393	2.0949	1.1003	1.8864	1.0419	1.9192	1.4351	1.6454		

Figur

Z = 1.7100			Z = 1.9000				Z = 2.1000			
PRESSURE SIDE			SUCTION SIDE		PRESSURE SIDE		SUCTION SIDE		PRESSURE SIDE	
Y _s	X _p	Y _p	X _s	Y _s	X _p	Y _p	X _s	Y _s	X _p	Y _p
011	0.5094	1.0903	0.8488	0.8540	0.6972	0.9817	1.0215	0.6386	0.8937	0.8078
102	0.5787	1.1863	0.9073	0.9435	0.7754	1.0546	1.0932	0.7093	0.9813	0.8575
345	0.6066	1.2258	0.9348	0.9841	0.8107	1.0885	1.1292	0.7432	1.0237	0.8828
988	0.6344	1.2654	0.9620	1.0248	0.8462	1.1223	1.1648	0.7773	1.0663	0.9078
428	0.6616	1.3053	0.9900	1.0649	0.8810	1.1567	1.2011	0.8107	1.1083	0.9336
867	0.6889	1.3451	1.0178	1.1052	0.9160	1.1910	1.2373	0.8442	1.1504	0.9592
804	0.7156	1.3853	1.0462	1.1450	0.9503	1.2257	1.2739	0.8771	1.1921	0.9854
742	0.7425	1.4254	1.0744	1.1849	0.9849	1.2603	1.3104	0.9102	1.2339	1.0115
176	0.7688	1.4657	1.1031	1.2244	1.0189	1.2953	1.3473	0.9428	1.2753	1.0380
612	0.7953	1.5061	1.1317	1.2640	1.0531	1.3302	1.3841	0.9754	1.3168	1.0645
043	0.8211	1.5467	1.1609	1.3031	1.0866	1.3657	1.4214	1.0075	1.3579	1.0916
475	0.8470	1.5874	1.1901	1.3422	1.1202	1.4011	1.4589	1.0392	1.3986	1.1190
904	0.8722	1.6283	1.2198	1.3809	1.1533	1.4369	1.4964	1.0710	1.4395	1.1463
333	0.8976	1.6693	1.2495	1.4196	1.1864	1.4727	1.5341	1.1025	1.4801	1.1740
760	0.9225	1.7104	1.2795	1.4580	1.2191	1.5089	1.5721	1.1336	1.5204	1.2021
86	0.9474	1.7516	1.3096	1.4963	1.2517	1.5451	1.6102	1.1646	1.5606	1.2302
08	0.9716	1.7932	1.3405	1.5340	1.2837	1.5819	1.6488	1.1948	1.6002	1.2591
30	0.9955	1.8350	1.3715	1.5716	1.3154	1.6189	1.6877	1.2247	1.6396	1.2884
47	1.0188	1.8770	1.4032	1.6086	1.3465	1.6564	1.7271	1.2539	1.6785	1.3183
64	1.0419	1.9192	1.4351	1.6454	1.3773	1.6941	1.7668	1.2829	1.7172	1.3485

Figure 222. Radial Turbine, Coordinates for Figure 208.

TABLE III				
HUB CONTOUR COORDINATES				
Z	R _H		Z	R _H
2.1000	1.2500		0.1496	2.1400
2.0109	1.2512		0.1440	2.1493
1.9214	1.2546		0.1394	2.3186
1.8327	1.2599		0.1358	2.2479
1.7434	1.2671		0.1331	2.2772
1.6544	1.2762		0.1013	2.3065
1.5654	1.2871		0.0904	2.3358
1.4850	1.2994		0.0803	2.3650
1.3950	1.3225		0.0710	2.3943
1.3050	1.3469		0.0624	2.4236
				*
1.2150	1.3785		0.0345	2.4529
1.1250	1.4116		0.0473	2.4822
1.0350	1.4483		0.0408	2.5115
0.9450	1.4889		0.0349	2.5407
0.8550	1.5338		0.0296	2.5700
				*
0.7650	1.5836		0.0249	2.5993
0.6750	1.6390		0.0206	2.6286
0.5850	1.7013		0.0169	2.6579
0.5216	1.7500		0.0137	2.6872
0.4862	1.7793		0.0108	2.7165
				*
0.4527	1.8086		0.0085	2.7458
0.4211	1.8379		0.0064	2.7750
0.3911	1.8672		0.0047	2.8043
0.3628	1.8965		0.0034	2.8336
0.3360	1.9257		0.0023	2.8629
				*
0.3106	1.9550		0.0015	2.8922
0.2867	1.9843		0.0009	2.9215
0.2641	2.0136		0.0005	2.9508
0.2428	2.0429		0.0002	2.9800
0.2228	2.0722		0.0001	3.0093
				*
0.2039	2.1015		0.0000	3.0386
0.1862	2.1308		0.0000	3.9000
				*

TABLE IV				
OUTSIDE EDGE CONTOUR COORDINATES				
Z	R _g		Z	R _g
0.2695	3.2000	*		
0.2695	3.0680			
0.2777	3.0220			
0.2786	3.0000			
0.2803	2.8819			
0.3077	2.8192			
0.3294	2.7578			
0.3573	2.6957			
0.3935	2.6336			
0.4373	2.5715			
0.4913	2.5093			
0.5273	2.4788			
0.5672	2.4467			
0.6030	2.4147			
0.6426	2.3829			
0.6808	2.3560			
1.0377	2.2285			
1.1445	2.2022			
1.2511	2.1936			
1.3575	2.1834			
1.4638	2.1756			
1.5700	2.1723			
1.6767	2.1699			
1.7822	2.1686			
1.8882	2.1681			
1.9941	2.1680			
2.1000	2.1680			

Figure 223. Radial Turbine, Coordinates for Figure 209.

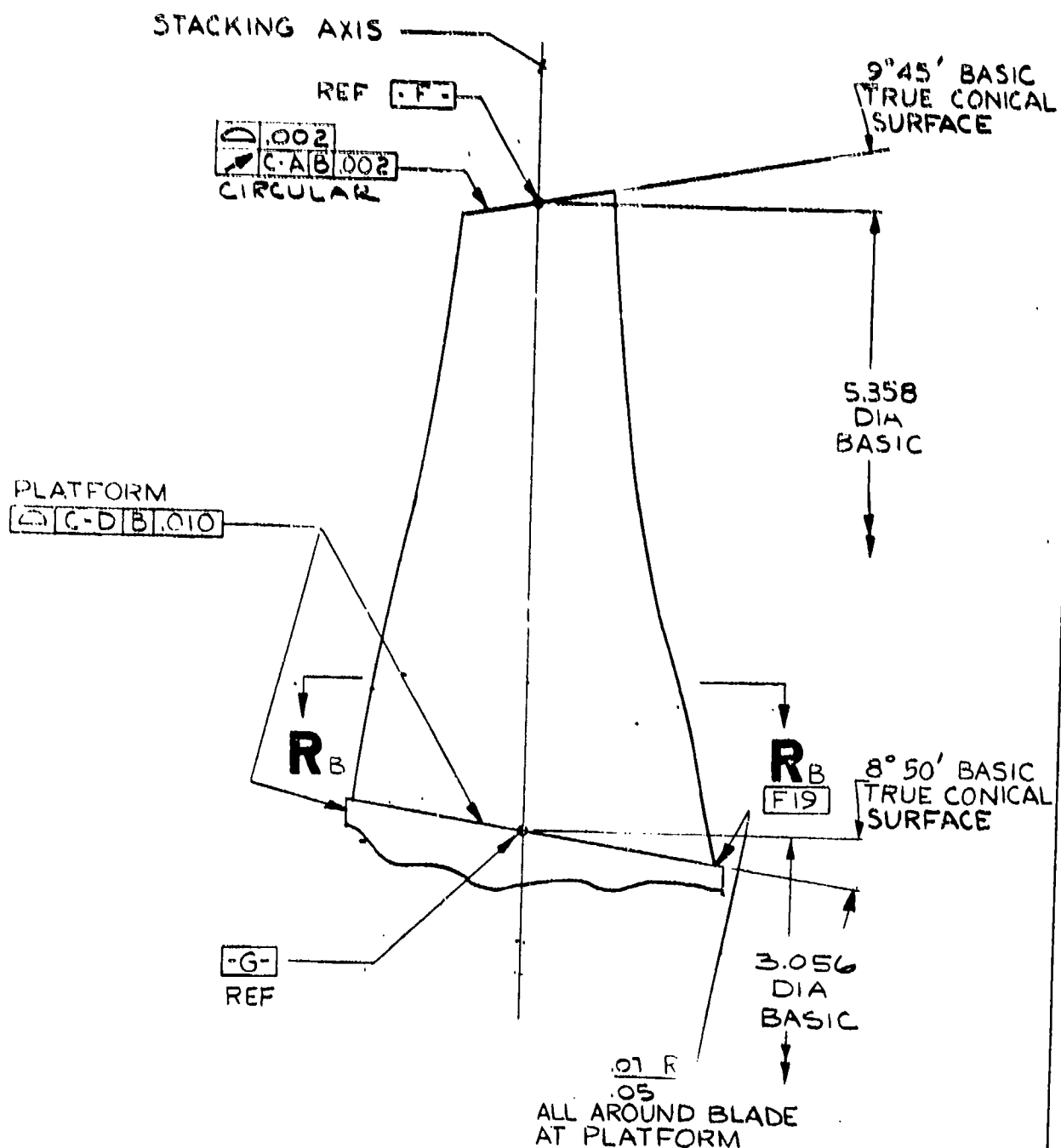
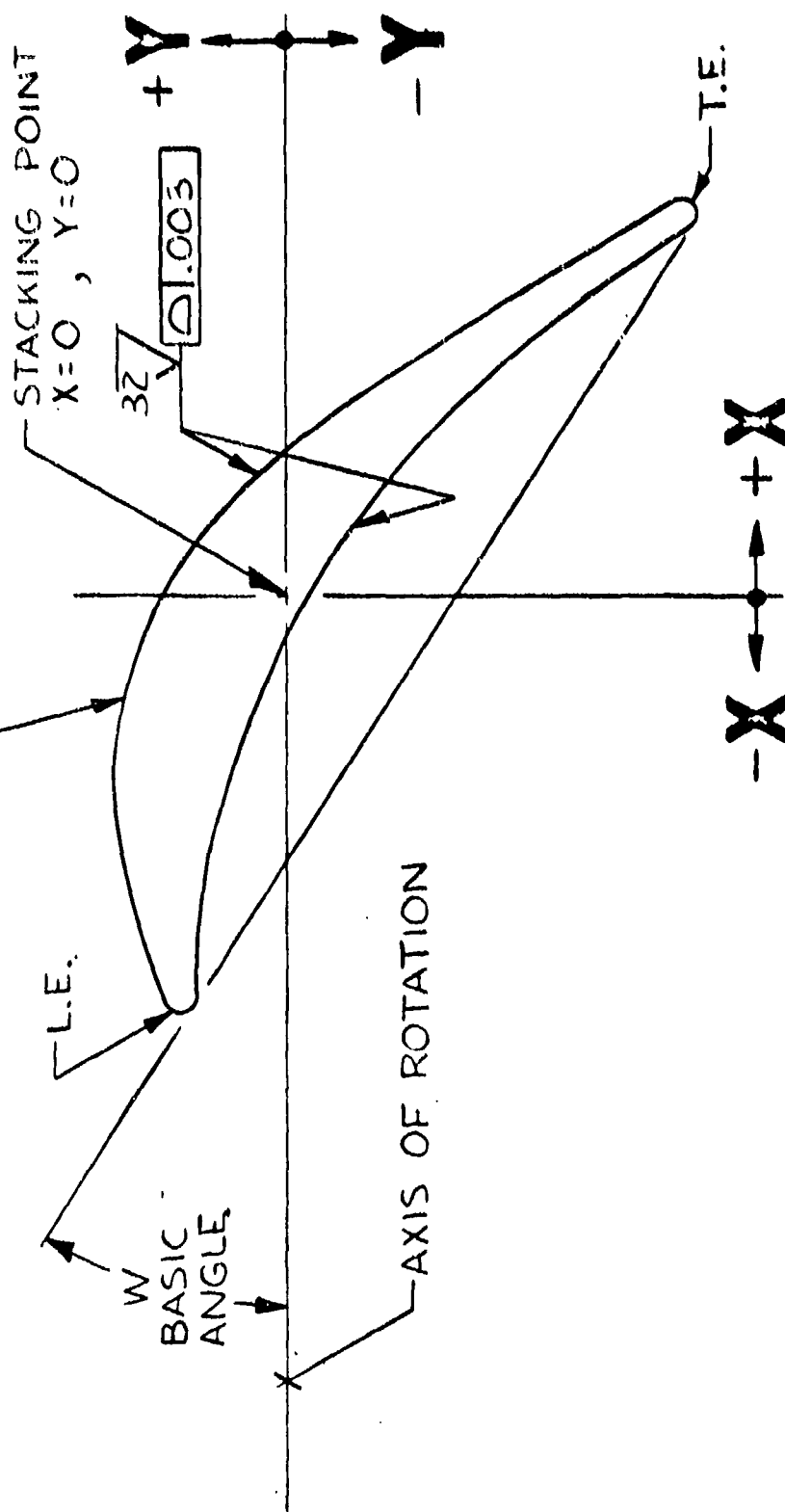


Figure 224. Axial Turbine.

FOR BASIC CONTOUR COORDINATES
SEE TABLE I E19



SECTION AT **R** B F16

Figure 225. Axial Turbine, Stacking.

DASH LINES INDICATE STRAIGHT LINE
ELEMENTS CONNECTING HUB & SHROUD
MEAN CONTOUR. ELEMENTS FROM 1 TO 15
PLUS THE LEADING & TRAILING EDGES
ARE NUMBERED IN TABLE II. BLADE 4.420 DI
SURFACE IS GENERATED BY FAIRING
SMOOTHLY ACROSS STRAIGHT LINE
ELEMENTS. NO SHARP BENDS OR CHANGES
IN CONTOUR

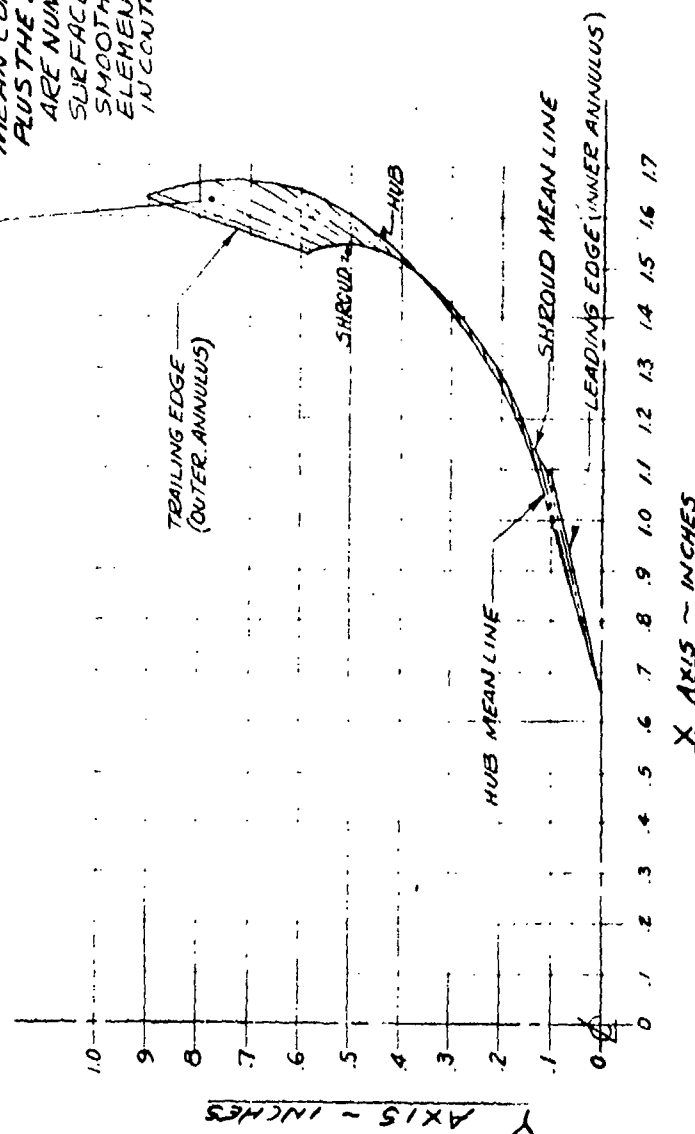


TABLE II

EL. NO.	MEAN LINE CONTOUR HUB		MEAN LINE CONTOUR SHROUD	
	X	Y	X	Y
1	0.660	0.000	1.097	0.104
2	0.707	0.019	1.104	0.111
3	0.763	0.038	1.116	0.121
4	0.865	0.068	1.142	0.138
5	0.978	0.095	1.175	0.154
6	1.111	0.138	1.225	0.173
7	1.240	0.190	1.273	0.195
8	1.365	0.258	1.337	0.230
9	1.485	0.349	1.402	0.278
10	1.567	0.452	1.454	0.326
11	1.631	0.564	1.500	0.383
12	1.663	0.651	1.530	0.434
13	1.680	0.750	1.548	0.482
14	1.670	0.832	1.550	0.538
15	1.644	0.891	1.543	0.561
16	1.640	0.898	1.535	0.583
17	1.637	0.904	1.532	0.591

Figure 226. Torque Converter, Impeller.

TABLE I

SECTION	FOR CONST PURPOSES									
	R ₁ =1.4130		R ₂ =1.4730		R ₃ =1.5771		R ₄ =1.6913		R ₅ =1.8054	
W	1°29'		4°04'		8°49'		14°28'		21°19'	
LER BASIC	.0143		.0136		.0126		.0118		.0112	
TER BASIC	.0103		.0101		.0099		.0097		.0094	
	X	Y	X	Y	X	Y	X	Y	X	Y
	-0.30564	-0.13435	-0.30260	-0.11739	-0.29534	-0.08773	-0.28443	-0.05505	-0.26975	-0.01627
	-0.27804	-0.10769	-0.27431	-0.09318	-0.26580	-0.06775	-0.25350	-0.03974	-0.23817	-0.00653
	-0.24748	-0.08465	-0.24338	-0.07244	-0.23422	-0.05095	-0.22117	-0.02730	-0.20589	0.00057
	-0.21441	-0.06574	-0.21025	-0.05557	-0.20095	-0.03763	-0.18774	-0.01788	-0.17314	0.00498
	-0.17974	-0.05006	-0.17571	-0.04181	-0.16662	-0.02717	-0.15363	-0.01106	-0.14015	0.00703
	-0.14385	-0.03704	-0.14013	-0.03070	-0.13158	-0.01937	-0.11916	-0.00689	-0.10710	0.00663
	-0.10699	-0.02704	-0.10375	-0.02253	-0.09603	-0.01437	-0.08450	-0.00537	-0.07417	0.00382
	-0.06943	-0.02004	-0.06682	-0.01727	-0.06018	-0.01214	-0.04903	-0.00646	-0.04153	-0.00138
	-0.03137	-0.01588	-0.02955	-0.01482	-0.02427	-0.01265	-0.01543	-0.01021	-0.00937	-0.00901
	0.00711	-0.01433	0.00794	-0.01500	0.01150	-0.01584	0.01846	-0.01670	0.02208	-0.01915
	0.04502	-0.01505	0.04537	-0.01801	0.04693	-0.02177	0.05170	-0.02585	0.05263	-0.03171
	0.08415	-0.01988	0.08251	-0.02386	0.08180	-0.03043	0.08405	-0.03759	0.08208	-0.04662
	0.12242	-0.02667	0.11926	-0.03225	0.11594	-0.04160	0.11532	-0.05182	0.11025	-0.06380
	0.16036	-0.03593	0.15548	-0.04311	0.14916	-0.05523	0.14527	-0.06849	0.13690	-0.08318
	0.19702	-0.04864	0.19047	-0.05704	0.18128	-0.07129	0.17422	-0.08687	0.16265	-0.10370
	0.23258	-0.06417	0.22426	-0.07366	0.21203	-0.08979	0.20161	-0.10745	0.18670	-0.12611
	0.26689	-0.08229	0.25669	-0.09275	0.24125	-0.11057	0.22730	-0.13008	0.20898	-0.15026
	0.29914	-0.10349	0.28717	-0.11461	0.26868	-0.13360	0.25138	-0.15438	0.22994	-0.17549
	0.32891	-0.12768	0.31531	-0.13917	0.29404	-0.15882	0.27368	-0.18032	0.24920	-0.20200
	0.35467	-0.15559	0.34006	-0.16685	0.31709	-0.18609	0.29483	-0.20718	0.26817	-0.22861
	0.35826	-0.15777	0.34355	-0.16907	0.32044	-0.18838	0.29790	-0.20950	0.27110	-0.23103
	0.36194	-0.15839	0.34718	-0.16975	0.32395	-0.18916	0.30120	-0.21042	0.27431	-0.23210
	0.36561	-0.15768	0.35081	-0.16912	0.32752	-0.18866	0.30461	-0.21017	0.27770	-0.23199
	0.36880	-0.15574	0.35399	-0.16726	0.33069	-0.18694	0.30773	-0.20876	0.28084	-0.23074
	0.37111	-0.15281	0.35632	-0.16441	0.33305	-0.18423	0.31018	-0.20638	0.28336	-0.22848
	0.37225	-0.14925	0.35751	-0.16092	0.33432	-0.18086	0.31167	-0.20331	0.28496	-0.22551
	0.36977	-0.14098	0.35521	-0.15271	0.33229	-0.17278	0.31012	-0.19476	0.28375	-0.21700
	0.33772	-0.10416	0.32219	-0.11277	0.29751	-0.12741	0.27345	-0.14342	0.24661	-0.15948
	0.30550	-0.06768	0.28901	-0.07321	0.26259	-0.08248	0.23664	-0.09261	0.20896	-0.10262
	0.27052	-0.03948	0.26077	-0.04193	0.23210	-0.04585	0.20370	-0.05009	0.17423	-0.05400
	0.24977	-0.01314	0.23068	-0.01249	0.19967	-0.01103	0.16869	-0.00937	0.13705	-0.00717
	0.21162	0.01856	0.19489	0.01813	0.16798	0.01773	0.14148	0.01734	0.11405	0.01735
	0.16981	0.04540	0.15559	0.04424	0.13303	0.04255	0.11131	0.04075	0.08838	0.03921
	0.12507	0.06699	0.11345	0.06543	0.09540	0.06303	0.07861	0.06046	0.06044	0.05803
	0.07812	0.08283	0.06909	0.08120	0.05557	0.07866	0.04372	0.07594	0.03048	0.07337
	0.02961	0.09248	0.02317	0.09113	0.01413	0.08908	0.00717	0.08688	-0.00106	0.08495
	-0.01963	0.09515	-0.02359	0.09450	-0.02830	0.09367	-0.03052	0.09281	-0.03374	0.09245
	-0.06865	0.09077	-0.07027	0.09117	-0.07094	0.09217	-0.06873	0.09330	-0.06709	0.09539
	-0.11628	0.07871	-0.11582	0.08058	-0.11287	0.08412	-0.10666	0.08804	-0.10050	0.09354
	-0.16117	0.05876	-0.15895	0.06248	-0.15295	0.06924	-0.14335	0.07669	-0.13323	0.08652
	-0.20171	0.03111	-0.19814	0.03694	-0.18983	0.04751	-0.17766	0.05910	-0.16438	0.07405
	-0.23578	-0.00494	-0.23169	0.00797	-0.22248	0.01975	-0.20932	0.03710	-0.19420	0.05839
	-0.26805	-0.04255	-0.26356	-0.03002	-0.25367	-0.00960	-0.23979	0.01352	-0.22320	0.04112
	-0.29878	-0.08127	-0.29401	-0.06628	-0.28309	-0.03995	-0.26936	-0.01100	-0.25164	0.02293
	-0.32961	-0.11932	-0.32443	-0.10148	-0.31345	-0.07026	-0.29845	-0.03589	-0.27955	0.00403
	-0.33157	-0.12465	-0.32665	-0.10642	-0.31644	-0.07543	-0.30207	-0.04020	-0.28367	0.00065
	-0.33142	-0.12969	-0.32685	-0.11123	-0.31680	-0.08085	-0.30329	-0.04517	-0.28568	-0.00377
	-0.32951	-0.13437	-0.32535	-0.11581	-0.31483	-0.08592	-0.30229	-0.05021	-0.28562	-0.00866
	-0.32609	-0.13807	-0.32234	-0.12057	-0.31092	-0.08969	-0.29927	-0.05455	-0.28351	-0.01306
	-0.32160	-0.14034	-0.31821	-0.12203	-0.30579	-0.09146	-0.29478	-0.05684	-0.27974	-0.01616
	-0.31660	-0.14089	-0.31348	-0.12290	-0.30038	-0.09091	-0.28965	-0.05719	-0.27501	-0.01738
LERC	-0.31752	-0.12679	-0.31342	-0.10939	-0.30434	-0.07895	-0.29141	-0.04542	-0.27464	-0.00606
TERC	+0.36181	-0.14784	+0.34725	-0.15935	+0.32436	-0.17903	+0.30219	-0.20058	+0.27573	-0.22245

A

BASIC AIRFOIL SECTION DATA

[illegible]

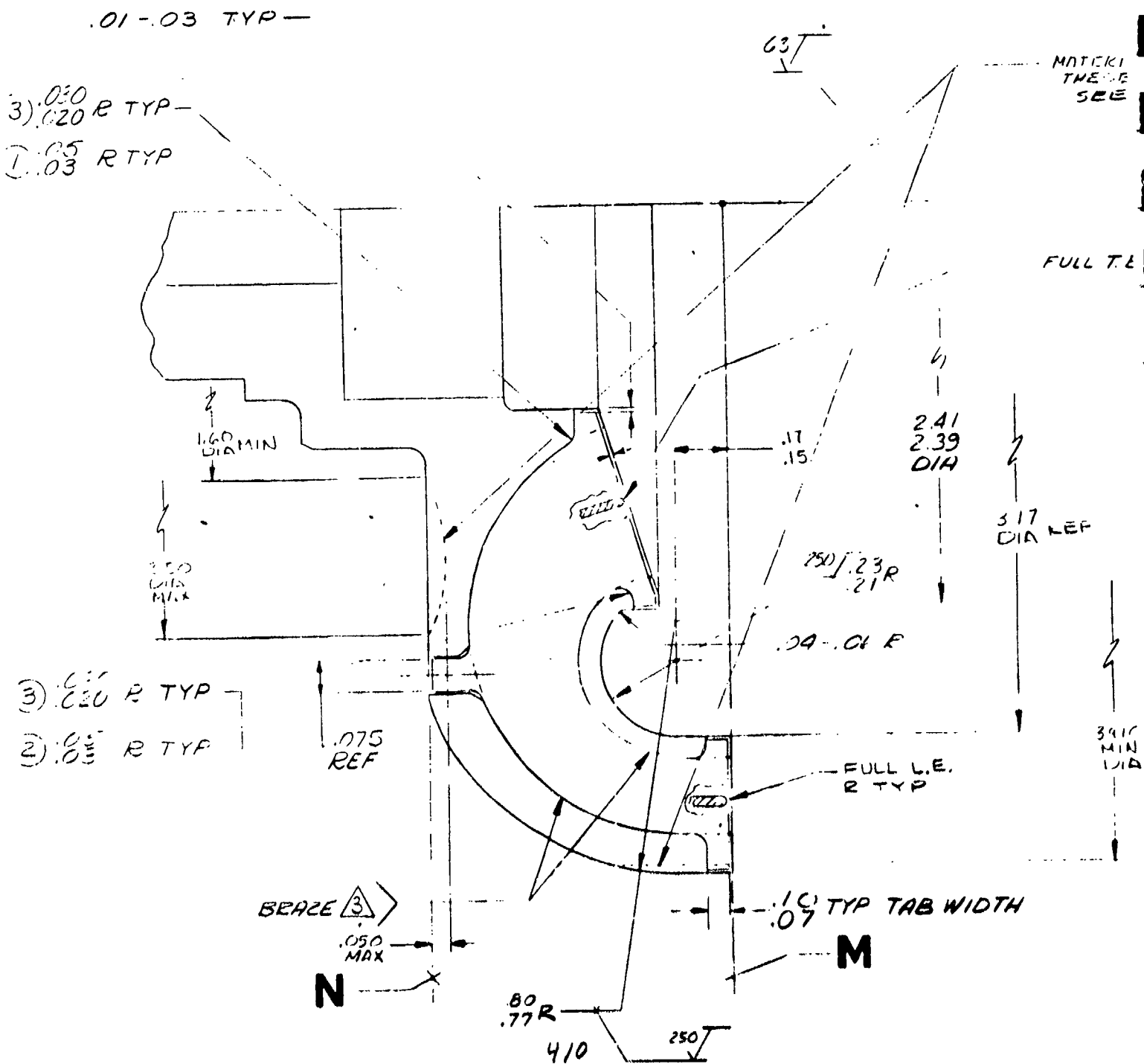
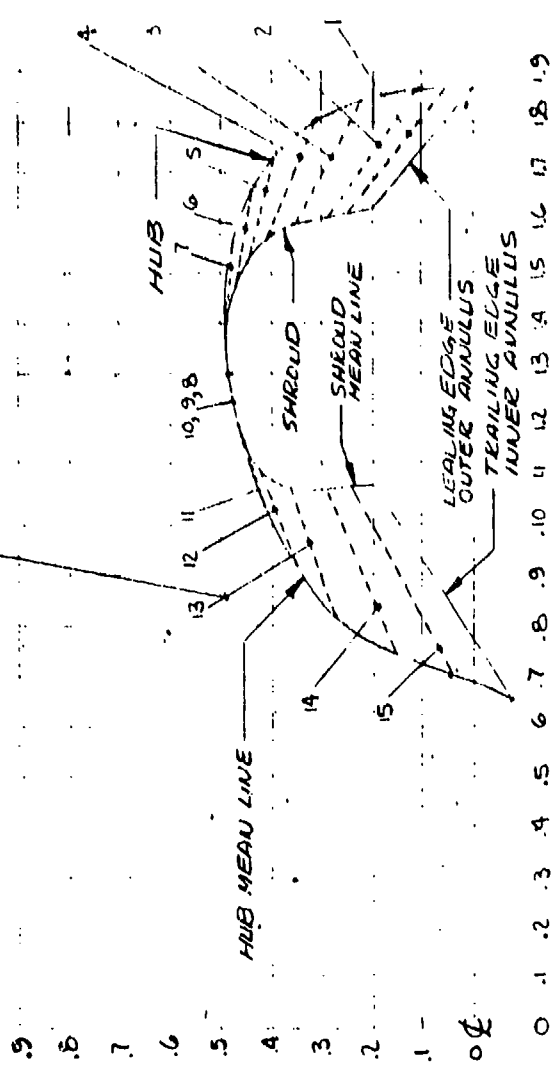


Figure 229. Torque Converter, Turbine.

NOTE: DASH LINES INDICATE STRAIGHT LINE ELEMENTS BETWEEN HUB AND SHROUD. ELEMENTS NUMBERED FROM 1 THRU 15 (I.E. & T.E. ARE ALSO STRAIGHT LINE ELEMENTS) BLADE SURFACE IS GENERATED BY FAIRING SMOOTHLY ACROSS STRAIGHT LINE ELEMENTS. NO SHARP BENDS OR RAPID CHANGES IN CONTOUR

TABLE II

MEAN LINE CONTOUR @ HUB		MEAN LINE CONTOUR @ SHROUD		ELEMENT NO.
X	Y	X	Y	
COORD.	COORD.	COORD.	COORD.	
1.8699	0.000	1.6297	-2.001	I.E
1.8691	-0.0579	1.6263	-2.258	1
1.8666	-1.118	1.6227	-2.505	2
1.848	-2.225	1.601	-3.500	3
1.811	-3.13	1.572	-4.076	4
1.745	-3.90	1.525	-4.455	5
1.670	-4.37	1.477	-4.702	6
1.560	-4.74	1.409	-4.836	7
1.445	-4.90	1.343	-4.85	8
1.306	-4.84	1.271	-4.80	9
1.171	-4.57	1.201	-4.67	10
1.043	-4.165	1.149	-4.475	11
.919	-3.49	1.107	-4.23	12
.823	-2.755	1.081	-3.87	13
.747	-1.55	1.076	-3.45	14
.7058	-0.405	1.061	-2.43	15
.6556	.0758	1.035	-2.009	T.E.



X AXIS ~ INCHES

MEAN LINE CONTOUR OF VANE - SEE NOTE 6
SCALE 4/1

Figure 230. Torque Converter, Turbine.

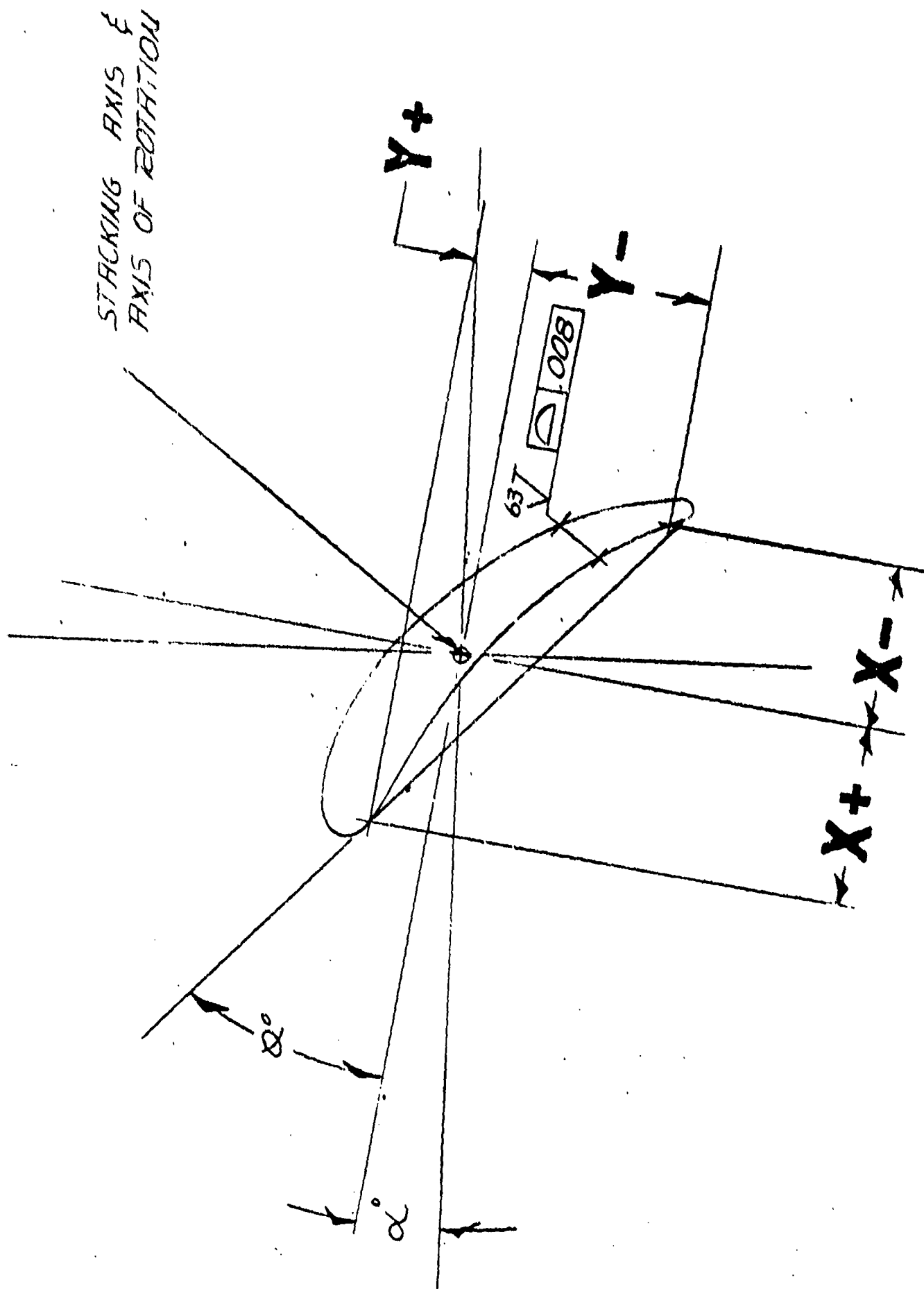
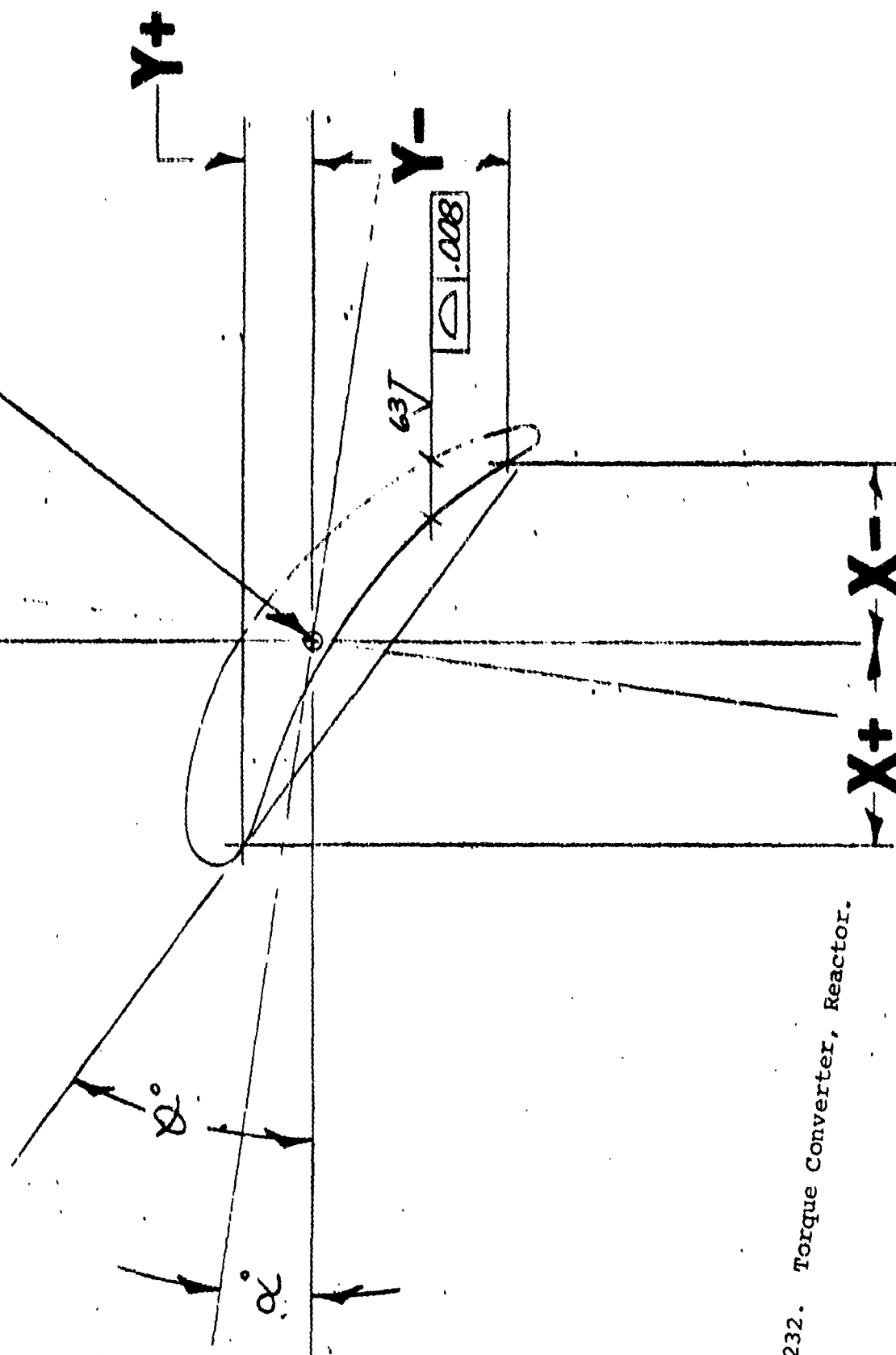


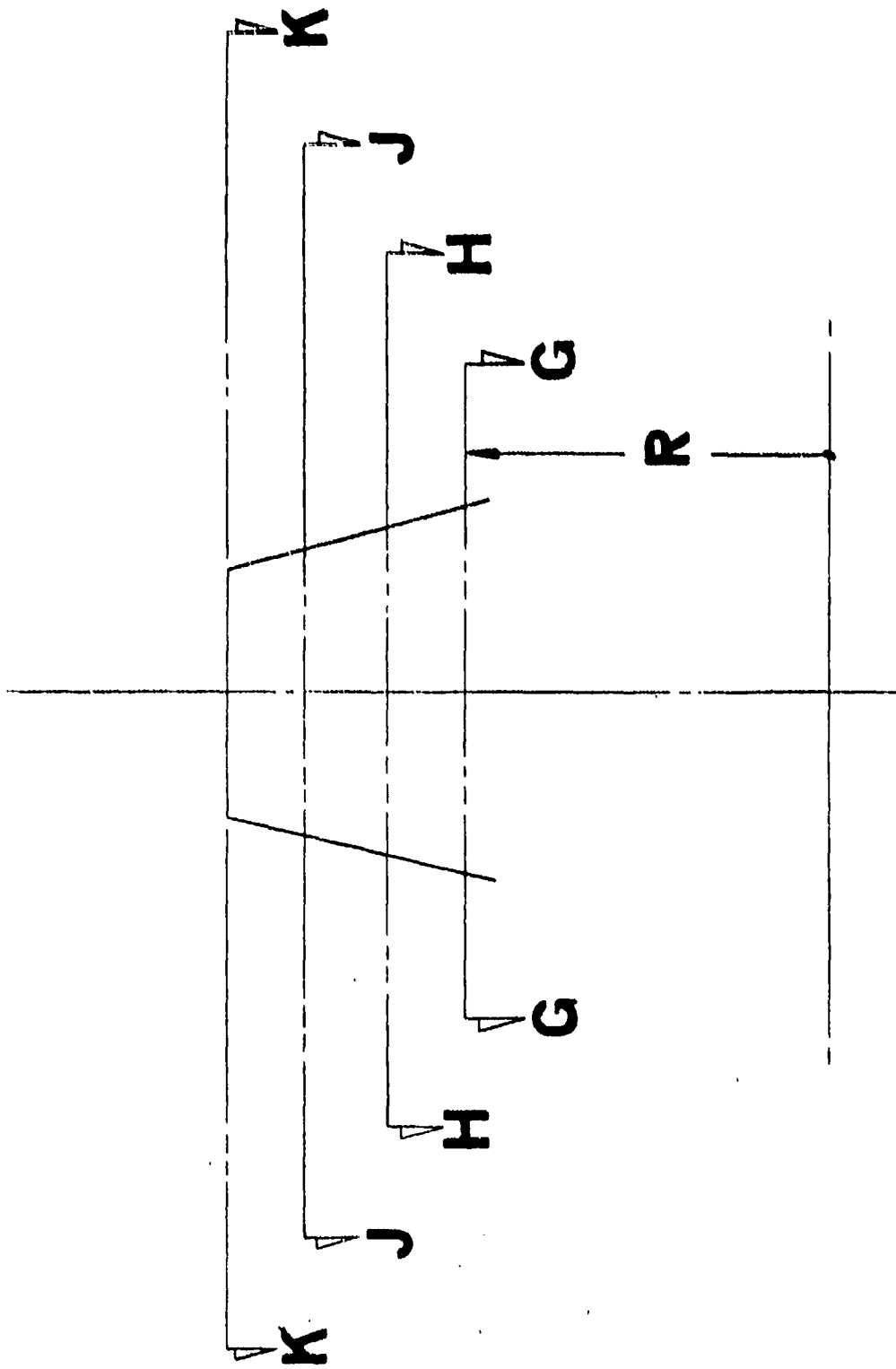
Figure 231. Torque Converter, Reactor.

STICKING AXIS
AXIS OF ROTATION



445

Figure 232. Torque Converter, Reactor.



VIEW OF TYPICAL AIRFOIL
 NO SCALE
 12 VANES EQUALLY SPACED

⊕	A-B	C	.010	TOTAL
⊕	4	⊕		

Figure 233. Torque Converter, Reactor.

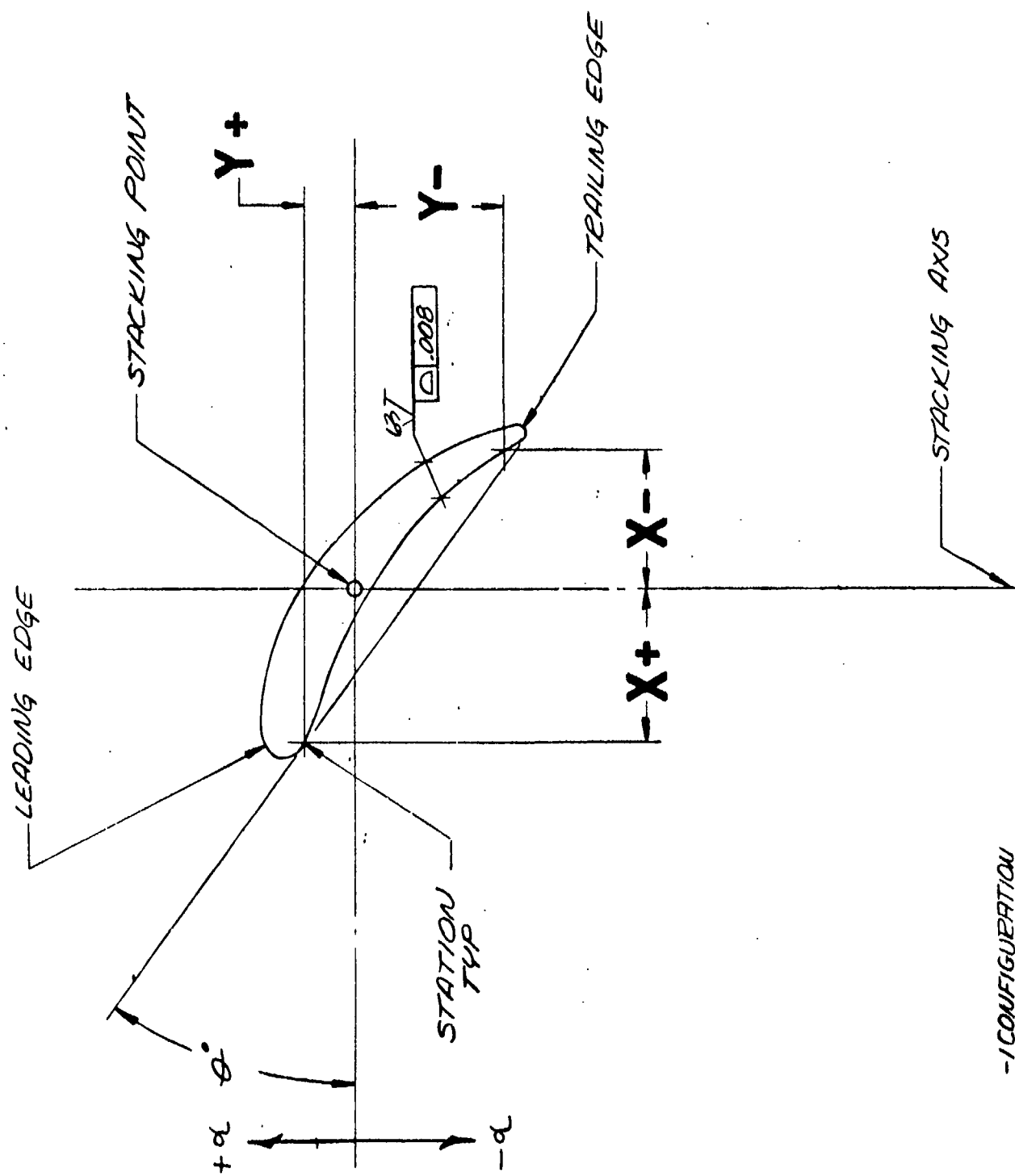


Figure 234. Torque Converter, Reactor.

-/CONFIGURATION

AIRFOIL DATA								
SECTION	G-G		H-H		J-J		K-K	
<i>R</i>	.660		.800		.950		1.093	
$\theta = \pm 30'$	35° 9'		36° 27'		38° 59'		42° 47'	
STATION	X	Y	X	Y	X	Y	X	Y
1	-.301	-.332	-.272	-.312	-.237	-.290	-.199	-.270
2	-.235	-.227	-.222	-.224	-.205	-.228	-.187	-.238
3	-.154	-.142	-.144	-.135	-.140	-.145	-.144	-.174
4	-.070	-.078	-.074	-.078	-.077	-.085	-.078	-.097
5	-.011	-.039	-.014	-.038	-.016	-.039	-.016	-.040
6	.066	.004	.074	.014	.061	.011	.028	.006
7	.122	.031	.136	.044	.117	.040	.062	.019
8	.178	.051	.192	.064	.173	.066	.118	.055
9	.268	.084	.259	.089	.227	.090	.172	.086
10	.306	.100	.273	.093	.239	.096	.209	.108
11	.319	.105	.278	.094	.242	.097	.215	.113
12	.332	.115	.294	.103	.256	.106	.223	.123
13	.341	.132	.304	.121	.264	.122	.227	.135
14	.342	.150	.305	.141	.264	.141	.223	.149
15	.334	.166	.299	.154	.258	.151	.216	.159
16	.321	.179	.284	.168	.244	.163	.205	.165
17	.302	.186	.265	.173	.228	.167	.196	.167
18	.287	.188	.255	.174	.219	.166	.184	.166
19	.246	.188	.239	.176	.203	.164	.136	.155
20	.136	.170	.157	.166	.138	.150	.074	.124
21	.074	.145	.092	.146	.073	.127	.013	.086
22	.009	.112	.022	.110	.012	.091	.023	.056
23	-.077	.056	-.074	.044	-.070	.029	-.066	.014
24	-.138	.002	-.134	-.011	-.130	-.031	-.125	-.057
25	-.216	-.089	-.199	-.089	-.185	-.110	-.179	-.151
26	-.282	-.200	-.260	-.203	-.234	-.212	-.208	-.227
27	-.332	-.322	-.299	-.303	-.260	-.282	-.221	-.262
28	-.331	-.329	-.298	-.307	-.260	-.287	-.221	-.271
29	-.327	-.335	-.294	-.314	-.256	-.293	-.217	-.275
30	-.321	-.339	-.289	-.318	-.252	-.297	-.214	-.277
31	-.314	-.340	-.283	-.319	-.246	-.297	-.207	-.277
32	-.305	-.337	-.276	-.317	-.240	-.295	-.201	-.275

Figure 235. Torque Converter, Reactor Airfoil Data.